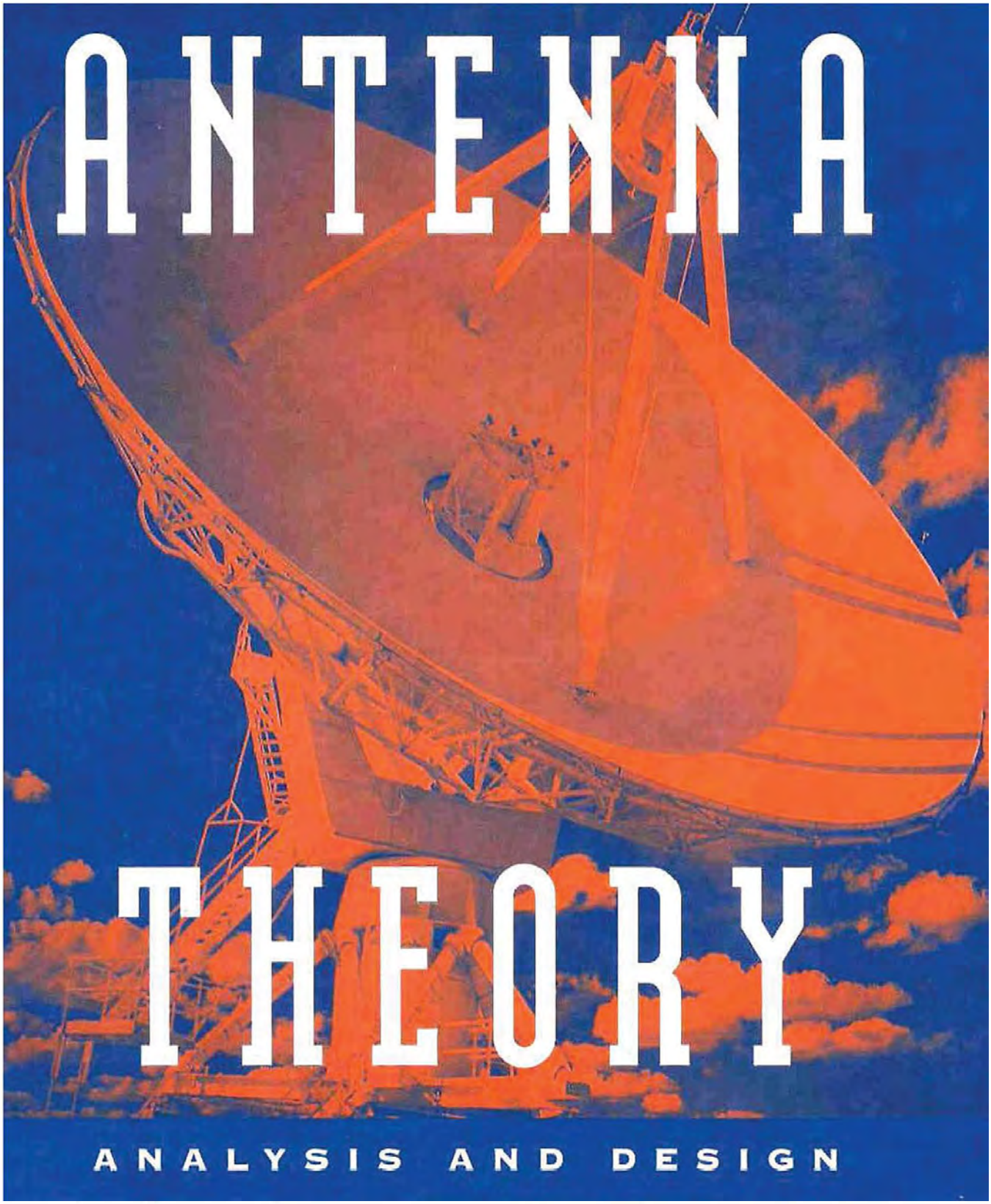


SECOND EDITION

CONSTANTINE A. BALANIS

INTEL-1045
U.S. Patent 7,151,430

ANTENNA THEORY

ANALYSIS AND DESIGN

SECOND EDITION



CONSTANTINE A. BALANIS
Arizona State University

JOHN WILEY & SONS, INC.
New York • Chichester • Brisbane • Toronto • Singapore

INTEL-1045
U.S. Patent 7,151,430

FRONT COVER PHOTO: Parabolic reflector (25-m diameter) of 27-element Very Large Array (VLA) radio telescope. National Radio Astronomy Observatory (NRAO), Socorro, New Mexico.

ACQUISITIONS EDITOR Steven Elliot
MARKETING MANAGER Jay Kirsch
SENIOR PRODUCTION EDITOR Tony VenGraitis
DESIGNER Harry Nolan
MANUFACTURING MANAGER Mark Cirillo
ILLUSTRATION Jamie Perea
PRODUCTION SERVICE Ingrao Associates
COVER PHOTOGRAPH Socorro Mexico, Telegraph Colour Library FPG. ©

This book was set in *Times Roman* by *Ruttle, Shaw & Wetherill*, and printed and bound by *Hamilton Printing*. The cover was printed by *New England Book Components*.

Recognizing the importance of preserving what has been written, it is a policy of John Wiley & Sons, Inc. to have books of enduring value published in the United States printed on acid-free paper, and we exert our best efforts to that end.

Copyright © 1982, 1997, by John Wiley & Sons, Inc.

All rights reserved. Published simultaneously in Canada.

Reproduction or translation of any part of this work beyond that permitted by Sections 107 and 108 of the 1976 United States Copyright Act without the permission of the copyright owner is unlawful. Requests for permission or further information should be addressed to the Permissions Department, John Wiley & Sons, Inc.

Library of Congress Cataloging in Publication Data:
Balanis, Constantine A., 1938–
Antenna theory : analysis and design / Constantine A. Balanis. — 2nd ed.
p. cm.
Includes index.
ISBN 0–471–59268–4 (cloth : alk. paper)
1. Antennas (Electronics) I. Title.
TK7871.6.B353 1997
621.382'4—dc20

Printed in the United States of America

10 9

INTEL-1045
U.S. Patent 7,151,430

To my mother, and to the memory of
my father, uncle, and aunt

About The Author

Constantine A. Balanis received his BSEE degree from Virginia Polytechnic Institute, Blacksburg, in 1964, his MEE degree from University of Virginia, Charlottesville, in 1966, and his PhD degree in electrical engineering from Ohio State University, Columbus, in 1969.

From 1964 to 1970 he was with the NASA Langley Research Center in Hampton, Virginia, and from 1970 to 1983 he was with the Department of Electrical Engineering, West Virginia University, Morgantown. In 1983 he joined Arizona State University, Tempe, and he is now Regents' Professor of Electrical Engineering. He teaches graduate and undergraduate courses in electromagnetic theory, antennas, and microwave circuits. His research interests are in low- and high-frequency numerical and computational techniques for antennas and scattering, electromagnetic wave propagation in microwave-integrated circuit tranmission lines, and multipath wave propagation. He received the Arizona State University Outstanding Graduate Mentor Award for 1996, the Graduate Teaching Excellence Award, School of Engineering, Arizona State University for 1987–1988, the 1989 IEEE Region 6 Individual Achievement Award, and the 1992 Special Professionalism Award of the IEEE Phoenix Section.

Dr. Balanis is a Fellow of IEEE, and a member of ASEE, Electromagnetics Academy, Sigma Xi, Tau Beta Pi, Eta Kappa Nu, and Phi Kappa Phi. He has served as the Associate Editor of the *IEEE Transactions on Antennas and Propagation* (1974–1977) and *IEEE Transactons on Geoscience and Remote Sensing* (1982–1984), Editor of the *Newsletter* for the IEEE Geoscience and Remote Sensing Society (1982–1983), Second Vice-President of the IEEE Geoscience and Remote Sensing Society (1984), and as Chairman of the Distinguished Lecturer Program (1988–91) and member of the Administrative Committee (1992–95), (1997–99) of the IEEE Antennas and Propagation Society. He is also the author of *Advanced Engineering Electromagnetics* (John Wiley & Sons, New York, 1989), and "Horn Antennas," Chapter 8 in *Antenna Handbook: Theory, Applications, and Design* (Y. T. Lo and S. W. Lee, Editors), Van Nostrand Reinhold Co., New York, 1988.



INTEL-1045
U.S. Patent 7,151,430

Preface

This second edition of *Antenna Theory* is designed to meet the needs of electrical engineering and physics students at the senior undergraduate and beginning graduate levels, and those of practicing engineers as well. The text presumes that the students have a knowledge of basic undergraduate electromagnetic theory, including Maxwell's equations and the wave equation, introductory physics, and differential and integral calculus. Mathematical techniques required for understanding some advanced topics in the later chapters are incorporated in the individual chapters or are included as appendices.

The second edition of the book has maintained all of the attractive features of the first edition. However there have been many new features added to this edition. In particular, an entire new chapter is devoted to the analysis and design of microstrip antennas; introductory material has been added for the Fourier transform (spectral domain) method, coupling, radar cross section for antennas, aperture-matched and multimode horns, near-field to far-field measurements, and compact range chamber designs and instrumentation for antenna and RCS measurements. There is an increase in design procedures and equations; FORTRAN computer programs at the end of most of the chapters that can be used for design and analysis; additional examples, end-of-chapter problems, and two- and three-dimensional illustrations; and updated material on Moment Method and mutual impedances. In addition, a computer program has been developed, based on the Finite Difference Time-Domain method to animate and visualize radiation. All the computer programs are contained in a 3.5-inch disc, which is included with the book.

The book's main objective is to introduce, in a unified manner, the fundamental principles of antenna theory and to apply them to the analysis, design, and measurements of antennas. Because there are so many methods of analysis and design and a plethora of antenna structures, applications are made to some of the most basic and practical configurations, such as linear dipoles, loops, arrays, broadband and frequency-independent antennas, aperture antennas, horn antennas, microstrip antennas, and reflector antennas.

Introductory material on analytical methods, such as the Moment method and Fourier transform (spectral) technique, is also included. These techniques, with the fundamental principles of antenna theory, can be used to analyze and design almost any antenna configuration. A chapter on antenna measurements introduces state-of-the-art methods used in the measurements of the most basic antenna characteristics (pattern, gain, directivity, radiation efficiency, impedance, current, and polarization) and updates progress made in antenna instrumentation, antenna range design, and scale modeling. Techniques and systems used in near- to far-field measurements and transformations are also discussed.

INTEL-1045
U.S. Patent 7,151,430

A sufficient number of topics have been covered, some for the first time in an undergraduate text, so that the book will serve not only as a text, but also as a reference for the practicing and design engineer and even the amateur radio buff. These include design procedures for Yagi-Uda and log-periodic arrays, horns, and microstrip patches; synthesis techniques using the Schelkunoff, Fourier transform, Woodward-Lawson, Tschebyscheff, and Taylor methods; radiation characteristics of corrugated, aperture-matched, and multimode horns; analysis and design of rectangular and circular microstrip patches; and matching techniques such as the binomial, Tschebyscheff, T-, gamma, and omega matches.

The text contains sufficient mathematical detail to enable the average undergraduate electrical engineering and physics students to follow, without too much difficulty, the flow of analysis and design. A certain amount of analytical detail, rigor, and thoroughness allows many of the topics to be traced to their origin. My experiences as a student, engineer, and teacher have shown that a text for this course must not be a book of unrelated formulas, and it must not resemble a "cookbook." This book begins with the most elementary material, develops underlying concepts needed for sequential topics, and progresses to more advanced methods and systems configurations. Each chapter is subdivided into sections or subsections whose individual headings clearly identify the antenna characteristic(s) discussed, examined, or illustrated.

A distinguished feature of this book is its three-dimensional graphical illustrations from the first edition, which have been expanded and supplemented in the second edition. In the past, antenna texts have displayed the three-dimensional energy radiated by an antenna by a number of separate two-dimensional patterns. With the advent and revolutionary advances in digital computations and graphical displays, an additional dimension has been introduced for the first time in an undergraduate antenna text by displaying the radiated energy of a given radiator by a single, three-dimensional graphical illustration. Such an image, formed by the graphical capabilities of the computer and available at most computational facilities, gives a clear view of the energy radiated in all space surrounding the antenna. It is hoped that this will lead to a better understanding of the underlying principles of radiation and that it will provide a clearer visualization of the pattern formation in all space.

In addition, there is an abundance of general graphical illustrations, design data, references, and additional problems. Many of the principles are illustrated with examples, graphical illustrations, and physical arguments. Although students are often convinced that they understand the principles, difficulties arise when they attempt to use them. An example, especially a graphical illustration, can often better illuminate those principles. As they say, "a picture is worth a thousand words."

Numerical techniques and computer solutions are illustrated and encouraged. A number of FORTRAN computer programs and subroutines are included at the end of Chapters 1, 2, 4, 5, 6, 8, 10, 11, 13, and 14. The program at the end of Chapter 1 can be used to animate and then visualize radiation by an infinite line source driven by a Gaussian pulse and an E-plane sectoral horn energized by a continuous cosinusoidal source. To accomplish this, the user needs the professional edition of MATLAB. All of the computer programs, especially those at the end of Chapters 6, 11, 13, and 14, have been developed to design, respectively, uniform and nonuniform arrays, log-periodic dipole arrays, horns, and microstrip patch antennas. In some cases, the computer programs also perform analysis on the designs. The programs at the end of Chapters 2, 4, 5, 8, and 10 are primarily developed for analysis. A computer disc with the source codes is included with the book. These can be used to perform routine calculations of complex functions and/or formulations, to carry out numerical integrations that cannot be performed in closed form, and to display solutions in graphical

INTEL-1045
U.S. Patent 7,151,430

form. The problems at the end of each chapter can be used to apply the underlying principles of antenna theory to the analysis and design of many practical radiators.

For course use, the text is intended primarily for a two-semester (or two- or three-quarter) sequence in antenna theory. The first course should be given at the senior undergraduate level and should cover most of the material in Chapters 1 through 7 and Chapter 16. The material in Chapters 8 through 15 should be covered in a beginning graduate-level course. Selected chapters and sections from the book can be covered in a single semester, without loss of continuity. However, it is almost essential that most of the material in Chapters 2 through 6 be covered in the first course and before proceeding to any more advanced topics. To cover all the material of the text in the proposed time frame would be, in some cases, a very ambitious task. Sufficient topics have been included, however, to make the text complete and to give the teacher the flexibility to emphasize, de-emphasize, or omit sections or chapters. Some of the chapters and sections can be omitted without loss of continuity.

In the entire book an $e^{j\omega t}$ time variation is assumed, and it is suppressed. The International System of Units, which is an expanded form of the rationalized MKS system, is used in the text. In some cases, the units of length are in meters (or centimeters) and in feet (or inches). Numbers in parentheses ( ) refer to equations, whereas those in brackets [ ] refer to references. For emphasis, the most important equations, once they are derived, are boxed. A Solutions Manual for all end of chapter problems is available for the instructor.

I would like to acknowledge the invaluable suggestions and constructive criticisms of the reviewers for the second edition of this book: Dr. Edward B. Joy of Georgia Tech, Dr. Stuart A. Long of University of Houston, Dr. David M. Pozar of University of Massachusetts, Dr. Ezekiel Bahar of the University of Nebraska and Dr. Paul E. Mayes of University of Illinois, Urbana, and those of the first edition from my colleague Dr. Thomas E. Tice of Arizona State University and Dr. Charlton H. Walter of TRW (formally of Ohio State University). Also I would like to acknowledge the suggestions, end of the chapter problems, and figures provided by my colleague Dr. James T. Aberle and Dr. Roger D. Radcliff of Ohio University.

The book, especially the graphical illustrations, computer programs, solutions to many of the problems, solutions manual, and proofreading of the galleys and page proofs would not have been possible without the contributions from many of my and other graduate students at Arizona State University. It is a pleasure to acknowledge those of Anastasis C. Polycarpou for the development of many of the computer programs for Chapters 6, 8, 13, and 14, and preparation of the computer disc; Seong-Ook and Jeong-Suk Park for completion of the solutions manual and proofreading the galleys and page proofs; Dr. Panayiotis A. Tirkas for the development of the computer programs for Yagi-Uda arrays and analysis of horns, and many of the new three-dimensional computer generated illustrations; William V. Andrew for the development of the animation-visualization computer program; Craig R. Birtcher for antenna pattern measurements, and material on near- to far-field measurements and compact ranges; Chris B. Bishop for the development of the computer program for the design and analysis of log-periodic dipole arrays; David M. Kokotoff for revising the Hallén's-Moment Method computer program; and Tamara Spreckic, Konstantinos D. Katsibas, and Jian Peng for proofreading the galleys and preparation of graphical illustrations.

Since many of the unique features of this book carry over from the first edition, I still acknowledge the contributions of my graduate students at West Virginia University, especially those of John L. Jeffrey. Many thanks go to all those professors, practicing engineers, and students, who over the years of the first edition provided invaluable suggestions and corrections. I also want to acknowledge the expert typing

INTEL-1045
U.S. Patent 7,151,430

by Linda S. Arneson of the additional material included in the revised manuscript and to Kathy Muckenhirn for handling many of the logistics during publication. Many thanks to Dr. Atef Z. Elsherbeni and Clayborne D. Taylor, Jr., of University of Mississippi for permitting and providing the use of the *2-D Antenna Pattern Plotter: Rectangular-Polar* computer program.

To the companies and individuals that provided illustrations and copyright permissions, I am most appreciative. I am also grateful to the staff of John Wiley & Sons, Inc., especially Steven Elliot, Wiley editor of electrical engineering, for the interest in the publication of the second edition. Special thanks also to Suzanne Ingrao of Ingrao Associates, production editor of this book, for her professional help. Finally, I must express my gratitude to Helen, Renie and Stephanie for proofreading the galleys and for their encouragement, patience, sacrifice and understanding for the many hours of neglect during the completion of the first and second editions of this book.

Constantine A. Balanis
Arizona State University
Tempe, AZ

INTEL-1045
U.S. Patent 7,151,430

Contents

Preface V

CHAPTER 1 ANTENNAS 1

1.1 Introduction 1
1.2 Types of Antennas 3
Wire Antennas; Aperture Antennas; Microstrip Antennas; Array Antennas; Reflector Antennas; Lens Antennas
1.3 Radiation Mechanism 7
Single Wire; Two-Wires; Dipole; Computer Animation-Visualization of Radiation Problems
1.4 Current Distribution on a Thin Wire Antenna 17
1.5 Historical Advancement 19
Antenna Elements; Methods of Analysis; Some Future Challenges
References 24
Computer Program—Animation-Visualization of Radiation Problems 27

CHAPTER 2 FUNDAMENTAL PARAMETERS OF ANTENNAS 28

2.1 Introduction 28
2.2 Radiation Pattern 28
Isotropic, Directional, and Omnidirectional Patterns; Principal Patterns; Radiation Pattern Lobes; Field Regions; Radian and Steradian
2.3 Radiation Power Density 35
2.4 Radiation Intensity 38
2.5 Directivity 39
Directional Patterns; Omnidirectional Patterns
2.6 Numerical Techniques 53
2.7 Gain 58
2.8 Antenna Efficiency 60
2.9 Half-Power Beamwidth 62
2.10 Beam Efficiency 63
2.11 Bandwidth 63
2.12 Polarization 64
Linear, Circular, and Elliptical Polarizations; Polarization Loss Factor and Efficiency

INTEL-1045
U.S. Patent 7,151,430

2.13 Input Impedance 73
2.14 Antenna Radiation Efficiency 78
2.15 Antenna Vector Effective Length and Equivalent areas 79
Vector Effective Length; Antenna Equivalent Areas
2.16 Maximum Directivity and Maximum Effective Area 84
2.17 Friis Transmission Equation and Radar Range Equation 86
Friis Transmission Equation; Radar Range Equation; Antenna Radar Cross Section
2.18 Antenna Temperature 98
References 101
Problems 102
Computer Program—2-D Antenna Pattern Plotter: Rectangular-Polar 113
Computer Program—Directivity 115

CHAPTER 3 RADIATION INTEGRALS AND AUXILIARY POTENTIAL FUNCTIONS 116

3.1 Introduction 116
3.2 The Vector Potential **A** for an Electric Current Source **J** 117
3.3 The Vector Potential **F** for a Magnetic Current Source **M** 119
3.4 Electric and Magnetic Fields for Electric (J) and Magnetic (M) Current Sources 120
3.5 Solution of the Inhomogeneous Vector Potential Wave Equation 121
3.6 Far-Field Radiation 125
3.7 Duality Theorem 126
3.8 Reciprocity and Reaction Theorems 127
Reciprocity for Two Antennas; Reciprocity for Radiation Patterns
References 132
Problems 132

CHAPTER 4 LINEAR WIRE ANTENNAS 133

4.1 Introduction 133
4.2 Infinitesimal Dipole 133
Radiated Fields; Power Density and Radiation Resistance; Radian Distance and Radian Sphere; Near-Field ($kr \ll 1$) Region; Intermediate-Field ($kr > 1$) Region; Far-Field ($kr \gg 1$) Region; Directivity
4.3 Small Dipole 143
4.4 Region Separation 145
Far-Field (Fraunhofer) Region; Radiating Near-Field (Fresnel) Region; Reactive Near-Field Region
4.5 Finite Length Dipole 151
Current Distribution; Radiated Fields: Element Factor, Space Factor, and Pattern Multiplication; Power Density, Radiation Intensity, and Radiation Resistance; Directivity; Input Resistance; Finite Feed Gap
4.6 Half-Wavelength Dipole 162
4.7 Linear Elements Near or on Infinite Perfect Conductors 164
Image Theory; Vertical Electric Dipole; Approximate Formulas for Rapid

INTEL-1045
U.S. Patent 7,151,430

Calculations and Design; Antennas for Mobile Communication Systems: Horizontal Electric Dipole
4.8 Ground Effects **181**
Vertical Electric Dipole; Horizontal Electric Dipole; Earth Curvature
References **194**
Problems **196**
Computer Program—Linear Dipole **202**

CHAPTER 5 LOOP ANTENNAS **203**

5.1 Introduction **203**
5.2 Small Circular Loop **204**
Radiated Fields; Small Loop and Infinitesimal Magnetic Dipole; Power Density and Radiation Resistance; Near-Field ($kr \ll 1$) Region; Far-Field ($kr \gg 1$) Region; Radiation Intensity and Directivity; Equivalent Circuit
5.3 Circular Loop of Constant Current **217**
Radiated Fields; Power Density, Radiation Intensity, Radiation Resistance, and Directivity
5.4 Circular Loop with Nonuniform Current **224**
Arrays; Design Procedure
5.5 Ground and Earth Curvature Effects for Circular Loops **230**
5.6 Polygonal Loop Antennas **233**
Square Loop; Triangular, Rectangular, and Rhombic Loops
5.7 Ferrite Loop **240**
Radiation Resistance; Ferrite-Loaded Receiving Loop
5.8 Mobile Communication Systems Applications **242**
References **242**
Problems **243**
Computer Program—Circular Loop **248**

CHAPTER 6 ARRAYS: LINEAR, PLANAR, AND CIRCULAR **249**

6.1 Introduction **249**
6.2 Two-Element Array **250**
6.3 *N*-Element Linear Array: Uniform Amplitude and Spacing **257**
Broadside Array; Ordinary End-Fire Array; Phased (Scanning) Array; Hansen-Woodyard End-Fire-Array
6.4 *N*-Element Linear Array: Directivity **276**
Broadside Array; Ordinary End-Fire Array; Hansen-Woodyard End-Fire Array
6.5 Design Procedure **282**
6.6 *N*-Element Linear Array: Three-Dimensional Characteristics **283**
N-Elements Along Z-Axis; N-Elements Along X- or Y-Axis
6.7 Rectangular-to-Polar Graphical Solution **287**
6.8 *N*-Element Linear Array: Uniform Spacing, Nonuniform Amplitude **288**
Array Factor; Binomial Array; Dolph-Tschebyscheff Array
6.9 Superdirectivity **306**
Efficiency and Directivity; Designs with Constraints

INTEL-1045
U.S. Patent 7,151,430

6.10 Planar Array 309
Array Factor: Beamwidth: Directivity
6.11 Design Considerations 321
6.12 Circular Array 324
Array Factor
References 328
Problems 329
Computer Program—Arrays 337

CHAPTER 7 ANTENNA SYNTHESIS AND CONTINUOUS SOURCES 339

7.1 Introduction 339
7.2 Continuous Sources 340
Line-Source: Discretization of Continuous Sources
7.3 Schelkunoff Polynomial Method 342
7.4 Fourier Transform Method 346
Line-Source; Linear Array
7.5 Woodward-Lawson Method 352
Line-Source; Linear Array
7.6 Taylor Line-Source (Tschebyscheff Error) 358
Design Procedure
7.7 Taylor Line-Source (One-Parameter) 362
7.8 Triangular, Cosine, and Cosine-Squared Amplitude Distributions 368
7.9 Line-Source Phase Distributions 371
7.10 Continuous Aperture Sources 373
Rectangular Aperture; Circular Aperture
References 375
Problems 376

CHAPTER 8 INTEGRAL EQUATIONS, MOMENT METHOD, AND SELF AND MUTUAL IMPEDANCES 379

8.1 Introduction 379
8.2 Integral Equation Method 380
Electrostatic Charge Distribution; Integral Equation
8.3 Finite Diameter Wires 388
Pocklington's Integral Equation; Hallén's Integral Equation; Source Modeling
8.4 Moment Method Solution 395
Basis Functions; Weighting (Testing) Functions
8.5 Self Impedance 403
Integral Equation-Moment Method; Induced EMF Method
8.6 Mutual Impedance Between Linear Elements 412
Integral Equation-Moment Method; Induced EMF Method
8.7 Mutual Coupling in Arrays 422
Coupling in the Transmitting Mode; Coupling in the Receiving Mode; Mutual Coupling on Array Performance; Coupling in an Infinite

INTEL-1045
U.S. Patent 7,151,430

Regular Array: Grating Lobes Considerations
References 434
Problems 436
Computer Program—Moment Method 438
Computer Program—Self and Mutual Impedances 439

CHAPTER 9 BROADBAND DIPOLES AND MATCHING TECHNIQUES 441

9.1 Introduction 441
9.2 Biconical Antenna 442
Radiated Fields; Input Impedance
9.3 Triangular Sheet, Bow-Tie, and Wire Simulation 447
9.4 Cylindrical Dipole 449
Bandwidth; Input Impedance; Resonance and Ground Plane Simulation; Radiation Patterns; Equivalent Radii; Dielectric Coating
9.5 Folded Dipole 458
9.6 Discone and Conical Skirt Monopole 462
9.7 Sleeve Dipole 464
9.8 Matching Techniques 466
Stub-Matching; Quarter-Wavelength Transformer; T-Match; Gamma Match; Omega Match; Baluns and Transformers
References 483
Problems 484

CHAPTER 10 TRAVELING WAVE AND BROADBAND ANTENNAS 488

10.1 Introduction 488
10.2 Traveling Wave Antennas 488
Long Wire; V Antenna; Rhombic Antenna
10.3 Broadband Antennas 505
Helical Antenna; Electric-Magnetic Dipole; Yagi-Uda Array of Linear Elements; Yagi-Uda Array of Loops
References 534
Problems 535
Computer Program—Yagi-Uda Array 541

CHAPTER 11 FREQUENCY INDEPENDENT ANTENNAS AND ANTENNA MINIATURIZATION 542

11.1 Introduction 542
11.2 Theory 543
11.3 Equiangular Spiral Antennas 545
Planar Spiral; Conical Spiral

INTEL-1045
U.S. Patent 7,151,430

11.4 Log-Periodic Antennas 551
Planar and Wire Surfaces; Dipole Array; Design of Dipole Array
11.5 Fundamental Limits of Electrically Small Antennas 566
References 570
Problems 571
Computer Program—Log-Periodic Dipole Array 573

CHAPTER 12 APERTURE ANTENNAS 575

12.1 Introduction 575
12.2 *Field Equivalence Principle: Huygens' Principle* 575
12.3 Radiation Equations 582
12.4 Directivity 584
12.5 Rectangular Apertures 584
Uniform Distribution on an Infinite Ground Plane; Uniform Distribution in Space; TE_{10}-Mode Distribution on an Infinite Ground Plane; Beam Efficiency
12.6 Circular Apertures 603
Uniform Distribution on an Infinite Ground Plane; TE_{11}-Mode Beam Efficiency
12.7 Design Considerations 611
Rectangular Aperture; Circular Aperture
12.8 Babinet's Principle 616
12.9 Fourier Transforms in Aperture Antenna Theory 620
Fourier Transforms-Spectral Domain; Radiated Fields; Asymptotic Evaluation of Radiated Field; Dielectric Covered Apertures; Aperture Admittance
12.10 Ground Plane Edge Effects: The Geometrical Theory of Diffraction 638
References 643
Problems 644

CHAPTER 13 HORN ANTENNAS 651

13.1 Introduction 651
13.2 *E*-Plane Sectoral Horn 651
Aperture Fields; Radiated Fields; Directivity
13.3 *H*-Plane Sectoral Horn 668
Aperture Fields; Radiated Fields; Directivity
13.4 Pyramidal Horn 682
Aperture Fields, Equivalent, and Radiated Fields; Directivity; Design Procedure
13.5 Conical Horn 695
13.6 Corrugated Horn 696
13.7 Aperture-Matched Horns 705
13.8 Multimode Horns 707
13.9 Dielectric-Loaded Horns 712
13.10 Phase Center 712
References 714
Problems 717
Computer Program—Pyramidal Horn: Analysis 720
Computer Program—Pyramidal Horn: Design 721

INTEL-1045
U.S. Patent 7,151,430

CHAPTER 14 MICROSTRIP ANTENNAS 722

14.1 Introduction 722
Basic Characteristics; Feeding Methods; Methods of Analysis
14.2 Rectangular Patch 727
Transmission-Line Model; Cavity Model; Directivity
14.3 Circular Patch 752
Electric and Magnetic Fields-TM^z_{mnp}; Resonant Frequencies; Design; Equivalent Current Densities and Fields Radiated; Conductance and Directivity; Resonant Input Resistance
14.4 Quality Factor, Bandwidth and Efficiency 760
14.5 Input Impedance 762
14.6 Coupling 764
14.7 Circular Polarization 767
14.8 Arrays and Feed Networks 772
References 776
Problems 779
Computer Program—Microstrip Antennas 784

CHAPTER 15 REFLECTOR ANTENNAS 785

15.1 Introduction 785
15.2 Plane Reflector 785
15.3 Corner Reflector 786
90° Corner Reflector; Other Corner Reflectors
15.4 Parabolic Reflector 794
Front-Fed Parabolic Reflector; Cassegrain Reflectors
15.5 Spherical Reflector 830
References 833
Problems 835

CHAPTER 16 ANTENNA MEASUREMENTS 839

16.1 Introduction 839
16.2 Antenna Ranges 840
Reflection Ranges; Free-Space Ranges; Compact Ranges; Near-Field/Far-Field Methods
16.3 Radiation Patterns 858
Instrumentation; Amplitude Pattern; Phase Measurements
16.4 Gain Measurements 865
Absolute-Gain Measurements; Gain-Transfer (Gain-Comparison) Measurements
16.5 Directivity Measurements 871
16.6 Radiation Efficiency 872
16.7 Impedance Measurements 873
16.8 Current Measurements 874
16.9 Polarization Measurements 875
16.10 Scale Model Measurements 880
References 881

INTEL-1045
U.S. Patent 7,151,430

Appendix I $f(x) = \frac{sin(x)}{x}$ 885

Appendix II $f_N(x) = \left|\frac{\sin(Nx)}{N\sin(x)}\right|$, $N = 1,3,5,10,20$ 887

Appendix III Cosine and Sine Integrals 889

Appendix IV Fresnel Integrals 893

Appendix V Bessel Functions 899

Appendix VI Identities 911

Appendix VII Vector Analysis 914

Appendix VIII Method of Stationary Phase 922

Appendix IX Television, Radio, Telephone, and Radar Frequency Spectrums 927

Index 931

INTEL-1045
U.S. Patent 7,151,430

CHAPTER

1

ANTENNAS

1.1 INTRODUCTION

An antenna is defined by Webster's Dictionary as "a usually metallic device (as a rod or wire) for radiating or receiving radio waves." The *IEEE Standard Definitions of Terms for Antennas* (IEEE Std 145-1983)* defines the antenna or aerial as "a means for radiating or receiving radio waves." In other words the antenna is the transitional structure between free-space and a guiding device, as shown in Figure 1.1. The guiding device or transmission line may take the form of a coaxial line or a hollow pipe (waveguide), and it is used to transport electromagnetic energy from the transmitting source to the antenna, or from the antenna to the receiver. In the former case we have a transmitting antenna and in the latter a receiving antenna.

A transmission-line Thevenin equivalent of the antenna system of Figure 1.1 in the transmitting mode is shown in Figure 1.2 where the source is represented by an ideal generator, the tramission line is represented by a line with characteristic impedance Z_c, and the antenna is represented by a load Z_A [$Z_A = (R_L + R_r) + jX_A$] connected to the transmission line. The Thevenin and Norton circuit equivalents of the antenna are also shown in Figure 2.21. The load resistance R_L is used to represent the conduction and dielectric losses associated with the antenna structure while R_r, referred to as the *radiation resistance*, is used to represent radiation by the antenna. The reactance X_A is used to represent the imaginary part of the impedance associated with radiation by the antenna. This is discussed more in detail in Sections 2.13 and 2.14. Under ideal conditions, energy generated by the source should be totally transferred to the radiation resistance R_r, which is used to represent radiation by the antenna. However, in a practical system there are conduction-dielectric losses due to the lossy nature of the transmission line and the antenna, as well as the due to reflections (mismatch) losses at the interface between the line and the antenna. Taking into account the internal impedance of the source and neglecting line and reflection (mismatch) losses, maximum power is delivered to the antenna under *conjugate matching*. This is discussed in Section 2.13.

**IEEE Transactions on Antennas and Propagation*, vols. AP-17, No. 3, May 1969; AP-22, No. 1, January 1974; and AP-31, No. 6, Part II, November 1983.

INTEL-1045
U.S. Patent 7,151,430

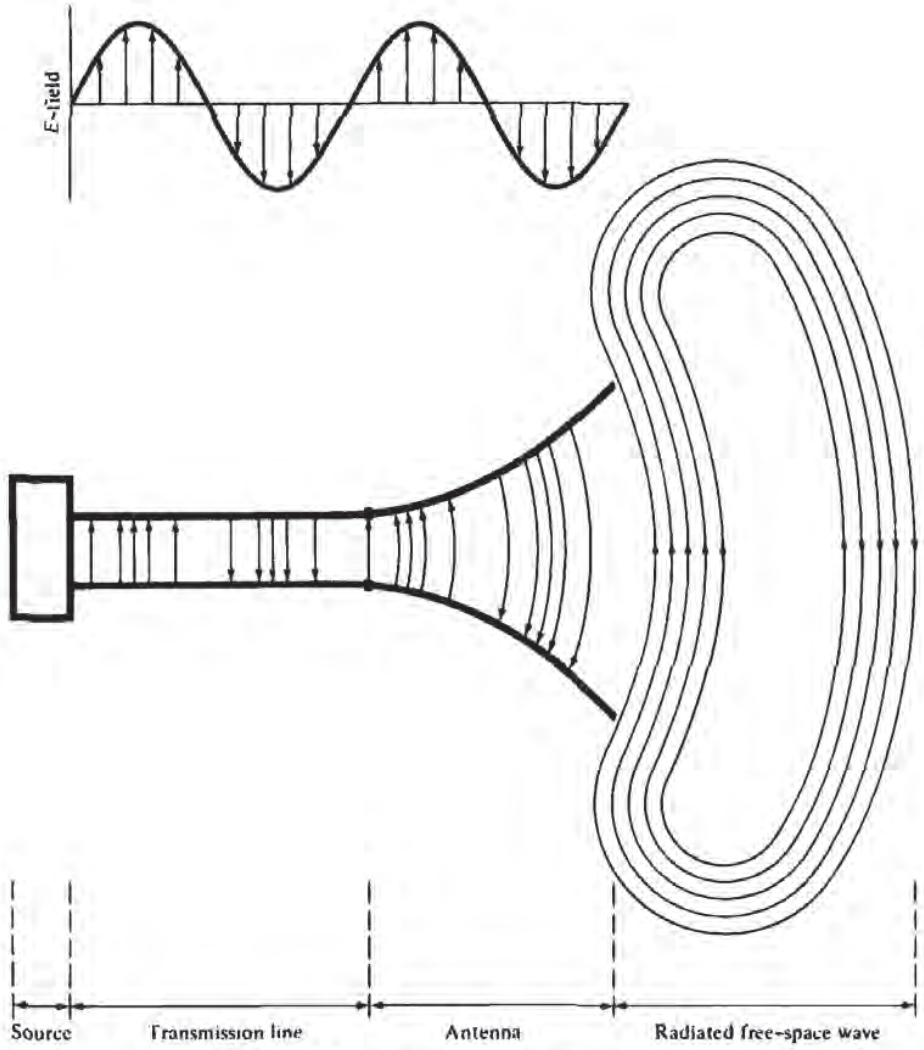


Figure 1.1 Antenna as a transition device.

The reflected waves from the interface create, along with the traveling waves from the source toward the antenna, constructive and destructive interference patterns, referred to as *standing waves*, inside the transmission line which represent pockets of energy concentrations and storage, typical of resonant devices. A typical standing wave pattern is shown dashed in Figure 1.2, while another is exhibited in Figure 1.15. If the antenna system is not properly designed, the transmission line could act to a large degree as an energy storage element instead of as a wave guiding and energy transporting device. If the maximum field intensities of the standing wave are sufficiently large, they can cause arching inside the transmission lines.

The losses due to the line, antenna, and the standing waves are undesirable. The losses due to the line can be minimized by selecting low-loss lines while those of the antenna can be decreased by reducing the loss resistance represented by R_L in Figure 1.2. The standing waves can be reduced, and the energy storage capacity of the line minimized, by matching the impedance of the antenna (load) to the characteristic impedance of the line. This is the same as matching loads to transmission lines, where

INTEL-1045
U.S. Patent 7,151,430

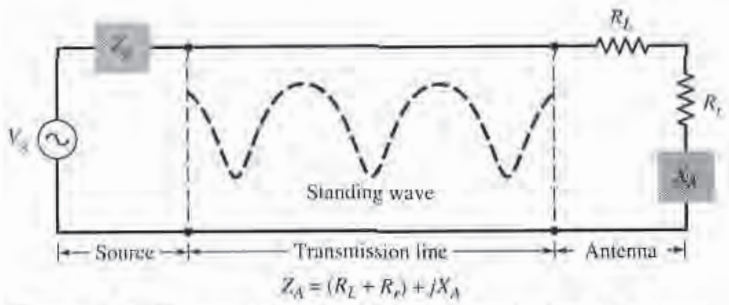


Figure 1.2 Transmission-line Thevenin equivalent of antenna in transmitting mode.

the load here is the antenna, and is discussed more in detail in Section 9.8. An equivalent similar to that of Figure 1.2 is used to represent the antenna system in the receiving mode where the source is replaced by a receiver. All other parts of the transmission-line equivalent remain the same. The radiation resistance R_r is used to represent in the receiving mode the transfer of energy from the free-space wave to the antenna. This is discussed in Section 2.13 and represented by the Thevenin and Norton circuit equivalents of Figure 2.20.

In addition to receiving or transmitting energy, an antenna in an advanced wireless system is usually required to *optimize* or *accentuate* the radiation energy in some directions and suppress it in others. *Thus the antenna must also serve as a directional device in addition to a probing device.* It must then take various forms to meet the particular need at hand, and it may be a piece of conducting wire, an aperture, a patch, an assembly of elements (array), a reflector, a lens, and so forth.

For wireless communication systems, the antenna is one of the most critical components. A good design of the antenna can relax system requirements and improve overall system performance. A typical example is TV for which the overall broadcast reception can be improved by utilizing a high-performance antenna. The antenna serves to a communication system the same purpose that eyes and eyeglasses serve to a human.

The field of antennas is vigorous and dynamic, and over the last 50 years antenna technology has been an indispensable partner of the communications revolution. Many major advances that occurred during this period are in common use today; however, many more issues and challenges are facing us today, especially since the demands for system performances are even greater. Many of the major advances in antenna technology that have been completed in the 1970s through the early 1990s, those that were underway in the early 1990s, and signals of future discoveries and breakthroughs were captured in a special issue of the *Proceedings of the IEEE* (Vol. 80, No. 1, January 1992) devoted to Antennas. The introductory paper of this special issue [1] provides a carefully structured, elegant discussion of the fundamental principles of radiating elements and has been written as an introduction for the nonspecialist and a review for the expert.

1.2 TYPES OF ANTENNAS

We will now introduce and briefly discuss some forms of the various antenna types in order to get a glance as to what will be encountered in the remainder of the book.

INTEL-1045
U.S. Patent 7,151,430

1.2.1 Wire Antennas

Wire antennas are familiar to the layman because they are seen virtually everywhere—on automobiles, buildings, ships, aircraft, spacecraft, and so on. There are various shapes of wire antennas such as a straight wire (dipole), loop, and helix which are shown in Figure 1.3. Loop antennas need not only be circular. They may take the form of a rectangle, square, ellipse, or any other configuration. The circular loop is the most common because of its simplicity in construction. Dipoles are discussed in more detail in Chapter 4, loops in Chapter 5, and helices in Chapter 10.

1.2.2 Aperture Antennas

Aperture antennas may be more familiar to the layman today than in the past because of the increasing demand for more sophisticated forms of antennas and the utilization of higher frequencies. Some forms of aperture antennas are shown in Figure 1.4. Antennas of this type are very useful for aircraft and spacecraft applications, because they can be very conveniently flush-mounted on the skin of the aircraft or spacecraft. In addition, they can be covered with a dielectric material to protect them from hazardous conditions of the environment. Waveguide apertures are discussed in more detail in Chapter 12 while horns are examined in Chapter 13.

1.2.3 Microstrip Antennas

Microstrip antennas became very popular in the 1970s primarily for spaceborne applications. Today they are used for government and commercial applications. These antennas consist of a metallic patch on a grounded substrate. The metallic patch can take many different configurations, as shown in Figure 14.2. However, the rectangular and circular patches, shown in Figure 1.5, are the most popular because of ease of

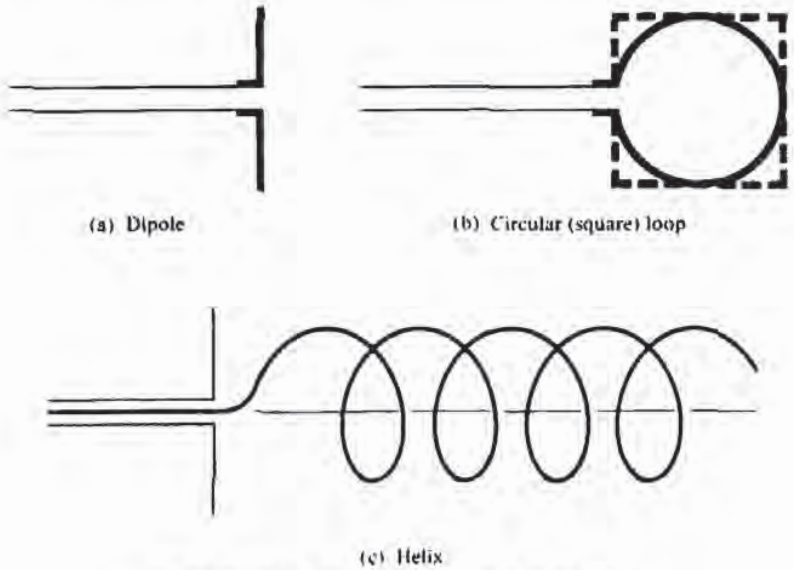


Figure 1.3 Wire antenna configurations.

INTEL-1045
U.S. Patent 7,151,430



(a) Pyramidal horn



(b) Conical horn



(c) Rectangular waveguide

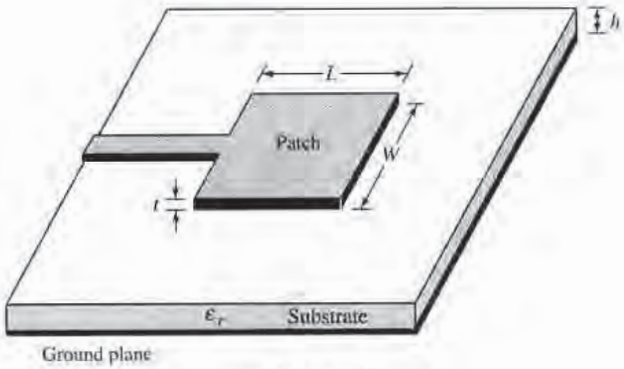
Figure 1.4 Aperture antenna configurations.

analysis and fabrication, and their attractive radiation characteristics, especially low cross-polarization radiation. The microstrip antennas are low-profile, comformable to planar and nonplanar surfaces, simple and inexpensive to fabricate using modern printed-circuit technology, mechanically robust when mounted on rigid surfaces, compatible with MMIC designs, and very versatile in terms of resonant frequency, polarization, pattern, and impedance. These antennas can be mounted on the surface of high-performance aircraft, spacecraft, satellites, missiles, cars, and even handheld mobile telephones. They are discussed in more detail in Chapter 14.

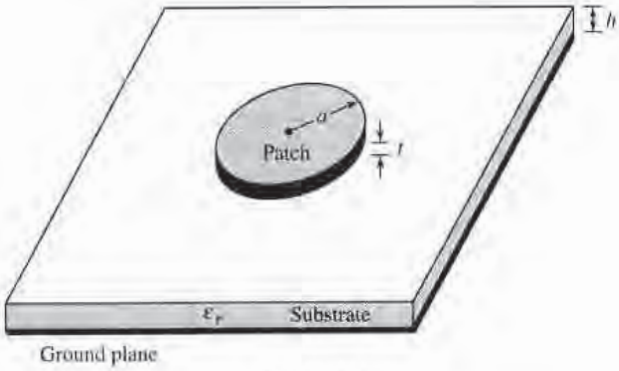
1.2.4 Array Antennas

Many applications require radiation characteristics that may not be achievable by a single element. It may, however, be possible that an aggregate of radiating elements in an electrical and geometrical arrangement (*an array*) will result in the desired radiation characteristics. The arrangement of the array may be such that the radiation from the elements adds up to give a radiation maximum in a particular direction or directions, minimum in others, or otherwise as desired. Typical examples of arrays

INTEL-1045
U.S. Patent 7,151,430



(a) Rectangular



(b) Circular

Figure 1.5 Rectangular and circular microstrip (patch) antennas.

are shown in Figure 1.6. Usually the term *array* is reserved for an arrangement in which the individual radiators are separate as shown in Figures 1.6(a–c). However the same term is also used to describe an assembly of radiators mounted on a continuous structure, shown in Figure 1.6(d).

1.2.5 Reflector Antennas

The success in the exploration of outer space has resulted in the advancement of antenna theory. Because of the need to communicate over great distances, sophisticated forms of antennas had to be used in order to transmit and receive signals that had to travel millions of miles. A very common antenna form for such an application is a parabolic reflector shown in Figures 1.7(a) and (b). Antennas of this type have been built with diameters as large as 305 m. Such large dimensions are needed to achieve the high gain required to transmit or receive signals after millions of miles of travel. Another form of a reflector, although not as common as the parabolic, is the corner reflector, shown in Figure 1.7(c). These antennas are examined in detail in Chapter 15.

INTEL-1045
U.S. Patent 7,151,430

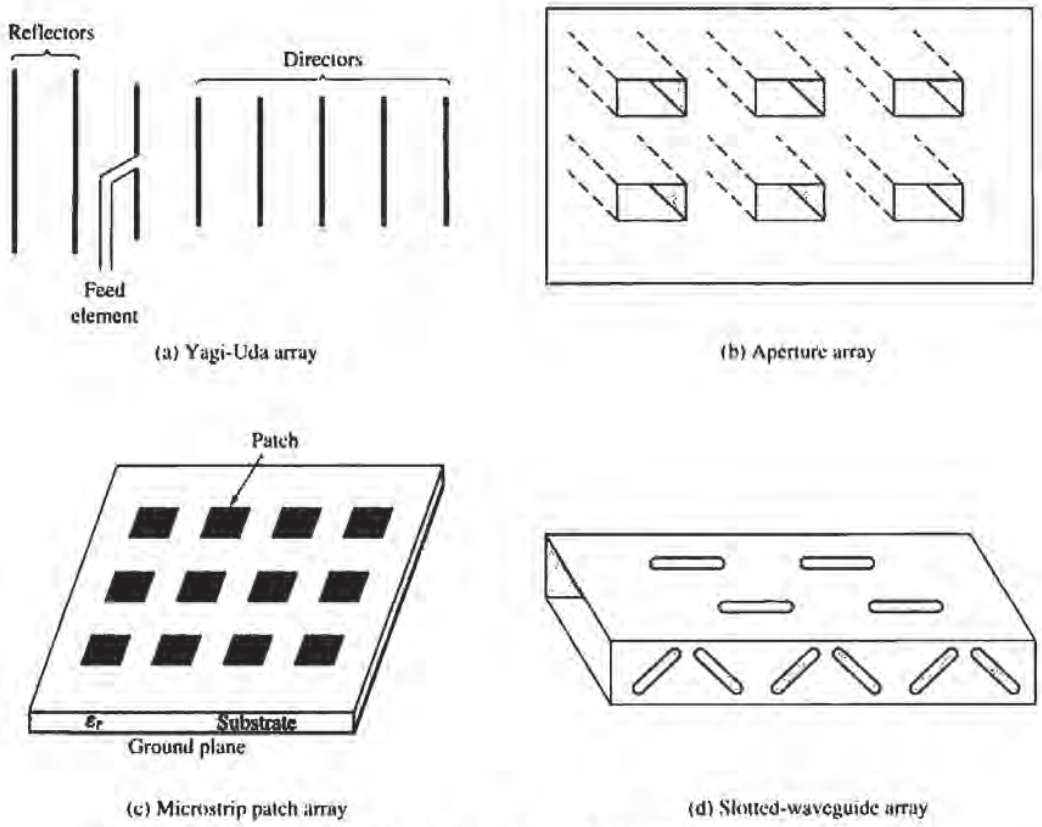


Figure 1.6 Typical wire, and aperture and microstrip array configurations.

1.2.6 Lens Antennas

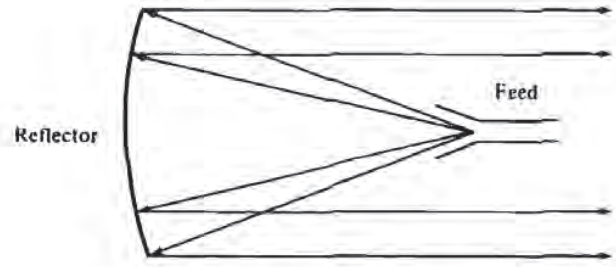
Lenses are primarily used to collimate incident divergent energy to prevent it from spreading in undesired directions. By properly shaping the geometrical configuration and choosing the appropriate material of the lenses, they can transform various forms of divergent energy into plane waves. They can be used in most of the same applications as are the parabolic reflectors, especially at higher frequencies. Their dimensions and weight become exceedingly large at lower frequencies. Lens antennas are classified according to the material from which they are constructed, or according to their geometrical shape. Some forms are shown in Figure 1.8 [2].

In summary, an ideal antenna is one that will radiate all the power delivered to it from the transmitter in a desired direction or directions. In practice, however, such ideal performances cannot be achieved but may be closely approached. Various types of antennas are available and each type can take different forms in order to achieve the desired radiation characteristics for the particular application. Throughout the book, the radiation characteristics of most of these antennas are discussed in detail.

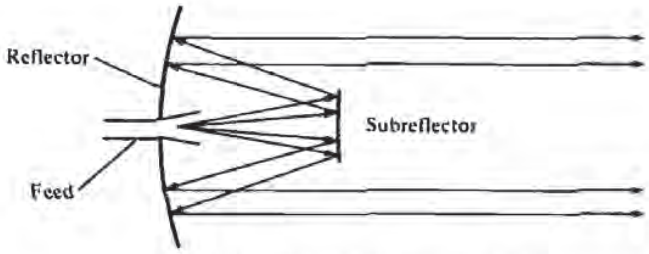
1.3 RADIATION MECHANISM

One of the first questions that may be asked concerning antennas would be "how is radiation accomplished?" In other words, how are the electromagnetic fields generated

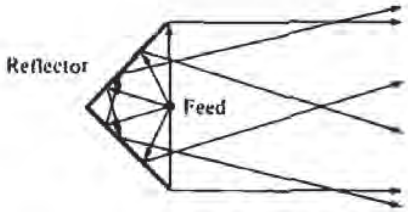
INTEL-1045
U.S. Patent 7,151,430



(a) Parabolic reflector with front feed



(b) Parabolic reflector with Cassegrain feed



(c) Corner reflector

Figure 1.7 Typical reflector configurations.

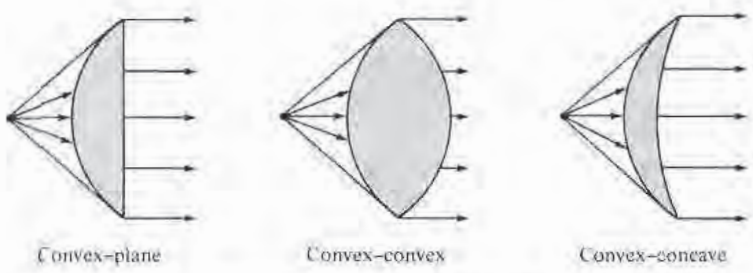
by the source, contained and guided within the transmission line and antenna, and finally "detached" from the antenna to form a free-space wave? The best explanation may be given by an illustration. However, let us first examine some basic sources of radiation.

1.3.1 Single Wire

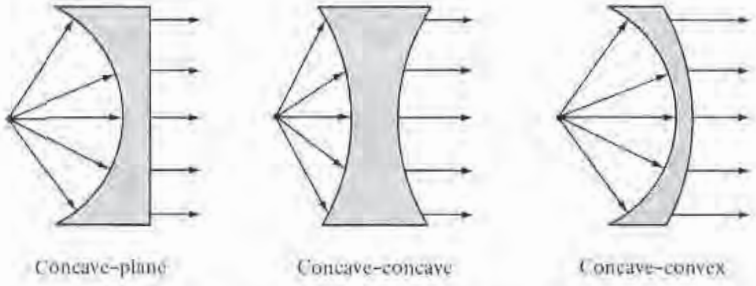
Conducting wires are material whose prominent characterisic is the motion of electric charges and the creation of current flow. Let us assume that an electric volume charge density, represented by q_v (coulombs/m^3), is distributed uniformly in a circular wire of cross-sectional area A and volume V, as shown in Figure 1.9. The total charge Q within volume V is moving in the z direction with a uniform velocity v_z (meters/sec). It can be shown that the current density J_z (amperes/m^2) over the cross section of the wire is given by [3]

$$J_z = q_v v_z \tag{1-1a}$$

INTEL-1045
U.S. Patent 7,151,430



(a) Lens antennas with index of refraction $n > 1$



(b) Lens antennas with index of refraction $n < 1$

Figure 1.8 Typical lens antenna configurations. (SOURCE: L. V. Blake, *Antennas*, Wiley, New York, 1966).

If the wire is made of an ideal electric conductor, the current density J_s (amperes/m) resides on the surface of the wire and it is given by

$$J_s = q_s v_z \tag{1-1b}$$

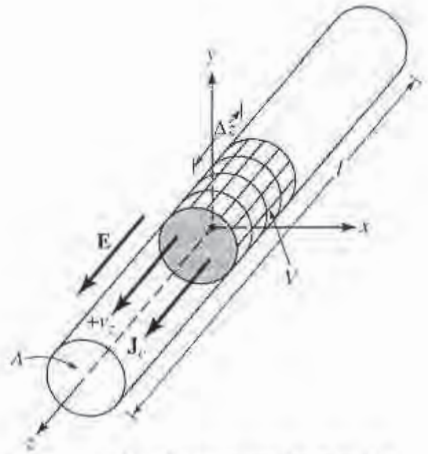


Figure 1.9 Charge uniformly distributed in a circular cross section cylinder.

where q_s (coulombs/m^2) is the surface charge density. If the wire is very thin (ideally zero radius), then the current in the wire can be represented by

$$I_z = q_l v_z \tag{1-1c}$$

where q_l (coulombs/m) is the charge per unit length.

Instead of examining all three current densities, we will primarily concentrate on the very thin wire. The conclusions apply to all three. If the current is time-varying, then the derivative of the current of (1-1c) can be written as

$$\frac{dI_z}{dt} = q_l \frac{dv_z}{dt} = q_l a_z \tag{1-2}$$

where $dv_z/dt = a_z$ (meters/sec^2) is the acceleration. If the wire is of length l, then (1-2) can be written as

$$\boxed{l\frac{dI_z}{dt} = lq_l \frac{dv_z}{dt} = lq_l a_z} \tag{1-3}$$

Equation (1-3) is the basic relation between current and charge, and it also serves as the fundamental relation of electromagnetic radiation [4], [5]. It simply states that *to create radiation, there must be a time-varying current or an acceleration (or deceleration) of charge.* We usually refer to currents in time-harmonic applications while charge is most often mentioned in transients. To create charge acceleration (or deceleration) the wire must be curved, bent, discontinuous or terminated [1], [4]. Periodic charge acceleration (or deceleration) or time varying current is also created when charge is oscillating in a time-harmonic motion, as shown in Figure 1.17 for a $\lambda/2$ dipole. Therefore:

1. If a charge is not moving, current is not created and there is no radiation.
2. If charge is moving with a uniform velocity:
   a. There is no radiation if the wire is straight, and infinite in extent.
   b. There is radiation if the wire is curved, bent, discontinuous, terminated, or truncated, as shown in Figure 1.10.
3. If charge is oscillating in a time-motion, it radiates even if the wire is straight.

A qualitative understanding of the radiation mechanism may be obtained by considering a pulse source attached to an open-ended conducting wire, which may be connected to the ground through a discrete load at its open end, as shown in Figure 1.10(d). When the wire is initially energized, the charges (free electrons) in the wire are set in motion by the electrical lines of force created by the source. When charges are accelerated in the source-end of the wire and decelerated (negative acceleration with respect to original motion) during reflection from its end, it is suggested that radiated fields are produced at each end and along the remaining part of the wire, [1], [4]. *Stronger radiation with a more broad frequency spectrum occurs if the pulses are of shorter or more compact duration while continuous time-harmonic oscillating charge produces, ideally, radiation of single frequency determined by the frequency of oscillation.* The acceleration of the charges is accomplished by the external source in which forces set the charges in motion and produce the associated field radiated. The deceleration of the charges at the end of the wire is accomplished by the internal

INTEL-1045
U.S. Patent 7,151,430

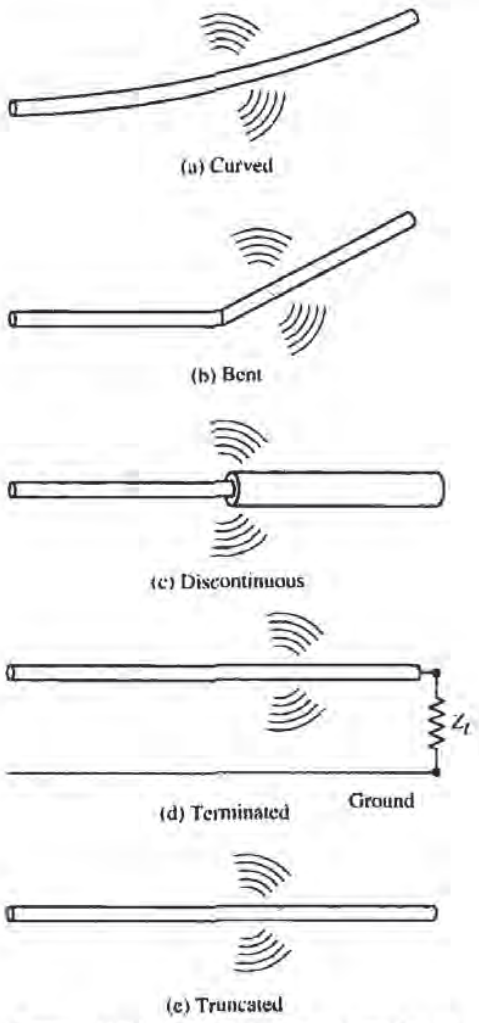


Figure 1.10 Wire configurations for radiation.

(self) forces associated with the induced field due to the buildup of charge concentration at the ends of the wire. The internal forces receive energy from the charge buildup as its velocity is reduced to zero at the ends of the wire. Therefore, charge acceleration due to an exciting electric field and deceleration due to impedance discontinuities or smooth curves of the wire are mechanisms responsible for electromagnetic radiation. While both current density ($\mathbf{J}_c$) and charge density (q_v) appear as source terms in Maxwell's equation, charge is viewed as a more fundamental quantity, especially for transient fields. Even though this interpretation of radiation is primarily used for transients, it can be used to explain steady-state radiation [4].

1.3.2 Two-Wires

Let us consider a voltage source connected to a two-conductor transmission line which is connected to an antenna. This is shown in Figure 1.11(a). Applying a voltage across

INTEL-1045
U.S. Patent 7,151,430

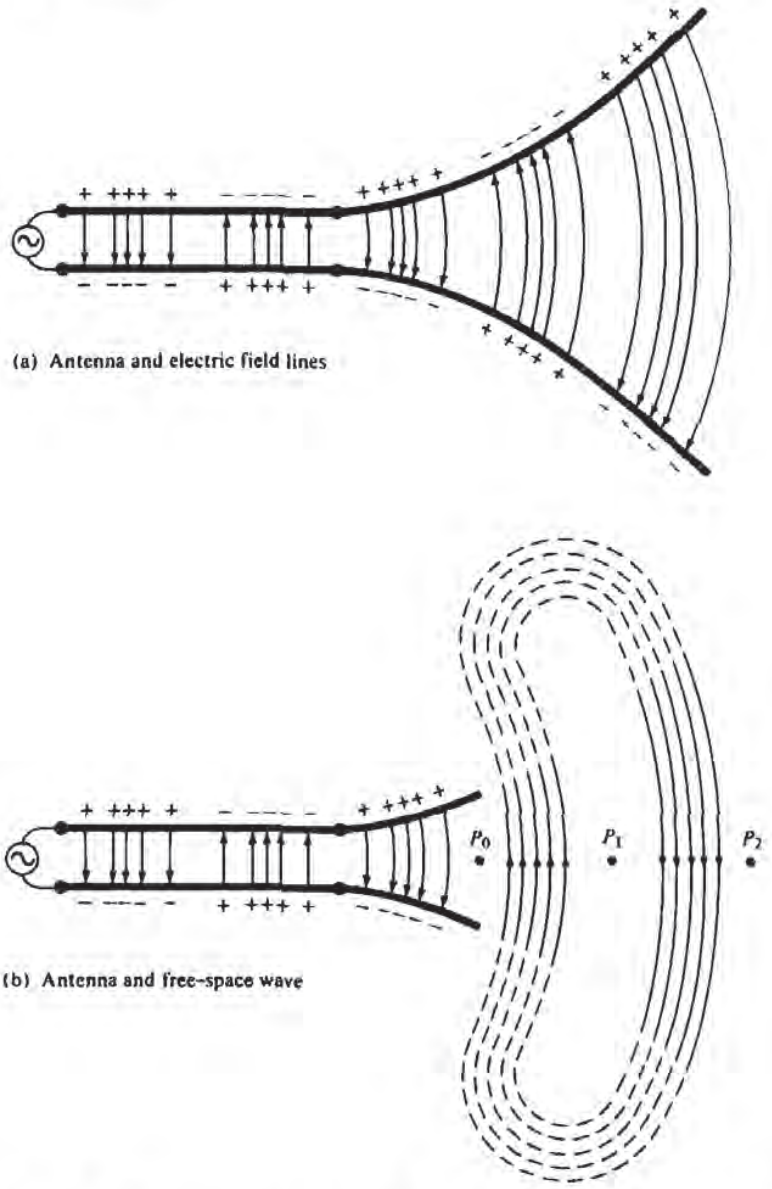


Figure 1.11 Source, transmission line, antenna, and detachment of electric field lines.

the two-conductor transmission line creates an electric field between the conductors. The electric field has associated with it electric lines of force which are tangent to the electric field at each point and their strength is proportional to the electric field intensity. The electric lines of force have a tendency to act on the free electrons (easily detachable from the atoms) associated with each conductor and force them to be displaced. The movement of the charges creates a current that in turn creates a magnetic field intensity. Associated with the magnetic field intensity are magnetic *lines of force which are tangent to the magnetic field.*

We have accepted that electric field lines start on positive charges and end on negative charges. They also can start on a positive charge and end at infinity, start at

INTEL-1045
U.S. Patent 7,151,430

infinity and end on a negative charge, or form closed loops neither starting or ending on any charge. Magnetic field lines always form closed loops encircling current-carrying conductors because there are no magnetic charges. In some mathematical formulations, it is often convenient to introduce magnetic charges and magnetic currents to draw a parallel between solutions involving electric and magnetic sources.

The electric field lines drawn between the two conductors help to exhibit the distribution of charge. If we assume that the voltage source is sinusoidal, we expect the electric field between the conductors to also be sinusoidal with a period equal to that of the applied source. The relative magnitude of the electric field intensity is indicated by the density (bunching) of the lines of force with the arrows showing the relative direction (positive or negative). The creation of time-varying electric and magnetic fields between the conductors forms electromagnetic waves which travel along the transmission line, as shown in Figure 1.11(a). The electromagnetic waves enter the antenna and have associated with them electric charges and corresponding currents. If we remove part of the antenna structure, as shown in Figure 1.11(b), free-space waves can be formed by "connecting" the open ends of the electric lines (shown dashed). The free-space waves are also periodic but a constant phase point P_0 moves outwardly with the speed of light and travels a distance of $\lambda/2$ (to P_1) in the time of one-half of a period. It has been shown [6] that close to the antenna the constant phase point P_0 moves faster than the speed of light but approaches the speed of light at points far away from the antenna (analogous to phase velocity inside a rectangular waveguide). Figure 1.12 displays the creation and travel of free-space

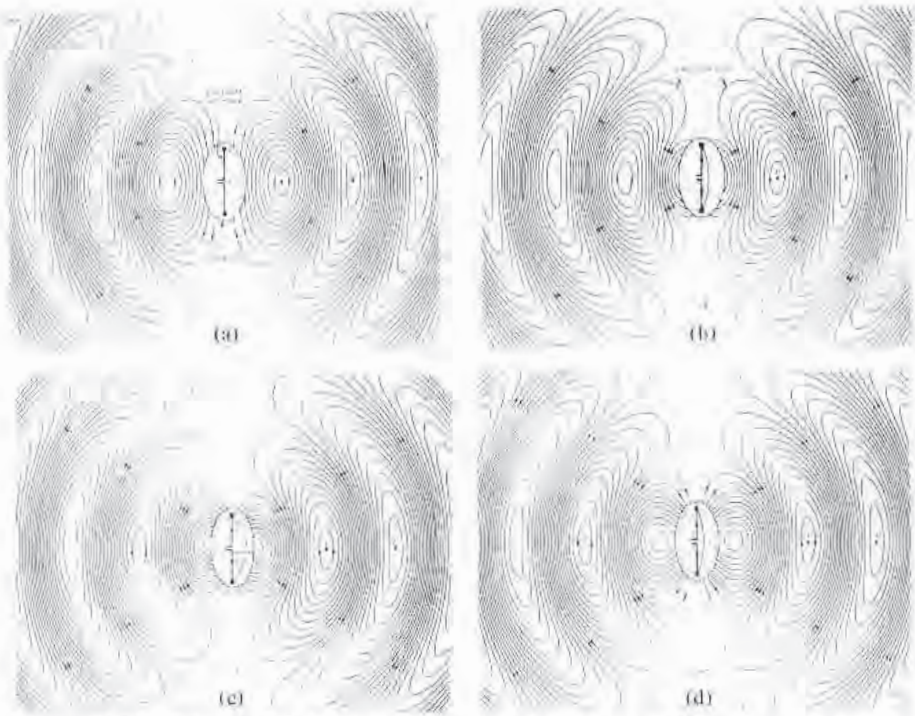


Figure 1.12 Electric field lines of free-space wave for a $\lambda/2$ antenna at $t = 0$, $T/8$, $T/4$, and $3T/8$. (SOURCE: J. D. Kraus and K. R. Carver, *Electromagnetics*, 2nd ed., McGraw-Hill, New York, 1973. Reprinted with permission of J. D. Kraus and John D. Cowan, Jr.)

INTEL-1045
U.S. Patent 7,151,430

waves by a prolate spheroid with $\lambda/2$ interfocal distance where λ is the wavelength. The free-space waves of a center-fed $\lambda/2$ dipole, except in the immediate vicinty of the antenna, are essentially the same as those of the prolate spheroid.

The question still unanswered is how the guided waves are detached from the antenna to create the free-space waves that are indicated as closed loops in Figures 1.11 and 1.12. Before we attempt to explain that, let us draw a parallel between the guided and free-space waves, and water waves [7] created by the dropping of a pebble in a calm body of water or initiated in some other manner. Once the disturbance in the water has been initiated, water waves are created which begin to travel outwardly. If the disturbance has been removed, the waves do not stop or extinguish themselves but continue their course of travel. If the disturbance persists, new waves are continuously created which lag in their travel behind the others. The same is true with the electromagnetic waves created by an electric disturbance. If the initial electric disturbance by the source is of a short duration, the created electromagnetic waves travel inside the transmission line, then into the antenna, and finally are radiated as free-space waves, even if the electric source has ceased to exist (as was with the water waves and their generating disturbance). If the electric disturbance is of a continuous nature, electromagnetic waves exist continuously and follow in their travel behind the others. This is shown in Figure 1.13 for a biconical antenna. When the electromagnetic waves are within the transmission line and antenna, their existence is associated with the presence of the charges inside the conductors. However, when the waves are radiated, they form closed loops and there are no charges to sustain their existence. *This leads us to conclude that electric charges are required to excite the fields but are not needed to sustain them and may exist in their absence. This is in direct analogy with water waves.*

1.3.3 Dipole

Now let us attempt to explain the mechanism by which the electric lines of force are detached from the antenna to form the free-space waves. This will again be illustrated

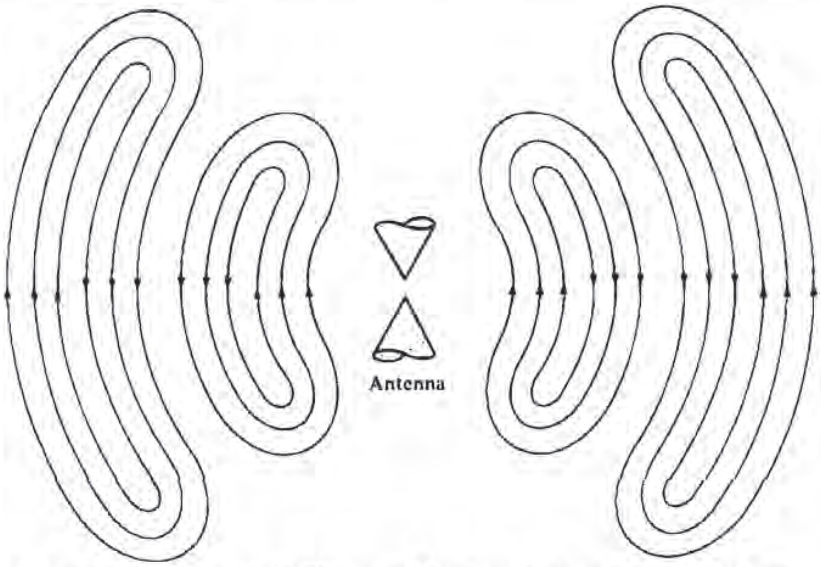


Figure 1.13 Electric field lines of free-space wave for biconical antenna.

INTEL-1045
U.S. Patent 7,151,430

by an example of a small dipole antenna where the time of travel is negligible. This is only necessary to give a better physical interpretation of the detachment of the lines of force. Although a somewhat simplified mechanism, it does allow one to visualize the creation of the free-space waves. Figure 1.14(a) displays the lines of force created between the arms of a small center-fed dipole in the first quarter of the period during which time the charge has reached its maximum value (assuming a sinusoidal time variation) and the lines have traveled outwardly a radial distance $\lambda/4$. For this example, let us assume that the number of lines formed are three. During the next quarter of the period, the original three lines travel an additional $\lambda/4$ (a total of $\lambda/2$ from the initial point) and the charge density on the conductors begins to diminish. This can be thought of as being accomplished by introducing opposite charges which at the end of the first half of the period have neutralized the charges on the conductors. The lines of force created by the opposite charges are three and travel a distance $\lambda/4$ during the second quarter of the first half, and they are shown dashed in Figure

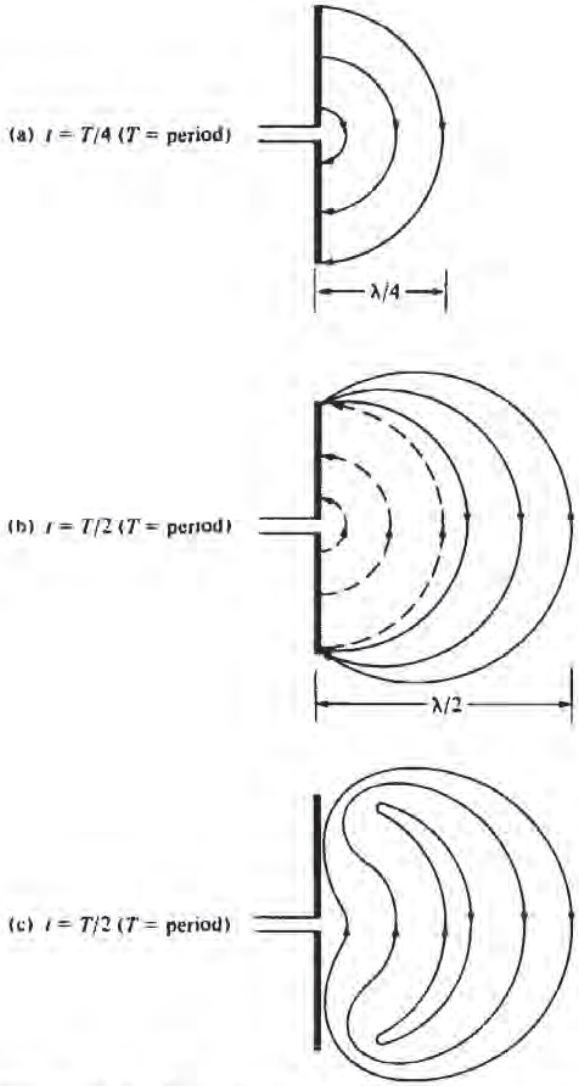


Figure 1.14 Formation and detachment of electric field lines for short dipole.

INTEL-1045
U.S. Patent 7,151,430

1.14(b). The end result is that there are three lines of force pointed upward in the first $\lambda/4$ distance and the same number of lines directed downward in the second $\lambda/4$. Since there is no net charge on the antenna, then the lines of force must have been forced to detach themselves from the conductors and to unite together to form closed loops. This is shown in Figure 1.14(c). In the remaining second half of the period, the same procedure is followed but in the opposite direction. After that, the process is repeated and continues indefinitely and electric field patterns, similar to those of Figure 1.22, are formed.

1.3.4 Computer Animation-Visualization of Radiation Problems

A difficulty that students usually confront is that the subject of electromagnetics is rather abstract, and it is hard to visualize electromagnetic wave propagation and interaction. With today's advanced numerical and computational methods, and computational and visualization software and hardware, this dilemma can, to a large extent, be minimized. To address this problem, we have developed and included in this book computer programs to animate and visualize three radiation problems. Descriptions of the computer programs are listed at the end of this chapter, and the computer programs are found on the computer disc included in this book. Each problem is solved using the Finite-Difference Time-Domain (FD-TD) method [8]-[10], a method which solves Maxwell's equations as a function of time in discrete time steps at discrete points in space. A picture of the fields can then be taken at each time step to create a movie which can be viewed as a function of time.

The three radiation problems that are animated and can be visualized using the computer program at the end of the chapter and included in the computer disc are:

a. *Infinite length line source (two-dimensional) excited by a single Gaussian pulse and radiating in an unbounded medium.*
b. *Infinite length line source (two-dimensional) excited by a single Gaussian pulse and radiating inside a perfectly electric conducting (PEC) square cylinder.*
c. *E-plane sectoral horn (two-dimensional form of Figure 13.2) excited by a continuous cosinusoidal voltage source and radiating in an unbounded medium.*

In order to animate and then visualize each of the three radiation problems, the user needs the professional edition of *MATLAB* [11] and the *MATLAB M-File*, found in the computer disc included in the book, to produce the corresponding FD-TD solution of each radiation problem. For each radiation problem, the *M-File* executed in *MATLAB* produces a movie by taking a picture of the computational domain every third time step. The movie is viewed as a function of time as the wave travels in the computational space.

A. Infinite Line Source in an Unbounded Medium

The first FD-TD solution is that of an infinite length line source excited by a single time-derivative Gaussian pulse, with a duration of approximately 0.4 nanoseconds, in a two-dimensional TM^z-computational domain. The unbounded medium is simulated using a six-layer Berenger Perfectly Matched Layer (PML) Absorbing Boundary Condition (ABC) [9], [10] to truncate the computational space at a finite distance without, in principle, creating any reflections. Thus, the pulse travels radially outward creating a *traveling* type of a wavefront. The outward moving wavefronts are easily

INTEL-1045
U.S. Patent 7,151,430

identified using the coloring scheme for the intensity (or gray scale for black and white monitors) when viewing the movie. The movie is created by the *MATLAB M-File* which produces the FD-TD solution by taking a picture of the computational domain every third time step. Each time step is 5 picoseconds while each FD-TD cell is 3 mm on a side. The movie is 37 frames long covering 185 picoseconds of elapsed time. The entire computational space is 15.3 cm by 15.3 cm and is modeled by 2500 square FD-TD cells (50×50), including 6 cells to implement the PML ABC.

B. Infinite Line Source in a PEC Square Cylinder

This problem is simulated similarly as that of the line source in an unbounded medium, including the characteristics of the pulse. The major difference is that the computational domain of this problem is truncated by PEC walls; *therefore there is no need for PML ABC*. For this problem the pulse travels in an outward direction and is reflected when it reaches the walls of the cylinder. The reflected pulse along with the radially outward traveling pulse interfere constructively and destructively with each other and create a *standing* type of a wavefront. The peaks and valleys of the modified wavefront can be easily identified when viewing the movie, using the colored or gray scale intensity schemes. Sufficient time is allowed in the movie to permit the pulse to travel from the source to the walls of the cylinder, return back to the source, and then return back to the walls of the cylinder. Each time step is 5 picoseconds and each FD-TD cell is 3 mm on a side. The movie is 70 frames long covering 350 picoseconds of elapsed time. The square cylinder, and thus the computational space, has a cross section of 15.3 cm by 15.3 cm and is modeled using an area 50 by 50 FD-TD cells.

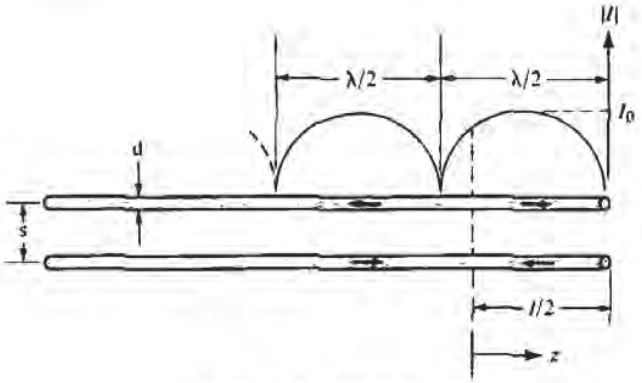
C. E-Plane Sectoral Horn in an Unbounded Medium

The *E*-plane sectoral horn is excited by a cosinusoidal voltage (CW) of 9.84 GHz in a TE^z computational domain, instead of the Gaussian pulse excitation of the previous two problems. The unbounded medium is implemented using an eight-layer Berenger PML ABC. The computational space is 25.4 cm by 25.4 cm and is modeled using 100 by 100 FD-TD cells (each square cell being 2.54 mm on a side). The movie is 70 frames long covering 296 picoseconds of elapsed time and is created by taking a picture every third frame. Each time step is 4.23 picoseconds in duration. The horn has a total flare angle of 52° and its flared section is 2.62 cm long, is fed by a parallel plate 1 cm wide and 4.06 cm long, and has an aperture of 3.56 cm.

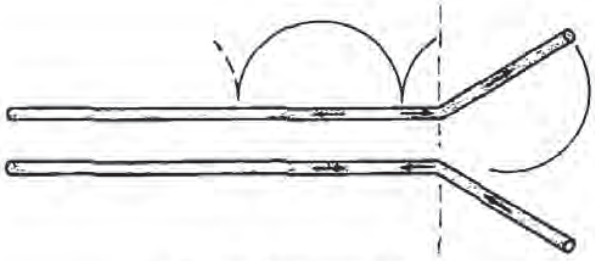
1.4 CURRENT DISTRIBUTION ON A THIN WIRE ANTENNA

In the preceding section we discussed the movement of the free electrons on the conductors representing the transmission line and the antenna. In order to illustrate the creation of the current distribution on a linear dipole, and its subsequent radiation, let us first begin with the geometry of a lossless two-wire transmission line, as shown in Figure 1.15(a). The movement of the charges creates a traveling wave current, of magnitude $I_0/2$, along each of the wires. When the current arrives at the end of each of the wires, it undergoes a complete reflection (equal magnitude and 180° phase reversal). The reflected traveling wave, when combined with the incident traveling wave, forms in each wire a pure standing wave pattern of sinusoidal form as shown in Figure 1.15(a). The current in each wire undergoes a 180° phase reversal between

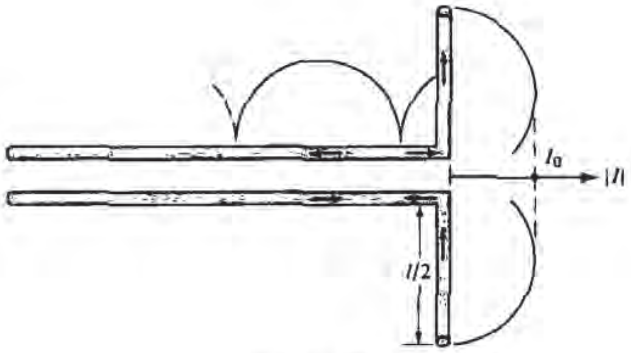
INTEL-1045
U.S. Patent 7,151,430



(a) Two-wire transmission line



(b) Flared transmission line



(c) Linear dipole

Figure 1.15 Current distribution on a lossless two-wire transmission line, flared transmission line, and linear dipole.

adjoining half cycles. This is indicated in Figure 1.15(a) by the reversal of the arrow direction. Radiation from each wire individually occurs because of the time-varying nature of the current and the termination of the wire.

For the two-wire balanced (symmetrical) transmission line, the current in a half-cycle of one wire is of the same magnitude but 180° out-of-phase from that in the corresponding half-cycle of the other wire. If in addition the spacing between the two wires is very small ($s \ll \lambda$), the fields radiated by the current of each wire are essentially cancelled by those of the other. The net result is an almost ideal (and desired) nonradiating transmission line.

INTEL-1045
U.S. Patent 7,151,430

As the section of the transmission line between $0 \leq z \leq l/2$ begins to flare, as shown in Figure 1.15(b), it can be assumed that the current distribution is essentially unaltered in form in each of the wires. However, because the two wires of the flared section are not necessarily close to each other, the fields radiated by one do not necessarily cancel those of the other. Therefore ideally there is a net radiation by the transmission line system.

Ultimately the flared section of the transmission line can take the form shown in Figure 1.15(c). This is the geometry of the widely used dipole antenna. Because of the standing wave current pattern, it is also classified as a standing wave antenna (as contrasted to the traveling wave antennas which will be discussed in detail in Chapter 10). If $l < \lambda$, the phase of the current standing wave pattern in each arm is the same throughout its length. In addition, spatially it is oriented in the same direction as that of the other arm as shown in Figure 1.15(c). Thus the fields radiated by the two arms of the dipole (vertical parts of a flared transmission line) will primarily reinforce each other toward most directions of observation (the phase due to the relative position of each small part of each arm must also be included for a complete description of the radiation pattern formation).

If the diameter of each wire is very small ($d \ll \lambda$), the ideal standing wave pattern of the current along the arms of the dipole is sinusoidal with a null at the end. However, its overall form depends on the length of each arm. For center-fed dipoles with $l \ll \lambda$, $l = \lambda/2$, $\lambda/2 < l < \lambda$ and $\lambda < l < 3\lambda/2$, the current patterns are illustrated in Figures 1.16(a–d). The current pattern of a very small dipole (usually $\lambda/50 < l \leq \lambda/10$) can be approximated by a triangular distribution since $\sin(kl/2) \approx kl/2$ when $kl/2$ is very small. This is illustrated in Figure 1.16(a).

Because of its cyclical spatial variations, the current standing wave pattern of a dipole longer than $\lambda (l > \lambda)$ undergoes 180° phase reversals between adjoining half-cycles. Therefore the current in all parts of the dipole does not have the same phase. This is demonstrated graphically in Figure 1.16(d) for $\lambda < l < 3\lambda/2$. In turn, the fields radiated by some parts of the dipole will not reinforce those of the others. As a result, significant interference and cancelling effects will be noted in the formation of the total radiation pattern.

For a time-harmonic varying system of radian frequency $\omega = 2\pi f$, the current standing wave patterns of Figure 1.16 represent the maximum current excitation for any time. The current variations, as a function of time, on a $\lambda/2$ center-fed dipole are shown in Figure 1.17 for $0 \leq t \leq T/2$ where T is the period. These variations can be obtained by multiplying the current standing wave pattern of Figure 1.16(b) by $\cos(\omega t)$.

1.5 HISTORICAL ADVANCEMENT

The history of antennas [12] dates back to James Clerk Maxwell who unified the theories of electricity and magnetism, and eloquently represented their relations through a set of profound equations best known as *Maxwell's Equations*. His work was first published in 1873 [13]. He also showed that light was electromagnetic and that both light and electromagnetic waves travel by wave disturbances of the same speed. In 1886, Professor Heinrich Rudolph Hertz demonstrated the first wireless electromagnetic system. He was able to produce in his laboratory at a wavelength of 4 meters a spark in the gap of a transmitting $\lambda/2$ dipole which was then detected as a spark in the gap of a nearby loop. It was not until 1901 that Guglielmo Marconi was able to send signals over large distances. He performed, in 1901, the first transatlantic

INTEL-1045
U.S. Patent 7,151,430

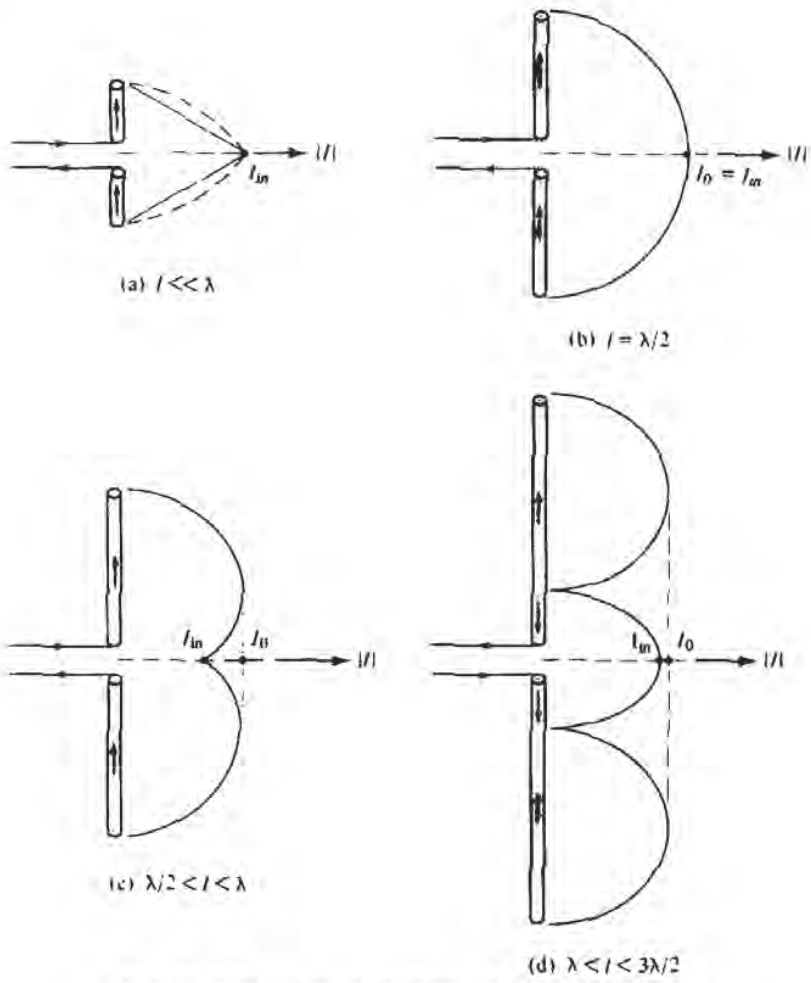


Figure 1.16 Current distribution on linear dipoles.

transmission from Poldhu in Cornwall, England, to St. John's Newfoundland. His transmitting antenna consisted of 50 vertical wires in the form of a fan connected to ground through a spark transmitter. The wires were supported horizontally by a guyed wire between two 60-m wooden poles. The receiving antenna at St. John's was a 200-m wire pulled and supported by a kite. This was the dawn of the antenna era.

From Marconi's inception through the 1940s, antenna technology was primarily centered on wire related radiating elements and frequencies up to about UHF. It was not until World War II that modern antenna technology was launched and new elements (such as waveguide apertures, horns, reflectors) were primarily introduced. Much of this work is captured in the book by Silver [14]. A contributing factor to this new era was the invention of microwave sources (such as the klystron and magnetron) with frequencies of 1 GHz and above.

While World War II launched a new era in antennas, advances made in computer architecture and technology during the 1960s through the 1990s have had a major impact on the advance of modern antenna technology, and they are expected to have an even greater influence on antenna engineering into the twenty-first century. Beginning primarily in the early 1960s, numerical methods were introduced that allowed

INTEL-1045
U.S. Patent 7,151,430

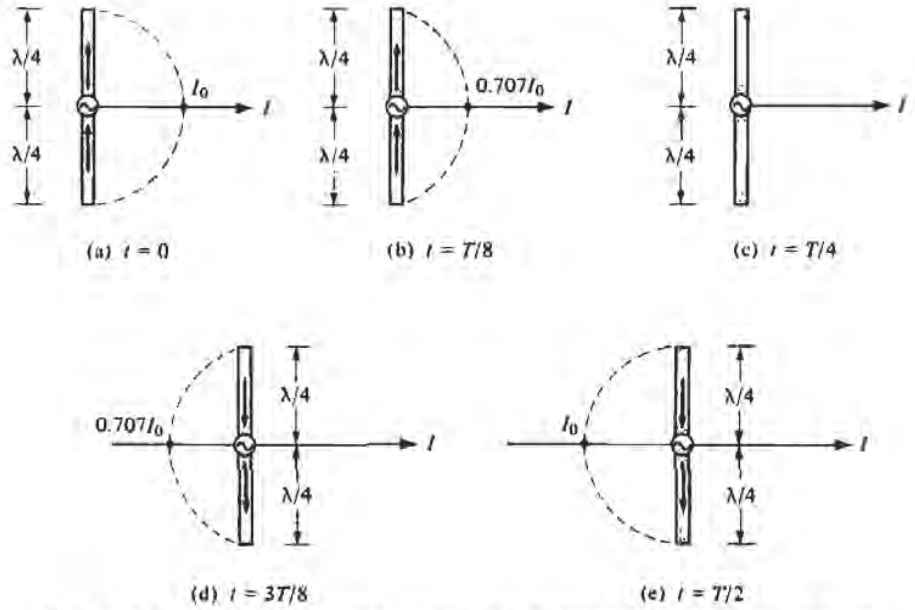


Figure 1.17 Current distribution on a $\lambda/2$ wire antenna for different times.

previously intractable complex antenna system configurations to be analyzed and designed very accurately. In addition, asymptotic methods for both low frequencies (e.g., Moment Method (MM), Finite-Difference, Finite-Element) and high frequencies (e.g., Geometrical and Physical Theories of Diffraction) were introduced, contributing significantly to the maturity of the antenna field. While in the past antenna design may have been considered a secondary issue in overall system design, today it plays a critical role. In fact, many system successes rely on the design and performance of the antenna. Also, while in the first half of this century antenna technology may have been considered almost a "cut and try" operation, today it is truly an engineering art. Analysis and design methods are such that antenna system performance can be predicted with remarkable accuracy. In fact, many antenna designs proceed directly from the initial design stage to the prototype without intermediate testing. The level of confidence has increased tremendously.

The widespread interest in antennas is reflected by the large number of books written on the subject [15]. These have been classified under four categories: Fundamental, Handbooks, Measurements, and Specialized. This is an outstanding collection of books, and it reflects the popularity of the antenna subject, especially since the 1950s. Because of space limitations, only a partial list is included here [2], [5], [7], [16]–[39], including the first edition of this book in 1982. Some of these books are now out of print.

1.5.1 Antenna Elements

Prior to World War II most antenna elements were of the wire type (long wires, dipoles, helices, rhombuses, fans, etc.), and they were used either as single elements or in arrays. During and after World War II, many other radiators, some of which may have been known for some and others of which were relatively new, were put into service. This created a need for better understanding and optimization of their radiation characteristics. Many of these antennas were of the aperture type (such as

INTEL-1045
U.S. Patent 7,151,430

open-ended waveguides, slots, horns, reflectors, lenses), and they have been used for communication, radar, remote sensing and deep space applications both on airborne and earth-based platforms. Many of these operate in the microwave region and are discussed in Chapters 12, 13, 15 and in [40].

Prior to the 1950s, antennas with broadband pattern and impedance characteristics had bandwidths not much greater than about 2:1. In the 1950s, a breakthrough in antenna evolution was created which extended the maximum bandwidth to as great as 40:1 or more. Because the geometries of these antennas are specified by angles instead of linear dimensions, they have ideally an infinite bandwidth. Therefore, they are referred to as *frequency independent*. These antennas are primarily used in the 10–10,000 MHz region in a variety of applications including TV, point-to-point communications, feeds for reflectors and lenses, and many others. This class of antennas is discussed in more detail in Chapter 11 and in [41].

It was not until almost 20 years later that a fundamental new radiating element, which has received a lot of attention and many applications since its inception, was introduced. This occurred in the early 1970s when the microstrip or patch antennas was reported. This element is simple, lightweight, inexpensive, low profile, and conformal to the surface. These antennas are discussed in more detail in Chapter 14 and in [42].

Major advances in millimeter wave antennas have been made in recent years, including integrated antennas where active and passive circuits are combined with the radiating elements in one compact unit (monolithic form). These antennas are discussed in [43].

Specific radiation pattern requirements usually cannot be achieved by single antenna elements, because single elements usually have relatively wide radiation patterns and low values of directivity. To design antennas with very large directivities, it is usually necessary to increase the electrical size of the antenna. This can be accomplished by enlarging the electrical dimensions of the chosen single element. However, mechanical problems are usually associated with very large elements. An alternative way to achieve large directivities, without increasing the size of the individual elements, is to use multiple single elements to form an *array*. An array is a sampled version of a very large single element. In an array, the mechanical problems of large single elements are traded for the electrical problems associated with the feed networks of arrays. However, with today's solid-state technology, very efficient and low-cost feed networks can be designed.

Arrays are the most versatile of antenna systems. They find wide applications not only in many spaceborne systems, but in many earthbound missions as well. In most cases, the elements of an array are identical; this is not necessary, but it is often more convenient, simpler, and more practical. With arrays, it is practical not only to synthesize almost any desired amplitude radiation pattern, but the main lobe can be scanned by controlling the relative phase excitation between the elements. This is most convenient for applications where the antenna system is not readily accessible, especially for spaceborne missions. The beamwidth of the main lobe along with the side lobe level can be controlled by the relative amplitude excitation (distribution) between the elements of the array. In fact, there is a trade-off between the beamwidth and the side lobe level base on the amplitude distribution. Analysis, design, and synthesis of arrays are discussed in Chapters 6 and 7. However, advances in array technology are reported in [44]–[48].

INTEL-1045
U.S. Patent 7,151,430

1.5.2 Methods of Analysis

There is plethora of antenna elements, many of which exhibit intricate configurations. To analyze each as a boundary-value problem and obtain solutions in closed form, the antenna structure must be described by an orthogonal curvilinear coordinate system. This places severe restrictions on the type and number of antenna systems that can be analyzed using such a procedure. Therefore, other exact or approximate methods are often pursued. Two methods that in the last three decades have been preeminent in the analysis of many previously intractable antenna problems are the *Integral Equation* (IE) method and the *Geometrical Theory of Diffraction* (GTD).

The Integral Equation method casts the solution to the antenna problem in the form of an integral (hence its name) where the unknown, usually the induced current density, is part of the integrand. Numerical techniques, such as the Moment Method (MM), are then used to solve for the unknown. Once the current density is found, the radiation integrals of Chapter 3 are used to find the fields radiated and other systems parameters. This method is most convenient for wire-type antennas and more efficient for structures that are small electrically. One of the first objectives of this method is to formulate the IE for the problem at hand. In general, there are two type of IE's. One is the *Electric Field Integral Equation (EFIE)*, and it is based on the boundary condition of the total tangential electric field. The other is the *Magnetic Field Integral Equation (MFIE)*, and it is based on the boundary condition that expresses the total electric current density induced on the surface in terms of the incident magnetic field. The MFIE is only valid for closed surfaces. For some problems, it is more convenient to formulate an EFIE, while for others it is more appropriate to use an MFIE. Advances, applications, and numerical issues of these methods are addressed in Chapter 8 and in [3] and [49].

When the dimensions of the radiating system are many wavelengths, low-frequency methods are not as computationally efficient. However, high-frequency asymptotic techniques can be used to analyze many problems that are otherwise mathematically intractable. One such method that has received considerable attention and application over the years is the GTD, which is an extension of geometrical optics (GO), and it overcomes some of the limitations of GO by introducing a diffraction mechanism. The Geometrical Theory of Diffraction is briefly discussed in Section 12.10. However, a detailed treatment is found in Chapter 13 of [3] while recent advances and applications are found in [50] and [51].

For structures that are not convenient to analyze by either of the two methods, a combination of the two is often used. Such a technique is referred to as a *hybrid method*, and it is described in detail in [52]. Another method, which has received a lot of attention in scattering, is the Finite-Difference Time-Domain (FDTD). This method has also been applied to antenna radiation problems [53]–[56]. A method that is beginning to gain momentum in its application to antenna problems is the Finite Element Method [57]–[61].

1.5.3 Some Future Challenges

Antenna engineering has enjoyed a very successful period during the 1940s–1990s. Responsible for its success have been the introduction and technological advances of some new elements of radiation, such as aperture antennas, reflectors, frequency

INTEL-1045
U.S. Patent 7,151,430

independent antennas, and microstrip antennas. Excitement has been created by the advancement of the low-frequency and high-frequency asymptotic methods, which has been instrumental in analyzing many previously intractable problems. A major factor in the success of antenna technology has been the advances in computer architecture and numerical computation methods. Today antenna engineering is considered a truly fine engineering art.

Although a certain level of maturity has been attained, there are many challenging opportunities and problems to be solved. Phased array architecture integrating monolithic MIC technology is still a most challenging problem. Integration of new materials into antenna technology offers many opportunities, and asymptotic methods will play key roles in their incorporation and system performance. Computational electromagnetics using supercomputing and parallel computing capabilities will model complex electromagnetic wave interactions, in both the frequency and time domains. Innovative antenna designs to perform complex and demanding system functions always remain a challenge. New basic elements are always welcome and offer refreshing opportunities. New applications include, but are not limited to cellular telephony, direct broadcast satellite systems, global positioning satellites (GPS), high-accuracy airborne navigation, global weather, earth resource systems, and others. Because of the many new applications, the lower portion of the EM spectrum has been saturated and the designs have been pushed to higher frequencies, including the millimeter wave frequency bands.

References

1. C. A. Balanis, "Antenna Theory: A Review," *Proc. IEEE*, Vol. 80, No. 1, pp. 7–23, January 1992.
2. L. V. Blake, *Antennas*, Wiley, New York, 1966, p. 289.
3. C. A. Balanis, *Advanced Engineering Electromagnetics*, Wiley, New York, 1989.
4. E. K. Miller and J. A. Landt, "Direct Time-Domain Techniques for Transient Radiation and Scattering from Wires," *Proc. IEEE*, Vol. 68, No. 11, pp. 1396–1423, November 1980.
5. J. D. Kraus, *Antennas*, McGraw-Hill, New York, 1988.
6. J. D. Kraus and K. R. Carver, *Electromagnetics*, McGraw-Hill, New York, 1973, pp. 648–650.
7. S. A. Schelkunoff and H. T. Friis, *Antenna Theory and Practice*, Wiley, New York, 1952.
8. K. S. Yee, "Numerical Solution of Initial Boundary Value Problems Involving Maxwell's Equations in Isotropic Media," *IEEE Trans. Antennas Propagat.*, Vol. AP-14, No. 3, pp. 302–307, May 1966.
9. J. P. Berenger, "A Perfectly Matched Layer for the Absorption of Electromagnetic Waves," *Journal Computational Physics*, Vol. 114, pp. 185–200, October 1994.
10. W. V. Andrew, C. A. Balanis and P. A. Tirkas, "A Comparison of the Berenger Perfectly Matched Layer and the Lindman Higher-Order ABC's for the FDTD Method," *IEEE Microwave and Guided Wave Letters*, Vol. 5, No. 6, pp. 192–194, June 1995.
11. *The Student Edition of MATLAB*: Version 4; User's Guide. The MATH WORKS, Inc., Prentice-Hall, Inc., Englewood Cliffs, NJ, 1995.
12. J. D. Kraus, "Antennas since Hertz and Marconi," *IEEE Trans. Antennas Propagat.*, Vol. AP-33, No. 2, pp. 131–137, February 1985.
13. J. C. Maxwell, *A Treatise on Electricity and Magnetism*, London, UK, Oxford Univ. Press, 1873, 1904.

INTEL-1045
U.S. Patent 7,151,430

14. S. Silver (Ed.), *Microwave Antenna Theory and Design*, MIT Radiation Lab. Series, Vol. 12, McGraw-Hill, New York, 1949.
15. S. Stutzman, "Bibliography for Antennas," *IEEE Antennas Propagat. Mag.*, Vol. 32, pp. 54–57, August 1990.
16. J. Aharoni, *Antennae*, London, UK, Oxford Univ. Press, 1946.
17. S. A. Schelkunoff, *Advanced Antenna Theory*, Wiley, New York, 1952.
18. E. A. Laport, *Radio Antenna Engineering*, McGraw-Hill, New York, 1952.
19. C. H. Walter, *Traveling Wave Antennas*, McGraw-Hill, New York, 1968.
20. E. Wolff, *Antenna Analysis*, Wiley, New York, 1966 (first edition), Artech House, Norwood, MA, 1988 (second edition).
21. W. L. Weeks, *Antenna Engineering*, McGraw-Hill, New York, 1968.
22. E. Jordan and K. Balmain, *Electromagnetic Waves and Radiating Systems*, Prentice-Hall, New York, 1968.
23. R. E. Collin and F. J. Zucker (Eds.), *Antenna Theory*, Parts 1 and 2, McGraw-Hill, New York, 1969.
24. W. V. T. Rusch and P. D. Potter, *Analysis of Reflector Antennas*, Academic Press, New York, 1970.
25. W. L. Stutzman and G. A. Thiele, *Antenna Theory and Design*, Wiley, New York, 1981.
26. R. S. Elliot, *Antenna Theory and Design*, Prentice-Hall, New York, 1981.
27. K. F. Lee, *Principles of Antenna Theory*, Wiley, New York, 1984.
28. R. E. Collin, *Antennas and Radiowave Propagation*, McGraw-Hill, New York, 1985.
29. T. A. Milligan, *Modern Antenna Design*, McGraw-Hill, New York, 1985.
30. J. R. Wait, *Introduction to Antennas and Propagation*, Hithin Herts, UK, IEE, 1966.
31. F. R. Connor, *Antennas*, Edward Arnold, London, 1989.
32. K. Chang (Ed.), *Handbook of Microwave and Optical Components*, Wiley-Interscience, New York, Vol. 1, Chapters 10–13, 1989.
33. R. C. Johnson and H. Jasik, *Antenna Engineering Handbook*, McGraw-Hill, New York, 1984.
34. R. C. Hansen (Ed.), *Microwave Scanning Antennas*, Vols. I–III, Academic Press, New York, 1964 (reprinted by Peninsula Publishing, Los Altos, CA).
35. A. W. Rudge, K. Milne, A. D. Olver, and P. Knight (Eds.), *The Handbook of Antenna Design*, Vols. 1 and 2, Peter Peregrinus, London, 1982.
36. Y. T. Lo and S. W. Lee (Eds.), *Antenna Handbook: Theory, Applications, and Design*, Van Nostrand Reinhold, New York, 1988.
37. I. J. Bahl and P. Bhartia, *Microstrip Antennas*, Artech House, Norwood, MA, 1980.
38. J. R. James and P. S. Hall (Eds.), *Handbook of Microstrip Antennas*, Vols. I and II, Peter Peregrinus, 1989.
39. D. M. Pozar, *Antenna Design Using Personal Computers*, Artech House, Norwood, MA, 1985.
40. W. V. T. Rusch, "The Current State of the Reflector Antenna Art-Entering the 1990's," *Proc. IEEE*, Vol. 80, No. 1, pp. 113–126, January 1992.
41. P. E. Mayes, "Frequency-Independent Antennas and Broad-Band Derivatives Thereof," *Proc. IEEE*, Vol. 80, No. 1, pp. 103–112, January 1992.
42. D. M. Pozar, "Microstrip Antennas," *Proc. IEEE*, Vol. 80, No. 1, pp. 79–91, January 1992.
43. F. K. Schwering, "Millimeter Wave Antennas," *Proc. IEEE*, Vol. 80, No. 1, pp. 92–102, January 1992.
44. W. H. Kummer, "Basic Array Theory," *Proc. IEEE*, Vol. 80, No. 1, pp. 127–140, January 1992.
45. R. C. Hansen, "Array Pattern Control and Synthesis," *Proc. IEEE*, Vol. 80, No. 1, pp. 141–151, January 1992.
46. W. F. Gabriel, "Adaptive Processing Array Systems," *Proc. IEEE*, Vol. 80, No. 1, pp. 152–162, January 1992.

INTEL-1045
U.S. Patent 7,151,430

47. R. J. Mailloux, "Antenna Array Architecture," *Proc. IEEE*, Vol. 80, No. 1, pp. 163–172, January 1992.
48. R. Tang and R. W. Burns, "Array Technology," *Proc. IEEE*, Vol. 80, No. 1, pp. 173–182, January 1992.
49. E. K. Miller and G. J. Burke, "Low-Frequency Computational Electromagnetics for Antenna Analysis," *Proc. IEEE*, Vol. 80, No. 1, pp. 24–43, January 1992.
50. P. H. Pathak, "High-Frequency Techniques for Antenna Analysis," *Proc. IEEE*, Vol. 80, No. 1, pp. 44–65, January 1992.
51. R. J. Marhefka and W. D. Burnside, "Antennas on Complex Platforms," *Proc. IEEE*, Vol. 80, No. 1, pp. 204–208, January 1992.
52. G. A. Thiele, "Overview of Selected Hybrid Methods in Radiating System Analysis," *Proc. IEEE*, Vol. 80, No. 1, pp. 66–78, January 1992.
53. J. C. Maloney, G. S. Smith, and W. R. Scott Jr., "Accurate Computation of the Radiation from Simple Antennas using the Finite-Difference Time-Domain Method," *IEEE Trans. Antennas Propagat.*, Vol. 38, No. 7, pp. 1059–1068, July 1990.
54. D. S. Katz, M. J. Piket-May, A. Taflove, and K. R. Umashankar, "FDTD Analysis of Electromagnetic Wave Radiation from Systems Containing Horn Antennas," *IEEE Trans. Antennas Propagat.*, Vol. 39, No. 8, pp. 1203–1212, August 1991.
55. P. A. Tirkas and C. A. Balanis, "Finite-Difference Time-Domain Techniques for Antenna Radiation," *IEEE Trans. Antennas Propagat.*, Vol. 40, No. 3, pp. 334–340, March 1992.
56. P. A. Tirkas and C. A. Balanis, "Contour Path FDTD Method for Analysis of Pyramidal Horns With Composite Inner E-Plane Walls," *IEEE Trans. Antennas Propagat.*, Vol. 42, No. 11, pp. 1476–1483, November 1994.
57. J. Jin, *The Finite Element Method in Electromagnetics*, John Wiley & Sons, Inc., 1993.
58. J. M. Jin and J. L. Volakis, "Scattering and Radiation Analysis of Three-Dimensional Cavity Arrays Via a Hybrid Finite-Element Method," *IEEE Trans. Antennas Propagat.*, Vol. 41, No. 11, pp. 1580–1586, November 1993.
59. D. T. McGrath and V. P. Pyati, "Phased Array Antenna Analysis with Hybrid Finite Element Method," *IEEE Trans. Antennas Propagat.*, Vol. 42, No. 12, pp. 1625–1630, December 1994.
60. W. Sun and C. A. Balanis, "Vector One-Way Wave Absorbing Boundary Condition for FEM Applications," *IEEE Trans. Antennas Propagat.*, Vol. 42, No. 6, pp. 872–878, June 1994.
61. E. W. Lucas and T. P. Fontana, "A 3-D Hybrid Finite Element/Boundary Element Method for the Unified Radiation and Scattering Analysis of General Infinite Periodic Arrays," *IEEE Trans. Antennas Propagat.*, Vol. 43, No. 2, pp. 145–153, February 1995.

INTEL-1045
U.S. Patent 7,151,430

COMPUTER PROGRAM
ANIMATION-VISUALIZATION OF RADIATION PROBLEMS

```
C***********************************************************
C THIS PROGRAM CONTAINS THREE SEPARATE ANIMATION-VISUALIZATION
C RADIATION PROBLEMS.
C      I.  LINE SOURCE-GAUSSIAN PULSE: UNBOUNDED MEDIUM
C      II.  LINE SOURCE-GAUSSIAN PULSE: PEC SQUARE CYLINDER
C      III. E-PLANE SECTORAL HORN: UNBOUNDED MEDIUM
C THE OBJECTIVE IS TO ALLOW THE USER TO ANIMATE AND THEN TO
C VISUALIZE RADIATION, AS A FUNCTION OF TIME, OF THREE DIFFERENT
C RADIATION PROBLEMS.
C      I.  LINE SOURCE-GAUSSIAN PULSE: UNBOUNDED MEDIUM
C THE FIRST ANIMATION-VISUALIZATION PROGRAM IS THAT OF A LINE
C SOURCE EXCITED BY A SINGLE GAUSSIAN PULSE RADIATING IN AN
C UNBOUNDED MEDIUM, USING THE FINITE-DIFFERENCE TIME-DOMAIN
C METHOD. THE UNBOUNDED MEDIUM IS SIMULATED USING A BERENGER
C PERFECTLY MATCHED LAYER (PML) ABSORBING BOUNDARY CONDITION
C (ABC) IN ORDER TO TRUNCATE THE COMPUTATIONAL DOMAIN. THE
C MATLAB M-FILE PRODUCES THE FD-TD SOLUTION OF AN INFINITE
C LENGTH LINE SOURCE EXCITED BY A TIME-DERIVATIVE GAUSSIAN
C PULSE IN A 2-D TM² COMPUTATIONAL DOMAIN. THE M-FILE PRODUCES A
C MOVIE WHICH IS 37 FRAMES LONG BY TAKING A PICTURE OF THE
C COMPUTATIONAL DOMAIN EVERY 3RD TIME STEP.
C      II.  LINE SOURCE-GAUSSIAN PULSE: PEC SQUARE CYLINDER
C THE SECOND ANIMATION-VISUALIZATION PROGRAM IS THAT OF A
C LINE SOURCE EXCITED BY A SINGLE GAUSSIAN PULSE RADIATING
C INSIDE A PERFECTLY ELECTRIC CONDUCTING (PEC) SQUARE CYLINDER,
C USING THE FINITE-DIFFERENCE TIME-DOMAIN METHOD. THE MATLAB
C M-FILE PRODUCES THE FD-TD SOLUTION OF AN INFINITE LENGTH LINE
C SOURCE EXCITED BY A TIME-DERIVATIVE GAUSSIAN PULSE IN A 2-D TM²
C COMPUTATIONAL DOMAIN. THE M-FILE PRODUCES A MOVIE WHICH IS
C 70 FRAMES LONG BY TAKING A PICTURE OF THE COMPUTATIONAL
C DOMAIN EVERY 3RD TIME STEP.
C      III. E-PLANE SECTORAL HORN: UNBOUNDED MEDIUM
C THE THIRD ANIMATION-VISUALIZATION PROGRAM IS THAT OF AN
C E-PLANE SECTORAL (2-D) HORN ANTENNA RADIATING INTO AN
C UNBOUNDED MEDIUM, USING THE FINITE-DIFFERENCE TIME-DOMAIN
C METHOD. THE UNBOUNDED MEDIUM IS SIMULATED USING A BERENGER
C PERFECTLY MATCHED LAYER (PML) ABSORBING BOUNDARY CONDITION
C (ABC) IN ORDER TO TRUNCATE THE COMPUTATIONAL DOMAIN. THE
C MATLAB M-FILE PRODUCES THE FD-TD SOLUTION OF THE E-PLANE
C SECTORAL (2-D) HORN ANTENNA EXCITED BY A SINUSOIDAL VOLTAGE IN
C A TE² COMPUTATIONAL DOMAIN. THE M-FILE PRODUCES A MOVIE WHICH
C IS 70 FRAMES LONG BY TAKING A PICTURE OF THE COMPUTATIONAL
C DOMAIN EVERY 3RD TIME STEP.
C **NOTE:
C IN ORDER TO ANIMATE AND THEN VISUALIZE THESE THREE RADIATION
C PROBLEMS, THE USER NEEDS THE PROFESSIONAL EDITION OF MATLAB
C AND THE MATLAB M-FILE FOUND IN THE INCLUDED COMPUTER DISC TO
C PRODUCE THE CORRESPONDING FD-TD SOLUTION OF EACH RADIATION
C PROBLEM. THE STUDENT EDITION WILL NOT WORK DUE TO THE
C RESTRICTIONS ON THE ARRAY SIZE. ADDITIONAL DETAILS ON THE USE
C OF EACH VISUALIZATION PROBLEM ARE FOUND IN THE COMPUTER DISC
C INCLUDED WITH THIS BOOK.
C***********************************************************
```


INTEL-1045
U.S. Patent 7,151,430

CHAPTER 2

FUNDAMENTAL PARAMETERS OF ANTENNAS

2.1 INTRODUCTION

To describe the performance of an antenna, definitions of various parameters are necessary. Some of the parameters are interrelated and not all of them need be specified for complete description of the antenna performance. Parameter definitions will be given in this chapter. Many of those in quotation marks are from the *IEEE Standard Definitions of Terms for Antennas* (IEEE Std 145-1983).* This is a revision of the IEEE Std 145-1973.

2.2 RADIATION PATTERN

An antenna *radiation pattern* or *antenna pattern* is defined as "a mathematical function or a graphical representation of the radiation properties of the antenna as a function of space coordinates. In most cases, the radiation pattern is determined in the far-field region and is represented as a function of the directional coordinates. Radiation properties include power flux density, radiation intensity, field strength, directivity phase or polarization." The radiation property of most concern is the two- or three-dimensional spatial distribution of radiated energy as a function of the observer's position along a path or surface of constant radius. A convenient set of coordinates is shown in Figure 2.1. A trace of the received power at a constant radius is called the *power pattern*. On the other hand, a graph of the spatial variation of the electric (or magnetic) field along a constant radius is called an amplitude *field pattern*. In practice, the three-dimensional pattern is measured and recorded in a series of two-dimensional patterns. However, for most practical applications, a few plots of the pattern as a function of θ for some particular values of ϕ, plus a few plots as a function of ϕ for some particular values of θ, give most of the useful and needed information.

IEEE Transactions on Antennas and Propagation, Vols. AP-17, No. 3, May 1969; Vol. AP-22, No. 1, January 1974; and Vol. AP-31, No. 6, Part II, November 1983.

INTEL-1045
U.S. Patent 7,151,430

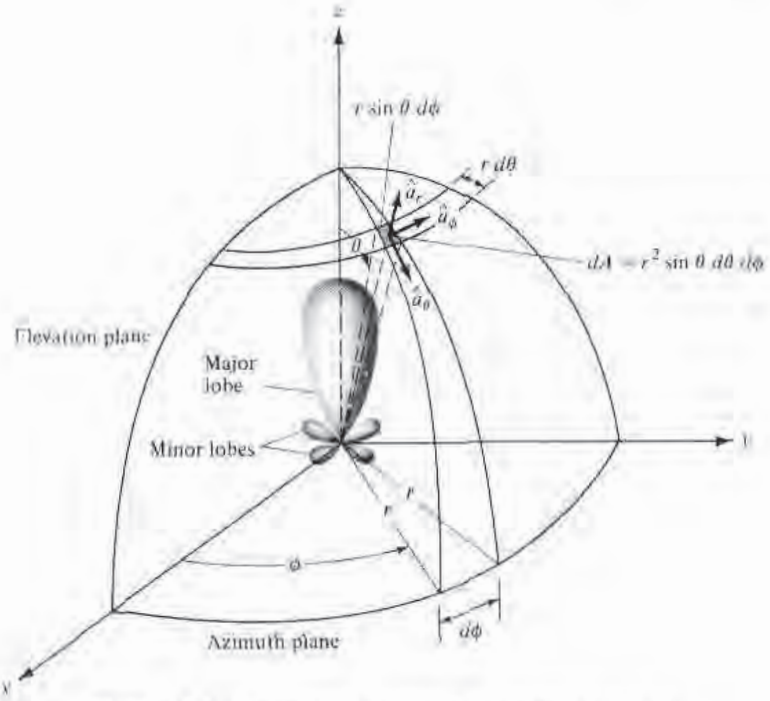


Figure 2.1 Coordinate system for antenna analysis.

2.2.1 Isotropic, Directional, and Omnidirectional Patterns

An *isotropic* radiator is defined as "a hypothetical lossless antenna having equal radiation in all directions." Although it is ideal and not physically realizable, it is often taken as a reference for expressing the directive properties of actual antennas. A *directional* antenna is one "having the property of radiating or receiving electromagnetic waves more effectively in some directions than in others. This term is usually applied to an antenna whose maximum directivity is significantly greater than that of a half-wave dipole." An example of an antenna with a directional radiation pattern is shown in Figure 2.2. It is seen that this pattern is nondirectional in the azimuth plane [$f(\phi)$, $\theta = \pi/2$] and directional in the elevation plane [$g(\theta)$, ϕ = constant]. This type of a pattern is designated as *omnidirectional*, and it is defined as one "having an essentially nondirectional pattern in a given plane (in this case in azimuth) and a directional pattern in any orthogonal plane (in this case in elevation)." An *omnidirectional* pattern is then a special type of a *directional* pattern.

2.2.2 Principal Patterns

For a linearly polarized antenna, performance is often described in terms of its principal *E*- and *H*-plane patterns. The *E-plane* is defined as "the plane containing the electric-field vector and the direction of maximum radiation," and the *H-plane* as "the plane containing the magnetic-field vector and the direction of maximum radiation." Although it is very difficult to illustrate the principal patterns without considering a specific example, it is the usual practice to orient most antennas so that at

INTEL-1045
U.S. Patent 7,151,430

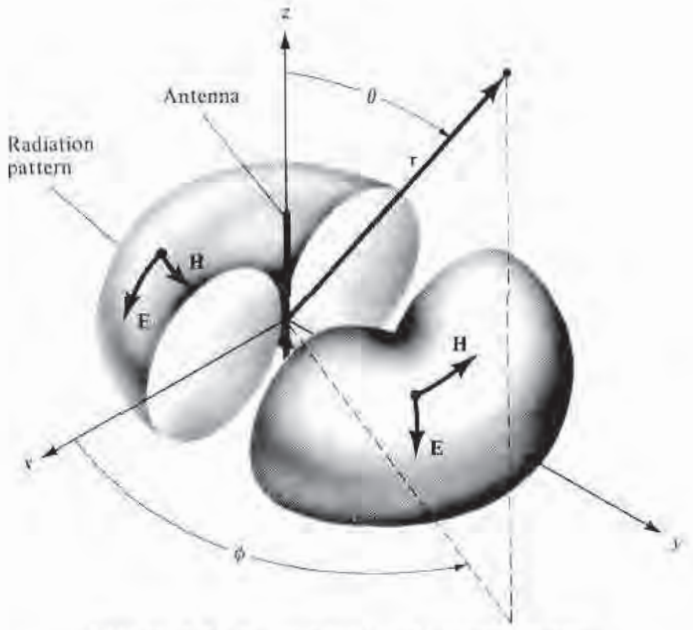


Figure 2.2 Omnidirectional antenna pattern.

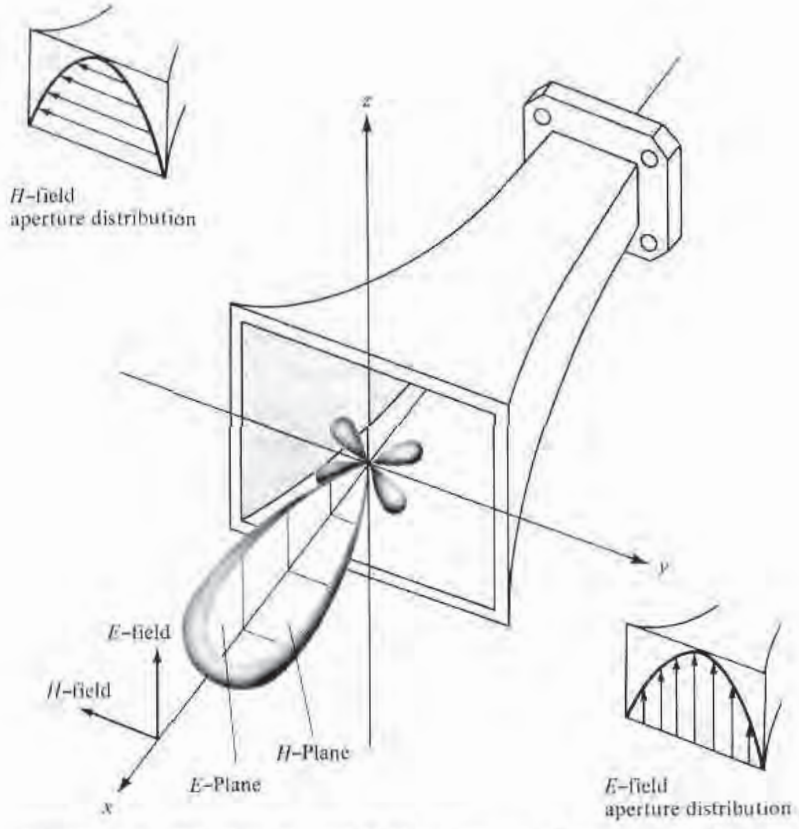


Figure 2.3 Principal E- and H-plane patterns for a pyramidal horn antenna.

least one of the principal plane patterns coincide with one of the geometrical principal planes. An illustration is shown in Figure 2.3. For this example, the x-z plane (elevation plane; $\phi = 0$) is the principal E-plane and the x-y plane (azimuthal plane: $\theta = \pi/2$) is the principal H-plane. Other coordinate orientations can be selected.

2.2.3 Radiation Pattern Lobes

Various parts of a radiation pattern are referred to as *lobes*, which may be subclassified into *major* or *main*, *minor*, *side*, and *back* lobes.

A *radiation lobe* is a "portion of the radiation pattern bounded by regions of relatively weak radiation intensity." Figure 2.4(a) demonstrates a symmetrical three-dimensional polar pattern with a number of radiation lobes. Some are of greater

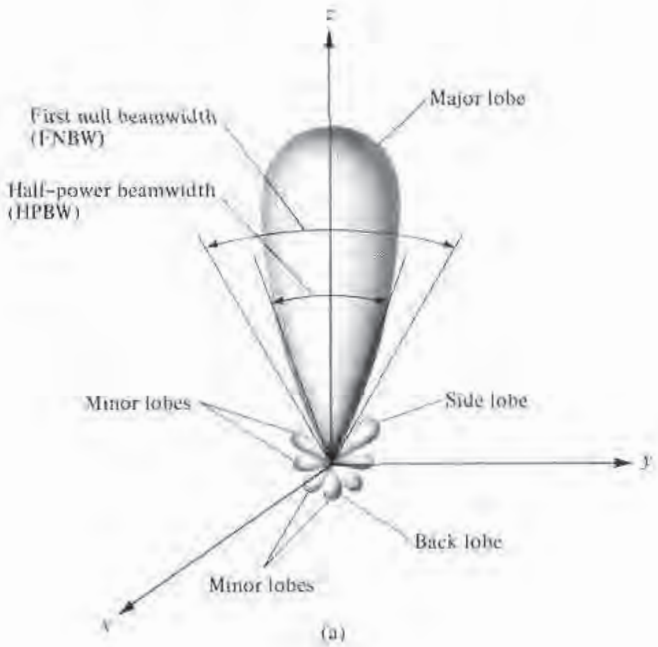


Figure 2.4 (a) Radiation lobes and beamwidths of an antenna pattern. (b) Linear plot of power pattern and its associated lobes and beamwidths.

INTEL-1045
U.S. Patent 7,151,430

radiation intensity than others, but all are classified as lobes. Figure 2.4(b) illustrates a linear two-dimensional pattern [one plane of Figure 2.4(a)] where the same pattern characteristics are indicated.

A computer program entitled *2-D ANTENNA PATTERN PLOTTER: RECTANGULAR-POLAR* [1] is included at the end of the chapter to plot two-dimensional *rectangular* and *polar* graphs, to represent single-plane antenna patterns similar to those exhibited in Figure 2.4(a,b) and elsewhere throughout the book. This program is well commented to assist the user in its implementation and only the executable part is included. Each pattern can be plotted in a linear or logarithmic (dB) scale. The program is provided courtesy of Dr. Elsherbeni and Taylor [1], and it is to be used only in conjunction with this book and for not any other purpose.

A *major lobe* (also called main beam) is defined as "the radiation lobe containing the direction of maximum radiation." In Figure 2.4 the major lobe is pointing in the $\theta = 0$ direction. In some antennas, such as split-beam antennas, there may exist more than one major lobe. A *minor lobe* is any lobe except a major lobe. In Figures 2.4(a) and (b) all the lobes with the exception of the major can be classified as minor lobes. A *side lobe* is "a radiation lobe in any direction other than the intended lobe." (Usually a side lobe is adjacent to the main lobe and occupies the hemisphere in the direction of the main beam.) A *back lobe* is "a radiation lobe whose axis makes an angle of approximately 180° with respect to the beam of an antenna." Usually it refers to a minor lobe that occupies the hemisphere in a direction opposite to that of the major (main) lobe.

Minor lobes usually represent radiation in undesired directions, and they should be minimized. Side lobes are normally the largest of the minor lobes. The level of minor lobes is usually expressed as a ratio of the power density in the lobe in question to that of the major lobe. This ratio is often termed the side lobe ratio or side lobe level. Side lobe levels of -20 dB or smaller are usually not desirable in most applications. Attainment of a side lobe level smaller than -30 dB usually requires very careful design and construction. In most radar systems, low side lobe ratios are very important to minimize false target indications through the side lobes.

2.2.4 Field Regions

The space surrounding an antenna is usually subdivided into three regions: (a) reactive near-field, (b) radiating near-field (Fresnel) and (c) far-field (Fraunhofer) regions as shown in Figure 2.5. These regions are so designated to identify the field structure in each. Although no abrupt changes in the field configurations are noted as the boundaries are crossed, there are distinct differences among them. The boundaries separating these regions are not unique, although various criteria have been established and are commonly used to identify the regions.

Reactive near-field region is defined as "that portion of the near-field region immediately surrounding the antenna wherein the reactive field predominates." For most antennas, the outer boundary of this region is commonly taken to exist at a distance $R < 0.62\sqrt{D^3/\lambda}$ from the antenna surface, where λ is the wavelength and D is the largest dimension of the antenna. "For a very short dipole, or equivalent radiator, the outer boundary is commonly taken to exist at a distance $\lambda/2\pi$ from the antenna surface."

Radiating near-field (Fresnel) region is defined as "that region of the field of an antenna between the reactive near-field region and the far-field region wherein radiation fields predominate and wherein the angular field distribution is dependent upon

INTEL-1045
U.S. Patent 7,151,430

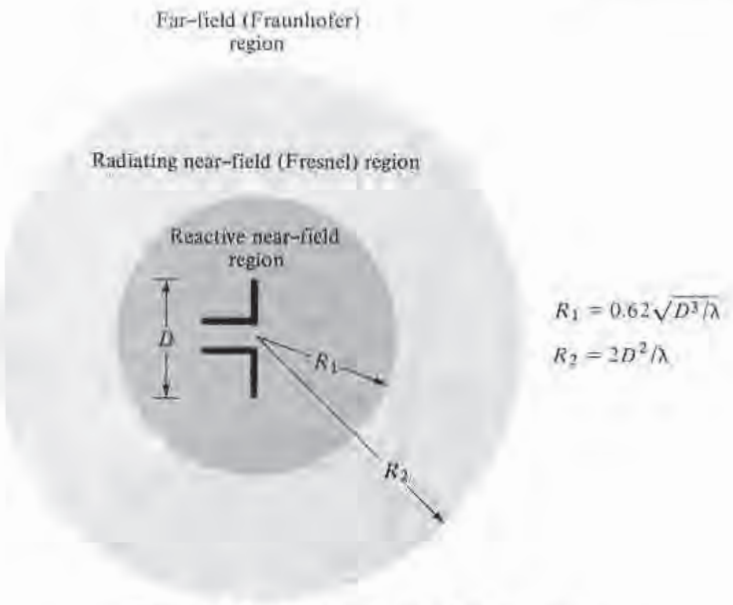


Figure 2.5 Field regions of an antenna.

the distance from the antenna. If the antenna has a maximum dimension that is not large compared to the wavelength, this region may not exist. For an antenna focused at infinity, the radiating near-field region is sometimes referred to as the Fresnel region on the basis of analogy to optical terminology. If the antenna has a maximum overall dimension which is very small compared to the wavelength, this field region may not exist." The inner boundary is taken to be the distance $R \geq 0.62\sqrt{D^3/\lambda}$ and the outer boundary the distance $R < 2D^2/\lambda$ where D is the largest* dimension of the antenna. This criterion is based on a maximum phase error of $\pi/8$. In this region the field pattern is, in general, a function of the radial distance and the radial field component may be appreciable.

Far-field (Fraunhofer) region is defined as "that region of the field of an antenna where the angular field distribution is essentially independent of the distance from the antenna. If the antenna has a maximum* overall dimension D, the far-field region is commonly taken to exist at distances greater than $2D^2/\lambda$ from the antenna, λ being the wavelength. The far-field patterns of certain antennas, such as multibeam reflector antennas, are sensitive to variations in phase over their apertures. For these antennas $2D^2/\lambda$ may be inadequate. In physical media, if the antenna has a maximum overall dimension, D, which is large compared to $\pi/|\gamma|$, the far-field region can be taken to begin approximately at a distance equal to $|\gamma|D^2/\pi$ from the antenna, γ being the propagation constant in the medium. For an antenna focused at infinity, the far-field region is sometimes referred to as the Fraunhofer region on the basis of analogy to optical terminology." In this region, the field components are essentially transverse and the angular distribution is independent of the radial distance where the measurements are made. The inner boundary is taken to be the radial distance $R = 2D^2/\lambda$ and the outer one at infinity.

To illustrate the pattern variation as a function of radial distance, in Figure 2.6 we have included three patterns of a parabolic reflector calculated at distances of $R = 2D^2/\lambda$, $4D^2/\lambda$, and infinity [2]. It is observed that the patterns are almost identical,

*To be valid, D must also be large compared to the wavelength ($D > \lambda$).

INTEL-1045
U.S. Patent 7,151,430

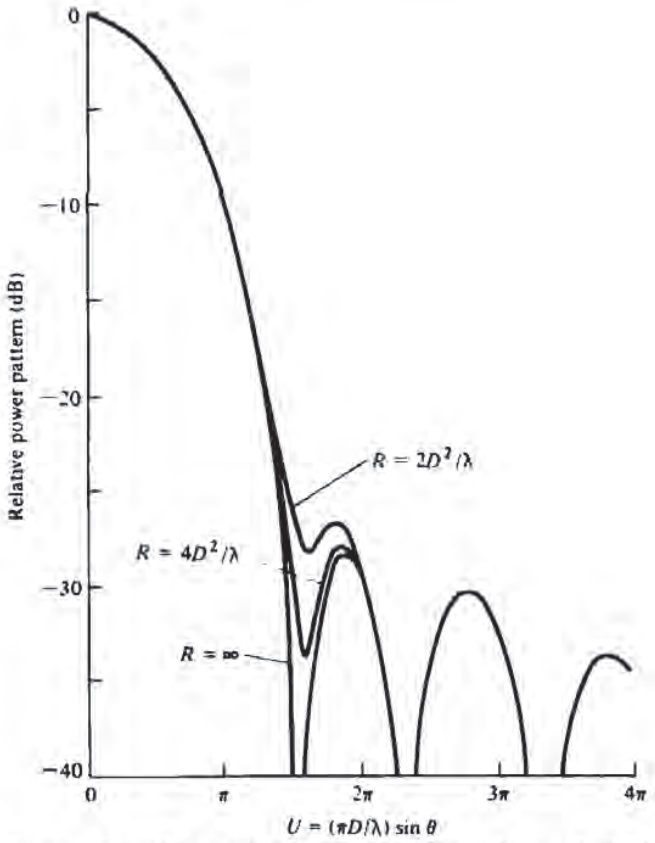


Figure 2.6 Calculated radiation patterns of a paraboloid antenna for different distances from the antenna. (SOURCE: J. S. Hollis, T. J. Lyon, and L. Clayton, Jr. (eds.), *Microwave Antenna Measurements*, Scientific-Atlanta, Inc., July 1970)

except for some differences in the pattern structure around the first null and at a level below 25 dB. Because infinite distances are not realizable in practice, the most commonly used criterion for minimum distance of far-field observations is $2D^2/\lambda$.

2.2.5 Radian and Steradian

The measure of a plane angle is a radian. One *radian* is defined as the plane angle with its vertex at the center of a circle of radius r that is subtended by an arc whose length is r. A graphical illustration is shown in Figure 2.7(a). Since the circumference of a circle of radius r is $C = 2\pi r$, there are 2π rad $(2\pi r/r)$ in a full circle.

The measure of a solid angle is a steradian. One *steradian* is defined as the solid angle with its vertex at the center of a sphere of radius r that is subtended by a spherical surface area equal to that of a square with each side of length r. A graphical illustration is shown in Figure 2.7(b). Since the area of a sphere of radius r is $A = 4\pi r^2$, there are 4π sr $(4\pi r^2/r^2)$ in a closed sphere.

The infinitesimal area dA on the surface of a sphere of radius r, shown in Figure 2.1, is given by

$$dA = r^2 \sin\theta \, d\theta \, d\phi \quad (\text{m}^2) \tag{2-1}$$

INTEL-1045
U.S. Patent 7,151,430

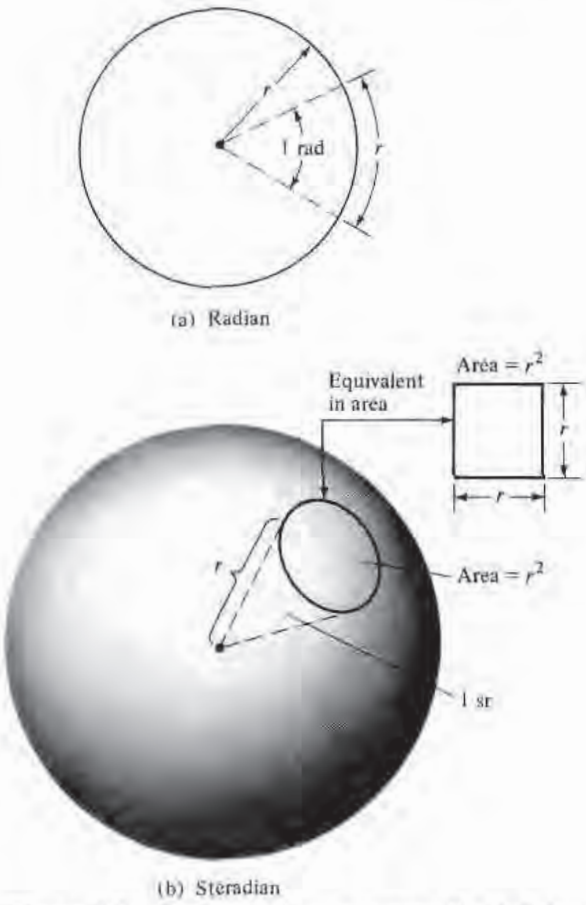


Figure 2.7 Geometrical arrangements for defining a radian and a steradian.

Therefore, the element of solid angle $d\Omega$ of a sphere can be written as

$$d\Omega = \frac{dA}{r^2} = \sin\theta\, d\theta\, d\phi \quad \text{(sr)} \tag{2-2}$$

2.3 RADIATION POWER DENSITY

Electromagnetic waves are used to transport information through a wireless medium or a guiding structure, from one point to the other. It is then natural to assume that power and energy are associated with electromagnetic fields. The quantity used to describe the power associated with an electromagnetic wave is the instantaneous Poynting vector defined as

$$\mathcal{W} = \mathcal{E} \times \mathcal{H} \tag{2-3}$$

$\mathcal{W}$ = instantaneous Poynting vector (W/m^2)
$\mathcal{E}$ = instantaneous electric field intensity (V/m)
$\mathcal{H}$ = instantaneous magnetic field intensity (A/m)

Note that script letters are used to denote instantaneous fields and quantities, while roman letters are used to represent their complex counterparts.

INTEL-1045
U.S. Patent 7,151,430

Since the Poynting vector is a power density, the total power crossing a closed surface can be obtained by integrating the normal component of the Poynting vector over the entire surface. In equation form

$$\mathcal{P} = \oiint_S \mathcal{W} \cdot d\mathbf{s} = \oiint_S \mathcal{W} \cdot \hat{\mathbf{n}}\, da \tag{2-4}$$

$\mathcal{P}$ = instantaneous total power (W)

$\hat{\mathbf{n}}$ = unit vector normal to the surface

da = infinitesimal area of the closed surface (m^2)

For applications of time varying fields, it is often more desirable to find the average power density which is obtained by integrating the instantaneous Poynting vector over one period and dividing by the period. For time harmonic variations of the form $e^{j\omega t}$, we define the complex fields $\mathbf{E}$ and $\mathbf{H}$ which are related to their instantaneous counterparts $\mathscr{E}$ and $\mathscr{H}$ by

$$\mathscr{E}(x, y, z; t) = \text{Re}[\mathbf{E}(x, y, z)e^{j\omega t}] \tag{2-5}$$

$$\mathscr{H}(x, y, z; t) = \text{Re}[\mathbf{H}(x, y, z)e^{j\omega t}] \tag{2-6}$$

Using the definitions of (2-5) and (2-6) and the identity $\text{Re}[\mathbf{E}e^{j\omega t}] = \frac{1}{2}[\mathbf{E}e^{j\omega t} + \mathbf{E}^*e^{-j\omega t}]$, (2-3) can be written as

$$\mathcal{W} = \mathscr{E} \times \mathscr{H} = \tfrac{1}{2}\,\text{Re}[\mathbf{E} \times \mathbf{H}^*] + \tfrac{1}{2}\,\text{Re}[\mathbf{E} \times \mathbf{H}e^{j2\omega t}] \tag{2-7}$$

The first term of (2-7) is not a function of time, and the time variations of the second are twice the given frequency. The time average Poynting vector (average power density) can be written as

$$\boxed{\mathbf{W}_{av}(x, y, z) = [\mathcal{W}(x, y, z; t)]_{av} = \tfrac{1}{2}\,\text{Re}[\mathbf{E} \times \mathbf{H}^*]} \quad (\text{W/m}^2) \tag{2-8}$$

The $\frac{1}{2}$ factor appears in (2-7) and (2-8) because the $\mathbf{E}$ and $\mathbf{H}$ fields represent peak values, and it should be omitted for RMS values.

A close observation of (2-8) may raise a question. If the real part of $(\mathbf{E} \times \mathbf{H}^*)/2$ represents the average (real) power density, what does the imaginary part of the same quantity represent? At this point it will be very natural to assume that the imaginary part must represent the reactive (stored) power density associated with the electromagnetic fields. In later chapters, it will be shown that the power density associated with the electromagnetic fields of an antenna in its far-field region is predominately real and will be referred to as *radiation density*.

Based upon the definition of (2-8), the average power radiated by an antenna (radiated power) can be written as

$$\boxed{\begin{aligned} P_{rad} = P_{av} &= \oiint_S \mathbf{W}_{rad} \cdot d\mathbf{s} = \oiint_S \mathbf{W}_{av} \cdot \hat{\mathbf{n}}\, da \\ &= \frac{1}{2} \oiint_S \text{Re}(\mathbf{E} \times \mathbf{H}^*) \cdot d\mathbf{s} \end{aligned}} \tag{2-9}$$

INTEL-1045
U.S. Patent 7,151,430

The power pattern of the antenna, whose definition was discussed in Section 2.2, is just a measure, as a function of direction, of the average power density radiated by the antenna. The observations are usually made on a large sphere of constant radius extending into the far-field. In practice, absolute power patterns are usually not desired. However, the performance of the antenna is measured in terms of the gain (to be discussed in a subsequent section) and in terms of relative power patterns. Three-dimensional patterns cannot be measured, but they can be constructed with a number of two-dimensional cuts.

Example 2.1

The radial component of the radiated power density of an antenna is given by

$$\mathbf{W}_{rad} = \hat{\mathbf{a}}_r W_r = \hat{\mathbf{a}}_r A_0 \sin\theta / r^2 \qquad (\mathrm{W/m^2})$$

where A_0 is the peak value of the power density, θ is the usual spherical coordinate, and $\hat{a}_r$ is the radial unit vector. Determine the total radiated power.

SOLUTION

For a closed surface, a sphere of radius r is chosen. To find the total radiated power, the radial component of the power density is integrated over its surface. Thus

$$P_{rad} = \oiint_S \mathbf{W}_{rad} \cdot \hat{\mathbf{n}}\, da$$

$$= \int_0^{2\pi} \int_0^{\pi} \left(\hat{\mathbf{a}}_r A_0 \frac{\sin\theta}{r^2}\right) \cdot (\hat{\mathbf{a}}_r r^2 \sin\theta\, d\theta\, d\phi) = \pi^2 A_0 \qquad (\mathrm{W})$$

A three-dimensional normalized plot of the average power density at a distance of $r = 1$ m is shown in Figure 2.2.

An isotropic radiator is an ideal source that radiates equally in all directions. Although it does not exist in practice, it provides a convenient isotropic reference with which to compare other antennas. Because of its symmetric radiation, its Poynting vector will not be a function of the spherical coordinate angles θ and ϕ. In addition, it will have only a radial component. Thus the total power radiated by it is given by

$$P_{rad} = \oiint_S \mathbf{W}_0 \cdot d\mathbf{s} = \int_0^{2\pi} \int_0^{\pi} [\hat{\mathbf{a}}_r W_0(r)] \cdot [\hat{\mathbf{a}}_r r^2 \sin\theta\, d\theta\, d\phi] = 4\pi r^2 W_0 \qquad (2\text{-}10)$$

and the power density by

$$\mathbf{W}_0 = \hat{\mathbf{a}}_r W_0 = \hat{\mathbf{a}}_r \left(\frac{P_{rad}}{4\pi r^2}\right) \qquad (\mathrm{W/m^2}) \qquad (2\text{-}11)$$

which is uniformly distributed over the surface of a sphere of radius r.

INTEL-1045
U.S. Patent 7,151,430

2.4 RADIATION INTENSITY

Radiation intensity in a given direction is defined as "the power radiated from an antenna per unit solid angle." The radiation intensity is a far-field parameter, and it can be obtained by simply multiplying the radiation density by the square of the distance. In mathematical form it is expressed as

$$\boxed{U = r^2 W_{rad}} \tag{2-12}$$

where

U = radiation intensity (W/unit solid angle)
W_{rad} = radiation density (W/m^2)

The radiation intensity is also related to the far-zone electric field of an antenna by

$$\begin{aligned} U(\theta, \phi) &= \frac{r^2}{2\eta} |\mathbf{E}(r, \theta, \phi)|^2 \simeq \frac{r^2}{2\eta} [|E_\theta(r, \theta, \phi)|^2 + |E_\phi(r, \theta, \phi)|^2] \\ &= \frac{1}{2\eta} [|E_\theta^\circ(\theta, \phi)|^2 + |E_\phi^\circ(\theta, \phi)|^2] \end{aligned} \tag{2-12a}$$

where

$\mathbf{E}(r, \theta, \phi)$ = far-zone electric field intensity of the antenna = $\mathbf{E}^\circ(\theta, \phi)\dfrac{e^{-jkr}}{r}$

E_θ, E_ϕ = far-zone electric field components of the antenna
η = intrinsic impedance of the medium

Thus the power pattern is also a measure of the radiation intensity.

The total power is obtained by integrating the radiation intensity, as given by (2-12), over the entire solid angle of 4π. Thus

$$P_{rad} = \oiint_\Omega U \, d\Omega = \int_0^{2\pi} \int_0^{\pi} U \sin\theta \, d\theta \, d\phi \tag{2-13}$$

where $d\Omega$ = element of solid angle = $\sin\theta \, d\theta \, d\phi$.

Example 2.2

For the problem of Example 2.1, find the total radiated power using (2-13).

SOLUTION

Using (2-12)

$$U = r^2 W_{rad} = A_0 \sin\theta$$

and by (2-13)

$$P_{rad} = \int_0^{2\pi} \int_0^{\pi} U \sin\theta \, d\theta \, d\phi = A_0 \int_0^{2\pi} \int_0^{\pi} \sin^2\theta \, d\theta \, d\phi = \pi^2 A_0$$

INTEL-1045
U.S. Patent 7,151,430

which is the same as that obtained in Example 2.1. A three-dimensional plot of the relative radiation intensity is also represented by Figure 2.2.

For an isotropic source, U will be independent of the angles θ and ϕ, as was the case for W_{rad}. Thus (2-13) can be written as

$$P_{rad} = \oint\!\!\oint_{\Omega} U_0 \, d\Omega = U_0 \oint\!\!\oint_{\Omega} d\Omega = 4\pi U_0 \tag{2-14}$$

or the radiation intensity of an isotropic source as

$$U_0 = \frac{P_{rad}}{4\pi} \tag{2-15}$$

2.5 DIRECTIVITY

In the 1983 version of the *IEEE Standard Definitions of Terms for Antennas*, there has been a substantive change in the definition of *directivity*, compared to the definition of the 1973 version. Basically the term *directivity* in the new 1983 version has been used to replace the term *directive gain* of the old 1973 version. In the new 1983 version the term *directive gain* has been deprecated. According to the authors of the new 1983 standards, "this change brings this standard in line with common usage among antenna engineers and with other international standards, notably those of the International Electrotechnical Commission (IEC)." Therefore *directivity of an antenna* defined as "the ratio of the radiation intensity in a given direction from the antenna to the radiation intensity averaged over all directions. The average radiation intensity is equal to the total power radiated by the antenna divided by 4π. If the direction is not specified, the direction of maximum radiation intensity is implied." Stated more simply, the directivity of a nonisotropic source is equal to the ratio of its radiation intensity in a given direction over that of an isotropic source. In mathematical form, using (2-15), it can be written as

$$\boxed{D = \frac{U}{U_0} = \frac{4\pi U}{P_{rad}}} \tag{2-16}$$

If the direction is not specified, it implies the direction of maximum radiation intensity (maximum directivity) expressed as

$$\boxed{D_{max} = D_0 = \frac{U|_{max}}{U_0} = \frac{U_{max}}{U_0} = \frac{4\pi U_{max}}{P_{rad}}} \tag{2-16a}$$

D = directivity (dimensionless)
D_0 = maximum directivity (dimensionless)
U = radiation intensity (W/unit solid angle)
U_{max} = maximum radiation intensity (W/unit solid angle)
U_0 = radiation intensity of isotropic source (W/unit solid angle)
P_{rad} = total radiated power (W)

INTEL-1045
U.S. Patent 7,151,430

For an isotropic source, it is very obvious from (2-16) or (2-16a) that the directivity is unity since U, U_{max}, and U_0 are all equal to each other.

For antennas with orthogonal polarization components, we define the *partial directivity of an antenna for a given polarization in a given direction* as "that part of the radiation intensity corresponding to a given polarization divided by the total radiation intensity averaged over all directions." With this definition for the partial directivity, then in a given direction "the total directivity is the sum of the partial directivities for any two orthogonal polarizations." For a spherical coordinate system, the total maximum directivity D_0 for the orthogonal θ and ϕ components of an antenna can be written as

$$D_0 = D_\theta + D_\phi \tag{2-17}$$

while the partial directivities D_θ and D_ϕ are expressed as

$$D_\theta = \frac{4\pi U_\theta}{(P_{rad})_\theta + (P_{rad})_\phi} \tag{2-17a}$$

$$D_\phi = \frac{4\pi U_\phi}{(P_{rad})_\theta + (P_{rad})_\phi} \tag{2-17b}$$

where

U_θ = radiation intensity in a given direction contained in θ field component
U_ϕ = radiation intensity in a given direction contained in ϕ field component
$(P_{rad})_\theta$ = radiated power in all directions contained in θ field component
$(P_{rad})_\phi$ = radiated power in all directions contained in ϕ field component

---

Example 2.3

As an illustration, find the maximum directivity of the antenna whose radiation intensity is that of Example 2.1. Write an expression for the directivity as a function of the directional angles θ and ϕ.

SOLUTION

The radiation intensity is given by

$$U = r^2 W_{rad} = A_0 \sin\theta$$

The maximum radiation is directed along $\theta = \pi/2$. Thus

$$U_{max} = A_0$$

In Example 2.1 it was found that

$$P_{rad} = \pi^2 A_0$$

Using (2-16a), we find that the maximum directivity is equal to

$$D_0 = \frac{4\pi U_{max}}{P_{rad}} = \frac{4}{\pi} = 1.27$$

INTEL-1045
U.S. Patent 7,151,430

Since the radiation intensity is only a function of θ, the directivity as a function of the directional angles is represented by

$$D = D_0 \sin\theta = 1.27 \sin\theta$$

Before proceeding with a more general discussion of directivity, it may be proper at this time to consider another example, compute its directivity, compare it with that of the previous example, and comment on what it actually represents. This may give the reader a better understanding and appreciation of the directivity.

Example 2.4

The radial component of the radiated power density of an infinitesimal linear dipole of length $l \ll \lambda$ is given by

$$\mathbf{W}_{av} = \hat{\mathbf{a}}_r W_r = \hat{\mathbf{a}}_r A_0 \sin^2\theta / r^2 \qquad (\text{W/m}^2)$$

where A_0 is the peak value of the power density, θ is the usual spherical coordinate, and $\hat{\mathbf{a}}_r$ is the radial unit vector. Determine the maximum directivity of the antenna and express the directivity as a function of the directional angles θ and ϕ.

SOLUTION

The radiation intensity is given by

$$U = r^2 W_r = A_0 \sin^2\theta$$

The maximum radiation is directed along $\theta = \pi/2$. Thus

$$U_{max} = A_0$$

The total radiated power is given by

$$P_{rad} = \oiint_{\Omega} U \, d\Omega = A_0 \int_0^{2\pi} \int_0^{\pi} \sin^2\theta \sin\theta \, d\theta \, d\phi = A_0\left(\frac{8\pi}{3}\right)$$

Using (2-16a), we find that the maximum directivity is equal to

$$D_0 = \frac{4\pi U_{max}}{P_{rad}} = \frac{4\pi A_0}{\frac{8\pi}{3}(A_0)} = \frac{3}{2}$$

which is greater than 1.27 found in Example 2.3. Thus the directivity is represented by

$$D = D_0 \sin^2\theta = 1.5 \sin^2\theta$$

At this time it will be proper to comment on the results of Examples 2.3 and 2.4. To better understand the discussion, we have plotted in Figure 2.8 the relative radiation

INTEL-1045
U.S. Patent 7,151,430

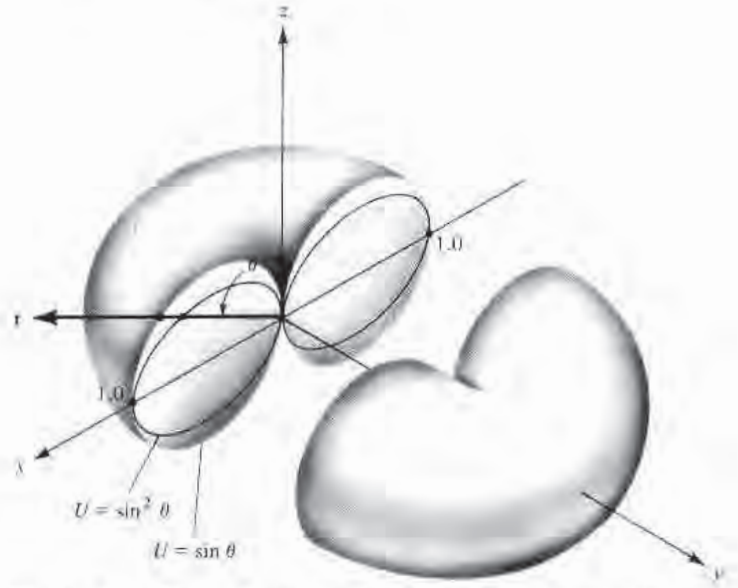


Figure 2.8 Three-dimensional radiation intensity patterns. (SOURCE: P. Lorrain and D. R. Corson, *Electromagnetic Fields and Waves*, 2nd ed., W. H. Freeman and Co. Copyright © 1970)

intensities of Example 2.3 ($U = A_0 \sin \theta$) and Example 2.4 ($U = A_0 \sin^2 \theta$) where A_0 was set equal to unity. We see that both patterns are omnidirectional but that of Example 2.4 has more directional characteristics (is narrower) in the elevation plane. Since the directivity is a "figure-of-merit" describing how well the radiator directs energy in a certain direction, it should be convincing from Figure 2.8 that the directivity of Example 2.4 should be higher than that of Example 2.3.

To demonstrate the significance of directivity, let us consider another example; in particular let us examine the directivity of a half-wavelength dipole ($l = \lambda/2$), which is derived in Section 4.6 of Chapter 4 and can be approximated by

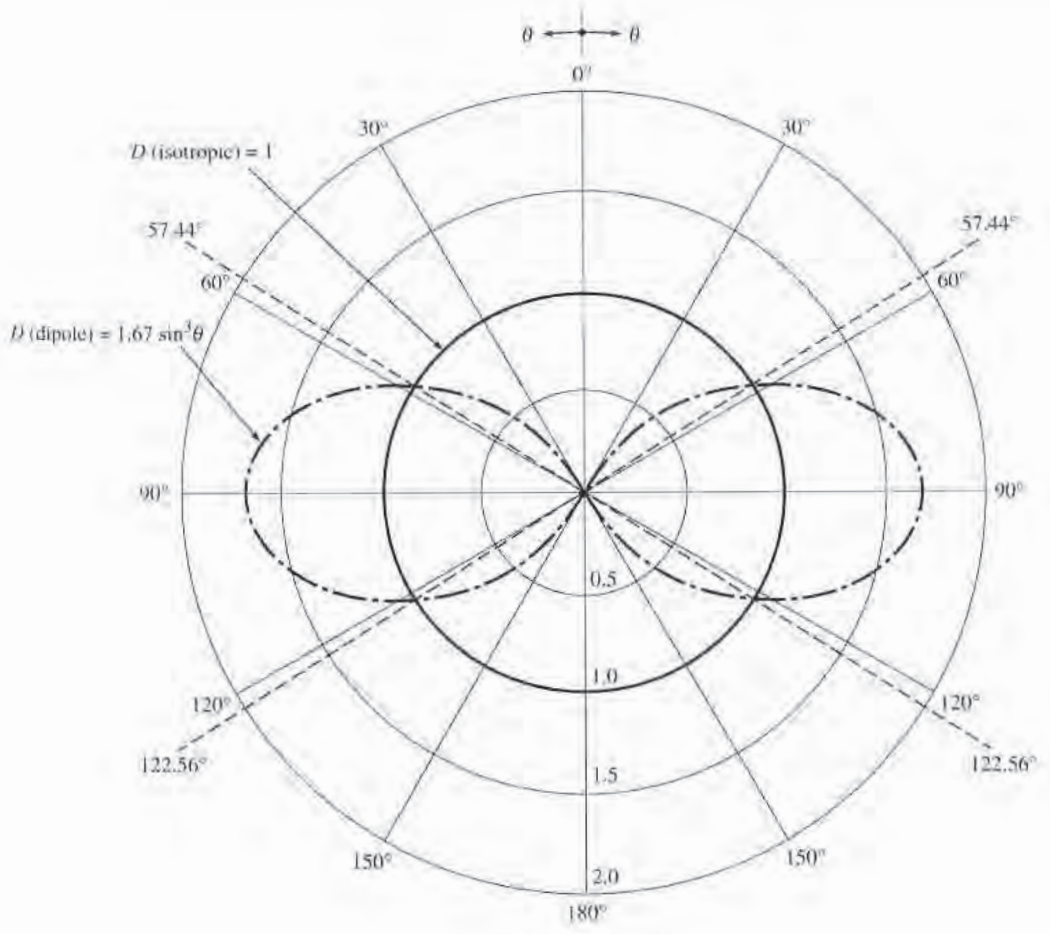
$$D = D_0 \sin^3 \theta = 1.67 \sin^3 \theta \tag{2-18}$$

since it can be shown that

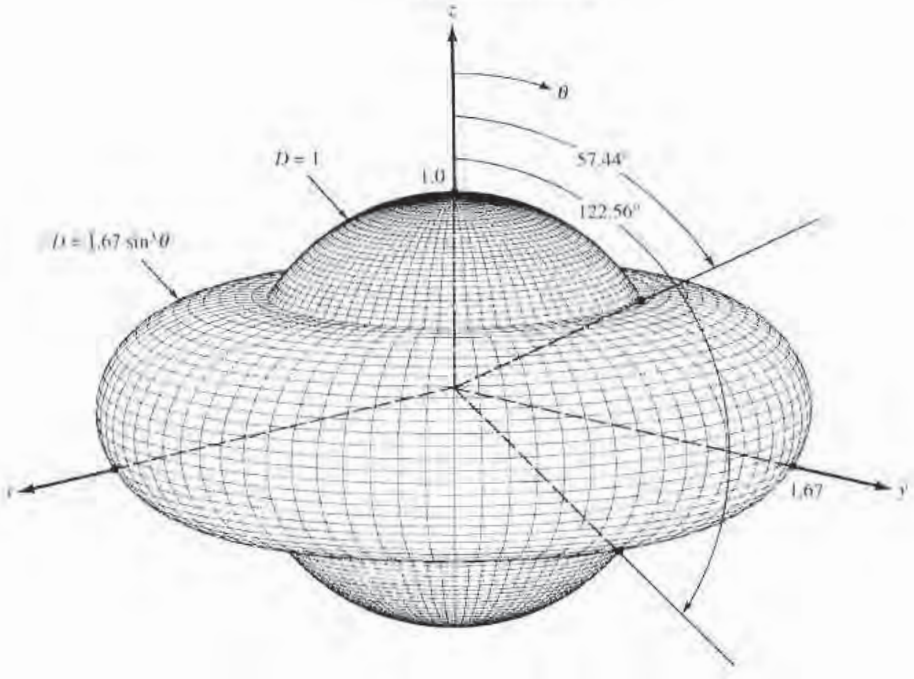
$$\sin^3 \theta \simeq \left[\frac{\cos\left(\frac{\pi}{2} \cos \theta\right)}{\sin \theta} \right]^2 \tag{2-18a}$$

where θ is measured from the axis along the length of the dipole. The values represented by (2-18) and those of an isotropic source ($D = 1$) are plotted two- and three-dimensionally in Figure 2.9(a,b). For the three-dimensional graphical representation of Figure 2.9(b), at each observation point only the largest value of the two directivities is plotted. It is apparent that when $\sin^{-1}(1/1.67)^{1/3} = 57.44° < \theta < 122.56°$, the dipole radiator has greater directivity (greater intensity concentration) in those directions than that of an isotropic source. Outside this range of angles, the isotropic radiator has higher directivity (more intense radiation). The maximum directivity of the dipole (relative to the isotropic radiator) occurs when $\theta = \pi/2$, and it is 1.67 (or

INTEL-1045
U.S. Patent 7,151,430



(a) Two-dimensional



(b) Three-dimensional

Figure 2.9 Two- and three-dimensional directivity patterns of a $\lambda/2$ dipole. (SOURCE: C. A. Balanis, "Antenna Theory: A Review." *Proc. IEEE*, Vol. 80, No. 1, January 1992. © 1992 IEEE.)

INTEL-1045
U.S. Patent 7,151,430

2.23 dB) more intense than that of the isotropic radiator (with the same radiated power).

The three-dimensional pattern of Figure 2.9(b), and similar ones, are included throughout the book to represent the three-dimensional radiation characteristics of antennas. These patterns are plotted using software developed in [3] and [4], and can be used to visualize the three-dimensional radiation pattern of the antenna. Many examples are demonstrated in [4]. The executable part of the computer program of [4] is included at the end of the chapter, courtesy of the authors Dr. Elsherbeni and Taylor, for use by the reader. The three-dimensional program of [4], along with the others, can be used effectively toward the design and synthesis of antennas, especially arrays, as demonstrated in [5] and [6].

The directivity of an isotropic source is unity since its power is radiated equally well in all directions. *For all other sources, the maximum directivity will always be greater than unity, and it is a relative "figure-of-merit" which gives an indication of the directional properties of the antenna as compared with those of an isotropic source.* In equation form, this is indicated in (2-16a). The directivity can be smaller than unity; in fact it can be equal to zero. For Examples 2.3 and 2.4, the directivity is equal to zero in the $\theta = 0$ direction. *The values of directivity will be equal to or greater than zero and equal to or less than the maximum directivity* ($0 \leq D \leq D_0$).

A more general expression for the directivity can be developed to include sources with radiation patterns that may be functions of both spherical coordinate angles θ and ϕ. In the previous examples we considered intensities that were represented by only one coordinate angle θ, in order not to obscure the fundamental concepts by the mathematical details. So it may now be proper, since the basic definitions have been illustrated by simple examples, to formulate the more general expressions.

Let the radiation intensity of an antenna be of the form

$$U = B_0 F(\theta, \phi) \simeq \frac{1}{2\eta} [|E_\theta^0(\theta, \phi)|^2 + |E_\phi^0(\theta, \phi)|^2] \tag{2-19}$$

where B_0 is a constant, and E_θ^0 and E_ϕ^0 are the antenna's far-zone electric field components. The maximum value of (2-19) is given by

$$U_{\max} = B_0 F(\theta, \phi)|_{\max} = B_0 F_{\max}(\theta, \phi) \tag{2-19a}$$

The total radiated power is found using

$$P_{\text{rad}} = \oiint_\Omega U(\theta, \phi)\, d\Omega = B_0 \int_0^{2\pi} \int_0^{\pi} F(\theta, \phi) \sin\theta\, d\theta\, d\phi \tag{2-20}$$

We now write the general expression for the directivity and maximum directivity using (2-16) and (2-16a), respectively, as

$$\boxed{D(\theta, \phi) = 4\pi \frac{F(\theta, \phi)}{\displaystyle\int_0^{2\pi} \int_0^{\pi} F(\theta, \phi) \sin\theta\, d\theta\, d\phi}} \tag{2-21}$$

$$\boxed{D_0 = 4\pi \frac{F(\theta, \phi)|_{\max}}{\displaystyle\int_0^{2\pi} \int_0^{\pi} F(\theta, \phi) \sin\theta\, d\theta\, d\phi}} \tag{2-22}$$

INTEL-1045
U.S. Patent 7,151,430

Equation (2-22) can also be written as

$$D_0 = \frac{4\pi}{\left[\int_0^{2\pi}\int_0^{\pi} F(\theta, \phi)\sin\theta\, d\theta\, d\phi\right] \Big/ F(\theta, \phi)|_{\max}} = \frac{4\pi}{\Omega_A} \tag{2-23}$$

where Ω_A is the beam solid angle, and it is given by

$$\Omega_A = \frac{1}{F(\theta, \phi)|_{\max}} \int_0^{2\pi}\int_0^{\pi} F(\theta, \phi)\sin\theta\, d\theta\, d\phi = \int_0^{2\pi}\int_0^{\pi} F_n(\theta, \phi)\sin\theta\, d\theta\, d\phi \tag{2-24}$$

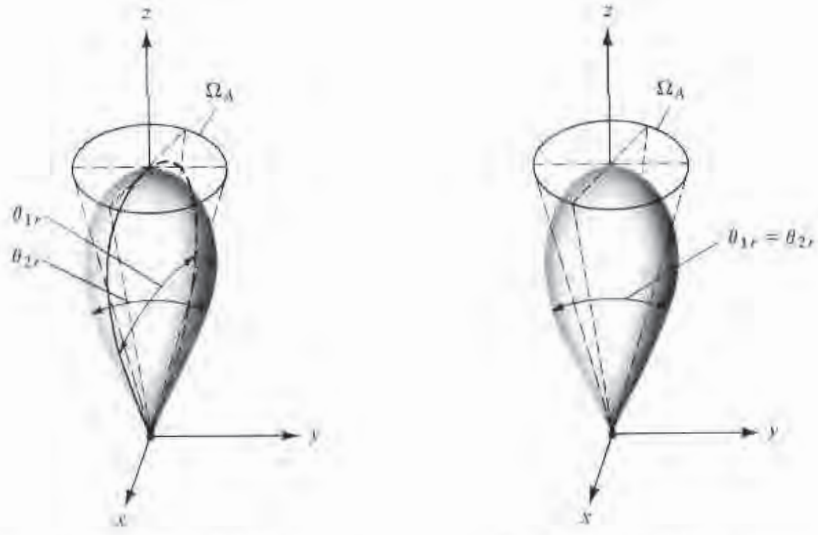
$$F_n(\theta, \phi) = \frac{F(\theta, \phi)}{F(\theta, \phi)|_{\max}} \tag{2-25}$$

Dividing by $F(\theta, \phi)|_{\max}$ merely normalizes the radiation intensity $F(\theta, \phi)$, and it makes its maximum value unity.

The beam solid angle Ω_A is defined as the solid angle through which all the power of the antenna would flow if its radiation intensity is constant (and equal to the maximum value of U) for all angles within Ω_A.

2.5.1 Directional Patterns

Instead of using the exact expression of (2-23) to compute the directivity, it is often convenient to derive simpler expressions, even if they are approximate, to compute the directivity. These can also be used for design purposes. For antennas with one narrow major lobe and very negligible minor lobes, the beam solid angle is approximately equal to the product of the half-power beamwidths in two perpendicular planes [7] shown in Figure 2.10(a). For a rotationally symmetric pattern, the half-power



(a) Nonsymmetrical pattern (b) Symmetrical pattern

Figure 2.10 Beam solid angles for nonsymmetrical and symmetrical radiation patterns.

INTEL-1045
U.S. Patent 7,151,430

beamwidths in any two perpendicular planes are the same, as illustrated in Figure 2.10(b).

With this approximation, (2-23) can be approximated by

$$D_0 = \frac{4\pi}{\Omega_A} = \frac{4\pi}{\Theta_{1r}\Theta_{2r}} \tag{2-26}$$

The beam solid angle Ω_A has been approximated by

$$\Omega_A \approx \Theta_{1r}\Theta_{2r} \tag{2-26a}$$

where

Θ_{1r} = half-power beamwidth in one plane (rad)
Θ_{2r} = half-power beamwidth in a plane at a right angle to the other (rad)

If the beamwidths are known in degress, (2-26) can be written as

$$D_0 \approx \frac{4\pi(180/\pi)^2}{\Theta_{1d}\Theta_{2d}} = \frac{41{,}253}{\Theta_{1d}\Theta_{2d}} \tag{2-27}$$

where

Θ_{1d} = half-power beamwidth in one plane (degrees)
Θ_{2d} = half-power beamwidth in a plane at a right angle to the other (degrees)

For planar arrays, a better approximation to (2-27) is [3]

$$D_0 \approx \frac{32{,}400}{\Omega_A(\text{degrees})^2} = \frac{32{,}400}{\Theta_{1d}\Theta_{2d}} \tag{2-27a}$$

The validity of (2-26) and (2-27) is based on a pattern that has only one major lobe and any minor lobes, if present, should be of very low intensity. For a pattern with two identical major lobes, the value of the maximum directivity using (2-26) or (2-27) will be twice its actual value. For patterns with significant minor lobes, the values of maximum directivity obtained using (2-26) or (2-27), which neglect any minor lobes, will usually be too high.

Example 2.5

The radiation intensity of the major lobe of many antennas can be adequately represented by

$$U = B_0 \cos\theta$$

where B_0 is the maximum radiation intensity. The radiation intensity exists only in the upper hemisphere ($0 \le \theta \le \pi/2$, $0 \le \phi \le 2\pi$), and it is shown in Figure 2.11. Find the maximum directivity using (2-26) or (2-27) and compare it with its exact value.

INTEL-1045
U.S. Patent 7,151,430

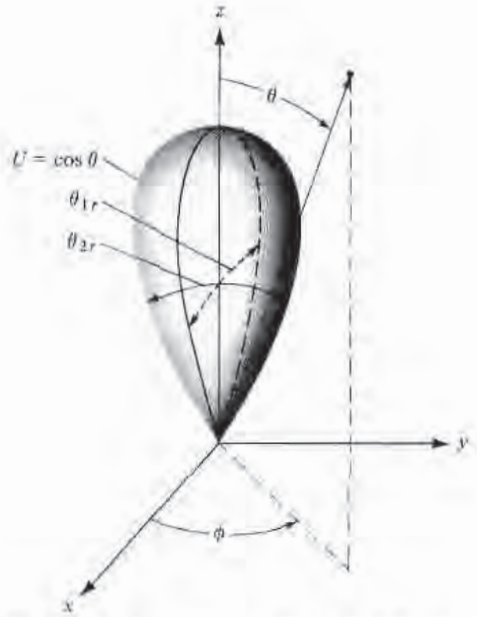


Figure 2.11 Radiation intensity pattern of the form $U = \cos\theta$ in the upper hemisphere.

SOLUTION

The half-power point of the pattern occurs at $\theta = 60°$. Thus the beamwidth in the θ direction is 120° or

$$\Theta_{1r} = \frac{2\pi}{3}$$

Since the pattern is independent of the ϕ coordinate, the beamwidth in the other plane is also equal to

$$\Theta_{2r} = \frac{2\pi}{3}$$

The maximum directivity, using (2-26), is then equal to

$$D_0 = \frac{4\pi}{(2\pi/3)^2} = \frac{9}{\pi} = 2.86$$

Now let us find the exact value of the maximum directivity and compare the results.

$$U = B_0 \cos\theta$$

$$U_{\max} = B_0 \cos\theta|_{\max} = B_0$$

$$P_{\text{rad}} = \int_0^{2\pi}\int_0^{\pi/2} B_0 \cos\theta \sin\theta \, d\theta \, d\phi = 2\pi B_0 \int_0^{\pi/2} \cos\theta \sin\theta \, d\theta$$

$$P_{\text{rad}} = \pi B_0 \int_0^{\pi/2} \sin(2\theta) \, d\theta = \pi B_0$$

$$D_0 = \frac{4\pi U_{\max}}{P_{\text{rad}}} = \frac{4\pi B_0}{\pi B_0} = 4 \qquad \text{(dimensionless)}$$

INTEL-1045
U.S. Patent 7,151,430

The exact maximum directivity is 4 and its approximate value, using (2-26), is 2.86. Better approximations can be obtained if the patterns have much narrower beamwidths, which will be demonstrated later in this section.

Many times it is desirable to express the directivity in decibels (dB) instead of dimensionless quantities. The expressions for converting the dimensionless quantities of directivity and maximum directivity to decibels (dB) are

$$D(\text{dB}) = 10 \log_{10}|D(\text{dimensionless})| \tag{2-28a}$$

$$D_0(\text{dB}) = 10 \log_{10}|D_0(\text{dimensionless})| \tag{2-28b}$$

It has also been proposed [9] that the maximum directivity of an antenna can also be obtained approximately by using the formula

$$\frac{1}{D_0} = \frac{1}{2}\left(\frac{1}{D_1} + \frac{1}{D_2}\right) \tag{2-29}$$

where

$$D_1 \simeq \frac{1}{\left[\dfrac{1}{2 \ln 2}\displaystyle\int_0^{\Theta_{1r}/2} \sin\theta\, d\theta\right]} \simeq \frac{16 \ln 2}{\Theta_{1r}^2} \tag{2-29a}$$

$$D_2 \simeq \frac{1}{\left[\dfrac{1}{2 \ln 2}\displaystyle\int_0^{\Theta_{2r}/2} \sin\theta\, d\theta\right]} \simeq \frac{16 \ln 2}{\Theta_{2r}^2} \tag{2-29b}$$

Θ_{1r} and Θ_{2r} are the half-power beamwidths (in radians) of the E- and H-planes, respectively. The formula of (2-29) will be referred to as the arithmetic mean of the maximum directivity. Using (2-29a) and (2-29b) we can write (2-29) as

$$\frac{1}{D_0} \simeq \frac{1}{2 \ln 2}\left(\frac{\Theta_{1r}^2}{16} + \frac{\Theta_{2r}^2}{16}\right) = \frac{\Theta_{1r}^2 + \Theta_{2r}^2}{32 \ln 2} \tag{2-30}$$

or

$$\boxed{D_0 \simeq \frac{32 \ln 2}{\Theta_{1r}^2 + \Theta_{2r}^2} = \frac{22.181}{\Theta_{1r}^2 + \Theta_{2r}^2}} \tag{2-30a}$$

$$D_0 \simeq \frac{22.181\,(180/\pi)^2}{\Theta_{1d}^2 + \Theta_{2d}^2} = \frac{72.815}{\Theta_{1d}^2 + \Theta_{2d}^2} \tag{2-30b}$$

where Θ_{1d} and Θ_{2d} are the half-power beamwidths in degrees. Equation (2-30a) is to be contrasted with (2-26) while (2-30b) should be compared with (2-27).

In order to make an evaluation and comparison of the accuracies of (2-26) and (2-30a), examples whose radiation intensities (power patterns) can be represented by

$$U(\theta, \phi) = \begin{cases} B_0 \cos^n(\theta) & 0 \le \theta \le \pi/2, \quad 0 \le \phi \le 2\pi \\ 0 & \text{elsewhere} \end{cases} \tag{2-31}$$

INTEL-1045
U.S. Patent 7,151,430

where $n = 1 - 10$, 11.28, 15, and 20 are considered. The maximum directivities were computed using (2-26) and (2-30a) and compared with the exact values as obtained using (2-22). The results are shown in Table 2.1. From the comparisons it is evident that the error due to Tai & Pereira's formula is always negative (i.e., it predicts lower values of maximum directivity than the exact ones) and monotonically decreases as n increases (the pattern becomes more narrow). However, the error due to Kraus' formula is negative for small values of n and positive for large values of n. For small values of n the error due to Kraus' formula is negative and positive for large values of n; the error is zero when $n = 5.497 \simeq 5.5$ (half-power beamwidth of 56.35°). In addition, for symmetrically rotational patterns the absolute error due to the two approximate formulas is identical when $n = 11.28$, which corresponds to a half-power beamwidth of 39.77°. From these observations we conclude that, Kraus' formula is more accurate for small values of n (broader patterns) while Tai & Pereira's is more accurate for large values of n (narrower patterns). Based on absolute error and symmetrically rotational patterns, Kraus' formula leads to smaller error for $n < 11.28$ (half-power beamwidth greater than 39.77°) while Tai & Pereira's leads to smaller error for $n > 11.28$ (half-power beamwidth smaller than 39.77°). The results are shown plotted in Figure 2.12 for $0 < n \leq 450$.

2.5.2 Omnidirectional Patterns

Some antennas (such as dipoles, loops, broadside arrays) exhibit omnidirectional patterns, as illustrated by the three-dimensional patterns in Figure 2.13 (a,b). As single-lobe directional patterns can be approximated by (2-31), omnidirectional patterns can often be approximated by

$$U = |\sin^n(\theta)| \qquad 0 \leq \theta \leq \pi, \quad 0 \leq \phi \leq 2\pi \tag{2-32}$$

where n represents both integer and noninteger values. The directivity of antennas with patterns represented by (2-32) can be determined in closed form using the

Table 2.1 COMPARISON OF EXACT AND APPROXIMATE VALUES OF MAXIMUM DIRECTIVITY FOR $U = \cos^n\theta$ POWER PATTERNS

n	Exact Equation (2-22)	Kraus Equation (2-26)	Kraus % Error	Tai and Pereira Equation (2-30a)	Tai and Pereira % Error
1	4	2.86	−28.50	2.53	−36.75
2	6	5.09	−15.27	4.49	−25.17
3	8	7.35	−8.12	6.48	−19.00
4	10	9.61	−3.90	8.48	−15.20
5	12	11.87	−1.08	10.47	−12.75
6	14	14.13	+0.93	12.46	−11.00
7	16	16.39	+2.48	14.47	−9.56
8	18	18.66	+3.68	16.47	−8.50
9	20	20.93	+4.64	18.47	−7.65
10	22	23.19	+5.41	20.47	−6.96
11.28	24.56	26.08	+6.24	23.02	−6.24
15	32	34.52	+7.88	30.46	−4.81
20	42	45.89	+9.26	40.46	−3.67

INTEL-1045
U.S. Patent 7,151,430

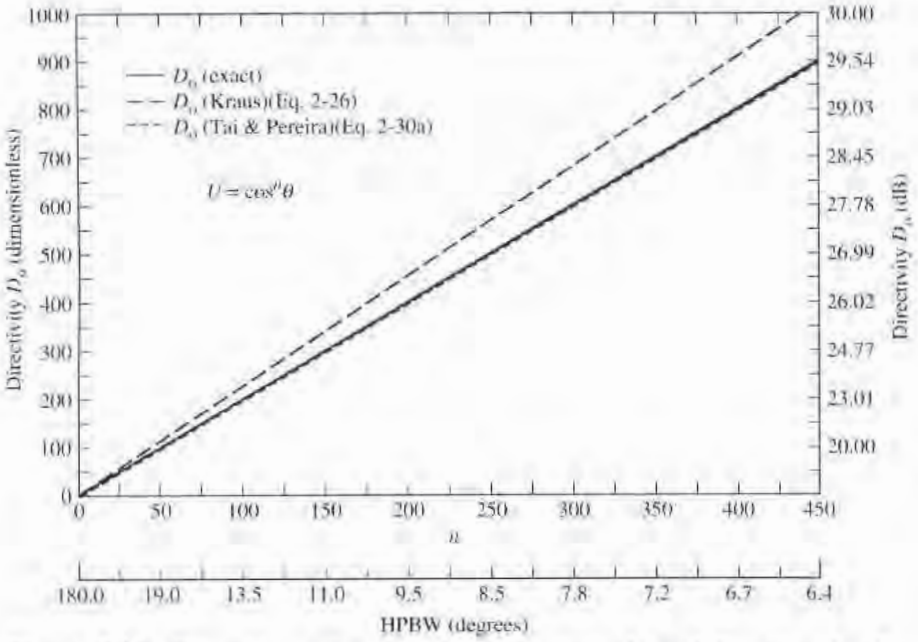


Figure 2.12 Comparison of exact and approximate values of directivity for directional $U = \cos^n\theta$ power patterns.

definition of (2-16a). However, as was done for the single-lobe patterns of Figure 2.10, approximate directivity formulas have been derived [10], [11] for antennas with omnidirectional patterns similar to the ones shown in Figure 2.13 whose main lobe is approximated by (2-32).The approximate directivity formula for an omnidirectional pattern as a function of the pattern half-power beamwidth (in degrees), which is reported by McDonald in [10], was derived based on the array factor of a broadside collinear array [see Section 6.4.1 and (6-38a)] and is given by

$$D_0 = \frac{101}{\text{HPBW (degrees)} - 0.0027\,[\text{HPBW (degrees)}]^2} \tag{2-33a}$$

However, that reported by Pozar in [11] is derived based on the exact values obtained using (2-32) and then representing the data in closed-form using curve-fitting, and it is given by

$$D_0 = -172.4 + 191\sqrt{0.818 + 1/\text{HPBW (degrees)}} \tag{2-33b}$$

The approximate formula of (2-33a) should, in general, be more accurate for omnidirectional patterns with minor lobes, as shown in Figure 2.13(a), while (2-33b) should be more accurate for omnidirectional patterns with minor lobes of very low intensity (ideally no minor lobes), as shown in Figure 2.13(b).

The approximate formulas of (2-33a) and (2-33b) can be used to design omnidirectional antennas with specified radiation pattern characteristics. To facilitate this procedure, the directivity of antennas with omnidirectional patterns approximated by (2-32) is plotted in Figure 2.14 versus n and the half-power beamwidth (in degrees).

INTEL-1045
U.S. Patent 7,151,430

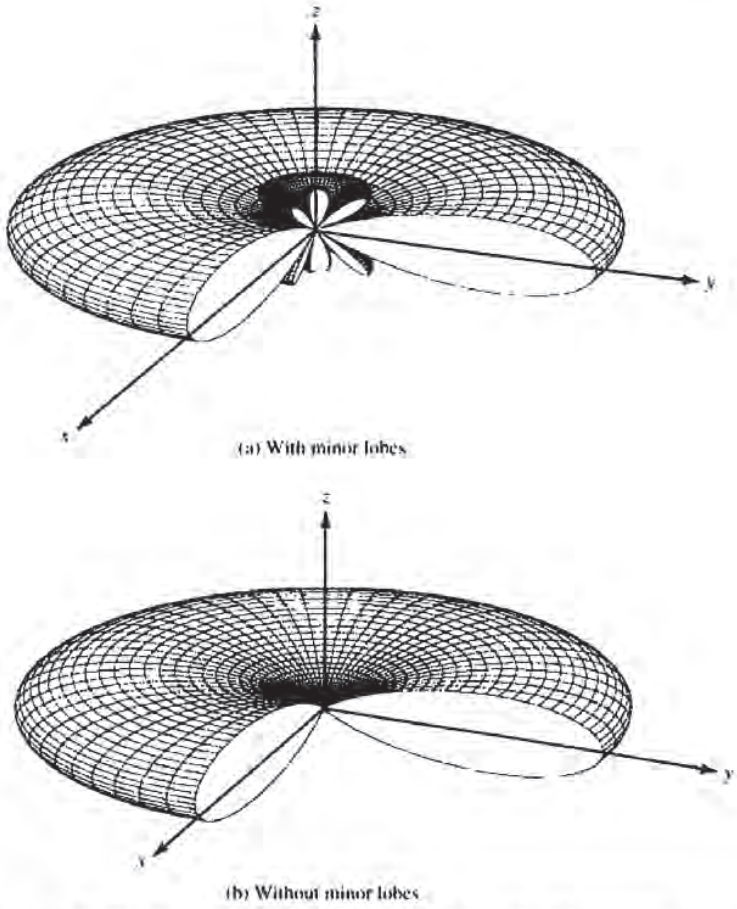


Figure 2.13 Omnidirectional patterns with and without minor lobes.

Three curves are plotted in Figure 2.14; one using (2-16a) and referred as *exact*, one using (2-33a) and denoted as *McDonald*, and the third using (2-33b) and denoted as *Pozar*. Thus, the curves of Figure 2.14 can be used for design purposes, as follows:

a. Specify the desired directivity and determine the value of n and half-power beamwidth of the omnidirectional antenna pattern, or

b. Specify the desired value of n or half-power beamwidth and determine the directivity of the omnidirectional antenna pattern.

To demonstrate the procedure, an example is taken.

Example 2.6

Design an antenna with omnidirectional amplitude pattern with a half-power beamwidth of 90°. Express its radiation intensity by $U = \sin^n\theta$. Determine the value of n and attempt to identify elements that exhibit such a pattern. Determine the directivity of the antenna using (2-16a), (2-33a), and (2-33b).

INTEL-1045
U.S. Patent 7,151,430

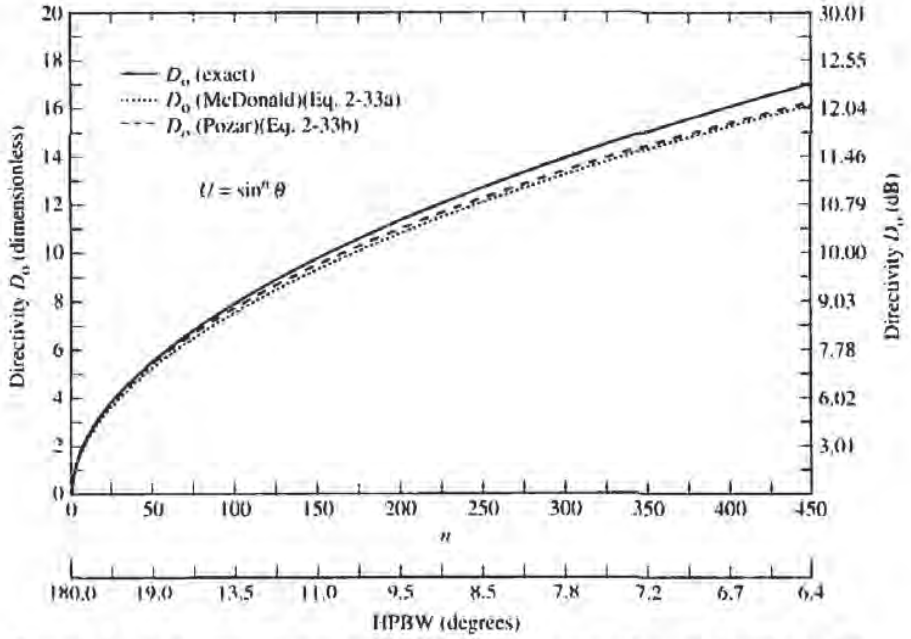


Figure 2.14 Comparison of exact and approximate values of directivity for omnidirectional $U = \sin^n\theta$ power patterns.

SOLUTION

Since the half-power beamwidth is 90°, the angle at which the half-power point occurs is $\theta = 45°$. Thus

$$U(\theta = 45°) = 0.5 = \sin^n(45°) = (0.707)^n$$

or

$$n = 2$$

Therefore, the radiation intensity of the omnidirectional antenna is represented by $U = \sin^2\theta$. An infinitesimal dipole (see Chapter 4) or a small circular loop (see Chapter 5) are two antennas which possess such a pattern.

Using the definition of (2-16a), the exact directivity is

$$U_{max} = 1$$

$$P_{rad} = \int_0^{2\pi}\int_0^{\pi} \sin^2\theta \sin\theta \, d\theta \, d\phi = \frac{8\pi}{3}$$

$$D_0 = \frac{4\pi}{8\pi/3} = \frac{3}{2} = 1.761 \text{ dB}$$

Since the half-power beamwidth is equal to 90°, then the directivity based on (2-33a) is equal to

$$D_0 = \frac{101}{90 - 0.0027\,(90)^2} = 1.4825 = 1.71 \text{ dB}$$

INTEL-1045
U.S. Patent 7,151,430

while that based on (2-33b) is equal to

$$D_0 = -172.4 + 191\sqrt{0.818 + 1/90} = 1.516 = 1.807 \text{ dB}$$

The value of n and the three values of the directivity can also be obtained using Figure 2.14, although they may not be as accurate as those given above because they have to be taken off the graph. However, the curves can be used for other problems.

2.6 NUMERICAL TECHNIQUES

For most practical antennas, their radiation patterns are so complex that closed form mathematical expressions are not available. Even in those cases where expressions are available, their form is so complex that integration to find the radiated power, required to compute the maximum directivity, cannot be performed. Instead of using the approximate expressions of Kraus, Tai and Pereira, McDonald or Pozar alternate and more accurate techniques may be desirable. With the high-speed computer systems now available, the answer may be to apply numerical methods.

Let us assume that the radiation intensity of a given antenna is separable, and it is given by

$$U = B_0 f(\theta)\, g(\phi) \tag{2-34}$$

where B_0 is a constant. The directivity for such a system is given by

$$D_0 = \frac{4\pi U_{\max}}{P_{\text{rad}}} \tag{2-35}$$

where

$$P_{\text{rad}} = B_0 \int_0^{2\pi} \left\{ \int_0^{\pi} f(\theta)\, g(\phi) \sin\theta\, d\theta \right\} d\phi \tag{2-36}$$

which can also be written as

$$P_{\text{rad}} = B_0 \int_0^{2\pi} g(\phi) \left\{ \int_0^{\pi} f(\theta) \sin\theta\, d\theta \right\} d\phi \tag{2-37}$$

If the integrations in (2-37) cannot be performed analytically, then from integral calculus we can write a series approximation

$$\int_0^{\pi} f(\theta) \sin\theta\, d\theta = \sum_{i=1}^{N} [f(\theta_i) \sin\theta_i]\, \Delta\theta_i \tag{2-38}$$

For N uniform divisions over the π interval,

$$\Delta\theta_i = \frac{\pi}{N} \tag{2-38a}$$

INTEL-1045
U.S. Patent 7,151,430

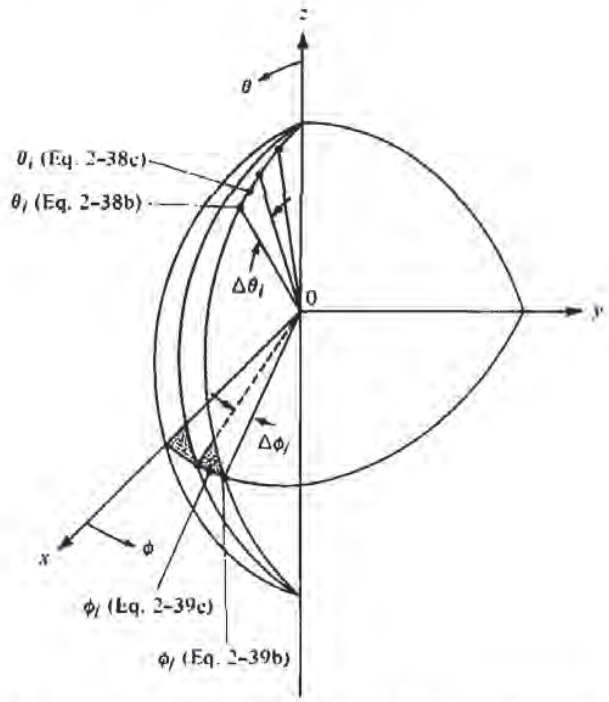


Figure 2.15 Digitization scheme of pattern in spherical coordinates.

Referring to Figure 2.15, θ_i can take many different forms. Two schemes are shown in Figure 2.15 such that

$$\theta_i = i\left(\frac{\pi}{N}\right), \qquad i = 1, 2, 3, \ldots, N \tag{2-38b}$$

or

$$\theta_i = \frac{\pi}{2N} + (i - 1)\frac{\pi}{N}, \qquad i = 1, 2, 3, \ldots, N \tag{2-38c}$$

In the former case, θ_i is taken at the trailing edge of each division; in the latter case, θ_i is selected at the middle of each division. The scheme that is more desirable will depend upon the problem under investigation. Many other schemes are available.

In a similar manner, we can write for the ϕ variations that

$$\int_0^{2\pi} g(\phi)\, d\phi = \sum_{j=1}^{M} g(\phi_j)\, \Delta\phi_j \tag{2-39}$$

where for M uniform divisions

$$\Delta\phi_j = \frac{2\pi}{M} \tag{2-39a}$$

INTEL-1045
U.S. Patent 7,151,430

Again referring to Figure 2.15

$$\phi_j = j\left(\frac{2\pi}{M}\right), \quad j = 1, 2, 3, \ldots, M \tag{2-39b}$$

or

$$\phi_j = \frac{2\pi}{2M} + (j-1)\frac{2\pi}{M}, \quad j = 1, 2, 3, \ldots, M \tag{2-39c}$$

Combining (2-38), (2-38a), (2-39), and (2-39a) we can write (2-37) as

$$P_{\text{rad}} = B_0\left(\frac{\pi}{N}\right)\left(\frac{2\pi}{M}\right)\sum_{j=1}^{M}\left\{g(\phi_j)\left[\sum_{i=1}^{N} f(\theta_i)\sin\theta_i\right]\right\} \tag{2-40}$$

The double summation of (2-40) is performed by adding for each value of j ($j = 1, 2, 3, \ldots, M$) all values of i ($i = 1, 2, 3, \ldots, N$). In a computer program flowchart, this can be performed by a loop within a loop. Physically, (2-40) can be interpreted by referring to Figure 2.15. It simply states that for each value of $g(\phi)$ at the azimuthal angle $\phi = \phi_j$, the values of $f(\theta)\sin\theta$ are added for all values of $\theta = \theta_i$ ($i = 1, 2, 3, \ldots, N$). The values of θ_i and ϕ_j can be determined by using either of the forms as given by (2-38b) or (2-38c) and (2-39b) or (2-39c).

Since the θ and ϕ variations are separable, (2-40) can also be written as

$$P_{\text{rad}} = B_0\left(\frac{\pi}{N}\right)\left(\frac{2\pi}{M}\right)\left[\sum_{j=1}^{M} g(\phi_j)\right]\left[\sum_{i=1}^{N} f(\theta_i)\sin\theta_i\right] \tag{2-41}$$

in which case each summation can be performed separately.

If the θ and ϕ variations are not separable, and the radiation intensity is given by

$$U = B_0 F(\theta, \phi) \tag{2-42}$$

the digital form of the radiated power can be written as

$$\boxed{P_{\text{rad}} = B_0\left(\frac{\pi}{N}\right)\left(\frac{2\pi}{M}\right)\sum_{j=1}^{M}\left[\sum_{i=1}^{N} F(\theta_i, \phi_j)\sin\theta_i\right]} \tag{2-43}$$

θ_i and ϕ_j take different forms, two of which were introduced and are shown pictorially in Figure 2.15. The evaluation and physical interpretation of (2-43) is similar to that of (2-40).

To examine the accuracy of the technique, two examples will be considered.

Example 2.7(a)

The radiation intensity of an antenna is given by

$$U(\theta, \phi) = \begin{cases} B_0 \sin\theta \sin^2\phi, & 0 \le \theta \le \pi, \quad 0 \le \phi \le \pi \\ 0 & \text{elsewhere} \end{cases}$$

INTEL-1045
U.S. Patent 7,151,430

Determine the maximum directivity numerically by using (2-41) with θ_i and ϕ_j of (2-38b) and (2-39b), respectively. Compare it with the exact value.

SOLUTION

Let us divide the θ and ϕ intervals each into 18 equals segments ($N = M = 18$). Since $0 \leq \phi \leq \pi$, then $\Delta\phi_j = \pi/M$ and (2-41) reduces to

$$P_{rad} = B_0\left(\frac{\pi}{18}\right)^2\left[\sum_{j=1}^{18}\sin^2\phi_j\right]\left[\sum_{i=1}^{18}\sin^2\theta_i\right]$$

with

$$\theta_i = i\left(\frac{\pi}{18}\right) = i(10°), \qquad i = 1, 2, 3, \ldots, 18$$

$$\phi_j = j\left(\frac{\pi}{18}\right) = j(10°), \qquad j = 1, 2, 3, \ldots, 18$$

Thus

$$P_{rad} = B_0\left(\frac{\pi}{18}\right)^2[\sin^2(10°) + \sin^2(20°) + \cdots + \sin^2(180°)]^2$$

$$P_{rad} = B_0\left(\frac{\pi}{18}\right)^2(9)^2 = B_0\left(\frac{\pi^2}{4}\right)$$

and

$$D_0 = \frac{4\pi U_{max}}{P_{rad}} = \frac{4\pi}{\pi^2/4} = \frac{16}{\pi} = 5.0929$$

The exact value is given by

$$P_{rad} = B_0\int_0^{\pi}\sin^2\phi\,d\phi\int_0^{\pi}\sin^2\theta\,d\theta = \frac{\pi}{2}\left(\frac{\pi}{2}\right)B_0 = \frac{\pi^2}{4}B_0$$

and

$$D_0 = \frac{4\pi U_{max}}{P_{rad}} = \frac{4\pi}{\pi^2/4} = \frac{16}{\pi} = 5.0929$$

Which is the same as the value obtained numerically!

Example 2.7(b)

Given the same radiation intensity as that in Example 2.7(a), determine the directivity using (2-41) with θ_i and ϕ_j of (2-38c) and (2-39c).

SOLUTION

Again using 18 divisions in each interval, we can write (2-41) as

$$P_{rad} = B_0\left(\frac{\pi}{18}\right)^2\left[\sum_{j=1}^{18}\sin^2\phi_j\right]\left[\sum_{i=1}^{18}\sin^2\theta_i\right]$$

INTEL-1045
U.S. Patent 7,151,430

with

$$\theta_i = \frac{\pi}{36} + (i-1)\frac{\pi}{18} = 5° + (i-1)\,10°, \qquad i = 1, 2, 3, \ldots, 18$$

$$\phi_j = \frac{\pi}{36} + (j-1)\frac{\pi}{18} = 5° + (j-1)\,10°, \qquad j = 1, 2, 3, \ldots, 18$$

Because of the symmetry of the divisions about the $\theta = \pi/2$ and $\phi = \pi/2$ angles, we can write

$$P_{\text{rad}} = B_0\left(\frac{\pi}{18}\right)^2\left[2\sum_{j=1}^{9}\sin^2\phi_j\right]\left[2\sum_{i=1}^{9}\sin^2\theta_i\right]$$

$$P_{\text{rad}} = B_0\left(\frac{\pi}{18}\right)^2 4[\sin^2(5°) + \sin^2(15°) + \cdots + \sin^2(85°)]^2$$

$$P_{\text{rad}} = B_0\left(\frac{\pi}{18}\right)^2 4(4.5)^2 = B_0\left(\frac{\pi}{18}\right)^2(81) = B_0\left(\frac{\pi^2}{4}\right)$$

which is identical to that of the previous example. Thus

$$D_0 = \frac{4\pi U_{\max}}{P_{\text{rad}}} = \frac{4\pi}{\pi^2/4} = \frac{16}{\pi} = 5.0929$$

which again is equal to the exact value!

It is interesting to note that decreasing the number of divisions (M and/or N) to 9, 6, 4, and even 2 leads to the same answer, which also happens to be the exact value! To demonstrate as to why the number of divisions does not affect the answer for this pattern, let us refer to Figure 2.16 where we have plotted the $\sin^2\phi$ function and divided the $0° \le \phi \le 180°$ interval into six divisions. The exact value of the directivity uses the area under the solid curve. Doing the problem numerically, we find the area under the rectangles, which is shown shaded. Because of the symmetrical nature of the function, it can be shown that the shaded area in section #1 (included in the numerical evaluation) is equal to the blank area in section #1′ (left out by the numerical method). The same is true for the areas in sections #2 and #2′, and #3 and #3′. Thus, there is a one-to-one compensation. Similar justification is applicable for the other number of divisions.

It should be emphasized that all functions, even though they may contain some symmetry, do not give the same answers independent of the number of divisions. As a matter of fact, in most cases the answer only approaches the exact value as the number of divisions is increased to a large number.

A FORTRAN computer program called DIRECTIVITY has been developed to compute the maximum directivity of any antenna whose radiation intensity is $U = F(\theta, \phi)$ based on the formulation of (2-43). The intensity function F does not have to be a function of both θ and ϕ. The numerical evaluations are made at the trailing edge, as defined by (2-38b) and (2-39b). The program is included at the end of this chapter. It contains a SUBROUTINE for which the intensity factor $U = F(\theta, \phi)$ for the required application must be specified by the user. As an illustration, the antenna

INTEL-1045
U.S. Patent 7,151,430

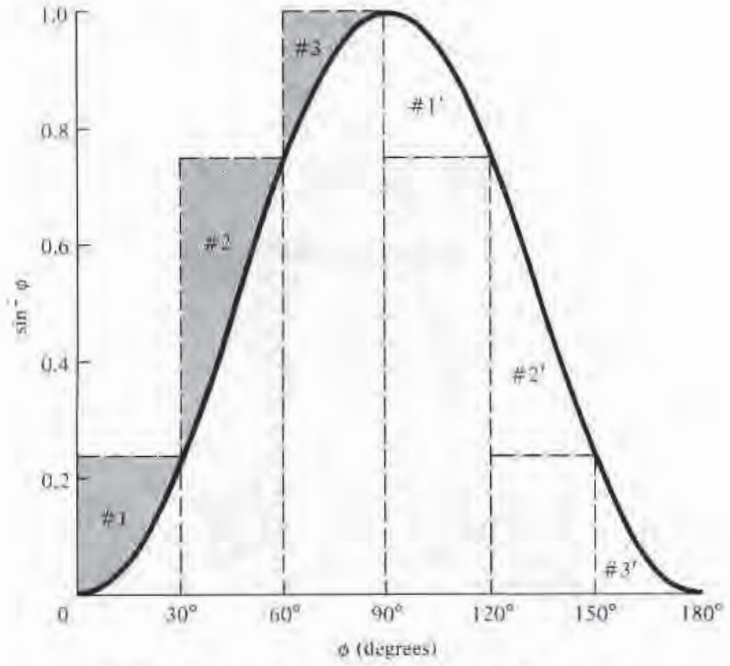


Figure 2.16 Digitized form of $\sin^2 \phi$ function.

intensity $U = \sin \theta \sin^2 \phi$ has been inserted in the subroutine. In addition, the upper and lower limits of θ and ϕ must be specified for each application of the same pattern.

2.7 GAIN

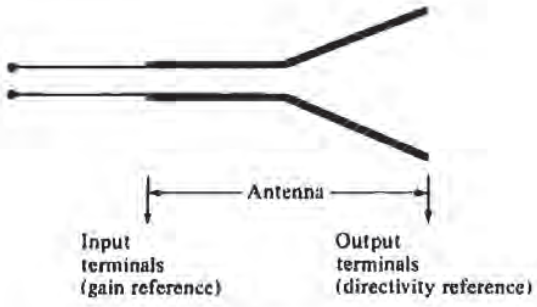
Another useful measure describing the performance of an antenna is the *gain*. Although the gain of the antenna is closely related to the directivity, it is a measure that takes into account the efficiency of the antenna as well as its directional capabilities. Remember that directivity is a measure that describes only the directional properties of the antenna, and it is therefore controlled only by the pattern.

Absolute gain of an antenna (in a given direction) is defined as "the ratio of the intensity, in a given direction, to the radiation intensity that would be obtained if the power accepted by the antenna were radiated isotropically. The radiation intensity corresponding to the isotropically radiated power is equal to the power accepted (input) by the antenna divided by 4π." In equation form this can be expressed as

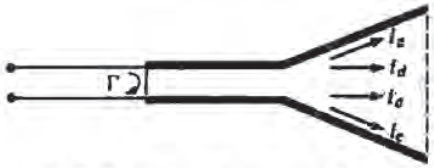
$$\text{gain} = 4\pi \frac{\text{radiation intensity}}{\text{total input (accepted) power}} = 4\pi \frac{U(\theta, \phi)}{P_{\text{in}}} \quad \text{(dimensionless)} \quad (2\text{-}44)$$

In most cases we deal with *relative gain*, which is defined as "the ratio of the power gain in a given direction to the power gain of a reference antenna in its referenced direction." The power input must be the same for both antennas. The reference antenna is usually a dipole, horn, or any other antenna whose gain can be

INTEL-1045
U.S. Patent 7,151,430



(a) Antenna reference terminals



(b) Reflection, conduction, and dielectric losses

Figure 2.17 Reference terminals and losses of an antenna.

calculated or it is known. In most cases, however, the reference antenna is a *lossless isotropic source*. Thus

$$G = \frac{4\pi U(\theta, \phi)}{P_{\text{in}} \text{ (lossless isotropic source)}} \qquad \text{(dimensionless)} \qquad (2\text{-}44a)$$

When the direction is not stated, the power gain is usually taken in the direction of maximum radiation.

Referring to Figure 2.17(a), we can write that the total radiated power (P_{rad}) is related to the total input power (P_{in}) by

$$P_{\text{rad}} = e_{cd} P_{\text{in}} \qquad (2\text{-}45)$$

where e_{cd} is the antenna radiation efficiency (dimensionless) which is defined in Section 2.14 by (2-90). According to the IEEE Standards, "gain does not include losses arising from impedance mismatches (reflection losses) and polarization mismatches (losses)." In this edition of the book, we will adhere, in terms of standardization, to this definition. But in the earlier edition we included both impedance (reflection) and polarization losses in the definition of the gain. These two losses are defined, respectively, by the reflection (mismatch) efficiency in (2-51) and (2-52), and by the polarization loss factor (PLF) in (2-71). Both are very important losses and they need to be included in the link calculations of a communication system to determine the received or radiated power, even if they are not included in the present definition of gain. Using (2-45) reduces (2-44a) to

$$G(\theta, \phi) = e_{cd}\left[4\pi \frac{U(\theta, \phi)}{P_{\text{rad}}}\right] \qquad (2\text{-}46)$$

INTEL-1045
U.S. Patent 7,151,430

which is related to the directivity of (2-21) by

$$\boxed{G(\theta, \phi) = e_{cd}\, D(\theta, \phi)} \tag{2-47}$$

In a similar manner, the maximum value of the gain is related to the maximum *directivity* by

$$\boxed{G_0 = G(\theta, \phi)|_{\max} = e_{cd}\, D(\theta, \phi)|_{\max} = e_{cd}\, D_0} \tag{2-47a}$$

As was done with the directivity, we can define the *partial gain of an antenna for a given polarization in a given direction* as "that part of the radiation intensity corresponding to a given polarization divided by the total radiation intensity that would be obtained if the power accepted by the antenna were radiated isotropically." With this definition for the partial directivity, then, in a given direction, "the total gain is the sum of the partial gains for any two orthogonal polarizations." For a spherical coordinate system, the total maximum gain G_0 for the orthogonal θ and ϕ components of an antenna can be written, in a similar form as was the maximum directivity in (2-17)–(2-17b), as

$$G_0 = G_\theta + G_\phi \tag{2-48}$$

while the partial gains G_θ and G_ϕ are expressed as

$$G_\theta = \frac{4\pi U_\theta}{P_{in}} \tag{2-48a}$$

$$G_\phi = \frac{4\pi U_\phi}{P_{in}} \tag{2-48b}$$

where

U_θ = radiation intensity in a given direction contained in E_θ field component

U_ϕ = radiation intensity in a given direction contained in E_ϕ field component

P_{in} = total input (accepted) power

For many practical antennas an approximate formula for the gain, corresponding to (2-27) or (2-27a) for the directivity, is

$$\boxed{G_0 \simeq \frac{30{,}000}{\Theta_{1d}\, \Theta_{2d}}} \tag{2-49}$$

In practice, whenever the term "gain" is used, it usually refers to the maximum gain as defined by (2-47a).

Usually the gain is given in terms of decibels instead of the dimensionless quantity of (2-47a). The conversion formula is given by

$$G_0(\text{dB}) = 10 \log_{10}[e_r\, D_0 \text{ (dimensionless)}] \tag{2-50}$$

2.8 ANTENNA EFFICIENCY

The total antenna efficiency e_0 is used to take into account losses at the input terminals and within the structure of the antenna. Such losses may be due, referring to Figure 2.17(b), to

INTEL-1045
U.S. Patent 7,151,430

1. reflections because of the mismatch between the transmission line and the antenna
2. I^2R losses (conduction and dielectric)

In general, the overall efficiency can be written as

$$\boxed{e_o = e_r e_c e_d} \tag{2-51}$$

where

e_o = total efficiency (dimensionless)
e_r = reflection (mismatch) efficiency = $(1 - |\Gamma|^2)$ (dimensionless)
e_c = conduction efficiency (dimensionless)
e_d = dielectric efficiency (dimensionless)
Γ = voltage reflection coefficient at the input terminals of the antenna [$\Gamma = (Z_{in} - Z_0)/(Z_{in} + Z_0)$ where Z_{in} = antenna input impedance, Z_0 = characteristic impedance of the transmission line]

Usually e_c and e_d are very difficult to compute, but they can be determined experimentally. Even by measurements they cannot be separated, and it is usually more convenient to write (2-51) as

$$e_o = e_r e_{cd} = e_{cd}(1 - |\Gamma|^2) \tag{2-52}$$

where $e_{cd} = e_c e_d$ = antenna radiation efficiency, which is used to relate the gain and directivity.

Example 2.8

A lossless resonant half-wavelength dipole antenna, with input impedance of 73 ohms, is to be connected to a transmission line whose characteristic impedance is 50 ohms. Assuming that the pattern of the antenna is given approximately by

$$U = B_0 \sin^3 \theta$$

find the overall maximum gain of this antenna.

SOLUTION

Let us first compute the maximum directivity of the antenna. For this

$$U|_{max} = U_{max} = B_0$$

$$P_{rad} = \int_0^{2\pi} \int_0^{\pi} U(\theta, \phi) \sin\theta \, d\theta \, d\phi = 2\pi B_0 \int_0^{\pi} \sin^4 \theta \, d\theta = B_0 \left(\frac{3\pi^2}{4}\right)$$

$$D_0 = 4\pi \frac{U_{max}}{P_{rad}} = \frac{16}{3\pi} = 1.697$$

Since the antenna was stated to be lossless, then the radiation efficiency

$$e_{cd} = 1$$

INTEL-1045
U.S. Patent 7,151,430

Thus, the total maximum gain, as defined in this edition and by IEEE, is equal to

$$G_0 = e_{cd} D_0 = 1(1.697) = 1.697$$
$$G_0(\text{dB}) = 10 \log_{10}(1.697) = 2.297$$

which is identical to the directivity because the antenna is lossless.

There is another loss factor which is not taken into account in the gain. That is the loss due to reflection or mismatch losses between the antenna (load) and the transmission line. This loss is accounted for by the reflection efficiency of (2-51) or (2-52), and it is equal to

$$e_r = (1 - |\Gamma|^2) = \left(1 - \left|\frac{73 - 50}{73 + 50}\right|^2\right) = 0.965$$
$$e_r(\text{dB}) = 10 \log_{10}(0.965) = -0.155$$

Thus, the overall efficiency is

$$e_0 = e_r e_{cd} = 0.965$$
$$e_0\,(\text{dB}) = -0.155$$

Thus, the overall losses are equal to 0.155 dB.

The gain in dB can also be obtained by converting the directivity and radiation efficiency in dB and then adding them. Thus,

$$e_{cd}(\text{dB}) = 10 \log_{10}(1.0) = 0$$
$$D_0(\text{dB}) = 10 \log_{10}(1.697) = 2.297$$
$$G_0(\text{dB}) = e_{cd}(\text{dB}) + D_0\,(\text{dB}) = 2.297$$

which is the same as obtained previously.

2.9 HALF-POWER BEAMWIDTH

The *half-power beamwidth* is defined as: "In a plane containing the direction of the maximum of a beam, the angle between the two directions in which the radiation intensity is one-half the maximum value of the beam." Often the term beamwidth is used to describe the angle between any two points on the pattern, such as the angle between the 10-dB points. In this case the specific points on the pattern must be described to avoid confusion. However the term *beamwidth* by itself is usually reversed to describe the 3-dB beamwidth.

The beamwidth of the antenna is a very important figure-of-merit, and it often used to as a tradeoff between it and the sidelobe level: that is, as the beamwidth decreases the sidelobe increases and vice versa. In addition, the beamwidth of the antenna is also used to describe the resolution capabilities of the antenna to distinguish between two adjacent radiating sources or radar targets. The most common resolution criterion states that *the resolution capability of an antenna to distinguish between two sources is equal to half the first null beamwidth (FNBW/2), which is usually used to approximate the half-power beamwidth (HPBW)* [7], [12]. That is, two sources separated by angular distances equal or greater than FNBW/2 ≈ HPBW of an antenna with a uniform distribution can be resolved. If the separation is smaller, then the antenna will tend to smooth the angular separation distance.

INTEL-1045
U.S. Patent 7,151,430

2.10 BEAM EFFICIENCY

Another parameter that is frequently used to judge the quality of transmitting and receiving antennas is the *beam efficiency*. For an antenna with its major lobe directed along the z-axis ($\theta = 0$), as shown in Figure 2.4(a), the beam efficiency (BE) is defined by

$$\text{BE} = \frac{\text{power transmitted (received) within cone angle } \theta_1}{\text{power transmitted (received) by the antenna}} \text{ (dimensionless)} \quad (2\text{-}53)$$

where θ_1 is the half-angle of the cone within which the percentage of the total power is to be found. Equation (2-53) can be written as

$$\text{BE} = \frac{\displaystyle\int_0^{2\pi}\int_0^{\theta_1} U(\theta, \phi) \sin\theta \, d\theta \, d\phi}{\displaystyle\int_0^{2\pi}\int_0^{\pi} U(\theta, \phi) \sin\theta \, d\theta \, d\phi} \quad (2\text{-}54)$$

If θ_1 is chosen as the angle where the first null or minimum occurs (see Figure 2.4), then the beam efficiency will indicate the amount of power in the major lobe compared to the total power. A very high beam efficiency (between the nulls or minimums), usually in the high 90s, is necessary for antennas used in radiometry, astronomy, radar, and other applications where received signals through the minor lobes must be minimized. The beam efficiencies of some typical circular and rectangular aperture antennas will be discussed in Chapter 12.

2.11 BANDWIDTH

The *bandwidth* of an antenna is defined as "the range of frequencies within which the performance of the antenna, with respect to some characteristic, conforms to a specified standard." The bandwidth can be considered to be the range of frequencies, on either side of a center frequency (usually the resonance frequency for a dipole), where the antenna characteristics (such as input impedance, pattern, beamwidth, polarization, side lobe level, gain, beam direction, radiation efficiency) are within an acceptable value of those at the center frequency. For broadband antennas, the bandwidth is usually expressed as the ratio of the upper-to-lower frequencies of acceptable operation. For example, a 10 : 1 bandwidth indicates that the upper frequency is 10 times greater than the lower. For narrowband antennas, the bandwidth is expressed as a percentage of the frequency difference (upper minus lower) over the center frequency of the bandwidth. For example, a 5% bandwidth indicates that the frequency difference of acceptable operation is 5% of the center frequency of the bandwidth.

Because the characteristics (input impedance, pattern, gain, polarization, etc.) of an antenna do not necessarily vary in the same manner or are even critically affected by the frequency, there is no unique characterization of the bandwidth. The specifications are set in each case to meet the needs of the particular application. Usually there is a distinction made between pattern and input impedance variations. Accordingly *pattern bandwidth* and *impedance bandwidth* are used to emphasize this distinction. Associated with pattern bandwidth are gain, side lobe level, beamwidth,

INTEL-1045
U.S. Patent 7,151,430

polarization, and beam direction while input impedance and radiation efficiency are related to impedance bandwidth. For example, the pattern of a linear dipole with overall length less than a half-wavelength ($l < \lambda/2$) is insensitive to frequency. The limiting factor for this antenna is its impedance, and its bandwidth can be formulated in terms of the Q. The Q of antennas or arrays with dimensions large compared to the wavelength, excluding superdirective designs, is near unity. Therefore the bandwidth is usually formulated in terms of beamwidth, side lobe level, and pattern characteristics. For intermediate length antennas, the bandwidth may be limited by either pattern or impedance variations, depending upon the particular application. For these antennas, a 2 : 1 bandwidth indicates a good design. For others, large bandwidths are needed. Antennas with very large bandwidths (like 40 : 1 or greater) have been designed in recent years. These are known as *frequency independent* antennas, and they are discussed in Chapter 11.

The above discussion presumes that the coupling networks (transformers, baluns, etc.) and/or the dimensions of the antenna are not altered in any manner as the frequency is changed. It is possible to increase the acceptable frequency range of a narrowband antenna if proper adjustments can be made on the critical dimensions of the antenna and/or on the coupling networks as the frequency is changed. Although not an easy or possible task in general, there are applications where this can be accomplished. The most common examples are the antenna of a car radio and the "rabbit ears" of a television. Both usually have adjustable lengths which can be used to tune the antenna for better reception.

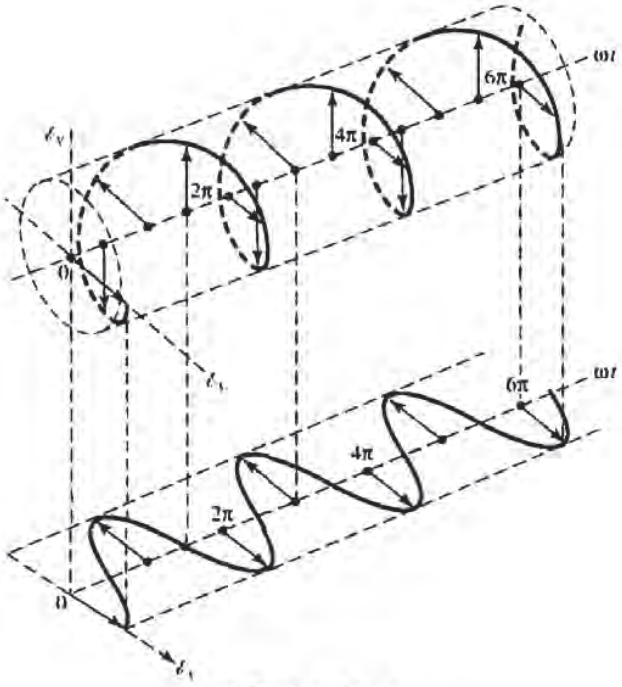
2.12 POLARIZATION

Polarization of an antenna in a given direction is defined as "the polarization of the wave transmitted (radiated) by the antenna. *Note:* When the direction is not stated, the polarization is taken to be the polarization in the direction of maximum gain." In practice, polarization of the radiated energy varies with the direction from the center of the antenna, so that different parts of the pattern may have different polarizations.

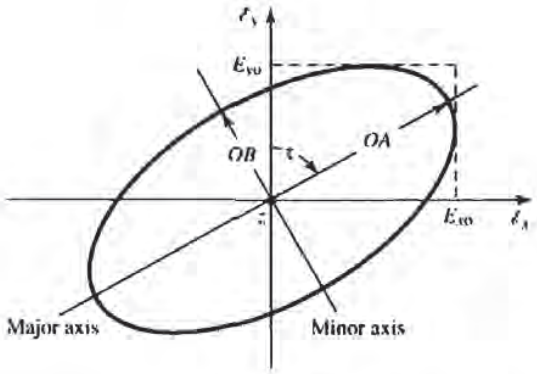
Polarization of a radiated wave is defined as "that property of an electromagnetic wave describing the time varying direction and relative magnitude of the electric-field vector; specifically, the figure traced as a function of time by the extremity of the vector at a fixed location in space, and the sense in which it is traced, *as observed along the direction of propagation.*" Polarization then is the curve traced by the end point of the arrow representing the instantaneous electric field. The field must be observed along the direction of propagation. A typical trace as a function of time is shown in Figures 2.18(a) and (b).

The polarization of a wave can be defined in terms of a wave *radiated (transmitted)* or *received* by an antenna in a given direction. The polarization of a wave *radiated* by an antenna in a specified direction at a point in the far field is defined as "the polarization of the (locally) plane wave which is used to represent the radiated wave at that point. At any point in the far field of an antenna the radiated wave can be represented by a plane wave whose electric field strength is the same as that of the wave and whose direction of propagation is in the radial direction from the antenna. As the radial distance approaches infinity, the radius of curvature of the radiated wave's phase front also approaches infinity and thus in any specified direction the wave appears locally as a plane wave." This is a far-field characteristic of waves

INTEL-1045
U.S. Patent 7,151,430



(a) Rotation of wave



(b) Polarization ellipse

Figure 2.18 Rotation of a plane electromagnetic wave and its polarization ellipse at $z = 0$ as a function of time.

radiated by all practical antennas, and it is illustrated analytically in Section 3.6 of Chapter 3. The polarization of a wave *received* by an antenna is defined as the "polarization of a plane wave, incident from a given direction and having a given power flux density, which results in maximum available power at the antenna terminals."

Polarization may be classified as linear, circular, or elliptical. If the vector that describes the electric field at a point in space as a function of time is always directed along a line, the field is said to be *linearly* polarized. In general, however, the figure

INTEL-1045
U.S. Patent 7,151,430

that the electric field traces is an ellipse, and the field is said to be elliptically polarized. Linear and circular polarizations are special cases of elliptical, and they can be obtained when the ellipse becomes a straight line or a circle, respectively. The figure of the electric field is traced in a *clockwise* (CW) or *counterclockwise* (CCW) sense. *Clockwise* rotation of the electric field vector is designated as *right-hand polarization* and *counterclockwise* as *left-hand polarization.*

In general, the polarization characteristics of an antenna can be represented by its *polarization pattern* whose one definition is "the spatial distribution of the polarizations of a field vector excited (radiated) by an antenna taken over its radiation sphere. When describing the polarizations over the radiation sphere, or portion of it, reference lines shall be specified over the sphere, in order to measure the tilt angles (see tilt angle) of the polarization ellipses and the direction of polarization for linear polarizations. An obvious choice, though by no means the only one, is a family of lines tangent at each point on the sphere to either the θ or ϕ coordinate line associated with a spherical coordinate system of the radiation sphere. At each point on the radiation sphere the polarization is usually resolved into a pair of orthogonal polarizations, the *co-polarization* and *cross polarization.* To accomplish this, the co-polarization must be specified at each point on the radiation sphere."

"For certain linearly polarized antennas, it is common practice to define the co-polarization in the following manner: First specify the orientation of the co-polar electric field vector at a pole of the radiation sphere. Then, for all other directions of interest (points on the radiation sphere), require that the angle that the co-polar electric field vector makes with each great circle line through the pole remain constant over that circle, the angle being that at the pole."

"In practice, the axis of the antenna's main beam should be directed along the polar axis of the radiation sphere. The antenna is then appropriately oriented about this axis to align the direction of its polarization with that of the defined co-polarization at the pole." "This manner of defining co-polarization can be extended to the case of elliptical polarization by defining the constant angles using the major axes of the polarization ellipses rather than the co-polar electric field vector. The sense of polarization (rotation) must also be specified."

The polarization of the wave radiated by the antenna can also be represented on the Poincaré sphere [7], [13]–[16]. Each point on the Poincaré sphere represents a unique polarization. The north pole represents left circular polarization, the south pole represents right circular, and points along the equator represent linear polarization of different tilt angles. All other points on the Poincaré sphere represent elliptical polarization. For details, see Figure 16.24 of Chapter 16.

The polarization of an antenna is measured using techniques described in Chapter 16.

2.12.1 Linear, Circular, and Elliptical Polarizations

The instantaneous field of a plane wave, traveling in the negative z direction, can be written as

$$\mathscr{E}(z; t) = \hat{\mathbf{a}}_x \mathscr{E}_x(z; t) + \hat{\mathbf{a}}_y \mathscr{E}_y(z; t) \tag{2-55}$$

According to (2-5), the instantaneous components are related to their complex counterparts by

INTEL-1045
U.S. Patent 7,151,430

$$\mathscr{E}_x(z;t) = \text{Re}[E_x e^{j(\omega t + kz)}] = \text{Re}[E_{xo} e^{j(\omega t + kz + \phi_x)}]$$
$$= E_{xo}\cos(\omega t + kz + \phi_x) \tag{2-56}$$
$$\mathscr{E}_y(z;t) = \text{Re}[E_y e^{j(\omega t + kz)}] = \text{Re}[E_{yo} e^{j(\omega t + kz + \phi_y)}]$$
$$= E_{yo}\cos(\omega t + kz + \phi_y) \tag{2-57}$$

where E_{xo} and E_{yo} are, respectively, the maximum magnitudes of the x and y components.

A. Linear Polarization

For the wave to have linear polarization, the time-phase difference between the two components must be

$$\Delta\phi = \phi_y - \phi_x = n\pi, \qquad n = 0, 1, 2, 3, \ldots \tag{2-58}$$

B. Circular Polarization

Circular polarization can be achieved *only* when the magnitudes of the two components are the same *and* the time-phase difference between them is odd multiples of $\pi/2$. That is,

$$|\mathscr{E}_x| = |\mathscr{E}_y| \rightharpoonup E_{xo} = E_{yo} \tag{2-59}$$
$$\Delta\phi = \phi_y - \phi_x = \begin{cases} +(\frac{1}{2} + 2n)\pi, \; n = 0, 1, 2, \ldots & \text{for CW} \quad (2\text{-}60) \\ -(\frac{1}{2} + 2n)\pi, \; n = 0, 1, 2, \ldots & \text{for CCW} \quad (2\text{-}61) \end{cases}$$

If the direction of wave propagation is reversed (i.e., $+z$ direction), the phases in (2-60) and (2-61) for CW and CCW rotation must be interchanged.

C. Elliptical Polarization

Elliptical polarization can be attained *only* when the time-phase difference between the two components is odd multiples of $\pi/2$ *and* their magnitudes are not the same *or* when the time-phase difference between the two components is not equal to multiples of $\pi/2$ (irrespective of their magnitudes). That is,

$$|\mathscr{E}_x| \neq |\mathscr{E}_y| \rightharpoonup E_{xo} \neq E_{yo}$$
$$\text{when } \Delta\phi = \phi_y - \phi_x = \begin{cases} +(\frac{1}{2} + 2n)\pi & \text{for CW} \quad (2\text{-}62a) \\ -(\frac{1}{2} + 2n)\pi & \text{for CCW} \quad (2\text{-}62b) \end{cases}$$
$$n = 0, 1, 2, \ldots$$

or

$$\Delta\phi = \phi_y - \phi_x \neq \pm\frac{n}{2}\pi = \begin{cases} > 0 & \text{for CW} \quad (2\text{-}63) \\ < 0 & \text{for CCW} \quad (2\text{-}64) \end{cases}$$
$$n = 0, 1, 2, 3, \ldots$$

For elliptical polarization, the curve traced at a given position as a function of time is, in general, a tilted ellipse, as shown in Figure 2.18(b). The ratio of the major axis to the minor axis is referred to as the axial ratio (AR), and it is equal to

$$\text{AR} = \frac{\text{major axis}}{\text{minor axis}} = \frac{OA}{OB}, \qquad 1 \leq \text{AR} \leq \infty \tag{2-65}$$

INTEL-1045
U.S. Patent 7,151,430

where

$$OA = \left[\frac{1}{2}\{E_{xo}^2 + E_{yo}^2 + [E_{xo}^4 + E_{yo}^4 + 2E_{xo}^2 E_{yo}^2 \cos(2\Delta\phi)]^{1/2}\}\right]^{1/2} \quad (2\text{-}66)$$

$$OB = \left[\frac{1}{2}\{E_{xo}^2 + E_{yo}^2 - [E_{xo}^4 + E_{yo}^4 + 2E_{xo}^2 E_{yo}^2 \cos(2\Delta\phi)]^{1/2}\}\right]^{1/2} \quad (2\text{-}67)$$

The tilt of the ellipse, *relative to the y axis*, is represented by the angle τ given by

$$\tau = \frac{\pi}{2} - \frac{1}{2}\tan^{-1}\left[\frac{2E_{xo}E_{yo}}{E_{xo}^2 - E_{yo}^2}\cos(\Delta\phi)\right] \quad (2\text{-}68)$$

When the ellipse is aligned with the principal axes [$\tau = n\pi/2$, $n = 0, 1, 2, \ldots$], the major (minor) axis is equal to $E_{xo}(E_{yo})$ or $E_{yo}(E_{xo})$ and the axial ratio is equal to E_{xo}/E_{yo} or E_{yo}/E_{xo}.

SUMMARY

We will summarize the preceding discussion on polarization by stating the general characteristics, and the *necessary and sufficient* conditions that the wave must have in order to possess *linear, circular* or *elliptical* polarization.

Linear Polarization *A time-harmonic wave is linearly polarized at a given point in space if the electric field (or magnetic field) vector at that point is always oriented along the same straight line at every instant of time.* This is accomplished if the field vector (electric or magnetic) possesses:

a. Only one component, or
b. Two orthogonal linear components that are in time phase or 180° (or multiples of 180°) out of phase.

Circular Polarization *A time-harmonic wave is circularly polarized at a given point in space if the electric (or magnetic) field vector at that point traces a circle as a function of time.*

The *necessary and sufficient* conditions to accomplish this are if the field vector (electric or magnetic) possesses all of the following:

a. The field must have two orthogonal linear components, and
b. The two components must have the same magnitude, and
c. The two components must have a time-phase difference of odd multiples of 90°.

The sense of rotation is always determined by rotating the phase-leading component toward the phase-lagging component and observing the field rotation as the wave is viewed as it travels away from the observer. If the rotation is clockwise, the wave is right-hand (or clockwise) circularly polarized; if the rotation is counterclockwise, the wave is left-hand (or counterclockwise) circularly polarized. The rotation of the phase-leading component toward the phase-lagging component should be done along the angular separation between the two components that is less than 180°. Phases equal to or greater than 0° and less than 180° should be considered leading whereas those equal to or greater than 180° and less than 360° should be considered lagging.

Elliptical Polarization *A time-harmonic wave is elliptically polarized if the tip of the field vector (electric or magnetic) traces an elliptical locus in space. At various*

INTEL-1045
U.S. Patent 7,151,430

instants of time the field vector changes continuously with time at such a manner as to describe an elliptical locus. It is right-hand (clockwise) elliptically polarized if the field vector rotates clockwise, and it is left-hand (counterclockwise) elliptically polarized if the field vector of the ellipse rotates counterclockwise [13]. The sense of rotation is determined using the same rules as for the circular polarization. In addition to the sense of rotation, elliptically polarized waves are also specified by their axial ratio whose magnitude is the ratio of the major to the minor axis.

A wave is elliptically polarized if it is not linearly or circularly polarized. Although *linear and circular polarizations are special cases of elliptical, usually in practice* elliptical polarization refers to other than linear or circular. The *necessary and sufficient* conditions to accomplish this are if the field vector (electric or magnetic) possesses all of the following:

a. The field must have two orthogonal linear components, and
b. The two components can be of the same or different magnitude.
c. (1) If the two components are not of the same magnitude, the time-phase difference between the two components must not be 0° or multiples of 180° (because it will then be linear). (2) If the two components are of the same magnitude, the time-phase difference between the two components must not be odd multiples of 90° (because it will then be circular).

If the wave is elliptically polarized with two components not of the same magnitude but with odd multiples of 90° time-phase difference, the polarization ellipse will not be tilted but it will be aligned with the principal axes of the field components. The major axis of the ellipse will align with the axis of the field component which is larger of the two, while the minor axis of the ellipse will align with the axis of the field component which is smaller of the two.

2.12.2 Polarization Loss Factor and Efficiency

In general, the polarization of the receiving antenna will not be the same as the polarization of the incoming (incident) wave. This is commonly stated as "polarization mismatch." The amount of power extracted by the antenna from the incoming signal will not be maximum because of the polarization loss. Assuming that the electric field of the incoming wave can be written as

$$\mathbf{E}_i = \hat{\boldsymbol{\rho}}_w E_i \tag{2-69}$$

where $\hat{\boldsymbol{\rho}}_w$ is the unit vector of the wave, and the polarization of the electric field of the receiving antenna can be expressed as

$$\mathbf{E}_a = \hat{\boldsymbol{\rho}}_a E_a \tag{2-70}$$

where $\hat{\boldsymbol{\rho}}_a$ is its unit vector (polarization vector), the polarization loss can be taken into account by introducing a *polarization loss factor* (PLF). It is defined, based on the polarization of the antenna in its transmitting mode, as

$$\text{PLF} = |\hat{\boldsymbol{\rho}}_w \cdot \hat{\boldsymbol{\rho}}_a|^2 = |\cos \psi_p|^2 \text{ (dimensionless)} \tag{2-71}$$

where ψ_p is the angle between the two unit vectors. The relative alignment of the polarization of the incoming wave and of the antenna is shown in Figure 2.19. If the

INTEL-1045
U.S. Patent 7,151,430

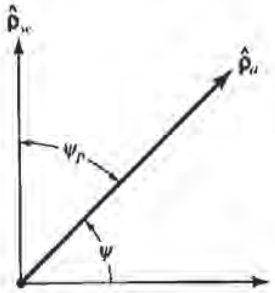


Figure 2.19 Polarization unit vectors of incident wave ($\hat{\rho}_w$) and antenna ($\hat{\rho}_a$), and polarization loss factor (PLF).

antenna is polarization matched, its PLF will be unity and the antenna will extract maximum power from the incoming wave.

Another figure-of-merit that is used to describe the polarization characteristics of a wave and that of an antenna is the *polarization efficiency (polarization mismatch* or *loss factor)* which is defined as "the ratio of the power received by an antenna from a given plane wave of arbitrary polarization to the power that would be received by the same antenna from a plane wave of the same power flux density and direction of propagation, whose state of polarization has been adjusted for a maximum received power." This is similar to the PLF and it is expressed as

$$p_e = \frac{|\boldsymbol{\ell}_e \cdot \mathbf{E}^{\text{inc}}|^2}{|\boldsymbol{\ell}_e|^2 |\mathbf{E}^{\text{inc}}|^2} \tag{2-71a}$$

where

$\boldsymbol{\ell}_e$ = vector effective length of the antenna
$\mathbf{E}^{\text{inc}}$ = incident electric field

The vector effective length $\boldsymbol{\ell}_e$ of the antenna has not yet been defined, and it is introduced in Section 2.15. It is a vector that describes the polarization characteristics of the antenna. Both the PLF and p_e lead to the same answers.

The conjugate (*) is not used in (2-71) or (2-71a) so that a right-hand circularly polarized incident wave (when viewed in its direction of propagation) is matched to right-hand circularly polarized receiving antenna (when its polarization is determined in the transmitting mode). Similarly, a left-hand circularly polarized wave will be matched to a left-hand circularly polarized antenna.

To illustrate the principle of polarization mismatch, two examples will be considered.

Example 2.9

The electric field of a linearly polarized electromagnetic wave given by

$$\mathbf{E}_i = \hat{\mathbf{a}}_x E_0(x, y) e^{-jkz}$$

is incident upon a linearly polarized antenna whose electric field polarization can be expressed as

$$\mathbf{E}_a = (\hat{\mathbf{a}}_x + \hat{\mathbf{a}}_y) E(r, \theta, \phi)$$

Find the polarization loss factor (PLF).

INTEL-1045
U.S. Patent 7,151,430

SOLUTION

For the incident wave

$$\hat{\boldsymbol{\rho}}_w = \hat{\mathbf{a}}_x$$

and for the antenna

$$\hat{\boldsymbol{\rho}}_a = \frac{1}{\sqrt{2}}(\hat{\mathbf{a}}_x + \hat{\mathbf{a}}_y)$$

The PLF is then equal to

$$\text{PLF} = |\hat{\boldsymbol{\rho}}_w \cdot \hat{\boldsymbol{\rho}}_a|^2 = |\hat{\mathbf{a}}_x \cdot \frac{1}{\sqrt{2}}(\hat{\mathbf{a}}_x + \hat{\mathbf{a}}_y)|^2 = \frac{1}{2}$$

which in dB is equal to

$$PLF(dB) = 10 \log_{10} PLF(dimensionless) = 10 \log_{10}(0.5) = -3$$

Even though in Example 2.9 both the incoming wave and the antenna are linearly polarized, there is a 3-dB loss in extracted power because the polarization of the incoming wave is not aligned with the polarization of the antenna. If the polarization of the incoming wave is orthogonal to the polarization of the antenna, then there will be no power extracted by the antenna from the incoming wave and the PLF will be zero or $-\infty$ dB. In Figures 2.20(a,b) we illustrate the polarization loss factors (PLF) of two types of antennas; wires and apertures.

We now want to consider an example where the polarization of the antenna and the incoming wave are described in terms of complex polarization vectors.

Example 2.10

A wave radiated by an antenna is traveling in the outward radial direction along the $+z$ axis. Its radiated field in the far-zone region is described by its spherical components, and its polarization is right-hand (clockwise) circularly polarized. This radiated field is impinging upon a receiving antenna whose polarization (in the transmitting mode, which is the mode the antenna polarization should always be specified according to the definition of IEEE) is also right-handed (clockwise) circularly polarized and whose polarization unit vector is represented by

$$\mathbf{E}_a = (\hat{\mathbf{a}}_\theta - j\hat{\mathbf{a}}_\phi)E(r, \theta, \phi)$$

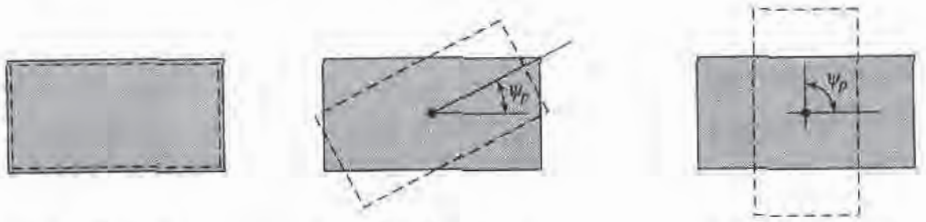
Determine the polarization loss factor (PLF).

SOLUTION

The polarization of the right-hand circularly polarized wave traveling along the $+z$ axis is described by the unit vector

$$\hat{\boldsymbol{\rho}}_w = \left(\frac{\hat{\mathbf{a}}_\theta + j\hat{\mathbf{a}}_\phi}{\sqrt{2}}\right)$$

INTEL-1045
U.S. Patent 7,151,430



(a) PLF for transmitting and receiving *aperture antennas*



(b) PLF for transmitting and receiving linear wire antennas

Figure 2.20 Polarization loss factors (PLF) for aperture and linear wire antennas.

while that of the antenna is represented by the unit vector

$$\hat{\rho}_a = \left(\frac{\hat{\mathbf{a}}_\theta - j\hat{\mathbf{a}}_\phi}{\sqrt{2}}\right)$$

Therefore the polarization loss factor is

$$\text{PLF} = |\hat{\rho}_w \cdot \hat{\rho}_a|^2 = \frac{1}{4}|1 + 1|^2 = 1 = 0 \text{ dB}$$

Since the polarization of the incoming wave matches (including the sense of rotation) the polarization of the receiving antenna, there should not be any losses. Obviously the answer matches the expectation.

Based upon the definitions of the wave transmitted and received by an antenna, the polarization of an antenna in the *receiving* mode is related to that in the *transmitting* mode as follows:

1. "In the same plane of polarization, the polarization ellipses have the same axial ratio, the same sense of polarization (rotation) and the same spatial orientation.

INTEL-1045
U.S. Patent 7,151,430

2. "Since their senses of polarization and spatial orientation are specified by viewing their polarization ellipses in the respective directions in which they are propagating, one should note that:
   a. Although their senses of polarization are the same, they would appear to be opposite if both waves were viewed in the same direction.
   b. Their tilt angles are such that they are the negative of one another with respect to a common reference."

Since the polarization of an antenna will almost always be defined in its transmitting mode, according to the IEEE Std 145-1983, "the receiving polarization may be used to specify the polarization characteristic of a nonreciprocal antenna which may transmit and receive arbitrarily different polarizations."

The polarization loss must always be taken into account in the link calculations design of a communication system because in some cases it may be a very critical factor. Link calculations of communication systems for outer space explorations are very stringent because of limitations in spacecraft weight. In such cases, power is a limiting consideration. The design must properly take into account all loss factors to ensure a successful operation of the system.

2.13 INPUT IMPEDANCE

Input impedance is defined as "the impedance presented by an antenna at its terminals or the ratio of the voltage to current at a pair of terminals or the ratio of the appropriate components of the electric to magnetic fields at a point." In this section we are primarily interested in the input impedance at a pair of terminals which are the input terminals of the antenna. In Figure 2.21(a) these terminals are designated as a–b. The ratio of the voltage to current at these terminals, with no load attached, defines the impedance of the antenna as

$$\boxed{Z_A = R_A + jX_A} \tag{2-72}$$

where

Z_A = antenna impedance at terminals a–b (ohms)
R_A = antenna resistance at terminals a–b (ohms)
X_A = antenna reactance at terminals a–b (ohms)

In general the resistive part of (2-72) consists of two components; that is

$$\boxed{R_A = R_r + R_L} \tag{2-73}$$

where

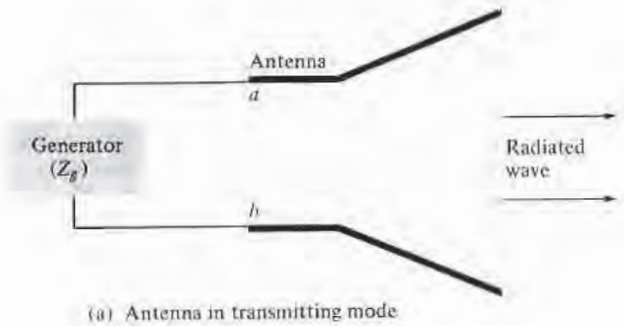
R_r = radiation resistance of the antenna
R_L = loss resistance of the antenna

The radiation resistance will be considered in more detail in later chapters, and it will be illustrated with examples.

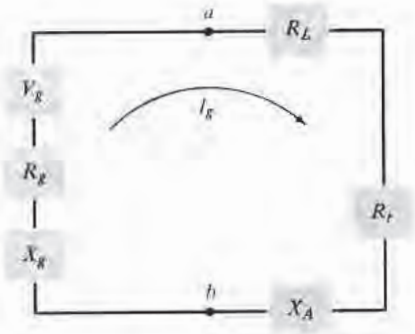
If we assume that the antenna is attached to a generator with internal impedance

$$Z_g = R_g + jX_g \tag{2-74}$$

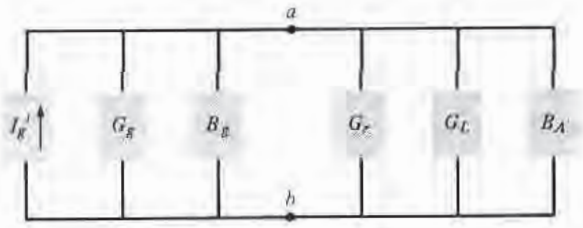
INTEL-1045
U.S. Patent 7,151,430



(a) Antenna in transmitting mode



(b) Thévenin equivalent



(c) Norton equivalent

Figure 2.21 Transmitting antenna and its equivalent circuits.

where

R_g = resistance of generator impedance (ohms)
X_g = reactance of generator impedance (ohms)

and the antenna is used in the transmitting mode, we can represent the antenna and generator by an equivalent circuit* shown in Figure 2.21(b). To find the amount of power delivered to R_r for radiation and the amount dissipated in R_L as heat ($I^2R_L/2$), we first find the current developed within the loop which is given by

$$I_g = \frac{V_g}{Z_t} = \frac{V_g}{Z_A + Z_g} = \frac{V_g}{(R_r + R_L + R_g) + j(X_A + X_g)} \quad (A) \qquad (2\text{-}75)$$

*This circuit can be used to represent small and simple antennas. It cannot be used for antennas with lossy dielectric or antennas over lossy ground because their loss resistance cannot be represented in series with the radiation resistance.

INTEL-1045
U.S. Patent 7,151,430

and its magnitude by

$$|I_g| = \frac{|V_g|}{[(R_r + R_L + R_g)^2 + (X_A + X_g)^2]^{1/2}} \tag{2-75a}$$

where V_g is the peak generator voltage. The power delivered to the antenna for radiation is given by

$$P_r = \frac{1}{2}|I_g|^2 R_r = \frac{|V_g|^2}{2}\left[\frac{R_r}{(R_r + R_L + R_g)^2 + (X_A + X_g)^2}\right] \quad (W) \tag{2-76}$$

and that dissipated as heat by

$$P_L = \frac{1}{2}|I_g|^2 R_L = \frac{|V_g|^2}{2}\left[\frac{R_L}{(R_r + R_L + R_g)^2 + (X_A + X_g)^2}\right] \quad (W) \tag{2-77}$$

The remaining power is dissipated as heat on the internal resistance R_g of the generator, and it is given by

$$P_g = \frac{|V_g|^2}{2}\left[\frac{R_g}{(R_r + R_L + R_g)^2 + (X_A + X_g)^2}\right] \quad (W) \tag{2-78}$$

The maximum power delivered to the antenna occurs when we have conjugate matching; that is when

$$R_r + R_L = R_g \tag{2-79}$$

$$X_A = -X_g \tag{2-80}$$

For this case

$$P_r = \frac{|V_g|^2}{2}\left[\frac{R_r}{4(R_r + R_L)^2}\right] = \frac{|V_g|^2}{8}\left[\frac{R_r}{(R_r + R_L)^2}\right] \tag{2-81}$$

$$P_L = \frac{|V_g|^2}{8}\left[\frac{R_L}{(R_r + R_L)^2}\right] \tag{2-82}$$

$$P_g = \frac{|V_g|^2}{8}\left[\frac{R_g}{(R_r + R_L)^2}\right] = \frac{|V_g|^2}{8}\left[\frac{1}{R_r + R_L}\right] = \frac{|V_g|^2}{8R_g} \tag{2-83}$$

From (2-81)–(2-83), it is clear that

$$P_g = P_r + P_L = \frac{|V_g|^2}{8}\left[\frac{R_g}{(R_r + R_L)^2}\right] = \frac{|V_g|^2}{8}\left[\frac{R_r + R_L}{(R_r + R_L)^2}\right] \tag{2-84}$$

The power supplied by the generator during conjugate matching is

$$P_s = \frac{1}{2}V_g I_g^* = \frac{1}{2}V_g\left[\frac{V_g^*}{2(R_r + R_L)}\right] = \frac{|V_g|^2}{4}\left[\frac{1}{R_r + R_L}\right] \quad (W) \tag{2-85}$$

Of the power that is provided by the generator, half is dissipated as heat in the internal resistance (R_g) of the generator and the other half is delivered to the antenna. This only happens when we have conjugate matching. Of the power that is delivered to the antenna, part is radiated through the mechanism provided by the radiation resistance and the other is dissipated as heat which influences part of the overall efficiency of the antenna. If the antenna is lossless ($e_{cd} = 1$), then half of the total power supplied by the generator is radiated by the antenna during conjugate matching, and the other

INTEL-1045
U.S. Patent 7,151,430

half is dissipated as heat in the generator. Thus, to radiate half of the available power through R_r you must dissipate the other half as heat in the generator through R_g. These two powers are, respectively, analogous to the power transferred to the load and the power scattered by the antenna in the receiving mode. In Figure 2.21 it is assumed that the generator is directly connected to the antenna. If there is a a transmission line between the two, which is usually the case, then Z_g represents the equivalent impedance of the generator transferred to the input terminals of the antenna using the impedance transfer equation. If, in addition, the transmission line is lossy, then the available power to be radiated by the antenna will be reduced by the losses of the transmission line. Figure 2.21(c) illustrates the Norton equivalent of the antenna and its source in the transmitting mode.

The use of the antenna in the receiving mode is shown in Figure 2.22(a). The incident wave impinges upon the antenna, and it induces a voltage V_T which is analogous to V_g of the transmitting mode. The Thevenin equivalent circuit of the antenna and its load is shown in Figure 2.22(b) and the Norton equivalent in Figure 2.22(c). The discussion for the antenna and its load in the receiving mode parallels that for the transmitting mode, and it will not be repeated here in detail. Some of the results will be summarized in order to discuss some subtle points. Following a procedure similar to that for the antenna in the transmitting mode, it can be shown using Figure 2.22 that in the receiving mode under conjugate matching ($R_r + R_L = R_T$ and $X_A = -X_T$) the powers delivered to R_T, R_r, and R_L are given, respectively, by

$$P_T = \frac{|V_T|^2}{8}\left[\frac{R_T}{(R_r + R_L)^2}\right] = \frac{|V_T|^2}{8}\left(\frac{1}{R_r + R_L}\right) = \frac{|V_T|^2}{8R_T} \tag{2-86}$$

$$P_r = \frac{|V_T|^2}{2}\left[\frac{R_r}{4(R_r + R_L)^2}\right] = \frac{|V_T|^2}{8}\left[\frac{R_r}{(R_r + R_L)^2}\right] \tag{2-87}$$

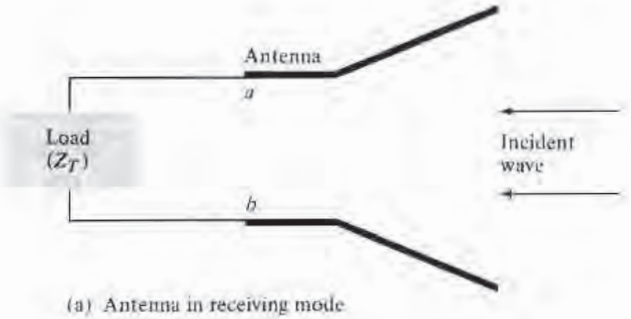
$$P_L = \frac{|V_T|^2}{8}\left[\frac{R_L}{(R_r + R_L)^2}\right] \tag{2-88}$$

while the *induced* (*collected* or *captured*) is

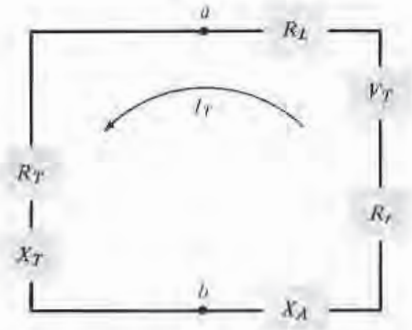
$$P_c = \frac{1}{2}V_T I_T^* = \frac{1}{2}V_T\left[\frac{V_T^*}{2(R_r + R_L)}\right] = \frac{|V_T|^2}{4}\left(\frac{1}{R_r + R_L}\right) \tag{2-89}$$

These are analogous, respectively, to (2-81)–(2-83) and (2-85). The power P_r of (2-87) delivered to R_r is referred to as *scattered* (or *reradiated*) power. It is clear through (2-86)–(2-89) that under conjugate matching of the total power collected or captured [P_c of (2-89)] half is delivered to the load R_T [P_T of (2-86)] and the other half is scattered or reradiated through R_r [P_r of (2-87)] and dissipated as heat through R_L [P_L of (2-88)]. If the losses are zero ($R_L = 0$), then half of the captured power is delivered to the load and the other half is scattered. This indicates that in order to deliver half of the power to the load you must scatter the other half. This becomes important when discussing effective equivalent areas and aperture efficiencies, especially for high directivity aperture antennas such as wave guides, horns, and reflectors with aperture efficiencies as high as 80 to 90%. Aperture efficiency (ϵ_{ap}) is defined by (2-100) and is the ratio of the maximum effective area to the physical area. The effective area is used to determine the power delivered to the load, which under conjugate matching is only one half of that intercepted; the other half is scattered and dissipated as heat. For a lossless antenna ($R_L = 0$) under conjugate matching, the maximum value of the effective area is equal to the physical area ($\epsilon_{ap} = 1$) and the

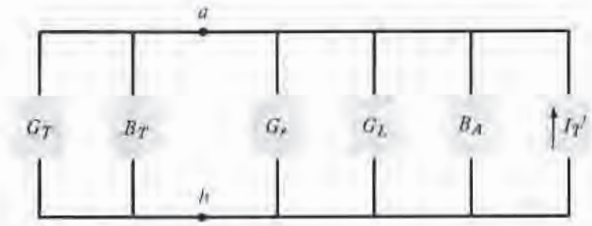
INTEL-1045
U.S. Patent 7,151,430



(a) Antenna in receiving mode



(b) Thevenin equivalent



(c) Norton equivalent

Figure 2.22 Antenna and its equivalent circuits in the receiving mode.

scattering area is also equal to the physical area. Thus half of the power is delivered to the load and the other half is scattered. Using (2-86) to (2-89) we conclude that even though the aperture efficiencies are higher than 50% (they can be as large as 100%) all of the power that is captured by the antenna is not delivered to the load but it includes that which is scattered plus dissipated as heat by the antenna. The most that can be delivered to the load is only half of that captured and that is only under conjugate matching and lossless transmission line.

The input impedance of an antenna is generally a function of frequency. Thus the antenna will be matched to the interconnecting transmission line and other associated equipment only within a bandwidth. In addition, the input impedance of the antenna depends on many factors including its geometry, its method of excitation, and its proximity to surrounding objects. Because of their complex geometries, only a limited number of practical antennas have been investigated analytically. For many others, the input impedance has been determined experimentally.

INTEL-1045
U.S. Patent 7,151,430

2.14 ANTENNA RADIATION EFFICIENCY

The antenna efficiency that takes into account the reflection, conduction, and dielectric losses was discussed in Section 2.8. The conduction and dielectric losses of an antenna are very difficult to compute and in most cases they are measured. Even with measurements, they are difficult to separate and they are usually lumped together to form the e_{cd} efficiency. The resistance R_L is used to represent the conduction-dielectric losses.

The *conduction-dielectric efficiency* e_{cd} is defined as *the ratio of the power delivered to the radiation resistance* R_r *to the power delivered to* R_r *and* R_L. Using (2-76) and (2-77), the radiation efficiency can be written as

$$e_{cd} = \left[\frac{R_r}{R_L + R_r}\right] \quad \text{(dimensionless)} \tag{2-90}$$

For a metal rod of length l and uniform cross-sectional area A, the dc resistance is given by

$$R_{dc} = \frac{1}{\sigma}\frac{l}{A} \quad \text{(ohms)} \tag{2-90a}$$

If the skin depth $\delta[\delta = \sqrt{2/(\omega\mu_0\sigma)}]$ of the metal is very small compared to the smallest diagonal of the cross section of the rod, the current is confined to a thin layer near the conductor surface. Therefore the high-frequency resistance can be written, based on a uniform current distribution, as

$$R_{hf} = \frac{l}{P}R_s = \frac{l}{P}\sqrt{\frac{\omega\mu_0}{2\sigma}} \quad \text{(ohms)} \tag{2-90b}$$

where P is the perimeter of the cross section of the rod ($P = C = 2\pi b$ for a circular wire of radius b). R_s is the conductor surface resistance, ω is the angular frequency, μ_0 is the permeability of free-space, and σ is the conductivity of the metal.

Example 2.11

A resonant half-wavelength dipole is made out of copper ($\sigma = 5.7 \times 10^7$ S/m) wire. Determine the conduction-dielectric (radiation) efficiency of the dipole antenna at $f = 100$ MHz if the radius of the wire b is $3 \times 10^{-4}\lambda$, and the radiation resistance of the $\lambda/2$ dipole is 73 ohms.

SOLUTION

At $f = 10^8$ Hz

$$\lambda = \frac{v}{f} = \frac{3 \times 10^8}{10^8} = 3 \text{ m}$$

$$l = \frac{\lambda}{2} = \frac{3}{2} \text{ m}$$

$$C = 2\pi b = 2\pi(3 \times 10^{-4})\lambda = 6\pi \times 10^{-4}\lambda$$

INTEL-1045
U.S. Patent 7,151,430

For a $\lambda/2$ dipole with a sinusoidal current distribution $R_L = \frac{1}{2}R_{hf}$ where R_{hf} is given by (2-90b). See Problem 2.44. Therefore,

$$R_L = \frac{1}{2}R_{hf} = \frac{0.25}{6\pi \times 10^{-4}}\sqrt{\frac{\pi(10^8)(4\pi \times 10^{-7})}{5.7 \times 10^7}} = 0.349 \text{ ohms}$$

Thus,

$$e_{cd}\,(\text{dimensionless}) = \frac{73}{73 + 0.349} = 0.9952 = 99.52\%$$

$$e_{cd}\,(\text{dB}) = 10\log_{10}(0.9905) = -0.02$$

2.15 ANTENNA VECTOR EFFECTIVE LENGTH AND EQUIVALENT AREAS

An antenna in the receiving mode, whether it is in the form of a wire, horn, aperture, array, dielectric rod, etc., is used to capture (collect) electromagnetic waves and to extract power from them, as shown in Figures 2.23(a) and (b). For each antenna, an equivalent length and a number of equivalent areas can then be defined.

These equivalent quantities are used to describe the receiving characteristics of an antenna, whether it be a linear or an aperture type, when a wave is incident upon the antenna.

2.15.1 Vector Effective Length

The effective length of an antenna, whether it be a linear or an aperture antenna, is a quantity that is used to determine the voltage induced on the open-circuit terminals of the antenna when a wave impinges upon it. The vector effective length $\boldsymbol{\ell}_e$ for an antenna is usually a complex vector quantity represented by

$$\boldsymbol{\ell}_e(\theta, \phi) = \hat{\mathbf{a}}_\theta \ell_\theta(\theta, \phi) + \hat{\mathbf{a}}_\phi \ell_\phi(\theta, \phi) \tag{2-91}$$

It should be noted that it is also referred to as the *effective height*. It is a far-field quantity and it is related to the *far-zone* field $\mathbf{E}_a$ radiated by the antenna, with current I_{in} in its terminals, by [13]–[18]

$$\mathbf{E}_a = \hat{\mathbf{a}}_\theta E_\theta + \hat{\mathbf{a}}_\phi E_\phi = -j\eta \frac{kI_{in}}{4\pi r}\boldsymbol{\ell}_e e^{-jkr} \tag{2-92}$$

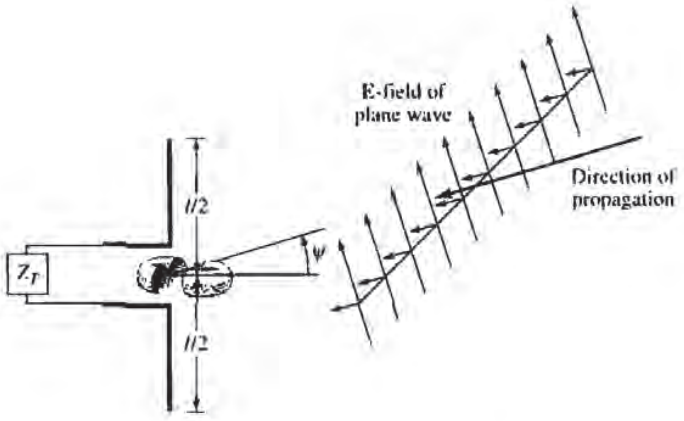
The effective length represents the antenna in its transmitting and receiving modes, and it is particularly useful in relating the open-circuit voltage V_{oc} of receiving antennas. This relation can be expressed as

$$V_{oc} = \mathbf{E}^i \cdot \boldsymbol{\ell}_e \tag{2-93}$$

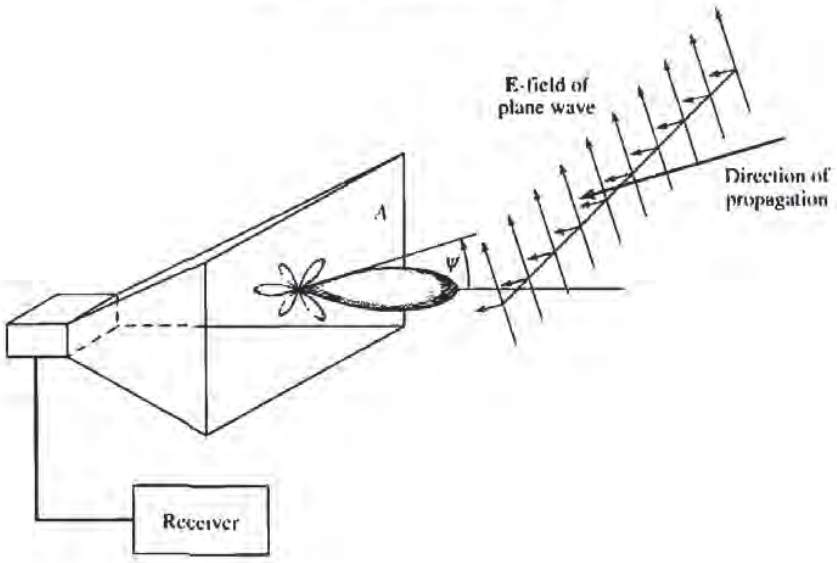
where

V_{oc} = open-circuit voltage at antenna terminals
$\mathbf{E}^i$ = incident electric field
$\boldsymbol{\ell}_e$ = vector effective length

INTEL-1045
U.S. Patent 7,151,430



(a) Dipole antenna in receiving mode



(b) Aperture antenna in receiving mode

Figure 2.23 Uniform plane wave incident upon dipole and aperture antennas.

In (2-93) V_{oc} can be thought of as the voltage induced in a linear antenna of length $l = \ell_e$ when ℓ_e and $\mathbf{E}^i$ are linearly polarized [19],[20]. From the relation of (2-93) the *effective length of a linearly polarized antenna receiving a plane wave in a given direction* is defined as "the ratio of the magnitude of the open-circuit voltage developed at the terminals of the antenna to the magnitude of the electric field strength in the direction of the antenna polarization. Alternatively, the effective length is the length of a thin straight conductor oriented perpendicular to the given direction and parallel to the antenna polarization, having a uniform current equal to that at the antenna terminals and producing the same far-field strength as the antenna in that direction."

In addition, as shown in Section 2.12.2, the antenna vector effective length is used to determine the polarization efficiency of the antenna. To illustrate the usefulness of the vector effective length, let us consider an example.

INTEL-1045
U.S. Patent 7,151,430

Example 2.12

The far-zone field radiated by a small dipole of length $l < \lambda/10$ and with a triangular current distribution, as shown in Figure 4.3, is derived in Section 4.3 of Chapter 4 and it is given by (4-36a), or

$$\mathbf{E}_a = \hat{\mathbf{a}}_\theta j\eta \frac{kI_{in}le^{-jkr}}{8\pi r} \sin\theta$$

Determine the vector effective length of the antenna.

SOLUTION

According to (2-92), the vector effective length is

$$\ell_e = -\hat{\mathbf{a}}_\theta \frac{l}{2} \sin\theta$$

This indicates, as it should, that the effective length is a function of the direction angle θ, and its maximum occurs when $\theta = 90°$. This tells us that the maximum open-circuit voltage at the dipole terminals occurs when the incident direction of the wave of Figure 2.23(a) impinging upon the small dipole antenna is normal to the axis (length) of the dipole ($\theta = 90°$). This is expected since the dipole has a radiation pattern whose maximum is in the $\theta = 90°$. In addition, the effective length of the dipole to produce the same output open-circuit voltage is only half (50%) of its physical length if it were replaced by a thin conductor having a uniform current distribution (it can be shown that the maximum effective length of an element with an ideal uniform current distribution is equal to its physical length).

2.15.2 Antenna Equivalent Areas

With each antenna, we can associate a number of equivalent areas. These are used to describe the power capturing characteristics of the antenna when a wave impinges on it. One of these equivalent areas is the *effective area (aperture)*, which in a given direction is defined as "the ratio of the available power at the terminals of a receiving antenna to the power flux density of a plane wave incident on the antenna from that direction, the wave being polarization matched to the antenna. If the direction is not specified, the direction of maximum radiation intensity is implied." In equation form it is written as

$$A_e = \frac{P_T}{W_i} = \frac{|I_T|^2 R_T/2}{W_i} \tag{2-94}$$

where

A_e = effective area (effective aperture) (m^2)
P_T = power delivered to the load (W)
W_i = power density of incident wave (W/m^2)

INTEL-1045
U.S. Patent 7,151,430

The effective aperture is the area which when multiplied by the incident power density gives the power delivered to the load. Using the equivalent of Figure 2.22, we can write (2-94) as

$$A_e = \frac{|V_T|^2}{2W_i}\left[\frac{R_T}{(R_r + R_L + R_T)^2 + (X_A + X_T)^2}\right] \tag{2-95}$$

Under conditions of maximum power transfer (conjugate matching), $R_r + R_L = R_T$ and $X_A = -X_T$, the effective area of (2-95) reduces to the maximum effective aperture given by

$$A_{em} = \frac{|V_T|^2}{8W_i}\left[\frac{R_T}{(R_L + R_r)^2}\right] = \frac{|V_T|^2}{8W_i}\left[\frac{1}{R_r + R_L}\right] \tag{2-96}$$

When (2-96) is multiplied by the incident power density, it leads to the maximum power delivered to the load of (2-86).

All of the power that is intercepted, collected, or captured by an antenna is not delivered to the load, as we have seen using the equivalent circuit of Figure 2.22. In fact, under conjugate matching only half of the captured power is delivered to the load; the other half is scattered and dissipated as heat. Therefore to account for the scattered and dissipated power we need to define, in addition to the effective area, the *scattering*, *loss* and *capture* equivalent areas. In equation form these can be defined similarly to (2-94)–(2-96) for the effective area.

The *scattering area* is defined as the equivalent area when multiplied by the incident power density is equal to the scattered or reradiated power. Under conjugate matching this is written, similar to (2-96), as

$$A_s = \frac{|V_T|^2}{8W_i}\left[\frac{R_r}{(R_L + R_r)^2}\right] \tag{2-97}$$

which when multiplied by the incident power density gives the scattering power of (2-87).

The *loss area* is defined as the equivalent area, which when multiplied by the incident power density leads to the power dissipated as heat through R_L. Under conjugate matching this is written, similar to (2-96), as

$$A_L = \frac{|V_T|^2}{8W_i}\left[\frac{R_L}{(R_L + R_r)^2}\right] \tag{2-98}$$

which when multiplied by the incident power density gives the dissipated power of (2-88).

Finally the *capture area* is defined as the equivalent area, which when multiplied by the incident power density leads to the total power captured, collected, or intercepted by the antenna. Under conjugate matching this is written, similar to (2-96), as

$$A_c = \frac{|V_T|^2}{8W_i}\left[\frac{R_T + R_r + R_L}{(R_L + R_r)^2}\right] \tag{2-99}$$

When (2-99) is multiplied by the incident power density, it leads to the captured power of (2-89). In general, the total capture area is equal to the sum of the other three, or

$$\textit{Capture Area} = \textit{Effective Area} + \textit{Scattering Area} + \textit{Loss Area}$$

INTEL-1045
U.S. Patent 7,151,430

This is apparent under conjugate matching using (2-96)–(2-99). However, it holds even under nonconjugate matching conditions.

Now that the equivalent areas have been defined, let us introduce the *aperture efficiency* ϵ_{ap} of an antenna, which is defined as the ratio of the maximum effective area A_{em} of the antenna to its physical area A_p, or

$$\epsilon_{ap} = \frac{A_{em}}{A_p} = \frac{\text{maximum effective area}}{\text{physical area}} \tag{2-100}$$

For aperture type antennas, such as waveguides, horns, and reflectors, the maximum effective area cannot exceed the physical area but it can equal it ($A_{em} \leq A_p$ or $0 \leq \epsilon_{ap} \leq 1$). Therefore the maximum value of the aperture efficiency cannot exceed unity (100 %). For a lossless antenna ($R_L = 0$) the maximum value of the scattering area is also equal to the physical area. Therefore even though the aperture efficiency is greater than 50%, for a lossless antenna under conjugate matching only half of the captured power is delivered to the load and the other half is scattered.

We can also introduce a *partial effective area* of an antenna *for a given polarization* in a given direction, which is defined as "the ratio of the available power at the terminals of a receiving antenna to the power flux density of a plane wave incident on the antenna from that direction and with a specified polarization differing from the receiving polarization of the antenna."

The effective area of an antenna is not necessarily the same as the physical aperture. It will be shown in later chapters that aperture antennas with constant amplitude and phase field distributions have maximum effective areas equal to the physical areas; they are smaller for nonconstant field distributions. In addition, the maximum effective area of wire antennas is greater than the physical area (if taken as the area of a cross section of the wire when split lengthwise along its diameter). Thus the wire antenna can capture much more power than is intercepted by its physical size! This should not come as a surprise. If the wire antenna would only capture the power incident on its physical size, it would be almost useless. So electrically, the wire antenna looks much bigger than its physical stature.

To illustrate the concept of effective area, especially as applied to a wire antenna, let us consider an example. In later chapters, we will consider examples of aperture antennas.

Example 2.13

A uniform plane wave is incident upon a very short lossless dipole ($l \ll \lambda$), as shown in Figure 2.23(a). Find the maximum effective area assuming that the radiation resistance of the dipole is $R_r = 80(\pi l/\lambda)^2$, and the incident field is linearly polarized along the axis of the dipole.

SOLUTION

For $R_L = 0$, the maximum effective area of (2-96) reduces to

$$A_{em} = \frac{|V_T|^2}{8W_i}\left[\frac{1}{R_r}\right]$$

INTEL-1045
U.S. Patent 7,151,430

Since the dipole is very short, the induced current can be assumed to be constant and of uniform phase. The induced voltage is

$$V_I = El$$

where

V_I = induced voltage on the dipole
E = electric field of incident wave
l = length of dipole

For a uniform plane wave, the incident power density can be written as

$$W_i = \frac{E^2}{2\eta}$$

where η is the intrinsic impedance of the medium ($\simeq 120\pi$ ohms for a free-space medium). Thus

$$A_{em} = \frac{(El)^2}{8(E^2/2\eta)(80\pi^2 l^2/\lambda^2)} = \frac{3\lambda^2}{8\pi} = 0.119\lambda^2$$

The above value is only valid for a lossless antenna (the losses of a short dipole are usually significant). If the loss resistance is equal to the radiation resistance ($R_L = R_r$) and the sum of the two is equal to the load (receiver) resistance ($R_T = R_r + R_L = 2R_r$), then the effective area is only one-half of the maximum effective area given above.

Let us now examine the significance of the effective area. From Example 2.13, the maximum effective area of a short dipole with $l \ll \lambda$ was equal to $A_{em} = 0.119\,\lambda^2$. Typical antennas that fall under this category are dipoles whose lengths are $l \leq \lambda/50$. For the purpose of demonstration, let us assume that $l = \lambda/50$. Because $A_{em} = 0.119\lambda^2 = lw_e = (\lambda/50)w_e$, the maximum effective electrical width of this dipole is $w_e = 5.95\lambda$. Typical physical diameters (widths) of wires used for dipoles may be about $w_p = \lambda/300$. Thus the maximum effective width w_e is about 1785 times larger than its physical width.

2.16 MAXIMUM DIRECTIVITY AND MAXIMUM EFFECTIVE AREA

To derive the relationship between directivity and maximum effective area, the geometrical arrangement of Figure 2.24 is chosen. Antenna 1 is used as a transmitter and 2 as a receiver. The effective areas and directivities of each are designated as A_1, A_2 and D_1, D_2. If antenna 1 were isotropic, its radiated power density at a distance R would be

$$W_0 = \frac{P_t}{4\pi R^2} \tag{2-101}$$

where P_t is the total radiated power. Because of the directive properties of the antenna, its actual density is

$$W_1 = W_0 D_1 = \frac{P_t D_1}{4\pi R^2} \tag{2-102}$$

INTEL-1045
U.S. Patent 7,151,430

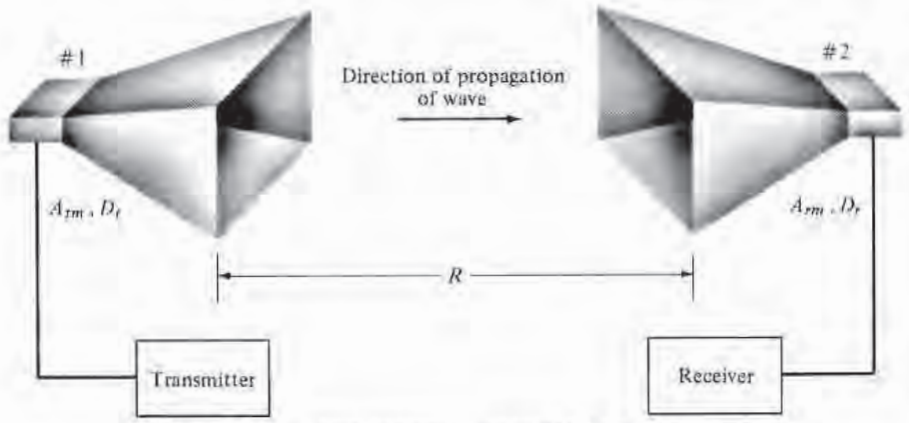


Figure 2.24 Two antennas separated by a distance R.

The power collected (received) by the antenna and transferred to the load would be

$$P_r = W_t A_r = \frac{P_t D_t A_r}{4\pi R^2} \tag{2-103}$$

or

$$D_t A_r = \frac{P_r}{P_t}(4\pi R^2) \tag{2-103a}$$

If antenna 2 is used as a transmitter, 1 as a receiver, and the intervening medium is linear, passive, and isotropic, we can write that

$$D_r A_t = \frac{P_r}{P_t}(4\pi R^2) \tag{2-104}$$

Equating (2-103a) and (2-104) reduces to

$$\frac{D_t}{A_t} = \frac{D_r}{A_r} \tag{2-105}$$

Increasing the directivity of an antenna increases its effective area in direct proportion. Thus, (2-105) can be written as

$$\frac{D_{0t}}{A_{tm}} = \frac{D_{0r}}{A_{rm}} \tag{2-106}$$

where A_{tm} and A_{rm} (D_{0t} and D_{0r}) are the *maximum* effective areas (directivities) of antennas 1 and 2, respectively.

If antenna 1 is isotropic, then $D_{0t} = 1$ and its maximum effective area can be expressed as

$$A_{tm} = \frac{A_{rm}}{D_{0r}} \tag{2-107}$$

Equation (2-107) states that the maximum effective area of an isotropic source is equal to the ratio of the maximum effective area to the maximum directivity of any other source. For example, let the other antenna be a very short ($l \ll \lambda$) dipole whose effective area ($0.119\lambda^2$ from Example 2.13) and maximum directivity (1.5) are known.

INTEL-1045
U.S. Patent 7,151,430

The maximum effective area of the isotropic source is then equal to

$$A_{im} = \frac{A_{em}}{D_{0r}} = \frac{0.119\lambda^2}{1.5} = \frac{\lambda^2}{4\pi} \tag{2-108}$$

Using (2-108), we can write (2-107) as

$$A_{em} = D_{0r} A_{im} = D_{0r} \left(\frac{\lambda^2}{4\pi}\right) \tag{2-109}$$

In general then, the *maximum effective aperture* (A_{em}) *of any antenna is related to its maximum directivity* (D_0) *by*

$$\boxed{A_{em} = \frac{\lambda^2}{4\pi} D_0} \tag{2-110}$$

Thus, when (2-110) is multiplied by the power density of the incident wave it leads to the maximum power that can be delivered to the load. This assumes that there are no conduction dielectric losses (radiation efficiency e_{cd} is unity), the antenna is matched to the load (reflection efficiency e_r is unity), and the polarization of the impinging wave matches that of the antenna (polarization loss factor PLF and polarization efficiency p_e are unity). If there are losses associated with an antenna, its maximum effective aperture of (2-110) must be modified to account for conduction-dielectric losses (radiation efficiency). Thus,

$$A_{em} = e_{cd} \left(\frac{\lambda^2}{4\pi}\right) D_0 \tag{2-111}$$

The maximum value of (2-111) assumes that the antenna is matched to the load and the incoming wave is polarization-matched to the antenna. If reflection and polarization losses are also included, then the maximum effective area of (2-111) is represented by

$$\boxed{\begin{aligned} A_{em} &= e_t \left(\frac{\lambda^2}{4\pi}\right) D_0 |\hat{\mathbf{p}}_w \cdot \hat{\mathbf{p}}_a|^2 \\ &= e_{cd}(1 - |\Gamma|^2) \left(\frac{\lambda^2}{4\pi}\right) D_0 |\hat{\mathbf{p}}_w \cdot \hat{\mathbf{p}}_a|^2 \end{aligned}} \tag{2-112}$$

2.17 FRIIS TRANSMISSION EQUATION AND RADAR RANGE EQUATION

The analysis and design of radar and communications systems often require the use of the *Friis Transmission Equation* and the *Radar Range Equation*. Because of the importance [21] of the two equations, a few pages will be devoted for their derivation.

2.17.1 Friis Transmission Equation

The Friis Transmission Equation relates the power received to the power transmitted between two antennas separated by a distance $R > 2D^2/\lambda$, where D is the largest dimension of either antenna. Referring to Figure 2.25, let us assume that the trans-

INTEL-1045
U.S. Patent 7,151,430

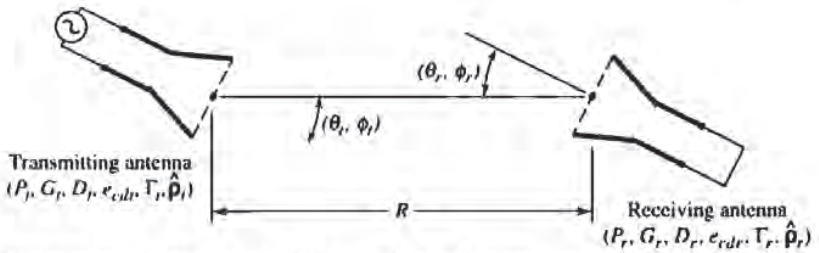


Figure 2.25 Geometrical orientation of transmitting and receiving antennas for Friis transmission equation.

mitting antenna is initially isotropic. If the input power at the terminals of the transmitting antenna is P_t, then its isotropic power density W_0 at distance R from the antenna is

$$W_0 = e_t \frac{P_t}{4\pi R^2} \tag{2-113}$$

where e_t is the radiation efficiency of the transmitting antenna. For a nonisotropic transmitting antenna, the power density of (2-113) in the direction θ_t, ϕ_t can be written as

$$W_t = \frac{P_t G_t(\theta_t,\phi_t)}{4\pi R^2} = e_t \frac{P_t D_t(\theta_t,\phi_t)}{4\pi R^2} \tag{2-114}$$

where $G_t(\theta_t, \phi_t)$ is the gain and $D_t(\theta_t, \phi_t)$ is the directivity of the transmitting antenna in the direction θ_t, ϕ_t. Since the effective area A_r of the antenna is related to its efficiency e_r and directivity D_r by

$$A_r = e_r D_r(\theta_r,\phi_r)\left(\frac{\lambda^2}{4\pi}\right) \tag{2-115}$$

the amount of power P_r collected by the receiving antenna can be written, using (2-114) and (2-115) as

$$P_r = e_r D_r(\theta_r,\phi_r)\frac{\lambda^2}{4\pi} W_t = e_t e_r \frac{\lambda^2 D_t(\theta_t,\phi_t) D_r(\theta_r,\phi_r) P_t}{(4\pi R)^2} |\hat{\rho}_t \cdot \hat{\rho}_r|^2 \tag{2-116}$$

or the ratio of the received to the input power as

$$\frac{P_r}{P_t} = e_t e_r \frac{\lambda^2 D_t(\theta_t, \phi_t) D_r(\theta_r,\phi_r)}{(4\pi R)^2} \tag{2-117}$$

The power received based on (2-117) assumes that the transmitting and receiving antennas are matched to their respective lines or loads (reflection efficiencies are unity) and the polarization of the receiving antenna is polarization-matched to the impinging wave (polarization loss factor and polarization efficiency are unity). If these two factors are also included, then the ratio of the received to the input power of (2-117) is represented by

$$\boxed{\frac{P_r}{P_t} = e_{cdt} e_{cdr}(1 - |\Gamma_t|^2)(1 - |\Gamma_r|^2)\left(\frac{\lambda}{4\pi R}\right)^2 D_t(\theta_t,\phi_t) D_r(\theta_r,\phi_r)|\hat{\rho}_t \cdot \hat{\rho}_r|^2} \tag{2-118}$$

INTEL-1045
U.S. Patent 7,151,430

For reflection and polarization-matched antennas aligned for maximum directional radiation and reception, (2-118) reduces to

$$\boxed{\frac{P_r}{P_t} = \left(\frac{\lambda}{4\pi R}\right)^2 G_{0t} G_{0r}} \tag{2-119}$$

Equations (2-117), (2-118), or (2-119) are known as the *Friis Transmission Equation*, and it relates the power P_r (delivered to the receiver load) to the input power of the transmitting antenna P_t. The term $(\lambda/4\pi R)^2$ is called the *free-space loss factor*, and it takes into account the losses due to the spherical spreading of the energy by the antenna.

2.17.2 Radar Range Equation

Now let us assume that the transmitted power is incident upon a target, as shown in Figure 2.26. We now introduce a quantity known as the *radar cross section* or *echo area* (σ) of a target which is defined as *the area intercepting that amount of power which, when scattered isotropically, produces at the receiver a density which is equal to that scattered by the actual target* [13]. In equation form

$$\lim_{R \to \infty} \left[\frac{\sigma W_t}{4\pi R^2}\right] = W_s \tag{2-120}$$

or

$$\boxed{\sigma = \lim_{R \to \infty} \left[4\pi R^2 \frac{W_s}{W_i}\right] = \lim_{R \to \infty} \left[4\pi R^2 \frac{|\mathbf{E}^s|^2}{|\mathbf{E}^i|^2}\right] = \lim_{R \to \infty} \left[4\pi R^2 \frac{|\mathbf{H}^s|^2}{|\mathbf{H}^i|^2}\right]} \tag{2-120a}$$

where

σ = radar cross section or echo area (m^2)
R = observation distance from target (m)
W_i = incident power density (W/m^2)
W_s = scattered power density (W/m^2)
$\mathbf{E}^i$ ($\mathbf{E}^s$) = incident (scattered) electric field (V/m)
$\mathbf{H}^i$ ($\mathbf{H}^s$) = incident (scattered) magnetic field (A/m)

Any of the definitions in (2-120a) can be used to derive the radar cross section of any antenna or target. For some polarization one of the definitions based either on the power density, electric field, or magnetic field may simplify the derivation, although all should give the same answers [13].

Using the definition of radar cross section, we can consider that the transmitted power incident upon the target is initially captured and then it is reradiated isotropically, insofar as the receiver is concerned. The amount of captured power P_c is obtained by multiplying the incident power density of (2-114) by the radar cross section σ, or

$$P_c = \sigma W_t = \sigma \frac{P_t G_t(\theta_t, \phi_t)}{4\pi R_1^2} = e_t \sigma \frac{P_t D_t(\theta_t, \phi_t)}{4\pi R_1^2} \tag{2-121}$$

INTEL-1045
U.S. Patent 7,151,430

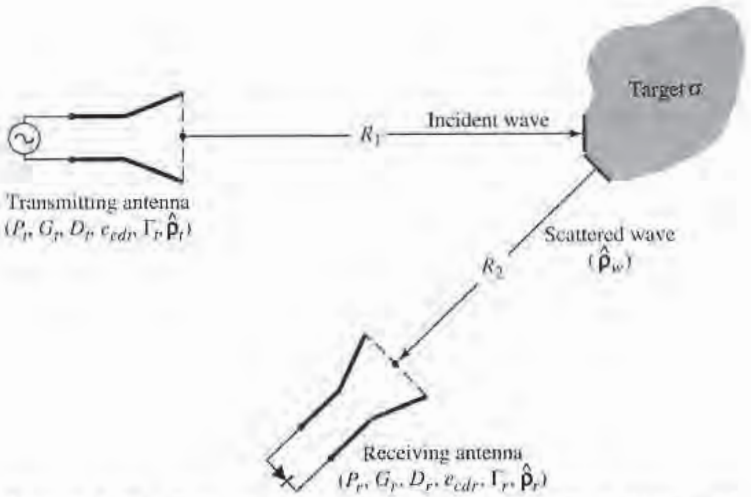


Figure 2.26 Geometrical arrangement of transmitter, target, and receiver for radar range equation.

The power captured by the target is reradiated isotropically, and the scattered power density can be written as

$$W_s = \frac{P_c}{4\pi R_2^2} = e_{cdt}\sigma \frac{P_t D_t(\theta_t,\phi_t)}{(4\pi R_1 R_2)^2} \tag{2-122}$$

The amount of power delivered to the receiver load is given by

$$P_r = A_r W_s = e_{cdt} e_{cdr} \sigma \frac{P_t D_t(\theta_t,\phi_t) D_r(\theta_r,\phi_r)}{4\pi} \left(\frac{\lambda}{4\pi R_1 R_2}\right)^2 \tag{2-123}$$

where A_r is the effective area of the receiving antenna as defined by (2-115).

Equation (2-123) can be written as the ratio of the received power to the input power, or

$$\frac{P_r}{P_t} = e_{cdt} e_{cdr} \sigma \frac{D_t(\theta_t,\phi_t) D_r(\theta_r,\phi_r)}{4\pi} \left(\frac{\lambda}{4\pi R_1 R_2}\right)^2 \tag{2-124}$$

Expression (2-124) is used to relate the received power to the input power, and it takes into account only conduction-dielectric losses (radiation efficiency) of the transmitting and receiving antennas. It does not include reflection losses (reflection efficiency) and polarization losses (polarization loss factor or polarization efficiency). If these two losses are also included, then (2-124) must be expressed as

$$\boxed{\frac{P_r}{P_t} = e_{cdt} e_{cdr} (1 - |\Gamma_t|^2)(1 - |\Gamma_r|^2)\, \sigma \frac{D_t(\theta_t,\phi_t)\, D_r(\theta_r,\phi_r)}{4\pi} \times \left(\frac{\lambda}{4\pi R_1 R_2}\right)^2 |\hat{\boldsymbol{\rho}}_w \cdot \hat{\boldsymbol{\rho}}_r|^2} \tag{2-125}$$

where

$\hat{\boldsymbol{\rho}}_w$ = polarization unit vector of the scattered waves

$\hat{\boldsymbol{\rho}}_r$ = polarization unit vector of the receiving antenna

INTEL-1045
U.S. Patent 7,151,430

For polarization-matched antennas aligned for maximum directional radiation and reception, (2-125) reduces to

$$\boxed{\frac{P_r}{P_t} = \sigma \frac{G_{0t} G_{0r}}{4\pi} \left[\frac{\lambda}{4\pi R_1 R_2}\right]^2} \tag{2-126}$$

Equation (2-124), or (2-125) or (2-126) is known as the *Radar Range Equation*. It relates the power P_r (delivered to the receiver load) to the input power P_t transmitted by an antenna, after it has been scattered by a target with a radar cross section (echo area) of σ.

Example 2.14

Two *lossless* X-band (8.2–12.4 GHz) horn antennas are separated by a distance of 100λ. The reflection coefficients at the terminals of the transmitting and receiving antennas are 0.1 and 0.2, respectively. The maximum directivities of the transmitting and receiving antennas (over isotropic) are 16 dB and 20 dB, respectively. Assuming that the input power in the lossless transmission line connected to the transmitting antenna is 2 W, and the antennas are aligned for maximum radiation between them and are polarization matched, find the power delivered to the load of the receiver.

SOLUTION

For this problem

$$\begin{aligned}
e_{cdt} &= e_{cdr} = 1 \quad \text{because antennas are lossless.} \\
|\hat{\boldsymbol{\rho}}_t \cdot \hat{\boldsymbol{\rho}}_r|^2 &= 1 \quad \text{because antennas are polarization matched} \\
D_t &= D_{0t} \\
D_r &= D_{0r}
\end{aligned} \Bigg\} \quad \text{because antennas are aligned for maximum radiation between them}$$

$$\begin{aligned}
D_{0t} &= 16 \text{ dB} \rightleftharpoons 39.81 \quad \textit{(dimensionless)} \\
D_{0r} &= 20 \text{ dB} \rightleftharpoons 100 \quad \text{(dimensionless)}
\end{aligned}$$

Using (2-125), we can write

$$\begin{aligned}
P_r &= [1 - (0.1)^2][1 - (0.2)^2][\lambda/4\pi(100\lambda)]^2(39.81)(100)(2) \\
&= 4.777 \text{ mW}
\end{aligned}$$

2.17.3 Antenna Radar Cross Section

The radar cross section, usually referred to as RCS, is a far-field parameter, which is used to characterize the scattering properties of a radar target. For a target, there is *monostatic* or *backscattering RCS* when the transmitter and receiver of Figure 2.26 are at the same location, and a *bistatic RCS when the transmitter and receiver are not* at the same location. In designing low-observable or low-profile (stealth) targets, it is the parameter that you attempt to minimize. For complex targets (such as aircraft,

INTEL-1045
U.S. Patent 7,151,430

spacecraft, missiles, ships, tanks, automobiles) it is a complex parameter to derive. In general, the RCS of a target is a function of the polarization of the incident wave, the angle of incidence, the angle of observation, the geometry of the target, the electrical properties of the target, and the frequency of operation. The units of RCS of three-dimensional targets are meters squared (m^2) or for normalized values decibels per squared meter (dBsm) or RCS per squared wavelength in decibels (RCS/λ^2 in dB). Representative values of some typical targets are shown in Table 2.2 [22]. Although the frequency was not stated, these numbers could be representative at X-band.

The RCS of a target can be controlled using primarily two basic methods: *shaping* and the use of *materials*. Shaping is used to attempt to direct the scattered energy toward directions other than the desired. However, for many targets shaping has to be compromised in order to meet other requirements, such as aerodynamic specifications for flying targets. Materials is used to trap the incident energy within the target and to dissipate part of the energy as heat or to direct it toward directions other than the desired. Usually both methods, shaping and materials, are used together in order to optimize the performance of a radar target. One of the "golden rules" to observe in order to achieve low RCS is to "*round corners, avoid flat and concave surfaces, and use material treatment in flare spots.*"

There are many methods of analysis to predict the RCS of a target [13], [22]–[33]. Some of them are full-wave methods, others are designated as asymptotic methods, either low-frequency or high-frequency, and some are considered as numerical methods. The methods of analysis are often contingent upon the shape, size, and material composition of the target. Some targets, because of their geometrical complexity, are often simplified and are decomposed into a number of basic shapes (such as strips, plates, cylinders, cones, wedges) which when put together represent a very good replica of the actual target. This has been used extensively and proved to be a very good approach. The topic is very extensive to be treated here in any detail, and the reader is referred to the literature [13], [22]–[33]. There is a plethora of references but because of space limitations, only a limited number is included here to get the reader started on the subject.

Table 2.2 RCS OF SOME TYPICAL TARGETS

	Typical RCSs [22]	
Object	RCS (m^2)	RCS (dBsm)
Pickup truck	200	23
Automobile	100	20
Jumbo jet airliner	100	20
Large bomber *or* commercial jet	40	16
Cabin cruiser boat	10	10
Large fighter aircraft	6	7.78
Small fighter aircraft *or* four-passenger jet	2	3
Adult male	1	0
Conventional winged missile	0.5	−3
Bird	0.01	−20
Insect	0.00001	−50
Advanced tactical fighter	0.000001	−60

INTEL-1045
U.S. Patent 7,151,430

Antennas individually are radar targets which many exhibit large radar cross section. In many applications, antennas are mounted on the surface of other complex targets (such as aircraft, spacecraft, satellites, missiles, automobiles) and become part of the overall radar target. In such configurations, many antennas, especially aperture types (such as waveguides, horns) become large contributors to the total RCS, monostatic or bistatic, of the target. Therefore in designing low-observable targets, the antenna type, location and contributions become an important consideration of the overall design.

The scattering and transmitting (radiation) characteristics of an antenna are related [34]–[36]. There are various methods which can be used to analyze the fields scattered by an antenna. The presentation here parallels that in [23], [37]–[40]. In general the electric field scattered by an antenna with a load impedance Z_L can be expressed by

$$\mathbf{E}^s(Z_L) = \mathbf{E}^s(0) - \frac{I_s}{I_t}\frac{Z_L}{Z_L + Z_A}\mathbf{E}^t \tag{2-127}$$

where

$\mathbf{E}^s(Z_L)$ = electric field scattered by antenna with a load Z_L

$\mathbf{E}^s(0)$ = electric field scattered by short-circuited antenna ($Z_L = 0$)

I_s = short-circuited current induced by the incident field on the antenna with $Z_L = 0$

I_t = antenna current in transmitting mode

$Z_A = R_A + jX_A$ = antenna input impedance

$\mathbf{E}^t$ = electric field radiated by the antenna in transmitting mode

By defining an antenna reflection coefficient of

$$\Gamma_A = \frac{Z_L - Z_A}{Z_L + Z_A} \tag{2-128}$$

the scattered field of (2-127) can be written as

$$\mathbf{E}^s(Z_L) = \mathbf{E}^s(0) - \frac{I_s}{I_t}\frac{1}{2}(1 + \Gamma_A)\mathbf{E}^t \tag{2-129}$$

Therefore according to (2-129) the scattered field by an antenna with a load Z_L is equal to the scattered field when the antenna is short-circuited ($Z_L = 0$) minus a term related to the reflection coefficient and the field transmitted by the antenna.

Green has expressed the field scattered by an antenna terminated with a load Z_L in a more convenient form which allows it to be separated into the *structural* and *antenna mode* scattering terms [23], [37]–[40]. This is accomplished by assuming that the antenna is loaded with a conjugate-matched impedance ($Z_L = Z_A^*$). Doing this generates using (2-127) another equation for the field scattered by the antenna with a load $Z_L = Z_A^*$. When this new equation is subtracted from (2-127) it eliminates the short-circuited scattered field, and we can write that the field scattered by the antenna with a load Z_L is

$$\mathbf{E}^s(Z_L) = \mathbf{E}^s(Z_A^*) - \frac{I_s}{I_t}\frac{\Gamma^* Z_A}{2R_A}\mathbf{E}^t \tag{2-130}$$

$$\Gamma^* = \frac{Z_L - Z_A^*}{Z_L + Z_A} \tag{2-130a}$$

INTEL-1045
U.S. Patent 7,151,430

where

$\mathbf{E}^s(Z_L)$ = electric field scattered by the antenna with load Z_L

$\mathbf{E}^s(Z_A^*)$ = electric field scattered by the antenna with a conjugate-matched load

$I(Z_A^*)$ = current induced by the incident wave at the terminals matched with a conjugate impedance load

Γ^* = conjugate-matched reflection coefficient

Z_L = load impedance attached to antenna terminals

For the short-circuited case and the conjugate-matched transmitting (radiating) case, the product of their currents and antenna impedance are related by [34]

$$I_s Z_A = I_m^*(Z_A + Z_A^*) = 2R_A I_m^* \tag{2-131}$$

where I_m^* is the scattering current when the antenna is conjugate-matched ($Z_L = Z_A^*$). Substituting (2-131) into (2-130) for I_s reduces (2-130) to

$$\mathbf{E}^s(Z_L) = \mathbf{E}^s(Z_A^*) - \frac{I_m^*}{I_t}\Gamma^*\mathbf{E}^t \tag{2-132}$$

It can also be shown that if the antenna is matched with a load Z_A (instead of Z_A^*), then (2-132) can be written as

$$\mathbf{E}^s(Z_L) = \mathbf{E}^s(Z_A) - \frac{I_m}{I_t}\Gamma_A\mathbf{E}^t \tag{2-133}$$

Therefore the field scattered by an antenna loaded with an impedance Z_L is related to the field radiated by the antenna in the transmitting mode in three different ways, as shown by (2-129), (2-132), and (2-133). According to (2-129) the field scattered by an antenna when it is loaded with an impedance Z_L is equal to the field scattered by the antenna when it is short-circuited ($Z_L = 0$) minus a term related to the antenna reflection coefficient and the field transmitted by the antenna. In addition, according to (2-132) the field scattered by an antenna when it is terminated with an impedance Z_L is equal to the field scattered by the antenna when it is conjugate matched with an impedance Z_A^* minus the field transmitted (radiated) times the conjugate reflection coefficient. The second term is weighted by the two currents. Alternatively, according to (2-133), the field scattered by the antenna when it is terminated with an impedance Z_L is equal to the field scattered by the antenna when it is matched with an impedance Z_A minus the field transmitted (radiated) times the reflection coefficient weighted by the two currents.

In (2-132) the first term consists of the *structural* scattering term and the second of the *antenna mode* scattering term. The *structural* scattering term is introduced by the currents induced on the surface of the antenna by the incident field when the antenna is conjugate-matched, and it is independent of the load impedance. The *antenna mode* scattering term is only a function of the radiation characteristics of the antenna, and its scattering pattern is the square of the antenna radiation pattern. The antenna mode depends on the power absorbed in the load of a lossless antenna and the power which is radiated by the antenna due to a load mismatch. This term vanishes when the antenna is conjugate-matched.

From the scattered field expression of (2-129), it can be shown that the total radar cross section of the antenna terminated with a load Z_L can be written as [40]

$$\sigma = |\sqrt{\sigma^s} - (1 + \Gamma_A)\sqrt{\sigma^a}e^{j\phi_r}|^2 \tag{2-134}$$

INTEL-1045
U.S. Patent 7,151,430

where

σ = total RCS with antenna terminated with Z_L
σ^s = RCS due to structural term
σ^a = RCS due to antenna mode term
ϕ_r = relative phase between the structural and antenna mode terms

If the antenna is short-circuited ($\Gamma_A = -1$), then according to (2-134)

$$\sigma_{\text{short}} = \sigma^s \tag{2-135}$$

If the antenna is open-circuited ($\Gamma_A = +1$), then according to (2-134)

$$\sigma_{\text{open}} = \left|\sqrt{\sigma^s} - 2\sqrt{\sigma^a}e^{j\phi_r}\right|^2 = \sigma_{\text{residual}} \tag{2-136}$$

Lastly, if the antenna is matched $Z_L = Z_A$ ($\Gamma_A = 0$), then according to (2-134)

$$\sigma_{\text{match}} = \left|\sqrt{\sigma^s} - \sqrt{\sigma^a}e^{j\phi_r}\right|^2 \tag{2-137}$$

Therefore under matched conditions, according to (2-137), the range of values (minimum to maximum) of the radar cross section is

$$\left|\sigma^s - \sigma^a\right| \le \sigma \le \left|\sigma^s + \sigma^a\right| \tag{2-138}$$

The minimum value occurring when the two RCSs are in-phase while the maximum occurs when they are out-of-phase.

Example 2.15

The structural RCS of a resonant wire dipole is in-phase and in magnitude slightly greater than four times that of the antenna mode. Relate the short-circuited, open-circuited and matched RCSs to that of the antenna mode.

SOLUTION

Using (2-135)

$$\sigma_{\text{short}} = 4\sigma_{\text{antenna}}$$

Using (2-136)

$$\sigma_{\text{open}} = 2\sigma_{\text{antenna}}(0) = 0 \text{ or very small}$$

The matched value is obtained using (2-137), or

$$\sigma_{\text{match}} = \sigma_{\text{antenna}}$$

To produce a zero RCS, (2-134) must vanish. This is accomplished if

$$Re(\Gamma_A) = -1 + \cos\phi_r\sqrt{\sigma^s/\sigma^a} \tag{2-139a}$$

$$Im(\Gamma_A) = -\sin\phi_r\sqrt{\sigma^s/\sigma^a} \tag{2-139b}$$

INTEL-1045
U.S. Patent 7,151,430

Assuming positive values of resistances, the real value of Γ_A cannot be greater than unity. Therefore there are some cases where the RCS cannot be reduced to zero by choosing Z_L. Because Z_A can be complex, there is no limit on the imaginary part of Γ_A.

In general, the structural and antenna mode scattering terms are very difficult to predict and usually require that the antenna is solved as a boundary-value problem. However, these two terms have been obtained experimentally utilizing the Smith chart [37]–[39]. The total radar cross section $\sigma_{i,j}$ of the antenna for any i,j receiver-transmitter polarization combination can be represented by

$$\sigma_{i,j} = \frac{\lambda_0^2}{4\pi} G_{0r} G_{0t} P_i P_j \left| A_{i,j} - \Gamma^* \right|^2 \tag{2-140}$$

where

G_{0r} = gain of the receiving antenna
G_{0t} = gain of the transmitting antenna
P_i = polarization efficiency of the receiving antenna
P_j = polarization efficiency of the transmitting antenna
$A_{i,j}$ = complex parameter independent of the load Z_L

$A_{i,j}$ and Γ^* can be plotted on the Smith chart for any polarization combination, and the changes of the phasor $|A_{i,j} - \Gamma^*|$ can be easily examined. Thus by measuring $\sigma_{i,j}$ for several values of Γ^*, then $A_{i,j}$ can be determined using the Smith chart [37]–[39].

Depending on the location of A on the Smith chart, any arbitrary antenna can be classified into one of three possible classes, as follows:

a. $|A| > 1$. For this class, A lies outside the boundary of the Smith chart, and it is not possible to reduce the scattered field to zero using any passive load. However, using a purely reactive load, a maximum or a minimum in the scattered field can be obtained. Antennas which fall into this class usually have a large structural scattering term due either to their construction or strongly excited antenna modes which do not couple to the terminals of interest.

b. $|A| = 1$. For this class, the values of A lie along the periphery of the Smith chart, and a reactive load can be found which will reduce the scattered field to zero. Thin linear dipole antennas with lengths equal or less than half a wavelength ($l \leq \lambda_0/2$) fall into this class.

c. $|A| < 1$. For this class, the values of A lie within the Smith chart, and a complex load can be found to reduce to zero the scattered field. However maximum scattering is obtained using a reactive load. Well designed parabolic reflectors fall into this class.

For a monostatic system the receiving and transmitting antennas are collocated. In addition, if the antennas are identical ($G_{0r} = G_{0t} = G_0$) and are polarization-matched ($P_i = P_j = 1$), then (2-140) for backscattering reduces to

$$\sigma = \frac{\lambda_0^2}{4\pi} G_0^2 |A - \Gamma^*|^2 \tag{2-141}$$

INTEL-1045
U.S. Patent 7,151,430

If the antenna is a thin dipole, then $A \simeq 1$ and (2-141) reduces to

$$\sigma \simeq \frac{\lambda_0^2}{4\pi} G_0^2 |1 - \Gamma^*|^2 = \frac{\lambda_0^2}{4\pi} G_0^2 \left| 1 - \frac{Z_L - Z_A^*}{Z_L + Z_A} \right| = \frac{\lambda_0^2}{4\pi} G_0^2 \left| \frac{2R_A}{Z_L + Z_A} \right|^2 \tag{2-142}$$

If in addition we assume that the dipole length is $l = \lambda_0/2$ and is short-circuited ($Z_L = 0$), then the normalized radar cross section of (2-142) is equal to

$$\frac{\sigma}{\lambda_0^2} = \frac{G_0^2}{\pi} = \frac{(1.643)^2}{\pi} = 0.8593 \simeq 0.86 \tag{2-143}$$

which agrees with experimental monostatic values reported in the literature [41], [42].

Shown in Figure 2.27 is the measured E-plane monostatic RCS of a half-wavelength dipole when it is matched to a load, short-circuited (straight wire) and open-circuited (gap at the feed). The aspect angle is measured from the normal to the wire. As expected, the RCS is a function of the observation (aspect) angle. Also it is apparent that there are appreciable differences between the three responses. Similar responses for the monostatic RCS of a pyramidal horn are shown in Figure 2.28(a) for the E-plane and in Figure 2.28(b) for the H-plane. The antenna is a commercial X-band (8.2-12.4 GHz) 20-dB standard gain horn with aperture dimension of 9.2 cm by 12.4 cm. The length of the horn is 25.6 cm. As for the dipole, there are differences between the three responses for each plane. It is seen that the short-circuited response exhibits the largest return.

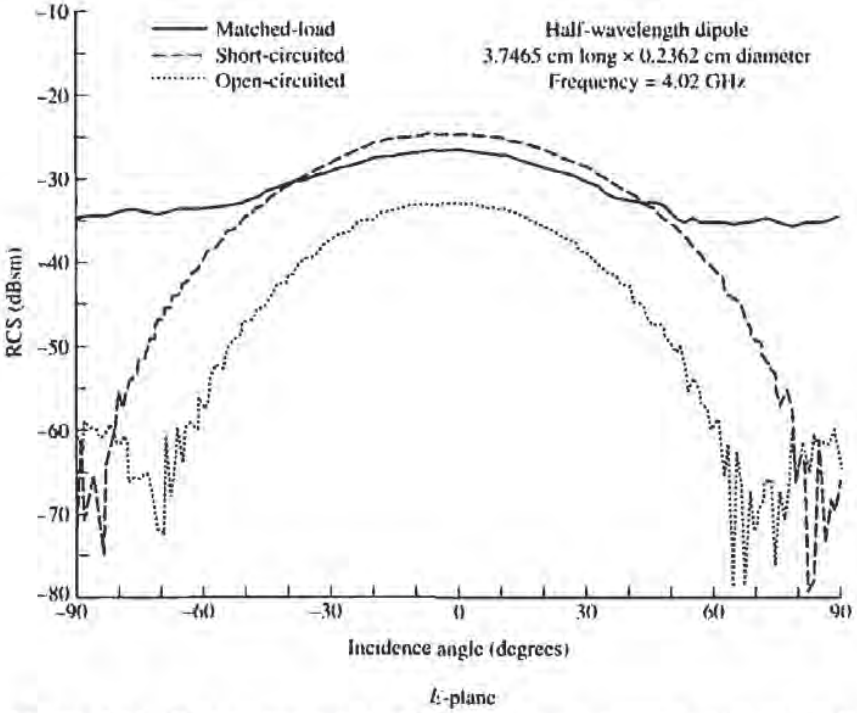
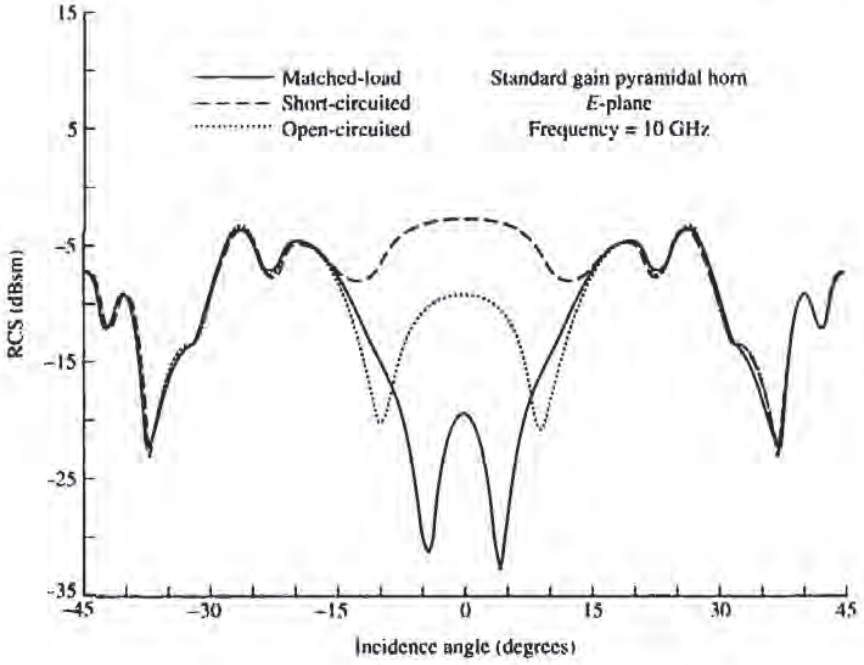
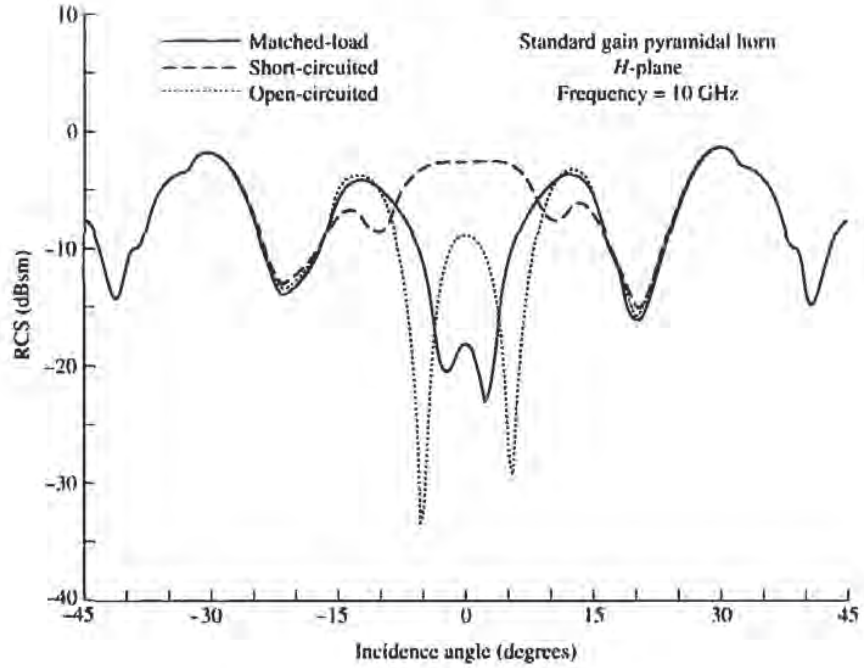


Figure 2.27 E-plane monostatic RCS ($\sigma_{\theta\theta}$) versus incidence angle for a half-wavelength dipole.

INTEL-1045
U.S. Patent 7,151,430



(a) E-plane ($\sigma_{\theta\theta}$)



(b) H-plane ($\sigma_{\phi\phi}$)

Figure 2.28 E- and H-plane monostatic RCS versus incidence angle for a pyramidal horn antenna.

INTEL-1045
U.S. Patent 7,151,430

Antenna RCS from model measurements [43] and microstrip patches [44], [45] have been reported.

2.18 ANTENNA TEMPERATURE

Every object with a physical temperature above absolute zero (0 K = −273°C) radiates energy [46]. The amount of energy radiated is usually represented by an equivalent temperature T_B, better known as brightness temperature, and it is defined as

$$T_B(\theta, \phi) = \epsilon(\theta, \phi)T_m = (1 - |\Gamma|^2)T_m \tag{2-144}$$

where

T_B = brightness temperature (equivalent temperature: K)
ϵ = emissivity (dimensionless)
T_m = molecular (physical) temperature (K)
$\Gamma(\theta, \phi)$ = reflection coefficient of the surface for the polarization of the wave

Since the values of emissivity are $0 \leq \epsilon \leq 1$, the maximum value the brightness temperature can achieve is equal to the molecular temperature. Usually the emissivity is a function of the frequency of operation, polarization of the emitted energy, and molecular structure of the object. Some of the better natural emitters of energy at microwave frequencies are (a) the ground with equivalent temperature of about 300 K and (b) the sky with equivalent temperature of about 5 K when looking toward zenith and about 100–150 K toward the horizon.

The brightness temperature emitted by the different sources is intercepted by antennas, and it appears at their terminals as an antenna temperature. The temperature appearing at the terminals of an antenna is that given by (2-144), after it is weighted by the gain pattern of the antenna. In equation form, this can be written as

$$T_A = \frac{\int_0^{2\pi}\int_0^{\pi} T_B(\theta, \phi)\, G(\theta, \phi) \sin\theta\, d\theta\, d\phi}{\int_0^{2\pi}\int_0^{\pi} G(\theta, \phi) \sin\theta\, d\theta\, d\phi} \tag{2-145}$$

where

T_A = antenna temperature (effective noise temperature of the antenna radiation resistance: K)
$G(\theta, \phi)$ = gain (power) pattern of the antenna

Assuming no losses or other contributions between the antenna and the receiver, the noise power transferred to the receiver is given by

$$P_r = kT_A\Delta f \tag{2-146}$$

where

P_r = antenna noise power (W)
k = Boltzmann's constant (1.38×10^{-23} J/K)

INTEL-1045
U.S. Patent 7,151,430

T_A = antenna temperature (K)
Δf = bandwidth (Hz)

If the antenna and transmission line are maintained at certain physical temperatures, and the transmission line between the antenna and receiver is lossy, the antenna temperature T_A as seen by the receiver through (2-146) must be modified to include the other contributions and the line losses. If the antenna itself is maintained at a certain physical temperature T_p and a transmission line of length l, constant physical temperature T_0 throughout its length, and uniform attenuation of α (Np/unit length) is used to connect an antenna to a receiver, as shown in Figure 2.29, the effective antenna temperature at the receiver terminals is given by

$$T_a = T_A e^{-2\alpha l} + T_{AP} e^{-2\alpha l} + T_0(1 - e^{-2\alpha l}) \tag{2-147}$$

where

$$T_{AP} = \left(\frac{1}{e_A} - 1\right) T_p \tag{2-147a}$$

T_a = antenna temperature at the receiver terminals (K)
T_A = antenna noise temperature at the antenna terminals (2-145) (K)
T_{AP} = antenna temperature at the antenna terminals due to physical temperature (2-147a) (K)
T_p = antenna physical temperature (K)
α = attenuation coefficient of transmission line (Np/m)
e_A = thermal efficiency of antenna (dimensionless)
l = length of transmission line (m)
T_0 = physical temperature of the transmission line (K)

The antenna noise power of (2-146) must also be modified and written as

$$P_r = kT_a\Delta f \tag{2-148}$$

where T_a is the antenna temperature at the receiver input as given by (2-147).

If the receiver itself has a certain noise temperature T_r (due to thermal noise in the receiver components), the *system noise power at the receiver terminals* is given by

$$P_s = k(T_a + T_r)\Delta f = kT_s\Delta f \tag{2-149}$$

where

P_s = system noise power (at receiver terminals)
T_a = antenna noise temperature (at receiver terminals)
T_r = receiver noise temperature (at receiver terminals)
$T_s = T_a + T_r$ = effective system noise temperature (at receiver terminals)

A graphical relation of all the parameters is shown in Figure 2.29. The effective system noise temperature T_s of radio astronomy antennas and receivers varies from very few degrees (typically $\simeq$ 10 K) to thousands of Kelvins depending upon the type

INTEL-1045
U.S. Patent 7,151,430

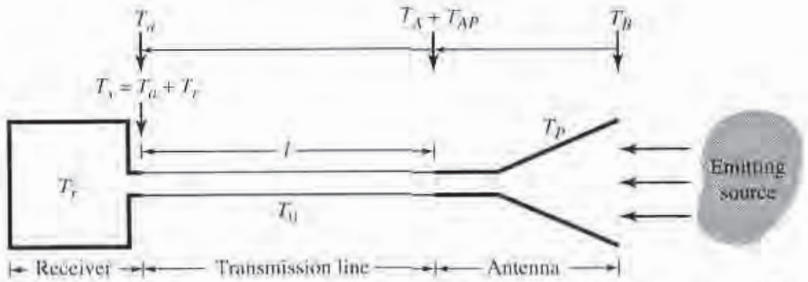


Figure 2.29 Antenna, transmission line, and receiver arrangement for system noise power calculation.

of antenna, receiver, and frequency of operation. Antenna temperature changes at the antenna terminals, due to variations in the target emissions, may be as small as a fraction of one degree. To detect such changes, the receiver must be very sensitive and be able to differentiate changes of a fraction of a degree.

Example 2.16

The effective antenna temperature of a target at the input terminals of the antenna is 150 K. Assuming that the antenna is maintained at a thermal temperature of 300 K and has a thermal efficiency of 99% and it is connected to a receiver through an *X*-band (8.2–12.4 GHz) rectangular waveguide of 10 m (loss of waveguide = 0.13 dB/m) and at a temperature of 300 K, find the effective antenna temperature at the receiver terminals.

SOLUTION

We first convert the attenuation coefficient from dB to Np by $\alpha(\text{dB/m}) = 20(\log_{10} e)\alpha(\text{Np/m}) = 20(0.434)\alpha(\text{Np/m}) = 8.68\alpha(\text{Np/m})$. Thus $\alpha(\text{Np/m}) = \alpha(\text{dB/m})/8.68 = 0.13/8.68 = 0.0149$. The effective antenna temperature at the receiver terminals can be written, using (2-147) and (2-147a), as

$$T_{AP} = 300\left(\frac{1}{0.99} - 1\right) = 3.03$$

$$T_a = 150e^{-0.149(2)} + 3.03e^{-0.149(2)} + 300[1 - e^{-0.149(2)}]$$
$$= 111.345 + 2.249 + 77.31 = 190.904 \text{ K}$$

The results of the above example illustrate that the antenna temperature at the input terminals of the antenna and at the terminals of the receiver can differ by quite a few degrees. For a smaller transmission line or a transmission line with much smaller losses, the difference can be reduced appreciably and can be as small as a fraction of a degree.

INTEL-1045
U.S. Patent 7,151,430

References

1. A. Z. Elsherbeni and C. D. Taylor Jr., "Antenna Pattern Plotter," Copyright © 1995, Electrical Engineering Department, The University of Mississippi, University, MS.
2. J. S. Hollis, T. J. Lyon, and L. Clayton Jr. (eds.), *Microwave Antenna Measurements*, Scientific-Atlanta, Inc., July 1970.
3. W. R. Scott Jr., "A General Program for Plotting Three-dimensional Antenna Patterns," *IEEE Antennas and Propagation Society Newsletter*, pp. 6–11, December 1989.
4. A. Z. Elsherbeni and C. D. Taylor Jr., "Interactive Antenna Pattern Visualization," Software Book in Electromagnetics, Vol. II, Chapter 8, CAEME Center for Multimedia Education, University of Utah, pp. 367–410, 1995.
5. A. Z. Elsherbeni and P. H. Ginn, "Interactive Analysis of Antenna Arrays," Software Book in Electromagnetics, Vol. II, Chapter 6, CAEME Center for Multimedia Education, University of Utah, pp. 337–366, 1995.
6. J. Romeu and R. Pujol, "Array," Software Book in Electromagnetics, Vol. II, Chapter 12, CAEME Center for Multimedia Education, University of Utah, pp. 467–481, 1995.
7. J. D. Kraus, *Antennas*, McGraw-Hill, New York, 1988.
8. R. S. Elliott, "Beamwidth and Directivity of Large Scanning Arrays," Last of Two Parts, *The Microwave Journal*, January 1964, pp. 74–82.
9. C.-T. Tai and C. S. Pereira, "An Approximate Formula for Calculating the Directivity of an Antenna," *IEEE Trans. Antennas Propagat.*, Vol. AP-24, No. 2, March 1976, pp. 235–236.
10. N. A. McDonald, "Approximate Relationship Between Directivity and Beamwidth for Broadside Collinear Arrays," *IEEE Trans. Antennas Propagat.*, Vol. AP-26, No. 2, pp. 340–341, March 1978.
11. D. M. Pozar, "Directivity of Omnidirectional Antennas," *IEEE Antennas and Propagation Magazine*, Vol. 35, No. 5, pp. 50–51, October 1993.
12. J. D. Kraus, Radio Astronomy, McGraw-Hill Book Co., pp. 170–171, 1966.
13. C. A. Balanis, *Advanced Engineering Electromagnetics*, John Wiley and Sons, New York, 1989.
14. H. Poincaré, *Theorie Mathematique de la Limiere*, Georges Carre, Paris, France, 1892.
15. G. A. Deschamps, "Part II—Geometrical Representation of the Polarization of a Plane Electromagnetic Wave," *Proc. IRE*, Vol. 39, pp. 540–544, May 1951.
16. E. F. Bolinder, "Geometrical Analysis of Partially Polarized Electromagnetic Waves," *IEEE Trans. Antennas Propagat.*, Vol. AP-15, No. 1, pp. 37–40, January 1967.
17. G. A. Deschamps and P. E. Mast, "Poincaré Sphere Representation of Partially Polarized Fields," *IEEE Trans. Antennas Propagat.*, Vol. AP-21, No. 4, pp. 474–478, July 1973.
18. G. Sinclair, "The Transmission and Reflection of Elliptically Polarized Waves," *Proc. IRE*, Vol. 38, pp. 148–151, February 1950.
19. C. A. Balanis, "Antenna Theory: A Review," *Proc. IEEE*, Vol. 80, No. 1, pp. 7–23, January 1992.
20. R. E. Collin, *Antennas and Radiowave Propagation*, McGraw-Hill Book Co., New York, 1985.
21. M. I. Skolnik, *Radar Systems*, Chapter 2, McGraw-Hill Book Co., New York, 1962.
22. J. A. Adam, "How to Design an "Invisible' Aircraft," *IEEE Spectrum*, pp. 26–31, April 1988.
23. G. T. Ruck, D. E. Barrick, W. D. Stuart, and C. K. Krichbaum, *Radar Cross Section Handbook*, Vols. 1, 2, Plenum Press, New York, 1970.
24. M. I. Skolnik (Ed.), *Radar Handbook*, Chapter 27, Section 6, pp. 27-19 to 27-40, McGraw-Hill Book Co., New York, 1970.
25. J. W. Crispin, Jr. and K. M. Siegel, *Methods of Radar Cross Section Analysis*, Academic Press, Inc., New York, 1968.

INTEL-1045
U.S. Patent 7,151,430

26. J. J. Bowman, T. B. A. Senior, and P. L. Uslenghi (Eds.), *Electromagnetic and Acoustic Scattering by Simple Shapes*, Amsterdam, The Netherlands: North-Holland, 1969.
27. E. F. Knott, M. T. Turley, and J. F. Shaeffer, *Radar Cross Section*, Artech House, Inc., Norwood, MA, 1985.
28. A. K. Bhattacharya and D. L. Sengupta, *Radar Cross Section Analysis and Control*, Artech House, Inc., Norwood, MA, 1991.
29. A. F. Maffett, *Topics for a Statistical Description of Radar Cross Section*, John Wiley and Sons, New York, 1989.
30. Special issue, *Proc. IEEE*, Vol. 53, No. 8, August 1965.
31. Special issue, *Proc. IEEE*, Vol. 77, No. 5, May 1989.
32. Special issue, *IEEE Trans. Antennas Propagat.*, Vol. 37, No. 5, May 1989.
33. W. R. Stone (ed.), *Radar Cross Sections of Complex Objects*, IEEE Press, New York, 1989.
34. A. F. Stevenson, "Relations between the transmitting and receiving properties of antennas," *Quart. Appl. Math.*, pp. 369–384, January 1948.
35. R. F. Harrington, "Theory of loaded scatterers," *Proc. IEE* (British), Vol. 111, pp. 617–623, April 1964.
36. R. E. Collin, "The receiving antenna," in *Antenna Theory, Part I*, (R. E. Collin and F. J. Zucker, Eds.), McGraw-Hill Book Co., 1969.
37. R. B. Green, "The effect of antenna installations on the echo area of an object," Report No. 1109-3, ElectroScience Lab., Ohio State Univ., Columbus, OH, September 1961.
38. R. B. Green "Scattering from conjugate-matched antennas," *IEEE Trans. Antennas Propagat.*, Vol. AP-14, No. 1, pp. 17–21, January 1966.
39. R. J. Garbacz, "The determination of antenna parameters by scattering cross-section measurements. III. Antenna Scattering Cross Section," Antenna Lab., Ohio State University, Report No. 1223-10, November 1962.
40. R. C. Hansen, "Relationships between antennas as scatterers and as radiators," *Proc. IEEE*, Vol. 77, No. 5, pp. 659–662, May 1989.
41. S. H. Dike and D. D. King, "Absorption gain and backscattering cross section of the cylindrical antenna," *Proc. IRE*, Vol. 40, 1952.
42. J. Sevick, "Experimental and theoretical results on the backscattering cross section of coupled antennas," Cruft Lab., Harvard Univ., Tech. Report No. 150, May 1952.
43. D. L. Moffatt, "Determination of antenna scattering properties from model measurements," Antenna Lab., Ohio State Univ., Report No. 1223-12, January 1964.
44. J. T. Aberle, Analysis of Probe-Fed Circular Microstrip Antennas, PhD Dissertation, University of Mass., Amherst, MA, 1989.
45. J. T. Aberle, D. M. Pozar, and C. R. Birtcher, "Evaluation of Input Impedance and Radar Cross Section of Probe-Fed Microstrip Patch Elements Using an Accurate Feed Model," *IEEE Trans. Antennas Propagat.*, Vol. 39, No. 12, pp. 1691–1696, December 1991.
46. J. D. Kraus, *Radio Astronomy*, McGraw-Hill, New York, 1966.

PROBLEMS

2.1. Derive (2-7) given the definitions of (2-5) and (2-6)

2.2. A hypothetical isotropic antenna is radiating in free space. At a distance of 100 m from the antenna, the total electric field (E_θ) is measured to be 5 V/m. Find
(a) the power density (W_{rad})
(b) the power radiated (P_{rad})

2.3. The maximum radiation intensity of a 90% efficiency antenna is 200 mW/unit solid angle. Find the directivity and gain (dimensionless and in dB) when the
(a) input power is 125.66 mW
(b) radiated power is 125.66 mW

INTEL-1045
U.S. Patent 7,151,430

2.4. The power radiated by a lossless antenna is 10 Watts. The directional characteristics of the antenna are represented by the radiation intensity of

$$U = B_0 \cos^3\theta \qquad \text{(W/unit solid angle)} \qquad 0 \le \theta \le \pi/2, \quad 0 \le \phi \le 2\pi$$

Find the
(a) maximum power density (in watts per square meter) at a distance of 1000 m (assume far field distance). Specify the angle where this occurs.
(b) directivity of the antenna (dimensionless and in dB)
(c) gain of the antenna (dimensionless and in dB)

2.5. In target-search ground-mapping radars it is desirable to have echo power received from a target, of constant cross section, to be independent of its range. For one such application, the desirable radiation intensity of the antenna is given by

$$U(\theta, \phi) = \left\{ \begin{array}{cc} 1 & 0° \le \theta < 20° \\ 0.342 \csc(\theta) & 20° \le \theta < 60° \\ 0 & 60° \le \theta \le 180° \end{array} \right\} 0° \le \phi \le 360°$$

Find the directivity (in dB) using the exact formula.

2.6. A beam antenna has half-power beamwidths of 30° and 35° in perpendicular planes intersecting at the maximum of the mainbeam. Find its approximate maximum effective aperture (in λ^2) using (a) Kraus' and (b) Tai and Pereira's formulas. The minor lobes are very small and can be neglected.

2.7. The normalized radiation intensity of a given antenna is given by
(a) $U = \sin\theta \sin\phi$ (b) $U = \sin\theta \sin^2\phi$
(c) $U = \sin\theta \sin^3\phi$ (d) $U = \sin^2\theta \sin\phi$
(e) $U = \sin^2\theta \sin^2\phi$ (f) $U = \sin^2\theta \sin^3\phi$
The intensity exists only in the $0 \le \theta \le \pi$, $0 \le \phi \le \pi$ region, and it is zero elsewhere. Find the
(a) exact directivity (dimensionless and in dB).
(b) azimuthal and elevation plane half-power beamwidths (in degrees).

2.8. Find the directivity (dimensionless and in dB) for the antenna of Problem 2.7 using
(a) Kraus' approximate formula (2-26)
(b) Tai and Pereira's approximate formula (2-30a)

2.9. For Problem 2.5, determine the approximate directivity (in dB) using
(a) Kraus' formula
(b) Tai and Pereira's formula.

2.10. The normalized radiation intensity of an antenna is rotationally symmetric in ϕ, and it is represented by

$$U = \left\{ \begin{array}{ll} 1 & 0° \le \theta < 30° \\ 0.5 & 30° \le \theta < 60° \\ 0.1 & 60° \le \theta < 90° \\ 0 & 90° \le \theta \le 180° \end{array} \right.$$

(a) What is the directivity (above isotropic) of the antenna (in dB)?
(b) What is the directivity (above an infinitesimal dipole) of the antenna (in dB)?

2.11. The radiation intensity of an antenna is given by

$$U(\theta, \phi) = \cos^4\theta \sin^2\phi$$

for $0 \le \theta \le \pi/2$ and $0 \le \phi \le 2\pi$ (i.e., in the upper half-space). It is zero in the lower half-space.
Find the
(a) exact directivity (dimensionless and in dB)
(b) elevation plane half-power beamwidth (in degrees)

INTEL-1045
U.S. Patent 7,151,430

2.12. The normalized radiation intensity of an antenna is symmetric, and it can be approximated by

$$U(\theta) = \begin{cases} 1 & 0° \le \theta < 30° \\ \dfrac{\cos(\theta)}{0.866} & 30° \le \theta < 90° \\ 0 & 90° \le \theta \le 180° \end{cases}$$

and it is independent of ϕ. Find the
(a) exact directivity by integrating the function
(b) approximate directivity using Kraus' formula

2.13. The maximum gain of a horn antenna is +20 dB, while the gain of its first sidelobe is −15 dB. What is the difference in gain between the maximum and first sidelobe:
(a) in dB
(b) as a ratio of the field intensities.

2.14. The normalized radiation intensity of an antenna is approximated by

$$U = \sin\theta$$

where $0 \le \theta \le \pi$, and $0 \le \phi \le 2\pi$. Determine the directivity using the
(a) exact formula
(b) formulas of (2-33a) by McDonald and (2-33b) by Pozar
(c) computer program DIRECTIVITY at the end of the chapter

2.15. Repeat Problem 2.14 for a $\lambda/2$ dipole whose normalized intensity is approximated by

$$U \simeq \sin^4\theta$$

Compare the value with that of (4-91) or 1.643 (2.156 dB).

2.16. The radiation intensity of a circular loop of radius and a of constant current is given by

$$U = J_1^2(ka\sin\theta), \qquad 0 \le \theta \le \pi \quad \text{and} \quad 0 \le \phi \le 2\pi$$

where $J_1(x)$ is the Bessel function of order 1. For a loop with radii of $a = \lambda/10$ and $\lambda/20$, determine the directivity using the:
(a) formulas (2-33a) by McDonald and (2-33b) by Pozar.
(b) computer program DIRECTIVITY at the end of the chapter.
A subroutine to compute the Bessel function can be found in the computer program at the end of Chapter 5. Compare the answers with that of a very small loop represented by 1.5 or 1.76 dB.

2.17. Find the directivity (dimensionless and in dB) for the antenna of Problem 2.7 using numerical techniques with 10° uniform divisions and with the field evaluated at the
(a) midpoint
(b) trailing edge of each division

2.18. Compute the directivity values of Problem 2.7 using the directivity computer program at the end of this chapter.

2.19. The far-zone electric field intensity (array factor) of an end-fire two-element array antenna, placed along the z-axis and radiating into free-space, is given by

$$E = \cos\left[\frac{\pi}{4}(\cos\theta - 1)\right]\frac{e^{-jkr}}{r}, \qquad 0 \le \theta \le \pi$$

Find the directivity using
(a) Kraus' approximate formula
(b) the DIRECTIVITY computer program at the end of this chapter

2.20. Repeat Problem 2.19 when

$$E = \cos\left[\frac{\pi}{4}(\cos\theta + 1)\right]\frac{e^{-jkr}}{r}, \qquad 0 \le \theta \le \pi$$

INTEL-1045
U.S. Patent 7,151,430

2.21. The radiation intensity is represented by

$$U = \begin{cases} U_0 \sin(\pi \sin\theta), & 0 \le \theta \le \pi/2 \quad \text{and} \quad 0 \le \phi \le 2\pi \\ 0 & \text{elsewhere} \end{cases}$$

Find the directivity
(a) exactly
(b) using the computer program DIRECTIVITY at the end of the chapter.

2.22. The radiation intensity of an aperture antenna, mounted on an infinite ground plane with z perpendicular to the aperture, is rotationally symmetric (not a function of ϕ), and it is given by

$$U = \left[\frac{\sin(\pi \sin\theta)}{\pi \sin\theta}\right]^2$$

Find the approximate directivity (dimensionless and in dB) using
(a) numerical integration. Use the DIRECTIVITY computer program at the end of this chapter.
(b) Kraus' formula
(c) Tai and Pereira's formula

2.23. The normalized far-zone field pattern of an antenna is given by

$$E = \begin{cases} (\sin\theta \cos^2\phi)^{1/2} & 0 \le \theta \le \pi \quad \text{and} \quad 0 \le \phi \le \pi/2, \\ & 3\pi/2 \le \phi \le 2\pi \\ 0 & \text{elsewhere} \end{cases}$$

Find the directivity using
(a) the exact expression
(b) Kraus' approximate formula
(c) Tai and Pereira's approximate formula
(d) the computer program DIRECTIVITY at the end of this chapter

2.24. The normalized field pattern of the main beam of a conical horn antenna, mounted on an infinite ground plane with z perpendicular to the aperture, is given by

$$\frac{J_1(ka \sin\theta)}{\sin\theta}$$

where a is its radius at the aperture. Assuming that $a = \lambda$, find the
(a) half-power beamwidth
(b) directivity using Kraus' approximate formula

2.25. A uniform plane wave, of a form similar to (2-55), is traveling in the positive z-axis. Find the polarization (linear, circular, or elliptical), sense of rotation (CW or CCW), axial ratio (AR), and tilt angle τ (in degrees) when
(a) $E_x = E_y$, $\Delta\phi = \phi_y - \phi_x = 0$ (b) $E_x \neq E_y$, $\Delta\phi = \phi_y - \phi_x = 0$
(c) $E_x = E_y$, $\Delta\phi = \phi_y - \phi_x = \pi/2$ (d) $E_x = E_y$, $\Delta\phi = \phi_y - \phi_x = -\pi/2$
(e) $E_x = E_y$, $\Delta\phi = \phi_y - \phi_x = \pi/4$ (f) $E_x = E_y$, $\Delta\phi = \phi_y - \phi_x = -\pi/4$
(g) $E_x = 0.5\,E_y$, $\Delta\phi = \phi_y - \phi_x = \pi/2$ (h) $E_x = 0.5\,E_y$, $\Delta\phi = \phi_y - \phi_x = -\pi/2$
In all cases, justify the answer.

2.26. Derive (2-66), (2-67), and (2-68).

2.27. Write a general expression for the polarization loss factor (PLF) of two linearly polarized antennas if
(a) both lie in the same plane
(b) both do not lie in the same plane

2.28. A linearly polarized wave traveling in the positive z-direction is incident upon a circularly polarized antenna. Find the polarization loss factor PLF (dimensionless and in dB) when the antenna is (based upon its transmission mode operation)
(a) right-handed (CW) (b) left-handed (CCW)

INTEL-1045
U.S. Patent 7,151,430

2.29. A circularly polarized wave, traveling in the positive z-direction, is incident upon a circularly polarized antenna. Find the polarization loss factor *PLF* (dimensionless and in dB) for right-hand (CW) and left-hand (CCW) wave and antenna.

2.30. The electric field radiated by a rectangular aperture, mounted on an infinite ground plane with z perpendicular to the aperture, is given by

$$\mathbf{E} = [\hat{\mathbf{a}}_\theta \cos\phi - \hat{\mathbf{a}}_\phi \sin\phi \cos\theta] f(r, \theta, \phi)$$

where $f(r, \theta, \phi)$ is a scalar function which describes the field variation of the antenna. Assuming that the receiving antenna is linearly polarized along the x-axis, find the polarization loss factor (PLF).

2.31. A circularly polarized wave, traveling in the $+z$-direction, is received by an elliptically polarized antenna whose reception characteristics near the main lobe are given approximately by

$$\mathbf{E}_a = [2\hat{\mathbf{a}}_x + j\hat{\mathbf{a}}_y] f(r, \theta, \phi)$$

Find the polarization loss factor PLF (dimensionless and in dB) when the incident wave is

(a) right-hand (CW)
(b) left-hand (CCW)

circularly polarized. Repeat the problem when

$$\mathbf{E}_a = [2\hat{\mathbf{a}}_x - j\hat{\mathbf{a}}_y] f(r, \theta, \phi)$$

In each case, what is the polarization of the antenna? How does it match with that of the wave?

2.32. A linearly polarized wave traveling in the negative z direction has a tilt angle (τ) of 45°. It is incident upon an antenna whose polarization characteristics are given by

$$\hat{\boldsymbol{\rho}}_a = \frac{4\hat{\mathbf{a}}_x + j\hat{\mathbf{a}}_y}{\sqrt{17}}$$

Find the polarization loss factor PLF (dimensionless and db).

2.33. An elliptically polarized wave traveling in the negative z-direction is received by a circularly polarized antenna whose main lobe is along the $\theta = 0$ direction. The unit vector describing the polarization of the incident wave is given by

$$\hat{\boldsymbol{\rho}}_w = \frac{2\hat{\mathbf{a}}_x + j\hat{\mathbf{a}}_y}{\sqrt{5}}$$

Find the polarization loss factor PLF (dimensionless and in dB) when the wave that would be transmitted by the antenna is

(a) right-hand CP
(b) left-hand CP

2.34. A CW circularly polarized uniform plane wave is traveling in the $+z$ direction. Find the polarization loss factor PLF (dimensionless and in dB) assuming the receiving antenna (in its transmitting mode) is

(a) CW circularly polarized
(b) CCW circularly polarized

2.35. A linearly polarized uniform plane wave traveling in the $+z$ direction, with a power density of 10 milliwatts per square meter, is incident upon a CW circularly polarized antenna whose gain is 10 dB at 10 GHz. Find the

(a) maximum effective area of the antenna (in square meters)
(b) power (in watts) that will be delivered to a load attached directly to the terminals of the antenna

2.36. A linearly polarized plane wave traveling along the negative z-axis is incident upon an elliptically polarized antenna (either CW or CCW). The axial ratio of the antenna

INTEL-1045
U.S. Patent 7,151,430

polarization ellipse is 2:1 and its major axis coincides with the principal x-axis. Find the polarization loss factor (PLF) assuming the incident wave is linearly polarized in the

(a) x-direction

(b) y-direction

2.37. A wave traveling normally outward from the page (toward the reader) is the resultant of two elliptically polarized waves, one with components of $\mathbf{E}$ given by:

$$\mathscr{E}_y' = 3\cos\omega t$$

$$\mathscr{E}_x' = 7\cos\left(\omega t + \frac{\pi}{2}\right)$$

and the other with components given by:

$$\mathscr{E}_y'' = 2\cos\omega t$$

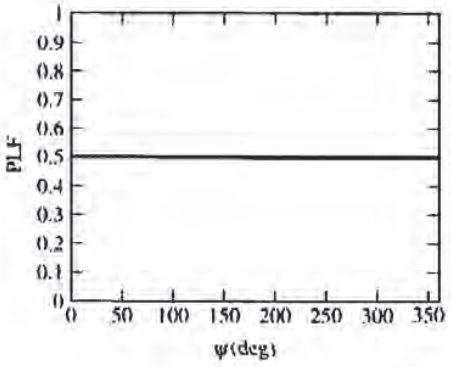
$$\mathscr{E}_x'' = 3\cos\left(\omega t - \frac{\pi}{2}\right)$$

(a) What is the axial ratio of the resultant wave?

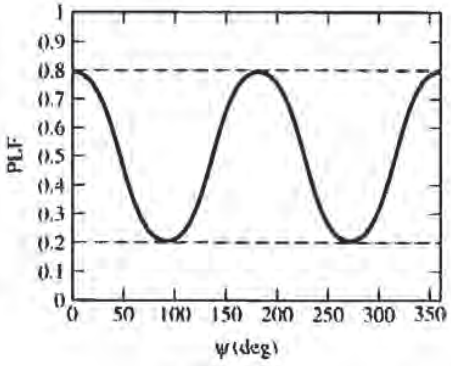
(b) Does the resultant vector $\mathbf{E}$ rotate clockwise or counterclockwise?

2.38. A linearly polarized antenna lying in the x-y plane is used to determine the polarization axial ratio of incoming plane waves traveling in the negative z-direction. The polarization of the antenna is described by the unit vector

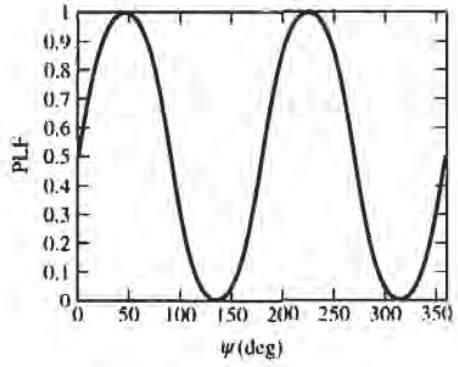
$$\hat{\boldsymbol{\rho}}_a = \hat{\mathbf{a}}_x \cos\psi + j\hat{\mathbf{a}}_y \sin\psi$$



(a) PLF versus ψ



(b) PLF versus ψ



(c) PLF versus ψ

INTEL-1045
U.S. Patent 7,151,430

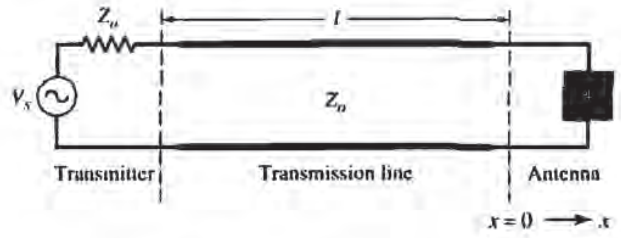
where ψ is an angle describing the orientation in the x-y plane of the receiving antenna. Below are the polarization loss factor (PLF) versus receiving antenna orientation curves obtained for three different incident plane waves. For each curve determine the axial ratio of the incident plane wave.

2.39. A $\lambda/2$ dipole, with a total loss resistance of 1 ohm, is connected to a generator whose internal impedance is $50 + j25$ ohms. Assuming that the peak voltage of the generator is 2 V and the impedance of the dipole, excluding the loss resistance, is $73 + j42.5$ ohms, find the power
(a) supplied by the source (real)
(b) radiated by the antenna
(c) dissipated by the antenna

2.40. The antenna and generator of Problem 2.39 are connected via a 50-ohm $\lambda/2$-long lossless transmission line. Find the power
(a) supplied by the source (real)
(b) radiated by the antenna
(c) dissipated by the antenna

2.41. An antenna with a radiation resistance of 48 ohms, a loss resistance of 2 ohms, and a reactance of 50 ohms is connected to a generator with open-circuit voltage of 10 V and internal impedance of 50 ohms via a $\lambda/4$-long transmission line with characteristic impedance of 100 ohms.
(a) Draw the equivalent circuit
(b) Determine the power supplied by the generator
(c) Determine the power radiated by the antenna

2.42. A transmitter, with an internal impedance Z_0 (real), is connected to an antenna through a lossless transmission line of length l and characteristic impedance Z_0. Find a *simple* expression for the ratio between the antenna gain and its realized gain.



$$V(x) = A\left[e^{-jkx} + \Gamma(0)e^{+jkx}\right]$$
$$I(x) = \frac{A}{Z_0}\left[e^{-jkx} - \Gamma(0)e^{+jkx}\right]$$

V_s = strength of voltage source
$Z_{in} = R_{in} + jX_{in}$ = input impedance of the antenna
$Z_0 = R_0$ = characteristic impedance of the line
$P_{accepted}$ = power accepted by the antenna $\{P_{accepted} = \mathrm{Re}[V(0)I^*(0)]\}$
$P_{available}$ = power delivered to a matched load [i.e., $Z_{in} = Z_0^* = Z_0$]

2.43. The input reactance of an infinitesimal linear dipole of length $\lambda/60$ and radius $a = \lambda/200$ is given by

$$X_{in} = -120\frac{[\ln(\ell/a) - 1]}{\tan(k\ell)}$$

Assuming the wire of the dipole is copper with a conductivityof 5.7×10^7 S/m, determine at $f = 1$ GHz the
(a) loss resistance
(b) radiation resistance
(c) radiation efficiency
(d) VSWR when the antenna is connected to a 50-ohm line

INTEL-1045
U.S. Patent 7,151,430

2.44. A dipole antenna consists of a circular wire of length l. Assuming the current distribution on the wire is cosinusoidal, i.e.,

$$I_s(z) = I_0 \cos\left(\frac{\pi}{l} z'\right) \qquad -l/2 \le z' \le l/2$$

where I_0 is a constant, derive an expression for the loss resistance R_L, which is one-half of (2-90b).

2.45. The E-field pattern of an antenna, independent of ϕ, varies as follows:

$$E = \begin{cases} 1 & 0° \le \theta \le 45° \\ 0 & 45° < \theta \le 90° \\ \frac{1}{2} & 90° < \theta \le 180° \end{cases}$$

(a) What is the directivity of this antenna?

(b) What is the radiation resistance of the antenna at 200 m from it if the field is equal to 10 V/m (rms) for $\theta = 0°$ at that distance and the terminal current is 5 A (rms)?

2.46. A 1-m long dipole antenna is driven by a 150 MHz source having a source resistance of 50 ohms and a voltage of 100 V. If the ohmic resistance of the antennas is given by $R_L = 0.625$ ohms, find:

(a) The current going into the antenna (I_{in})

(b) The average power dissipated by the antenna

(c) The average power radiated by the antenna

(d) The radiation efficiency of the antenna

2.47. Show that the effective length of a linear antenna can be written as

$$l_e = \sqrt{\frac{A_e |Z_t|^2}{\eta R_t}}$$

which for a lossless antenna and maximum power transfer reduces to

$$l_e = 2\sqrt{\frac{A_{em} R_t}{\eta}}$$

A_e and A_{em} represent, respectively, the effective and maximum effective apertures of the antenna while η is the intrinsic impedance of the medium.

2.48. An antenna has a maximum effective aperture of 2.147 m^2 at its operating frequency of 100 MHz. It has no conduction or dielectric losses. The input impedance of the antenna itself is 75 ohms, and it is connected to a 50-ohm transmission line. Find the directivity of the antenna system ("system" meaning includes any effects of connection to the transmission line). Assume no polarization losses.

2.49. An incoming wave, with a uniform power density equal to 10^{-3} W/m^2 is incident normally upon a lossless horn antenna whose directivity is 20 dB. At a frequency of 10 GHz, determine the very maximum possible power that can be expected to be delivered to a receiver or a load connected to the horn antenna. There are no losses between the antenna and the receiver or load.

2.50. For an X-band (8.2–12.4 GHz) rectangular horn, with aperture dimensions of 5.5 cm and 7.4 cm, find its maximum effective aperture (in cm^2) when its gain (over isotropic) is

(a) 14.8 dB at 8.2 GHz

(b) 16.5 dB at 10.3 GHz

(c) 18.0 dB at 12.4 GHz

2.51. A 30-dB, right-circularly polarized antenna in a radio link radiates 5 W of power at 2 GHz. The receiving antenna has an impedance mismatch at its terminals, which leads to a VSWR of 2. The receiving antenna is about 95% efficient and has a field pattern near the beam maximum given by $\mathbf{E}_R = (2\hat{\mathbf{a}}_\theta + j\hat{\mathbf{a}}_\phi) F_R(\theta, \phi)$. The distance between

INTEL-1045
U.S. Patent 7,151,430

the two antennas is 4,000 km, and the receiving antenna is required to deliver 10^{-14} W to the receiver. Determine the maximum effective aperture of the receiving antenna.

2.52. The radiation intensity of an antenna can be approximated by

$$U(\theta, \phi) = \begin{cases} \cos^4(\theta) & 0° \le \theta < 90° \\ 0 & 90° \le \theta \le 180° \end{cases} \quad \text{with } 0° \le \phi \le 360°$$

Determine the maximum effective aperture (*in* m^2) of the antenna if its frequency of operation is $f = 10$ GHz.

2.53. A communication satellite is in stationary (synchronous) orbit about the earth (assume altitude of 22,300 statute miles). Its transmitter generates 8.0 W. Assume the transmitting antenna is isotropic. Its signal is received by the 210-ft diameter tracking paraboloidal antenna on the earth at the NASA tracking station at Goldstone, California. Also assume no resistive loss in either antenna, perfect polarization match, and perfect impedance match at both antennas. At a frequency of 2 GHz, determine the:
(a) power density (in watts/m^2) incident on the receiving antenna.
(b) power received by the ground-based antenna whose gain is 60 dB.

2.54. A lossless ($e_{cd} = 1$) antenna is operating at 100 MHz and its maximum effective aperture is 0.7162 m^2 at this frequency. The input impedence of this antenna is 75 ohms, and it is attached to a 50-ohm transmission line. Find the directivity (dimensionless) of this antenna if it is polarization matched.

2.55. A resonant, lossless ($e_{cd} = 1.0$) half-wavelength dipole antenna, having a directivity of 2.156 dB, has an input impedance of 73 ohms and is connected to a lossless, 50 ohms transmission line. A wave, having the same polarization as the antenna, is incident upon the antenna with a power density of 5 W/m^2 at a frequency of 10 MHz. Find the received power available at the end of the transmission line.

2.56. Two *X*-band (8.2–12.4 GHz) rectangular horns, with aperture dimensions of 5.5 cm and 7.4 cm and each with a gain of 16.3 dB (over isotropic) at 10 GHz, are used as transmitting and receiving antennas. Assuming that the input power is 200 mW, the VSWR of each is 1.1, the conduction-dielectric efficiency is 100%, and the antennas are polarization-matched, find the maximum received power when the horns are separated *in air by*
(a) 5 m
(b) 50 m
(c) 500 m

2.57. Transmitting and receiving antennas operating at 1 GHz with gains (over isotropic) of 20 and 15 dB, respectively, are separated by a distance of 1 km. Find the maximum power delivered to the load when the input power is 150 W. Assume that the
(a) antennas are polarization-matched
(b) transmitting antenna is circularly polarized (either right- or left-hand) and the receiving antenna is linearly polarized.

2.58. Two lossless, polarization matched antennas are aligned for maximum radiation between them, and are separated by a distance of 50λ. The antennas are matched to their transmission lines and have directivities of 20 dB. Assuming that the power at the input terminals of the transmitting antenna is 10 W, find the power at the terminals of the receiving antenna.

2.59. Repeat Problem 2.58 for two antennas with 30 dB directivities and separated by 100λ. The power at the input terminals is 20 W.

2.60. Transmitting and receiving antennas operating at 1 GHz with gains of 20 and 15 dB, respectively, are separated by a distance of 1 km. Find the power delivered to the load when the input power is 150 W. Assume the PLF = 1.

2.61. A series of microwave repeater links operating at 10 GHz are used to relay television signals into a valley that is surrounded by steep mountain ranges. Each repeater consists of a receiver, transmitter, antennas and associated equipment. The transmitting and

INTEL-1045
U.S. Patent 7,151,430

receiving antennas are identical horns, each having gain over isotropic of 15 dB. The repeaters are separated in distance by 10 km. For acceptable signal-to-noise ratio, the power received at each repeater must be greater than 10 nW. Loss due to polarization mismatch is not expected to exceed 3 dB. Assume matched loads and free space propagation conditions. Determine the minimum transmitter power that should be used.

2.62. A one-way communication system, operating at 100 MHz, uses two identical $\lambda/2$ vertical, resonant, and lossless dipole antennas as transmitting and receiving elements separated by 10 km. In order for the signal to be detected by the receiver, the power level at the receiver terminals must be at least 1 μW. Each antenna is connected to the transmitter and receiver by a lossless 50-Ω transmission line. Assuming the antennas are polarization-matched and are aligned so that the maximum intensity of one is directed toward the maximum radiation intensity of the other, determine the minimum power that must be generated by the transmitter so that the signal will be detected by the receiver. Account for the proper losses from the transmitter to the receiver.

2.63. In a long-range microwave communication system operating at 9 GHz, the transmitting and receiving antennas are identical, and they are separated by 10,000 m. To meet the signal-to-noise ratio of the receiver, the received power must be at least 10 μW. Assuming the two antennas are aligned for maximum reception to each other, including being polarization matched, what should the gains (in dB) of the transmitting and receiving antennas be when the input power to the transmitting antenna is 10 W?

2.64. A rectangular *X*-band horn, with aperture dimensions of 5.5 cm and 7.4 cm and a gain of 16.3 dB (over isotropic) at 10 GHz, is used to transmit and receive energy scattered from a perfectly conducting sphere of radius $a = 5\lambda$. Find the maximum scattered power delivered to the load when the distance between the horn and the sphere is
(a) 200λ
(b) 500λ
Assume that the input power is 200 mW, and the radar cross section is equal to the geometrical cross section.

2.65. A radar antenna, used for both transmitting and receiving, has a gain of 150 (dimensionless) at its operating frequency of 5 GHz. It transmits 100 kW, and is aligned for maximum directional radiation and reception to a target 1 km away having a radar cross section of 3 m^2. The received signal matches the polarization of the transmitted signal. Find the received power.

2.66. In an experiment to determine the radar cross-section of a Tomahawk cruise missle, a 1,000 W, 300 MHz signal was transmitted toward the target, and the received power was measured to be 0.1425 mW. The same antenna, whose gain was 75, was used for both transmitting and receiving. The polarizations of both signals were identical (PLF = 1), and the distance between the antenna and missile was 500 m. What is the radar cross section of the cruise missile?

2.67. Repeat Problem 2.66 for a radar system with 1,000 W, 100 MHz transmitted signal, 0.01 W received signal, an antenna with a gain of 75, and separation between the antenna and target of 700 m.

2.68. Transmitting and receiving antennas operating at 1 GHz with gains (over isotropic) of 20 and 15 dB, respectively, are separated by a distance of 1 km. Find the maximum power delivered to the load when the input power is 150 W. Assume that the
(a) antennas are polarization-matched
(b) transmitting antenna is circularly polarized (either right- or left-hand) and the receiving antenna is linearly polarized.

2.69. The maximum radar cross section of a resonant linear $\lambda/2$ dipole is approximately $0.86\lambda^2$. For a monostatic system (i.e., transmitter and receiver at the same location), find the received power (in W) if the transmitted power is 100 W, the distance of the dipole from the transmitting and receiving antennas is 100 m, the gain of the transmitting and receiving antennas is 15 dB each, and the frequency of operation is 3 GHz. Assume a polarization loss factor of -1 dB.

INTEL-1045
U.S. Patent 7,151,430

2.70. The effective antenna temperature of an antenna looking toward zenith is approximately 5 K. Assuming that the temperature of the transmission line (waveguide) is 72°F, find the effective temperature at the receiver terminals when the attenuation of the transmission line is 4 dB/100 ft and its length is
(a) 2 ft
(b) 100 ft
Compare it to a receiver noise temperature of about 54 K.

2.71. Derive (2-147). Begin with an expression that assumes that the physical temperature and the attenuation of the transmission line are not constant.

INTEL-1045
U.S. Patent 7,151,430

COMPUTER PROGRAM
2-D ANTENNA PATTERN PLOTTER: RECTANGULAR - POLAR

```
C**********************************************************************
C            THIS PROGRAM IS COPYRIGHTED BY
C
C                        Copyright (c) 1995
C              Atef Z. Elsherbeni and Clayborne D. Taylor, Jr.
C                    Electrical Engineering Department
C              The University of Mississippi, University, MS 38677
C
C PERMISSION IS GRANTED, FOR THE EXECUTABLE PART OF THE
C PROGRAM, TO THE AUTHOR OF THIS BOOK BY THE AUTHORS
C OF THE PROGRAM, TO BE USED IN CONJUNCTION WITH THIS
C BOOK AND NOT FOR ANY OTHER PURPOSE.
C
C  THIS PROGRAM IS A GENERAL PURPOSE 2D RECTANGULAR
C  AND POLAR PATTERN PLOTTER.  THE USER INTERFACE FOR
C  DOS MAKES THE PROGRAM EASY TO USE.  HOWEVER, THERE
C  ARE FEW THINGS THE USER SHOULD KNOW TO USE THE
C  PROGRAM EFFECTIVELY.
C
C THE FORMAT FOR A DATA FILE MUST CONTAIN 2-COLUMN DATA.
C BASICALLY, THE FILED IS READ THROUGH A FORTRAN FREE-FORMAT
C SPECIFICATION.  IF ANY ERRORS OCCUR DURING THE READ PROCESS,
C IT IS ABORTED WITH NO PLOT GIVEN.  THE FIRST COLUMN MUST BE THE
C ANGLE (in degrees).  THE SECOND COLUMN SHOULD BE THE FIELD VALUE
C THE MAXIMUM NUMBER OF POINTS THAT MAY BE READ IS CURRENTLY
C 2048 POINTS.  IF THE FILED IS LONGER, ONLY THE FIRST 2048 POINTS
C WILL BE PLOTTED.
C
C WHEN IN THE PLOT WINDOW "ON TOP", A PULL-DOWN MENU IS
C ACCESSIBLE BY HOLDING THE LEFT MOUSE BUTTON DOWN ON THE
C SMALL BOX IN THE TOP LEFT CORNER OF THE WINDOW.  FROM THERE,
C THE TYPE OF PLOT OR THE PLOT OPTIONS MAY BE SELECTED.  WHEN
C EDITING THE LABEL TEXT, GREEK CHARACTERS ARE AVAILABLE BY
C  FIRST TYPING THE \' KEY AND FOLLOW BY TYPING 'A'-'Z' OR 'a'-'z'.
C  A POSTSCRIPT FILE NAMED 'FONTLIST.PS' CONTAINING THE GREEK
C FONT KEY EQUIVALENTS MAY BE PRINTED FOR REFERENCE.  ALSO NOTE
C THAT THE ~ SYMBOL FROM THE KEYBOARD HAS BEEN REPLACED BY
C THE DEGREE SYMBOL.
C
C HARD COPY OUTPUT IS ONLY AVAILABLE FOR POSTSCRIPT
C DEVICES.  BEFORE PRINTING A PLOT, MAKE SURE THE
C PRINTER OPTIONS ARE ON THE DESIRED SETTINGS.  THIS IS
C DONE BY SELECTION OF THE 'PRINTER SETUP' OPTION.
C OUTPUT IS WRITTEN TO A FILE BY DEFAULT.  PRESSING ANY
C OF THE PORT BUTTONS WILL CHANGE THE OUTPUT TO THAT
C PORT.  NOTE THAT THE SERIAL PRINTERS CONNECTED
C THROUGH THE COM PORTS MUST BE PROPERLY CONFIGURE
C THROUGH DOS BEFORE RUNNING THE PROGRAM.  ALSO NOTE
C THAT COLOR POSTSCRIPT IS SUPPORTED BY SELECTING THE
C "COLOR" BUTTON.
C
C
```

(continued on next page)

INTEL-1045
U.S. Patent 7,151,430

```
C                                                          (continued)
C
C                                  DISCLAIMER
C  THE INFORMATION AND CODE IS PROVIDED AS DESCRIBED
C  ABOVE WITHOUT WARRANTY OF ANY KIND.  THE AUTHORS
C  WILL NOT BE LIABLE FOR ANY DAMAGES WHATSOEVER
C  INCLUDING DIRECT, INDIRECT, INCIDENTAL, CONSEQUENTIAL,
C  LOSS OF BUSINESS PROFITS OR SPECIAL DAMAGES DIRECTLY
C  OR INDIRECTLY RELATED TO THE USE OF THIS SOFTWARE.
C
C
C  *  THE PROTECTED MODE RUN-TIME DOS-EXTENDER IS THE
C     PROPERTY OF RATIONAL SYSTEMS, INC.
C
C  ** THE FONTS USED BY THIS SOFTWARE PACKAGE ARE THE
C     PROPERTY OF ADOBE SYSTEMS, INC.
C
C  FOR ADDITIONAL INFORMATION CONCERNING THIS CODE,
C  CONTACT THE AUTHORS OF THE CODE AT THE ABOVE ADDRESS
C
C*****************************************************************
```


INTEL-1045
U.S. Patent 7,151,430

COMPUTER PROGRAM - DIRECTIVITY

```
C*****************************************************************
C
C THIS IS A FORTRAN PROGRAM THAT COMPUTES THE:
C
C     I.  RADIATED POWER
C     II. MAXIMUM DIRECTIVITY
C
C OF ANY ANTENNA. THE MAXIMUM DIRECTIVITY IS CALCULATED
C USING THE TRAILING EDGE METHOD IN INCREMENTS OF 1° IN
C THETA AND 1° IN PHI.
C
C
C          **INPUT PARAMETERS
C          1. TL, TU:  LOWER AND UPPER LIMITS IN THETA (in degrees)
C          2. PL, PU:  LOWER AND UPPER LIMITS IN PHI (in degrees)
C          3. F(THETA, PHI): THE RADIATION INTENSITY FUNCTION
C
C          **NOTE
C          THE RADIATION INTENSITY FUNCTION F MUST BE PROVIDED
C          FOR A GIVEN ANTENNA, AND SHOULD BE INSERTED INTO
C          THE SUBROUTINE U.
C
C          **EXAMPLE
C          IF THE ANTENNA IS RADIATING ONLY IN THE UPPER
C          HEMISPHERE, THE LIMITS ON THETA ARE 0 AND 90 (degrees)
C          AND THE LIMITS IN PHI ARE 0 AND 360 (degrees)
C
C*****************************************************************
```


INTEL-1045
U.S. Patent 7,151,430

CHAPTER 3

RADIATION INTEGRALS AND AUXILIARY POTENTIAL FUNCTIONS

3.1 INTRODUCTION

In the analysis of radiation problems, the usual procedure is to specify the sources and then require the fields radiated by the sources. This is in contrast to the synthesis problem where the radiated fields are specified, and we are required to find the sources.

It is a very common practice in the analysis procedure to introduce auxiliary functions, known as *vector potentials,* which will aid in the solution of the problems. The most common vector potential functions are the **A** (magnetic vector potential) and **F** (electric vector potential). Another pair is the Hertz potentials $\mathbf{\Pi}_e$ and $\mathbf{\Pi}_h$. *Although the electric and magnetic field intensities* (**E** *and* **H**) *represent physically measurable quantities, among most engineers the potentials are strictly mathematical tools.* The introduction of the potentials often simplifies the solution even though it may require determination of additional functions. While it is possible to calculate the **E** and **H** fields directly from the source-current densities **J** and **M**, as shown in Figure 3.1, it is usually much simpler to calculate the auxiliary potential functions first and then determine the **E** and **H**. This two-step procedure is also shown in Figure 3.1.

The one-step procedure, through path 1, relates the **E** and **H** fields to **J** and **M** by integral relations. The two-step procedure, through path 2, relates the **A** and **F** (or $\mathbf{\Pi}_e$ and $\mathbf{\Pi}_h$) potentials to **J** and **M** by integral relations. The **E** and **H** are then determined simply by differentiating **A** and **F** (or $\mathbf{\Pi}_e$ and $\mathbf{\Pi}_h$). Although the two-step procedure requires both integration and differentiation, where path 1 requires only integration, the integrands in the two-step procedure are much simpler.

The most difficult operation in the two-step procedure is the integration to determine **A** and **F** (or $\mathbf{\Pi}_e$ and $\mathbf{\Pi}_h$). Once the vector potentials are known, then **E** and **H** can always be determined because any well-behaved function, no matter how complex, can always be differentiated.

INTEL-1045
U.S. Patent 7,151,430

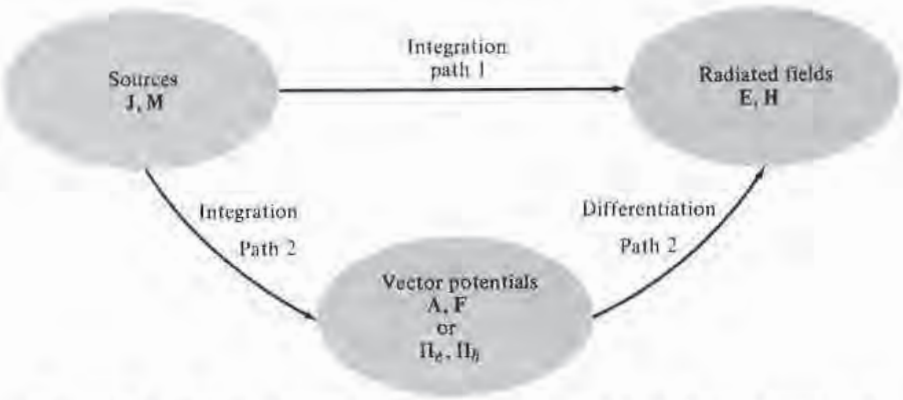


Figure 3.1 Block diagram for computing radiated fields from electric and magnetic sources.

The integration required to determine the potential functions is restricted over the bounds of the sources **J** and **M**. This will result in the **A** and **F** (or $\mathbf{\Pi}_e$ and $\mathbf{\Pi}_h$) to be functions of the observation point coordinates; the differentiation to determine **E** and **H** must be done in terms of the observation point coordinates. The integration in the one-step procedure also requires that its limits be determined by the bounds of the sources.

The vector Hertz potential $\mathbf{\Pi}_e$ is analogous to **A** and $\mathbf{\Pi}_h$ is analogous to **F**. The functional relation between them is a proportionality constant which is a function of the frequency and the constitutive parameters of the medium. In the solution of a problem, only one set, **A** and **F** or $\mathbf{\Pi}_e$ and $\mathbf{\Pi}_h$, is required. The author prefers the use of **A** and **F**, which will be used throughout the book. The derivation of the functional relations between **A** and $\mathbf{\Pi}_e$, and **F** and $\mathbf{\Pi}_h$ are assigned at the end of the chapter as problems. (Problems 3.1 and 3.2).

3.2 THE VECTOR POTENTIAL A FOR AN ELECTRIC CURRENT SOURCE J

The vector potential **A** is useful in solving for the EM field generated by a given harmonic electric current **J**. The magnetic flux **B** is always solenoidal; that is, $\nabla \cdot \mathbf{B} = 0$. Therefore, it can be represented as the curl of another vector because it obeys the vector identity

$$\nabla \cdot \nabla \times \mathbf{A} = 0 \tag{3-1}$$

where **A** is an arbitrary vector. Thus we define

$$\mathbf{B}_A = \mu \mathbf{H}_A = \nabla \times \mathbf{A} \tag{3-2}$$

or

$$\boxed{\mathbf{H}_A = \frac{1}{\mu} \nabla \times \mathbf{A}} \tag{3-2a}$$

where subscript A indicates the field due to the **A** potential. Substituting (3-2a) into Maxwell's curl equation

$$\nabla \times \mathbf{E}_A = -j\omega\mu \mathbf{H}_A \tag{3-3}$$

INTEL-1045
U.S. Patent 7,151,430

reduces it to

$$\nabla \times \mathbf{E}_A = -j\omega\mu\mathbf{H}_A = -j\omega\,\nabla \times \mathbf{A} \tag{3-4}$$

which can also be written as

$$\nabla \times [\mathbf{E}_A + j\omega\mathbf{A}] = 0 \tag{3-5}$$

From the vector identity

$$\nabla \times (-\nabla\,\phi_e) = 0 \tag{3-6}$$

and (3-5), it follows that

$$\mathbf{E}_A + j\omega\mathbf{A} = -\nabla\,\phi_e \tag{3-7}$$

or

$$\boxed{\mathbf{E}_A = -\nabla\,\phi_e - j\omega\mathbf{A}} \tag{3-7a}$$

The scalar function ϕ_e represents an arbitrary electric scalar potential which is a function of position.

Taking the curl of both sides of (3-2) and using the vector identity

$$\nabla \times \nabla \times \mathbf{A} = \nabla(\nabla \cdot \mathbf{A}) - \nabla^2\mathbf{A} \tag{3-8}$$

reduces it to

$$\nabla \times (\mu\mathbf{H}_A) = \nabla(\nabla \cdot \mathbf{A}) - \nabla^2\mathbf{A} \tag{3-8a}$$

For a homogeneous medium, (3-8a) reduces to

$$\mu\nabla \times \mathbf{H}_A = \nabla(\nabla \cdot \mathbf{A}) - \nabla^2\mathbf{A} \tag{3-9}$$

Equating Maxwell's equation

$$\boxed{\nabla \times \mathbf{H}_A = \mathbf{J} + j\omega\epsilon\mathbf{E}_A} \tag{3-10}$$

to (3-9) leads to

$$\mu\mathbf{J} + j\omega\mu\epsilon\mathbf{E}_A = \nabla(\nabla \cdot \mathbf{A}) - \nabla^2\mathbf{A} \tag{3-11}$$

Substituting (3-7a) into (3-11) reduces it to

$$\begin{aligned}\nabla^2\mathbf{A} + k^2\mathbf{A} &= -\mu\mathbf{J} + \nabla(\nabla \cdot \mathbf{A}) + \nabla(j\omega\mu\epsilon\phi_e) \\ &= -\mu\mathbf{J} + \nabla(\nabla \cdot \mathbf{A} + j\omega\mu\epsilon\phi_e)\end{aligned} \tag{3-12}$$

where $k^2 = \omega^2\mu\epsilon$.

In (3-2), the curl of **A** was defined. Now we are at liberty to define the divergence of **A**, which is independent of its curl. In order to simplify (3-12), let

$$\boxed{\nabla \cdot \mathbf{A} = -j\omega\epsilon\mu\phi_e \Rightarrow \phi_e = -\frac{1}{j\omega\mu\epsilon}\nabla \cdot \mathbf{A}} \tag{3-13}$$

which is known as the *Lorentz condition.* Substituting (3-13) into (3-12) leads to

$$\boxed{\nabla^2\mathbf{A} + k^2\mathbf{A} = -\mu\mathbf{J}} \tag{3-14}$$

INTEL-1045
U.S. Patent 7,151,430

In addition, (3-7a) reduces to

$$\boxed{\mathbf{E}_A = -\nabla\phi_e - j\omega\mathbf{A} = -j\omega\mathbf{A} - j\frac{1}{\omega\mu\epsilon}\nabla(\nabla\cdot\mathbf{A})} \tag{3-15}$$

Once $\mathbf{A}$ is known, $\mathbf{H}_A$ can be found from (3-2a) and $\mathbf{E}_A$ from (3-15). $\mathbf{E}_A$ can just as easily be found from Maxwell's equation (3-10) with $\mathbf{J} = 0$. It will be shown later how to find $\mathbf{A}$ in terms of the current density $\mathbf{J}$. It will be a solution to the inhomogeneous Helmholtz equation of (3-14).

3.3 THE VECTOR POTENTIAL F FOR A MAGNETIC CURRENT SOURCE M

Although magnetic currents appear to be physically unrealizable, equivalent magnetic currents arise when we use the volume or the surface equivalence theorems. The fields generated by a harmonic magnetic current in a homogeneous region, with $\mathbf{J} = 0$ but $\mathbf{M} \neq 0$, must satisfy $\nabla\cdot\mathbf{D} = 0$. Therefore, $\mathbf{E}_F$ can be expressed as the curl of the vector potential $\mathbf{F}$ by

$$\boxed{\mathbf{E}_f = -\frac{1}{\epsilon}\nabla\times\mathbf{F}} \tag{3-16}$$

Substituting (3-16) into Maxwell's curl equation

$$\nabla\times\mathbf{H}_F = j\omega\epsilon\mathbf{E}_F \tag{3-17}$$

reduces it to

$$\nabla\times(\mathbf{H}_F + j\omega\mathbf{F}) = 0 \tag{3-18}$$

From the vector identity of (3-6), it follows that

$$\boxed{\mathbf{H}_F = -\nabla\phi_m - j\omega\mathbf{F}} \tag{3-19}$$

where ϕ_m represents an arbitrary magnetic scalar potential which is a function of position. Taking the curl of (3-16)

$$\nabla\times\mathbf{E}_F = -\frac{1}{\epsilon}\nabla\times\nabla\times\mathbf{F} = -\frac{1}{\epsilon}[\nabla\,\nabla\cdot\mathbf{F} - \nabla^2\mathbf{F}] \tag{3-20}$$

and equating it to Maxwell's equation

$$\boxed{\nabla\times\mathbf{E}_F = -\mathbf{M} - j\omega\mu\mathbf{H}_F} \tag{3-21}$$

leads to

$$\nabla^2\mathbf{F} + j\omega\mu\epsilon\mathbf{H}_F = \nabla\,\nabla\cdot\mathbf{F} - \epsilon\mathbf{M} \tag{3-22}$$

Substituting (3-19) into (3-22) reduces it to

$$\nabla^2\mathbf{F} + k^2\mathbf{F} = -\epsilon\mathbf{M} + \nabla(\nabla\cdot\mathbf{F}) + \nabla(j\omega\mu\epsilon\phi_m) \tag{3-23}$$

INTEL-1045
U.S. Patent 7,151,430

By letting

$$\boxed{\nabla \cdot \mathbf{F} = -j\omega\mu\epsilon\phi_m \rightsquigarrow \phi_m = -\frac{1}{j\omega\mu\epsilon}\nabla \cdot \mathbf{F}} \tag{3-24}$$

reduces (3-23) to

$$\boxed{\nabla^2\mathbf{F} + k^2\mathbf{F} = -\epsilon\mathbf{M}} \tag{3-25}$$

and (3-19) to

$$\boxed{\mathbf{H}_F = -j\omega\mathbf{F} - \frac{j}{\omega\mu\epsilon}\nabla(\nabla \cdot \mathbf{F})} \tag{3-26}$$

Once $\mathbf{F}$ is known, $\mathbf{E}_F$ can be found from (3-16) and $\mathbf{H}_F$ from (3-26) or (3-21) with $\mathbf{M} = 0$. It will be shown later how to find $\mathbf{F}$ once $\mathbf{M}$ is known. It will be a solution to the inhomogeneous Helmholtz equation of (3-25).

3.4 ELECTRIC AND MAGNETIC FIELDS FOR ELECTRIC (J) AND MAGNETIC (M) CURRENT SOURCES

In the previous two sections we have developed equations that can be used to find the electric and magnetic fields generated by an electric current source $\mathbf{J}$ and a magnetic current source $\mathbf{M}$. The procedure requires that the auxiliary potential functions $\mathbf{A}$ and $\mathbf{F}$ generated, respectively, by $\mathbf{J}$ and $\mathbf{M}$ are found first. In turn, the corresponding electric and magnetic fields are then determined ($\mathbf{E}_A$, $\mathbf{H}_A$ due to $\mathbf{A}$ and $\mathbf{E}_F$, $\mathbf{H}_F$ due to $\mathbf{F}$). The total fields are then obtained by the superposition of the individual fields due to $\mathbf{A}$ and $\mathbf{F}$ ($\mathbf{J}$ and $\mathbf{M}$).

In summary form, the procedure that can be used to find the fields is as follows:

Summary

1. Specify $\mathbf{J}$ and $\mathbf{M}$ (electric and magnetic current density sources).
2. **a.** Find $\mathbf{A}$ (due to $\mathbf{J}$) using

$$\boxed{\mathbf{A} = \frac{\mu}{4\pi}\iiint_V \mathbf{J}\frac{e^{-jkR}}{R}dv'} \tag{3-27}$$

which is a solution of the inhomogeneous vector wave equation of (3-14).

b. Find $\mathbf{F}$ (due to $\mathbf{M}$) using

$$\boxed{\mathbf{F} = \frac{\epsilon}{4\pi}\iiint_V \mathbf{M}\frac{e^{-jkR}}{R}dv'} \tag{3-28}$$

which is a solution of the inhomogeneous vector wave equation of (3-25). In (3-27) and (3-28), $k^2 = \omega^2\mu\epsilon$ and R is the distance from any point in the source to the observation point. In a latter section, we will demonstrate that (3-27) is a solution to (3-14) as (3-28) is to (3-25).

INTEL-1045
U.S. Patent 7,151,430

3. **a.** Find $\mathbf{H}_A$ using (3-2a) and $\mathbf{E}_A$ using (3-15). $\mathbf{E}_A$ can also be found using Maxwell's equation of (3-10) with $\mathbf{J} = 0$.
   b. Find $\mathbf{E}_F$ using (3-16) and $\mathbf{H}_F$ using (3-26). $\mathbf{H}_F$ can also be found using Maxwell's equation of (3-21) with $\mathbf{M} = 0$.
4. The total fields are then given by

$$\boxed{\mathbf{E} = \mathbf{E}_A + \mathbf{E}_F = -j\omega\mathbf{A} - j\frac{1}{\omega\mu\epsilon}\nabla(\nabla \cdot \mathbf{A}) - \frac{1}{\epsilon}\nabla \times \mathbf{F}} \tag{3-29}$$

or

$$\boxed{\mathbf{E} = \mathbf{E}_A + \mathbf{E}_F = \frac{1}{j\omega\epsilon}\nabla \times \mathbf{H}_A - \frac{1}{\epsilon}\nabla \times \mathbf{F}} \tag{3-29a}$$

and

$$\boxed{\mathbf{H} = \mathbf{H}_A + \mathbf{H}_F = \frac{1}{\mu}\nabla \times \mathbf{A} - j\omega\mathbf{F} - j\frac{1}{\omega\mu\epsilon}\nabla(\nabla \cdot \mathbf{F})} \tag{3-30}$$

or

$$\boxed{\mathbf{H} = \mathbf{H}_A + \mathbf{H}_F = \frac{1}{\mu}\nabla \times \mathbf{A} - \frac{1}{j\omega\mu}\nabla \times \mathbf{E}_F} \tag{3-30a}$$

Whether (3-15) or (3-10) is used to find $\mathbf{E}_A$ and (3-26) or (3-21) to find $\mathbf{H}_F$ depends largely upon the problem. In many instances one may be more complex than the other or vice versa. In computing fields in the far-zone, it will be easier to use (3-15) for $\mathbf{E}_A$ and (3-26) for $\mathbf{H}_F$ because, as it will be shown, the second term in each expression becomes negligible in that region.

3.5 SOLUTION OF THE INHOMOGENEOUS VECTOR POTENTIAL WAVE EQUATION

In the previous section we indicated that the solution of the inhomogeneous vector wave equation of (3-14) is (3-27).

To derive it, let us assume that a source with current density J_z, which in the limit is an infinitesimal source, is placed at the origin of a x, y, z coordinate system, as shown in Figure 3.2(a). Since the current density is directed along the z-axis (J_z), only an A_z component will exist. Thus we can write (3-14) as

$$\nabla^2 A_z + k^2 A_z = -\mu J_z \tag{3-31}$$

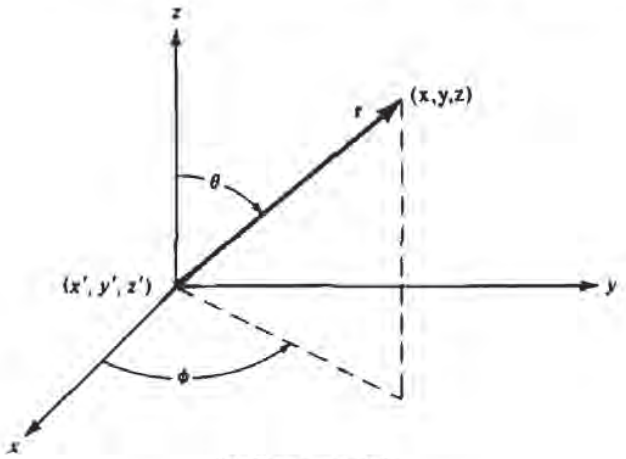
At points removed from the source ($J_z = 0$), the wave equation reduces to

$$\nabla^2 A_z + k^2 A_z = 0 \tag{3-32}$$

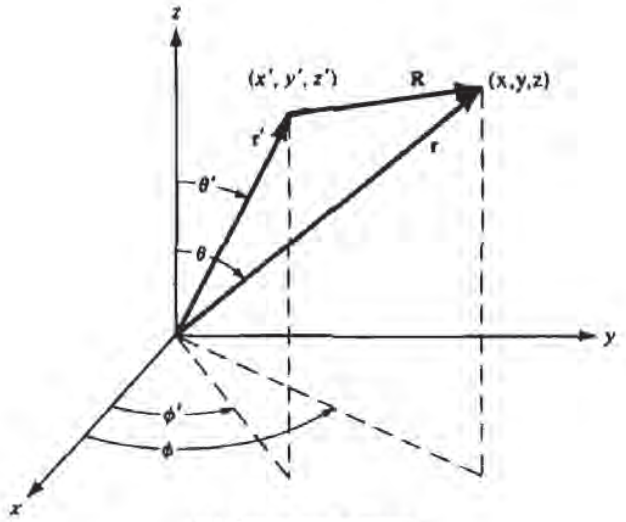
Since in the limit the source is a point, it requires that A_z is not a function of direction (θ and ϕ); in a spherical coordinate system, $A_z = A_z(r)$ where r is the radial distance. Thus (3-32) can be written as

$$\nabla^2 A_z(r) + k^2 A_z(r) = \frac{1}{r^2}\frac{\partial}{\partial r}\left[r^2\frac{\partial A_z(r)}{\partial r}\right] + k^2 A_z(r) = 0 \tag{3-33}$$

INTEL-1045
U.S. Patent 7,151,430



(a) Source at origin



(b) Source not at origin

Figure 3.2 Coordinate systems for computing radiating fields.

which when expanded reduces to

$$\frac{d^2A_z(r)}{dr^2} + \frac{2}{r}\frac{dA_z(r)}{dr} + k^2A_z(r) = 0 \tag{3-34}$$

The partial derivative has been replaced by the ordinary derivative since A_z is only a function of the radial coordinate.

The differential equation of (3-34) has two independent solutions

$$A_{z1} = C_1\frac{e^{-jkr}}{r} \tag{3-35}$$

$$A_{z2} = C_2\frac{e^{+jkr}}{r} \tag{3-36}$$

Equation (3-35) represents an outwardly (in the radial direction) traveling wave and (3-36) describes an inwardly traveling wave (assuming an $e^{j\omega t}$ time variation). For

INTEL-1045
U.S. Patent 7,151,430

this problem, the source is placed at the origin with the radiated fields traveling in the outward radial direction. Therefore, we choose the solution of (3-35), or

$$A_z = A_{z1} = C_1 \frac{e^{-jkr}}{r} \tag{3-37}$$

In the static case ($\omega = 0, k = 0$), (3-37) simplifies to

$$A_z = \frac{C_1}{r} \tag{3-38}$$

which is a solution to the wave equation of (3-32), (3-33), or (3-34) when $k = 0$. Thus at points removed from the source, the time-varying and the static solutions of (3-37) and (3-38) differ only by the e^{-jkr} factor; or the time-varying solution of (3-37) can be obtained by multiplying the static solution of (3-38) by e^{-jkr}.

In the presence of the source ($J_z \neq 0$) and $k = 0$ the wave equation of (3-31) reduces to

$$\nabla^2 A_z = -\mu J_z \tag{3-39}$$

This equation is recognized to be Poisson's equation whose solution is widely documented. The most familiar equation with Poisson's form is that relating the scalar electric potential ϕ to the electric charge density ρ. This is given by

$$\nabla^2 \phi = -\frac{\rho}{\epsilon} \tag{3-40}$$

whose solution is

$$\phi = \frac{1}{4\pi\epsilon} \iiint_V \frac{\rho}{r}\, dv' \tag{3-41}$$

where r is the distance from any point on the charge density to the observation point. Since (3-39) is similar in form to (3-40), its solution is similar to (3-41), or

$$A_z = \frac{\mu}{4\pi} \iiint_{V'} \frac{J_z}{r}\, dv' \tag{3-42}$$

Equation (3-42) represents the solution to (3-31) when $k = 0$ (static case). Using the comparative analogy between (3-37) and (3-38), the time-varying solution of (3-31) can be obtained by multiplying the static solution of (3-42) by e^{-jkr}. Thus

$$\boxed{A_z = \frac{\mu}{4\pi} \iiint_V J_z \frac{e^{-jkr}}{r}\, dv'} \tag{3-43}$$

which is a solution to (3-31).

If the current densities were in the x- and y-directions (J_x and J_y), the wave equation for each would reduce to

$$\nabla^2 A_x + k^2 A_x = -\mu J_x \tag{3-44}$$

$$\nabla^2 A_y + k^2 A_y = -\mu J_y \tag{3-45}$$

INTEL-1045
U.S. Patent 7,151,430

with corresponding solutions similar in form to (3-43), or

$$A_x = \frac{\mu}{4\pi}\iiint_V J_x \frac{e^{-jkr}}{r}\,dv' \tag{3-46}$$

$$A_y = \frac{\mu}{4\pi}\iiint_V J_y \frac{e^{-jkr}}{r}\,dv' \tag{3-47}$$

The solutions of (3-43), (3-46), and (3-47) allow us to write the solution to the vector wave equation of (3-14) as

$$\mathbf{A} = \frac{\mu}{4\pi}\iiint_V \mathbf{J} \frac{e^{-jkr}}{r}\,dv' \tag{3-48}$$

If the source is removed from the origin and placed at a position represented by the primed coordinates (x', y', z'), as shown in Figure 3.2(b), (3-48) can be written as

$$\mathbf{A}(x, y, z) = \frac{\mu}{4\pi}\iiint_V \mathbf{J}(x', y', z') \frac{e^{-jkR}}{R}\,dv' \tag{3-49}$$

where the primed coordinates represent the source, the unprimed the observation point, and R the distance from any point on the source to the observation point. In a similar fashion we can show that the solution of (3-25) is given by

$$\mathbf{F}(x, y, z) = \frac{\epsilon}{4\pi}\iiint_V \mathbf{M}(x', y', z') \frac{e^{-jkR}}{R}\,dv' \tag{3-50}$$

If $\mathbf{J}$ and $\mathbf{M}$ represent linear densities (m^{-1}), (3-49) and (3-50) reduce to surface integrals, or

$$\mathbf{A} = \frac{\mu}{4\pi}\iint_S \mathbf{J}_s(x', y', z') \frac{e^{-jkR}}{R}\,ds' \tag{3-51}$$

$$\mathbf{F} = \frac{\epsilon}{4\pi}\iint_S \mathbf{M}_s(x', y', z') \frac{e^{-jkR}}{R}\,ds' \tag{3-52}$$

For electric and magnetic currents $\mathbf{I}_e$ and $\mathbf{I}_m$, they in turn reduce to line integrals of the form

$$\mathbf{A} = \frac{\mu}{4\pi}\int_C \mathbf{I}_e(x', y', z') \frac{e^{-jkR}}{R}\,dl' \tag{3-53}$$

INTEL-1045
U.S. Patent 7,151,430

$$\boxed{\mathbf{F} = \frac{\epsilon}{4\pi}\int_C \mathbf{I}_m(x', y', z')\frac{e^{-jkR}}{R}\,dl'} \tag{3-54}$$

3.6 FAR-FIELD RADIATION

The fields radiated by antennas of finite dimensions are spherical waves. For these radiators, a general solution to the vector wave equation of (3-14) in spherical components, each as a function of r, θ, ϕ, takes the general form of

$$\mathbf{A} = \hat{\mathbf{a}}_r A_r(r, \theta, \phi) + \hat{\mathbf{a}}_\theta A_\theta(r, \theta, \phi) + \hat{\mathbf{a}}_\phi A_\phi(r, \theta, \phi) \tag{3-55}$$

The amplitude variations of r in each component of (3-55) are of the form $1/r^n$, $n = 1, 2, \ldots$ [1]. Neglecting higher order terms of $1/r^n$ ($1/r^n = 0$, $n = 2, 3, \ldots$) reduces (3-55) to

$$\mathbf{A} \simeq [\hat{\mathbf{a}}_r A_r'(\theta, \phi) + \hat{\mathbf{a}}_\theta A_\theta'(\theta, \phi) + \hat{\mathbf{a}}_\phi A_\phi'(\theta, \phi)]\frac{e^{-jkr}}{r}, \qquad r \to \infty \tag{3-56}$$

The r variations are separable from those of θ and ϕ. This will be demonstrated in the chapters that follow by many examples.

Substituting (3-56) into (3-15) reduces it to

$$\mathbf{E} = \frac{1}{r}\{-j\omega e^{-jkr}[\hat{\mathbf{a}}_r(0) + \hat{\mathbf{a}}_\theta A_\theta'(\theta, \phi) + \hat{\mathbf{a}}_\phi A_\phi'(\theta, \phi)]\} + \frac{1}{r^2}\{\cdots\} + \cdots \tag{3-57}$$

The radial E-field component has no $1/r$ terms, because its contributions from the first and second terms of (3-15) cancel each other.

Similarly, by using (3-56), we can write (3-2a) as

$$\mathbf{H} = \frac{1}{r}\left\{j\frac{\omega}{\eta}e^{-jkr}[\hat{\mathbf{a}}_r(0) + \hat{\mathbf{a}}_\theta A_\phi'(\theta, \phi) - \hat{\mathbf{a}}_\phi A_\theta'(\theta, \phi)]\right\} + \frac{1}{r^2}\{\cdots\} + \cdots \tag{3-57a}$$

where $\eta = \sqrt{\mu/\epsilon}$ is the intrinsic impedance of the medium.

Neglecting higher order terms of $1/r^n$, the radiated **E**- and **H**-fields have only θ and ϕ components. They can be expressed as

Far-Field Region

$$\left.\begin{aligned} E_r &\simeq 0 \\ E_\theta &\simeq -j\omega A_\theta \\ E_\phi &\simeq -j\omega A_\phi \end{aligned}\right\} \Rightarrow \boxed{\mathbf{E}_A \simeq -j\omega\mathbf{A}} \tag{3-58a}$$

(for the θ and ϕ components only since $E_r \simeq 0$)

$$\left.\begin{aligned} H_r &= 0 \\ H_\theta &\simeq +j\frac{\omega}{\eta}A_\phi \simeq -\frac{E_\phi}{\eta} \\ H_\phi &\simeq -j\frac{\omega}{\eta}A_\theta \simeq +\frac{E_\theta}{\eta} \end{aligned}\right\} \Rightarrow \boxed{\mathbf{H}_A \simeq \frac{\hat{\mathbf{a}}_r}{\eta} \times \mathbf{E}_A = -j\frac{\omega}{\eta}\hat{\mathbf{a}}_r \times \mathbf{A}} \tag{3-58b}$$

(for the θ and ϕ components only since $H_r \simeq 0$)

Radial field components exist only for higher order terms of $1/r^n$.

INTEL-1045
U.S. Patent 7,151,430

In a similar manner, the far-zone fields due to a magnetic source **M** (potential **F**) can be written as

Far-Field Region

$$\left.\begin{aligned} H_r &\simeq 0 \\ H_\theta &\simeq -j\omega F_\theta \\ H_\phi &\simeq -j\omega F_\phi \end{aligned}\right\} \Rightarrow \boxed{\mathbf{H}_F = -j\omega\,\mathbf{F}} \quad \text{(3-59a)}$$

(for the θ and ϕ components only since $H_r \simeq 0$)

$$\left.\begin{aligned} E_r &\simeq 0 \\ E_\theta &\simeq -j\omega\eta F_\phi = \eta H_\phi \\ E_\phi &\simeq +j\omega\eta F_\theta = -\eta H_\theta \end{aligned}\right\} \Rightarrow \boxed{\mathbf{E}_F = -\eta\hat{\mathbf{a}}_r \times \mathbf{H}_F = j\omega\eta\hat{\mathbf{a}}_r \times \mathbf{F}} \quad \text{(3-59b)}$$

(for the θ and ϕ components only since $E_r \simeq 0$)

Simply stated, *the corresponding far-zone* **E**- *and* **H**-*field components are orthogonal to each other and form TEM* (*to r*) *mode fields.* This is a very useful relation, and it will be adopted in the chapters that follow for the solution of the far-zone radiated fields. The far-zone (far-field) region for a radiator is defined in Figure 2.5. Its smallest radial distance is $2D^2/\lambda$ where D is the largest dimension of the radiator.

3.7 DUALITY THEOREM

When two equations that describe the behavior of two different variables are of the same mathematical form, their solutions will also be identical. The variables in the two equations that occupy identical positions are known as *dual* quantities and a solution of one can be formed by a systematic interchange of symbols to the other. This concept is known as the *duality theorem.*

Comparing Equations (3-2a), (3-3), (3-10), (3-14), and (3-15) to (3-16), (3-17), (3-21), (3-25), and (3-26), respectively, it is evident that they are to each other dual equations and their variables dual quantities. Thus knowing the solutions to one set (i.e., $\mathbf{J} \neq 0$, $\mathbf{M} = 0$), the solution to the other set ($\mathbf{J} = 0$, $\mathbf{M} \neq 0$) can be formed by a proper interchange of quantities. The dual equations and their dual quantities are listed in Tables 3.1 and 3.2 for electric and magnetic sources, respectively. Duality

Table 3.1 DUAL EQUATIONS FOR ELECTRIC (J) AND MAGNETIC (M) CURRENT SOURCES

Electric Sources ($\mathbf{J} \neq 0$, $\mathbf{M} = 0$)	Magnetic Sources ($\mathbf{J} = 0$, $\mathbf{M} \neq 0$)
$\nabla \times \mathbf{E}_A = -j\omega\mu\mathbf{H}_A$	$\nabla \times \mathbf{H}_F = j\omega\epsilon\mathbf{E}_F$
$\nabla \times \mathbf{H}_A = \mathbf{J} + j\omega\epsilon\mathbf{E}_A$	$-\nabla \times \mathbf{E}_F = \mathbf{M} + j\omega\mu\mathbf{H}_F$
$\nabla^2\mathbf{A} + k^2\mathbf{A} = -\mu\mathbf{J}$	$\nabla^2\mathbf{F} + k^2\mathbf{F} = -\epsilon\mathbf{M}$
$\mathbf{A} = \dfrac{\mu}{4\pi}\iiint_V \mathbf{J}\dfrac{e^{-jkR}}{R}\,dv'$	$\mathbf{F} = \dfrac{\epsilon}{4\pi}\iiint_V \mathbf{M}\dfrac{e^{-jkR}}{R}\,dv'$
$\mathbf{H}_A = \dfrac{1}{\mu}\nabla \times \mathbf{A}$	$\mathbf{E}_F = -\dfrac{1}{\epsilon}\nabla \times \mathbf{F}$
$\mathbf{E}_A = -j\omega\mathbf{A} - j\dfrac{1}{\omega\mu\epsilon}\nabla(\nabla \cdot \mathbf{A})$	$\mathbf{H}_F = -j\omega\mathbf{F} - j\dfrac{1}{\omega\mu\epsilon}\nabla(\nabla \cdot \mathbf{F})$

INTEL-1045
U.S. Patent 7,151,430

Table 3.2 DUAL QUANTITIES FOR ELECTRIC (J) AND MAGNETIC (M) CURRENT SOURCES

Electric Sources ($\mathbf{J} \neq 0$, $\mathbf{M} = 0$)	Magnetic Sources ($\mathbf{J} = 0$, $\mathbf{M} \neq 0$)
$\mathbf{E}_A$	$\mathbf{H}_F$
$\mathbf{H}_A$	$-\mathbf{E}_F$
$\mathbf{J}$	$\mathbf{M}$
$\mathbf{A}$	$\mathbf{F}$
ϵ	μ
μ	ϵ
k	k
η	$1/\eta$
$1/\eta$	η

only serves as a guide to form mathematical solutions. It can be used in an abstract manner to explain the motion of magnetic charges giving rise to magnetic currents, when compared to their dual quantities of moving electric charges creating electric currents. It must, however, be emphasized that this is purely mathematical in nature since it is known as of today, that there are no magnetic charges or currents in nature.

3.8 RECIPROCITY AND REACTION THEOREMS

We are all well familiar with the reciprocity theorem, as applied to circuits, which states that "in any network composed of linear, bilateral, lumped elements, if one places a constant **current** *(voltage)* generator between two **nodes** *(in any branch)* and places a **voltage** *(current)* meter between any other two **nodes** *(in any other branch)*, makes observation of the meter reading, then interchanges the locations of the source and the meter, the meter reading will be unchanged" [2]. We want now to discuss the reciprocity theorem as it applies to electromagnetic theory. This is done best by the use of Maxwell's equations.

Let us assume that within a linear and isotropic medium, but not necessarily homogeneous, there exist two sets of sources $\mathbf{J}_1$, $\mathbf{M}_1$, and $\mathbf{J}_2$, $\mathbf{M}_2$ which are allowed to radiate simultaneously or individually inside the same medium at the frequency and produce fields $\mathbf{E}_1$, $\mathbf{H}_1$ and $\mathbf{E}_2$, $\mathbf{H}_2$, respectively. It can be shown [1], [3] that the sources and fields satisfy

$$-\nabla \cdot (\mathbf{E}_1 \times \mathbf{H}_2 - \mathbf{E}_2 \times \mathbf{H}_1) = \mathbf{E}_1 \cdot \mathbf{J}_2 + \mathbf{H}_2 \cdot \mathbf{M}_1 - \mathbf{E}_2 \cdot \mathbf{J}_1 - \mathbf{H}_1 \cdot \mathbf{M}_2 \tag{3-60}$$

which is called the *Lorentz Reciprocity Theorem* in differential form.

Taking a volume integral of both sides of (3-60) and using the divergence theorem on the left side, we can write it as

$$-\oint\!\!\!\oint_S (\mathbf{E}_1 \times \mathbf{H}_2 - \mathbf{E}_2 \times \mathbf{H}_1) \cdot d\mathbf{s}'$$

$$= \iiint_V (\mathbf{E}_1 \cdot \mathbf{J}_2 + \mathbf{H}_2 \cdot \mathbf{M}_1 - \mathbf{E}_2 \cdot \mathbf{J}_1 - \mathbf{H}_1 \cdot \mathbf{M}_2)\, dv' \tag{3-61}$$

which is designated as the *Lorentz Reciprocity Theorem* in integral form.

INTEL-1045
U.S. Patent 7,151,430

For a source-free ($\mathbf{J}_1 = \mathbf{J}_2 = \mathbf{M}_1 = \mathbf{M}_2 = 0$) region, (3-60) and (3-61) reduce, respectively, to

$$\boxed{\nabla \cdot (\mathbf{E}_1 \times \mathbf{H}_2 - \mathbf{E}_2 \times \mathbf{H}_1) = 0} \tag{3-62}$$

and

$$\boxed{\oiint_S (\mathbf{E}_1 \times \mathbf{H}_2 - \mathbf{E}_2 \times \mathbf{H}_1) \cdot d\mathbf{s}' = 0} \tag{3-63}$$

Equations (3-62) and (3-63) are special cases of the Lorentz Reciprocity Theorem and must be satisfied in source-free regions.

As an example of where (3-62) and (3-63) may be applied and what they would represent, consider a section of a waveguide where two different modes exist with fields $\mathbf{E}_1$, $\mathbf{H}_1$ and $\mathbf{E}_2$, $\mathbf{H}_2$. For the expressions of the fields for the two modes to be valid, they must satisfy (3-62) and/or (3-63).

Another useful form of (3-61) is to consider that the fields ($\mathbf{E}_1$, $\mathbf{H}_1$, $\mathbf{E}_2$, $\mathbf{H}_2$) and the sources ($\mathbf{J}_1$, $\mathbf{M}_1$, $\mathbf{J}_2$, $\mathbf{M}_2$) are within a medium that is enclosed by a sphere of infinite radius. Assume that the sources are positioned within a finite region and that the fields are observed in the far field (ideally at infinity). Then the left side of (3-61) is equal to zero, or

$$\oiint_S (\mathbf{E}_1 \times \mathbf{H}_2 - \mathbf{E}_2 \times \mathbf{H}_1) \cdot d\mathbf{s}' = 0 \tag{3-64}$$

which reduces (3-61) to

$$\iiint_V (\mathbf{E}_1 \cdot \mathbf{J}_2 + \mathbf{H}_2 \cdot \mathbf{M}_1 - \mathbf{E}_2 \cdot \mathbf{J}_1 - \mathbf{H}_1 \cdot \mathbf{M}_2)\, dv' = 0 \tag{3-65}$$

Equation 3-65 can also be written as

$$\boxed{\iiint_V (\mathbf{E}_1 \cdot \mathbf{J}_2 - \mathbf{H}_1 \cdot \mathbf{M}_2)\, dv' = \iiint_V (\mathbf{E}_2 \cdot \mathbf{J}_1 - \mathbf{H}_2 \cdot \mathbf{M}_1)\, dv'} \tag{3-66}$$

The reciprocity theorem, as expressed by (3-66), is the most useful form.

A close observation of (3-61) will reveal that it does not, in general, represent relations of power because no conjugates appear. The same is true for the special cases represented by (3-63) and (3-66). Each of the integrals in (3-66) can be interpreted as a coupling between a set of fields and a set of sources, which produce another set of fields. This coupling has been defined as *Reaction* [4] and each of the integrals in (3-66) are denoted by

$$\langle 1, 2 \rangle = \iiint_V (\mathbf{E}_1 \cdot \mathbf{J}_2 - \mathbf{H}_1 \cdot \mathbf{M}_2)\, dv \tag{3-67}$$

$$\langle 2, 1 \rangle = \iiint_V (\mathbf{E}_2 \cdot \mathbf{J}_1 - \mathbf{H}_2 \cdot \mathbf{M}_1)\, dv \tag{3-68}$$

INTEL-1045
U.S. Patent 7,151,430

The relation $\langle 1, 2\rangle$ of (3-67) relates the reaction (coupling) of fields $(\mathbf{E}_1, \mathbf{H}_1)$, which are produced by sources $\mathbf{J}_1$, $\mathbf{M}_1$ to sources $(\mathbf{J}_2, \mathbf{M}_2)$, which produce fields $\mathbf{E}_2$, $\mathbf{H}_2$; $\langle 2, 1\rangle$ relates the reaction (coupling) of fields $(\mathbf{E}_2, \mathbf{H}_2)$ to sources $(\mathbf{J}_1, \mathbf{M}_1)$. For reciprocity to hold, it requires that the reaction (coupling) of one set of sources with the corresponding fields of another set of sources must be equal to the reaction (coupling) of the second set of sources with the corresponding fields of the first set of sources, and vice versa. In equation form, it is written as

$$\langle 1, 2\rangle = \langle 2, 1\rangle \tag{3-69}$$

3.8.1 Reciprocity for Two Antennas

There are many applications of the reciprocity theorem. To demonstrate its potential, an antenna example will be considered. Two antennas, whose input impedances are Z_1 and Z_2, are separated by a linear and isotropic (but not necessarily homogeneous) medium, as shown in Figure 3.3. One antenna (#1) is used as a transmitter and the other (#2) as a receiver. The equivalent network of each antenna is given in Figure 3.4. The internal impedance of the generator Z_g is assumed to be the conjugate of the impedance of antenna #1 ($Z_g = Z_1^* = R_1 - jX_1$) while the load impedance Z_L is equal to the conjugate of the impedance of antenna #2 ($Z_L = Z_2^* = R_2 - jX_2$). These assumptions are made only for convenience.

The power delivered by the generator to antenna #1 is given by

$$P_1 = \frac{1}{2}\operatorname{Re}[V_1 I_1^*] = \frac{1}{2}\operatorname{Re}\left[\left(\frac{V_g Z_1}{Z_1 + Z_g}\right)\frac{V_g^*}{(Z_1 + Z_g)^*}\right] = \frac{|V_g|^2}{8R_1} \tag{3-70}$$

If the transfer admittance of the combined network consisting of the generator impedance, antennas, and load impedance is Y_{21}, the current through the load is $V_g Y_{21}$ and the power delivered to the load is

$$P_2 = \tfrac{1}{2}\operatorname{Re}[Z_2(V_g Y_{21})(V_g Y_{21})^*] = \tfrac{1}{2} R_2 |V_g|^2 |Y_{21}|^2 \tag{3-71}$$

The ratio of (3-69) to (3-68) is

$$\frac{P_2}{P_1} = 4R_1 R_2 |Y_{21}|^2 \tag{3-72}$$

In a similar manner, we can show that when antenna #2 is transmitting and #1 is receiving, the power ratio of P_1/P_2 is given by

$$\frac{P_1}{P_2} = 4R_2 R_1 |Y_{12}|^2 \tag{3-73}$$

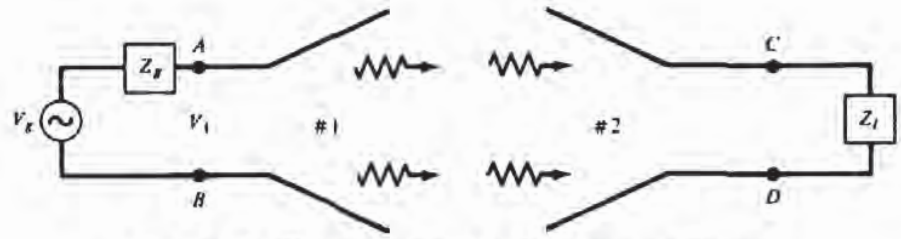


Figure 3.3 Transmitting and receiving antenna systems.

INTEL-1045
U.S. Patent 7,151,430

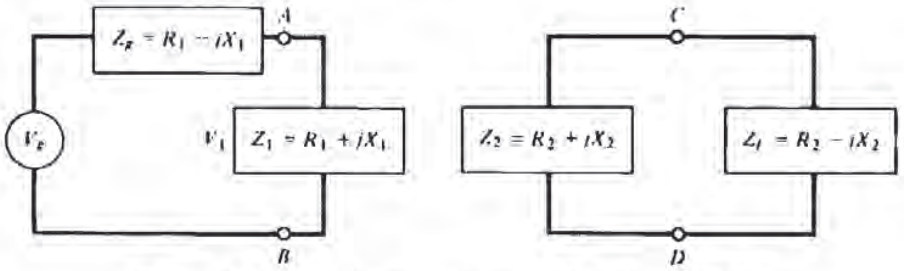


Figure 3.4 Two antenna systems with conjugate loads.

Under conditions of reciprocity ($Y_{12} = Y_{21}$), the power delivered in either direction is the same.

3.8.2 Reciprocity for Radiation Patterns

The radiation pattern is a very important antenna characteristic. Although it is usually most convenient and practical to measure the pattern in the receiving mode, it is identical, because of reciprocity, to that of the transmitting mode.

Reciprocity for antenna patterns is general provided the materials used for the antennas and feeds, and the media of wave propagation are linear. Nonlinear devices, such as diodes, can make the antenna system nonreciprocal. The antennas can be of any shape or size, and they do not have to be matched to their corresponding feed lines or loads provided there is a distinct single propagating mode at each port. The only other restriction for reciprocity to hold is for the antennas in the transmit and receive modes are polarization matched, including the sense of rotation. This is necessary so that the antennas can transmit and receive the same field components, and thus total power. If the antenna that is used as a probe to measure the fields radiated by the antenna under test is not of the same polarization, then in some situations the transmit and receive patterns can still be the same. For example, if the transmit antenna is circularly polarized and the probe antenna is linearly polarized, then if the linearly polarized probe antenna is used twice and it is oriented one time to measure the θ-component and the other the ϕ-component, then the sum of the two components can represent the pattern of the circularly polarized antenna in either the transmit or receive modes. During this procedure, the power level and sensitivities must be held constant.

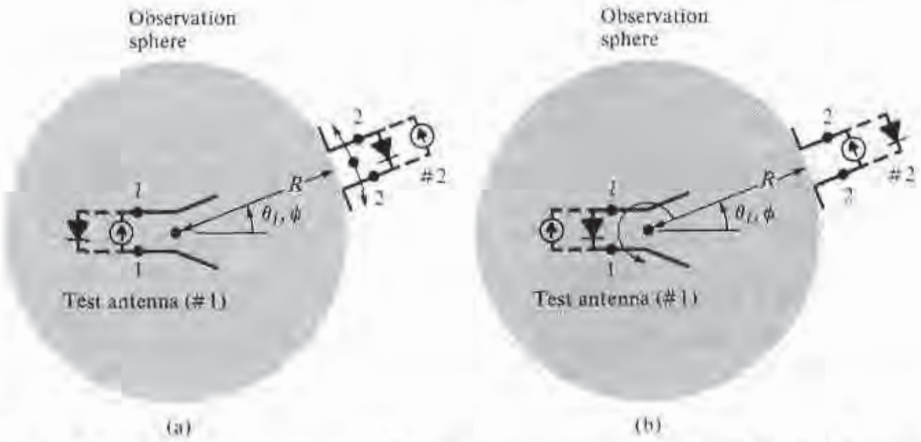
To detail the procedure and foundation of pattern measurements and reciprocity, let us refer to Figures 3.5(a) and (b). The antenna under test is #1 while the probe antenna (#2) is oriented to transmit or receive maximum radiation. The voltages and currents V_1, I_1 at terminals 1–1 of antenna #1 and V_2, I_2 at terminals 2–2 of antenna #2 are related by

$$\begin{aligned} V_1 &= Z_{11}I_1 + Z_{12}I_2 \\ V_2 &= Z_{21}I_1 + Z_{22}I_2 \end{aligned} \tag{3-74}$$

where

Z_{11} = self-impedance of antenna #1
Z_{22} = self-impedance of antenna #2
Z_{12}, Z_{21} = mutual impedances between antennas #1 and #2

INTEL-1045
U.S. Patent 7,151,430



(a) (b)

Figure 3.5 Antenna arrangement for pattern measurements and reciprocity theorem.

If a current I_1 is applied at the terminals 1–1 and voltage V_2 (designated as V_{2oc}) is measured at the *open* ($I_2 = 0$) terminals of antenna #2, then an equal voltage V_{1oc} will be measured at the *open* ($I_1 = 0$) terminals of antenna #1 provided the current I_2 of antenna #2 is equal to I_1. In equation form, we can write

$$Z_{21} = \left.\frac{V_{2oc}}{I_1}\right|_{I_2=0} \tag{3-75a}$$

$$Z_{12} = \left.\frac{V_{1oc}}{I_2}\right|_{I_1=0} \tag{3-75b}$$

If the medium between the two antennas is linear, passive, isotropic, and the waves monochromatic, then because of reciprocity

$$Z_{21} = \left.\frac{V_{2oc}}{I_1}\right|_{I_2=0} = \left.\frac{V_{1oc}}{I_2}\right|_{I_1=0} = Z_{12} \tag{3-76}$$

If in addition $I_1 = I_2$, then

$$V_{2oc} = V_{1oc} \tag{3-77}$$

The above are valid for any position and any mode of operation between the two antennas.

Reciprocity will now be reviewed for two modes of operation. In one mode, antenna #1 is held stationary while #2 is allowed to move on the surface of a constant radius sphere, as shown in Figure 3.5(a). In the other mode, antenna #2 is maintained stationary while #1 pivots about a point, as shown in Figure 3.5(b).

In the mode of Figure 3.5(a), antenna #1 can be used either as a transmitter or receiver. In the transmitting mode, while antenna #2 is moving on the constant radius sphere surface, the open terminal voltage V_{2oc} is measured. In the receiving mode, the open terminal voltage V_{1oc} is recorded. The three-dimensional plots of V_{2oc} and V_{1oc}, as a function of θ and ϕ, have been defined in Section 2.2 as *field patterns*. Since the three-dimensional graph of V_{2oc} is identical to that of V_{1oc} (due to reciprocity), the *transmitting* (V_{2oc}) *and receiving* (V_{1oc}) field patterns are also equal. The same conclusion can be arrived at if antenna #2 is allowed to remain stationary while #1 rotates, as shown in Figure 3.5(b).

INTEL-1045
U.S. Patent 7,151,430

The conditions of reciprocity hold whether antenna #1 is used as a transmitter and #2 as a receiver *or* antenna #2 as a transmitter and #1 as a receiver. In practice, the most convenient mode of operation is that of Figure 3.5(b) with the test antenna used as a receiver. Antenna #2 is usually placed in the far-field of the test antenna (#1), and vice-versa, in order that its radiated fields are plane waves in the vicinity of #1.

The receiving mode of operation of Figure 3.5(b) for the test antenna is most widely used to measure antenna patterns, because the transmitting equipment is in most cases bulky and heavy while the receiver is small and lightweight. In some cases, the receiver is nothing more than a simple diode detector. The transmitting equipment usually consists of sources and amplifiers. To make precise measurements, especially at microwave frequencies, it is necessary to have frequency and power stabilities. Therefore, the equipment must be placed on stable and vibration-free platforms. This can best be accomplished by allowing the transmitting equipment to be held stationary and the receiving equipment to rotate.

An excellent manuscript on test procedures for antenna measurements of amplitude, phase, impedance, polarization, gain, directivity, efficiency, and others has been published by IEEE [5]. A condensed summary of it is found in [6], and a review is presented in Chapter 15 of this text.

References

1. R. F. Harrington, *Time-Harmonic Electromagnetic Fields*, McGraw-Hill, New York, 1961.
2. P. E. Mayes, personal communication.
3. C. A. Balanis, *Advanced Engineering Electromagnetics*, John Wiley & Sons, New York, 1989.
4. V. H. Rumsey, "The Reaction Concept in Electromagnetic Theory," *Physical Review*, Series 2, Vol. 94, No. 6, pp. 1483–1491, June 15, 1954.
5. *IEEE Standard Test Procedures for Antennas*, IEEE Std 149-1979, IEEE, Inc., New York, 1979.
6. W. H. Kummer and E. S. Gillespie, "Antenna Measurements–1978," *Proc. IEEE*, Vol. 66, No. 4, April 1978, pp. 483–507.

PROBLEMS

3.1. If $\mathbf{H}_e = j\omega\epsilon\nabla \times \mathbf{\Pi}_e$, where $\mathbf{\Pi}_e$ is the electric Hertzian potential, show that

(a) $\nabla^2\mathbf{\Pi}_e + k^2\mathbf{\Pi}_e = j\dfrac{1}{\omega\epsilon}\mathbf{J}$ (b) $\mathbf{E}_e = k^2\mathbf{\Pi}_e + \nabla(\nabla \cdot \mathbf{\Pi}_e)$

(c) $\mathbf{\Pi}_e = -j\dfrac{1}{\omega\mu\epsilon}\mathbf{A}$

3.2. If $\mathbf{E}_h = -j\omega\mu\nabla \times \mathbf{\Pi}_h$, where $\mathbf{\Pi}_h$ is the magnetic Hertzian potential, show that

(a) $\nabla^2\mathbf{\Pi}_h + k^2\mathbf{\Pi}_h = j\dfrac{1}{\omega\mu}\mathbf{M}$ (b) $\mathbf{H}_h = k^2\mathbf{\Pi}_h + \nabla(\nabla \cdot \mathbf{\Pi}_h)$

(c) $\mathbf{\Pi}_h = -j\dfrac{1}{\omega\mu\epsilon}\mathbf{F}$

3.3. Verify that (3-35) and (3-36) are solutions to (3-34).

3.4. Show that (3-42) is a solution to (3-39) and (3-43) is a solution to (3-31).

3.5. Verify (3-57) and (3-57a).

3.6. Derive (3-60) and (3-61).

INTEL-1045
U.S. Patent 7,151,430

CHAPTER

4

LINEAR WIRE ANTENNAS

4.1 INTRODUCTION

Wire antennas, linear or curved, are some of the oldest, simplest, cheapest, and in many cases the most versatile for many applications. It should not then come as a surprise to the reader that we begin our analysis of antennas by considering some of the oldest, simplest, and most basic configurations. Initially we will try to minimize the complexity of the antenna structure and geometry to keep the mathematical details to a minimum.

4.2 INFINITESIMAL DIPOLE

An infinitesimal linear wire ($l \ll \lambda$) is positioned symmetrically at the origin of the coordinate system and oriented along the z axis, as shown in Figure 4.1(a). Although infinitesimal dipoles are not very practical, they are used to represent capacitor-plate (also referred to as *top-hat-loaded*) antennas. In addition, they are utilized as building blocks of more complex geometries. The wire, in addition to being very small ($l \ll \lambda$), is very thin ($a \ll \lambda$). The current is assumed to be constant and given by

$$\mathbf{I}(z') = \hat{\mathbf{a}}_z I_0 \tag{4-1}$$

where I_0 = constant.

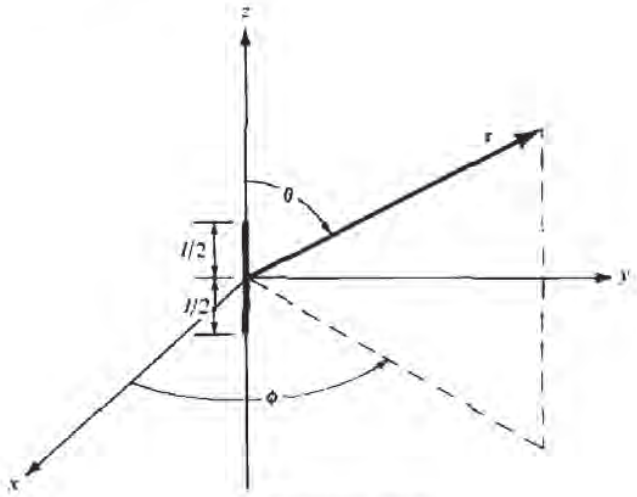
4.2.1 Radiated Fields

To find the fields radiated by the current element, the two-step procedure of Figure 3.1 is used. It will be required to determine first **A** and **F** and then find the **E** and **H**. The functional relation between **A** and the source **J** is given by (3-49), (3-51), or (3-53). Similar relations are available for **F** and **M**, as given by (3-50), (3-52), and (3-54).

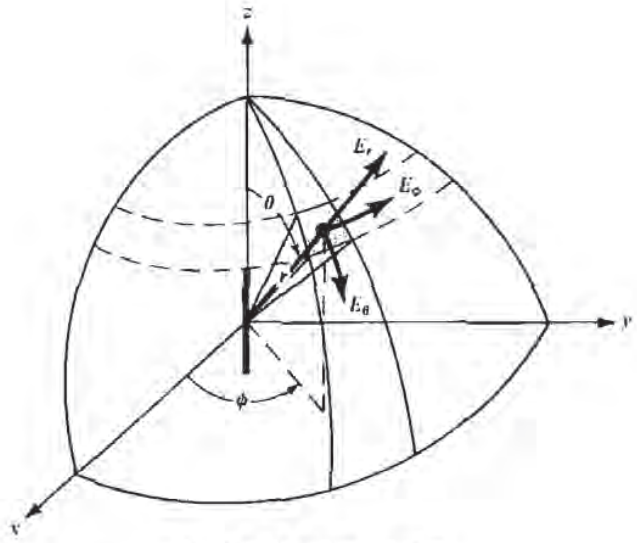
Since the source only carries an electric current $\mathbf{I}_e$, $\mathbf{I}_m$ and the potential function **F** are zero. To find **A** we write

$$\mathbf{A}(x, y, z) = \frac{\mu}{4\pi} \int_C \mathbf{I}_e(x', y', z') \frac{e^{-jkR}}{R} dl' \tag{4-2}$$

INTEL-1045
U.S. Patent 7,151,430



(a) Infinitesimal dipole



(b) Electric field orientation

Figure 4.1 Geometrical arrangement of an infinitesimal dipole and its associated electric field components on a spherical surface.

where (x, y, z) represent the observation point coordinates, (x', y', z') represent the coordinates of the source, R is the distance from any point on the source to the observation point, and path C is along the length of the source. For the problem of Figure 4.1

$$\mathbf{I}_e(x', y', z') = \hat{\mathbf{a}}_z I_0 \tag{4-3a}$$

$$x' = y' = z' = 0 \quad \text{(infinitesimal dipole)} \tag{4-3b}$$

$$R = \sqrt{(x - x')^2 + (y - y')^2 + (z - z')^2} = \sqrt{x^2 + y^2 + z^2}$$
$$= r = \text{constant} \tag{4-3c}$$

$$dl' = dz' \tag{4-3d}$$

INTEL-1045
U.S. Patent 7,151,430

so we can write (4-2) as

$$\boxed{\mathbf{A}(x, y, z) = \hat{\mathbf{a}}_z \frac{\mu I_0}{4\pi r} e^{-jkr} \int_{-l/2}^{+l/2} dz' = \hat{\mathbf{a}}_z \frac{\mu I_0 l}{4\pi r} e^{-jkr}} \tag{4-4}$$

The next step of the procedure is to find $\mathbf{H}_A$ using (3-2a) and then $\mathbf{E}_A$ using (3-15) or (3-10) with $\mathbf{J} = 0$. To do this, it is often much simpler to transform (4-4) from rectangular to spherical components and then use (3-2a) and (3-15) or (3-10) in spherical coordinates to find $\mathbf{H}$ and $\mathbf{E}$.

The transformation between rectangular and spherical components is given, in matrix form, by (see Appendix VII)

$$\begin{bmatrix} A_r \\ A_\theta \\ A_\phi \end{bmatrix} = \begin{bmatrix} \sin\theta\cos\phi & \sin\theta\sin\phi & \cos\theta \\ \cos\theta\cos\phi & \cos\theta\sin\phi & -\sin\theta \\ -\sin\phi & \cos\phi & 0 \end{bmatrix} \begin{bmatrix} A_x \\ A_y \\ A_z \end{bmatrix} \tag{4-5}$$

For this problem, $A_x = A_y = 0$, so (4-5) using (4-4) reduces to

$$A_r = A_z \cos\theta = \frac{\mu I_0 l e^{-jkr}}{4\pi r} \cos\theta \tag{4-6a}$$

$$A_\theta = -A_z \sin\theta = -\frac{\mu I_0 l e^{-jkr}}{4\pi r} \sin\theta \tag{4-6b}$$

$$A_\phi = 0 \tag{4-6c}$$

Using the symmetry of the problem (no variations in ϕ), (3-2a) can be expanded in spherical coordinates and written in simplified form as

$$\mathbf{H} = \hat{\mathbf{a}}_\phi \frac{1}{\mu r} \left[\frac{\partial}{\partial r}(rA_\theta) - \frac{\partial A_r}{\partial \theta} \right] \tag{4-7}$$

Substituting (4-6a)–(4-6c) into (4-7) reduces it to

$$\boxed{\begin{aligned} H_r &= H_\theta = 0 \qquad (4\text{-}8a) \\ H_\phi &= j \frac{k I_0 l \sin\theta}{4\pi r} \left[1 + \frac{1}{jkr} \right] e^{-jkr} \qquad (4\text{-}8b) \end{aligned}}$$

The electric field $\mathbf{E}$ can now be found using (3-15) or (3-10) with $\mathbf{J} = 0$. That is,

$$\mathbf{E} = \mathbf{E}_A = -j\omega\mathbf{A} - j\frac{1}{\omega\mu\epsilon} \nabla(\nabla \cdot \mathbf{A}) = \frac{1}{j\omega\epsilon} \nabla \times \mathbf{H} \tag{4-9}$$

Substituting (4-6a)–(4-6c) or (4-8a)–(4-8b) into (4-9) reduces it to

$$\boxed{\begin{aligned} E_r &= \eta \frac{I_0 l \cos\theta}{2\pi r^2} \left[1 + \frac{1}{jkr} \right] e^{-jkr} \qquad (4\text{-}10a) \\ E_\theta &= j\eta \frac{k I_0 l \sin\theta}{4\pi r} \left[1 + \frac{1}{jkr} - \frac{1}{(kr)^2} \right] e^{-jkr} \qquad (4\text{-}10b) \\ E_\phi &= 0 \qquad (4\text{-}10c) \end{aligned}}$$

INTEL-1045
U.S. Patent 7,151,430

The **E**- and **H**-field components are valid everywhere, except on the source itself, and they are sketched in Figure 4.1(b) on the surface of a sphere of radius r. It is a straightforward exercise to verify Equations (4-10a)–(4-10c), and this is left as an exercise to the reader (Prob. 4.9).

4.2.2 Power Density and Radiation Resistance

The input impedance of an antenna, which consists of real and imaginary parts, was discussed in Section 2.13. For a lossless antenna, the real part of the input impedance was designated as radiation resistance. It is through the mechanism of the radiation resistance that power is transferred from the guided wave to the free-space wave. To find the input resistance for a lossless antenna, the Poynting vector is formed in terms of the **E**- and **H**-fields radiated by the antenna. By integrating the Poynting vector over a closed surface (usually a sphere of constant radius), the total power radiated by the source is found. The real part of it is related to the input resistance.

For the infinitesimal dipole, the complex Poynting vector can be written using (4-8a)–(4-8b) and (4-10a)–(4-10c) as

$$\begin{aligned} \mathbf{W} &= \tfrac{1}{2}(\mathbf{E} \times \mathbf{H}^*) = \tfrac{1}{2}(\hat{\mathbf{a}}_r E_r + \hat{\mathbf{a}}_\theta E_\theta) \times (\hat{\mathbf{a}}_\phi H_\phi^*) \\ &= \tfrac{1}{2}(\hat{\mathbf{a}}_r E_\theta H_\phi^* - \hat{\mathbf{a}}_\theta E_r H_\phi^*) \end{aligned} \tag{4-11}$$

whose radial W_r and transverse W_θ components are given, respectively, by

$$W_r = \frac{\eta}{8}\left|\frac{I_0 l}{\lambda}\right|^2 \frac{\sin^2\theta}{r^2}\left[1 - j\frac{1}{(kr)^3}\right] \tag{4-12a}$$

$$W_\theta = j\eta\frac{k|I_0 l|^2 \cos\theta \sin\theta}{16\pi^2 r^3}\left[1 + \frac{1}{(kr)^2}\right] \tag{4-12b}$$

The complex power moving in the radial direction is obtained by integrating (4-11)–(4-12b) over a closed sphere of radius r. Thus it can be written as

$$P = \oiint_S \mathbf{W} \cdot d\mathbf{s} = \int_0^{2\pi}\int_0^{\pi} (\hat{\mathbf{a}}_r W_r + \hat{\mathbf{a}}_\theta W_\theta) \cdot \hat{\mathbf{a}}_r r^2 \sin\theta \, d\theta \, d\phi \tag{4-13}$$

which reduces to

$$P = \int_0^{2\pi}\int_0^{\pi} W_r r^2 \sin\theta \, d\theta \, d\phi = \eta\frac{\pi}{3}\left|\frac{I_0 l}{\lambda}\right|^2\left[1 - j\frac{1}{(kr)^3}\right] \tag{4-14}$$

The transverse component W_θ of the power density does not contribute to the integral. Thus (4-14) does not represent the total complex power radiated by the antenna. Since W_θ, as given by (4-12b), is purely imaginary, it will not contribute to any real radiated power. However, it does contribute to the imaginary (reactive) power which along with the second term of (4-14) can be used to determine the total reactive power of the antenna. The reactive power density, which is most dominant for small values of kr, has both radial and transverse components. It merely changes between outward and inward directions to form a standing wave at a rate of twice per cycle. It also moves in the transverse direction as suggested by (4-12b).

INTEL-1045
U.S. Patent 7,151,430

Equation (4-13), which gives the real and imaginary power that is moving outwardly, can also be written as [4]

$$P = \frac{1}{2}\iint_S \mathbf{E} \times \mathbf{H}^* \cdot d\mathbf{s} = \eta\left(\frac{\pi}{3}\right)\left|\frac{I_0 l}{\lambda}\right|^2\left[1 - j\frac{1}{(kr)^3}\right]$$

$$= P_{\text{rad}} + j2\omega(\tilde{W}_m - \tilde{W}_e) \tag{4-15}$$

where

P = power (in radial direction)
P_{rad} = time-average power radiated
$\tilde{W}_m$ = time-average magnetic energy density (in radial direction)
$\tilde{W}_e$ = time-average electric energy density (in radial direction)
$2\omega(\tilde{W}_m - \tilde{W}_e)$ = time-average imaginary (reactive) power (in radial direction)

From (4-14)

$$P_{\text{rad}} = \eta\left(\frac{\pi}{3}\right)\left|\frac{I_0 l}{\lambda}\right|^2 \tag{4-16}$$

and

$$2\omega(\tilde{W}_m - \tilde{W}_e) = -\eta\left(\frac{\pi}{3}\right)\left|\frac{I_0 l}{\lambda}\right|^2 \frac{1}{(kr)^3} \tag{4-17}$$

It is clear from (4-17) that the radial electric energy must be larger than the radial magnetic energy. For large values of kr ($kr \gg 1$ or $r \gg \lambda$), the reactive power diminishes and vanishes when $kr = \infty$.

Since the antenna radiates its real power through the radiation resistance, for the infinitesimal dipole it is found by equating (4-16) to

$$\boxed{P_{\text{rad}} = \eta\left(\frac{\pi}{3}\right)\left|\frac{I_0 l}{\lambda}\right|^2 = \frac{1}{2}|I_0|^2 R_r} \tag{4-18}$$

where R_r is the radiation resistance. Equation (4-18) reduces to

$$\boxed{R_r = \eta\left(\frac{2\pi}{3}\right)\left(\frac{l}{\lambda}\right)^2 = 80\pi^2\left(\frac{l}{\lambda}\right)^2} \tag{4-19}$$

for a free-space medium ($\eta \simeq 120\pi$). It should be pointed out that the radiation resistance of (4-19) represents the total radiation resistance since (4-12b) does not contribute to it.

For a wire antenna to be classified as an infinitesimal dipole, its overall length must be very small (usually $l \leq \lambda/50$).

Example 4.1

Find the radiation resistance of an infinitesimal dipole whose overall length is $l = \lambda/50$.

INTEL-1045
U.S. Patent 7,151,430

SOLUTION

Using (4-19)

$$R_r = 80\pi^2\left(\frac{l}{\lambda}\right)^2 = 80\pi^2\left(\frac{1}{50}\right)^2 = 0.316 \text{ ohms}$$

Since the radiation resistance of an infinitesimal dipole is about 0.3 ohms, it will present a very large mismatch when connected to practical transmission lines, many of which have characteristic impedances of 50 or 75 ohms. The reflection efficiency (e_r) and hence the overall efficiency (e_t) will be very small.

The reactance of an infinitesimal dipole is capacitive. This can be illustrated by considering the dipole as a flared open-circuited transmission line, as discussed in Section 1.4. Since the input impedance of an open-circuited transmission line a distance $l/2$ from its open end is given by $Z_{in} = -jZ_c \cot(\beta l/2)$, where Z_c is its characteristic impedance, it will always be negative (capacitive) for $l \ll \lambda$.

4.2.3 Radian Distance and Radian Sphere

The **E**- and **H**-fields for the infinitesimal dipole, as represented by (4-8a)–(4-8b) and (4-10a)–(4-10c), are valid everywhere (except on the source itself). An inspection of these equations reveals the following:

(a) At a distance $r = \lambda/2\pi$ (or $kr = 1$), which is referred to as the *radian distance*, the magnitude of the first and second terms within the brackets of (4-8b) and (4-10a) is the same. Also at the radian distance the magnitude of all three terms within the brackets of (4-10b) is identical; the only term that contributes to the total field is the second, because the first and third terms cancel each other. This is illustrated in Figure 4.2.

(b) At distances less than the radian distance $r < \lambda/2\pi$ ($kr < 1$), the magnitude of the second term within the brackets of (4-8b) and (4-10a) is greater than the first term and begins to dominate as $r \ll \lambda/2\pi$. For (4-10b) and $r < \lambda/2\pi$, the magnitude of the third term within the brackets is greater than the magnitude of the first and second terms while the magnitude of the second term is greater than that of the first one; each of these terms begins to dominate as $r \ll \lambda/2\pi$. This is illustrated in Figure 4.2. The region $r < \lambda/2\pi$ ($kr < 1$) is referred to as the *near-field* region.

(c) At distances greater than the radian distance $r > \lambda/2\pi$ ($kr > 1$), the first term within the brackets of (4-8b) and (4-10a) is greater than the magnitude of the second term and begins to dominate as $r \gg \lambda/2\pi (kr \gg 1)$. For (4-10b) and $r > \lambda/2\pi$, the first term within the brackets is greater than the magnitude of the second and third terms while the magnitude of the second term is greater than that of the third; each of these terms begins to dominate as $r \gg \lambda/2\pi$. This is illustrated in Figure 4.2. The region $r > \lambda/2\pi$ ($kr > 1$) is referred to as the *intermediate-field* region while that for $r \gg \lambda/2\pi$ ($kr \gg 1$) is referred to as the *far-field* region.

INTEL-1045
U.S. Patent 7,151,430

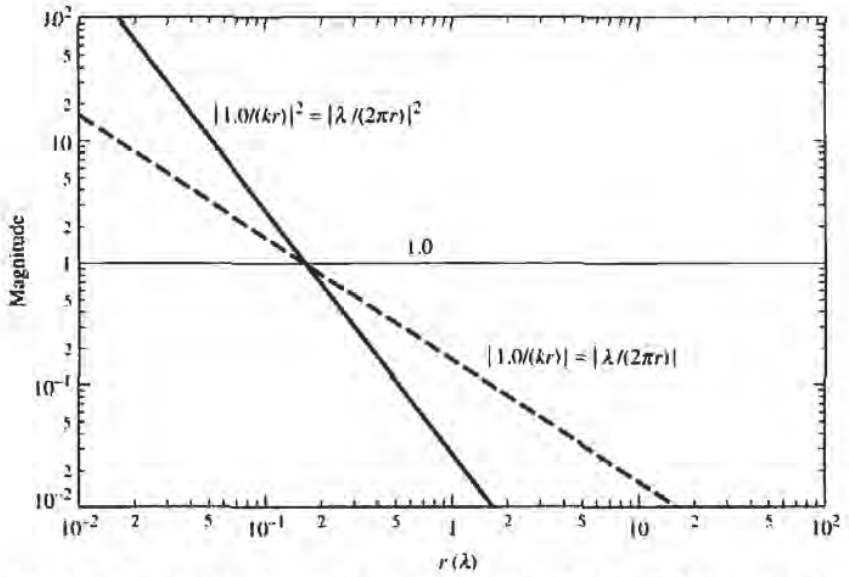


Figure 4.2 Magnitude variation, as a function of the radial distance, of the field terms radiated by an infinitesimal dipole.

(d) The sphere with radius equal to the radian distance ($r = \lambda/2\pi$) is referred as the *radian sphere*, and it defines the region within which the reactive power density is greater than the radiated power density [1]–[3]. For an antenna, the radian sphere represents the volume occupied mainly by the stored energy of the antenna's electric and magnetic fields. Outside the radian sphere the radiated power density is greater than the reactive power density and begins to dominate as $r \gg \lambda/2\pi$. Therefore the radian sphere can be used as a reference, and it defines the transition between stored energy pulsating primarily in the θ direction [represented by (4-12b)] and energy radiating in the radial (r) direction [represented by the first term of (4-12a); the second term represents stored energy pulsating in the radial (r) direction].

4.2.4 Near-Field ($kr \ll 1$) Region

An inspection of (4-8a)–(4-8b) and (4-10a)–(4-10c) reveals that for $kr \ll \lambda$ or $r \ll \lambda/2\pi$ they can be reduced in much simpler form and can be approximated by

$$E_r \simeq -j\eta \frac{I_0 l e^{-jkr}}{2\pi k r^3} \cos\theta \qquad \text{(4-20a)}$$

$$E_\theta \simeq -j\eta \frac{I_0 l e^{-jkr}}{4\pi k r^3} \sin\theta \qquad \text{(4-20b)}$$

$$kr \ll 1$$

$$E_\phi = H_r = H_\theta = 0 \qquad \text{(4-20c)}$$

$$H_\phi \simeq \frac{I_0 l e^{-jkr}}{4\pi r^2} \sin\theta \qquad \text{(4-20d)}$$

The E-field components, E_r and E_θ, are in time-phase but they are in time phase quadrature with the H-field component H_ϕ; therefore there is no time-average power

INTEL-1045
U.S. Patent 7,151,430

flow associated with them. This is demonstrated by forming the time-average power density as

$$\mathbf{W}_{av} = \tfrac{1}{2}\mathrm{Re}[\mathbf{E} \times \mathbf{H}^*] = \tfrac{1}{2}\mathrm{Re}[\hat{\mathbf{a}}_r E_\theta H^*_\phi - \hat{\mathbf{a}}_\theta E_r H^*_\phi] \tag{4-21}$$

which by using (4-20a)–(4-20d) reduces to

$$\mathbf{W}_{av} = \frac{1}{2}\mathrm{Re}\left[-\hat{\mathbf{a}}_r j\frac{\eta}{k}\left|\frac{I_0 l}{4\pi}\right|^2 \frac{\sin^2\theta}{r^5} + \hat{\mathbf{a}}_\theta j\frac{\eta}{k}\frac{|I_0 l|^2}{8\pi^2}\frac{\sin\theta\cos\theta}{r^5}\right] = 0 \tag{4-22}$$

The condition of $kr \ll 1$ can be satisfied at moderate distances away from the antenna provided that the frequency of operation is very low. Equations (4-20a) and (4-20b) are similar to those of a static electric dipole and (4-20d) to that of a static current element. Thus we usually refer to (4-20a)–(4-20d) as the *quasistationary fields.*

4.2.5 Intermediate-Field ($kr > 1$) Region

As the values of kr begin to increase and become greater than unity, the terms that were dominant for $kr \ll 1$ become smaller and eventually vanish. For moderate values of kr the E-field components lose their in-phase condition and approach time-phase quadrature. Since their magnitude is not the same, in general, they form a rotating vector whose extremity traces an ellipse. This is analogous to the polarization problem except that the vector rotates in a plane parallel to the direction of propagation and is usually referred to as the *cross field.* At these intermediate values of kr, the E_θ and H_ϕ components approach time-phase, which is an indication of the formation of time-average power flow in the outward (radial) direction (radiation phenomenon).

As the values of kr become moderate ($kr > 1$), the field expressions can be approximated again but in a different form. In contrast to the region where $kr \ll 1$, the first term within the brackets in (4-8b) and (4-10a) becomes more dominant and the second term can be neglected. The same is true for (4-10b) where the second and third terms become less dominant than the first. Thus we can write for $kr > 1$

$$E_r \simeq \eta\frac{I_0 l e^{-jkr}}{2\pi r^2}\cos\theta \tag{4-23a}$$

$$E_\theta \simeq j\eta\frac{kI_0 l e^{-jkr}}{4\pi r}\sin\theta \tag{4-23b}$$

$$E_\phi = H_r = H_\theta = 0 \tag{4-23c}$$

$$H_\phi \simeq j\frac{kI_0 l e^{jkr}}{4\pi r}\sin\theta \tag{4-23d}$$

$kr > 1$

The total electric field is given by

$$\mathbf{E} = \hat{\mathbf{a}}_r E_r + \hat{\mathbf{a}}_\theta E_\theta \tag{4-24}$$

whose magnitude can be written as

$$|\mathbf{E}| = \sqrt{|E_r|^2 + |E_\theta|^2} \tag{4-25}$$

INTEL-1045
U.S. Patent 7,151,430

4.2.6 Far-Field ($kr \gg 1$) Region

Since (4-23a)–(4-23d) are valid only for values of $kr > 1$ ($r > \lambda$), then E_r will be smaller than E_θ because E_r is inversely proportional to r^2 where E_θ is inversely proportional to r. In a region where $kr \gg 1$, (4-23a)–(4-23d) can be simplified and approximated by

$$E_\theta \simeq j\eta \frac{kI_0 le^{-jkr}}{4\pi r} \sin\theta \qquad (4\text{-}26a)$$

$$E_r \simeq E_\phi \simeq H_r = H_\theta = 0 \qquad (4\text{-}26b)$$

$$H_\phi \simeq j \frac{kI_0 le^{-jkr}}{4\pi r} \sin\theta \qquad (4\text{-}26c)$$

$kr \gg 1$

The ratio of E_θ to H_ϕ is equal to

$$Z_w = \frac{E_\theta}{H_\phi} \simeq \eta \qquad (4\text{-}27)$$

where

Z_w = wave impedance

η = intrinsic impedance ($377 \simeq 120\pi$ ohms for free-space)

The **E**- and **H**-field components are perpendicular to each other, transverse to the radial direction of propagation, and the r variations are separable from those of θ and ϕ. The shape of the pattern is not a function of the radial distance r, and the fields form a *T*ransverse *E*lectro*M*agnetic (TEM) wave whose wave impedance is equal to the intrinsic impedance of the medium. As it will become even more evident in later chapters, this relationship is applicable in the far-field region of all antennas of finite dimensions. Equations (4-26a)–(4-26c) can also be derived using the procedure outlined and relationships developed in Section 3.6. This is left as an exercise to the reader (Prob. 4.11).

Example 4.2

For an infinitesimal dipole determine and interpret the vector effective length. At what incidence angle does the open-circuit maximum voltage occurs at the output terminals of the dipole if the electric field intensity of the incident wave is 10 mvolts/meter? The length of the dipole is 10 cm.

SOLUTION

Using (4-26a) and the effective length as defined by (2-92), we can write that

$$E_\theta = j\eta \frac{kI_0 le^{-jkr}}{4\pi r} \sin\theta = -\hat{\mathbf{a}}_\theta j\eta \frac{kI_0 e^{-jkr}}{4\pi r} \cdot (-\hat{\mathbf{a}}_\theta l \sin\theta)$$

$$= -\hat{\mathbf{a}}_\theta j\eta \frac{kI_0 e^{-jkr}}{4\pi r} \cdot \ell_e$$

INTEL-1045
U.S. Patent 7,151,430

Therefore, the effective length is

$$\ell_v = -\hat{\mathbf{a}}_\theta l \sin\theta$$

whose maximum value occurs when $\theta = 90°$, and it is equal to l. Therefore, to achieve maximum output the wave must be incident upon the dipole at a normal incidence angle ($\theta = 90°$).

The open-circuit maximum voltage is equal to

$$V_{oc}\Big|_{\max} = |\mathbf{E}^i \cdot \ell_e|_{\max} = |\hat{\mathbf{a}}_\theta 10 \times 10^{-3} \cdot (-\hat{\mathbf{a}}_\theta l \sin\theta)|_{\max}$$
$$= 10 \times 10^{-3} l \simeq 10^{-3} \text{ volts}$$

4.2.7 Directivity

The real power P_{rad} radiated by the dipole was found in Section 4.2.2, as given by (4-16). The same expression can be obtained by first forming the average power density, using (4-26a)–(4-26c). That is,

$$\mathbf{W}_{\text{av}} = \frac{1}{2}\text{Re}(\mathbf{E} \times \mathbf{H}^*) = \hat{\mathbf{a}}_r \frac{1}{2\eta}|E_\theta|^2 = \hat{\mathbf{a}}_r \frac{\eta}{2}\left|\frac{kI_0 l}{4\pi}\right|^2 \frac{\sin^2\theta}{r^2} \tag{4-28}$$

Integrating (4-28) over a closed sphere of radius r reduces it to (4-16). This is left as an exercise to the reader (Prob. 4.10).

Associated with the average power density of (4-28) is a radiation intensity U which is given by

$$U = r^2 W_{\text{av}} = \frac{\eta}{2}\left(\frac{kI_0 l}{4\pi}\right)^2 \sin^2\theta = \frac{r^2}{2\eta}|E_\theta(r, \theta, \phi)|^2 \tag{4-29}$$

and it conforms with (2-12a). The normalized pattern of (4-29) is shown in Figure 4.3. The maximum value occurs at $\theta = \pi/2$ and it is equal to

$$U_{\max} = \frac{\eta}{2}\left(\frac{kI_0 l}{4\pi}\right)^2 \tag{4-30}$$

Using (4-16) and (4-30), the directivity reduces to

$$\boxed{D_0 = 4\pi \frac{U_{\max}}{P_{\text{rad}}} = \frac{3}{2}} \tag{4-31}$$

and the maximum effective aperture to

$$\boxed{A_{em} = \left(\frac{\lambda^2}{4\pi}\right) D_0 = \frac{3\lambda^2}{8\pi}} \tag{4-32}$$

The radiation resistance of the dipole can be obtained by the definition of (4-18). Since the radiated power obtained by integrating (4-28) over a closed sphere is the same as that of (4-16), the radiation resistance using it will also be the same as obtained previously and given by (4-19).

Integrating the complex Poynting vector over a closed sphere, as was done in (4-13), results in the power (real and imaginary) directed in the radial direction. Any

INTEL-1045
U.S. Patent 7,151,430

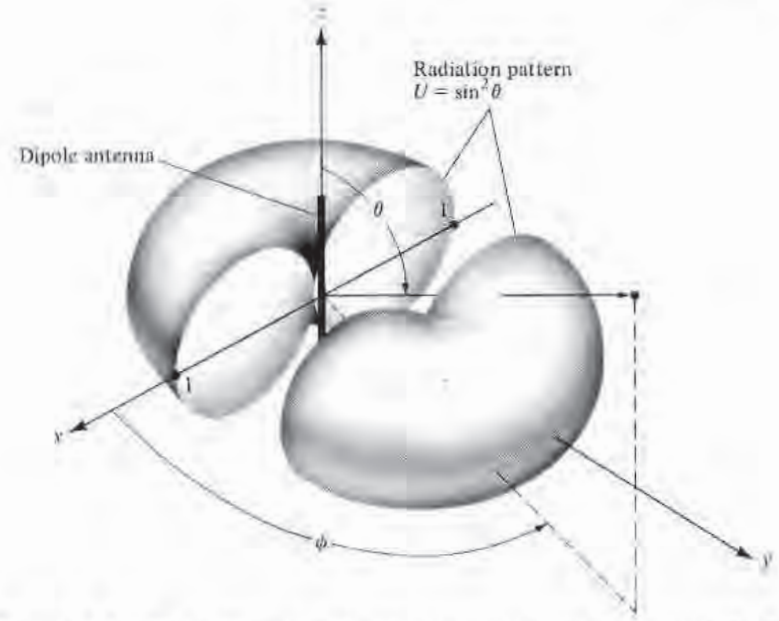


Figure 4.3 Three-dimensional radiation pattern of infinitesimal dipole.

transverse components of power density, as given by (4-12b), will not be captured by the integration even though they are part of the overall power. Because of this limitation, this method cannot be used to derive the input reactance of the antenna.

4.3 SMALL DIPOLE

The creation of the current distribution on a thin wire was discussed in Section 1.4, and it was illustrated with some examples in Figure 1.16. The radiation properties of an infinitesimal dipole, which is usually taken to have a length $l \leq \lambda/50$, were discussed in the previous section. Its current distribution was assumed to be constant. Although a constant current distribution is not realizable (other than top-hat-loaded elements), it is a mathematical quantity that is used to represent actual current distributions of antennas that have been incremented into many small lengths.

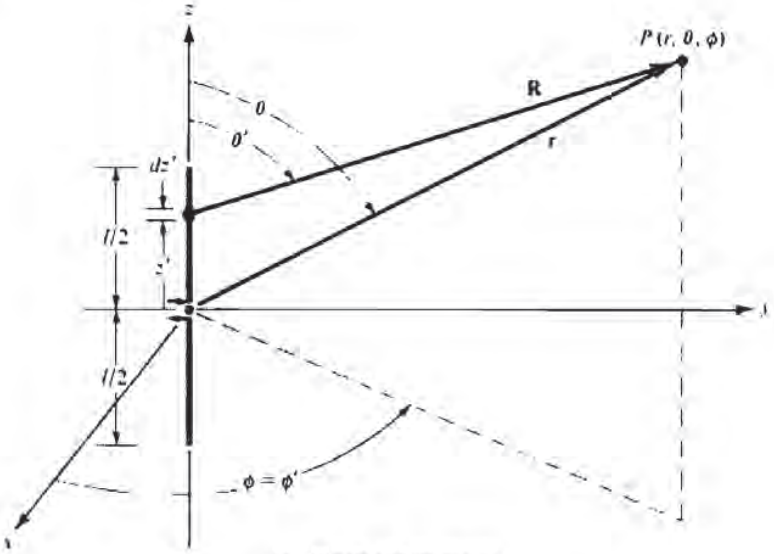
A better approximation of the current distribution of wire antennas, whose lengths are usually $\lambda/50 < l \leq \lambda/10$, is the triangular variation of Figure 1.16(a). The sinusoidal variations of Figures 1.16(b)–(c) are more accurate representations of the current distribution of any length wire antenna.

The most convenient geometrical arrangement for the analysis of a dipole is usually to have it positioned symmetrically about the origin with its length directed along the z-axis, as shown in Figure 4.4(a). This is not necessary, but it is usually the most convenient. The current distribution of a small dipole ($\lambda/50 < l \leq \lambda/10$) is shown in Figure 4.4(b), and it is given by

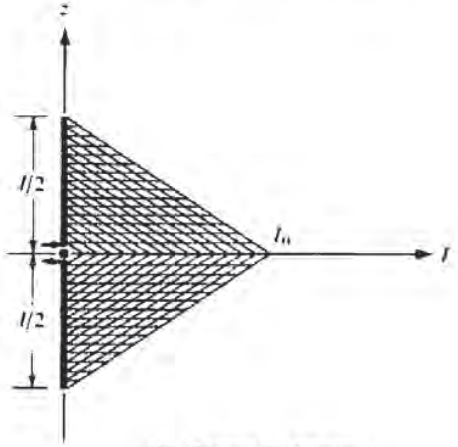
$$\mathbf{I}_e(x', y', z') = \begin{cases} \hat{\mathbf{a}}_z I_0 \left(1 - \dfrac{2}{l} z'\right), & 0 \leq z' \leq l/2 \\ \hat{\mathbf{a}}_z I_0 \left(1 + \dfrac{2}{l} z'\right), & -l/2 \leq z' \leq 0 \end{cases} \tag{4-33}$$

where $I_0 =$ constant.

INTEL-1045
U.S. Patent 7,151,430



(a) Dipole and geometry



(b) Current distribution

Figure 4.4 Geometrical arrangement of dipole and current distribution.

Following the procedure established in the previous section, the vector potential of (4-2) can be written using (4-33) as

$$\mathbf{A}(x, y, z) = \frac{\mu}{4\pi}\left[\hat{\mathbf{a}}_z \int_{-l/2}^{0} I_0\left(1 + \frac{2}{l}z'\right)\frac{e^{-jkR}}{R}\,dz' + \hat{\mathbf{a}}_z \int_{0}^{l/2} I_0\left(1 - \frac{2}{l}z'\right)\frac{e^{-jkR}}{R}\,dz'\right] \tag{4-34}$$

Because the overall length of the dipole is very small (usually $l \leq \lambda/10$), the values of R for different values of z' along the length of the wire ($-l/2 \leq z' \leq l/2$) are not much different from r. Thus R can be approximated by $R \simeq r$ throughout the integration path. The maximum phase error in (4-34) by allowing $R = r$ for $\lambda/50 < l \leq \lambda/10$, will be $kl/2 = \pi/10$ rad $= 18°$ for $l = \lambda/10$. Smaller values will occur for the other lengths. As it will be shown in the next section, this amount of phase error

INTEL-1045
U.S. Patent 7,151,430

is usually considered negligible and has very little effect on the overall radiation characteristics. Performing the integration, (4-34) reduces to

$$\mathbf{A} = \hat{\mathbf{a}}_z A_z = \hat{\mathbf{a}}_z \frac{1}{2}\left[\frac{\mu I_0 l e^{-jkr}}{4\pi r}\right] \tag{4-35}$$

which is one-half of that obtained in the previous section for the infinitesimal dipole and given by (4-4).

The potential function given by (4-35) becomes a more accurate approximation as $kr \to \infty$. This is also the region of most practical interest, and it has been designated as the *far-field* region. Since the potential function for the triangular distribution is one-half of the corresponding one for the constant (uniform) current distribution, the corresponding fields of the former are one-half of the latter. Thus we can write the **E**- and **H**-fields radiated by a small dipole as

$$E_\theta \simeq j\eta \frac{kI_0 l e^{-jkr}}{8\pi r} \sin\theta \tag{4-36a}$$

$$E_r \simeq E_\phi = H_r = H_\theta = 0 \qquad kr \gg 1 \tag{4-36b}$$

$$H_\phi \simeq j \frac{kI_0 l e^{-jkr}}{8\pi r} \sin\theta \tag{4-36c}$$

with the wave impedance equal, as before, to (4-27).

Since the directivity of an antenna is controlled by the relative shape of the field or power pattern, the directivity and maximum effective area of this antenna are the same as the ones with the constant current distribution given by (4-31) and (4-32), respectively.

The radiation resistance of the antenna is strongly dependent upon the current distribution. Using the procedure established for the infinitesimal dipole, it can be shown that for the small dipole its radiated power is one-fourth ($\frac{1}{4}$) of (4-18). Thus the radiation resistance reduces to

$$\boxed{R_r = \frac{2P_{\text{rad}}}{|I_0|^2} = 20\pi^2\left(\frac{l}{\lambda}\right)^2} \tag{4-37}$$

which is also one-fourth ($\frac{1}{4}$) of that obtained for the infinitesimal dipole as given by (4-19). Their relative patterns (shapes) are the same and are shown in Figure 4.3.

4.4 REGION SEPARATION

Before we attempt to solve for the fields radiated by a finite dipole of any length, it would be very desirable to discuss the separation of the space surrounding an antenna into three regions; namely, the *reactive near-field*, *radiating near-field* (*Fresnel*) and the *far-field* (*Fraunhofer*) which were introduced briefly in Section 2.2. This is necessary because for a dipole antenna of any length and any current distribution, it will become increasingly difficult to solve for the fields everywhere. Approximations can be made, especially for the far-field (Fraunhofer) region which is usually the one of most practical interest, to simplify the formulation to yield closed form solutions. The same approximations used to simplify the formulation of the fields radiated by a finite

INTEL-1045
U.S. Patent 7,151,430

dipole are also used to formulate the fields radiated by most practical antennas. So it will be very important to introduce them properly and understand their implications upon the solution.

The difficulties in obtaining closed form solutions that are valid everywhere for any practical antenna stem from the inability to perform the integration of

$$\mathbf{A}(x, y, z) = \frac{\mu}{4\pi} \int_C \mathbf{I}_e(x', y', z') \frac{e^{-jkR}}{R} dl' \tag{4-38}$$

where

$$R = \sqrt{(x - x')^2 + (y - y')^2 + (z - z')^2} \tag{4-38a}$$

For a finite dipole with sinusoidal current distribution, the integral of (4-38) can be reduced to a closed form that is valid everywhere! This will be shown in Chapter 8. The length R is defined as the distance from any point on the source to the observation point. The integral of (4-38) was used to solve for the fields of infinitesimal and small dipoles in Sections 4.1 and 4.2. However in the first case (infinitesimal dipole) $R = r$ and in the second case (small dipole) R was approximated by r ($R \simeq r$) because the length of the dipole was restricted to be $l \leq \lambda/10$. The major simplification of (4-38) will be in the approximation of R.

A very thin dipole of finite length l is symmetrically positioned about the origin with its length directed along the z-axis, as shown in Figure 4.5(a). Because the wire is assumed to be very thin ($x' = y' = 0$), we can write (4-38) as

$$R = \sqrt{(x - x')^2 + (y - y')^2 + (z - z')^2} = \sqrt{x^2 + y^2 + (z - z')^2} \tag{4-39}$$

which when expanded can be written as

$$R = \sqrt{(x^2 + y^2 + z^2) + (-2zz' + z'^2)} = \sqrt{r^2 + (-2rz' \cos\theta + z'^2)} \tag{4-40}$$

where

$$r^2 = x^2 + y^2 + z^2 \tag{4-40a}$$

$$z = r\cos\theta \tag{4-40b}$$

Using the binomial expansion, we can write (4-40) in a series

$$R = r - z'\cos\theta + \frac{1}{r}\left(\frac{z'^2}{2}\sin^2\theta\right) + \frac{1}{r^2}\left(\frac{z'^3}{2}\cos\theta\sin^2\theta\right) + \cdots \tag{4-41}$$

whose higher order terms become less significant provided $r \gg z'$.

4.4.1 Far-Field (Fraunhofer) Region

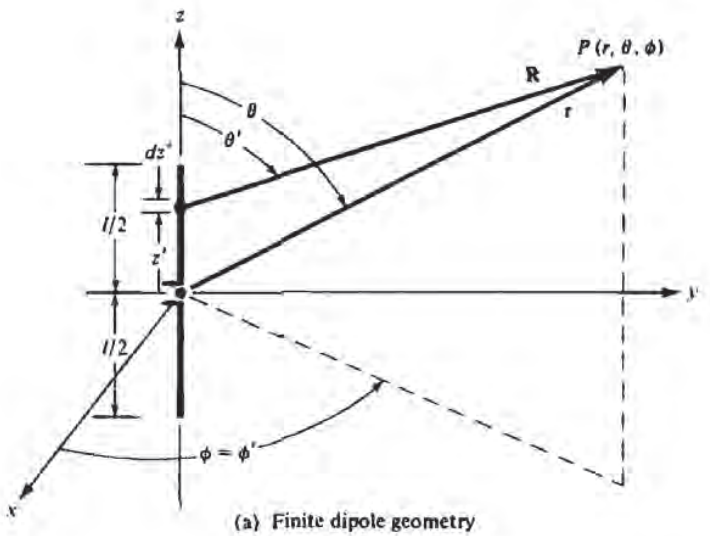
The most convenient simplification of (4-41), other than $R = r$, will be to approximate it by its first two terms, or

$$R = r - z'\cos\theta \tag{4-42}$$

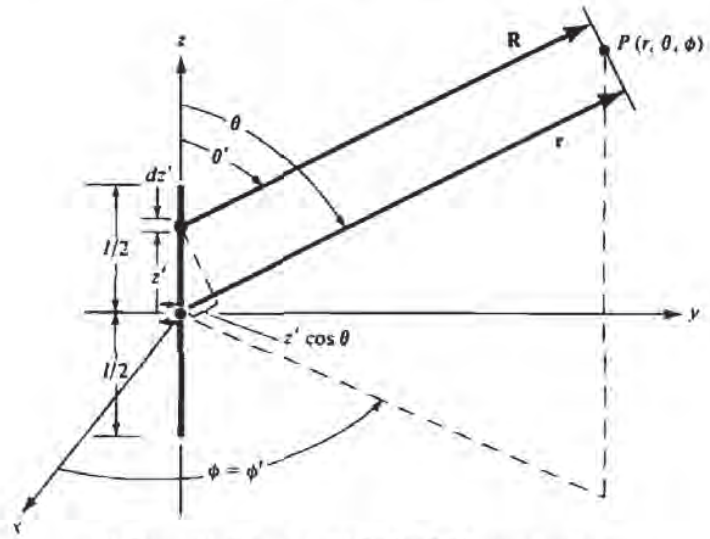
The most significant neglected term of (4-41) is the third whose maximum value is

$$\frac{1}{r}\left(\frac{z'^2}{2}\sin^2\theta\right)_{\max} = \frac{z'^2}{2r} \qquad \text{when } \theta = \pi/2 \tag{4-43}$$

INTEL-1045
U.S. Patent 7,151,430



(a) Finite dipole geometry



(b) Geometrical arrangement for far-field approximations

Figure 4.5 Finite dipole geometry and far-field approximations.

When (4-43) attains its maximum value, the fourth term of (4-41) vanishes because $\theta = \pi/2$. It can be shown that the higher order terms not shown in (4-41) also vanish. Therefore approximating (4-41) by (4-42) introduces a *maximum* error given by (4-43).

It has been shown by many investigators through numerous examples that for most practical antennas, *with overall lengths greater than a wavelength* ($l > \lambda$), a maximum total phase error of $\pi/8$ rad (22.5°) is not very detrimental in their analytical formulation. Using that as a criterion we can write, using (4-43), that the maximum phase error should always be

$$\frac{k(z')^2}{2r} \leq \frac{\pi}{8} \tag{4-44}$$

INTEL-1045
U.S. Patent 7,151,430

which for $-l/2 \leq z' \leq l/2$ reduces to

$$r \geq 2\left(\frac{l^2}{\lambda}\right) \tag{4-45}$$

Equation (4-45) simply states that to maintain the maximum phase error of an antenna equal to or less than $\pi/8$ rad (22.5°), the observation distance r must equal or be greater than $2l^2/\lambda$ where l is the largest* dimension of the antenna structure. The usual simplification for the far-field region is to approximate the R in the exponential (e^{-jkR}) of (4-38) by (4-42) and the R in the denominator of (4-38) by $R \simeq r$. These simplifications are designated as the far-field approximations and are usually denoted in the literature as

Far-field Approximations

$$\begin{aligned} R &= r - z'\cos\theta \quad && \text{for phase terms} \\ R &= r && \text{for amplitude terms} \end{aligned} \tag{4-46}$$

provided r satisfies (4-45).

It may be advisable to illustrate the approximation (4-46) geometrically. For $R \simeq r - z'\cos\theta$, where θ is the angle measured from the z-axis, the radial vectors $\mathbf{R}$ and $\mathbf{r}$ must be parallel to each other, as shown in Figure 4.5(b). For any other antenna whose maximum dimension is D, the approximation of (4-46) is valid provided the observations are made at a distance

$$r \geq 2D^2/\lambda \tag{4-47}$$

For an aperture antenna the maximum dimension is taken to be its diagonal.

For most practical antennas, whose overall length is large compared to the wavelength, these are adequate approximations which have been shown by many investigators through numerous examples to give valid results in pattern predictions. Some discrepancies are evident in regions of low intensity (usually below -25 dB). This is illustrated in Figure 2.6 where the patterns of a paraboloidal antenna for $R = \infty$ and $R = 2D^2/\lambda$ differ at levels below -25 dB. Allowing R to have a value of $R = 4D^2/\lambda$ gives better results.

It would seem that the approximation of R in (4-46) for the amplitude is more severe than that for the phase. However a close observation reveals this is not the case. Since the observations are made at a distance where r is very large, any small error in the approximation of the denominator (amplitude) will not make much difference in the answer. However, because of the periodic nature of the phase (repeats every 2π rad), it can be a major fraction of a period. The best way to illustrate it will be to consider an example.

Example 4.3

For an antenna with an overall length $l = 5\lambda$, the observations are made at $r = 60\lambda$. Find the errors in phase and amplitude using (4-46).

*Provided the overall length (l) of the antenna is large compared to the wavelength [see IEEE Standard Definitions of Terms for Antennas, IEEE Std (145-1983)].

INTEL-1045
U.S. Patent 7,151,430

SOLUTION

For $\theta = 90°$, $z' = 2.5\lambda$, and $r = 60\lambda$, (4-40) reduces to

$$R_1 = \lambda\sqrt{(60)^2 + (2.5)^2} = 60.052\lambda$$

and (4-46) to

$$R_2 = r = 60\lambda$$

Therefore the phase difference is

$$\Delta\phi = k\Delta R = \frac{2\pi}{\lambda}(R_1 - R_2) = 2\pi(0.052) = 0.327 \text{ rad} = 18.74°$$

which in an appreciable fraction ($\simeq \frac{1}{20}$) of a full period (360°).

The difference of the inverse values of R is

$$\frac{1}{R_2} - \frac{1}{R_1} = \frac{1}{\lambda}\left(\frac{1}{60} - \frac{1}{60.052}\right) = \frac{1.44 \times 10^{-5}}{\lambda}$$

which should always be a very small value.

4.4.2 Radiating Near-Field (Fresnel) Region

If the observation point is chosen to be smaller than $r = 2l^2/\lambda$, the maximum phase error by the approximation of (4-46) is greater than $\pi/8$ rad (22.5°) which may be undesirable in many applications. If it is necessary to choose observation distances smaller than (4-45), another term (the third) in the series solution of (4-41) must be retained to maintain a maximum phase error of $\pi/8$ rad (22.5°). Doing this, the infinite series of (4-41) can be approximated by

$$R \simeq r - z' \cos\theta + \frac{1}{r}\left(\frac{z'^2}{2}\sin^2\theta\right) \tag{4-48}$$

The most significant term that we are neglecting from the infinite series of (4-41) is the fourth. To find the maximum phase error introduced by the omission of the next most significant term, the angle θ at which this occurs must be found. To do this, the neglected term is differentiated with respect to θ and the result is set equal to zero. Thus

$$\frac{\partial}{\partial\theta}\left[\frac{1}{r^2}\left(\frac{z'^3}{2}\cos\theta\sin^2\theta\right)\right] = \frac{z'^3}{2r^2}\sin\theta[-\sin^2\theta + 2\cos^2\theta] = 0 \tag{4-49}$$

The angle $\theta = 0$ is not chosen as a solution because for that value the fourth term is equal to zero. In other words, $\theta = 0$ gives the minimum error. The maximum error occurs when the second term of (4-49) vanishes; that is when

$$[-\sin^2\theta + 2\cos^2\theta]_{\theta=\theta_1} = 0 \tag{4-50}$$

INTEL-1045
U.S. Patent 7,151,430

or

$$\theta_1 = \tan^{-1}(\pm\sqrt{2}) \tag{4-50a}$$

If the maximum phase error is allowed to be equal or less than $\pi/8$ rad, the distance r at which this occurs can be found from

$$\frac{kz'^3}{2r^2}\cos\theta\sin^2\theta\Big|_{\substack{z'=l/2\\ \theta=\tan^{-1}\sqrt{2}}} = \frac{\pi}{\lambda}\frac{l^3}{8r^2}\left(\frac{1}{\sqrt{3}}\right)\left(\frac{2}{3}\right) = \frac{\pi}{12\sqrt{3}}\left(\frac{l^3}{\lambda r^2}\right) \le \frac{\pi}{8} \tag{4-51}$$

which reduces to

$$r^2 \ge \frac{2}{3\sqrt{3}}\left(\frac{l^3}{\lambda}\right) = 0.385\left(\frac{l^3}{\lambda}\right) \tag{4-52}$$

or

$$r \ge 0.62\sqrt{l^3/\lambda} \tag{4-52a}$$

A value of r greater than that of (4-52a) will lead to an error less than $\pi/8$ rad (22.5°). Thus the region where the first three terms of (4-41) are significant, and the omission of the fourth introduces a maximum phase error of $\pi/8$ rad (22.5°), is defined by

$$2l^2/\lambda > r \ge 0.62\sqrt{l^3/\lambda} \tag{4-53}$$

where l is the length of the antenna. This region is designated as *radiating near-field* because the radiating power density is greater than the reactive power density and the field pattern (its shape) is a function of the radial distance r. This region is also called the *Fresnel region* because the field expressions in this region reduce to Fresnel integrals.

The discussion has centered around the finite length antenna of length l with the observation considered to be a point source. If the antenna is not a line source, l in (4-53) must represent the largest dimension of the antenna (which for an aperture is the diagonal). Also if the transmitting antenna has maximum length l_t and the receiving antenna has maximum length l_r, then the *sum of* l_t *and* l_r must be used in place of l in (4-53).

The boundaries for separating the far-field (Fraunhofer), the radiating near-field (Fresnel), and the reactive near-field regions are not very rigid. Other criteria have also been established [4] but the ones introduced here are the most "popular." Also the fields, as the boundaries from one region to the other are crossed, do not change abruptly but undergo a very gradual transition.

4.4.3 Reactive Near-Field Region

If the distance of observation is smaller than the inner boundary of the Fresnel region, this region is usually designated as *reactive near-field* with inner and outer boundaries defined by

$$0.62\sqrt{l^3/\lambda} > r > 0 \tag{4-54}$$

where l is the length of the antenna. In this region the reactive power density predominates, as was demonstrated in Section 4.1 for the infinitesimal dipole.

INTEL-1045
U.S. Patent 7,151,430

In summary, the space surrounding an antenna is divided into three regions whose boundaries are determined by

reactive near-field $[0.62\sqrt{D^3/\lambda} > r > 0]$	(4-55a)
radiating near-field (Fresnel) $[2D^2/\lambda > r \geq 0.62\sqrt{D^3/\lambda}]$	(4-55b)
far-field (Fraunhofer) $[\infty \geq r \geq 2D^2/\lambda]$	(4-55c)

where D is the largest dimension of the antenna ($D = l$ for a wire antenna).

4.5 FINITE LENGTH DIPOLE

The techniques that were developed previously can also be used to analyze the radiation characteristics of a linear dipole of any length. To reduce the mathematical complexities, it will be assumed in this chapter that the dipole has a negligible diameter (ideally zero). This is a good approximation provided the diameter is considerably smaller than the operating wavelength. Finite radii dipoles will be analyzed in Chapters 8 and 9.

4.5.1 Current Distribution

For a very thin dipole (ideally zero diameter), the current distribution can be written, to a good approximation, as

$$\mathbf{I}_e(x' = 0, y' = 0, z') = \begin{cases} \hat{\mathbf{a}}_z I_0 \sin\left[k\left(\frac{l}{2} - z'\right)\right], & 0 \leq z' \leq l/2 \\ \hat{\mathbf{a}}_z I_0 \sin\left[k\left(\frac{l}{2} + z'\right)\right], & -l/2 \leq z' \leq 0 \end{cases} \tag{4-56}$$

This distribution assumes that the antenna is *center-fed and the current vanishes at the end points* ($z' = \pm l/2$). Experimentally it has been verified that the current in a center-fed wire antenna has sinusoidal form with nulls at the end points. For $l = \lambda/2$ and $\lambda/2 < l < \lambda$ the current distribution of (4-56) is shown plotted in Figures 1.16(b) and 1.12(c), respectively. The geometry of the antenna is that shown in Figure 4.5.

4.5.2 Radiated Fields: Element Factor, Space Factor, and Pattern Multiplication

For the current distribution of (4-56) it will be shown in Chapter 8 that closed form expressions for the **E**- and **H**-fields can be obtained which are valid in all regions (any observation point except on the source itself). In general, however, this is not the case. Usually we are limited to the far-field region, because of the mathematical complications provided in the integration of the vector potential **A** of (4-2). Since closed form solutions, which are valid everywhere, cannot be obtained for many antennas, the observations will be restricted to the far-field region. This will be done first in order to illustrate the procedure. In some cases, even in that region it may become impossible to obtain closed form solutions.

The finite dipole antenna of Figure 4.5 is subdivided into a number of infinitesimal

INTEL-1045
U.S. Patent 7,151,430

dipoles of length $\Delta z'$. As the number of subdivisions is increased, each infinitesimal dipole approaches a length dz'. For an infinitesimal dipole of length dz' positioned along the z-axis at z', the electric and magnetic field components in the far-field are given, using (4-26a)–(4-26c), as

$$dE_\theta \simeq j\eta \frac{kI_e(x', y', z')e^{-jkR}}{4\pi R} \sin\theta\, dz' \tag{4-57a}$$

$$dE_r \simeq dE_\phi = dH_r = dH_\theta = 0 \tag{4-57b}$$

$$dH_\phi \simeq j \frac{kI_e(x', y', z')e^{-jkR}}{4\pi R} \sin\theta\, dz' \tag{4-57c}$$

where R is given by (4-39) or (4-40).

Using the far-field approximations given by (4-46), (4-57a) can be written as

$$dE_\theta \simeq j\eta \frac{kI_e(x', y', z')e^{-jkr}}{4\pi r} \sin\theta e^{+jkz'\cos\theta} dz' \tag{4-58}$$

Summing the contributions from all the infinitesimal elements, the summation reduces, in the limit, to an integration. Thus

$$\boxed{E_\theta = \int_{-l/2}^{+l/2} dE_\theta = j\eta \frac{ke^{-jkr}}{4\pi r} \sin\theta \left[\int_{-l/2}^{+l/2} I_e(x', y', z') e^{jkz'\cos\theta} dz' \right]} \tag{4-58a}$$

The factor outside the brackets is designated as the *element factor* and that within the brackets as the *space factor*. For this antenna, the element factor is equal to the field of a unit length infinitesimal dipole located at a reference point (the origin). In general, the element factor depends on the type of current and its direction of flow while the space factor is a function of the current distribution along the source.

The total field of the antenna is equal to the product of the element and space factors. This is referred to as *pattern multiplication* for continuously distributed sources, and it can be written as

$$\boxed{\text{total field} = (\text{element factor}) \times (\text{space factor})} \tag{4-59}$$

The pattern multiplication for continuous sources is analogous to the pattern multiplication of (6-5) for discrete-element antennas (arrays).

For the current distribution of (4-56), (4-58a) can be written as

$$E_\theta \simeq j\eta \frac{kI_0 e^{-jkr}}{4\pi r} \sin\theta \left\{ \int_{-l/2}^{0} \sin\left[k\left(\frac{l}{2} + z'\right)\right] e^{+jkz'\cos\theta} dz' + \int_{0}^{+l/2} \sin\left[k\left(\frac{l}{2} - z'\right)\right] e^{+jkz'\cos\theta} dz' \right\} \tag{4-60}$$

Each one of the integrals in (4-60) can be integrated using

$$\int e^{\alpha x} \sin(\beta x + \gamma)\, dx = \frac{e^{\alpha x}}{\alpha^2 + \beta^2} [\alpha \sin(\beta x + \gamma) - \beta \cos(\beta x + \gamma)] \tag{4-61}$$

where

$$\alpha = \pm jk \cos\theta \tag{4-61a}$$

INTEL-1045
U.S. Patent 7,151,430

$$\beta = \pm k \tag{4-61b}$$

$$\gamma = kl/2 \tag{4-61c}$$

After some mathematical manipulations, (4-60) takes the form of

$$\boxed{E_\theta \simeq j\eta \frac{I_0 e^{-jkr}}{2\pi r}\left[\frac{\cos\left(\frac{kl}{2}\cos\theta\right) - \cos\left(\frac{kl}{2}\right)}{\sin\theta}\right]} \tag{4-62a}$$

In a similar manner, or by using the established relationship between the E_θ and H_ϕ in the far-field as given by (3-58b) or (4-27), the total H_ϕ component can be written as

$$\boxed{H_\phi \simeq \frac{E_\theta}{\eta} \simeq j\frac{I_0 e^{-jkr}}{2\pi r}\left[\frac{\cos\left(\frac{kl}{2}\cos\theta\right) - \cos\left(\frac{kl}{2}\right)}{\sin\theta}\right]} \tag{4-62b}$$

4.5.3 Power Density, Radiation Intensity, and Radiation Resistance

For the dipole, the average Poynting vector can be written as

$$\mathbf{W}_{av} = \frac{1}{2}\text{Re}[\mathbf{E}\times\mathbf{H}^*] = \frac{1}{2}\text{Re}[\hat{\mathbf{a}}_\theta E_\theta \times \hat{\mathbf{a}}_\phi H_\phi^*] = \frac{1}{2}\text{Re}\left[\hat{\mathbf{a}}_\theta E_\theta \times \hat{\mathbf{a}}_\phi \frac{E_\theta^*}{\eta}\right]$$

$$\mathbf{W}_{av} = \hat{\mathbf{a}}_r W_{av} = \hat{\mathbf{a}}_r \frac{1}{2\eta}|E_\theta|^2 = \eta\frac{|I_0|^2}{8\pi^2 r^2}\left[\frac{\cos\left(\frac{kl}{2}\cos\theta\right) - \cos\left(\frac{kl}{2}\right)}{\sin\theta}\right]^2 \tag{4-63}$$

and the radiation intensity as

$$U = r^2 W_{av} = \eta\frac{|I_0|^2}{8\pi^2}\left[\frac{\cos\left(\frac{kl}{2}\cos\theta\right) - \cos\left(\frac{kl}{2}\right)}{\sin\theta}\right]^2 \tag{4-64}$$

The normalized (to 0 dB) elevation power patterns, as given by (4-64) for $l = \lambda/4$, $\lambda/2$, $3\lambda/4$, and λ are shown plotted in Figure 4.6. The current distribution of each is given by (4-56). The power patterns for an infinitestimal dipole $l \ll \lambda$ ($U \sim \sin^2\theta$) is also included for comparison. As the length of the antenna increases, the beam becomes narrower. Because of that, the directivity should also increase with length. It is found that the 3-dB beamwidth of each is equal to

$$\begin{aligned}
&l \ll \lambda && \text{3-db beamwidth} = 90^\circ \\
&l = \lambda/4 && \text{3-dB beamwidth} = 87^\circ \\
&l = \lambda/2 && \text{3-dB beamwidth} = 78^\circ \\
&l = 3\lambda/4 && \text{3-dB beamwidth} = 64^\circ \\
&l = \lambda && \text{3-dB beamwidth} = 47.8^\circ
\end{aligned} \tag{4-65}$$

INTEL-1045
U.S. Patent 7,151,430

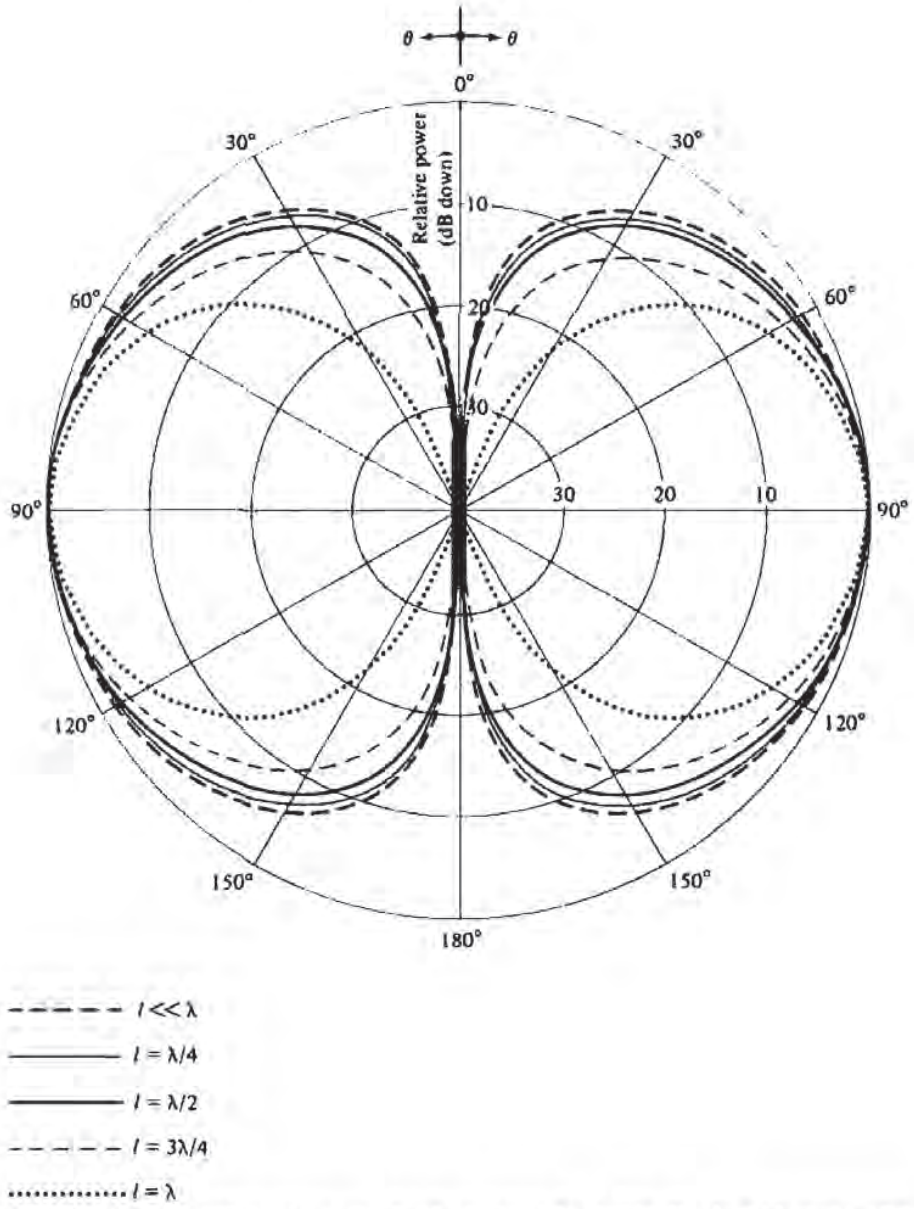
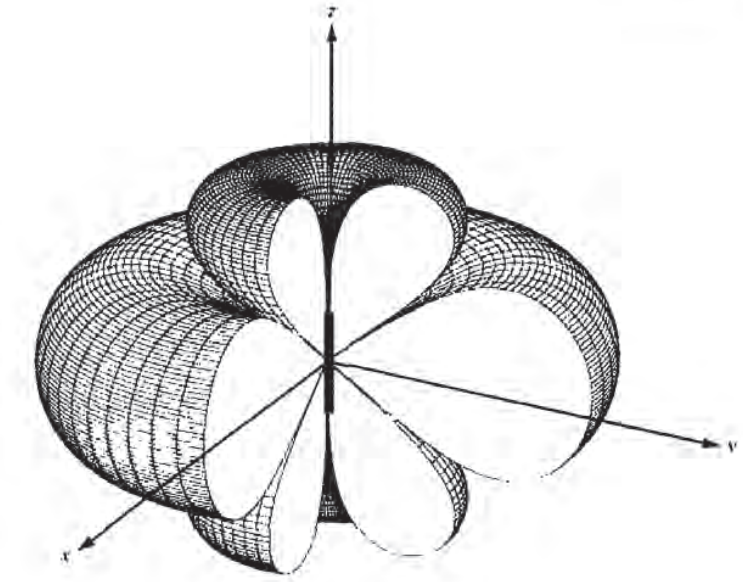


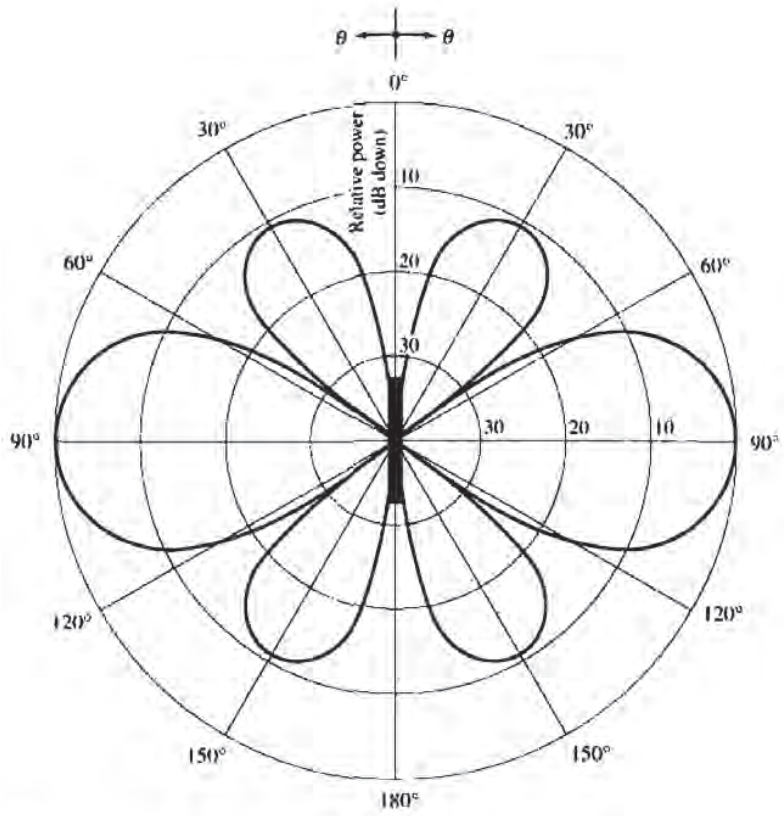
Figure 4.6 *Elevation plane amplitude patterns for a thin dipole with sinusoidal current distribution ($l = \lambda/4, \lambda/2, 3\lambda/4, \lambda$).*

As the length of the dipole increases beyond one wavelength ($l > \lambda$), the number of lobes begin to increase. The normalized power pattern for a dipole with $l = 1.25\lambda$ is shown in Figure 4.7. In Figure 4.7(a) the three-dimensional pattern is illustrated using the software from [5], while in Figure 4.7(b) the two-dimensional (elevation pattern) is depicted. For the three-dimensional illustration a 90° angular section of the pattern has been omitted to illustrate the elevation plane directional pattern variations. The current distribution for the dipoles with $l = \lambda/4, \lambda/2, \lambda, 3\lambda/2$, and 2λ, as given by (4-56), is shown in Figure 4.8.

INTEL-1045
U.S. Patent 7,151,430



(a) Three-dimensional



(b) Two-dimensional

Figure 4.7 Three- and two-dimensional amplitude patterns for a thin dipole of $l = 1.25\lambda$ and sinusoidal current distribution.

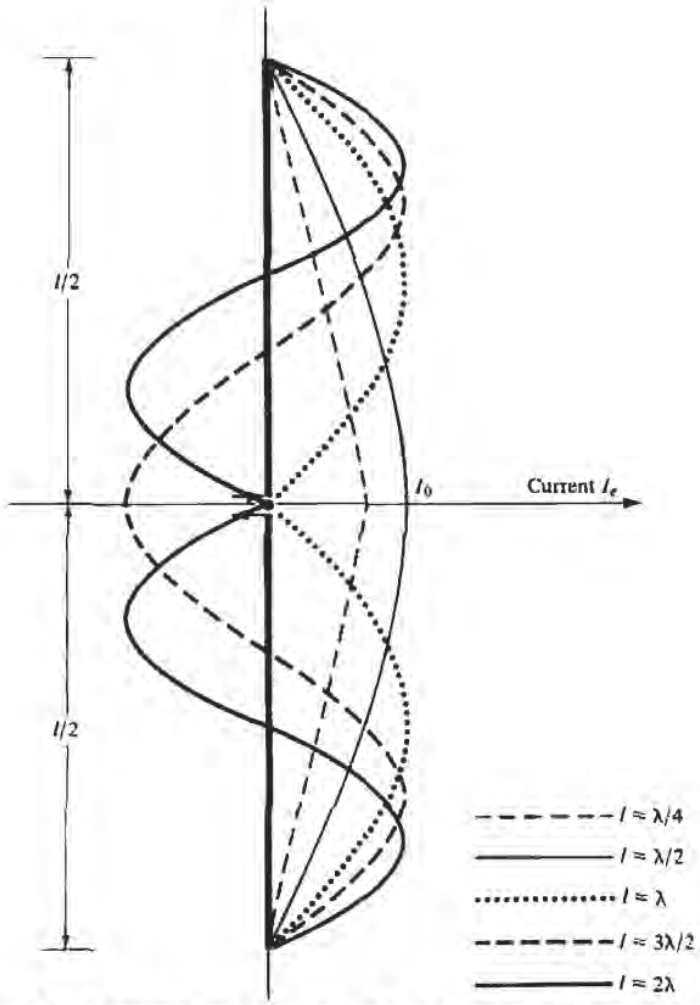


Figure 4.8 Current distributions along the length of a linear wire antenna.

To find the total power radiated, the average Poynting vector of (4-63) is integrated over a sphere of radius r. Thus

$$P_{\text{rad}} = \oiint_S \mathbf{W}_{\text{av}} \cdot d\mathbf{s} = \int_0^{2\pi} \int_0^{\pi} \hat{\mathbf{a}}_r W_{\text{av}} \cdot \hat{\mathbf{a}}_r r^2 \sin\theta \, d\theta \, d\phi$$

$$= \int_0^{2\pi} \int_0^{\pi} W_{\text{av}} r^2 \sin\theta \, d\theta \, d\phi \tag{4-66}$$

Using (4-63), we can write (4-66) as

$$P_{\text{rad}} = \int_0^{2\pi} \int_0^{\pi} W_{\text{av}} r^2 \sin\theta \, d\theta \, d\phi$$

$$= \eta \frac{|I_0|^2}{4\pi} \int_0^{\pi} \frac{\left[\cos\left(\frac{kl}{2}\cos\theta\right) - \cos\left(\frac{kl}{2}\right)\right]^2}{\sin\theta} d\theta \tag{4-67}$$

INTEL-1045
U.S. Patent 7,151,430

After some extensive mathematical manipulations, it can be shown that (4-67) reduces to

$$P_{\text{rad}} = \eta\frac{|I_0|^2}{4\pi}\{C + \ln(kl) - C_i(kl) + \tfrac{1}{2}\sin(kl)[S_i(2kl) - 2S_i(kl)] + \tfrac{1}{2}\cos(kl)[C + \ln(kl/2) + C_i(2kl) - 2C_i(kl)]\} \tag{4-68}$$

where $C = 0.5772$ (Euler's constant) and $C_i(x)$ and $S_i(x)$ are the cosine and sine integrals (see Appendix III) given by

$$C_i(x) = -\int_x^\infty \frac{\cos y}{y}\,dy = \int_\infty^x \frac{\cos y}{y}\,dy \tag{4-68a}$$

$$S_i(x) = \int_0^x \frac{\sin y}{y}\,dy \tag{4-68b}$$

The derivation of (4-68) from (4-67) is assigned as a problem at the end of the chapter (Prob. 4.17). $C_i(x)$ is related to $C_{in}(x)$ by

$$C_{in}(x) = \ln(\gamma x) - C_i(x) = \ln(\gamma) + \ln(x) - C_i(x) = 0.5772 + \ln(x) - C_i(x) \tag{4-69}$$

where

$$C_{in}(x) = \int_0^x \left(\frac{1 - \cos y}{y}\right)dy \tag{4-69a}$$

$C_i(x)$, $S_i(x)$ and $C_{in}(x)$ are tabulated in Appendix III.

The radiation resistance can be obtained using (4-18) and (4-68) and can be written as

$$R_r = \frac{2P_{\text{rad}}}{|I_0|^2} = \frac{\eta}{2\pi}\{C + \ln(kl) - C_i(kl) + \tfrac{1}{2}\sin(kl) \times [S_i(2kl) - 2S_i(kl)] + \tfrac{1}{2}\cos(kl) \times [C + \ln(kl/2) + C_i(2kl) - 2C_i(kl)]\} \tag{4-70}$$

Shown in Figure 4.9 is a plot of R_r as a function of l (in wavelengths) when the antenna is radiating into free-space ($\eta \simeq 120\pi$).

4.5.4 Directivity

As was illustrated in Figure 4.6, the radiation pattern of a dipole becomes more directional as its length increases. When the overall length is greater than about one wavelength, the number of lobes increases and the antenna loses its directional properties. The parameter that is used as a "figure-of-merit" for the directional properties of the antenna is the directivity which was defined in Section 2.5.

INTEL-1045
U.S. Patent 7,151,430

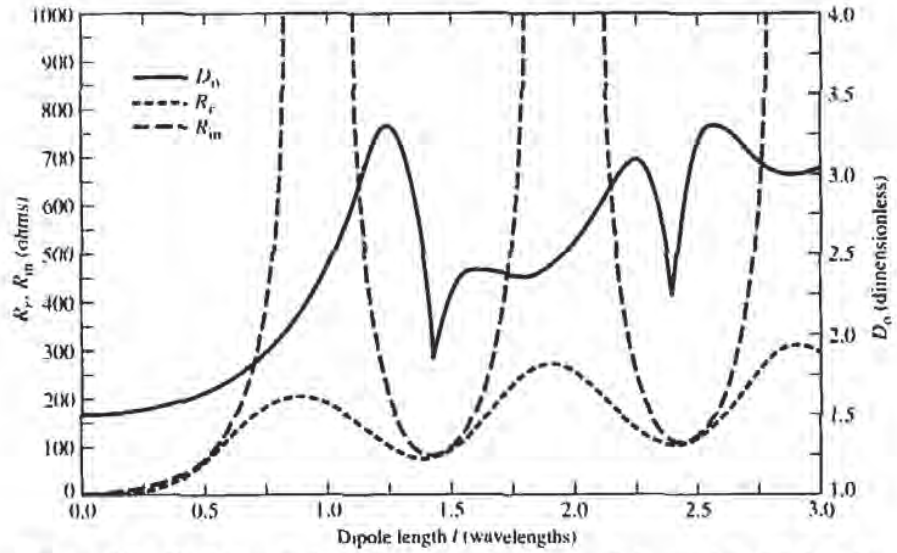


Figure 4.9 *Radiation resistance, input resistance and directivity of a thin dipole with sinusoidal current distribution.*

The directivity was defined mathematically by (2-22), or

$$D_0 = 4\pi \frac{F(\theta, \phi)|_{\max}}{\int_0^{2\pi} \int_0^{\pi} F(\theta, \phi) \sin\theta \, d\theta \, d\phi} \tag{4-71}$$

where $F(\theta, \phi)$ is related to the radiation intensity U by (2-19), or

$$U = B_0 F(\theta, \phi) \tag{4-72}$$

From (4-64), the dipole antenna of length l has

$$F(\theta, \phi) = F(\theta) = \left[\frac{\cos\left(\frac{kl}{2}\cos\theta\right) - \cos\left(\frac{kl}{2}\right)}{\sin\theta} \right]^2 \tag{4-73}$$

and

$$B_0 = \eta \frac{|I_0|^2}{8\pi^2} \tag{4-73a}$$

Because the pattern is not a function of ϕ, (4-71) reduces to

$$D_0 = \frac{2F(\theta)|_{\max}}{\int_0^{\pi} F(\theta) \sin\theta \, d\theta} \tag{4-74}$$

Equation (4-74) can be written, using (4-67), (4-68), and (4-73), as

$$D_0 = \frac{2F(\theta)|_{\max}}{Q} \tag{4-75}$$

INTEL-1045
U.S. Patent 7,151,430

where

$$Q = \{C + \ln(kl) - C_i(kl) + \tfrac{1}{2}\sin(kl)[S_i(2kl) - 2S_i(kl)] + \tfrac{1}{2}\cos(kl)[C + \ln(kl/2) + C_i(2kl) - 2C_i(kl)]\} \quad (4\text{-}75a)$$

The maximum value of $F(\theta)$ varies and depends upon the length of the dipole.

Values of the directivity, as given by (4-75) and (4-75a), have been obtained for $0 < l \leq 3\lambda$ and are shown plotted in Figure 4.9. The corresponding values of the maximum effective aperture are related to the directivity by

$$A_{em} = \frac{\lambda^2}{4\pi} D_0 \quad (4\text{-}76)$$

4.5.5 Input Resistance

In Section 2.13 the input impedance was defined as "the ratio of the voltage to current at a pair of terminals or the ratio of the appropriate components of the electric to magnetic fields at a point." The real part of the input impedance was defined as the input resistance which for a lossless antenna reduces to the radiation resistance, a result of the radiation of real power.

In Section 4.2.2, the radiation resistance of an infinitesimal dipole was derived using the definition of (4-18). The radiation resistance of a dipole of length l with sinusoidal current distribution, of the form given by (4-56), is expressed by (4-70). By this definition, the radiation resistance is referred to the maximum current which for some lengths ($l = \lambda/4, 3\lambda/4, \lambda$, etc.) does not occur at the input terminals of the antenna (see Figure 4.8). To refer the radiation resistance to the input terminals of the antenna, the antenna itself is first assumed to be lossless ($R_L = 0$). Then the power at the input terminals is equated to the power at the current maximum.

Referring to Figure 4.10, we can write

$$\frac{|I_{in}|^2}{2} R_{in} = \frac{|I_0|^2}{2} R_r \quad (4\text{-}77)$$

or

$$R_{in} = \left[\frac{I_0}{I_{in}}\right]^2 R_r \quad (4\text{-}77a)$$

where

R_{in} = radiation resistance at input (feed) terminals
R_r = radiation resistance at current maximum Eq. (4-70)
I_0 = current maximum
I_{in} = current at input terminals

For a dipole of length l, the current at the input terminals (I_{in}) is related to the current maximum (I_0) referring to Figure 4.10, by

$$I_{in} = I_0 \sin\left(\frac{kl}{2}\right) \quad (4\text{-}78)$$

INTEL-1045
U.S. Patent 7,151,430

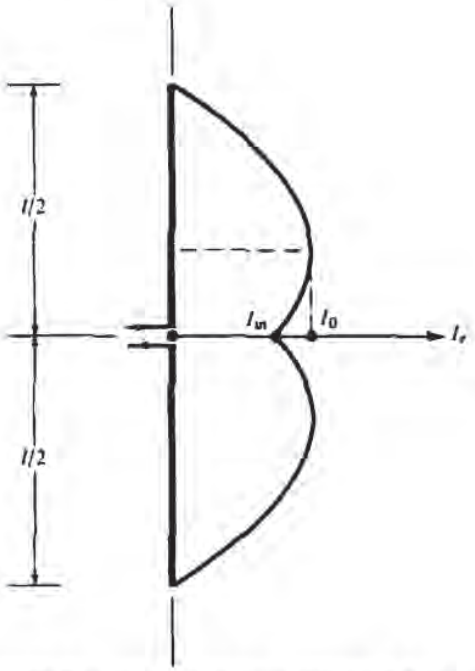


Figure 4.10 Current distribution of a linear wire antenna when current maximum does not occur at the input terminals.

Thus the input radiation resistance of (4-77a) can be written as

$$R_{in} = \frac{R_r}{\sin^2\left(\frac{kl}{2}\right)} \tag{4-79}$$

Values of R_{in} for $0 < l \leq 3\lambda$ are shown in Figure 4.9.

To compute the radiation resistance (in ohms), directivity (dimensionless and in dB), and input resistance (in ohms) for a dipole of length l, a FORTRAN computer program has been developed. The program is based on the definitions of each as given by (4-70), (4-71), and (4-79). The radiated power P_{rad} is computed by numerically integrating (over a closed sphere) the radiation intensity of (4-72)–(4-73a). The program is included at the end of this chapter and in the computer disc made available with the book. The length of the dipole (in wavelengths) must be inserted as an input.

When the overall length of the antenna is a multiple of λ (i.e., $l = n\lambda$, $n = 1, 2, 3, \ldots$), it is apparent from (4-56) and from Figure 4.8 that $I_{in} = 0$. That is,

$$I_{in} = I_0 \sin\left[k\left(\frac{l}{2} \pm z'\right)\right]\Bigg|_{\substack{z'=0 \\ l=n\lambda,\, n=0,1,2,}} = 0 \tag{4-80}$$

which indicates that the radiation resistance at the input terminals, as given by (4-77a) or (4-79) is infinite. In practice this is not the case because the current distribution does not follow an exact sinusoidal distribution, especially at the feed point. It has, however, very high values. Two of the primary factors which contribute

INTEL-1045
U.S. Patent 7,151,430

to the nonsinusoidal current distribution on an actual wire antenna are the nonzero radius of the wire and finite gap spacing at the terminals.

The radiation resistance and input resistance, as predicted, respectively, by (4-70) and (4-79), are based on the ideal current distribution of (4-56) and do not account for the finite radius of the wire or the gap spacing at the feed. Although the radius of the wire does not strongly influence the resistances, the gap spacing at the feed does play a significant role especially when the current at and near the feed point is small.

4.5.6 Finite Feed Gap

To analytically account for a nonzero current at the feed point for antennas with a finite gap at the terminals, Schelkunoff and Friis [6] have changed the current of (4-56) by including a quadrature term in the distribution. The additional term is inserted to take into account the effects of radiation on the antenna current distribution. In other words, once the antenna is excited by the "ideal" current distribution of (4-56), electric and magnetic fields are generated which in turn disturb the "ideal" current distribution. This reaction is included by modifying (4-56) to

$$\mathbf{I}_e(x', y', z') = \begin{cases} \hat{\mathbf{a}}_z \left\{ I_0 \sin\left[k\left(\frac{l}{2} - z'\right)\right] + jpI_0\left[\cos(kz') - \cos\left(\frac{k}{2}l\right)\right]\right\}, \\ \qquad\qquad 0 \le z' \le l/2 \\ \hat{\mathbf{a}}_z \left\{ I_0 \sin\left[k\left(\frac{l}{2} + z'\right)\right] + jpI_0\left[\cos(kz') - \cos\left(\frac{k}{2}l\right)\right]\right\}, \\ \qquad\qquad -l/2 \le z' \le 0 \end{cases} \tag{4-81}$$

where p is a coefficient that is dependent upon the overall length of the antenna and the gap spacing at the terminals. The values of p become smaller as the radius of the wire and the gap decrease.

When $l = \lambda/2$,

$$\mathbf{I}_e(x', y', z') = \hat{\mathbf{a}}_z I_0(1 + jp)\cos(kz') \qquad 0 \le |z'| \le \lambda/4 \tag{4-82}$$

and for $l = \lambda$

$$\mathbf{I}_e(x', y', z') = \begin{cases} \hat{\mathbf{a}}_z I_0\{\sin(kz') + jp[1 + \cos(kz')]\} & 0 \le z' \le \lambda/2 \\ \hat{\mathbf{a}}_z I_0\{-\sin(kz') + jp[1 + \cos(kz')]\} & -\lambda/2 \le z' \le 0 \end{cases} \tag{4-83}$$

Thus for $l = \lambda/2$ the shape of the current is not changed while for $l = \lambda$ it is modified by the second term which is more dominant for small values of z'.

The variations of the current distribution and impedances, especially of wire-type antennas, as a function of the radius of the wire and feed gap spacing can be easily taken into account by using advanced computational methods and numerical techniques, especially Integral Equations and Moment Method [7]–[12], which are introduced in Chapter 8.

To illustrate the point, the current distribution of an $l = \lambda/2$ and $l = \lambda$ dipole has been computed using an integral equation formulation with a moment method

INTEL-1045
U.S. Patent 7,151,430

numerical solution, and it is shown in Figure 8.13(b) where it is compared with the ideal distribution of (4-56) and other available data. For the moment method solution, a gap at the feed has been inserted. As expected and illustrated in Figure 8.13(b), the current distribution for the $l = \lambda/2$ dipole based on (4-56) is not that different from that based on the moment method. This is also illustrated by (4-82). Therefore the input resistance based on these two methods will not be that different. However, for the $l = \lambda$ dipole, the current distribution based on (4-56) is quite different, especially at and near the feed point, compared to that based on the moment method, as shown in Figure 8.13(b). This is expected since the current distribution based on the ideal current distribution is zero at the feed point; for practical antennas it is very small. Therefore the gap at the feed plays an important role on the current distribution at and near the feed point. In turn, the values of the input resistance based on the two methods will be quite different, since there is a significant difference in the current between the two methods. This is discussed further in Chapter 8.

4.6 HALF-WAVELENGTH DIPOLE

One of the most commonly used antennas is the half-wavelength ($l = \lambda/2$) dipole. Because its radiation resistance is 73 ohms, which is very near the 75-ohm characteristic impedance of some transmission lines, its matching to the line is simplified especially at resonance. Because of its wide acceptance in practice, we will examine in a little more detail its radiation characteristics.

The electric and magnetic field components of a half-wavelength dipole can be obtained from (4-62a) and (4-62b) by letting $l = \lambda/2$. Doing this, they reduce to

$$E_\theta \simeq j\eta \frac{I_0 e^{-jkr}}{2\pi r}\left[\frac{\cos\left(\frac{\pi}{2}\cos\theta\right)}{\sin\theta}\right] \tag{4-84}$$

$$H_\phi \simeq j\frac{I_0 e^{-jkr}}{2\pi r}\left[\frac{\cos\left(\frac{\pi}{2}\cos\theta\right)}{\sin\theta}\right] \tag{4-85}$$

In turn, the time-average power density and radiation intensity can be written, respectively, as

$$W_{av} = \eta\frac{|I_0|^2}{8\pi^2 r^2}\left[\frac{\cos\left(\frac{\pi}{2}\cos\theta\right)}{\sin\theta}\right]^2 = \eta\frac{|I_0|^2}{8\pi^2 r^2}\sin^3\theta \tag{4-86}$$

and

$$U = r^2 W_{av} = \eta\frac{|I_0|^2}{8\pi^2}\left[\frac{\cos\left(\frac{\pi}{2}\cos\theta\right)}{\sin\theta}\right]^2 = \eta\frac{|I_0|^2}{8\pi^2}\sin^3\theta \tag{4-87}$$

INTEL-1045
U.S. Patent 7,151,430

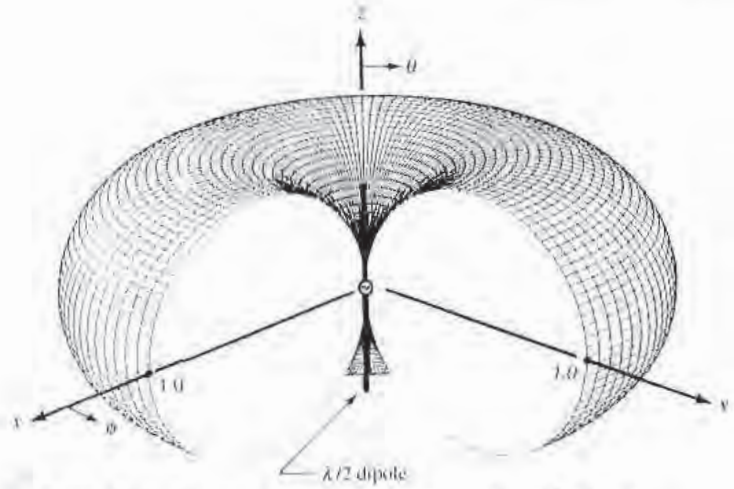


Figure 4.11 Three-dimensional pattern of a $\lambda/2$ dipole. (SOURCE: C. A. Balanis, "Antenna Theory: A Review" *Proc. IEEE*, Vol. 80, No 1, Jan. 1992, © 1992 IEEE.)

whose two-dimensional pattern is shown plotted in Figure 4.6 while the three-dimensional pattern is depicted in Figure 4.11. For the three-dimensional pattern of Figure 4.11, a 90° angular sector has been removed to illustrate the figure-eight elevation plane pattern variations.

The total power radiated can be obtained as a special case of (4-67), or

$$P_{\text{rad}} = \eta \frac{|I_0|^2}{4\pi} \int_0^{\pi} \frac{\cos^2\left(\frac{\pi}{2}\cos\theta\right)}{\sin\theta} d\theta \tag{4-88}$$

which when integrated reduces, as a special case of (4-68), to

$$P_{\text{rad}} = \eta \frac{|I_0|^2}{8\pi} \int_0^{2\pi} \left(\frac{1-\cos y}{y}\right) dy = \eta \frac{|I_0|^2}{8\pi} C_{\text{in}}(2\pi) \tag{4-89}$$

By the definition of $C_{\text{in}}(x)$, as given by (4-69), $C_{\text{in}}(2\pi)$ is equal to

$$C_{\text{in}}(2\pi) = 0.5772 + \ln(2\pi) - C_i(2\pi) = 0.5772 + 1.838 - (-0.02) \simeq 2.435 \tag{4-90}$$

where $C_i(2\pi)$ is obtained from the tables in Appendix III.

Using (4-87), (4-89), and (4-90), the directivity of the half-wavelength dipole reduces to

$$\boxed{D_0 = 4\pi \frac{U_{\max}}{P_{\text{rad}}} = 4\pi \frac{U|_{\theta=\pi/2}}{P_{\text{rad}}} = \frac{4}{C_{\text{in}}(2\pi)} = \frac{4}{2.435} \simeq 1.643} \tag{4-91}$$

The corresponding maximum effective area is equal to

$$\boxed{A_{em} = \frac{\lambda^2}{4\pi} D_0 = \frac{\lambda^2}{4\pi}(1.643) = 0.13\lambda^2} \tag{4-92}$$

INTEL-1045
U.S. Patent 7,151,430

and the radiation resistance, for a free-space medium ($\eta = 120\pi$), is given by

$$R_r = \frac{2P_{rad}}{|I_0|^2} = \frac{\eta}{4\pi} C_{in}(2\pi) = 30(2.435) \simeq 73 \tag{4-93}$$

The radiation resistance of (4-93) is also the radiation resistance at the input terminals (input resistance) since the current maximum for a dipole of $l = \lambda/2$ occurs at the input terminals (see Figure 4.8). As it will be shown in Chapter 8, the imaginary part (reactance) associated with the input impedance of a dipole is a function of its length (for $l = \lambda/2$, it is equal to $j42.5$). Thus the total input impedance for $l = \lambda/2$ is equal to $Z_{in} = 73 + j42.5$. To reduce the imaginary part of the input impedance to zero, the antenna is matched or reduced in length until the reactance vanishes. The latter is most commonly used in practice for half-wavelength dipoles.

Depending on the radius of the wire, the length of the dipole for first resonance is about $l = 0.47\lambda$ to 0.48λ; the thinner the wire, the closer the length is to 0.48λ. Thus, for thicker wires, a larger segment of the wire has to be removed from $\lambda/2$ to achieve resonance.

4.7 LINEAR ELEMENTS NEAR OR ON INFINITE PERFECT CONDUCTORS

Thus far we have considered the radiation characteristics of antennas radiating into an unbounded medium. The presence of an obstacle, especially when it is near the radiating element, can significantly alter the overall radiation properties of the antenna system. In practice the most common obstacle that is always present, even in the absence of anything else, is the ground. Any energy from the radiating element directed toward the ground undergoes a reflection. The amount of reflected energy and its direction are controlled by the geometry and constitutive parameters of the ground.

In general, the ground is a lossy medium ($\sigma \neq 0$) whose effective conductivity increases with frequency. Therefore it should be expected to act as a very good conductor above a certain frequency, depending primarily upon its moisture content. To simplify the analysis, it will first be assumed that the ground is a perfect electric conductor, flat, and infinite in extent. The effects of finite conductivity and earth curvature will be incorporated later. The same procedure can also be used to investigate the characteristics of any radiating element near any other infinite, flat, perfect electric conductor. Although infinite structures are not realistic, the developed procedures can be used to simulate very large (electrically) obstacles. The effects that finite dimensions have on the radiation properties of a radiating element can be conveniently accounted for by the use of the Geometrical Theory of Diffraction (Chapter 12, Section 12.10) and/or the Moment Method (Chapter 8, Section 8.4).

4.7.1 Image Theory

To analyze the performance of an antenna near an infinite plane conductor, virtual sources (images) will be introduced to account for the reflections. As the name implies, these are not real sources but imaginary ones, which when combined with the real

INTEL-1045
U.S. Patent 7,151,430

sources, form an equivalent system. For analysis purposes only, the equivalent system gives the same radiated field on and above the conductor as the actual system itself. Below the conductor, the equivalent system does not give the correct field. However, in this region the field is zero and there is no need for the equivalent.

To begin the discussion, let us assume that a vertical electric dipole is placed a distance h above an infinite, flat, perfect electric conductor as shown in Figure 4.12(a). The arrow indicates the polarity of the source. Energy from the actual source is radiated in all directions in a manner determined by its unbounded medium directional properties. For an observation point P_1, there is a direct wave. In addition, a wave from the actual source radiated toward point R_1 of the interface undergoes a reflection. The direction is determined by the law of reflection ($\theta_1^i = \theta_1^r$) which assures that the energy in homogeneous media travels in straight lines along the shortest paths. This wave will pass through the observation point P_1. By extending its actual path below the interface, it will seem to originate from a virtual source positioned a distance h below the boundary. For another observation point P_2 the point of reflection is R_2, but the virtual source is the same as before. The same is concluded for all other observation points above the interface.

The amount of reflection is generally determined by the respective constitutive parameters of the media below and above the interface. For a perfect electric conductor below the interface, the incident wave is completely reflected and the field below the boundary is zero. According to the boundary conditions, the tangential components of the electric field must vanish at all points along the interface. Thus for an incident electric field with vertical polarization shown by the arrows, the polarization of the reflected waves must be as indicated in the figure to satisfy the boundary conditions. To excite the polarization of the reflected waves, the virtual source must also be vertical and with a polarity in the same direction as that of the actual source (thus a reflection coefficient of $+1$).

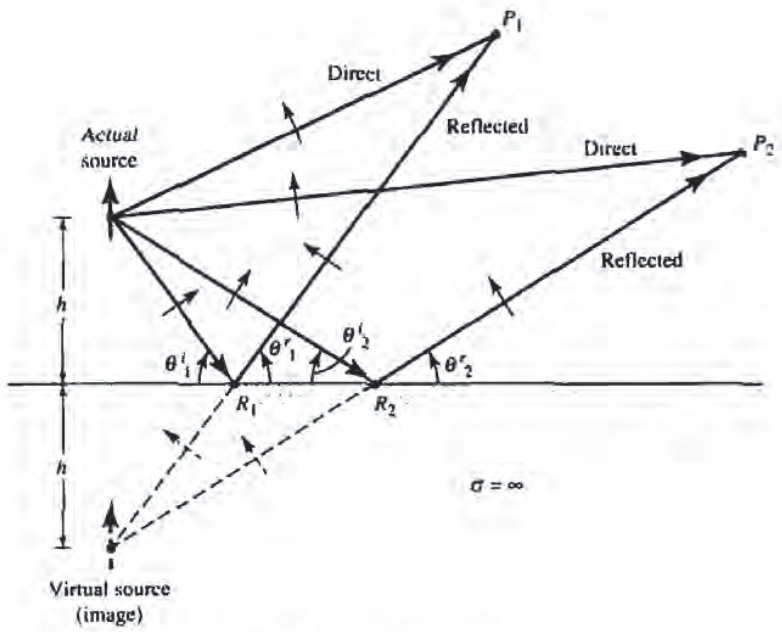
Another orientation of the source will be to have the radiating element in a horizontal position, as shown in Figure 4.21. Following a procedure similar to that of the vertical dipole, the virtual source (image) is also placed a distance h below the interface but with a 180° polarity difference relative to the actual source (thus a reflection coefficient of -1).

In addition to electric sources, artificial equivalent "magnetic" sources and magnetic conductors have been introduced to aid in the analyses of electromagnetic boundary value problems. Figure 4.13(a) displays the sources and their images for an electric plane conductor. The single arrow indicates an electric element and the double a magnetic one. The direction of the arrow identifies the polarity. Since many problems can be solved using duality, Figure 4.13(b) illustrates the sources and their images when the obstacle is an infinite, flat, perfect "magnetic" conductor.

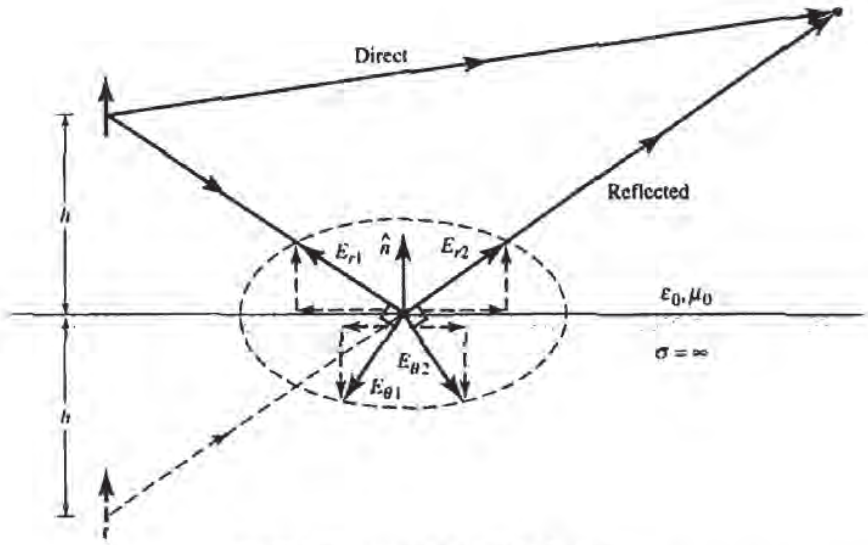
4.7.2 Vertical Electric Dipole

The analysis procedure for vertical and horizontal electric and magnetic elements near infinite electric and magnetic plane conductors, using image theory, was illustrated graphically in the previous section. Based on the graphical model of Figure 4.12, the mathematical expressions for the fields of a vertical linear element near a perfect electric conductor will now be developed. For simplicity, only far-field observations will be considered.

INTEL-1045
U.S. Patent 7,151,430



(a) Vertical electric dipole



(b) Field components at point of reflection

Figure 4.12 Vertical electric dipole above an infinite, flat, perfect electric conductor.

Referring to the geometry of Figure 4.14(a), the far-zone direct component of the electric field of the infinitesimal dipole of length l, constant current I_0, and observation point P is given according to (4-26a) by

$$E_\theta^d = j\eta \frac{kI_0 l e^{-jkr_1}}{4\pi r_1} \sin \theta_1 \tag{4-94}$$

INTEL-1045
U.S. Patent 7,151,430

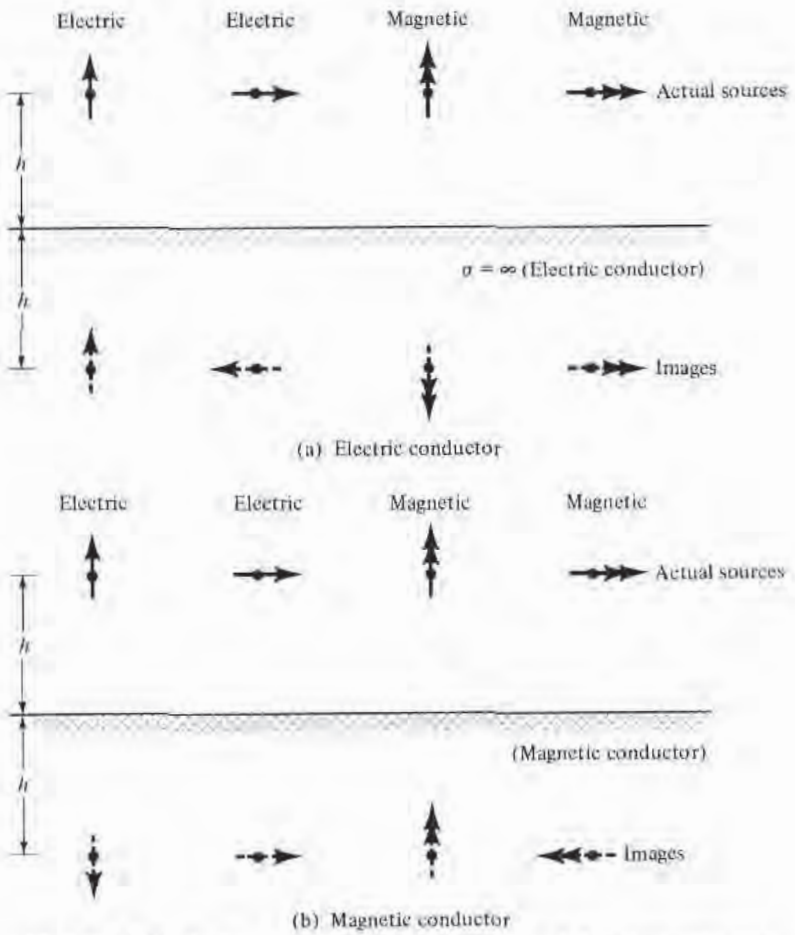


Figure 4.13 Electric and magnetic sources and their images near electric and magnetic conductors.

The reflected component can be accounted for by the introduction of the virtual source (image), as shown in Figure 4.14(a), and it can be written as

$$E_\theta^r = jR_v\eta\frac{kI_0le^{-jkr_2}}{4\pi r_2}\sin\theta_2 \tag{4-95}$$

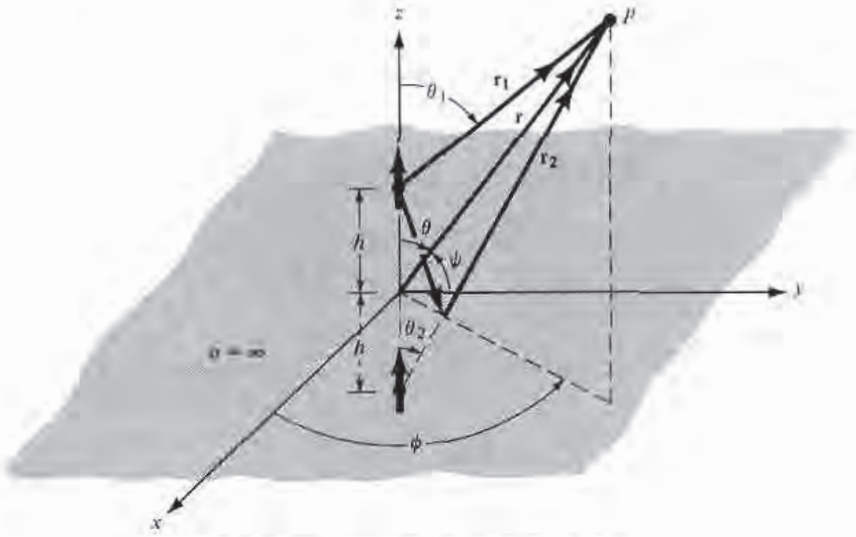
or

$$E_\theta' = j\eta\frac{kI_0le^{-jkr_2}}{4\pi r_2}\sin\theta_2 \tag{4-95a}$$

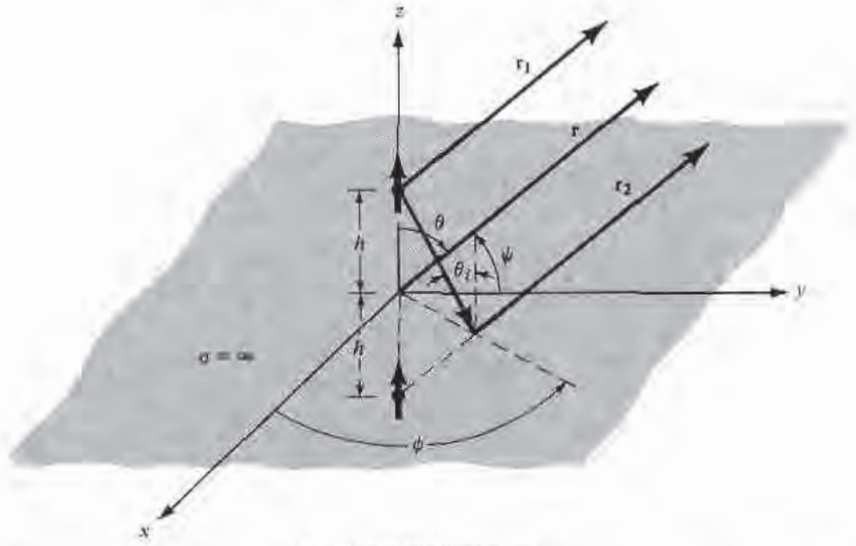
since the reflection coefficient R_v is equal to unity.

The total field above the interface ($z \geq 0$) is equal to the sum of the direct and reflected components as given by (4-94) and (4-95a). Since a field cannot exist inside a perfect electric conductor, it is equal to zero below the interface. To simplify the expression for the total electric field, it is referred to the origin of the coordinate system ($z = 0$).

INTEL-1045
U.S. Patent 7,151,430



(a) Vertical electric dipole above ground plane



(b) Far-field observations

Figure 4.14 Vertical electric dipole above infinite perfect electric conductor.

In general, we can write that

$$r_1 = [r^2 + h^2 - 2rh\cos\theta]^{1/2} \tag{4-96a}$$

$$r_2 = [r^2 + h^2 - 2rh\cos(\pi - \theta)]^{1/2} \tag{4-96b}$$

For far-field observations ($r \gg h$), (4-96a) and (4-96b) reduce using the binomial expansion to

$$r_1 \simeq r - h\cos\theta \tag{4-97a}$$

$$r_2 \simeq r + h\cos\theta \tag{4-97b}$$

As shown in Figure 4.14(b), geometrically (4-97a) and (4-97b) represent parallel lines. Since the amplitude variations are not as critical

INTEL-1045
U.S. Patent 7,151,430

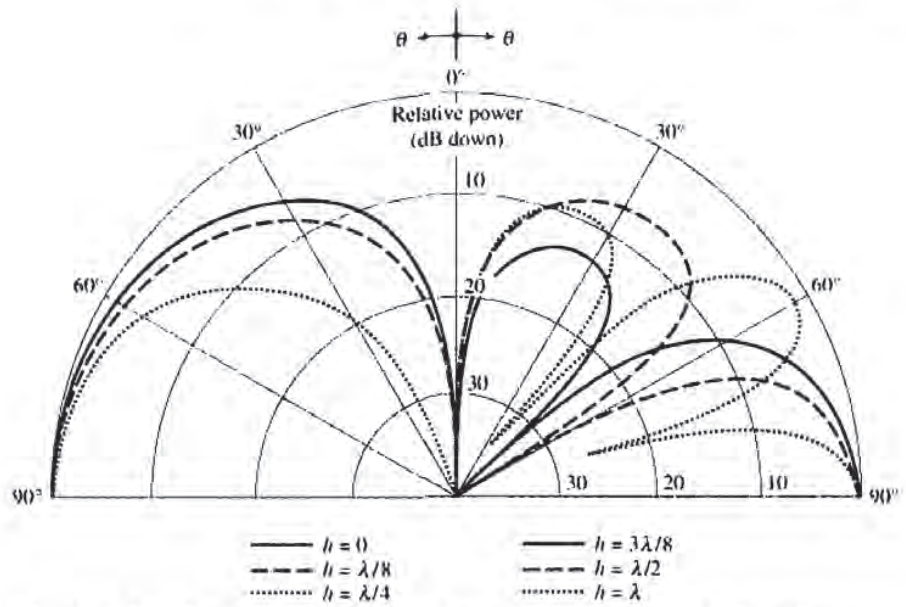


Figure 4.15 Elevation plane amplitude patterns of a vertical infinitesimal electric dipole for different heights above an infinite perfect electric conductor.

$$r_1 \simeq r_2 \simeq r \qquad \text{for amplitude variations} \tag{4-98}$$

Using (4-97a)–(4-98), the sum of (4-94) and (4-95a) can be written as

$$\left.\begin{aligned} E_\phi &\simeq j\eta \frac{kI_0 l e^{-jkr}}{4\pi r} \sin\theta |2\cos(kh\cos\theta)| \qquad z \geq 0 \\ E_\phi &= 0 \qquad\qquad\qquad\qquad\qquad\qquad\qquad\quad z < 0 \end{aligned}\right\} \tag{4-99}$$

It is evident that the total electric field is equal to the product of the field of a single source positioned symmetrically about the origin and a factor [within the brackets in (4-99)] which is a function of the antenna height (h) and the observation angle (θ). This is referred to as *pattern multiplication* and the factor is known as the *array factor*. This will be developed and discussed in more detail and for more complex configurations in Chapter 6.

The shape and amplitude of the field is not only controlled by the field of the single element but also by the positioning of the element relative to the ground. To examine the field variations as a function of the height h, the normalized (to 0 dB) power patterns for $h = 0$, $\lambda/8$, $\lambda/4$, $3\lambda/8$, $\lambda/2$, and λ have been plotted in Figure 4.15. Because of symmetry, only half of each pattern is shown. For $h > \lambda/4$ more minor lobes, in addition to the major ones, are formed. As h attains values greater than λ, an even greater number of minor lobes is introduced. These are shown in Figure 4.16 for $h = 2\lambda$ and 5λ. The introduction of the additional lobes in Figure 4.16 is usually called *scalloping*. In general, the total number of lobes is equal to the integer that is closest to

$$\boxed{\text{number of lobes} \simeq \frac{2h}{\lambda} + 1} \tag{4-100}$$

INTEL-1045
U.S. Patent 7,151,430

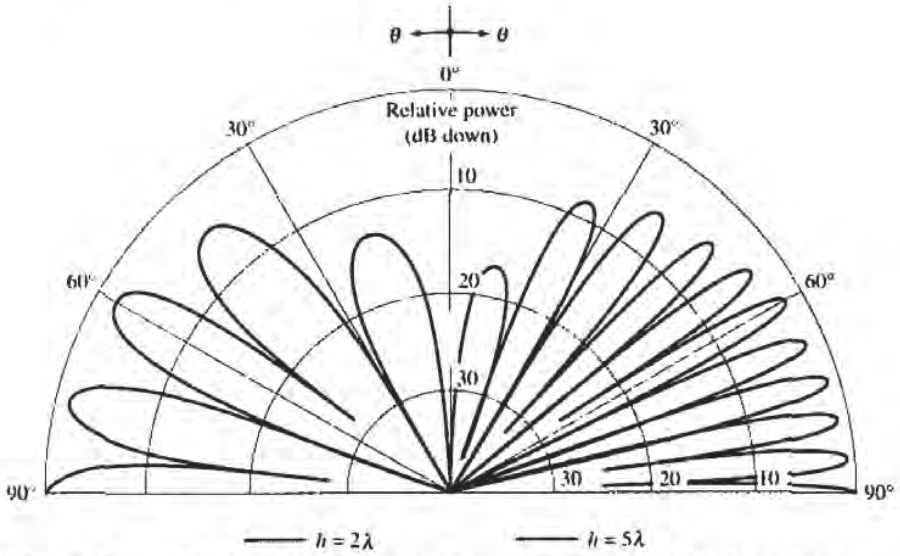


Figure 4.16 Elevation plane amplitude patterns of a vertical infinitesimal electric dipole for heights of 2λ and 5λ above an infinite perfect electric conductor.

Since the total field of the antenna system is different from that of a single element, the directivity and radiation resistance are also different. To derive expressions for them, we first find the total radiated power over the upper hemisphere of radius r using

$$P_{\text{rad}} = \oiint_S \mathbf{W}_{\text{av}} \cdot d\mathbf{s} = \frac{1}{2\eta}\int_0^{2\pi}\int_0^{\pi/2} |E_\theta|^2 r^2 \sin\theta \, d\theta \, d\phi$$

$$= \frac{\pi}{\eta}\int_0^{\pi/2} |E_\theta|^2 r^2 \sin\theta \, d\theta \tag{4-101}$$

which simplifies, with the aid of (4-99), to

$$P_{\text{rad}} = \pi\eta \left|\frac{I_0 l}{\lambda}\right|^2 \left[\frac{1}{3} - \frac{\cos(2kh)}{(2kh)^2} + \frac{\sin(2kh)}{(2kh)^3}\right] \tag{4-102}$$

As $kh \to \infty$ the radiated power, as given by (4-102), is equal to that of an isolated element. However, for $kh \to 0$, it can be shown by expanding the sine and cosine functions into series that the power is twice that of an isolated element. Using (4-99), the radiation intensity can be written as

$$U = r^2 W_{\text{av}} = r^2\left(\frac{1}{2\eta}|E_\theta|^2\right) = \frac{\eta}{2}\left|\frac{I_0 l}{\lambda}\right|^2 \sin^2\theta \cos^2(kh\cos\theta) \tag{4-103}$$

The maximum value of (4-103) occurs at $\theta = \pi/2$ and is given, excluding $kh \to \infty$, by

$$U_{\max} = U|_{\theta=\pi/2} = \frac{\eta}{2}\left|\frac{I_0 l}{\lambda}\right|^2 \tag{4-103a}$$

INTEL-1045
U.S. Patent 7,151,430

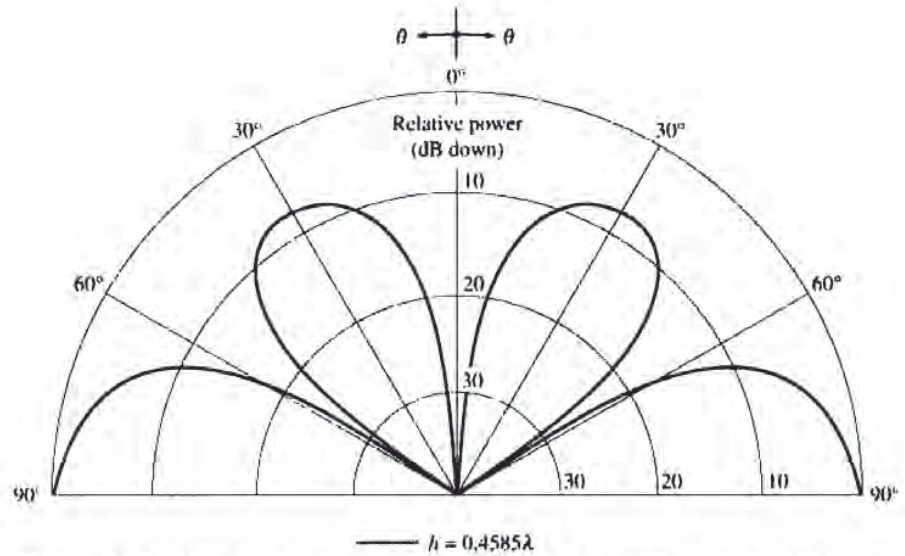


Figure 4.17 Elevation plane amplitude pattern of a vertical infinitesimal electric dipole at a height of 0.4585λ above an infinite perfect electric conductor.

which is four times greater than that of an isolated element. With (4-102) and (4-103a), the directivity can be written as

$$D_0 = \frac{4\pi U_{\max}}{P_{\text{rad}}} = \frac{2}{\left[\frac{1}{3} - \frac{\cos(2kh)}{(2kh)^2} + \frac{\sin(2kh)}{(2kh)^3}\right]} \tag{4-104}$$

whose value for $kh = 0$ is 3. The maximum value occurs when $kh = 2.881$ ($h = 0.4585\lambda$), and it is equal to 6.566 which is greater than four times that of an isolated element (1.5). The pattern for $h = 0.4585\lambda$ is shown plotted in Figure 4.17 while the directivity, as given by (4-104), is displayed in Figure 4.18 for $0 \le h \le 5\lambda$.

Using (4-102), the radiation resistance can be written as

$$R_r = \frac{2P_{\text{rad}}}{|I_0|^2} = 2\pi\eta\left(\frac{l}{\lambda}\right)^2\left[\frac{1}{3} - \frac{\cos(2kh)}{(2kh)^2} + \frac{\sin(2kh)}{(2kh)^3}\right] \tag{4-105}$$

whose value for $kh \to \infty$ is the same and for $kh = 0$ is twice that of the isolated element as given by (4-19). When $kh = 0$, the value of R_r as given by (4-105) is only one-half the value of an $l' = 2l$ isolated element according to (4-19). The radiation resistance, as given by (4-105), is plotted in Figure 4.18 for $0 \le h \le 5\lambda$ when $l = \lambda/50$ and the element is radiating into free-space ($\eta \simeq 120\pi$). It can be compared to the value of $R_r = 0.316$ ohms for the isolated element of Example 4.1.

In practice, a wide use has been made of a quarter-wavelength monopole ($l = \lambda/4$) mounted above a ground plane, as shown in Figure 4.19(a). For analysis purposes, a $\lambda/4$ image is introduced and it forms the $\lambda/2$ equivalent of Figure 4.19(b). It should be emphasized that the $\lambda/2$ equivalent of Figure 4.19(b) gives the correct field values for the actual system of Figure 4.19(a) only above the interface ($z \ge 0$, $0 \le \theta \le \pi/2$). Thus, the far-zone electric and magnetic fields for the $\lambda/4$ monopole above the ground plane are given, respectively, by (4-84) and (4-85).

INTEL-1045
U.S. Patent 7,151,430

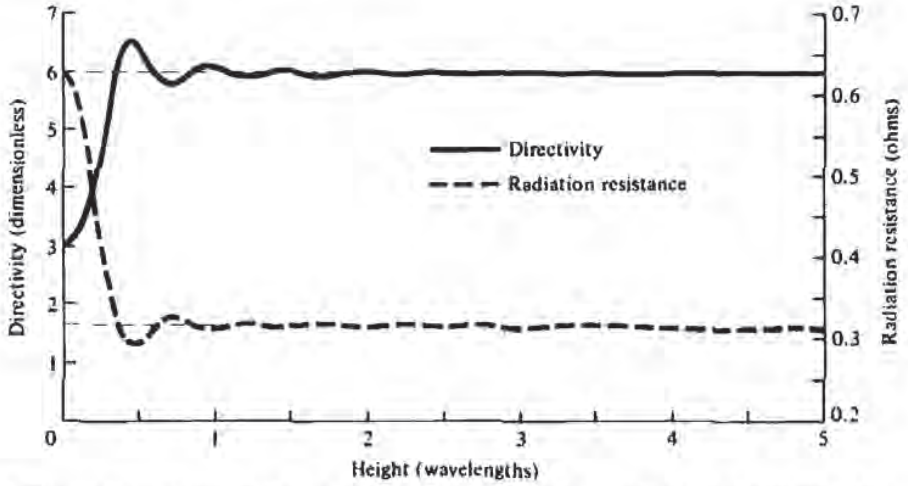
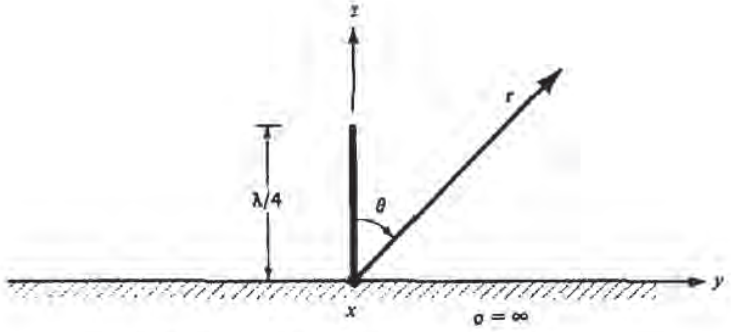
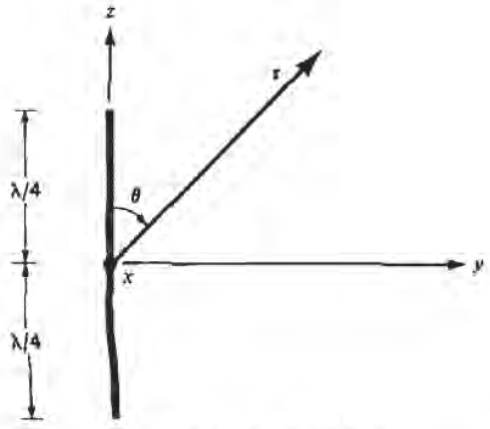


Figure 4.18 Directivity and radiation resistance of a vertical infinitesimal electric dipole as a function of its height above an infinite perfect electric conductor.



(a) λ/4 monopole on infinite electric conductor



(b) Equivalent of λ/4 monopole on infinite electric conductor

Figure 4.19 Quarter-wavelength monopole on an infinite perfect electric conductor.

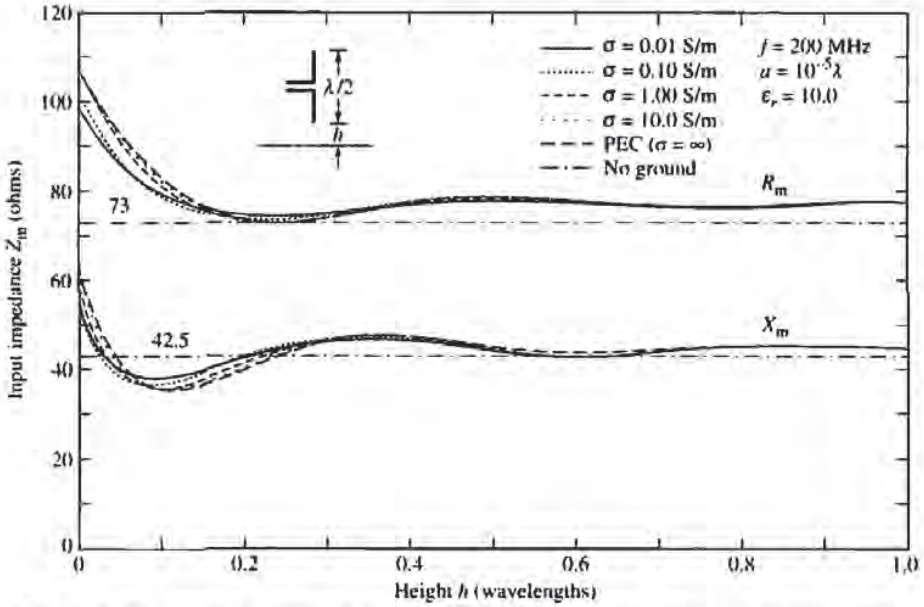


Figure 4.20 Input impedance of a vertical $\lambda/2$ dipole above a flat lossy electric conducting surface.

From the discussions of the resistance of an infinitesimal dipole above a ground plane for $kh = 0$, it follows that the input impedance of a $\lambda/4$ monopole above a ground plane is equal to one-half that of an isolated $\lambda/2$ dipole. Thus, referred to the current maximum, the input impedance Z_{im} is given by

$$Z_{im}\,(\text{monopole}) = \tfrac{1}{2}\,Z_{im}\,(\text{dipole}) = \tfrac{1}{2}[73 + j42.5] = 36.5 + j21.25 \quad (4\text{-}106)$$

where $73 + j42.5$ is the input impedance (and also the impedance referred to the current maximum) of a $\lambda/2$ dipole.

The same procedure can be followed for any other length. The input impedance $Z_{im} = R_{im} + jX_{im}$ (referred to the current maximum) of a vertical $\lambda/2$ dipole placed near a flat lossy electric conductor, as a function of height above the ground plane, is plotted in Figure 4.20, for $0 \leq h \leq \lambda$. Conductivity values considered were 10^{-2}, 10^{-1}, 1, 10 S/m, and infinity (PEC). It is apparent that the conductivity does not strongly influence the impedance values. The conductivity values used are representative of dry to wet earth. It is observed that the values of the resistance and reactance approach, as the height increases, the corresponding ones of the isolated element (73 ohms for the resistance and 42.5 ohms for the reactance).

4.7.3 Approximate Formulas for Rapid Calculations and Design

Although the input resistance of a dipole of any length can be computed using (4-70) and (4-79), while that of the corresponding monopole using (4-106), very good answers can be obtained using simpler but approximate expressions. Defining G as

$$G = kl/2 \text{ for dipole} \quad (4\text{-}107a)$$

$$G = kl \text{ for monopole} \quad (4\text{-}107b)$$

INTEL-1045
U.S. Patent 7,151,430

where l is the total length of each respective element, it has been shown that the input resistance of the dipole and monopole can be computed approximately using [10]

$$\underline{0 < G < \pi/4}$$

(maximum input resistance of dipole is less than 12.337 ohms)

$$R_{in}\,(\text{dipole}) = 20G^2 \qquad 0 < l < \lambda/4 \tag{4-108a}$$

$$R_{in}\,(\text{monopole}) = 10G^2 \qquad 0 < l < \lambda/8 \tag{4-108b}$$

$$\underline{\pi/4 \leq G < \pi/2}$$

(maximum input resistance of dipole is less than 76.383 ohms)

$$R_{in}\,(\text{dipole}) = 24.7G^{2.5} \qquad \lambda/4 \leq l < \lambda/2 \tag{4-109a}$$

$$R_{in}\,(\text{monopole}) = 12.35G^{2.5} \qquad \lambda/8 \leq l < \lambda/4 \tag{4-109b}$$

$$\underline{\pi/2 \leq G < 2}$$

(maximum input resistance of dipole is less than 200.53 ohms)

$$R_{in}\,(\text{dipole}) = 11.14G^{4.17} \qquad \lambda/2 \leq l < 0.6366\lambda \tag{4-110a}$$

$$R_{in}\,(\text{monopole}) = 5.57G^{4.17} \qquad \lambda/4 \leq l < 0.3183\lambda \tag{4-110b}$$

Besides being much simpler in form, these formulas are much more convenient in design (synthesis) problems where the input resistance is given and it is desired to determine the length of the element. These formulas can be verified by plotting the actual resistance versus length on a log–log scale and observe the slope of the line [13]. For example, the slope of the line for values of G up to about $\pi/4 = 0.75$ is 2.

Example 4.4

Determine the length of the dipole whose input resistance is 50 ohms. Verify the answer.

SOLUTION

Using (4-109a)

$$50 = 24.7G^{2.5}$$

or

$$G = 1.3259 = kl/2$$

Therefore

$$l = 0.422\lambda$$

Using (4-70) and (4-79) R_{in} for 0.422λ is 45.816 ohms, which closely agrees with the desired value of 50 ohms. To obtain 50 ohms using (4-70) and (4-79), $l = 0.4363\lambda$.

INTEL-1045
U.S. Patent 7,151,430

4.7.4 Antennas for Mobile Communication Systems

The dipole and monopole are two of the most widely used antennas for wireless mobile communication systems [14]–[17]. An array of dipole elements is extensively used as an antenna at the base station of a land mobile system while the monopole, because of its broadband characteristics and simple construction, is perhaps to most common antenna element for portable equipments, such as cellular telephones, cordless telephones, automobiles, trains, etc. The radiation efficiency and gain characteristics of both of these elements are strongly influenced by their electrical length which is related to the frequency of operation. In a hand-held unit, such as a cellular telephone, the position of the monopole element on the unit influences the pattern while it does not strongly affect the input impedance and resonant frequency. In addition to its use in mobile communication systems, the quarter-wavelength monopole is very popular in many other applications. An alternative to the monopole for the hand-held unit is the loop, which is discussed in Chapter 5. Other elements include the inverted F, planar inverted F antenna (PIFA), microstrip (patch), spiral, and others [14]–[17].

4.7.5 Horizontal Electric Dipole

Another dipole configuration is when the linear element is placed horizontally relative to the infinite electric ground plane, as shown in Figure 4.21. The analysis procedure of this is identical to the one of the vertical dipole. Introducing an image and assuming far-field observations, as shown in Figure 4.22(a,b), the direct component can be written as

$$E_{\psi}^{d} = j\eta \frac{kI_0 l e^{-jkr_1}}{4\pi r_1} \sin\psi \tag{4-111}$$

and the reflected one by

$$E_{\psi}^{r} = jR_h \eta \frac{kI_0 l e^{-jkr_2}}{4\pi r_2} \sin\psi \tag{4-112}$$

or

$$E_{\psi}^{r} = -j\eta \frac{kI_0 l e^{-jkr_2}}{4\pi r_2} \sin\psi \tag{4-112a}$$

since the reflection coefficient is equal to $R_h = -1$.

To find the angle ψ, which is measured from the y-axis toward the observation point, we first form

$$\cos\psi = \hat{\mathbf{a}}_y \cdot \hat{\mathbf{a}}_r = \hat{\mathbf{a}}_y \cdot (\hat{\mathbf{a}}_x \sin\theta\cos\phi + \hat{\mathbf{a}}_y \sin\theta\sin\phi + \hat{\mathbf{a}}_z \cos\theta) = \sin\theta\sin\phi \tag{4-113}$$

from which we find

$$\sin\psi = \sqrt{1 - \cos^2\psi} = \sqrt{1 - \sin^2\theta\sin^2\phi} \tag{4-114}$$

INTEL-1045
U.S. Patent 7,151,430

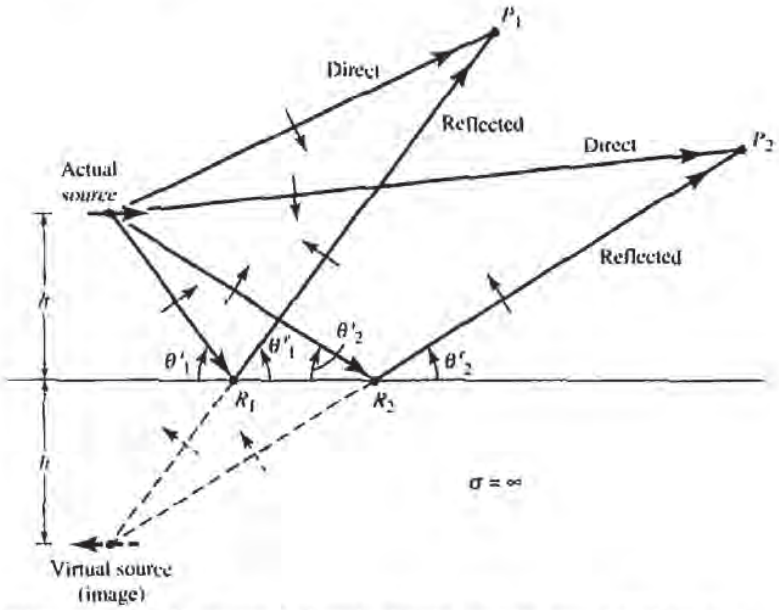


Figure 4.21 Horizontal electric dipole, and its associated image, above an infinite, flat, perfect electric conductor.

Since for far-field observations

$$\left.\begin{aligned} r_1 &\simeq r - h\cos\theta \\ r_2 &\simeq r + h\cos\theta \end{aligned}\right\} \quad \text{for phase variations} \tag{4-115a}$$

$$r_1 \simeq r_2 \simeq r \quad \text{for amplitude variations} \tag{4-115b}$$

the total field, which is valid only above the ground plane ($z \geq h$; $0 \leq \theta \leq \pi/2$, $0 \leq \phi \leq 2\pi$), can be written as

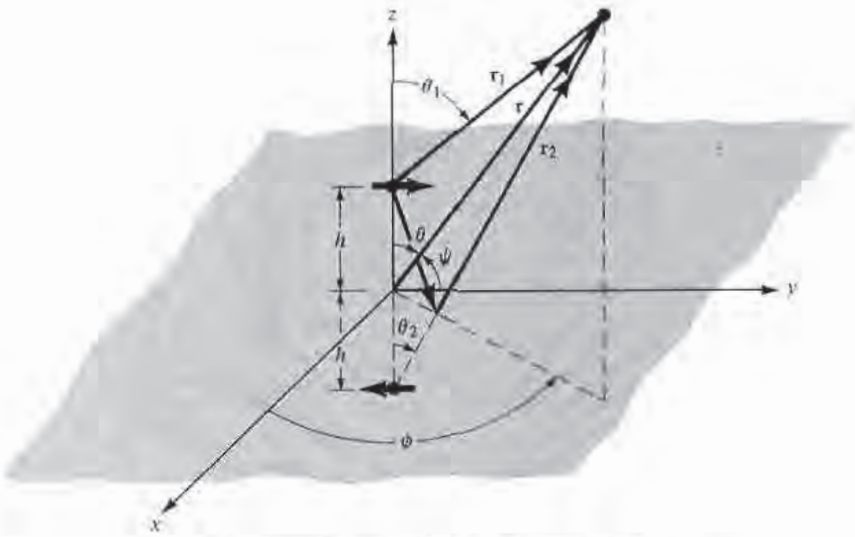
$$E_\phi = E_\phi^i + E_\phi^r = j\eta \frac{kI_0 le^{-jkr}}{4\pi r} \sqrt{1 - \sin^2\theta \sin^2\phi}\,[2j\sin(kh\cos\theta)] \tag{4-116}$$

Equation (4-116) again consists of the product of the field of a single isolated element placed symmetrically at the origin and a factor (within the brackets) known as the *array factor*. This again is the pattern multiplication rule which is discussed in more detail in Chapter 6.

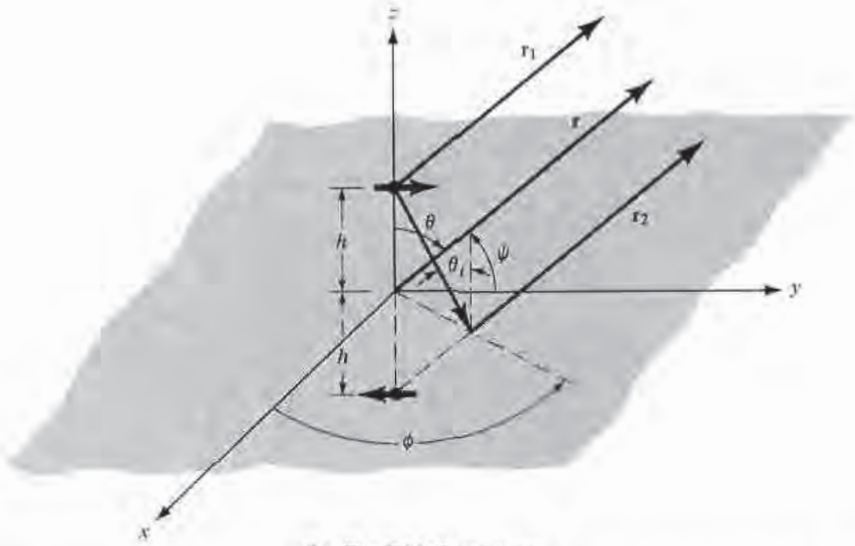
To examine the variations of the total field as a function of the element height above the ground plane, the two-dimensional elevation plane patterns (normalized to 0 dB) for $\phi = 90°$ (y-z plane) when $h = 0$, $\lambda/8$, $\lambda/4$, $3\lambda/8$, $\lambda/2$, and λ are plotted in Figure 4.23. Since this antenna system is not symmetric, the azimuthal plane (x-y plane) pattern will not be isotropic.

To obtain a better visualization of the radiation intensity in all directions above the interface, the three-dimensional pattern for $h = \lambda$ is shown plotted in Figure 4.24. The radial distance on the x-y plane represents the elevation angle θ from 0° to 90°, and the z-axis represents the normalized amplitude of the radiation field intensity from

INTEL-1045
U.S. Patent 7,151,430



(a) Horizontal electric dipole above ground plane



(b) Far-field observations

Figure 4.22 Horizontal electric dipole above an infinite perfect electric conductor.

0 to 1. The azimuthal angle ϕ ($0 \leq \phi \leq 2\pi$) is measured from the x- toward the y-axis on the x-y plane.

As the height increases beyond one wavelength ($h > \lambda$), a larger number of lobes is again formed. This is illustrated in Figure 4.25 for $h = 2\lambda$ and 5λ. The scalloping effect is evident here, as in Figure 4-16 for the vertical dipole. The total number of lobes is equal to the integer that most closely is equal to

$$\boxed{\text{number of lobes} = 2\left(\frac{h}{\lambda}\right)} \tag{4-117}$$

with unity being the smallest number.

INTEL-1045
U.S. Patent 7,151,430

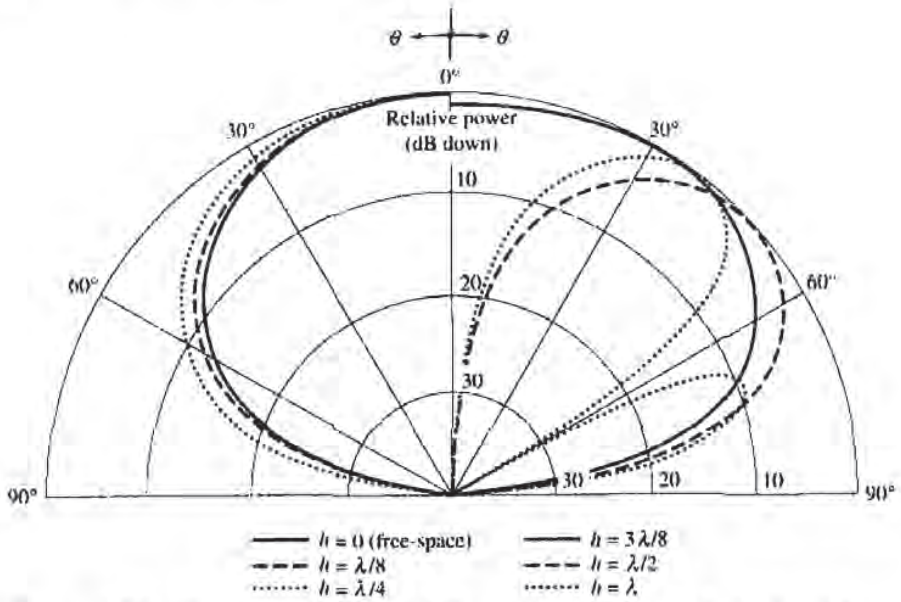


Figure 4.23 Elevation plane ($\phi = 90°$) amplitude patterns of a horizontal infinitesimal electric dipole for different heights above an infinite perfect electric conductor.

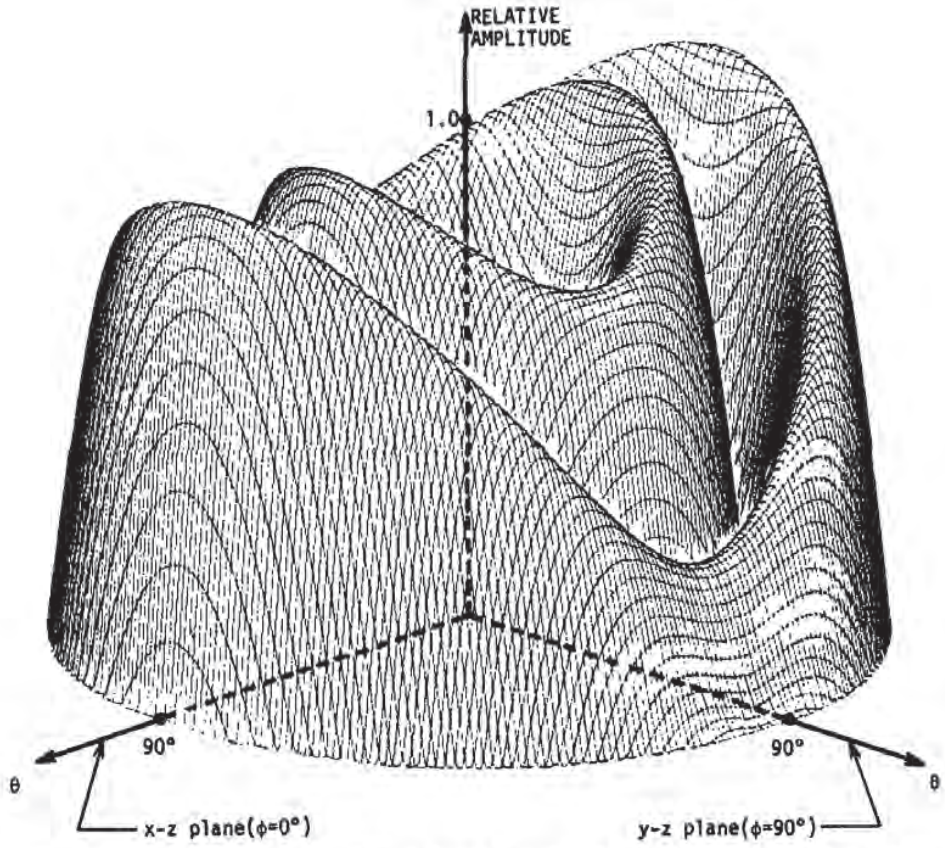


Figure 4.24 Three-dimensional amplitude pattern of an infinitesimal horizontal dipole a distance $h = \lambda$ above an infinite perfect electric conductor.

INTEL-1045
U.S. Patent 7,151,430

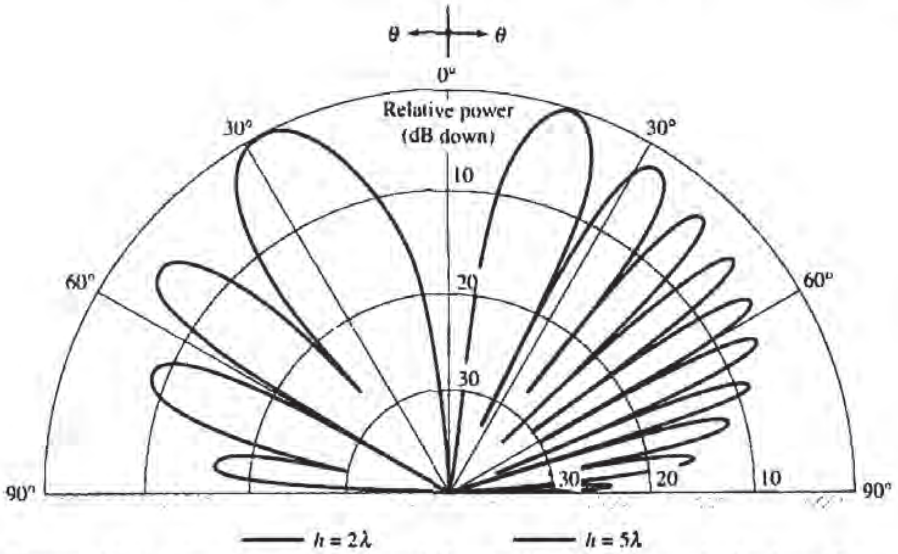


Figure 4.25 Elevation plane ($\phi = 90°$) amplitude patterns of a horizontal infinitesimal electric dipole for heights 2λ and 5λ above an infinite perfect electric conductor.

Following a procedure similar to the one performed for the vertical dipole, the radiated power can be written as

$$P_{rad} = \eta \frac{\pi}{2} \left| \frac{I_0 l}{\lambda} \right|^2 \left[\frac{2}{3} - \frac{\sin(2kh)}{2kh} - \frac{\cos(2kh)}{(2kh)^2} + \frac{\sin(2kh)}{(2kh)^3} \right] \tag{4-118}$$

and the radiation resistance as

$$R_r = \eta \pi \left(\frac{l}{\lambda} \right)^2 \left[\frac{2}{3} - \frac{\sin(2kh)}{2kh} - \frac{\cos(2kh)}{(2kh)^2} + \frac{\sin(2kh)}{(2kh)^3} \right] \tag{4-119}$$

By expanding the sine and cosine functions into series, it can be shown that (4-119) reduces for small values of kh to

$$R_r \overset{kh \to 0}{=} \eta \pi \left(\frac{l}{\lambda} \right)^2 \left[\frac{2}{3} - \frac{2}{3} + \frac{8}{15} \left(\frac{2\pi h}{\lambda} \right)^2 \right] = \eta \frac{32\pi^3}{15} \left(\frac{l}{\lambda} \right)^2 \left(\frac{h}{\lambda} \right)^2 \tag{4-120}$$

For $kh \to \infty$, (4-119) reduces to that of an isolated element. The radiation resistance, as given by (4-119), is plotted in Figure 4.26 for $0 \le h \le 5\lambda$ when $l = \lambda/50$ and the antenna is radiating into free space ($\eta \simeq 120\pi$).

The radiation intensity is given by

$$U \simeq \frac{r^2}{2\eta} |E_\phi|^2 = \frac{\eta}{2} \left| \frac{I_0 l}{\lambda} \right|^2 (1 - \sin^2 \theta \sin^2 \phi) \sin^2(kh \cos \theta) \tag{4-121}$$

The maximum value of (4-121) depends on the value of kh (whether $kh \le \pi/2$, $h \le \lambda/4$ or $kh > \pi/2$, $h > \lambda/4$). It can be shown that the maximum of (4-121) is:

$$U_{max} = \begin{cases} \dfrac{\eta}{2} \left| \dfrac{I_0 l}{\lambda} \right|^2 \sin^2(kh) & kh \le \pi/2 \ (h \le \lambda/4) \\ & (\theta = 0°) \end{cases} \tag{4-122a}$$

$$\begin{cases} \dfrac{\eta}{2} \left| \dfrac{I_0 l}{\lambda} \right|^2 & kh > \pi/2 \ (h > \lambda/4) \\ & [\phi = 0° \text{ and } \sin(kh \cos \theta_{max}) = 1 \\ & \text{or } \theta_{max} = \cos^{-1}(\pi/2kh)] \end{cases} \tag{4-122b}$$

INTEL-1045
U.S. Patent 7,151,430

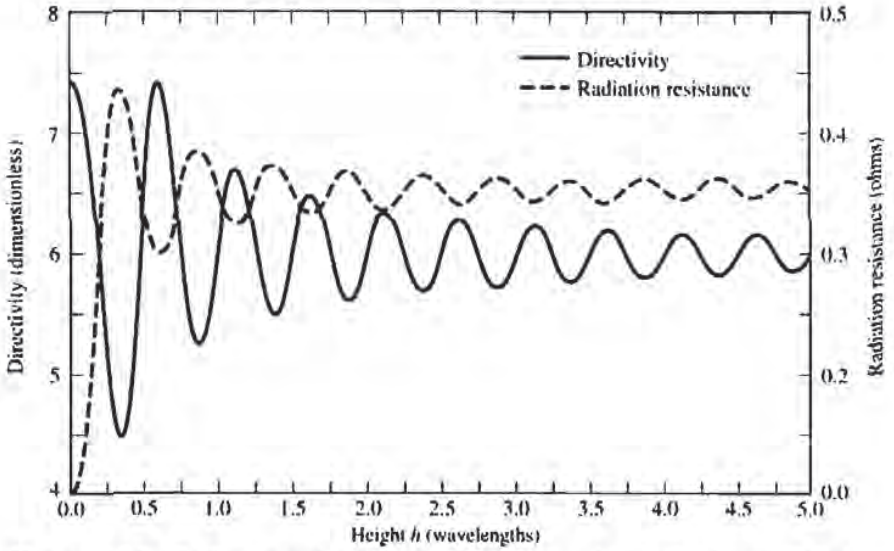


Figure 4.26 Radiation resistance and directivity gain of a horizontal infinitesimal electric dipole as a function of its height above an infinite perfect electric conductor.

Using (4-118) and (4-122a), (4-122b), the directivity can be written as

$$D_0 = \frac{4\pi U_{\max}}{P_{\text{rad}}} = \begin{cases} \dfrac{4\sin^2(kh)}{R(kh)} & kh \le \pi/2 \ (h \le \lambda/4) \quad (4\text{-}123a) \\ \dfrac{4}{R(kh)} & kh > \pi/2 \ (h > \lambda/4) \quad (4\text{-}123b) \end{cases}$$

where

$$R(kh) = \left[\frac{2}{3} - \frac{\sin(2kh)}{2kh} - \frac{\cos(2kh)}{(2kh)^2} + \frac{\sin(2kh)}{(2kh)^3}\right] \quad (4\text{-}123c)$$

For small values of kh ($kh \to 0$), (4-123a) reduces to

$$D_0 \overset{kh\to 0}{=} \frac{4\sin^2(kh)}{\left[\frac{2}{3} - \frac{2}{3} + \frac{8}{15}(kh)^2\right]} = 7.5\left(\frac{\sin kh}{kh}\right)^2 \quad (4\text{-}124)$$

For $h = 0$ the element is shorted and it does not radiate. The directivity, as given by (4-123a), (4-123b) is plotted for $0 \le h \le 5\lambda$ in Figure 4.26. It exhibits a maximum value of 7.5 for small values of h. Maximum values of 6 occur when $h \simeq (0.725 + n/2)\lambda$, $n = 0, 1, 2, 3, \ldots$.

The input impedance $Z_{\text{in}} = R_{\text{in}} + jX_{\text{in}}$ (referred to the current maximum) of a horizontal $\lambda/2$ dipole above a flat lossy electric conductor is shown plotted in Figure 4.27 for $0 \le h \le \lambda$. Conductivities of 10^{-2}, 10^{-1}, 1, 10 S/m, and infinity (PEC) were considered. It is apparent that the conductivity does have a more pronounced effect on the impedance values, compared to those of the vertical dipole shown in Figure 4.20. The conductivity values used are representative of those of the dry to wet earth. The values of the resistance and reactance approach, as the height increases, the

INTEL-1045
U.S. Patent 7,151,430

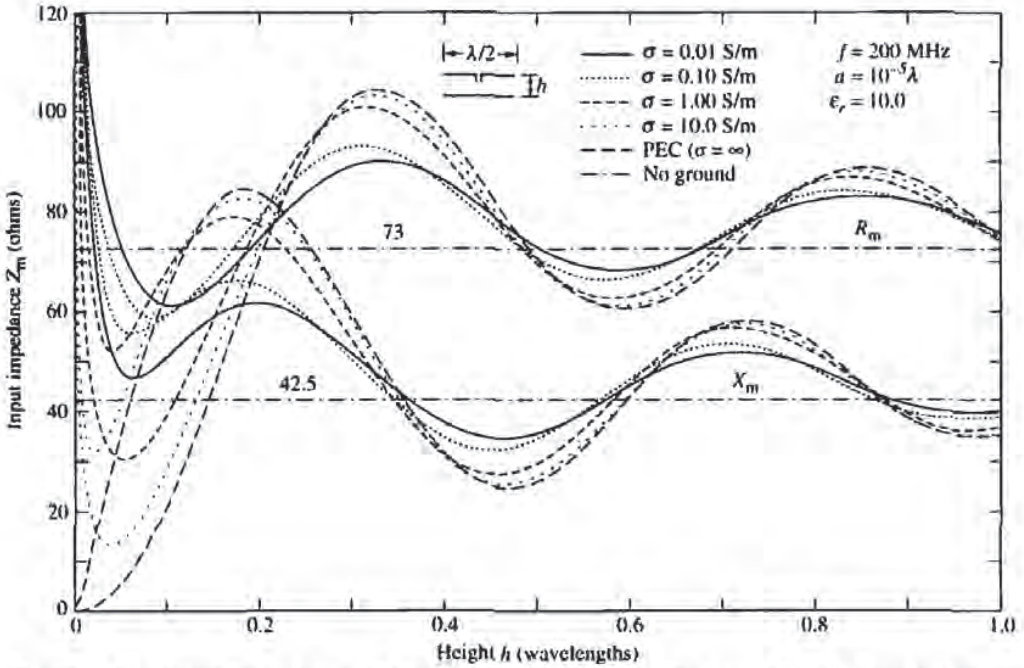


Figure 4.27 Input impedance of a horizontal $\lambda/2$ above a flat lossy electric conducting surface.

corresponding values of the isolated element (73 ohms for the resistance and 42.5 ohms for the reactance).

4.8 GROUND EFFECTS

In the previous two sections the variations of the radiation characteristics (pattern, radiation resistance, directivity) of infinitesimal vertical and horizontal linear elements were examined when they were placed above plane perfect electric conductors. Although ideal electric conductors ($\sigma = \infty$) are not realizable, their effects can be used as guidelines for good conductors ($\sigma \gg \omega\epsilon$, where ϵ is the permittivity of the medium).

One obstacle that is not an ideal conductor, and it is always present in any antenna system, is the ground (earth). In addition, the earth is not a plane surface. To simplify the analysis, however, the earth will initially be assumed to be flat. For pattern analysis, this is a very good engineering approximation provided the radius of the earth is large compared to the wavelength and the observation angles are greater than about $57.3/(ka)^{1/3}$ degrees from grazing (a is the earth radius) [18]. Usually these angles are greater than about 3°.

In general, the characteristics of an antenna at low (LF) and medium (MF) frequencies are profoundly influenced by the lossy earth. This is particularly evident in the input resistance. When the antenna is located at a height that is small compared to the skin depth of the conducting earth, the input resistance may even be greater than its free-space values [18]. This leads to antennas with very low efficiencies. Improvements in the efficiency can be obtained by placing radial wires or metallic disks on the ground.

The analytical procedures that are introduced to examine the ground effects are

INTEL-1045
U.S. Patent 7,151,430

based on the geometrical optics models of the previous sections. The image (virtual) source is again placed a distance h below the interface to account for the reflection. However, for each polarization nonunity reflection coefficients are introduced which, in general, will be a function of the angles of incidence and the constitutive parameters of the two media. Although plane wave reflection coefficients are used, even though spherical waves are radiated by the source, the error is small for conducting media [19]. The spherical nature of the wavefront begins to dominate the reflection phenomenon at grazing angles (i.e., as the point of reflection approaches the horizon) [20]. If the height (h) of the antenna above the interface is much less than the skin depth $\delta[\delta = \sqrt{2/(\omega\mu\sigma)}]$ of the ground, the image depth h below the interface should be increased [19] by a complex distance $\delta(1 - j)$.

The geometrical optics formulations are valid provided the sources are located inside the lossless medium. When the sources are placed within the ground, the formulations should include possible surface-wave contributions. Exact boundary-value solutions, based on Sommerfeld integral formulations, are available [18]. However they are too complex to be included in an introductory chapter.

4.8.1 Vertical Electric Dipole

The field radiated by an electric infinitesimal dipole when placed above the ground can be obtained by referring to the geometry of Figures 4.14(a) and (b). Assuming the earth is flat and the observations are made in the far-field, the direct component of the field is given by (4-94) and the reflected by (4-95) where the reflection coefficient $R_\perp$ is given by

$$R_\perp = \frac{\eta_0 \cos\theta_i - \eta_1 \cos\theta_t}{\eta_0 \cos\theta_i + \eta_1 \cos\theta_t} = -R_\parallel \tag{4-125}$$

where $R_\parallel$ is the reflection coefficient for parallel polarization [7] and

$\eta_0 = \sqrt{\dfrac{\mu_0}{\epsilon_0}}$ = intrinsic impedance of free-space (air)

$\eta_1 = \sqrt{\dfrac{j\omega\mu_1}{\sigma_1 + j\omega\epsilon_1}}$ = intrinsic impedance of the ground

θ_i = angle of incidence (relative to the normal)

θ_t = angle of refraction (relative to the normal)

The angles θ_i and θ_t are related by Snell's law of refraction

$$\gamma_0 \sin\theta_i = \gamma_1 \sin\theta_t \tag{4-126}$$

where

$\gamma_0 = jk_0$ = propagation constant for free-space (air)

k_0 = phase constant for free-space (air)

$\gamma_1 = (\alpha_1 + jk_1)$ = propagation constant for the ground

α_1 = attenuation constant for the ground

k_1 = phase constant for the ground

INTEL-1045
U.S. Patent 7,151,430

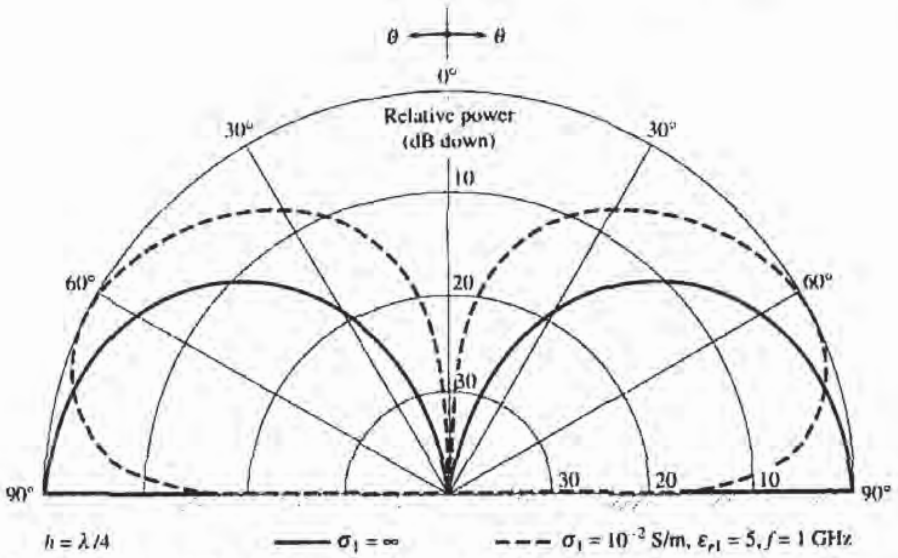


Figure 4.28 Elevation plane amplitude patterns of an infinitesimal verticle dipole above a perfect electric conductor ($\sigma_1 = \infty$) and a flat earth ($\sigma_1 = 0.01$ S/m, $\epsilon_{r1} = 5, f = 1$ GHz).

Using the far-field approximations of (4-97a)–(4-98), the total electric field above the ground ($z \geq 0$) can be written as

$$E_\theta = j\eta \frac{kI_0 l e^{-jkr}}{4\pi r} \sin\theta [e^{jkh\cos\theta} + R_v e^{-jkh\cos\theta}] \qquad z \geq 0 \qquad (4\text{-}127)$$

where R_v is given by (4-125).

The permittivity and conductivity of the earth are strong functions of the ground's geological constituents, especially its moisture. Typical values for the relative permittivity ϵ_r (dielectric constant) are in the range of 5–100 and for the conductivity σ in the range of $10^{-4} - 1$ S/m.

A normalized (to 0 dB) pattern for an infinitesimal dipole above the ground with $h = \lambda/4$, $\epsilon_{r1} = 5$, $f = 1$ GHz, $\sigma_1 = 10^{-2}$ S/m is shown plotted in Figure 4.28 (dashed curves) where it is compared with that (solid curve) of a perfect conductor ($\sigma_1 = \infty$). In the presence of the ground, the radiation toward the vertical direction ($60° > \theta > 0°$) is more intense that for the perfect electric conductor, but it vanishes for grazing angles ($\theta = 90°$). The null field toward the horizon ($\theta = 90°$) is formed because the reflection coefficient R_v approaches -1 as $\theta_i \to 90°$. Thus the ground effects on the pattern of a vertically polarized antenna are significantly different from those of a perfect conductor.

Significant changes also occur in the impedance. Because the formulation for the impedance is much more complex [18], it will not be presented here. Graphical illustrations for the impedance change of a vertical dipole placed a height h above a homogeneous lossy half-space, as compared to those in free-space, are shown in Figure 4.29. They are based on numerical results obtained by Vogler and Noble [21]. The variations in impedance are expressed in terms of changes in resistance ($\Delta R/R_0$) and in reactance ($\Delta X/R_0$), where R_0 is the radiation resistance of an infinitesimal

INTEL-1045
U.S. Patent 7,151,430

dipole radiating in an infinite free-space [as given by (4-19)]. The parameter N_1 is defined by

$$N_1 = \sqrt{\frac{\sigma_1 + j\omega\epsilon_1}{j\omega\epsilon_0}} = |N_1|e^{-j\left(\frac{\pi}{4} - \psi\right)} \tag{4-128}$$

where σ_1, ϵ_1 are the conductivity and permittivity, respectively, of the homogeneous lossy half-space, ϵ_0 is the free-space permittivity, and ψ is phase angle of N_1.

The curve in Figure 4.29(a) represents the data for a perfectly conducting ($|N_1| = \infty$) half-space. As expected, the magnitude of $\Delta R/R_0$ approaches unity as $2k_0h \to 0$, which corresponds to doubling the radiation resistance, while the magnitude of ΔX approaches infinity as $2k_0\text{h} \to 0$. The curves for both ΔR and ΔX become oscillatory as $2k_0h$ exceeds approximately π or the height h exceeds $\lambda_0/4$.

For the finite conductivity half-space, the $\psi = \pi/4$ curves correspond to a perfect dielectric half-space ($\sigma_1 = 0$) while the $\psi = 0$ curves represent negligible displacement currents in the lossy half-space. The curves for $|N_1^2| = 100$ are not too different from that of a perfectly conducting half-space ($|N_1| = \infty$). Significant changes are evident as the values of $|N_1^2|$ decrease particularly in the resistive portion of the $\psi = 0$ curves.

The curves of Figure 4.29 can be used as design data to determine the changes in the input impedance of an infinitesimal vertical dipole when it is placed above a lossy medium. To demonstrate the procedure, let us consider the following example.

Example 4.5

An infinitesimal vertical dipole of length $l = \lambda_0/50$ is placed a height $h = \lambda_0/10$ above the earth. Assume the earth is locally flat with a dielectric constant of 4 and conductivity of 10^{-3} S/m at a frequency of 100 MHz. Determine the changes in input resistance and reactance of the dipole.

SOLUTION

For a frequency of 100 MHz

$$\frac{\sigma_1}{\omega\epsilon_1} = \frac{10^{-3}}{2\pi \times 10^8 \times 4 \times 8.854 \times 10^{-12}} = 1.99 \times 10^{-3} \ll 1$$

Therefore according to (4-125)

$$N_1 \simeq \sqrt{\frac{\epsilon_1}{\epsilon_0}} = \sqrt{4} = 2$$

or

$$|N_1|^2 = 4$$

$$\frac{\pi}{4} - \psi = 0$$

INTEL-1045
U.S. Patent 7,151,430

For a height of $\lambda_0/10$

$$2k_0h = 2\left(\frac{2\pi}{\lambda_0}\right)\left(\frac{\lambda_0}{10}\right) = 1.257$$

Using Figure 4.29(d) and the curve for $\pi/4 - \psi = 0$ at $2k_0h = 1.257$, the relative changes in resistance and reactance are, respectively, equal to

$$\frac{\Delta R}{R_0} \simeq 0.767$$

$$\frac{\Delta X}{R_0} \simeq 1.2$$

Since for a $\lambda_0/50$ dipole the radiation resistance according to (4-19) and Example 4.1 is equal to

$$R_r = R_0 = 0.316 \text{ ohms}$$

then the changes in resistance and reactance are, respectively, equal to

$$\Delta R = 0.767(0.316) = 0.242 \text{ ohms}$$
$$\Delta X = 1.2(0.316) = 0.379 \text{ ohms}$$

4.8.2 Horizontal Electric Dipole

The analytical formulation of the horizontal dipole above the ground can also be obtained in a similar manner as for the vertical electric dipole. Referring to Figure 4.22(a) and (b), the direct component is given by (4-111) and the reflected by (4-112) where the reflection coefficient R_h is given by

$$R_h = \begin{cases} R_\perp \text{ for } \phi = 0°, 180° \text{ plane} \\ R_\parallel \text{ for } \phi = 90°, 270° \text{ plane} \end{cases} \tag{4-129}$$

where $R_\parallel$ is the reflection coefficient for parallel polarization, as given by (4-125), and $\perp$ is the reflection coefficient for perpendicular polarization given by [7].

$$R_\perp = \frac{\eta_1 \cos\theta_i - \eta_0 \cos\theta_t}{\eta_1 \cos\theta_i + \eta_0 \cos\theta_t} \tag{4-129a}$$

The angles θ_i and θ_t are again related by Snell's law of refraction as given by (4-126).

Using the far-field approximations of (4-115a) and 4-115b), the total field above the ground ($z \geq h$) can be written as

$$E_\phi = j\eta \frac{kI_0 e^{-jkr}}{4\pi r} \sqrt{1 - \sin^2\theta \sin^2\phi}\,[e^{jkh\cos\theta} + R_h e^{-jkh\cos\theta}],\ z \geq h \tag{4-130}$$

where R_h is given by (4-129).

The normalized (to 0 dB) pattern in the y-z plane ($\phi = 90°$) for $h = \lambda/4$ is shown plotted in Figure 4.30 (dashed curve) where it is compared with that (solid curve) of a perfect conductor ($\sigma_1 = \infty$). In the space above the interface, the relative

INTEL-1045
U.S. Patent 7,151,430

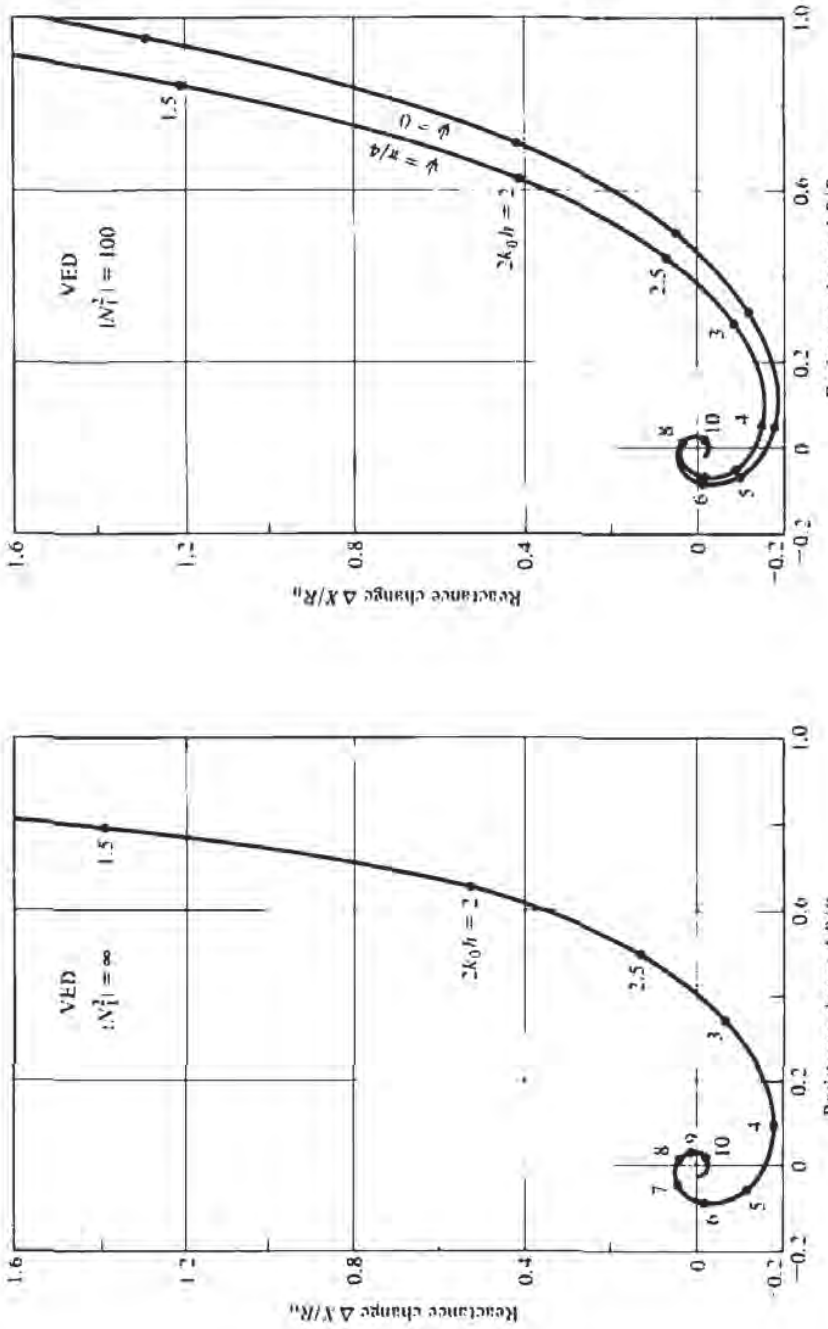


Figure 4.29 Vertical electric dipole (VED) impedance as a function of height above a homogeneous lossy half-space. (SOURCE: R. E. Collin and F. J. Zucker (eds.), *Antenna Theory Part 2*, McGraw-Hill, New York, 1969).

INTEL-1045
U.S. Patent 7,151,430

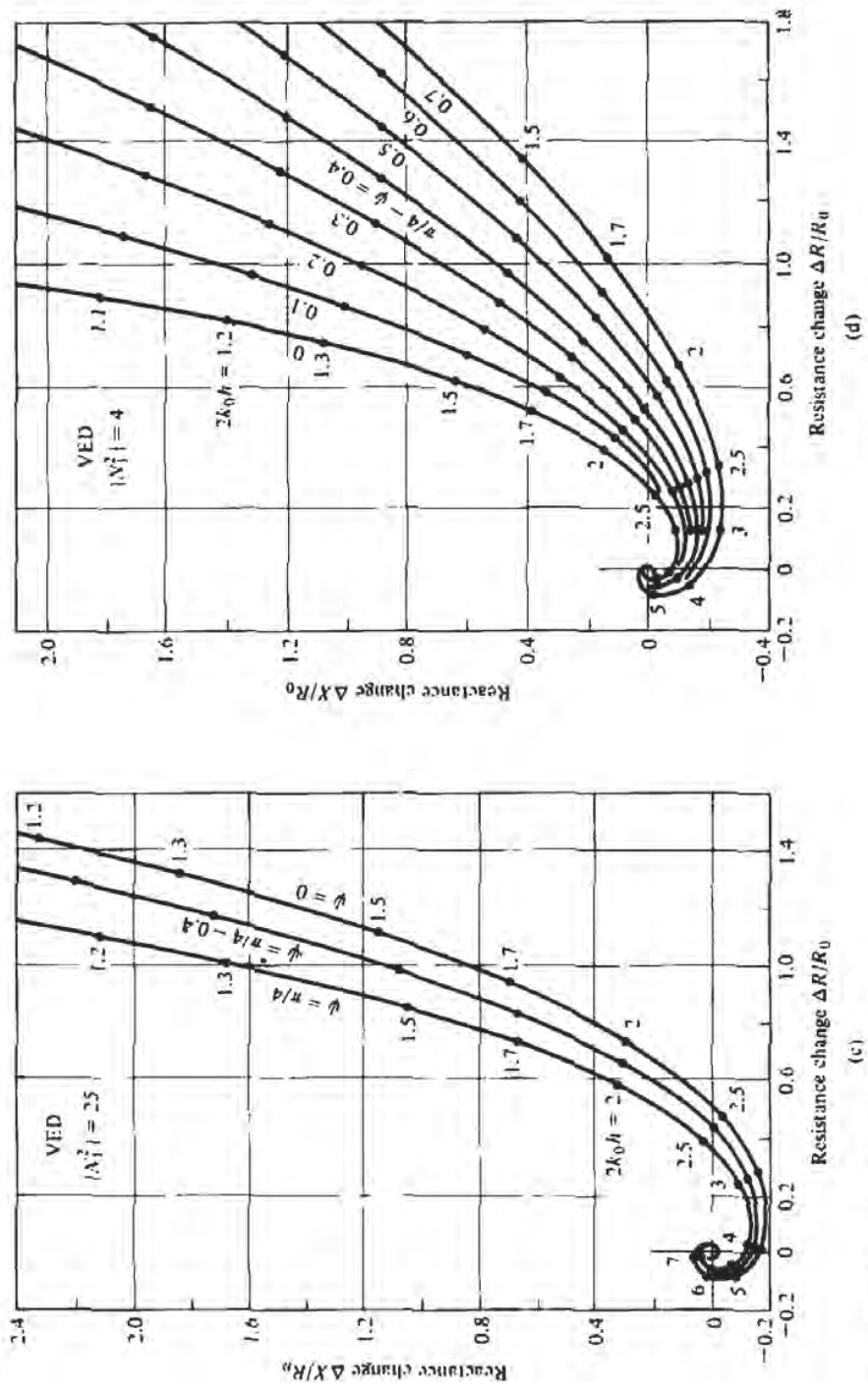


Figure 4.29 (continued)

INTEL-1045
U.S. Patent 7,151,430

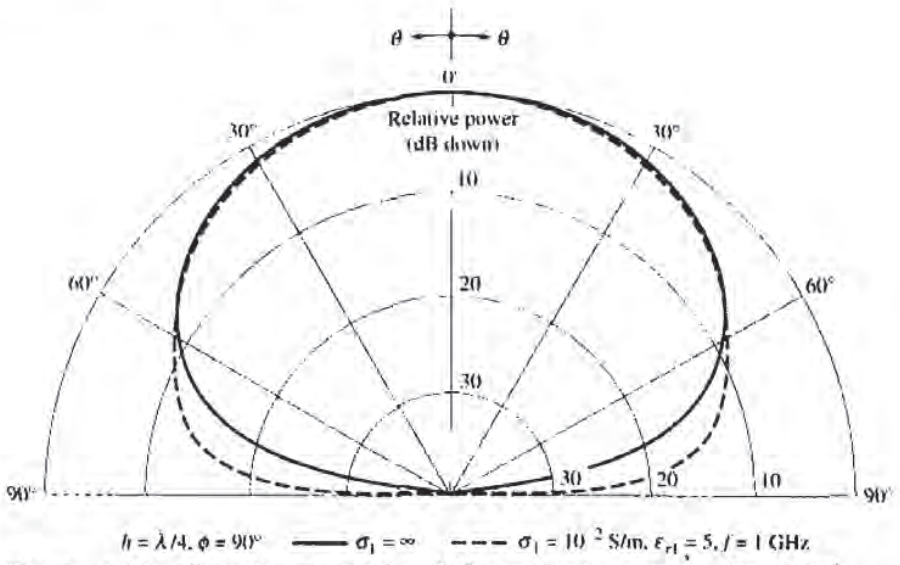


Figure 4.30 Elevation plane ($\phi = 90°$) amplitude patterns of an infinitesimal horizontal dipole above a perfect electric conductor ($\sigma_1 = \infty$) and a flat earth ($\sigma_1 = 0.01$ S/m, $\epsilon_{r1} = 5$, $f = 1$ GHz).

pattern in the presence of the ground is not significantly different from that of a perfect conductor. This becomes more evident by examining R_h as given by (4-129). For a ground medium, the values of R_h for most observation angles are not much different from -1 (the value of R_h for a perfect conductor). For grazing angles ($\theta_i \rightarrow 90°$), the values of R_h for the lossy ground approach -1 very rapidly. Thus the relative pattern of a horizontal dipole above a lossy surface is not significantly different from that above a perfect conductor.

4.8.3 Earth Curvature

Antenna pattern measurements on aircraft can be made using either scale models or full scale in-flight. Scale model measurements usually are made indoors using electromagnetic anechoic chambers, as described in Chapter 16. The indoor facilities provide a controlled environment, and all-weather capability, security, and minimize electromagnetic interference. However, scale model measurements may not always simulate real-life outdoor conditions, such as the reflecting surface of sea water. Therefore full-scale model measurements may be necessary. For in-flight measurements, reflecting surfaces, such as sea water, introduce reflections, which usually interfere with the direct signal. These unwanted signals are usually referred to as *multipath*. Therefore the total measured signal in an outdoor system configuration is the combination of the direct signal and that due to multipath, and usually it cannot be easily separated in its parts using measuring techniques. Since the desired signal is that due to the direct path, it is necessary to be able to subtract from the total response the contributions due to multipath. This can be accomplished by developing analytical models to predict the contributions due to multipath, which can then be subtracted from the total signal in order to be left with the desired direct path signal. In this section we will briefly describe techniques that have been used to accomplish this [22], [23].

INTEL-1045
U.S. Patent 7,151,430

The analytical formulations of Sections 4.8.1 and 4.8.2 for the patterns of vertical and horizontal dipoles assume that the earth is flat. This is a good approximation provided the curvature of the earth is large compared to the wavelength and the angle of observation is greater than about 3° from grazing [or more accurately greater than about $57.3/(ka)^{1/3}$ degrees, where a is the radius of the earth] from grazing [24]. The curvature of the earth has a tendency to spread out (weaken, diffuse, diverge) the reflected energy more than a corresponding flat surface. The spreading of the reflected energy from a curved surface as compared to that from a flat surface is taken into account by introducing a divergence factor D [20], [22], [23], defined as

$$D = \text{divergence factor} = \frac{\text{reflected field from curved surface}}{\text{reflected field from flat surface}} \tag{4-131}$$

The formula for D can be derived using purely geometrical considerations. It is accomplished by comparing the ray energy density in a small cone reflected from a sphere near the principal point of reflection with the energy density the rays (within the same cone) would have if they were reflected from a plane surface. Based on the geometrical optics energy conservation law for a bundle of rays within a cone, the reflected rays within the cone will subtend a circle on a perpendicular plane for reflections from a flat surface, as shown in Figure 4.31(a). However, according to the geometry of Figure 4.31(b), it will subtend an ellipse for a spherical reflecting surface. Therefore the divergence factor of (4-131) can also be defined as

$$D = \frac{E_s^r}{E_f^r} \approx \left[\frac{\text{area contained in circle}}{\text{area contained in ellipse}}\right]^{1/2} \tag{4-132}$$

where

E_s^r = reflected field from spherical surface

E_f^r = reflected field from flat surface

Using the geometry of Figure 4.32, the divergence factor can be written as [7] and [23]

$$D = \frac{\sqrt{\dfrac{\rho_1^r \rho_2^r}{(\rho_1^r + s)(\rho_2^r + s)}}}{\dfrac{s'}{s' + s}} \tag{4-133}$$

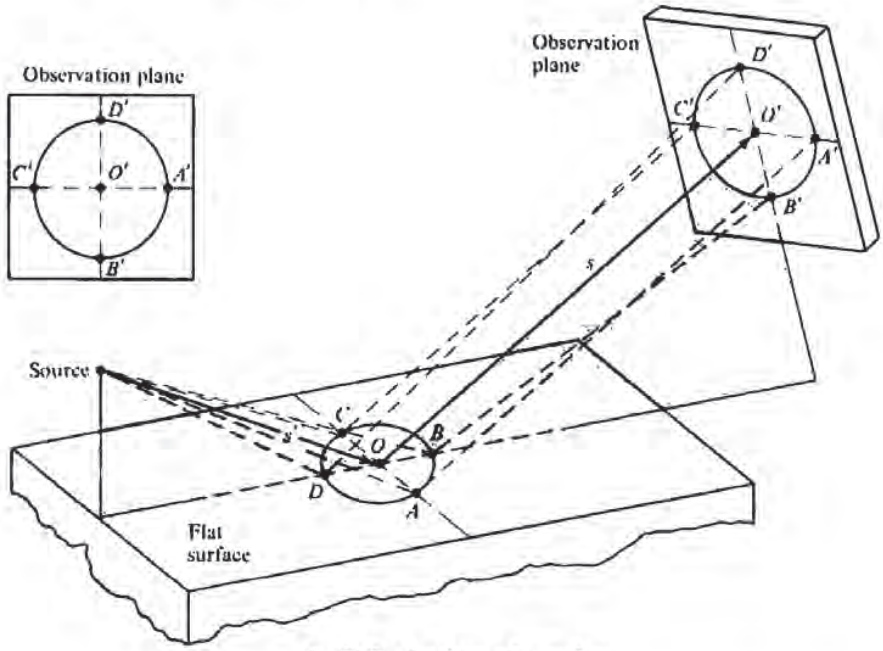
where ρ_1^r and ρ_2^r are the principal radii of curvature of the reflected wavefront at the point of reflection and are given, according to the geometry of Figure 4.32, by

$$\frac{1}{\rho_1^r} = \frac{1}{s'} + \frac{1}{\rho \sin \psi} + \sqrt{\frac{1}{(\rho \sin \psi)^2} - \frac{4}{a^2}} \tag{4-133a}$$

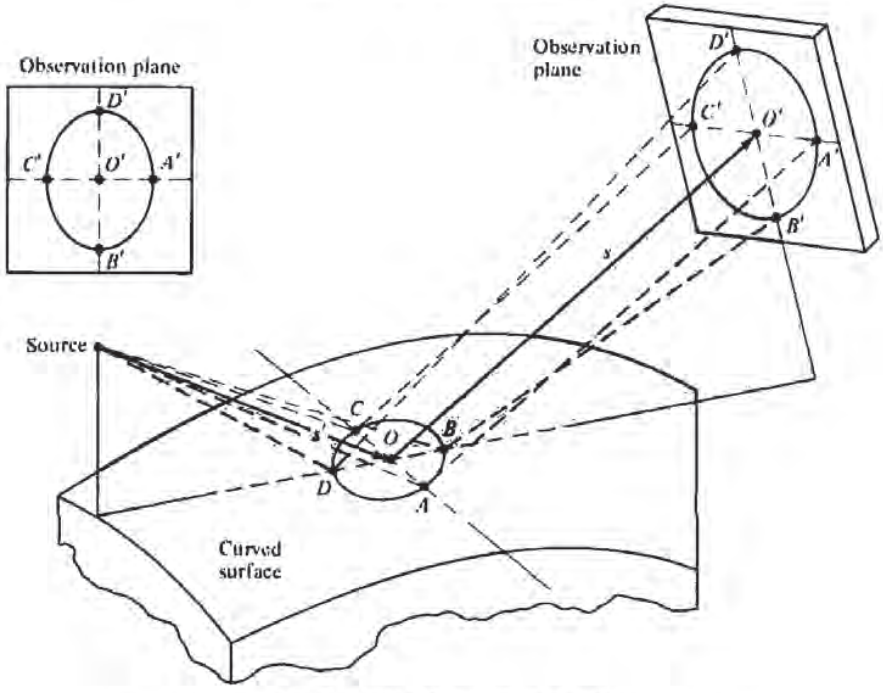
$$\frac{1}{\rho_2^r} = \frac{1}{s'} + \frac{1}{\rho \sin \psi} - \sqrt{\frac{1}{(\rho \sin \psi)^2} - \frac{4}{a^2}} \tag{4-133b}$$

$$\rho = \frac{a}{1 + \sin^2 \psi} \tag{4-133c}$$

INTEL-1045
U.S. Patent 7,151,430



(a) Reflection from a flat surface



(b) Reflection from a spherical surface

Figure 4.31 Reflection from a flat and spherical surfaces.

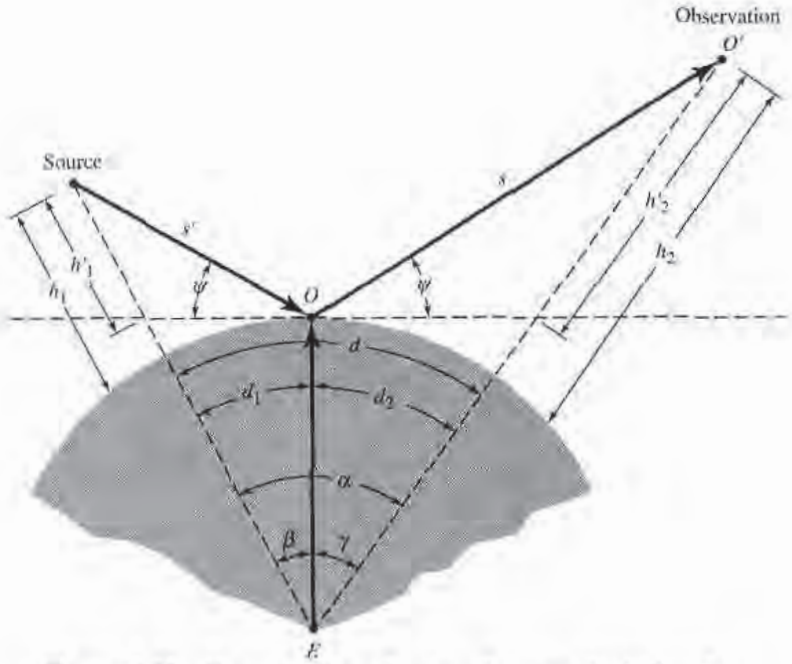


Figure 4.32 Geometry for reflections from a spherical surface.

A simplified form of the divergence factor is that of [25]

$$D \cong \left[1 + \frac{2s's}{a(s' + s)\sin\psi}\right]^{-1/2} \cdot \left[1 + \frac{2s's}{a(s' + s)}\right]^{-1/2} \tag{4-134}$$

Both (4-133) and (4-134) take into account the earth curvature in two orthogonal planes.

Assuming that the divergence of rays in the azimuthal plane (plane vertical to the page) is negligible, the divergence factor can be written as

$$D = \left[1 + 2\frac{ss'}{ad\tan\psi}\right]^{-1/2} \tag{4-135}$$

where ψ is the grazing angle. Thus the divergence factor of (4-135) takes into account energy spreading primarily in the elevation plane. According to Figure 4.32

h_1' = height of the source above the earth (with respect to the tangent at the point of reflection)

h_2' = height of the observation point above the earth (with respect to the tangent at the point of reflection)

d = range (along the surface of the earth) between the source and the observation point

a = radius of the earth (3,959 mi). Usually a $\frac{4}{3}$ radius (= 5,280 mi) is used.

ψ = reflection angle (with respect to the tangent at the point of reflection).

d_1 = distance (along the surface of the earth) from the source to the reflection point

d_2 = distance (along the surface of the earth) from the observation point to the reflection point

INTEL-1045
U.S. Patent 7,151,430

The divergence factor can be included in the formulation of the fields radiated by a vertical or a horizontal dipole, in the presence of the earth, by modifying (4-127) and (4-130) and writing them, respectively, as

$$E_\theta = j\eta \frac{kI_0 l e^{-jkr}}{4\pi r} \sin\theta [e^{jkh\cos\theta} + DR_v e^{-jkh\cos\theta}] \tag{4-136a}$$

$$E_\psi = j\eta \frac{kI_0 l e^{-jkr}}{4\pi r} \sqrt{1 - \sin^2\theta \sin^2\phi}\, [e^{jkh\cos\theta} + DR_h e^{-jkh\cos\theta}] \tag{4-136b}$$

While the previous formulations are valid for smooth surfaces, they can still be used with rough surfaces, provided the surface geometry satisfies the Rayleigh criterion [20] and [25]

$$h_m < \frac{\lambda}{8 \sin\psi} \tag{4-137}$$

where h_m is the maximum height of the surface roughness. Since the dividing line between a smooth and a rough surface is not that well defined, (4-137) should only be used as a guideline.

The *coherent* contributions due to scattering by a surface with Gaussian rough surface statistics can be approximately accounted for by modifying the vertical and horizontal polarization smooth surface reflection coefficients of (4-125) and (4-129) and express them as

$$R^s_{v,h} = R_{v,h} e^{-2(k_0 h_0 \cos\theta_i)^2} \tag{4-138}$$

where

$R^s_{v,h}$ = reflection coefficient of a rough surface for either vertical or horizontal polarization

$R_{v,h}$ = reflection coefficient of a smooth surface for either vertical (4-125) or horizontal (4-129) polarization

h_0^2 = mean-square roughness height

A *slightly rough surface* is defined as one whose rms height is much smaller than the wavelength, while a *very rough surface* is defined as one whose rms height is much greater than the wavelength.

Plots of the divergence factor as a function of the grazing angle ψ (or as a function of the observation point h_2') for different source heights are shown in Figure 4.33. It is observed that the divergence factor is somewhat different and smaller than unity for small grazing angles, and it approaches unity as the grazing angle becomes larger. The variations of D displayed in Figure 4.33 are typical but not unique. For different positions of the source and observation point, the variations will be somewhat different. More detailed information on the variation of the divergence factor and its effect on the overall field pattern is available [23].

The most difficult task usually involves the determination of the reflection point from a knowledge of the heights of the source and observation points, and the range d between them. Procedures to do this have been developed [20], [22]–[26].

However, the one presented here is more accurate and does not require either

INTEL-1045
U.S. Patent 7,151,430

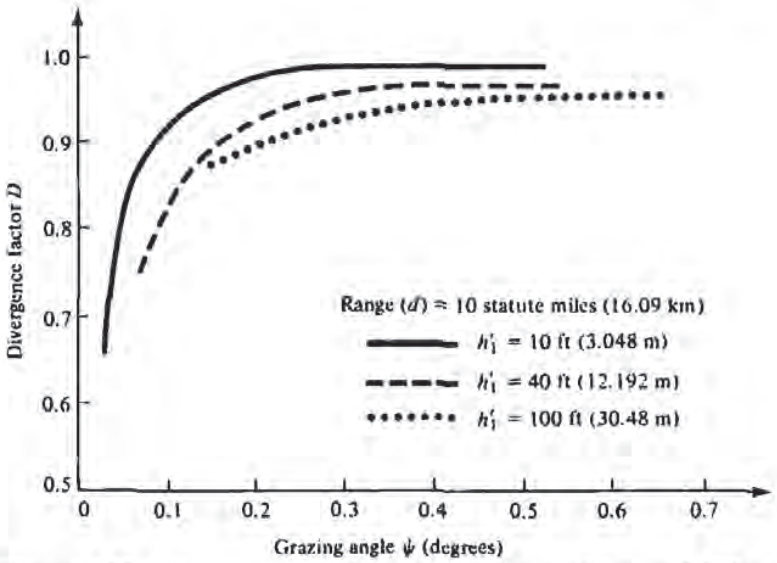


Figure 4.33 Divergence factor for a 4/3 radius earth (a_e = 5,280 mi = 8,497.3 km) as a function of grazing angle ψ.

iterative or graphical solutions. To find d_1 and d_2 (given d, h_1, and h_2), the cubic equation of [20] is utilized

$$2d_1^3 - 3dd_1^2 + [d^2 - 2a(h_1 + h_2)]d_1 + 2ah_1d = 0 \tag{4-139}$$

with solution given by

$$d_1 = \frac{d}{2} + p\cos\left(\frac{\Omega + \pi}{3}\right) \tag{4-139a}$$

$$d_2 = d - d_1 \tag{4-139b}$$

$$p = \frac{2}{\sqrt{3}}\sqrt{a(h_1 + h_2) + \left(\frac{d}{2}\right)^2} \tag{4-139c}$$

$$\Omega = \cos^{-1}\left[\frac{2a(h_1 - h_2)d}{p^3}\right] \tag{4-139d}$$

Equation (4-139) is valid provided that $\alpha - \beta$ is small, such that $\sin(\alpha - \beta) \approx \alpha - \beta$, $\cos(\alpha - \beta) \approx 1 - (\alpha - \beta)^2/2$, $\sin\beta \approx \beta$, and $\cos\beta \approx 1 - (\beta)^2/2$. Once d_1 and d_2 are found, then successively β, γ, s', s, ψ, r_1, r_2, α_1^r, α_1^d, α_2^r, and α_2^d can be determined using the geometry of Figure 4.31.

Using the analytical model developed here, computations were made to see how well the predictions compared with measurements. For the computations it was assumed that the reflecting surface is sea water possessing a dielectric constant of 81 and a conductivity of 4.64 S/m [22], [23]. To account for atmospheric refraction, a 4/3 earth was assumed [20], [22], [27] so the atmosphere above the earth can be considered homogeneous with propagation occurring along straight lines.

For computations using the earth as the reflecting surface, all three divergence

INTEL-1045
U.S. Patent 7,151,430

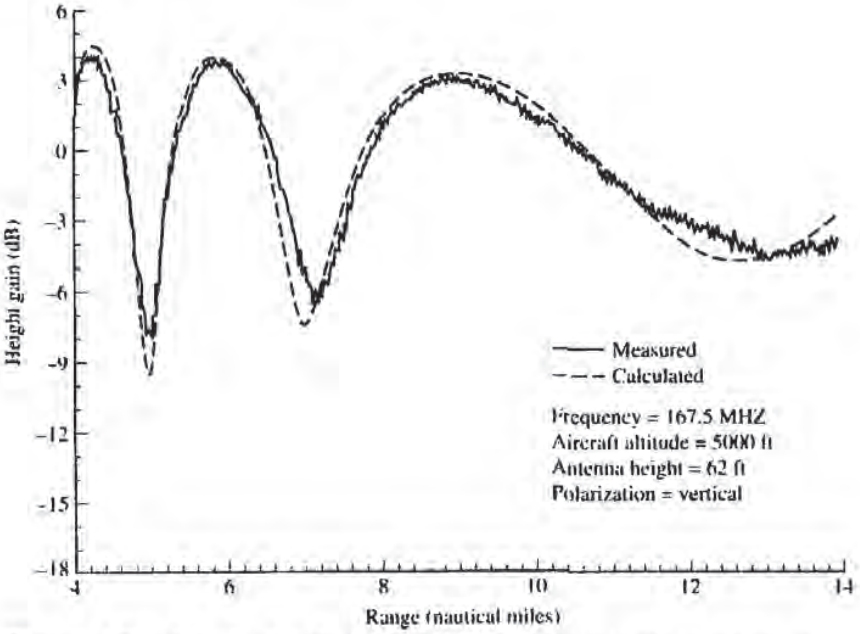


Figure 4.34 Measured and calculated height gain over the ocean (ϵ_r = 81, σ = 4.64 S/m) for vertical polarization.

factors of (4-133)–(4-135) gave the same results. However, for nonspherical reflecting surfaces and for those with smaller radii of curvature, the divergence factor of (4-133) is slightly superior followed by (4-134) and then by (4-135). In Figure 4.34 we display and compare the predicted and measured *height gain* versus range d ($4 < d < 14$ nautical miles) for a vertical-vertical polarization system configuration at a frequency of 167.5 MHz. The *height gain* is defined as the ratio of the total field in the presence of the earth divided by the total field in the absence of the earth. A good agreement is noted between the two. The peaks and nulls are formed by constructive and destructive interferences between the direct and reflected components. If the reflecting surface were perfectly conducting, the maximum height gain would be 2 (6 dB). Because the modeled reflecting surface of Figure 4.34 was sea water with a dielectric constant of 81 and a conductivity of 4.64 S/m, the maximum height gain is less than 6 dB. The measurements were taken by aircraft and facilities of the Naval Air Warfare Center, Patuxent River, MD. Additional measurements were made but are not included here; they can be found in [28] and [29].

References

1. W. A. Wheeler, "The Spherical Coil as an Inductor, Shield, or Antenna," *Proc. IRE*, Vol. 46, pp. 1595–1602, September 1958 (correction, Vol. 48, p. 328, March 1960).
2. W. A. Wheeler, "The Radiansphere Around a Small Antenna," *Proc. IRE*, Vol. 47, pp. 1325–1331, August 1959.
3. W. A. Wheeler, "Small Antennas," *IEEE Trans. Antennas Propagat.*, Vol. AP-23, No. 4, pp. 462–469, July 1975.
4. C. H. Walter, *Traveling Wave Antennas*, McGraw-Hill, 1965, pp. 32–44.

INTEL-1045
U.S. Patent 7,151,430

5. W. R. Scott, Jr., "A General Program for Plotting Three-Dimensional Antenna Patterns," *IEEE Antennas and Propagation Society Newsletter*, pp. 6–11, December 1989.
6. S. K. Schelkunoff and H. T. Friis, *Antennas: Theory and Practice*, Wiley, New York, 1952, pp. 229–244, 351–353.
7. C. A. Balanis, *Advanced Engineering Electromagnetics*, John Wiley & Sons, Inc., New York, 1989.
8. R. F. Harrington, "Matrix Methods for Field Problems," *Proc. IEEE*, Vol. 55, No. 2, pp. 136–149, February 1967.
9. R. F. Harrington, *Field Computation by Moment Methods*, Macmillan, New York, 1968.
10. R. Mittra (Ed.), *Computer Techniques for Electromagnetics*, Pergamon, New York, 1973.
11. J. Moore and P. Pizer (Eds.), *Moment Methods in Electromagnetics: Techniques and Applications*, Letchworth, UK: Research Studies Press, 1984.
12. J. J. Wang, *Generalized Moment Methods in Electromagnetics*, John Wiley & Sons, Inc., New York, 1991.
13. R. F. Schwartz, "Input Impedance of a Dipole or Monopole," *The Microwave Journal*, Vol. 15, No. 12, p. 22, December 1972.
14. K. Fujimoto and J. R. James, *Mobile Antenna Systems Handbook*, Artech House, Norwood, MA, 1994.
15. M. A. Jensen and Y. Rahmat-Samii, "Performance Analysis of Antennas for Hand-Held Transceivers Using FDTD," *IEEE Trans. Antennas Propagat.*, Vol. 42, No. 8, pp. 1106–1113, August 1994.
16. M. A. Jensen and Y. Rahmat-Samii, "EM Interaction of Handset Antennas and a Human in Personal Communications," *Proc. IEEE*, Vol. 83, No. 1, pp. 7–17, January 1995.
17. C. A. Balanis, K. D. Katsibas and P. A. Tirkas, "Antenna Considerations for Wireless Communication Systems and Networks," 5th International Conference on Advances in Communication and Control (ComCon 5), June 26–30, 1995, Rethymnon, Crete, Greece.
18. R. E. Collin and F. J. Zucker (eds.), *Antenna Theory Part 2*, Chapters 23 and 24 (by J. R. Wait), McGraw-Hill, New York, 1969.
19. P. R. Bannister, "Image Theory Results for the Mutual Impedance of Crossing Earth Return Circuits," *IEEE Trans. Electromagn. Compat.*, Vol. 15, No. 4, 1973, pp. 158–160.
20. D. E. Kerr, *Propagation of Short Radio Waves*, MIT Radiation Laboratory Series, McGraw-Hill, New York, 1951, Vol. 13, pp. 98–109, 112–122, 396–444.
21. L. E. Vogler and J. L. Noble, "Curves of Input Impedance Change due to Ground for Dipole Antennas," U.S. National Bureau of Standards, Monograph 72, January 31, 1964.
22. H. R. Reed and C. M. Russell, *Ultra High Frequency Propagation*, Boston Technical Publishers, Inc., Lexington, Mass., 1964, Chapter 4, pp. 102–116.
23. C. A. Balanis, R. Hartenstein, and D. DeCarlo, "Multipath Interference for In-Flight Antenna Measurements," *IEEE Trans. Antennas Propagat.*, Vol. AP-32, No. 1, pp. 100–104, January 1984.
24. J. R. Wait and A. M. Conda, "Pattern of an Antenna on a Curved Lossy Surface," *IRE Trans. Antennas Propagat.*, Vol. AP-6, No. 4, October 1958, pp. 348–359.
25. P. Beckmann and A. Spizzichino, *The Scattering of Electromagnetic Waves from Rough Surfaces*, MacMillan, New York, 1963.
26. G. May, "Determining the Point of Reflection on MW Radio Links," *Microwave Journal*, Vol. 20, No. 9, September 1977, pp. 74, 76.
27. D. T. Paris and F. K. Hurd, *Basic Electromagnetic Theory*, McGraw-Hill Book Co., pp. 385–386, 1969.
28. C. A. Balanis, "Multipath Interference in Airborne Antenna Measurements," Final Report, prepared for Naval Air Station, Patuxent River, Maryland, May 28, 1982.
29. D. DeCarlo, "Automation of In-Flight Antenna Measurements," MSEE Problem Report, Dept. of Electrical Engineering, West Virginia University, July 1980.

INTEL-1045
U.S. Patent 7,151,430

PROBLEMS

4.1. A horizontal infinitesimal electric dipole of constant current I_0 is placed symmetrically about the origin and directed along the x-axis. Derive the
(a) far-zone fields radiated by the dipole
(b) directivity of the antenna

4.2. Repeat Problem 4.1 for a horizontal infinitesimal electric dipole directed along the y-axis.

4.3. For Problem 4.1 determine the polarization of the radiated far-zone electric fields (E_θ, E_ϕ) and normalized amplitude pattern in the following planes:
(a) $\phi = 0°$
(b) $\phi = 90°$
(c) $\theta = 90°$

4.4. Repeat Problem 4.3 for the horizontal infinitesimal electric dipole of Problem 4.2, which is directed along the y-axis.

4.5. An infinitesimal magnetic dipole of constant current I_m and length l is symmetrically placed about the origin along the z-axis. Find the
(a) spherical **E**- and **H**-field components radiated by the dipole in all space
(b) directivity of the antenna

4.6. For the infinitesimal magnetic dipole of Problem 4.5, find the far-zone fields when the element is placed along the
(a) x-axis
(b) y-axis

4.7. An infinitesimal electric dipole is centered at the origin and lies on the x-y plane along a line which is at an angle of 45° with respect to the x-axis. Find the far-zone electric and magnetic fields radiated. The answer should be a function of spherical coordinates.

4.8. Repeat Problem 4.7 for an infinitesimal magnetic dipole.

4.9. Derive (4-10a)–(4-10c) using (4-8a)–(4-9).

4.10. Derive the radiated power of (4-16) by forming the average power density, using (4-26a)–(4-26c), and integrating it over a sphere of radius r.

4.11. Derive the far-zone fields of an infinitesimal electric dipole, of length l and constant current I_0, using (4-4) and the procedure outlined in Section 3.6. Compare the results with (4-26a)–(4-26c).

4.12. Derive the fifth term of (4-41).

4.13. For an antenna with a maximum linear dimension of D, find the inner and outer boundaries of the Fresnel region so that the maximum phase error does not exceed
(a) $\pi/16$ rad
(b) $\pi/4$ rad
(c) 18°
(d) 15°

4.14. The boundaries of the far-field (Fraunhofer) and Fresnel regions were selected based on a maximum phase error of 22.5°, which occur, respectively, at directions of 90° and 54.74° from the axis along the largest dimension of the antenna. For an antenna of maximum length of 5λ, what do these maximum phase errors reduce to at an angle of 30° from the axis along the length of the antenna? Assume that the phase error in each case is totally contributed by the respective first higher order term that is being neglected in the infinite series expansion of the distance from the source to the observation point.

4.15. The current distribution on a terminated and matched long linear (traveling wave) antenna of length l, positioned along the z-axis and fed at its one end, is given by

$$\mathbf{I} = \hat{\mathbf{a}}_z I_0 e^{-jkz'}, \quad 0 \le z' \le l$$

where I_0 is a constant. Derive expressions for the
(a) far-zone spherical electric and magnetic field components
(b) radiation power density

INTEL-1045
U.S. Patent 7,151,430

4.16. A line source of infinite length and constant current I_0 is positioned along the z-axis. Find the
(a) vector potential **A**
(b) cylindrical **E**- and **H**-field components radiated

$$\text{Hint: } \int_{-\infty}^{+\infty} \frac{e^{-j\beta\sqrt{b^2+t^2}}}{\sqrt{b^2+t^2}}\,dt = -j\pi H_0^{(2)}(\beta b)$$

where $H_0^{(2)}(\alpha x)$ is the Hankel function of the second kind of order zero.

4.17. Show that (4-67) reduces to (4-68) and (4-88) to (4-89).

4.18. A thin linear dipole of length l is placed symmetrically about the z-axis. Find the far-zone spherical electric and magnetic components radiated by the dipole whose current distribution can be approximated by

(a) $I_z(z') = \begin{cases} I_0\left(1 + \dfrac{2}{l}z'\right), & -l/2 \le z' \le 0 \\ I_0\left(1 - \dfrac{2}{l}z'\right), & 0 \le z' \le l/2 \end{cases}$

(b) $I_z(z') = I_0 \cos\left(\dfrac{\pi}{l}z'\right), \quad -l/2 \le z' \le l/2$

(c) $I_z(z') = I_0 \cos^2\left(\dfrac{\pi}{l}z'\right), \quad -l/2 \le z' \le l/2$

4.19. A center-fed electric dipole of length l is attached to a balanced lossless transmission line whose characteristic impedance is 50 ohms. Assuming the dipole is resonant at the given length, find the input VSWR when
(a) $l = \lambda/4$ (b) $l = \lambda/2$
(c) $l = 3\lambda/4$ (d) $l = \lambda$

4.20. Use the equations in the book or the computer program at the end of the chapter. Find the radiation efficiency of resonant linear electric dipoles of length
(a) $l = \lambda/50$ (b) $l = \lambda/4$
(c) $l = \lambda/2$ (d) $l = \lambda$
Assume that each dipole is made out of copper [$\sigma = 5.7 \times 10^7$ S/m], has a radius of $10^{-4}\lambda$, and is operating at $f = 10$ MHz. Use the computer program at the end of the chapter to find the radiation resistances.

4.21. Write the far-zone electric and magnetic fields radiated by a magnetic dipole of $l = \lambda/2$ aligned with the z-axis. Assume a sinusoidal magnetic current with maximum value I_{mo}.

4.22. A resonant center-fed dipole is connected to a 50-ohm line. It is desired to maintain the input VSWR = 2.
(a) What should the largest input resistance of the dipole be to maintain the VSWR = 2?
(b) What should the length (in wavelengths) of the dipole be to meet the specification?
(c) What is the radiation resistance of the dipole?

4.23. The radiation field of a particular antenna is given by:

$$\mathbf{E} = \hat{\mathbf{a}}_\theta j\omega\mu k \sin\theta \frac{I_0 A_1 e^{-jkr}}{4\pi r} + \hat{\mathbf{a}}_\phi \omega\mu \sin\theta \frac{I_0 A_2 e^{-jkr}}{2\pi r}$$

The values A_1 and A_2 depend on the antenna geometry. Obtain an expression for the radiation resistance. What is the polarization of the antenna?

INTEL-1045
U.S. Patent 7,151,430

4.24. For a $\lambda/2$ dipole placed symmetrical along the z-axis, determine the
(a) vector effective height
(b) maximum value (magnitude) of the vector effective height
(c) ratio (in percent) of the maximum value (magnitude) of the vector effective height to its total length
(d) maximum open-circuit output voltage when a uniform plane wave with an electric field of

$$\mathbf{E}^i|_{\theta=90^\circ} = -\hat{\mathbf{a}}_\theta 10^{-3} \text{ volts/wavelength}$$

impinges at broadside incidence on the dipole

4.25. A $\lambda/2$ dipole situated with its center at the origin radiates a time-averaged power of 600 W at a frequency of 300 MHz. A second $\lambda/2$ dipole is placed with its center at a point $P(r, \theta, \phi)$, where $r = 200$ m, $\theta = 90^\circ$, $\phi = 40^\circ$. It is oriented so that its axis is parallel to that of the transmitting antenna. What is the available power at the terminals of the second (receiving) dipole?

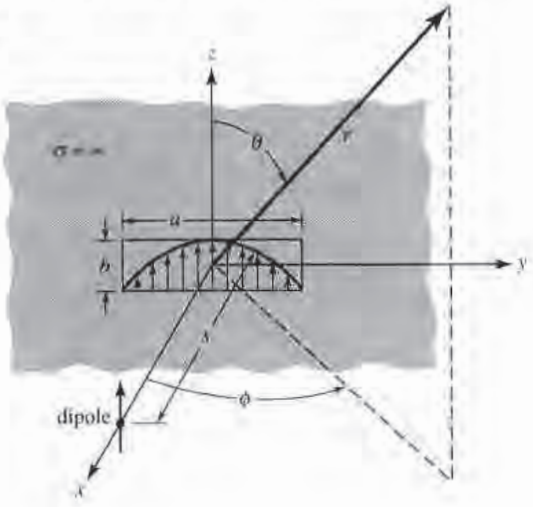
4.26. A half-wave dipole is radiating into free space. The coordinate system is defined so that the origin is at the center of the dipole and the z-axis is aligned with the dipole. Input power to the dipole is 100 W. Assuming an overall efficiency of 50%, find the power density (in W/m^2) at $r = 500$ m, $\theta = 60^\circ$, $\phi = 0^\circ$.

4.27. The input impedance of a $\lambda/2$ dipole, assuming the input (feed) terminals are at the center of the dipole, is equal to $73 + j42.5$. Assuming the dipole is lossless, find the
(a) input impedance (real and imaginary parts) assuming the input (feed) terminals have been shifted to a point on the dipole which is $\lambda/8$ from either end point of the dipole length
(b) capacitive or inductive reactance that must be placed across the new input terminals of part (a) so that the dipole is self-resonant
(c) VSWR at the new input terminals when the self-resonant dipole of part (b) is connected to a "twin-lead" 300-ohm line

4.28. A linear half-wavelength dipole is operating at a frequency of 1 GHz, determine the capacitance *or* inductance that must be placed *across* the input terminals of the dipole so that the antenna becomes resonant (make the total input impedance real). What is then the VSWR of the resonant half-wavelength dipole when it is connected to a 50-ohm line?

4.29. The field radiated by an infinitesimal electric dipole, placed along the z-axis a distance s along the x-axis, is incident upon a waveguide aperture antenna of dimensions a and b, mounted on an infinite ground plane, as shown in the figure. The normalized electric field radiated by the aperture in the E-plane (x-z plane; $\phi = 0^\circ$) is given by

$$\mathbf{E} = -\hat{\mathbf{a}}_\theta j \frac{\omega\mu b I_0 e^{-jkr}}{4\pi r} \frac{\sin\left(\frac{kb}{2}\cos\theta\right)}{\frac{kb}{2}\cos\theta}$$



INTEL-1045
U.S. Patent 7,151,430

Assuming the dipole and aperture antennas are in the far field of each other, determine the polarization loss (in dB) between the two antennas.

4.30. We are given the following information about antenna A:

(a) When A is transmitting, its radiated far-field expression for the E field is given by:

$$\mathbf{E}_a(z) = E_0 \frac{e^{-jkz}}{4\pi z}\left(\frac{\hat{\mathbf{a}}_x + j\hat{\mathbf{a}}_y}{\sqrt{2}}\right) \qquad V/m$$

(b) When A is receiving an incident plane wave given by:

$$\mathbf{E}_1(z) = \hat{\mathbf{a}}_y e^{jkz} \qquad V/m$$

its open-circuit voltage is $V_1 = 4e^{j20^\circ}$ V.

If we use the same antenna to receive a second incident plane given by:

$$\mathbf{E}_2(z) = 10(2\hat{\mathbf{a}}_x + \hat{\mathbf{a}}_y E^{j30^\circ})e^{jkz} \qquad V/m$$

find its received open-circuit voltage V_2.

4.31. A 3-cm long dipole carries a phasor current $I_0 = 10e^{j60}$ A. Assuming that $\lambda = 5$ cm, determine the E- and H-fields at 10 cm away from the dipole and at $\theta = 45^\circ$.

4.32. The radiation resistance of a thin, lossless linear electric dipole of length $l = 0.6\lambda$ is 120 ohms. What is the input resistance?

4.33. A lossless, resonant, center-fed $3\lambda/4$ linear dipole, radiating in free space is attached to a balanced, lossless transmission line whose characteristic impedence is 300 ohms. *Calculate* the

(a) radiation resistance (referred to the current maximum)

(b) input impedance (referred to the input terminals)

(c) VSWR on the transmission line

For parts (a) and (b) use the computer program at the end of the chapter.

4.34. Repeat Problem 4.33 for a center-fed $5\lambda/8$ dipole.

4.35. A dipole antenna, with a triangular current distribution, is used for communication with submarines at a frequency of 150 kHz. The overall length of the dipole is 200 m, and its radius is 1 m. Assume a loss resistance of 2 ohms in series with the radiation resistance of the antenna.

(a) Evaluate the input impedance of the antenna including the loss resistance. The input reactance can be approximated by

$$X_{in} \simeq -j120\,\frac{[\ln(l/2a) - 1]}{\tan(\pi l/\lambda)}$$

(b) Evaluate the radiation efficiency of the antenna.

(c) Evaluate the radiation power factor of the antenna.

(d) Design a conjugate-matching network to provide a perfect match between the antenna and a 50 ohms transmission line. Give the value of the series reactance X and the turns ratio n of the ideal transformer.

(e) Assuming a conjugate match, evaluate the instantaneous 2 : 1 VSWR bandwidth of the antenna.

4.36. Derive (4-102) using (4-99).

4.37. Determine the smallest height that an infinitesimal vertical electric dipole of $l = \lambda/50$ must be placed above an electric ground plane so that its pattern has only one null (aside from the null toward the vertical), and it occurs at 30° from the vertical. For that height, find the directivity and radiation resistance.

4.38. A $\lambda/50$ linear dipole is placed vertically at a height $h = 2\lambda$ above an infinite electric ground plane. Determine the angles (in degrees) where all the nulls of its pattern occur.

4.39. A linear infinitesimal dipole of length l and constant current is placed vertically a distance h above an infinite electric ground plane. Find the first five smallest heights

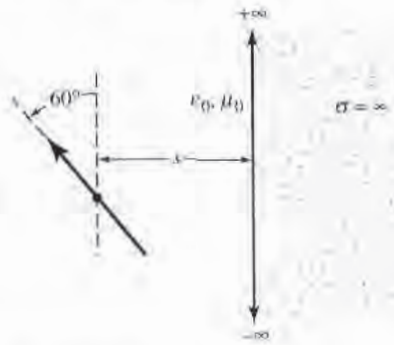
INTEL-1045
U.S. Patent 7,151,430

(in ascending order) so that a null is formed (for each height) in the far-field pattern at an angle of 60° from the vertical.

4.40. A vertical infinitesimal linear dipole is placed a distance $h = 3\lambda/2$ above an infinite perfectly conducting flat ground plane. Determine the
(a) angles (*in degrees* from the vertical) where the *array factor* of the system will achieve its *maximum* value
(b) angle (*in degrees* from the vertical) where the maximum of the *total field* will occur
(c) relative (compared to its maximum) field strength (*in dB*) of the total field at the angles where the array factor of the system achieves its maximum value (as obtained in part a)

4.41. A half-wavelength dipole is placed vertically on an infinite electric ground plane. Assuming that the dipole is fed at its base, find the
(a) radiation impedance (referred to the current maximum)
(b) input impedance (referred to the input terminals)
(c) VSWR when the antenna is connected to a lossless 50-ohm transmission line

4.42. An infinitesimal dipole of length ℓ is placed a distance s from an air-conductor interface and at an angle of $\theta = 60°$ from the vertical axis, as shown in the figure. Determine the location and direction of the image source which can be used to account for reflections. Be very clear in indicating the location and direction of the image. Your answer can be in the form of a very clear sketch.



4.43. It is desired to design an antenna system, which utilizes a vertical infinitesimal dipole of length ℓ placed a height h above a flat, perfect electric conductor of infinite extent. The design specifications require that the pattern of the array factor of the source and its image has only one maximum, and that maximum is pointed at an angle of 60° from the vertical. Determine (in wavelengths) the height of the source to achieve this desired design specification.

4.44. A very short ($l \leq \lambda/50$) vertical electric dipole is mounted on a pole a height h above the ground, which is assumed to be flat, perfectly conducting, and of infinite extent. The dipole is used as a transmitting antenna in a VHF ($f = 50$ MHz) ground-to-air communication system. In order for the communication system transmitting antenna signal not to interfere with a nearby radio station, it is necessary to place a null in the vertical dipole system pattern at an angle of 80° from the vertical. What should the shortest height (in meters) of the dipole be to achieve the desired specifications?

4.45. Derive (4-118) using (4-116).

4.46. An infinitesimal horizontal electric dipole of length $l = \lambda/50$ is placed parallel to the y-axis a height h above an infinite electric ground plane.
(a) Find the smallest height h (excluding $h = 0$) that the antenna must be elevated so that a null in the $\phi = 90°$ plane will be formed at an angle of $\theta = 45°$ from the vertical axis.
(b) For the height of part (a), determine the (1) radiation resistance and (2) directivity (for $\theta = 0°$) of the antenna system.

INTEL-1045
U.S. Patent 7,151,430

4.47. A horizontal $\lambda/50$ infinitesimal dipole of constant current and length l is placed parallel to the y-axis a distance $h = 0.707\lambda$ above an infinite electric ground plane. Find *all* the nulls formed by the antenna system in the $\phi = 90°$ plane.

4.48. An infinitesimal magnetic dipole is placed vertically a distance h above an infinite, perfectly conducting electric ground plane. Derive the far-zone fields radiated by the element above the ground plane.

4.49. Repeat Problem 4.48 for an electric dipole above an infinite, perfectly conducting magnetic ground plane.

4.50. Repeat Problem 4.48 for a magnetic dipole above an infinite, perfectly conducting magnetic ground plane.

4.51. An infinitesimal vertical electric dipole is placed at height h above an infinite PMC (perfect magnetic conductor) ground plane.

(a) Find the smallest height h (excluding $h = 0$) to which the antenna must be elevated so that a null is formed at an angle $\theta = 60°$ from the vertical axis

(b) For the value of h found in part (a), determine

1. the directive gain of the antenna in the $\theta = 45°$ direction
2. the radiation resistance of the antenna normalizd to the intrinsic impedance of the medium above the ground plane

Assume that the length of the antenna is $l = \frac{\lambda}{100}$.

4.52. A vertical $\lambda/2$ dipole, operating at 1 GHz, is placed a distance of 5 m (with respect to the tangent at the point of reflections) above the earth. Find the total field at a point 20 km from the source ($d = 20 \times 10^3$ m), at a height of 1,000 m (with respect to the tangent) above the ground. Use a $\frac{4}{3}$ radius earth and assume that the electrical parameters of the earth are $\epsilon_r = 5$, $\sigma = 10^{-2}$ S/m.

4.53. Two astronauts equipped with handheld radios land on different parts of a large asteroid. The radios are identical and transmit 5 W average power at 300 MHz. Assume the asteroid is a smooth sphere with physical radius of 1,000 km, has no atmosphere, and *consists of a lossless dielectric material with relative permittivity* $\epsilon_r = 9$. *Assume that* the radios' antennas can be modeled as vertical infinitesimal electric dipoles. Determine the signal power (in microwatts) received by each radio from the other, if the astronauts are separated by a range (distance along the asteroid's surface) of 2 km, and hold their radios vertically at heights of 1.5 m above the asteroid's surface.

Additional Information Required to Answer this Question: Prior to landing on the asteroid the astronauts calibrated their radios. Separating themselves in outer space by 10 km, the astronauts found the received signal power at each radio from the other was 10 microwatts, when both antennas were oriented in the same direction.

4.54. A satellite S transmitts an electromagnetic wave, at 10 GHz, via its transmitting antenna. The characteristics of the satellite-based transmitter are:

(a) The power radiated from the satellite antenna is 10 W.

(b) The distance between the satellite antenna and a point A on the earth's surface is 3.7×10^7 m, and

(c) The satellite transmitting antenna directivity in the direction SA is 50 dB

Ignoring ground effects,

1. Determine the magnitude of the E-field at A.
2. If the receiver at point A is a $\lambda/2$ dipole, what would be the voltage reading at the terminals of the antenna?

4.55. Derive (4-134) based on geometrical optics as presented in section 13.2 of [7].

INTEL-1045
U.S. Patent 7,151,430

COMPUTER PROGRAM - LINEAR DIPOLE

```
C*****************************************************************
C
C THIS IS A FORTRAN PROGRAM THAT COMPUTES THE:
C
C     I.   MAXIMUM DIRECTIVITY (DIMENSIONLESS AND IN dB)
C     II.  RADIATION RESISTANCE
C     III. INPUT RESISTANCE
C
C FOR A SYMMETRICAL DIPOLE OF FINITE LENGTH. THE DIPOLE IS
C RADIATING IN FREE SPACE.
C
C THE DIRECTIVITY, RADIATION RESISTANCE AND INPUT
C RESISTANCE ARE CALCULATED USING THE TRAILING EDGE
C METHOD IN INCREMENTS OF 1° IN THETA.
C
C
C          **INPUT PARAMETERS
C          1. L: DIPOLE LENGTH (in wavelengths)
C
C          **NOTE
C          THE FAR-ZONE ELECTRIC FIELD COMPONENT E_θ
C          EXISTS FOR 0°≤ Θ ≤180° AND 0°≤ Φ ≤360°.
C
C
C*****************************************************************
```


INTEL-1045
U.S. Patent 7,151,430

CHAPTER 5

LOOP ANTENNAS

5.1 INTRODUCTION

Another simple, inexpensive, and very versatile antenna type is the loop antenna. Loop antennas take many different forms such as a rectangle, square, triangle, ellipse, circle, and many other configurations. Because of the simplicity in analysis and construction, the circular loop is the most popular and has received the widest attention. It will be shown that a small loop (circular or square) is equivalent to an infinitesimal magnetic dipole whose axis is perpendicular to the plane of the loop. That is, the fields radiated by an electrically small circular or square loop are of the same mathematical form as those radiated by an infinitesimal magnetic dipole.

Loop antennas are usually classified into two categories, electrically small and electrically large. Electrically small antennas are those whose overall length (number of turns times circumference) is usually less than about one-tenth of a wavelength ($N \times C < \lambda/10$). However, electrically large loops are those whose circumference is about a free-space wavelength ($C \sim \lambda$). Most of the applications of loop antennas are in the HF (3–30 MHz), VHF (30–300 MHz), and UHF (300–3,000 MHz) bands. When used as field probes, they find applications even in the microwave frequency range.

Loop antennas with electrically small circumferences or perimeters have small radiation resistances that are usually smaller than their loss resistances. Thus they are very poor radiators, and they are seldom employed for transmission in radio communication. When they are used in any such application, it is usually in the receiving mode, such as in portable radios and pagers, where antenna efficiency is not as important as the signal-to-noise ratio. They are also used as probes for field measurements and as directional antennas for radiowave navigation. The field pattern of electrically small antennas of any shape (circular, elliptical, rectangular, square, etc.) is similar to that of an infinitesimal dipole with a null perpendicular to the plane of the loop and with its maximum along the plane of the loop. As the overall length of the loop increases and its circumference approaches one free-space wavelength, the maximum of the pattern shifts from the plane of the loop to the axis of the loop which is perpendicular to its plane.

INTEL-1045
U.S. Patent 7,151,430

The radiation resistance of the loop can be increased, and made comparable to the characteristic impedance of practical transmission lines, by increasing (electrically) its perimeter and/or the number of turns. Another way to increase the radiation resistance of the loop is to insert, within its circumference or perimeter, a ferrite core of very high permeability which will raise the magnetic field intensity and hence the radiation resistance. This forms the so-called ferrite loop.

Electrically large loops are used primarily in directional arrays, such as in helical antennas (see Section 10.3.1), Yagi-Uda arrays (see Section 10.3.3), quad arrays (see Section 10.3.4), and so on. For these and other similar applications, the maximum radiation is directed toward the axis of the loop forming an end-fire antenna. To achieve such directional pattern characteristics, the circumference (perimeter) of the loop should be about one free-space wavelength. The proper phasing between turns enhances the overall directional properties.

5.2 SMALL CIRCULAR LOOP

The most convenient geometrical arrangement for the field analysis of a loop antenna is to position the antenna symmetrically on the x-y plane, at $z = 0$, as shown in Figure 5.1(a). The wire is assumed to be very thin and the current distribution is given by

$$I_\phi = I_0 \tag{5-1}$$

where I_0 is a constant. Although this type of current distribution is accurate only for a loop antenna with a very small circumference, a more complex distribution makes the mathematical formulation quite cumbersome.

5.2.1 Radiated Fields

To find the fields radiated by the loop, the same procedure is followed as for the linear dipole. The potential function $\mathbf{A}$ given by (3-53) as

$$\mathbf{A}(x, y, z) = \frac{\mu}{4\pi}\int_C \mathbf{I}_e(x', y', z')\frac{e^{-jkR}}{R}dl' \tag{5-2}$$

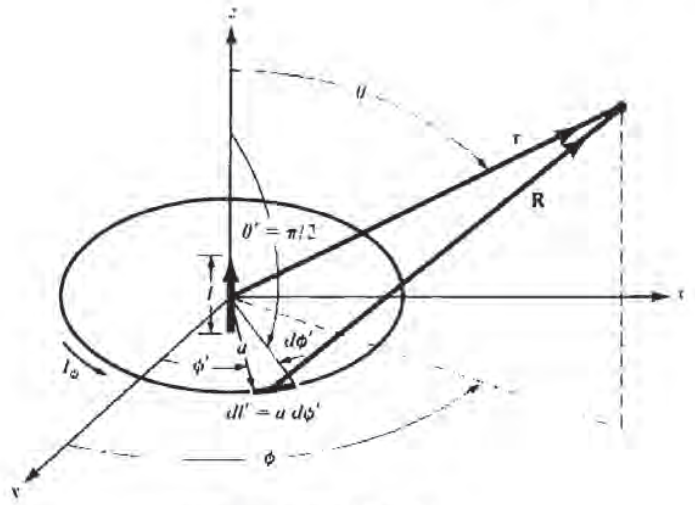
is first evaluated. Referring to Figure 5.1(a), R is the distance from any point on the loop to the observation point and dl' is an infinitesimal section of the loop antenna. In general, the current distribution $\mathbf{I}_e(x', y', z')$ can be written as

$$\mathbf{I}_e(x', y', z') = \hat{\mathbf{a}}_x I_x(x', y', z') + \hat{\mathbf{a}}_y I_y(x', y', z') + \hat{\mathbf{a}}_z I_z(x', y', z') \tag{5-3}$$

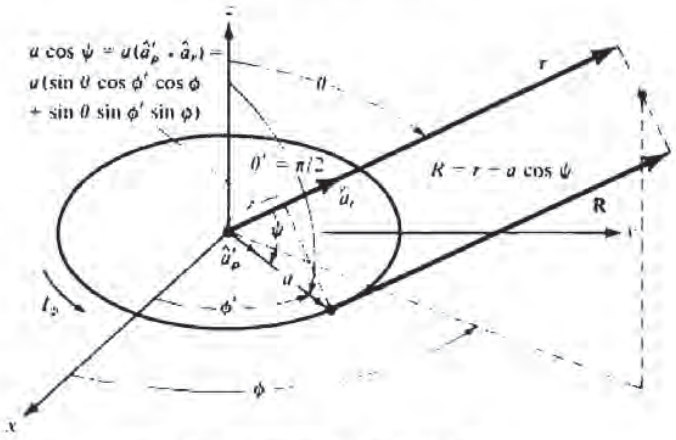
whose form is more convenient for linear geometries. For the circular loop antenna of Figure 5.1(a), whose current is directed along a circular path, it would be more convenient to write the rectangular current components of (5-3) in terms of the cylindrical components using the transformation (see Appendix VII)

$$\begin{bmatrix} I_x \\ I_y \\ I_z \end{bmatrix} = \begin{bmatrix} \cos\phi' & -\sin\phi' & 0 \\ \sin\phi' & \cos\phi' & 0 \\ 0 & 0 & 1 \end{bmatrix}\begin{bmatrix} I_\rho \\ I_\phi \\ I_z \end{bmatrix} \tag{5-4}$$

INTEL-1045
U.S. Patent 7,151,430



(a) Geometry for circular loop



(b) Geometry for far-field observations

Figure 5.1 Geometrical arrangement for loop antenna analysis.

which when expanded can be written as

$$\left.\begin{aligned} I_x &= I_\rho \cos\phi' - I_\phi \sin\phi' \\ I_y &= I_\rho \sin\phi' + I_\phi \cos\phi' \\ I_z &= I_z \end{aligned}\right\} \tag{5-5}$$

Since the radiated fields are usually determined in spherical components, the rectangular unit vectors of (5-3) are transformed to spherical unit vectors using the transformation matrix given by (4-5). That is,

$$\left.\begin{aligned} \hat{\mathbf{a}}_x &= \hat{\mathbf{a}}_r \sin\theta\cos\phi + \hat{\mathbf{a}}_\theta \cos\theta\cos\phi - \hat{\mathbf{a}}_\phi \sin\phi \\ \hat{\mathbf{a}}_y &= \hat{\mathbf{a}}_r \sin\theta\sin\phi + \hat{\mathbf{a}}_\theta \cos\theta\sin\phi + \hat{\mathbf{a}}_\phi \cos\phi \\ \hat{\mathbf{a}}_z &= \hat{\mathbf{a}}_r \cos\theta - \hat{\mathbf{a}}_\theta \sin\theta \end{aligned}\right\} \tag{5-6}$$

INTEL-1045
U.S. Patent 7,151,430

Substituting (5-5) and (5-6) in (5-3) reduces it to

$$\begin{aligned}\mathbf{I}_c &= \hat{\mathbf{a}}_r[I_\rho \sin\theta\cos(\phi-\phi') + I_\phi \sin\theta\sin(\phi-\phi') + I_z\cos\theta] \\ &+ \hat{\mathbf{a}}_\theta[I_\rho\cos\theta\cos(\phi-\phi') + I_\phi\cos\theta\sin(\phi-\phi') - I_z\sin\theta] \\ &+ \hat{\mathbf{a}}_\phi[-I_\rho\sin(\phi-\phi') + I_\phi\cos(\phi-\phi')]\end{aligned} \tag{5-7}$$

It should be emphasized that the source coordinates are designated as primed (ρ', ϕ', z') and the observation coordinates as unprimed (r, θ, ϕ). For the circular loop, the current is flowing in the ϕ direction (I_ϕ) so that (5-7) reduces to

$$\mathbf{I}_c = \hat{\mathbf{a}}_r I_\phi \sin\theta\sin(\phi-\phi') + \hat{\mathbf{a}}_\theta I_\phi\cos\theta\sin(\phi-\phi') + \hat{\mathbf{a}}_\phi I_\phi\cos(\phi-\phi') \tag{5-8}$$

The distance R, from any point on the loop to the observation point, can be written as

$$R = \sqrt{(x-x')^2 + (y-y')^2 + (z-z')^2} \tag{5-9}$$

Since

$$\begin{aligned} x &= r\sin\theta\cos\phi \\ y &= r\sin\theta\sin\phi \\ z &= r\cos\theta \\ x^2 + y^2 + z^2 &= r^2 \\ x' &= a\cos\phi' \\ y' &= a\sin\phi' \\ z' &= 0 \\ x'^2 + y'^2 + z'^2 &= a^2 \end{aligned} \tag{5-10}$$

(5-9) reduces to

$$R = \sqrt{r^2 + a^2 - 2ar\sin\theta\cos(\phi-\phi')} \tag{5-11}$$

By referring to Figure 5.1(a), the differential element length is given by

$$dl' = a\,d\phi' \tag{5-12}$$

Using (5-8), (5-11), and (5-12), the ϕ-component of (5-2) can be written as

$$A_\phi = \frac{a\mu}{4\pi}\int_0^{2\pi} I_\phi\cos(\phi-\phi')\frac{e^{-jk\sqrt{r^2+a^2-2ar\sin\theta\cos(\phi-\phi')}}}{\sqrt{r^2+a^2-2ar\sin\theta\cos(\phi-\phi')}}\,d\phi' \tag{5-13}$$

Since the current I_ϕ as given by (5-1) is constant, the field radiated by the loop will not be a function of the observation angle ϕ. Thus any observation angle ϕ can be chosen; for simplicity $\phi = 0$. Therefore (5-13) can be written as

$$A_\phi = \frac{a\mu I_0}{4\pi}\int_0^{2\pi}\cos\phi'\frac{e^{-jk\sqrt{r^2+a^2-2ar\sin\theta\cos\phi'}}}{\sqrt{r^2+a^2-2ar\sin\theta\cos\phi'}}\,d\phi' \tag{5-14}$$

The integration of (5-14) cannot be carried out without any approximations. For small loops, the function

$$f = \frac{e^{-jk\sqrt{r^2+a^2-2ar\sin\theta\cos\phi'}}}{\sqrt{r^2+a^2-2ar\sin\theta\cos\phi'}} \tag{5-15}$$

INTEL-1045
U.S. Patent 7,151,430

which is part of the integrand of (5-14), can be expanded in a Maclaurin series in a using

$$f \simeq f(0) + f'(0)\,a + \frac{1}{2!}f''(0)\,a^2 + \cdots + \frac{1}{(n-1)!}f^{(n-1)}(0)\,a^{n-1} + \cdots \tag{5-15a}$$

where $f'(0) = \partial f/\partial a|_{a=0}$, $f''(0) = \partial^2 f/\partial a^2|_{a=0}$, and so forth. Taking into account only the first two terms of (5-15a), or

$$f(0) = \frac{e^{-jkr}}{r} \tag{5-15b}$$

$$f'(0) = \left(\frac{jk}{r} + \frac{1}{r^2}\right) e^{-jkr} \sin\theta \cos\phi' \tag{5-15c}$$

$$f \simeq \left[\frac{1}{r} + a\left(\frac{jk}{r} + \frac{1}{r^2}\right) \sin\theta \cos\phi'\right] e^{-jkr} \tag{5-15d}$$

reduces (5-14) to

$$A_\phi \simeq \frac{a\mu I_0}{4\pi} \int_0^{2\pi} \cos\phi' \left[\frac{1}{r} + a\left(\frac{jk}{r} + \frac{1}{r^2}\right) \sin\theta \cos\phi'\right] e^{-jkr}\, d\phi'$$

$$A_\phi \simeq \frac{a^2\mu I_0}{4} e^{-jkr} \left(\frac{jk}{r} + \frac{1}{r^2}\right) \sin\theta \tag{5-16}$$

In a similar manner, the r- and θ-components of (5-2) can be written as

$$A_r \simeq \frac{a\mu I_0}{4\pi} \sin\theta \int_0^{2\pi} \sin\phi' \left[\frac{1}{r} + a\left(\frac{jk}{r} + \frac{1}{r^2}\right) \sin\theta \cos\phi'\right] e^{-jkr}\, d\phi' \tag{5-16a}$$

$$A_\theta \simeq -\frac{a\mu I_0}{4\pi} \cos\theta \int_0^{2\pi} \sin\phi' \left[\frac{1}{r} + a\left(\frac{jk}{r} + \frac{1}{r^2}\right) \sin\theta \cos\phi'\right] e^{-jkr}\, d\phi' \tag{5-16b}$$

which when integrated reduce to zero. Thus

$$\mathbf{A} \simeq \hat{\mathbf{a}}_\phi A_\phi = \hat{\mathbf{a}}_\phi \frac{a^2\mu I_0}{4} e^{-jkr} \left[\frac{jk}{r} + \frac{1}{r^2}\right] \sin\theta$$

$$= \hat{\mathbf{a}}_\phi j \frac{k\mu a^2 I_0 \sin\theta}{4r} \left[1 + \frac{1}{jkr}\right] e^{-jkr} \tag{5-17}$$

Substituting (5-17) into (3-2a) reduces the magnetic field components to

$$H_r = j\frac{ka^2 I_0 \cos\theta}{2r^2} \left[1 + \frac{1}{jkr}\right] e^{-jkr} \tag{5-18a}$$

$$H_\theta = -\frac{(ka)^2 I_0 \sin\theta}{4r} \left[1 + \frac{1}{jkr} - \frac{1}{(kr)^2}\right] e^{-jkr} \tag{5-18b}$$

$$H_\phi = 0 \tag{5-18c}$$

INTEL-1045
U.S. Patent 7,151,430

Using (3-15) or (3-10) with $\mathbf{J} = 0$, the corresponding electric field components can be written as

$$\boxed{E_r = E_\theta = 0} \tag{5-19a}$$

$$\boxed{E_\phi = \eta \frac{(ka)^2 I_0 \sin\theta}{4r}\left[1 + \frac{1}{jkr}\right] e^{-jkr}} \tag{5-19b}$$

5.2.2 Small Loop and Infinitesimal Magnetic Dipole

A comparison of (5-18a)–(5-19b) with those of the infinitesimal magnetic dipole indicates that they have similar forms. In fact, the electric and magnetic field components of an infinitesimal magnetic dipole of length l and constant "magnetic" current I_m are given by

$$E_r = E_\theta = H_\phi = 0 \tag{5-20a}$$

$$E_\phi = -j \frac{kI_m l \sin\theta}{4\pi r}\left[1 + \frac{1}{jkr}\right] e^{-jkr} \tag{5-20b}$$

$$H_r = \frac{I_m l \cos\theta}{2\pi\eta r^2}\left[1 + \frac{1}{jkr}\right] e^{-jkr} \tag{5-20c}$$

$$H_\theta = j \frac{kI_m l \sin\theta}{4\pi\eta r}\left[1 + \frac{1}{jkr} - \frac{1}{(kr)^2}\right] e^{-jkr} \tag{5-20d}$$

These can be obtained from the fields of an infinitesimal electric dipole, (4-8a)–(4-10c). When (5-20a)–(5-20d) are compared with (5-18a)–(5-19b), they indicate that *a magnetic dipole of magnetic moment $I_m l$ is equivalent to a small electric loop of radius a and constant electric current I_0 provided that*

$$\boxed{I_m l = jS\omega\mu I_0} \tag{5-21}$$

where $S = \pi a^2$ (area of the loop). Thus, for analysis purposes, the small electric loop can be replaced by a small linear magnetic dipole of constant current. The geometrical equivalence is illustrated in Figure 5.1(a) where the magnetic dipole is directed along the z-axis which is also perpendicular to the plane of the loop.

5.2.3 Power Density and Radiation Resistance

The fields radiated by a small loop, as given by (5-18a)–(5-19b), are valid everywhere except at the origin. As was discussed in Section 4.1 for the infinitesimal dipole, the power in the region very close to the antenna (near-field, $kr \ll 1$) is predominantly reactive and in the far-field ($kr \gg 1$) is predominantly real. To illustrate this for the loop, the complex power density

$$\begin{aligned} \mathbf{W} &= \tfrac{1}{2}(\mathbf{E} \times \mathbf{H}^*) = \tfrac{1}{2}[(\hat{\mathbf{a}}_\phi E_\phi) \times (\hat{\mathbf{a}}_r H^*_r + \hat{\mathbf{a}}_\theta H^*_\theta)] \\ &= \tfrac{1}{2}(-\hat{\mathbf{a}}_r E_\phi H^*_\theta + \hat{\mathbf{a}}_\theta E_\phi H^*_r) \end{aligned} \tag{5-22}$$

INTEL-1045
U.S. Patent 7,151,430

is first formed. When (5-22) is integrated over a closed sphere, only its radial component given by

$$W_r = \eta \frac{(ka)^4}{32} |I_0|^2 \frac{\sin^2 \theta}{r^2} \left[1 + j \frac{1}{(kr)^3} \right] \tag{5-22a}$$

contributes to the complex power P_r. Thus

$$P_r = \oiint_S \mathbf{W} \cdot d\mathbf{s} = \eta \frac{(ka)^4}{32} |I_0|^2 \int_0^{2\pi} \int_0^{\pi} \left[1 + j \frac{1}{(kr)^3} \right] \sin^3 \theta \, d\theta \, d\phi \tag{5-23}$$

which reduces to

$$P_r = \eta \left(\frac{\pi}{12} \right) (ka)^4 |I_0|^2 \left[1 + j \frac{1}{(kr)^3} \right] \tag{5-23a}$$

and whose real part is equal to

$$P_{\text{rad}} = \eta \left(\frac{\pi}{12} \right) (ka)^4 |I_0|^2 \tag{5-23b}$$

For small values of kr ($kr \ll 1$), the second term within the brackets of (5-23a) is dominant which makes the power mainly reactive. In the far-field ($kr \gg 1$), the second term within the brackets diminishes which makes the power real. A comparison between (5-23a) with (4-14) indicates a difference in sign between the terms within the brackets. Whereas for the infinitesimal dipole the radial power density in the near-field is capacitive, for the small loop it is inductive. This indicates that the radial magnetic energy is larger than the electric energy.

The radiation resistance of the loop is found by equating (5-23b) to $|I_0|^2 R_r/2$. Doing this, the radiation resistance can be written as

$$\boxed{R_r = \eta \left(\frac{\pi}{6} \right) (k^2 a^2)^2 = \eta \frac{2\pi}{3} \left(\frac{kS}{\lambda} \right)^2 = 20\pi^2 \left(\frac{C}{\lambda} \right)^4 = 31.171 \left(\frac{S^2}{\lambda^4} \right)} \tag{5-24}$$

where $S = \pi a^2$ is the area and $C = 2\pi a$ is the circumference of the loop.

The radiation resistance as given by (5-24) is only for a single-turn loop. If the loop antenna has N turns wound so that the magnetic field passes through all the loops, the radiation resistance is equal to that of single turn multiplied by N^2. That is,

$$\boxed{R_r = \eta \left(\frac{2\pi}{3} \right) \left(\frac{kS}{\lambda} \right)^2 N^2 = 20\pi^2 \left(\frac{C}{\lambda} \right)^4 N^2 = 31.171 \, N^2 \left(\frac{S^2}{\lambda^4} \right)} \tag{5-24a}$$

Even though the radiation resistance of a single turn loop may be small, the overall value can be increased by including many turns. This is a very desirable and practical mechanism that is not available for the infinitesimal dipole.

Example 5.1

Find the radiation resistance of a single-turn and an 8-turn small circular loop. The radius of the loop is $\lambda/25$ and the medium is free-space.

INTEL-1045
U.S. Patent 7,151,430

SOLUTION

$$S = \pi a^2 = \pi\left(\frac{\lambda}{25}\right)^2 = \frac{\pi\lambda^2}{625}$$

$$R_r \text{ (single turn)} = 120\pi\left(\frac{2\pi}{3}\right)\left(\frac{2\pi^2}{625}\right)^2 = 0.788 \text{ ohms}$$

$$R_r \text{ (8 turns)} = 0.788(8)^2 = 50.43 \text{ ohms}$$

The radiation and loss resistances of an antenna determine the radiation efficiency, as defined by (2-90). The loss resistance of a single-turn small loop is, in general, much larger than its radiation resistance; thus the corresponding radiation efficiencies are very low and depend on the loss resistance. To increase the radiation efficiency, multiturn loops are often employed. However, because the current distribution in a multiturn loop is quite complex, great confidence has not yet been placed in analytical methods for determining the radiation efficiency. Therefore greater reliance has been placed on experimental procedures. Two experimental techniques that can be used to measure the radiation efficiency of a small multiturn loop are those that are usually referred to as the *Wheeler method* and the *Q method* [1].

Usually it is assumed that the loss resistance of a small loop is the same as that of a straight wire whose length is equal to the circumference of the loop, and it is computed using (2-90b). Although this assumption is adequate for single-turn loops, it is not valid for multiturn loops. In a multiturn loop, the current is not uniformly distributed around the wire but depends on the skin and proximity effects [2]. In fact, for close spacings between turns, the contribution to the loss resistance due to the proximity effect can be larger than that due to the skin effect.

The total ohmic resistance for an N-turn circular loop antenna with loop radius a, wire radius b, and loop separation $2c$, shown in Figure 5.2(a) is given by [3]

$$R_{\text{ohmic}} = \frac{Na}{b}R_s\left(\frac{R_p}{R_0} + 1\right) \tag{5-25}$$

where

$$R_s = \sqrt{\frac{\omega\mu_0}{2\sigma}} = \text{surface impedance of conductor}$$

$$R_p = \text{ohmic resistance per unit length due to proximity effect}$$

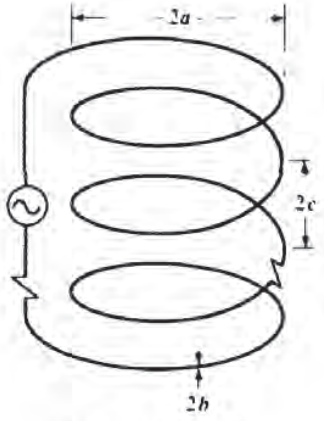
$$R_0 = \frac{NR_s}{2\pi b} = \text{ohmic skin effect resistance per unit length (ohms/m)}$$

The ratio of R_p/R_0 has been computed [3] as a function of the spacing c/b for loops with $2 \le N \le 8$ and it is shown plotted in Figure 5.2(b). It is evident that for close spacing the ohmic resistance is twice as large as that in the absence of the proximity effect ($R_p/R_0 = 0$).

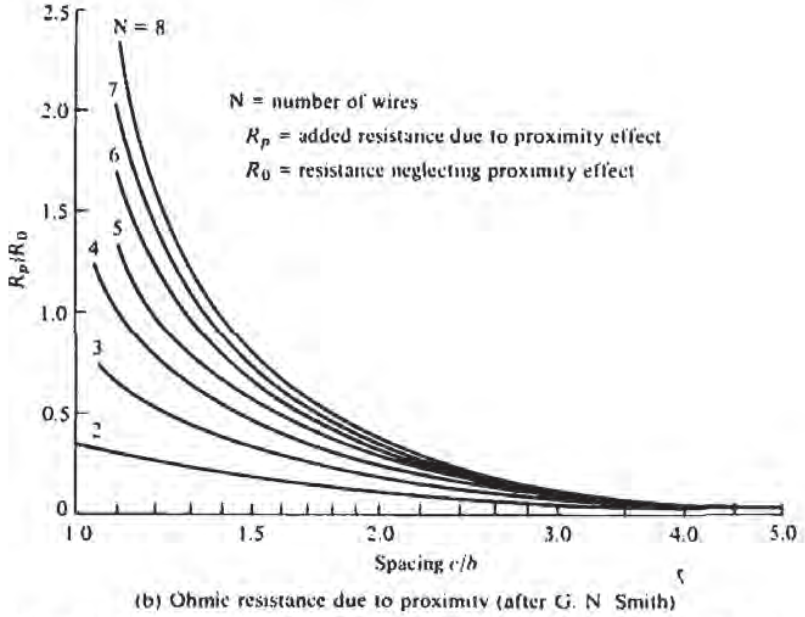
Example 5.2

Find the radiation efficiency of a single-turn and an 8-turn small circular loop at $f = 100$ MHz. The radius of the loop is $\lambda/25$, the radius of the wire is $10^{-4}\lambda$, and

INTEL-1045
U.S. Patent 7,151,430



(a) N-turn circular loop



(b) Ohmic resistance due to proximity (after G. N. Smith)

Figure 5.2 N-turn circular loop and ohmic resistance due to proximity effect. (SOURCE: G. S. Smith, "Radiation Efficiency of Electrically Small Multiturn Loop Antennas," *IEEE Trans. Antennas Propagat.*, Vol. AP-20, No. 5, pp. 656-657, Sept. 1972© (1972) IEEE).

the turns are spaced $4 \times 10^{-4}\lambda$ apart. Assume the wire is copper with a conductivity of 5.7×10^7 (S/m) and the antenna is radiating into free-space.

SOLUTION

From Example 5.1

$$R_r \text{ (single turn)} = 0.788 \text{ ohms}$$

$$R_r \text{ (8 turns)} = 50.43 \text{ ohms}$$

INTEL-1045
U.S. Patent 7,151,430

The loss resistance for a single turn is given, according to (2-90b), by

$$R_L = R_{hf} = \frac{a}{b}\sqrt{\frac{\omega\mu_0}{2\sigma}} = \frac{1}{25(10^{-4})}\sqrt{\frac{\pi(10^8)(4\pi \times 10^{-7})}{5.7 \times 10^7}}$$
$$= 1.053 \text{ ohms}$$

and the radiation efficiency, according to (2-90), by

$$e_{cd} = \frac{0.788}{0.788 + 1.053} = 0.428 = 42.8\%$$

From Figure 5.2(b)

$$\frac{R_R}{R_0} = 0.38$$

and from (5-25)

$$R_r = R_{\text{ohmic}} = \frac{8}{25(10^{-4})}\sqrt{\frac{\pi(10^8)(4\pi \times 10^{-7})}{5.7 \times 10^7}}(1.38) = 11.62$$

Thus

$$e_{cd} = \frac{50.43}{50.43 + 11.62} = 0.813 = 81.3\%$$

5.2.4 Near-Field ($kr \ll 1$) Region

The expressions for the fields, as given by (5-18a)–(5-19b), can be simplified if the observations are made in the near-field ($kr \ll 1$). As for the infinitesimal dipole, the predominant term in each expression for the field in the near-zone region is the last one within the parentheses of (5-18a)–(5-19b). Thus for $kr \ll 1$

$$H_r \simeq \frac{a^2 I_0 e^{-jkr}}{2r^3}\cos\theta \qquad \text{(5-26a)}$$

$$H_\theta \simeq \frac{a^2 I_0 e^{-jkr}}{4r^3}\sin\theta \qquad \text{(5-26b)}$$

$$H_\phi = E_r = E_\theta = 0 \qquad \text{(5-26c)}$$

$$E_\phi \simeq -j\frac{a^2 k I_0 e^{-jkr}}{4r^2}\sin\theta \qquad \text{(5-26d)}$$

$kr \ll 1$

The two **H**-field components are in time-phase. However, they are in time quadrature with those of the electric field. This indicates that the average power (real power) is zero, as for the infinitesimal electric dipole. The condition of $kr \ll 1$ can be satisfied at moderate distances away from the antenna provided the frequency of operation is very low. The fields of (5-26a)–(5-26d) are usually referred to as *quasi-stationary*.

INTEL-1045
U.S. Patent 7,151,430

5.2.5 Far-Field ($kr \gg 1$) Region

The other space of interest where the fields can be approximated is the far-field ($kr \gg 1$) region. In contrast to the near-field, the dominant term in (5-18a)–(5-19b) for $kr \gg 1$ is the first one within the parentheses. Since for $kr > 1$ the H_r component will be inversely proportional to r^2 whereas H_θ will be inversely proportional to r, for large values of kr ($kr \gg 1$) the H_r component will be small compared to H_θ. Thus it can be assumed that it is approximately equal to zero. Therefore for $kr \gg 1$,

$$\left.\begin{aligned} H_\theta &\simeq -\frac{k^2a^2I_0e^{-jkr}}{4r}\sin\theta = -\frac{\pi SI_0e^{-jkr}}{\lambda^2 r}\sin\theta \qquad (5\text{-}27a)\\ E_\phi &\simeq \eta\frac{k^2a^2I_0e^{-jkr}}{4r}\sin\theta = \eta\frac{\pi SI_0e^{-jkr}}{\lambda^2 r}\sin\theta \qquad (5\text{-}27b) \end{aligned}\right\} kr \gg 1$$

$$H_r \simeq H_\phi = E_r = E_\theta = 0 \qquad (5\text{-}27c)$$

where $S = \pi a^2$ is the geometrical area of the loop.

Forming the ratio of $-E_\phi/H_\theta$, the wave impedance can be written as

$$Z_w = -\frac{E_\phi}{H_\theta} \simeq \eta \qquad (5\text{-}28)$$

where

Z_w = wave impedance

η = intrinsic impedance

As for the infinitesimal dipole, the **E**- and **H**-field components of the loop in the far-field ($kr \gg 1$) region are perpendicular to each other and transverse to the direction of propagation. They form a *T*ransverse *E*lectro *M*agnetic (TEM) field whose wave impedance is equal to the intrinsic impedance of the medium. Equations (5-27a)–(5-27c) can also be derived using the procedure outlined and relationships developed in Section 3.6. This is left as an exercise to the reader (Prob. 5.5).

5.2.6 Radiation Intensity and Directivity

The real power P_{rad} radiated by the loop was found in Section 5.2.3 and is given by (5-23b). The same expression can be obtained by forming the average power density, using (5-27a)–(5-27c), and integrating it over a closed sphere of radius r. This is left as an exercise to the reader (Prob. 5.4). Associated with the radiated power P_{rad} is an average power density $\mathbf{W}_{av}$. It has only a radial component W_r which is related to the radiation intensity U by

$$U = r^2W_r = \frac{\eta}{2}\left(\frac{k^2a^2}{4}\right)^2|I_0|^2\sin^2\theta = \frac{r^2}{2\eta}|E_\phi(r,\theta,\phi)|^2 \qquad (5\text{-}29)$$

and it conforms to (2-12a). The normalized pattern of the loop, as given by (5-29), is identical to that of the infinitesimal dipole shown in Figure 4.2. The maximum value occurs at $\theta = \pi/2$, and it is given by

$$U_{max} = U|_{\theta=\pi/2} = \frac{\eta}{2}\left(\frac{k^2a^2}{4}\right)^2|I_0|^2 \qquad (5\text{-}30)$$

INTEL-1045
U.S. Patent 7,151,430

Using (5-30) and (5-23b), the directivity of the loop can be written as

$$\boxed{D_0 = 4\pi \frac{U_{\max}}{P_{\text{rad}}} = \frac{3}{2}} \tag{5-31}$$

and its maximum effective aperture as

$$\boxed{A_{em} = \left(\frac{\lambda^2}{4\pi}\right) D_0 = \frac{3\lambda^2}{8\pi}} \tag{5-32}$$

It is observed that the directivity, and as a result the maximum effective area, of a small loop is the same as that of an infinitesimal electric dipole. This should be expected since their patterns are identical.

The far-field expressions for a small loop, as given by (5-27a)–(5-27c), will be obtained by another procedure in the next section. In that section a loop of any radius but of constant current will be analyzed. Closed form solutions will be possible only in the far-field region. The small loop far-field expressions will then be obtained as a special case of that problem.

Example 5.3

The radius of a small loop of constant current is $\lambda/25$. Find the physical area of the loop and compare it with its maximum effective aperture.

SOLUTION

$$S\,(\text{physical}) = \pi a^2 = \pi\left(\frac{\lambda}{25}\right)^2 = \frac{\pi\lambda^2}{625} = 5.03 \times 10^{-3}\lambda^2$$

$$A_{em} = \frac{3\lambda^2}{8\pi} = 0.119\lambda^2$$

$$\frac{A_{em}}{S} = \frac{0.119\lambda^2}{5.03 \times 10^{-3}\lambda^2} = 23.66$$

Electrically the loop is about 24 times larger than its physical size, which should not be surprising. To be effective, a small loop must be larger electrically than its physical size.

5.2.7 Equivalent Circuit

A small loop is primarily inductive, and it can be represented by a lumped element equivalent circuit similar to those of Figure 2.22.

INTEL-1045
U.S. Patent 7,151,430

A. Transmitting Mode

The equivalent circuit for its input impedance when the loop is used as a transmitting antenna is that shown in Figure 5.3. This is similar to the equivalent circuit of Figure 2.22(b). Therefore its input impedance Z_{in} is represented by

$$Z_{in} = R_{in} + jX_{in} = (R_r + R_L) + j(X_A + X_i) \tag{5-33}$$

where

R_r = radiation resistance as given by (5-24)
R_L = loss resistance of loop conductor
X_A = external inductive reactance of loop antenna = ωL_A
X_i = internal high-frequency reactance of loop conductor = ωL_i

In Figure 5.3 the capacitor C_r is used in parallel to (5-33) to resonate the antenna; it can also be used to represent distributed stray capacitances. In order to determine the capacitance of C_r at resonance, it is easier to represent (5-33) by its equivalent admittance Y_{in} of

$$Y_{in} = G_{in} + jB_{in} = \frac{1}{Z_{in}} = \frac{1}{R_{in} + jX_{in}} \tag{5-34}$$

where

$$G_{in} = \frac{R_{in}}{R_{in}^2 + X_{in}^2} \tag{5-34a}$$

$$B_{in} = -\frac{X_{in}}{R_{in}^2 + X_{in}^2} \tag{5-34b}$$

At resonance, the susceptance B_r of the capacitor C_r must be chosen to eliminate the imaginary part B_{in} of (5-34) and (5-34a). This is accomplished by choosing C_r according to

$$C_r = \frac{B_r}{2\pi f} = -\frac{B_{in}}{2\pi f} = \frac{1}{2\pi f}\frac{X_{in}}{R_{in}^2 + X_{in}^2} \tag{5-35}$$

Under resonance the input impedance Z'_{in} is then equal to

$$Z'_{in} = R'_{in} = \frac{1}{G_{in}} = \frac{R_{in}^2 + X_{in}^2}{R_{in}} = R_{in} + \frac{X_{in}^2}{R_{in}} \tag{5-36}$$

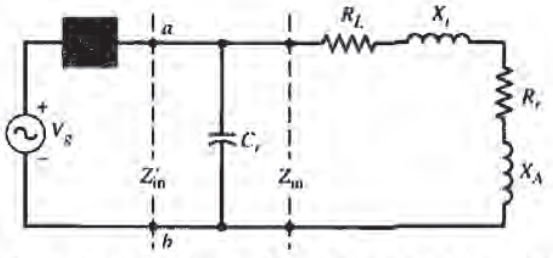


Figure 5.3 Equivalent circuit of loop antenna in transmitting mode.

INTEL-1045
U.S. Patent 7,151,430

The loss resistance R_L of the loop conductor can be computed using techniques illustrated in Example 5.2. The inductive reactance X_A of the loop is computed using the inductance L_A of:

Circular loop of radius a and wire radius b:

$$L_A = \mu_0 a\left[\ln\left(\frac{8a}{b}\right) - 2\right] \tag{5-37a}$$

Square loop with sides a and wire radius b:

$$L_A = 2\mu_0\frac{a}{\pi}\left[\ln\left(\frac{a}{b}\right) - 0.774\right] \tag{5-37b}$$

The internal reactance of the loop conductor X_i can be found using the internal inductance L_i of the loop which for a single turn can be approximated by

$$L_i = \frac{l}{\omega P}\sqrt{\frac{\omega\mu_0}{2\sigma}} = \frac{a}{\omega b}\sqrt{\frac{\omega\mu_0}{2\sigma}} \tag{5-38}$$

where l is the length and P is the perimeter of the wire of the loop

B. Receiving Mode

The loop antenna is often used as a receiving antenna or as a probe to measure magnetic flux density. Therefore when a plane wave impinges upon it, as shown in Figure 5.4(a), an open-circuit voltage develops across its terminals. This open-circuit voltage is related according to (2-93) to its vector effective length and incident electric field. This open-circuit voltage is proportional to the incident magnetic flux density B_z^i, which is normal to the plane of the loop. Assuming the incident field is uniform over the plane of the loop, the open-circuit voltage for a single-turn loop can be written as [5]

$$V_{oc} = j\omega\pi a^2 B_z^i \tag{5-39}$$

Defining in Figure 5.4(a) the plane of incidence as the plane formed by the z axis and radical vector, then the open-circuit voltage of (5-39) can be related to the magnitude of the incident magnetic and electric fields by

$$V_{oc} = j\omega\pi a^2\mu_0 H^i\cos\psi_i\sin\theta_i = jk_0\pi a^2 E^i\cos\psi_i\sin\theta_i \tag{5-39a}$$

where ψ_i is the angle between the direction of the magnetic field of the incident plane wave and the plane of incidence, as shown in Figure 5.4(a).

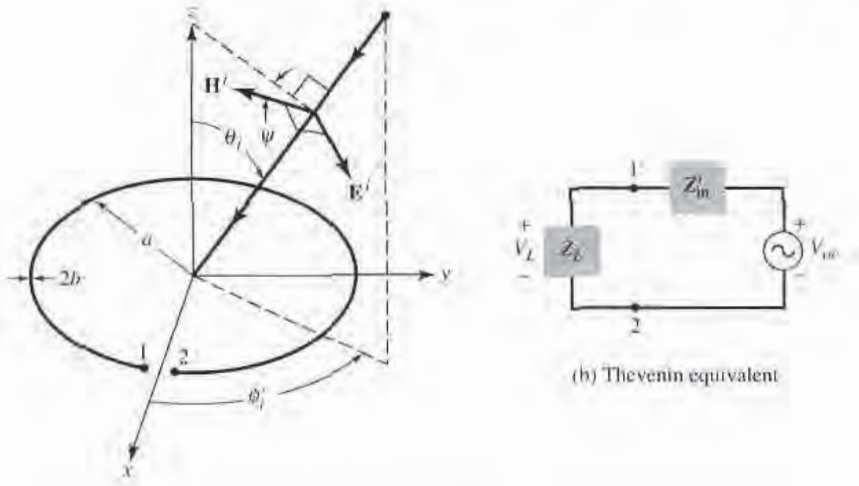
Since the open-circuit voltage is also related to the vector effective length by (2-93), then the effective length for a single turn loop can be written as

$$\ell_e = \hat{\mathbf{a}}_\psi l_e = \hat{\mathbf{a}}_\phi jk_0\pi a^2\cos\psi_i\sin\theta_i = \hat{\mathbf{a}}_\phi jk_0 S\cos\psi_i\sin\theta_i \tag{5-40}$$

where S is the area of the loop. The factor $\cos\psi_i\sin\theta_i$ is introduced because the open-circuit voltage is proportional to the magnetic flux density component B_z^i which is normal to the plane of the loop.

When a load impedance Z_L is connected to the output terminals of the loop as shown in Figure 5.4(b), the voltage V_L across the load impedance Z_L is related to the input impedance Z_{in}^l of Figure 5.4(b) and the open-circuit voltage of (5-39a) by

INTEL-1045
U.S. Patent 7,151,430



(a) Plane wave incident on a receiving loop (G.S. Smith, "Loop Antennas," Copyright © 1984, McGraw-Hill, Inc. Permission by McGraw-Hill, Inc.)

(b) Thevenin equivalent

Figure 5.4 Loop antenna and its equivalent in receiving mode.

$$V_L = V_{oc}' \frac{Z_L}{Z_{in}' + Z_L} \tag{5-41}$$

5.3 CIRCULAR LOOP OF CONSTANT CURRENT

Let us now reconsider the loop antenna of Figure 5.1(a) but with a radius that may not necessarily be small. The current in the loop will again be assumed to be constant, as given by (5-1). For this current distribution, the vector potential is given by (5-14). Without using the small radius approximation, the integration in (5-14) cannot be carried out. However, if the observations are restricted in the far-field ($r \gg a$) region, the small radius approximation is not needed to integrate (5-14).

Although the uniform current distribution along the perimeter of the loop is only valid provided the circumference is less than about 0.2λ (radius less than about 0.03λ), the procedure developed here for a constant current can be followed to find the far zone fields of any size loop with not necessarily uniform current.

5.3.1 Radiated Fields

To find the fields in the far-field region, the distance R can be approximated by

$$R = \sqrt{r^2 + a^2 - 2ar \sin\theta \cos\phi'} \approx \sqrt{r^2 - 2ar \sin\theta \cos\phi'} \qquad \text{for} \quad r \gg a \tag{5-42}$$

which can be reduced, using the binomial expansion, to

$$\left.\begin{aligned} R &\simeq r\sqrt{1 - \frac{2a}{r}\sin\theta\cos\phi'} = r - a\sin\theta\cos\phi' = r - a\cos\psi_0 \\ &\qquad\qquad \text{for phase terms} \\ R &\simeq r \qquad\qquad \text{for amplitude terms} \end{aligned}\right\} \tag{5-43}$$

INTEL-1045
U.S. Patent 7,151,430

since

$$\cos\psi_0 = \hat{\mathbf{a}}_\rho' \cdot \hat{\mathbf{a}}_r \big|_{\phi=0} = (\hat{\mathbf{a}}_x \cos\phi' + \hat{\mathbf{a}}_y \sin\phi') \cdot (\hat{\mathbf{a}}_x \sin\theta\cos\phi + \hat{\mathbf{a}}_y \sin\theta\sin\phi + \hat{\mathbf{a}}_z \cos\theta)\big|_{\phi=0} = \sin\theta\cos\phi' \tag{5-43a}$$

The geometrical relation between R and r, for any observation angle ϕ in the far-field region, is shown in Figure 5.1(b). For observations at $\phi = 0$, it simplifies to that given by (5-43) and shown in Figure 5.5. Thus (5-14) can be written as

$$A_\phi = \frac{a\mu I_0 e^{-jkr}}{4\pi r}\int_0^{2\pi} \cos\phi' e^{+jka\sin\theta\cos\phi'}\, d\phi' \tag{5-44}$$

and it can be separated into two terms as

$$A_\phi = \frac{a\mu I_0 e^{-jkr}}{4\pi r}\left[\int_0^{\pi} \cos\phi' e^{+jka\sin\theta\cos\phi'}\, d\phi' + \int_{\pi}^{2\pi} \cos\phi' e^{+jka\sin\theta\cos\phi'}\, d\phi'\right] \tag{5-45}$$

The second term within the brackets can be rewritten by making a change of variable of the form

$$\phi' = \phi'' + \pi \tag{5-46}$$

Thus (5-45) can also be written as

$$A_\phi = \frac{a\mu I_0 e^{-jkr}}{4\pi r}\left[\int_0^{\pi} \cos\phi' e^{+jka\sin\theta\cos\phi'}\, d\phi' - \int_0^{\pi} \cos\phi'' e^{-jka\sin\theta\cos\phi''}\, d\phi''\right] \tag{5-47}$$

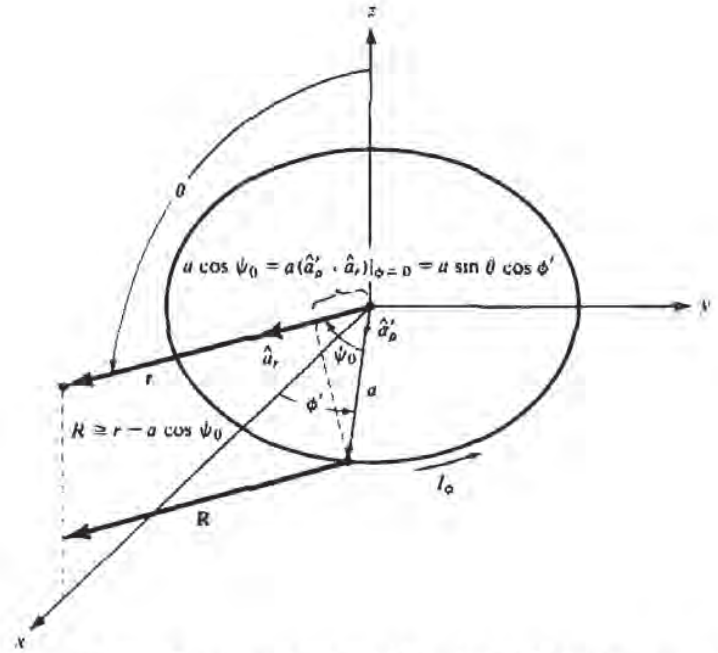


Figure 5.5 Geometry for far-field analysis of a loop antenna.

INTEL-1045
U.S. Patent 7,151,430

Each of the integrals in (5-47) can be integrated by the formula (see Appendix V)

$$\pi j^n J_n(z) = \int_0^{\pi} \cos(n\phi) e^{+jz\cos\phi}\, d\phi \tag{5-48}$$

where $J_n(z)$ is the Bessel function of the first kind of order n. Using (5-48) reduces (5-47) to

$$A_\phi \simeq \frac{a\mu I_0 e^{-jkr}}{4\pi r} |\pi j J_1(ka \sin\theta) - \pi j J_1(-ka \sin\theta)| \tag{5-49}$$

The Bessel function of the first kind and order n is defined (see Appendix V) by the infinite series

$$J_n(z) = \sum_{m=0}^{\infty} \frac{(-1)^m (z/2)^{n+2m}}{m!(m+n)!} \tag{5-50}$$

By a simple substitution into (5-50), it can be shown that

$$J_n(-z) = (-1)^n J_n(z) \tag{5-51}$$

which for $n = 1$ is equal to

$$J_1(-z) = -J_1(z) \tag{5-52}$$

Using (5-52) we can write (5-49) as

$$A_\phi \simeq j \frac{a\mu I_0 e^{-jkr}}{2r} J_1(ka \sin\theta) \tag{5-53}$$

The next step is to find the **E**- and **H**-fields associated with the vector potential of (5-53). Since (5-53) is only valid for far-field observations, the procedure outlined in Section 3.6 can be used. The vector potential **A**, as given by (5-53), is of the form suggested by (3-56). That is, the r variations are separable from those of θ and ϕ. Therefore according to (3-58a)–(3-58b) and (5-53)

$$E_r \simeq E_\theta = 0 \tag{5-54a}$$

$$E_\phi \simeq \frac{ak\eta I_0 e^{-jkr}}{2r} J_1(ka \sin\theta) \tag{5-54b}$$

$$H_r \simeq H_\phi = 0 \tag{5-54c}$$

$$H_\theta \simeq -\frac{E_\phi}{\eta} = -\frac{akI_0 e^{-jkr}}{2r} J_1(ka \sin\theta) \tag{5-54d}$$

5.3.2 Power Density, Radiation Intensity, Radiation Resistance, and Directivity

The next objective for this problem will be to find the power density, radiation intensity, radiation resistance, and directivity. To do this, the time-average power density is formed. That is,

$$\mathbf{W}_{av} = \frac{1}{2}\text{Re}[\mathbf{E} \times \mathbf{H}^*] = \frac{1}{2}\text{Re}[\hat{\mathbf{a}}_\phi E_\phi \times \hat{\mathbf{a}}_\theta H_\theta^*] = \hat{\mathbf{a}}_r \frac{1}{2\eta}|E_\phi|^2 \tag{5-55}$$

INTEL-1045
U.S. Patent 7,151,430

which can be written using (5-54b) as

$$\mathbf{W}_{av} = \hat{\mathbf{a}}_r W_r = \hat{\mathbf{a}}_r \frac{(a\omega\mu)^2|I_0|^2}{8\eta r^2} J_1^2(ka \sin\theta) \tag{5-56}$$

with the radiation intensity given by

$$U = r^2 W_r = \frac{(a\omega\mu)^2|I_0|^2}{8\eta} J_1^2(ka \sin\theta) \tag{5-57}$$

The radiation patterns for $a = \lambda/10$, $\lambda/5$, and $\lambda/2$ are shown in Figure 5.6. These patterns indicate that the field radiated by the loop along its axis ($\theta = 0°$) is zero. Also the shape of these patterns is similar to that of a linear dipole with $l \leq \lambda$ (a

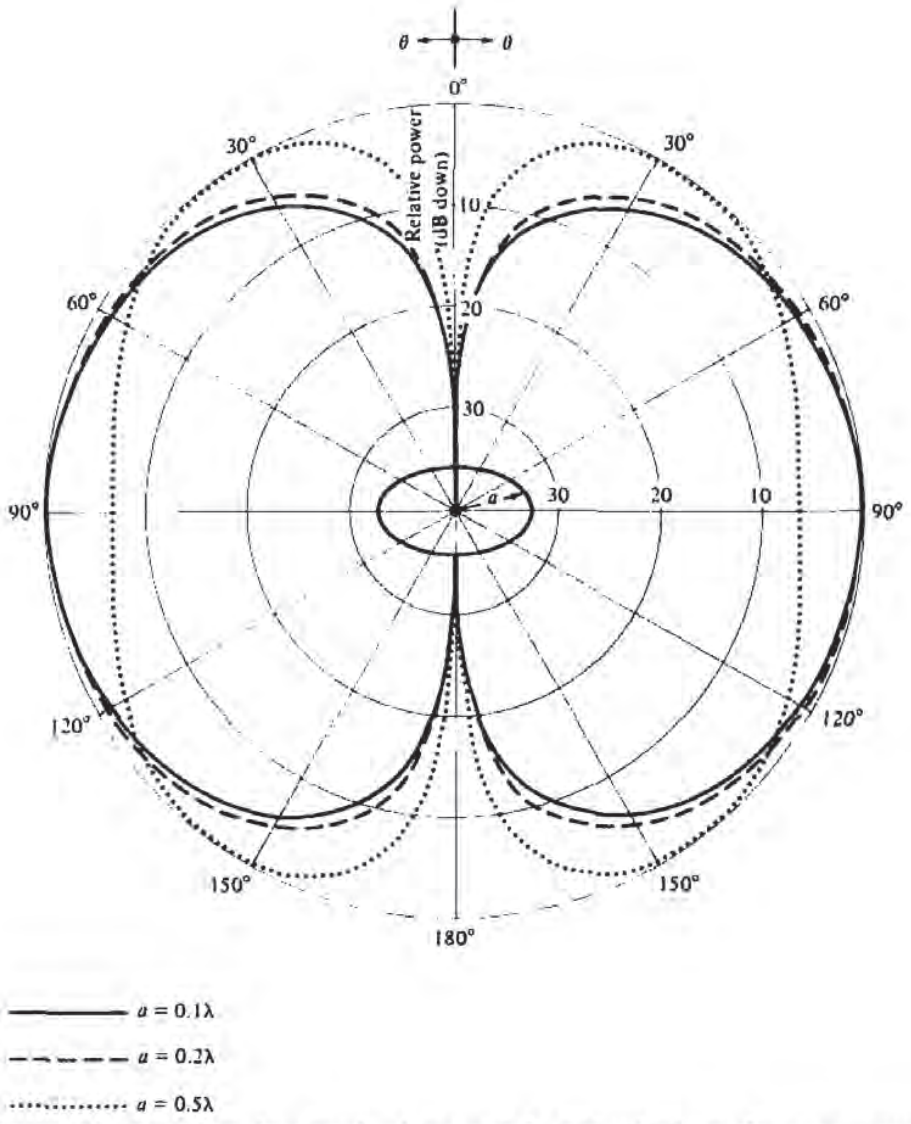


Figure 5.6 Elevation plane amplitude patterns for a circular loop of constant current ($a = 0.1\lambda$, 0.2λ, and 0.5λ).

INTEL-1045
U.S. Patent 7,151,430

figure-eight shape). As the radius a increases beyond 0.5λ, the field intensity along the plane of the loop ($\theta = 90°$) diminishes and eventually it forms a null when $a \approx 0.61\lambda$. This is left as an exercise to the reader for verification (Prob. 5.13). Beyond $a = 0.61\lambda$, the radiation along the plane of the loop begins to intensify and the pattern attains a multilobe form.

The patterns represented by (5-57) (some of them are illustrated in Figure 5.6) assume that the current distribution, no matter what the loop size, is constant. This is not a valid assumption if the loop circumference C ($C = 2\pi a$) exceeds about 0.2λ (i.e., $a > 0.032\lambda$) [6]. For radii much greater than about 0.032λ, the current variation along the circumference of the loop begins to attain a distribution that is best represented by a Fourier series [5]. Although a most common assumption is that the current distribution is nearly cosinusoidal, it is not satisfactory particulary near the driving point of the antenna.

It has been shown [7] that when the circumference of the loop is about one wavelength ($C \approx \lambda$), its maximum radiation is along its axis ($\theta = 0°$) which is perpendicular to the plane of the loop. This feature of the loop antenna has been utilized to design Yagi-Uda arrays whose basic elements (feed, directors, and reflectors) are circular loops [8]–[10]. Because of its many applications, the one wavelength circumference circular loop antenna is considered as fundamental as a half-wavelength dipole.

The radiated power can be written using (5-56) as

$$P_{\text{rad}} = \iint_S \mathbf{W}_{\text{av}} \cdot d\mathbf{s} = \frac{\pi(a\omega\mu)^2|I_0|^2}{4\eta} \int_0^{\pi} J_1^2(ka \sin\theta) \sin\theta \, d\theta \tag{5-58}$$

The integral in (5-58) cannot be integrated exactly. However, it can be rewritten [11] as

$$\int_0^{\pi} J_1^2(ka \sin\theta) \sin\theta \, d\theta = \frac{1}{ka} \int_0^{2ka} J_2(x) \, dx \tag{5-59}$$

Even though (5-59) still cannot be integrated, approximations can be made depending upon the values of the upper limit (the radius of the loop).

A. Large Loop Approximation ($a \geq \lambda/2$)

To evaluate (5-59), the first approximation will be to assume that the radius of the loop is large ($a \geq \lambda/2$). For that case, the integral in (5-59) can be approximated by

$$\int_0^{\pi} J_1^2(ka \sin\theta) \sin\theta \, d\theta = \frac{1}{ka} \int_0^{2ka} J_2(x) \, dx \approx \frac{1}{ka} \tag{5-60}$$

and (5-58) by

$$P_{\text{rad}} \approx \frac{\pi(a\omega\mu)^2|I_0|^2}{4\eta(ka)} \tag{5-61}$$

The maximum radiation intensity occurs when $ka \sin\theta = 1.84$ so that

$$U|_{\max} = \frac{(a\omega\mu)^2|I_0|^2}{8\eta} J_1^2(ka \sin\theta)|_{ka\sin\theta = 1.84} = \frac{(a\omega\mu)^2|I_0|^2}{8\eta}(0.584)^2 \tag{5-62}$$

INTEL-1045
U.S. Patent 7,151,430

Thus

$$R_r = \frac{2P_{\text{rad}}}{|I_0|^2} = \frac{2\pi(a\omega\mu)^2}{4\eta(ka)} = \eta\left(\frac{\pi}{2}\right)ka = 60\pi^2(ka) = 60\pi^2\left(\frac{C}{\lambda}\right) \quad (5\text{-}63a)$$

$$D_0 = 4\pi\frac{U_{\max}}{P_{\text{rad}}} = 4\pi\frac{ka(0.584)^2}{2\pi} = 2ka(0.584)^2 = 0.682\left(\frac{C}{\lambda}\right) \quad (5\text{-}63b)$$

$$A_{em} = \frac{\lambda^2}{4\pi}D_0 = \frac{\lambda^2}{4\pi}\left[0.682\left(\frac{C}{\lambda}\right)\right] = 5.43 \times 10^{-2}\lambda C \quad (5\text{-}63c)$$

where C (circumference) $= 2\pi a$ and $\eta \simeq 120\pi$.

B. Intermediate Loop Approximation ($\lambda/6\pi \leq a < \lambda/2$)
If the radius of the loop is $\lambda/6\pi \leq a < \lambda/2$, the integral of (5-59) can be approximated by

$$\int_0^{\pi} J_1^2(ka\sin\theta)\sin\theta\, d\theta = \frac{1}{ka}\int_0^{2ka} J_2(x)\, dx$$
$$\simeq \frac{1}{ka}\left[-2J_1(2ka) + \int_0^{2ka} J_0(y)\, dy\right] \quad (5\text{-}64)$$

where $J_0(y)$ is the Bessel function of the first kind of zero order. No further simplifications can be made. The integral of $J_0(y)$ appearing in (5-64) is a tabulated function which is included in Appendix V. The radiation resistance, directivity, and maximum effective area can be found using (5-64) to evaluate the P_{rad} of (5-58).

C. Small Loop Approximation ($a < \lambda/6\pi$)
If the radius of the loop is small ($a < \lambda/6\pi$), the expressions for the fields as given by (5-54a)–(5-54d) can be simplified. To do this, the Bessel function $J_1(ka\sin\theta)$ is expanded, by the definition of (5-50), in an infinite series of the form (see Appendix V)

$$J_1(ka\sin\theta) = \tfrac{1}{2}(ka\sin\theta) - \tfrac{1}{16}(ka\sin\theta)^3 + \cdots \quad (5\text{-}65)$$

For small values of ka ($ka < \frac{1}{3}$), (5-65) can be approximated by its first term, or

$$J_1(ka\sin\theta) \simeq \frac{ka\sin\theta}{2} \quad (5\text{-}65a)$$

Thus (5-54a)–(5-54d) can be written as

$$\left.\begin{aligned} E_r &\simeq E_\theta = 0 && (5\text{-}66a)\\ E_\phi &\simeq \frac{a^2\omega\mu k I_0 e^{-jkr}}{4r}\sin\theta = \eta\frac{a^2k^2I_0e^{-jkr}}{4r}\sin\theta && (5\text{-}66b)\\ H_r &\simeq H_\phi = 0 && (5\text{-}66c)\\ H_\theta &\simeq -\frac{a^2\omega\mu k I_0 e^{-jkr}}{4\eta r}\sin\theta = -\frac{a^2k^2I_0e^{-jkr}}{4r}\sin\theta && (5\text{-}66d)\end{aligned}\right\} a < \lambda/6\pi$$

INTEL-1045
U.S. Patent 7,151,430

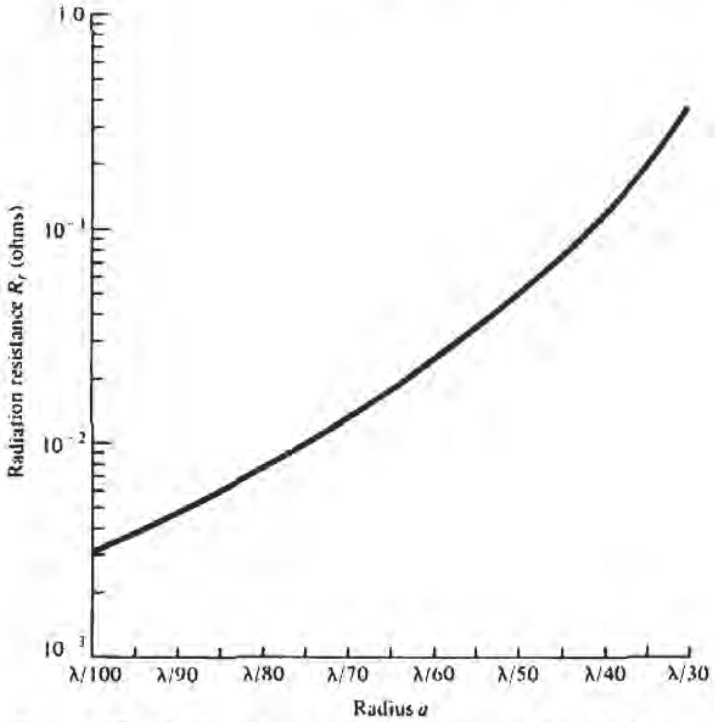


Figure 5.7 Radiation resistance for a constant current circular loop antenna based on the approximation of (5-65a).

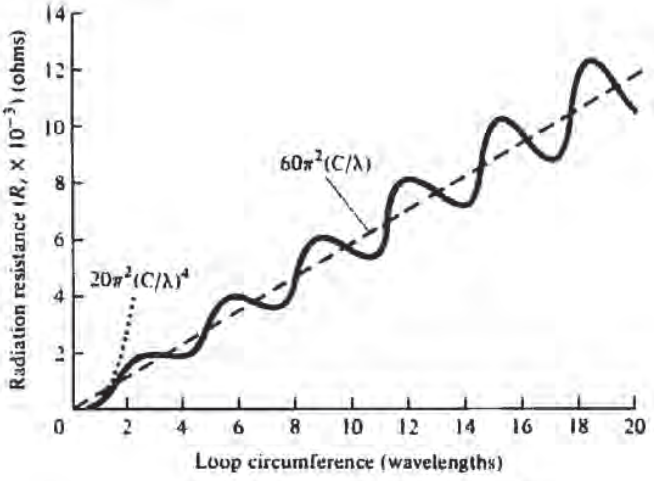
which are identical to those of (5-27a)–(5-27c). Thus the expressions for the radiation resistance, radiation intensity, directivity, maximum effective aperture, and radiation resistance are those given by (5-24), (5-29), (5-31), and (5-32).

To demonstrate the variation of the radiation resistance as a function of the radius a of the loop, it is plotted in Figure 5.7 for $\lambda/100 \leq a \leq \lambda/30$, based on the approximation of (5-65a). It is evident that the values are extremely low (less than 1 ohm), and they are usually smaller than the loss resistances of the wires. These radiation resistances also lead to large mismatch losses when connected to practical transmission lines of 50 or 75 ohms. To increase the radiation resistance, it would require multiple turns as suggested by (5-24a). This, however, also increases the loss resistance which contributes to the inefficiency of the antenna. A plot of the radiation resistance for $0 < ka = C/\lambda < 20$, based on the evaluation of (5-59) by numerical techniques, is shown in Figure 5.8. The dashed line represents the values based on the large loop approximation of (5-60) and the dotted ($\cdots\cdots$) represents the values based on the small loop approximation of (5-65a).

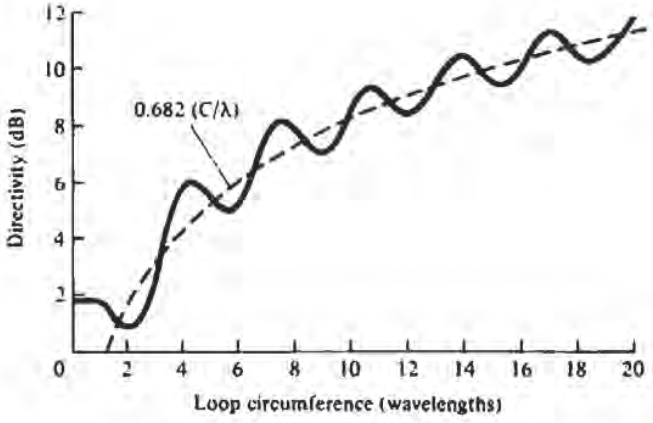
In addition to the real part of the input impedance, there is also an imaginary component which would increase the mismatch losses even if the real part is equal to the characteristic impedance of the lossless transmission line. However, the imaginary component can always, in principle at least, be eliminated by connecting a reactive element (capacitive or inductive) across the terminals of the loop to make the antenna a resonant circuit.

To facilitate the computations for the directivity and radiation resistance of a circular loop with a constant current distribution, a FORTRAN computer program has

INTEL-1045
U.S. Patent 7,151,430



(a) Radiation resistance of circular loop



(b) Directivity of circular loop

Figure 5.8 Radiation resistance and directivity for circular loop of constant current. (SOURCE: E. A. Wolff, *Antenna Analysis*, Wiley, New York, 1966)

been developed. The program utilizes (5-62) and (5-58) to compute the directivity [(5-58) is integrated numerically]. The program requires as an input the radius of the loop (in wavelengths). A Bessel function subroutine is contained within the program. A listing of the program is included at the end of this chapter and in the computer disc included with the book.

5.4 CIRCULAR LOOP WITH NONUNIFORM CURRENT

The analysis in the previous sections was based on a uniform current, which would be a valid approximation when the radius of the loop is small electrically (usually $a < 0.03\lambda$). As the dimensions of the loop increase, the current variations along the circumference of the loop must be taken into account. As stated previously, a very common assumption for the current distribution is a cosinusoidal variation [12], [13]. This, however, is not a satisfactory approximation particularly near the driving point

INTEL-1045
U.S. Patent 7,151,430

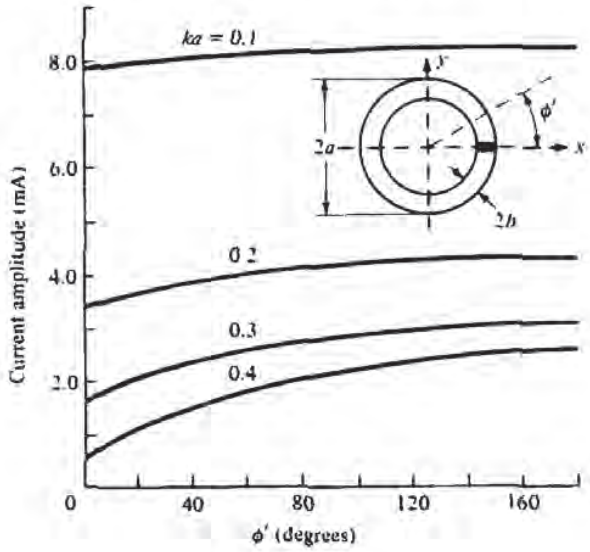
of the antenna [6]. A better distribution would be to represent the current by a Fourier series [14]

$$I(\phi') = I_0 + 2\sum_{n=1}^{M} I_n \cos(n\phi') \tag{5-67}$$

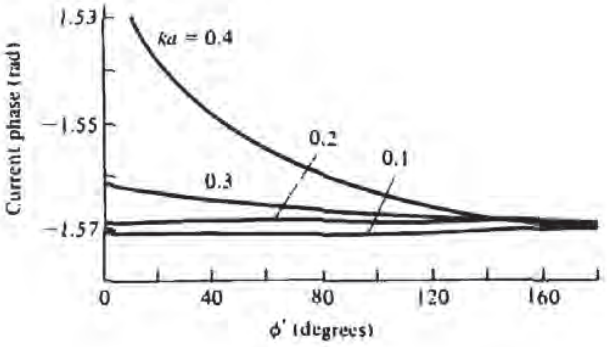
where ϕ' is measured from the feed point of the loop along the circumference, as shown at the inset of Figure 5.9.

A complete analysis of the fields radiated by a loop with nonuniform current distribution is somewhat complex, laborious, and quite lengthy. Instead of attempting to include the analytical formulations, which are cumbersome but well documented in the cited references, a number of graphical illustrations of numerical and experimental data is presented. These curves can be used in facilitating designs.

To illustrate that the current distribution of a wire loop antenna is not uniform unless its radius is very small, the magnitude and phase of it have been plotted in Figure 5.9 as a function of ϕ' (in degrees). The loop circumference C is $ka = C/\lambda$



(a) Magnitude



(b) Phase

Figure 5.9 Current magnitude and phase distributions on small circular loop antennas. (SOURCE: J. E. Storer, "Impedance of Thin-Wire Loop Antennas," *AIEE Trans.*, Vol. 75, November 1956. © 1956 IEEE)

INTEL-1045
U.S. Patent 7,151,430

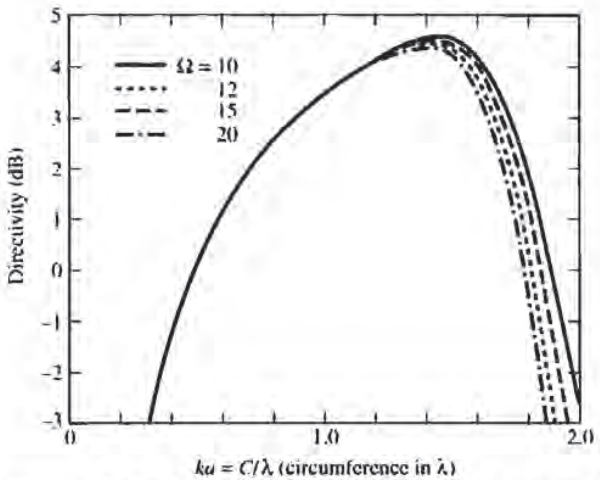


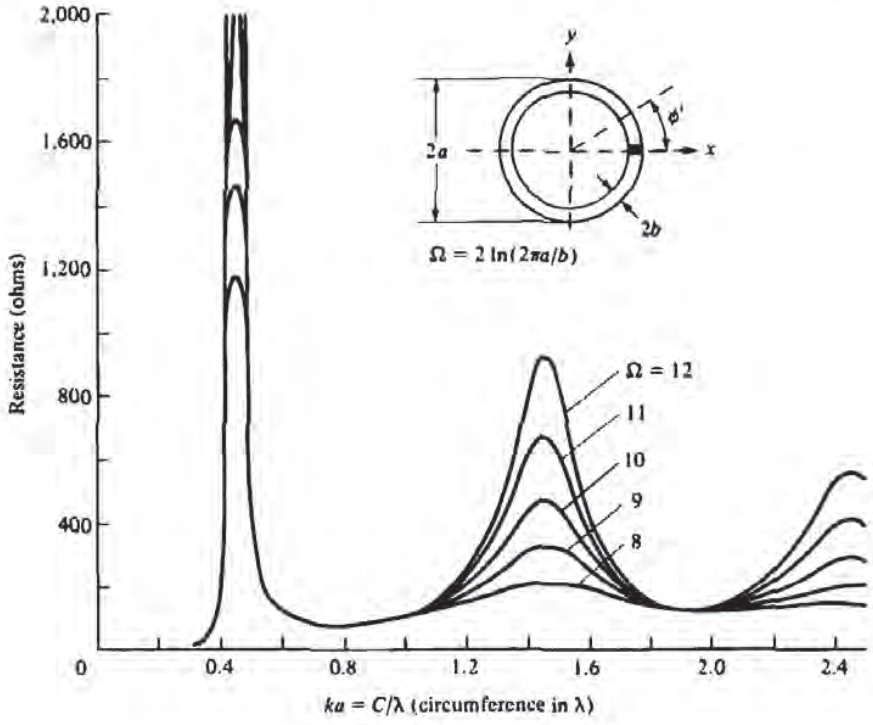
Figure 5.10 Directivity of circular-loop antenna for $\theta = 0, \pi$ versus electrical size (circumference/wavelength). (SOURCE: G. S. Smith, "Loop Antennas," copyright © McGraw-Hill, Inc. Permission by McGraw-Hill, Inc.)

$= 0.1, 0.2, 0.3$, and 0.4 and the wire size was chosen so that $\Omega = 2 \ln(2\pi a/b) = 10$. It is apparent that for $ka = 0.1$ the current is nearly uniform. For $ka = 0.2$ the variations are slightly greater and become even larger as ka increases. On the basis of these results, loops much larger than $ka = 0.2$ (radius much greater than 0.03–0.04λ) cannot be considered small.

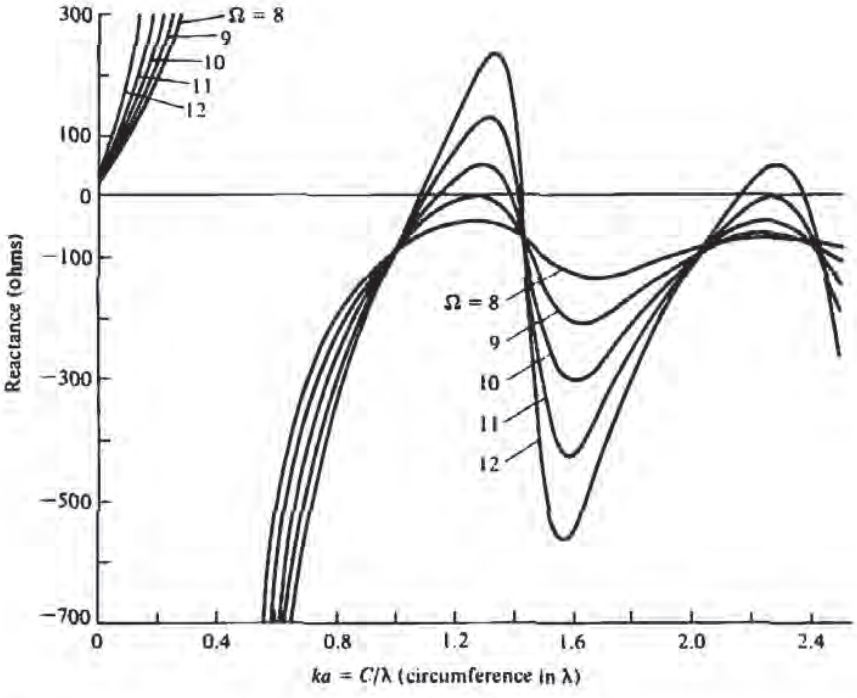
As was indicated earlier, the maximum of the pattern for a loop antenna shifts from the plane of the loop ($\theta = 90°$) to its axis ($\theta = 0°, 180°$) as the circumference of the loop approaches one wavelength. Based on the nonuniform current distribution of (5-67), the directivity of the loop along $\theta = 0°$ has been computed, and it is plotted in Figure 5.10 versus the circumference of the loop in wavelengths [5]. The maximum directivity is about 4.5 dB, and it occurs when the circumference is about 1.4λ. For a one wavelength circumference, which is usually the optimum design for a helical antenna, the directivity is about 3.4 dB. It is also apparent that the directivity is basically independent of the radius of the wire, as long as the circumference is equal or less than about 1.3 wavelengths; there are differences in directivity as a function of the wire radius for greater circumferences.

Computed impedances, based on the Fourier series representation of the current, are shown plotted in Figure 5.11. The input resistance and reactance are plotted as a function of the circumference C (in wavelengths) for $0 \leq ka = C/\lambda \leq 2.5$. The diameter of the wire was chosen so that $\Omega = 2 \ln(2\pi a/b) = 8, 9, 10, 11$, and 12. It is apparent that the first antiresonance occurs when the circumference of the loop is about $\lambda/2$, and it is extremely sharp. It is also noted that as the loop wire increases in thickness, there is a rapid disappearance of the resonances. As a matter of fact, for $\Omega < 9$ there is only one antiresonance point. These curves (for $C > \lambda$) are similar, both qualitatively and quantitatively, to those of a linear dipole. The major difference is that the loop is more capacitive (by about 130 ohms) than a dipole. This shift in reactance allows the dipole to have several resonances and antiresonances while moderately thick loops ($\Omega < 9$) have only one antiresonance. Also small loops are primarily inductive while small dipoles are primarily capacitive. The resistance curves for the loop and the dipole are very similar.

INTEL-1045
U.S. Patent 7,151,430



(a) Resistance



(b) Reactance

Figure 5.11 Input impedance of circular loop antennas. (SOURCE: J. E. Stover. "Impedance of Thin-Wire Loop Antennas." *AIEE Trans.*, Vol. 75, November 1956. © 1956 IEEE).

INTEL-1045
U.S. Patent 7,151,430

To verify the analytical formulations and the numerical computations, loop antennas were built and measurements of impedance were made [6]. The measurements were conducted using a half-loop over an image plane, and it was driven by a two-wire line. An excellent agreement between theory and experiment was indicated everywhere except near resonances where computed conductance curves were slightly higher than those measured. This is expected since ohmic losses were not taken into account in the analytical formulation. It was also noted that the measured susceptance curve was slightly displaced vertically by a constant value. This can be attributed to the "end effect" of the experimental feeding line and the "slice generator" used in the analytical modeling of the feed. For a dipole, the correction to the analytical model is usually a negative capacitance in shunt with the antenna [15]. A similar correction for the loop would result in a better agreement between the computed and measured susceptances. Computations for a half-loop above a ground plane were also performed by J. E. Jones [16] using the Moment Method.

The radiation resistance of a loop antenna, with a cosinusoidal current distribution, was computed [17] by evaluating triple integrals numerically. The results are shown in Figure 5.12 where they are compared with those of a uniform current distribution. It is evident that when the circumference of the loop is less than about 0.8λ, the constant current radiation resistances agree quite well with those of the cosinusoidal distribution.

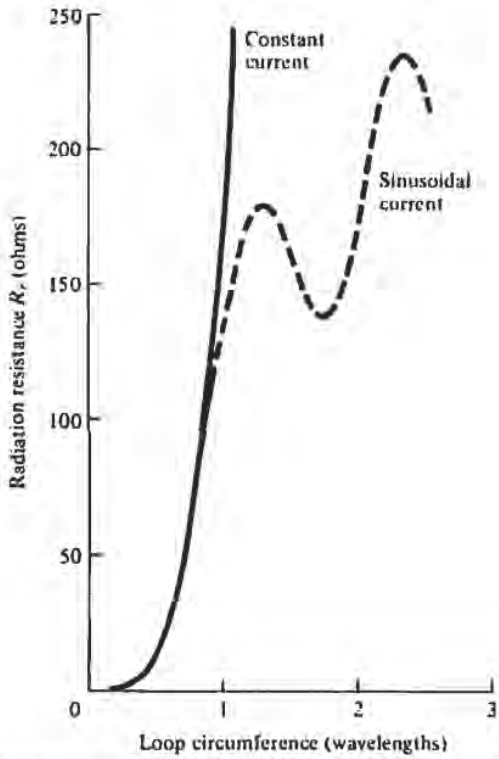


Figure 5.12 Radiation resistance of circular loop with constant and sinusoidal current distributions. (SOURCE: A. Richtscheid, "Calculation of the Radiation Resistance of Loop Antennas with Sinusoidal Current Distribution," *IEEE Trans. Antennas Propagat.*, Vol. AP-24, November 1976. © 1976 IEEE)

INTEL-1045
U.S. Patent 7,151,430

5.4.1 Arrays

In addition to be used as single elements, loop antennas are widely used in arrays. Two of the most popular arrays of loop antennas are the helical antenna and the Yagi-Uda array. The loop is also widely used to form a solenoid which in conjunction with a ferrite cylindrical rod within its circumference is used as a receiving antenna and as a tuning element, especially in transistor radios. This is discussed in Section 5.7.

The helical antenna, which is discussed in more detail in Section 10.3.1, is a wire antenna, which is wound in the form of a helix, as shown in Figure 10.13. It is shown that it can be modeled approximately by a series of loops and vertical dipoles, as shown in Figure 10.14. The helical antenna possesses in general elliptical polarization, but it can be designed to achieve nearly circular polarization. There are two primary modes of operation for a helix, the normal mode and the axial mode. The helix operates in its normal mode when its overall length is small compared to the wavelength, and it has a pattern with a null along its axis and the maximum along the plane of the loop. This pattern (figure eight type in the elevation plane) is similar to that of a dipole or a small loop. The helix operates in the axial mode when the circumference of the loop is between $3/4\lambda < C < 4/3\lambda$ with an optimum design when the circumference is nearly one wavelength. When the circumference of the loop approaches one wavelength, the maximum of the pattern is along its axis. In addition, the phasing among the turns is such that overall the helix forms an end-fire antenna with attractive impedance and polarization characteristics. In general, the helix is a popular communication antenna in the VHF and UHF bands.

The Yagi-Uda antenna is primarily an array of linear dipoles with one element serving as the feed while the others act as parasitic. However this arrangement has been extended to include arrays of loop antennas, as shown in Figure 10.27. As for the helical antenna, in order for this array to perform as an endfire array, the circumference of each of the elements is near one wavelength. More details can be found in Section 10.3.4 and especially in [8]–[10]. A special case is the quad antenna which is very popular amongst ham radio operators. It consists of two square loops, one serving as the excitation while the other is acting as a reflector; there are no directors. The overall perimeter of each loop is one wavelength.

5.4.2 Design Procedure

The design of small loops is based on the equations for the radiation resistance (5-24), (5-24a), directivity (5-31), maximum effective aperture (5-32), resonance capacitance (5-35), resonance input impedance (5-36) and inductance (5-37a), (5-37b). In order to resonate the element, the capacitor C_r of Figure 5.3 is chosen based on (5-35) so as to cancel out the imaginary part of the input impedance Z_{in}.

For large loops with a nonuniform current distribution, the design is accomplished using the curves of Figure 5.10 for the axial directivity and those of Figure 5.11 for the impedance. To resonate the loop, usually a capacitor in parallel or an inductor in series is added, depending on the radius of the loop and that of the wire.

Example 5.4

Design a resonant loop antenna to operate at 100 MHz so that the pattern maximum is along the axis of the loop. Determine the radius of the loop and that of the wire (in

INTEL-1045
U.S. Patent 7,151,430

meters), the axial directivity (in dB), and the parallel lumped element (capacitor in parallel or inductor in series) that must be used in order to resonate the antenna.

SOLUTION

In order for the pattern maximum to be along the axis of the loop, the circumference of the loop must be large compared to the wavelength. Therefore the current distribution will be nonuniform. To accomplish this, Figure 5.11(a) should be used. There is not only one unique design which meets the specifications, but there are many designs that can accomplish the goal.

One design is to select a circumference where the loop is self-resonant, and there is no need for a resonant capacitor. For example, referring to Figure 5.11(b) and choosing an $\Omega = 12$, the circumference of the loop is nearly 1.125λ. Since the free-space wavelength at 100 MHz is 3 meters, then the circumference is

$$\text{circumference} \simeq 1.125(3) = 3.375 \text{ meters}$$

while the radius of the loop is

$$\text{radius} = a = \frac{3.375}{2\pi} = 0.5371 \text{ meters}$$

The radius of the wire is obtained using

$$\Omega = 12 = 2 \ln\left(\frac{2\pi a}{b}\right)$$

or

$$\frac{a}{b} = 64.2077$$

Therefore the radius of the wire is

$$b = \frac{a}{64.2077} = \frac{0.5371}{64.2077} = 0.8365 \text{ cm} = 8.365 \times 10^{-3} \text{ meters}$$

Using Figure 5.10, the axial directivity for this design is approximately 3.6 dB. Using Figure 5.11(a), the input impedance is approximately

$$Z_{in} = Z'_{in} \simeq 125 \text{ ohms}$$

Since the antenna chosen is self-resonant, there is no need for a lumped element to resonate the radiator.

Another design will be to use another circumference where the loop is not self resonant. This will necessitate the use of a capacitor C_r to resonate the antenna. This is left as an end of the chapter exercise.

5.5 GROUND AND EARTH CURVATURE EFFECTS FOR CIRCULAR LOOPS

The presence of a lossy medium can drastically alter the performance of a circular loop. The parameters mostly affected are the pattern, directivity, input impedance,

INTEL-1045
U.S. Patent 7,151,430

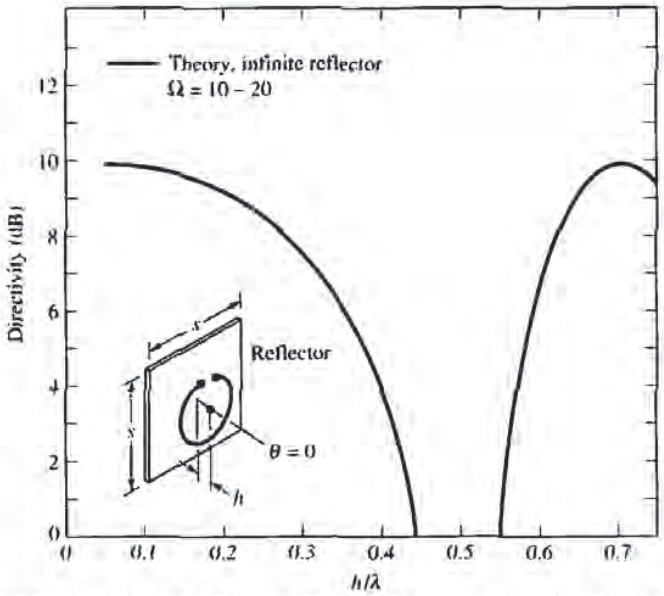


Figure 5.13 Directivity of circular-loop antenna, $C = ka = 1$, for $\theta = 0$ versus distance from reflector h/λ. Theoretical curve is for infinite planar reflector; measured points are for square reflector. (SOURCE: G. S. Smith, "Loop Antennas," copyright © McGraw-Hill, Inc. *Permission by McGraw-Hill, Inc.*)

and antenna efficiency. The amount of energy dissipated as heat by the lossy medium directly affects the antenna efficiency. As for the linear elements, geometrical optics techniques can be used to analyze the radiation characteristics of loops in the presence of conducting surfaces. The reflections are taken into account by introducing appropriate image (virtual) sources. Divergence factors are introduced to take into account the effects of the ground curvature. Because the techniques are identical to the formulations of Section 4.8, they will not be repeated here. The reader is directed to that section for the details. It should be pointed out, however, that a horizontal loop has horizontal polarization in contrast to the vertical polarization of a vertical electric dipole. Exact boundary-value solutions, based on Sommerfeld integral formulations, are available [16]. However they are too complex to be included in an introductory chapter.

By placing the loop above a reflector, the pattern is made unidirectional and the directivity is increased. To simplify the problem, initially the variations of the axial directivity ($\theta = 0°$) of a circular loop with a circumference of one wavelength ($ka = 1$) when placed horizontally a height h above an infinite in extent perfect electric conductor are examined as a function of the height above the ground plane. These were obtained using image theory and the array factor of two loops, and they are shown for $10 < \Omega < 20$ in Figure 5.13[5], [18]. Since only one curve is shown for $10 < \Omega < 20$, it is evident that the directivity variations as a function of the height are not strongly dependent on the radius of the wire of the loop. It is also apparent that for $0.05\lambda < h < 0.2\lambda$ and $0.65\lambda < h < 0.75\lambda$ the directivity is about 9 dB. For the same size loop, the corresponding variations of the impedance as a function of the height are shown in Figure 5.14[5], [18]. While the directivity variations are not strongly influenced by the radius of the wire, the variations of the impedance do show a dependence on the radius of the wire of the loop for $10 < \Omega < 20$.

INTEL-1045
U.S. Patent 7,151,430

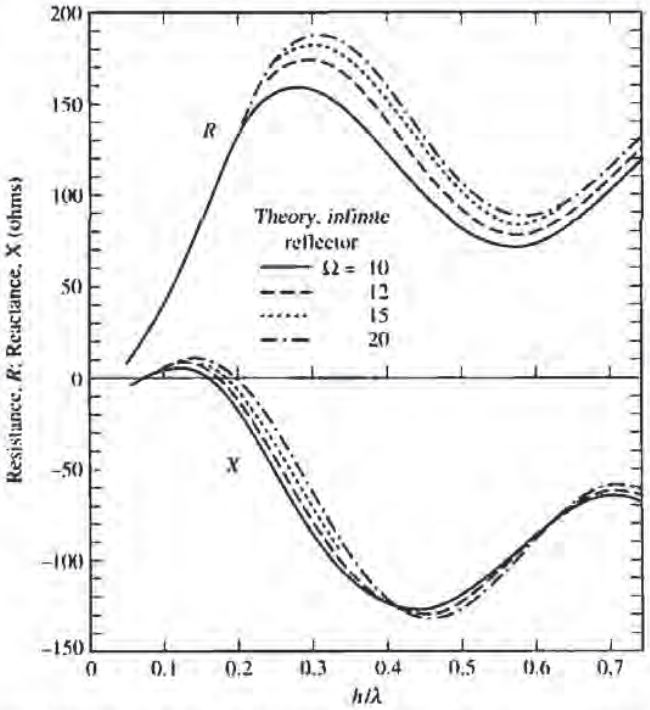


Figure 5.14 Input impedance of circular-loop antenna $C = ka = 1$ versus distance from reflector h/λ. Theoretical curves are for infinite planar reflector; measured points are for square reflector. (SOURCE: G. S. Smith, "Loop Antennas," copyright © 1984, McGraw-Hill, Inc. Permission by McGraw-Hill, Inc.)

A qualitative criterion that can be used to judge the antenna performance is the *ratio of the radiation resistance in free-space to that in the presence of the homogeneous lossy medium* [19]. This is a straightforward but very tedious approach. A much simpler method [20] is to find directly the self-impedance changes (real and imaginary) that result from the presence of the conducting medium.

Since a small horizontal circular loop is equivalent to a small vertical magnetic dipole (see Section 5.2.2), computations [21] were carried out for a vertical magnetic dipole placed a height h above a homogeneous lossy half-space. The changes in the self-impedance, normalized with respect to the free-space radiation resistance R_0 given by (5-24), are shown plotted in Figure 5.15. The parameter N_1 is defined by (4-124).

As for the vertical electric dipole, the magnitude changes of $\Delta R/R_0$ in Figure 5.15(a) approach unity as the height h of the antenna above a perfectly conducting ($|N_1^2| = \infty$) ground plane approaches zero ($2k_0h \to 0$). For the magnetic dipole (or the loop) this corresponds to a vanishing resistance. Also, as expected, the magnitude of ΔX approaches infinity as $2k_0h \to 0$. Both ΔR and ΔX become oscillatory as $2k_0h$ exceeds approximately π or when h exceeds about $\lambda_0/4$.

The effect the finite conductivity has on the resistance (ΔR) and reactance (ΔX) changes for $|N_1^2| = 100, 25, 4$ are shown in Figures 5.15(b) and (c). Significant modifications, compared to those of a perfect conductor, are indicated. The effects that a stratified lossy half-space have on the characteristics of a horizontal small circular loop have also been investigated and documented [22]. It was found that when a resonant loop is close to the interface, the changes in the input admittance as a function of the antenna height and the electrical properties of the lossy medium

INTEL-1045
U.S. Patent 7,151,430

were very pronounced. This suggests that a resonant loop can be used effectively to sense and to determine the electrical properties of an unknown geological structure.

5.6 POLYGONAL LOOP ANTENNAS

The most attractive polygonal loop antennas are the square, rectangular, triangular, and rhombic. These antennas can be used for practical applications such as for aircraft, missiles, and communications systems. However, because of their more complex structure, theoretical analyses seem to be unsuccessful [23]. Thus the application of these antennas has received much less attention. However design curves, computed using the Moment Method, do exist [24] and can be used to design polygonal loop antennas for practical applications. Usually the circular loop has been used in the UHF range because of its higher directivity while triangular and square loops have been applied in the HF and UHF bands because of advantages in their mechanical construction. Broadband impedance characteristics can be obtained from the different polygonal loops.

5.6.1 Square Loop

Next to the circular loop, the square loop is the simplest loop configuration. The far-field pattern for a small loop, in each of its principal planes, can be obtained by assuming that each of its sides is a small linear dipole of constant current I_0 and length l. Referring to Figure 5.16, the field in the y-z plane is given according to (4-26a) by

$$E_\phi = E_{\phi 1} + E_{\phi 2} = -j\eta \frac{kI_0 l}{4\pi}\left[\frac{e^{-jkr_1}}{r_1} - \frac{e^{-jkr_2}}{r_2}\right] \tag{5-68}$$

since the pattern of each element is omnidirectional in that plane. Using the far-field approximations of

$$\left.\begin{aligned} r_1 &\simeq r - \frac{l}{2}\sin\theta \\ r_2 &\simeq r + \frac{l}{2}\sin\theta \end{aligned}\right\} \quad \text{for phase variations} \tag{5-68a}$$

$$r_1 \simeq r_2 \simeq r \quad \text{for amplitude variations} \tag{5-68b}$$

(5-68) can be written as

$$E_\phi = \eta \frac{kI_0 l e^{-jkr}}{2\pi r}\sin\left(\frac{kl}{2}\sin\theta\right) \tag{5-69}$$

For small values of l ($l < \lambda/50$), (5-69) reduces to

$$\boxed{E_\phi = \eta \frac{(kl)^2 I_0 e^{-jkr}}{4\pi r}\sin\theta = \eta \frac{\pi S I_0 e^{-jkr}}{\lambda^2 r}\sin\theta} \tag{5-70}$$

where $S = l^2$ is the geometrical area of the loop. The corresponding magnetic field is given by

$$H_\theta = -\frac{E_\phi}{\eta} = -\frac{\pi S I_0 e^{-jkr}}{\lambda^2 r}\sin\theta \tag{5-71}$$

INTEL-1045
U.S. Patent 7,151,430

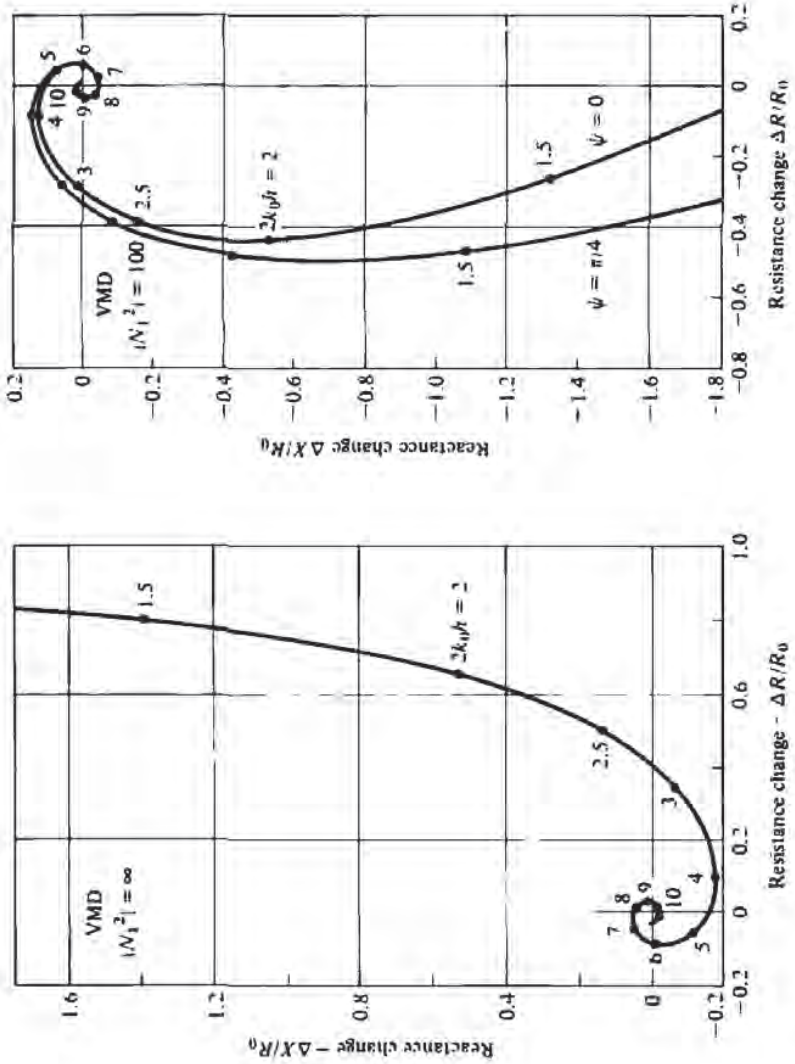


Figure 5.15 Vertical magnetic dipole (VMD) (or small horizontal loop) impedance change as a function of height above a homogeneous lossy half-space. (SOURCE: R. E. Collin and F. J. Zucker (eds.), *Antenna Theory Part 2*, McGraw-Hill, New York, 1969).

INTEL-1045
U.S. Patent 7,151,430

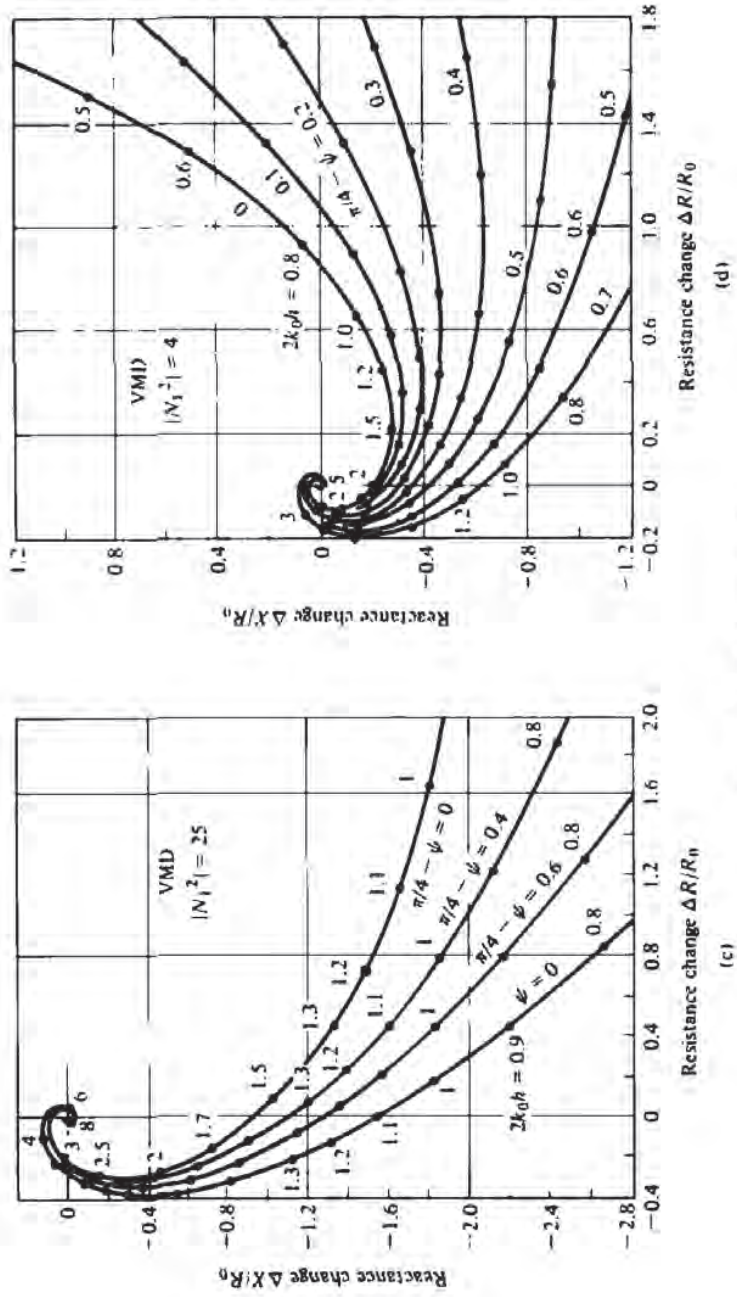


Figure 5.15 (continued)

INTEL-1045
U.S. Patent 7,151,430

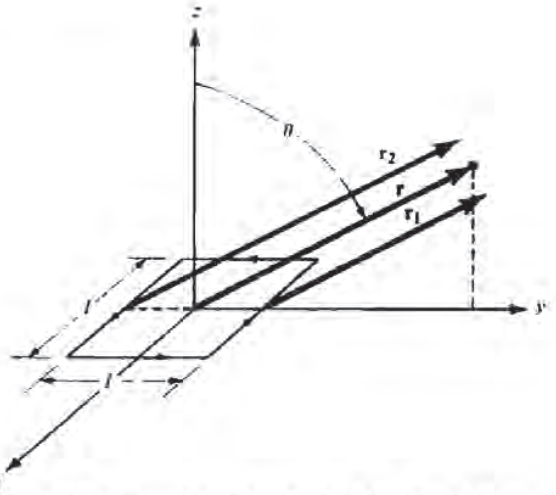


Figure 5.16 Square loop geometry for far-field observations on the y-z plane.

Equations (5-70) and (5-71) are identical to (5-27b) and (5-27a), respectively, for the small circular loop. Thus the far-zone principal-plane fields of a small square loop are identical to those of a small circular loop. The fields in the other planes are more difficult to obtain, and they will not be attempted here. However design curves are included which can be used for practical design applications.

5.6.2 Triangular, Rectangular, and Rhombic Loops

Shown in Figure 5.17 are the polygonal loops for which design data will be presented. They consist of top- and base-driven triangular loops, a rectangular loop, and a rhombic loop. The top-driven triangular loop has its feed at the top corner of the isosceles triangle while the base-driven configuration has its terminals at the base. The rectangular loop has its feed at the center of one of its sides while the rhombic configuration has its terminals at one of its corners.

The parameter β defines the angle of the top corner of the isosceles triangle for the triangular and rhombic loops while $\gamma = W/H$ is used to identify the relative side dimensions of the rectangular loop. The perimeter of each loop is given by P; for the rectangular loop, $P = 2(H + W)$. For all configurations, the radius of the wire is b.

Shown in Figure 5.18 are the input impedance ($Z = R + jX$) variations, as a function of P (in wavelengths), of the four configurations shown in Figure 5.17. The interval between adjacent points on each curve is $\Delta P/\lambda = 0.2$. Depending on the parameters β or γ, the input resistance of polygonal loops near the resonance frequency changes drastically. The reactance goes to zero when a loop approaches a short-circuited $\lambda/2$ long transmission line. In design then, the shape of the loop can be chosen so that the input impedance is equal to the characteristic impedance of the transmission line. Although the curves in Figure 5.18 are for specific wire radii, the impedance variations of the polygonal antennas as a function of the wire diameter are similar to those of the dipole.

Because the radius of the impedance locus for the $\beta = 60°$ of the top-driven triangular loop [Figure 5.18(a)] is smaller than for the other values of β, the $\beta = 60°$

INTEL-1045
U.S. Patent 7,151,430

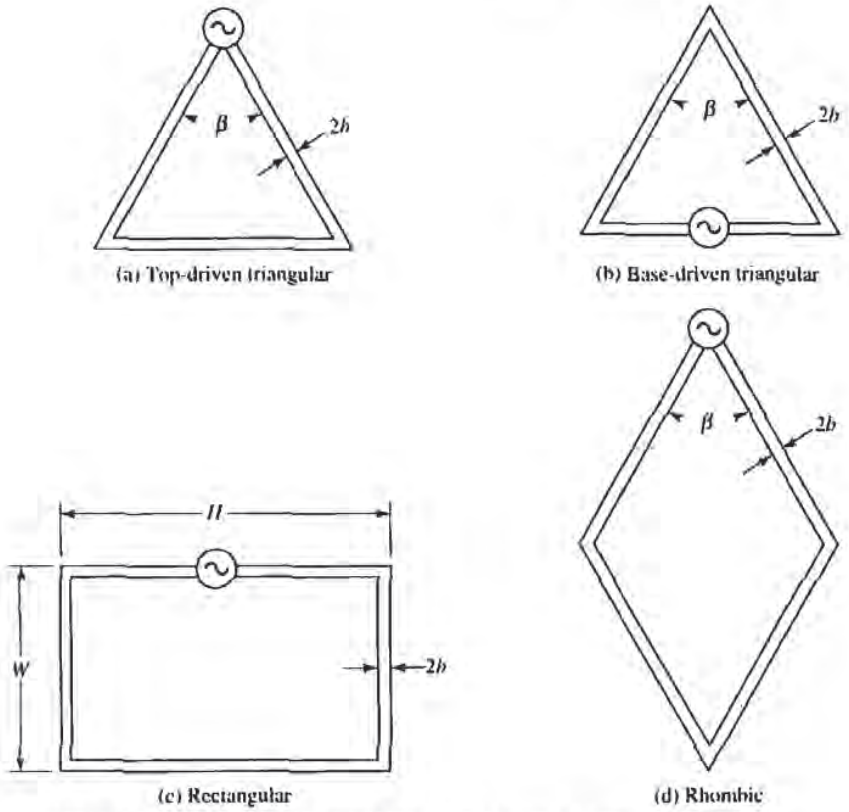


Figure 5.17 Typical configurations of polygonal loop antennas. (SOURCE: T. Tsukiji and S. Tou, "On Polygonal Loop Antennas," *IEEE Trans. Antennas Propagat.*, Vol. AP-28, No. 4, July 1980. © 1980 IEEE)

has the broadest impedance bandwidth compared with other triangular shapes or with the same shape but different feed points. Similar broadband impedance characteristics are indicated in Figure 5.18(c) for a rectangular loop with $\gamma = 0.5$ (the side with the feed point is twice as large as the other).

It can then be concluded that if the proper shape and feed point are chosen, a polygonal loop can have broadband impedance characteristics. The most attractive are the top-driven triangular loop with $\beta = 60°$ and the rectangular loop with $\gamma = 0.5$. A 50–70 ohm coaxial cable can be matched with a triangular loop with $\beta = 40°$. Rectangular loops with greater directivities, but with less ideal impedance characteristics, are those with larger values of γ.

The frequency characteristics of a polygonal loop can be estimated by inspecting its current distribution. When the current standing wave pattern has, at its antiresonant frequency, a null at a sharp corner of the loop, the loop has a very low current standing wave and, hence, broadband impedance characteristics.

Radiation patterns for the $\beta = 60°$ top- and base-driven triangular loops and the $\gamma = 4$ rectangular loop, for various values of P (in wavelengths), were also computed [24]. It was noted that for low frequencies near the resonance, the patterns of the top- and base-driven triangular loops were not too different. However, for higher frequencies the base-driven triangular loop had a greater gain than its corresponding top-driven configuration. In general, rectangular loops with larger γ's have greater gains.

INTEL-1045
U.S. Patent 7,151,430

Figure 5.18 Input impedances of polygonal loop antennas. (SOURCE: T. Tsukiji and S. Tou, "On Polygonal Loop Antennas," *IEEE Trans. Antennas Propagat.*, Vol. AP-28, No. 4, July 1980, © 1980 IEEE)

INTEL-1045
U.S. Patent 7,151,430

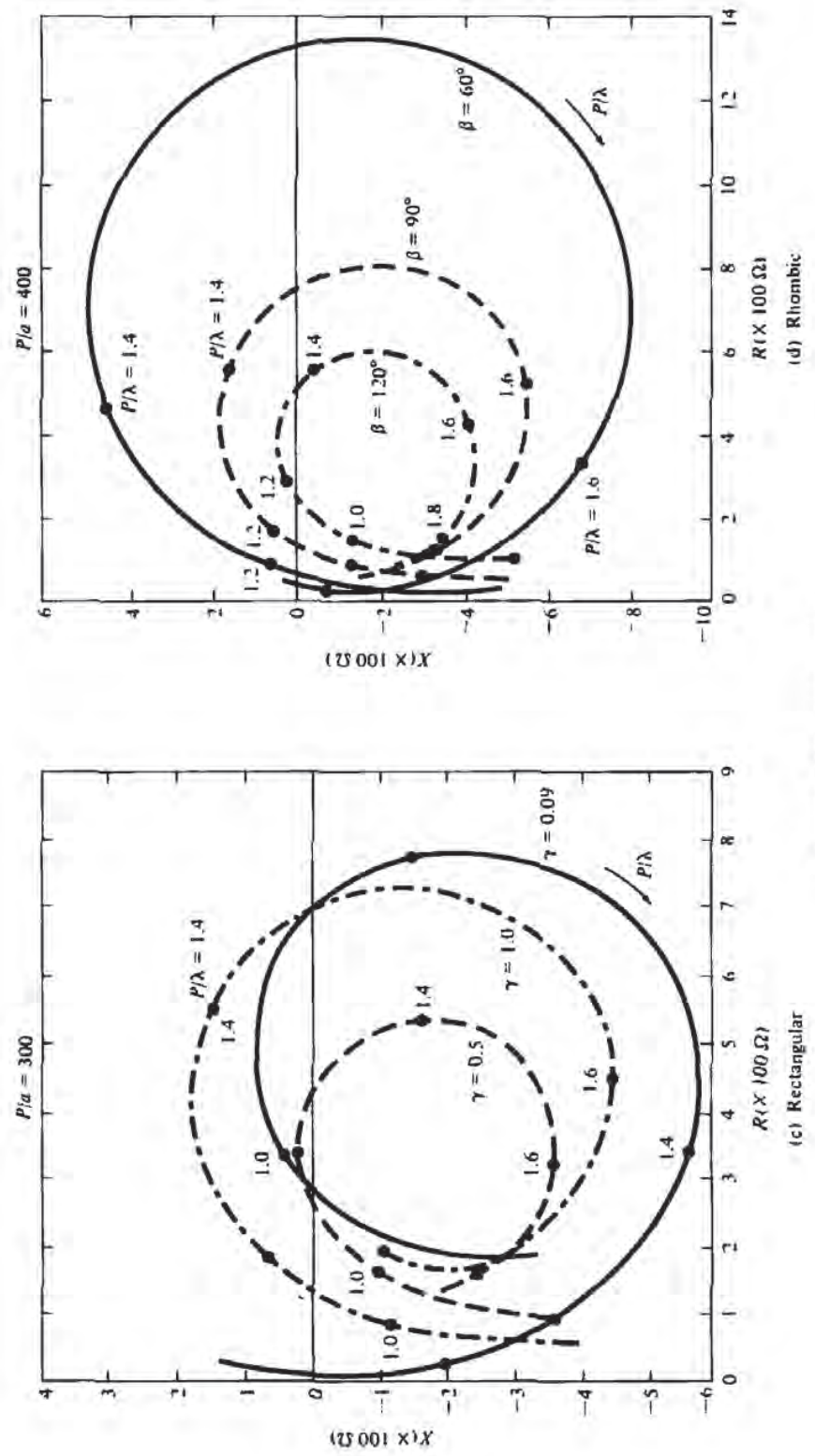


Figure 5.18 (continued)

INTEL-1045
U.S. Patent 7,151,430

5.7 FERRITE LOOP

Because the loss resistance is comparable to the radiation resistance, electrically small loops are very poor radiators and are seldom used in the transmitting mode. However, they are often used for receiving signals, such as in radios and pagers, where the signal-to-noise ratio is much more important than the efficiency.

5.7.1 Radiation Resistance

The radiation resistance, and in turn the antenna efficiency, can be raised by increasing the circumference of the loop. Another way to increase the radiation resistance, without increasing the electrical dimensions of the antenna, would be to insert within its circumference a ferrite core that has a tendency to increase the magnetic flux, the magnetic field, the open-circuit voltage, and in turn the radiation resistance of the loop [25]–[27]. This is the so-called *ferrite loop* and the ferrite material can be a rod of very few inches in length. The radiation resistance of the ferrite loop is given by

$$\frac{R_f}{R_r} = \left(\frac{\mu_{ce}}{\mu_0}\right)^2 = \mu_{cer}^2 \tag{5-72}$$

where

R_f = radiation resistance of ferrite loop
R_r = radiation resistance of air core loop
μ_{ce} = effective permeability of ferrite core
μ_0 = permeability of free-space
μ_{cer} = relative effective permeability of ferrite core

Using (5-24), the radiation resistance of (5-72) for a single-turn small ferrite loop can be written as

$$\boxed{R_f = 20\pi^2 \left(\frac{C}{\lambda}\right)^4 \left(\frac{\mu_{ce}}{\mu_0}\right)^2 = 20\pi^2 \left(\frac{C}{\lambda}\right)^2 \mu_{cer}^2} \tag{5-73}$$

and for an N-turn loop, using (5-24a), as

$$\boxed{R_f = 20\pi^2 \left(\frac{C}{\lambda}\right)^4 \left(\frac{\mu_{ce}}{\mu_0}\right)^2 N^2 = 20\pi^2 \left(\frac{C}{\lambda}\right)^4 \mu_{cer}^2 N^2} \tag{5-74}$$

The relative effective permeability of the ferrite core μ_{cer} is related to the relative intrinsic permeability of the unbounded ferrite material μ_{fr} ($\mu_{fr} = \mu_f/\mu_0$) by

$$\mu_{cer} = \frac{\mu_{ce}}{\mu_0} = \frac{\mu_{fr}}{1 + D(\mu_{fr} - 1)} \tag{5-75}$$

where D is the demagnetization factor which has been found experimentally for different core geometries, as shown in Figure 5.19. For most ferrite material, the relative intrinsic permeability μ_{fr} is very large ($\mu_{fr} \gg 1$) so that the relative effective permeability of the ferrite core μ_{cer} is approximately inversely proportional to the

INTEL-1045
U.S. Patent 7,151,430

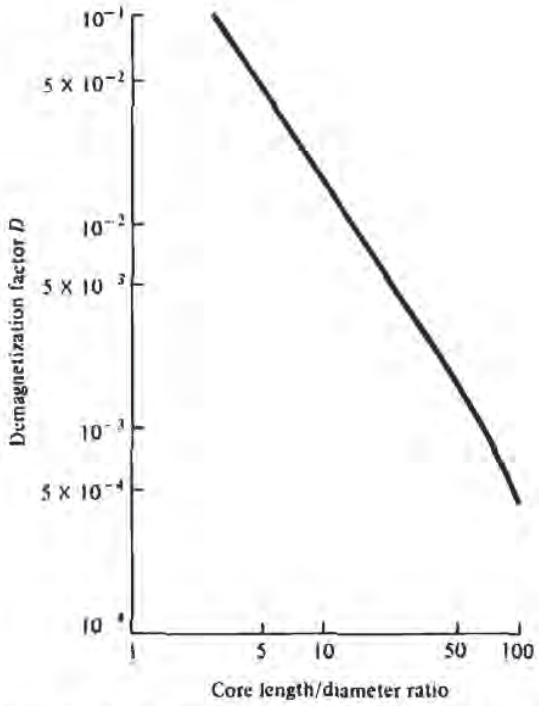


Figure 5.19 Demagnetization factor as a function of core length/diameter ratio. (SOURCE: E. A. Wolff, *Antenna Analysis*, Wiley, New York, 1966)

demagnetization factor, or $\mu_{eff} \sim 1/D = D^{-1}$. In general, the demagnetization factor is a function of the geometry of the ferrite core. For example, the demagnetization factor for a sphere is $D = \frac{1}{3}$ while that for an ellipsoid of length $2l$ and radius a, such that $l \gg a$, is

$$D = \left(\frac{a}{l}\right)^2 \left[\ln\left(\frac{2l}{a}\right) - 1\right] \tag{5-75a}$$

5.7.2 Ferrite-Loaded Receiving Loop

Because of their smallness, ferrite loop antennas of few turns wound around a small ferrite rod are used as antennas especially in pocket transistor radios. The antenna is usually connected in parallel with the RF amplifier tuning capacitance and, in addition to acting as an antenna, it furnishes the necessary inductance to form a tuned circuit. Because the inductance is obtained with only few turns, the loss resistance is kept small. Thus the Q is usually very high, and it results in high selectivity and greater induced voltage.

The equivalent circuit for a ferrite loaded loop antenna is similar to that of Figure 5.3 except that a loss resistance R_M, in addition to R_L, is needed to account for the power losses in the ferrite core. Expressions for the loss resistance R_M and inductance L_A for the ferrite loaded loop of N turns can be found in [4] and depend on some empirical factors which are determined from an average of experimental results. The inductance L_i is the same as that of the unloaded loop.

INTEL-1045
U.S. Patent 7,151,430

5.8 MOBILE COMMUNICATION SYSTEMS APPLICATIONS

As was indicated in Section 4.7.4 of Chapter 4, the monopole is one of the most widely used elements for handheld units of mobile communication systems. An alternative to the monopole is the loop, [28]–[31], which has been often used in pagers but has found very few applications in handheld transceivers. This is probably due to loop's high resistance and inductive reactance which are more difficult to match to standard feed lines. The fact that loop antennas are more immune to noise makes them more attractive for an interfering and fading environment, like that of mobile communication systems. In addition, loop antennas become more viable candidates for wireless communication systems which utilize devices operating at higher frequency bands, particularly in designs where balanced amplifiers must interface with the antenna. Relative to top side of the handheld unit, such as the telephone, the loop can be placed either horizontally [29] or vertically [31]. Either configuration presents attractive radiation characteristics for land-based mobile systems.

References

1. E. H. Newman, P. Bohley, and C. H. Walter, "Two Methods for Measurement of Antenna Efficiency," *IEEE Trans. Antennas Propagat.*, Vol. AP-23, No. 4, July 1975, pp. 457–461.
2. G. S. Smith, "Radiation Efficiency of Electrically Small Multiturn Loop Antennas," *IEEE Trans. Antennas Propagat.*, Vol. AP-20, No. 5, September 1972, pp. 656–657.
3. G. S. Smith, "The Proximity Effect in Systems of Parallel Conductors," *J. Appl. Phys.*, Vol. 43, No. 5, May 1972, pp. 2196–2203.
4. J. D. Kraus, *Electromagnetics*, 4th ed., McGraw-Hill Book Co., New York, 1992.
5. G. S. Smith, "Loop Antennas," Chapter 5 in *Antenna Engineering Handbook*, second edition, McGraw-Hill Book Co., New York, 1984.
6. J. E. Storer, "Impedance of Thin-Wire Loop Antennas," *AIEE Trans.*, (Part I. Communication and Electronics), Vol. 75, Nov. 1956, pp. 606–619.
7. S. Adachi and Y. Mushiake, "Studies of Large Circular Loop Antenna," Sci. Rep. Research Institute of Tohoku University (RITU), B, 9, 2, 1957, pp. 79–103.
8. S. Ito, N. Inagaki, and T. Sekiguchi, "An Investigation of the Array of Circular-Loop Antennas," *IEEE Trans. Antennas Propagat.*, Vol. AP-19, No. 4, July 1971, pp. 469–476.
9. A. Shoamanesh and L. Shafai, "Properties of Coaxial Yagi Loop Arrays," *IEEE Trans. Antennas Propagat.*, Vol. AP-26, No. 4, pp. 547–550, July 1978.
10. A. Shoamanesh and L. Shafai, "Design Data for Coaxial Yagi Array of Circular Loops," *IEEE Trans. Antennas Propagat.*, Vol. AP-27, pp. 711–713, September 1979.
11. G. N. Watson, *A Treatise on the Theory of Bessel Functions*, Cambridge University Press, London, 1922.
12. J. E. Lindsay, Jr., "A Circular Loop Antenna with Non-Uniform Current Distribution," *IRE Trans. Antennas Propagat.*, Vol. AP-8, No. 4, July 1960, pp. 438–441.
13. E. A. Wolff, *Antenna Analysis*, Wiley, New York, 1966.
14. H. C. Pocklington, "Electrical Oscillations in Wire," *Cambridge Philosophical Society Proceedings*, London, England, Vol. 9, 1897, p. 324.
15. R. King, "Theory of Antennas Driven from Two-Wire Line," *Journal of Applied Physics*, Vol. 20, 1949, p. 832.
16. D. G. Fink (ed.), *Electronics Engineers' Handbook*, Section 18, "Antennas" (by W. F. Croswell), McGraw-Hill, New York, pp. 18–22.
17. A. Richtscheid, "Calculation of the Radiation Resistance of Loop Antennas with Sinu-

INTEL-1045
U.S. Patent 7,151,430

soidal Current Distribution," *IEEE Trans. Antennas Propagat.*, Vol. AP-24, No. 6, Nov. 1976, pp. 889–891.
18. K. Iizuka, R. W. P. King, and C. W. Harrison, Jr., "Self- and Mutual Admittances of Two Identical Circular Loop Antennas in a Conducting Medium and in Air," *IEEE Trans. Antennas Propagat.*, Vol. AP-14, No. 4, pp. 440–450, July 1966.
19. R. E. Collin and F. J. Zucher (eds.), *Antenna Theory Part 2*, Chapter 23 (by J. R. Wait), McGraw-Hill, New York, 1969.
20. J. R. Wait, "Possible Influence of the Ionosphere on the Impedance of a Ground-Based Antenna," *J. Res. Natl. Bur. Std.* (U.S.), Vol. 66D, September–October 1962, pp. 563–569.
21. L. E. Vogler and J. L. Noble, "Curves of Input Impedance Change Due to Ground for Dipole Antennas," *U.S. National Bureau of Standards, Monograph 72, January 31, 1964.*
22. D. C. Chang, "Characteristics of a Horizontal Circular Loop Antenna over a Multilayered, Dissipative Half-Space," *IEEE Trans. Antennas Propagat.*, Vol. AP-21, No. 6, November 1973, pp. 871–874.
23. R. W. P. King, "Theory of the Center-Driven Square Loop Antenna," *IRE Trans. Antennas Propagat.*, Vol. AP-4, No. 4, July 1956, p. 393.
24. T. Tsukiji and S. Tou, "On Polygonal Loop Antennas," *IEEE Trans. Antennas Propagat.*, Vol. AP-28, No. 4, July 1980, pp. 571–575.
25. M. A. Islam, "A Theoretical Treatment of Low-Frequency Loop Antennas with Permeable Cores," *IEEE Trans. Antennas Propagat.*, Vol. AP-11, No. 2, March 1963, pp. 162–169.
26. V. H. Rumsey and W. L. Weeks, "Electrically Small Ferrite Loaded Loop Antennas," *IRE Convention Record*, Vol. 4, Part 1, 1956, pp. 165–170.
27. E. A. Wolff, *Antenna Analysis*, Wiley, New York, 1966, pp. 75–89.
28. K. Fujimoto and J. R. James, *Mobile Antenna Systems Handbook*, Artech House, Norwood, MA, 1994.
29. M. A. Jensen and Y. Rahmat-Samii, "Performance Analysis of Antennas for Hand-Held Transceivers Using FDTD," *IEEE Trans. Antennas Propagat.*, Vol. 42, No. 8, pp. 1106–1113, August 1994.
30. M. A. Jensen and Y. Rahmat-Samii, "EM Interaction of Handset Antennas and a Human in Personal Communications," *Proc. IEEE*, Vol. 83, No. 1, pp. 7–17, January 1995.
31. C. A. Balanis, K. D. Katsibas and P. A. Tirkas, "Antenna Considerations for Wireless Communication Systems and Networks," Fifth International Conference on Advances in Communication and Control (ComCon 5), June 26–30, 1995, Rethymnon, Crete, Greece.

PROBLEMS

5.1. Derive
(a) (5-18a)–(5-18c) using (5-17) and (3-2a)
(b) (5-19a)–(5-19b) using (5-18a)–(5-18c)

5.2. Write the fields of an infinitesimal linear magnetic dipole of constant current I_m, length l, and positioned along the z-axis. Use the fields of an infinitesimal electric dipole, (4-8a)–(4-10c), and apply the principle of duality. Compare with (5-20a)–(5-20d).

5.3. Find the radiation efficiency of a single-turn and a 4-turn circular loop each of radius $\lambda/(10\pi)$ and operating at 10 MHz. The radius of the wire is $10^{-3}\lambda$ and the turns are spaced $3 \times 10^{-3}\lambda$ apart. Assume the wire is copper with a conductivity of 5.7×10^7 S/m, and the antenna is radiating into free-space.

5.4. Find the power radiated by a small loop by forming the average power density, using (5-27a)–(5-27c), and integrating over a sphere of radius r. Compare the answer with (5-23b).

INTEL-1045
U.S. Patent 7,151,430

5.5. For a small loop of constant current, derive its far-zone fields using (5-17) and the procedure outlined and relationships developed in Section 3.6. Compare the answers with (5-27a)–(5-27b).

5.6. Design a lossless resonant circular loop operating at 10 MHz so that its single turn radiation resistance is 0.73 ohms. The resonant loop is to be connected to a matched load through a balanced "twin-lead" 300-ohm transmission line.
(a) Determine the radius of the loop (in meters and wavelengths).
(b) To minimize the matching reflections between the resonant loop and the 300-ohm transmission line, determine the closest number of integer turns the loop must have.
(c) For the loop of part b, determine the maximum power that can be expected to be delivered to a receiver matched-load if the incident wave is polarization matched to the lossless resonant loop. The power density of the incident wave is 10^{-6} watts/m^2.

5.7. A resonant 6-turn loop of *closely spaced turns* is operating at 50 MHz. The radius of the loop is $\lambda/30$, and the loop is connected to a 50-ohm transmission line. The radius of the wire is $\lambda/300$, its conductivity is $\sigma = 5.7 \times 10^7$ S/m, and the spacing between the turns is $\lambda/100$. Determine the
(a) directivity of the antenna (in dB)
(b) radiation efficiency taking into account the proximity effects of the turns
(c) reflection efficiency
(d) gain of the antenna (in dB)

5.8. Find the radiation efficiency (in percent) of an 8-turn circular loop antenna operating at 30 MHz. The radius of each turn is $a = 15$ cm, the radius of the wire is $b = 1$ mm, and the spacing between turns is $2c = 3.6$ mm. Assume the wire is copper ($\sigma = 5.7 \times 10^7$ S/m), and the antenna is radiating into free space. Account for the *proximity effect*.

5.9. A very small circular loop of radius $a (a < \lambda/6\pi)$ and constant current I_0 is symmetrically placed about the origin at $x = 0$ and with the plane of its area parallel to the y-z plane. Find the
(a) spherical **E**- and **H**-field components radiated by the loop in the far-zone
(b) directivity of the antenna

5.10. Repeat Problem 5.9 when the plane of the loop is parallel to the x-z plane at $y = 0$.

5.11. Using the computer program at the end of this chapter, compute the radiation resistance and the directivity of a circular loop of constant current with a radius of
(a) $a = \lambda/50$ (b) $a = \lambda/10$
(c) $a = \lambda/4$ (d) $a = \lambda/2$

5.12. A constant current circular loop of radius $a = 5\lambda/4$ is placed on the x-y plane. Find the *two* smallest angles (excluding $\theta = 0°$) where a null is formed in the far-field pattern.

5.13. Design a circular loop of constant current such that its field intensity vanishes only at $\theta = 0°$ ($\theta = 180°$) and 90°. Find its
(a) radius
(b) radiation resistance
(c) directivity

5.14. Design a constant current circular loop so that its first minimum, aside from $\theta = 0°$, in its far-field pattern is at 30° from a normal to the plane of the loop. Find the
(a) smallest radius of the antenna (in wavelengths)
(b) relative (to the maximum) radiation intensity (in dB) in the plane of the loop

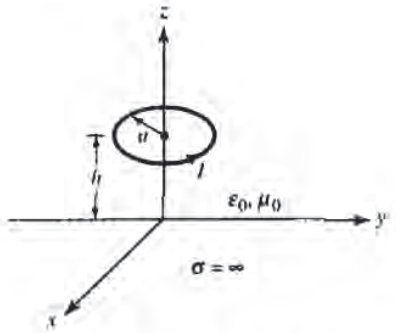
5.15. Design a constant current circular loop so that its pattern has a null in the plane of the loop, and two nulls above and two nulls below the plane of the loop. Find the
(a) radius of the loop
(b) angles where the nulls occur

INTEL-1045
U.S. Patent 7,151,430

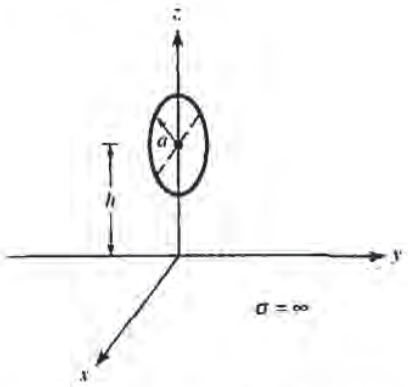
5.16. *A constant current circular loop is placed on the x-y plane. Find the far-field position,* relative to that of the loop, that a linearly polarized probe antenna must have so that the polarization loss factor (PLF) is maximized.

5.17. A very small ($a \ll \lambda$) circular loop of constant current is placed a distance h above an infinite electric ground plane. Assuming z is perpendicular to the ground plane, find the total far-zone field radiated by the loop when its plane is parallel to the
(a) x-z plane
(b) y-z plane

5.18. A very small loop antenna ($a \ll \lambda/30$) of constant current is placed a height h above a flat, perfectly conducting ground plane of infinite extent. The area plane of the loop is parallel to the interface (x-y plane). For far-field observations
(a) find the total electric field radiated by the loop in the presence of the ground plane
(b) all the angles (in degrees) from the vertical to the interface where the total field will vanish when the height is λ
(c) the smallest nonzero height (in λ) such that the total far-zone field exhibits a null at an angle of 60° from the vertical



5.19. A small circular loop, with its area parallel to the x-z plane, is placed a height h above an infinite flat perfectly electric conducting ground plane. Determine
(a) the array factor for the equivalent problem which allows you to find the total field on and above the ground plane
(b) angle(s) θ (in degrees) where the array factor will vanish when the loop is placed at a height $\lambda/2$ above the ground plane



5.20. For the loop of Problem 5.17(a), find the smallest height h so that a null is formed in the y-z plane at an angle of 45° above the ground plane.

INTEL-1045
U.S. Patent 7,151,430

5.21. A small single-turn circular loop of radius $a = 0.05\lambda$ is operating at 300 MHz. Assuming the radius of the wire is $10^{-4}\lambda$, determine the
(a) loss resistance
(b) radiation resistance
(c) loop inductance
Show that the loop inductive reactance is much greater than the loss resistance and radiation resistance indicating that a small loop acts primarily as an inductor.

5.22. Determine the radiation resistance of a single-turn small loop, assuming the geometrical shape of the loop is
(a) rectangular with dimensions a and b ($a, b \ll \lambda$)
(b) elliptical with major axis a and minor axis b ($a, b, \ll \lambda$)

5.23. Show that for the rectangular loop the radiation resistance is represented by

$$R_r = 31.171 \left(\frac{a^2 b^2}{\lambda^4}\right)$$

while for the elliptical loop is represented by

$$R_r = 31.171 \left(\frac{\pi^2 a^2 b^2}{16\lambda^4}\right)$$

Assuming the direction of the magnetic field of the incident plane wave coincides with the plane of incidence, derive the effective length of a small circular loop of radius a based on the definition of (2-92). Show that its effective length is

$$\mathbf{l}_e = \hat{\mathbf{a}}_\phi jkS \sin(\theta)$$

where $S = \pi a^2$.

5.24. A circular loop of nonconstant current distribution, with circumference of 1.4λ, is attached to a 300-ohm line. Assuming the radius of the wire is $1.555 \times 10^{-2}\lambda$, find the
(a) input impedance of the loop
(b) VSWR of the system
(c) inductance or capacitance that must be placed across the feed points so that the loop becomes resonant at $f = 100$ MHz

5.25. A very popular antenna for amateur radio operators is a square loop antenna (referred to as *quad antenna*) whose circumference is one wavelength. Assuming the radiation characteristics of the square loop are well represented by those of a circular loop:
(a) What is the input impedance (real and imaginary parts) of the antenna?
(b) What element (inductor or capacitor), and of what value, must be placed in series with the loop at the feed point to resonate the radiating element at a frequency of 1 GHz?
(c) What is the input VSWR, having the inductor or capacitor in place, if the loop is connected to a 78-ohm coaxial cable?

5.26. Design circular loops of wire radius b, which resonate at the first resonance. Find
(a) four values of a/b where the first resonance occurs (a is the radius of the loop)
(b) the circumference of the loops and the corresponding radii of the wires for the antennas of part (a)

5.27. Consider a circular loop of wire of radius a on the x–y plane and centered about the origin. Assume the current on the loop is given by

$$I_\phi(\phi') = I_0 \cos(\phi')$$

INTEL-1045
U.S. Patent 7,151,430

(a) Show that the far-zone electric field of the loop is given by

$$E_\theta = \frac{j\eta ka}{2} I_0 \frac{e^{-jkr}}{r} \frac{J_1(ka \sin\theta)}{ka \sin\theta} \cos\theta \sin\phi$$

$$E_\phi = \frac{j\eta ka}{2} I_0 \frac{e^{-jkr}}{r} J_1'(ka \sin\theta) \cos\phi$$

where

$$J_1'(x) = \frac{dJ_1(x)}{dx}$$

(b) Evaluate the radiation intensity $U(\theta, \phi)$ in the direction $\theta = 0$ and $\phi = \frac{\pi}{2}$ as a function of ka.

5.28. A very small circular loop, of constant current and radius of $\lambda_0/25$, is placed a height h above a perfect conductor and it is radiating in free-space.

(a) Find the smallest height h ($h < \lambda_0$) where the changes of its reactance are the smallest.

(b) At the height from part (a), find the radiation resistance of the loop.

5.29. A single-turn small loop of constant current I_0, radius $a = \lambda_0/(10\pi)$, and wire radius $b = \lambda_0/(500\pi)$ is placed a height h above a lossy ground plane, with the plane of the loop parallel to the ground. Assuming the lossy medium is flat earth with a conductivity of $\sigma_1 = 10^{-4}$ S/m, relative permittivity (dielectric constant) of $\epsilon_{r1} = 4$, and an operating frequency of 1 GHz, find the

(a) input resistance and reactance of the loop, assuming the wire of the loop is perfectly conducting and the loop is radiating in air (neglect ground effects)

(b) changes in the input resistance and input reactance when the loop is placed a height $h = 0.06\lambda_0$ above a flat, lossy earth

(c) total input resistance and input reactance when the loop is placed a distance $h = 0.06\lambda_0$ above a flat, lossy earth

(d) input reflection coefficient when the loop is connected to a 300-ohm "twin-lead" transmission line

(e) input VSWR when the loop is connected to the 300-ohm transmission line

INTEL-1045
U.S. Patent 7,151,430

COMPUTER PROGRAM - CIRCULAR LOOP

```
C*****************************************************************
C
C THIS IS A FORTRAN PROGRAM THAT COMPUTES THE:
C
C      I.   MAXIMUM DIRECTIVITY (DIMENSIONLESS AND IN dB)
C      II.  RADIATION RESISTANCE
C
C FOR A SMALL (CONSTANT CURRENT) LOOP. THE LOOP IS
C RADIATING INTO FREE SPACE.
C
C THE DIRECTIVITY AND RADIATION RESISTANCE ARE
C CALCULATED USING THE TRAILING EDGE METHOD IN
C INCREMENTS OF 1° IN THETA.
C
C
C           **INPUT PARAMETERS
C           1. A: LOOP RADIUS (in wavelengths)
C
C           **NOTE
C           THE FAR-ZONE ELECTRIC FIELD COMPONENT E_φ
C           EXISTS FOR 0°≤ Θ ≤180° AND 0°≤ Φ ≤360°.
C
C
C*****************************************************************
```


INTEL-1045
U.S. Patent 7,151,430

CHAPTER

6

ARRAYS: LINEAR, PLANAR, AND CIRCULAR

6.1 INTRODUCTION

In the previous chapter, the radiation characteristics of single-element antennas were discussed and analyzed. Usually the radiation pattern of a single element is relatively wide, and each element provides low values of directivity (gain). In many applications it is necessary to design antennas with very directive characteristics (very high gains) to meet the demands of long distance communication. This can only be accomplished by increasing the electrical size of the antenna.

Enlarging the dimensions of single elements often leads to more directive characteristics. Another way to enlarge the dimensions of the antenna, without necessarily increasing the size of the individual elements, is to form an assembly of radiating elements in an electrical and geometrical configuration. This new antenna, formed by multielements, is referred to as an *array*. In most cases, the elements of an array are identical. This is not necessary, but it is often convenient, simpler, and more practical. The individual elements of an array may be of any form (wires, apertures, etc.).

The total field of the array is determined by the vector addition of the fields radiated by the individual elements. This assumes that the current in each element is the same as that of the isolated element. This is usually not the case and depends on the separation between the elements. To provide very directive patterns, it is necessary that the fields from the elements of the array interfere constructively (add) in the desired directions and interfere destructively (cancel each other) in the remaining space. Ideally this can be accomplished, but practically it is only approached. In an array of identical elements, there are five controls that can be used to shape the overall pattern of the antenna. These are:

1. the geometrical configuration of the overall array (linear, circular, rectangular, spherical, etc.)
2. the relative displacement between the elements
3. the excitation amplitude of the individual elements
4. the excitation phase of the individual elements
5. the relative pattern of the individual elements

INTEL-1045
U.S. Patent 7,151,430

The influence that each one of the above has on the overall radiation characteristics will be the subject of this chapter. In many cases the techniques will be illustrated with examples.

The simplest and one of the most practical arrays is formed by placing the elements along a line. To simplify the presentation and give a better physical interpretation of the techniques, a two-element array will first be considered. The analysis of an N-element array will then follow. Two-dimensional analysis will be the subject at first. In latter sections, three-dimensional techniques will be introduced.

6.2 TWO-ELEMENT ARRAY

Let us assume that the antenna under investigation is an array of two infinitesimal horizontal dipoles positioned along the z-axis, as shown in Figure 6.1(a). The total field radiated by the two elements, assuming no coupling between the elements, is equal to the sum of the two and in the y-z plane it is given by

$$\mathbf{E}_t = \mathbf{E}_1 + \mathbf{E}_2 = \hat{\mathbf{a}}_\theta j\eta \frac{kI_0 l}{4\pi}\left\{\frac{e^{-j[kr_1 - (\beta/2)]}}{r_1}\cos\theta_1 + \frac{e^{-j[kr_2 + (\beta/2)]}}{r_2}\cos\theta_2\right\} \tag{6-1}$$

where β is the difference in phase excitation between the elements. The magnitude excitation of the radiators is identical. Assuming far-field observations and referring to Figure 6.1(b),

$$\theta_1 \simeq \theta_2 \simeq \theta \tag{6-2a}$$

$$\left.\begin{aligned} r_1 &\simeq r - \frac{d}{2}\cos\theta \\ r_2 &\simeq r + \frac{d}{2}\cos\theta \end{aligned}\right\} \quad \text{for phase variations} \tag{6-2b}$$

$$r_1 \simeq r_2 \simeq r \qquad \text{for amplitude variations} \tag{6-2c}$$

Equation 6-1 reduces to

$$\mathbf{E}_t = \hat{\mathbf{a}}_\theta j\eta \frac{kI_0 l e^{-jkr}}{4\pi r}\cos\theta\left[e^{+j(kd\cos\theta + \beta/2)} + e^{-j(kd\cos\theta + \beta/2)}\right]$$

$$\mathbf{E}_t = \hat{\mathbf{a}}_\theta j\eta \frac{kI_0 l e^{-jkr}}{4\pi r}\cos\theta\, 2\cos\left[\frac{1}{2}(kd\cos\theta + \beta)\right] \tag{6-3}$$

It is apparent from (6-3) that the total field of the array is equal to the field of a single element positioned at the origin multiplied by a factor which is widely referred to as the *array factor*. Thus for the two-element array of constant amplitude, the array factor is given by

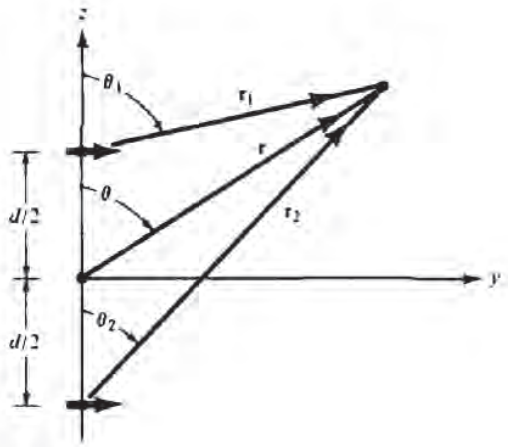
$$\text{AF} = 2\cos[\tfrac{1}{2}(kd\cos\theta + \beta)] \tag{6-4}$$

which in normalized form can be written as

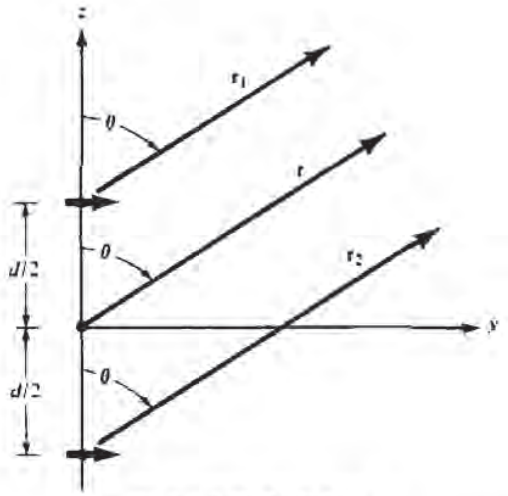
$$(\text{AF})_n = \cos[\tfrac{1}{2}(kd\cos\theta + \beta)] \tag{6-4a}$$

The array factor is a function of the geometry of the array and the excitation phase. By varying the separation d and/or the phase β between the elements, the characteristics of the array factor and of the total field of the array can be controlled.

INTEL-1045
U.S. Patent 7,151,430



(a) Two infinitesimal dipoles



(b) Far-field observations

Figure 6.1 Geometry of a two-element array positioned along the z-axis.

It has been illustrated that the far-zone field of a uniform two-element array of identical elements is equal to the *product of the field of a single element, at a selected reference point (usually the origin), and the array factor of that array.* That is,

$$\boxed{\mathbf{E}(\text{total}) = [\mathbf{E}(\text{single element at reference point})] \times [\text{array factor}]} \quad (6\text{-}5)$$

This is referred to as *pattern multiplication* for arrays of identical elements, and it is analogous to the pattern multiplication of (4-59) for continuous sources. Although it has been illustrated only for an array of two elements, each of identical magnitude, it is also valid for arrays with any number of identical elements which do not necessarily have identical magnitudes, phases, and/or spacings between them. This will be demonstrated in this chapter by a number of different arrays.

Each array has its own array factor. The array factor, in general, is a function of the number of elements, their geometrical arrangement, their relative magnitudes, their relative phases, and their spacings. The array factor will be of simpler form if

INTEL-1045
U.S. Patent 7,151,430

the elements have identical amplitudes, phases, and spacings. Since the array factor does not depend on the directional characteristics of the radiating elements themselves, it can be formulated by replacing the actual elements with isotropic (point) sources. Once the array factor has been derived using the point-source array, the total field of the actual array is obtained by the use of (6-5). Each point-source is assumed to have the amplitude, phase, and location of the corresponding element it is replacing.

In order to synthesize the total pattern of an array, the designer is not only required to select the proper radiating elements but the geometry (positioning) and excitation of the individual elements. To illustrate the principles, let us consider some examples.

Example 6.1

Given the array of Figures 6.1(a) and (b), find the nulls of the total field when $d = \lambda/4$ and

(a) $\beta = 0$

(b) $\beta = +\dfrac{\pi}{2}$

(c) $\beta = -\dfrac{\pi}{2}$

SOLUTION

(a) $\beta = 0$

The normalized field is given by

$$E_{tn} = \cos\theta \cos\left(\frac{\pi}{4}\cos\theta\right)$$

The nulls are obtained by setting the total field equal to zero, or

$$E_{tn} = \cos\theta \cos\left(\frac{\pi}{4}\cos\theta\right)\Big|_{\theta=\theta_n} = 0$$

Thus

$$\cos\theta_n = 0 \Rightarrow \theta_n = 90°$$

and

$$\cos\left(\frac{\pi}{4}\cos\theta_n\right) = 0 \Rightarrow \frac{\pi}{4}\cos\theta_n = \frac{\pi}{2}, -\frac{\pi}{2} \Rightarrow \theta_n = \text{does not exist}$$

The only null occurs at $\theta = 90°$ and is due to the pattern of the individual elements. The array factor does not contribute any additional nulls because there is not enough separation between the elements to introduce a phase difference of 180° between the elements, for any observation angle.

(b) $\beta = +\dfrac{\pi}{2}$

INTEL-1045
U.S. Patent 7,151,430

The normalized field is given by

$$E_m = \cos\theta \cos\left[\frac{\pi}{4}(\cos\theta + 1)\right]$$

The nulls are found from

$$E_m = \cos\theta \cos\left[\frac{\pi}{4}(\cos\theta + 1)\right]\Big|_{\theta=\theta_n} = 0$$

Thus

$$\cos\theta_n = 0 \Rightarrow \theta_n = 90°$$

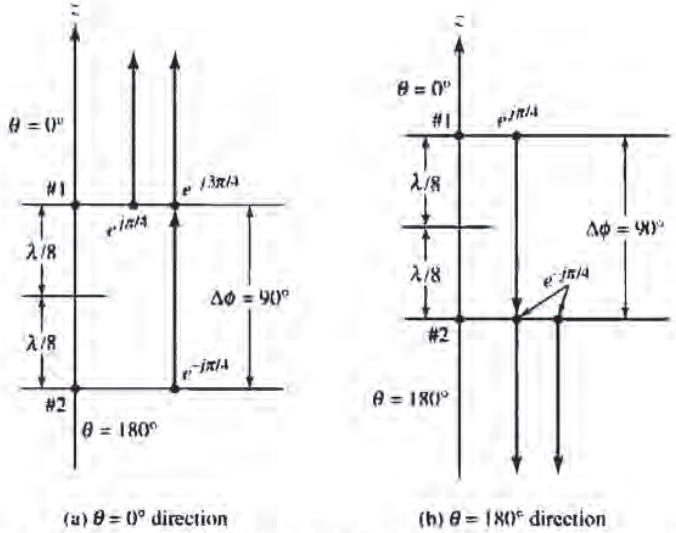
and

$$\cos\left[\frac{\pi}{4}(\cos\theta + 1)\right]\Big|_{\theta=\theta_n} = 0 \Rightarrow \frac{\pi}{4}(\cos\theta_n + 1) = \frac{\pi}{2} \Rightarrow \theta_n = 0°$$

and

$$\Rightarrow \frac{\pi}{4}(\cos\theta_n + 1) = -\frac{\pi}{2} \Rightarrow \theta_n = \text{does not exist}$$

The nulls of the array occur at $\theta = 90°$ and $0°$. The null at $0°$ is introduced by the arrangement of the elements (array factor). This can also be shown by physical reasoning, as shown in Figure 6.2(a). The element in the negative z-axis has an initial phase lag of $90°$ relative to the other element. As the wave from that element travels toward the positive z-axis ($\theta = 0°$ direction). it undergoes an additional $90°$ phase retardation when it arrives at the other element on the positive z-axis. Thus there is a total of $180°$ phase difference between the waves of the two elements when travel is



(a) $\theta = 0°$ direction (b) $\theta = 180°$ direction

Figure 6.2 Phase accumulation for two-element array for null formation toward $\theta = 0°$ and $180°$.

INTEL-1045
U.S. Patent 7,151,430

toward the positive z-axis ($\theta = 0°$). The waves of the two elements are in phase when they travel in the negative z-axis ($\theta = 180°$), as shown in Figure 6.2(b).

(c) $\beta = -\dfrac{\pi}{2}$

The normalized field is given by

$$E_m = \cos\theta \cos\left[\frac{\pi}{4}(\cos\theta - 1)\right]$$

and the nulls by

$$E_m = \cos\theta \cos\left[\frac{\pi}{4}(\cos\theta - 1)\right]\Big|_{\theta=\theta_n} = 0$$

Thus

$$\cos\theta_n = 0 \Rightarrow \theta_n = 90°$$

and

$$\cos\left[\frac{\pi}{4}(\cos\theta_n - 1)\right] = 0 \Rightarrow \frac{\pi}{4}(\cos\theta_n - 1) = \frac{\pi}{2} \Rightarrow \theta_n = \text{does not exist}$$

and

$$\Rightarrow \frac{\pi}{4}(\cos\theta_n - 1) = -\frac{\pi}{2} \Rightarrow \theta_n = 180°$$

The nulls occur at 90° and 180°. The element at the positive z-axis has a phase lag of 90° relative to the other, and the phase difference is 180° when travel is restricted toward the negative z-axis. There is no phase difference when the waves travel toward the positive z-axis. A diagram similar to that of Figure 6.2 can be used to illustrate this case.

To better illustrate the pattern multiplication rule, the normalized patterns of the single element, the array factor, and the total array for each of the above array examples are shown in Figures 6.3, 6.4(a), and 6.4(b). In each figure, the total pattern of the array is obtained by multiplying the pattern of the single element by that of the array factor. *In each case, the pattern is normalized to its own maximum.* Since the array factor for the example of Figure 6.3 is nearly isotropic (within 3 dB), the element pattern and the total pattern are almost identical in shape. The largest magnitude difference between the two is about 3 dB, and for each case it occurs toward the direction along which the phases of the two elements are in phase quadrature (90° out of phase). For Figure 6.3 this occurs along $\theta = 0°$ while for Figures 6.4(a,b) this occurs along $\theta = 90°$. Because the array factor for Figure 6.4(a) is of cardioid form, its corresponding element and total patterns are considerably different. In the total pattern, the null at $\theta = 90°$ is due to the element pattern while that toward $\theta = 0°$ is due to the array factor. Similar results are displayed in Figure 6.4(b).

INTEL-1045
U.S. Patent 7,151,430

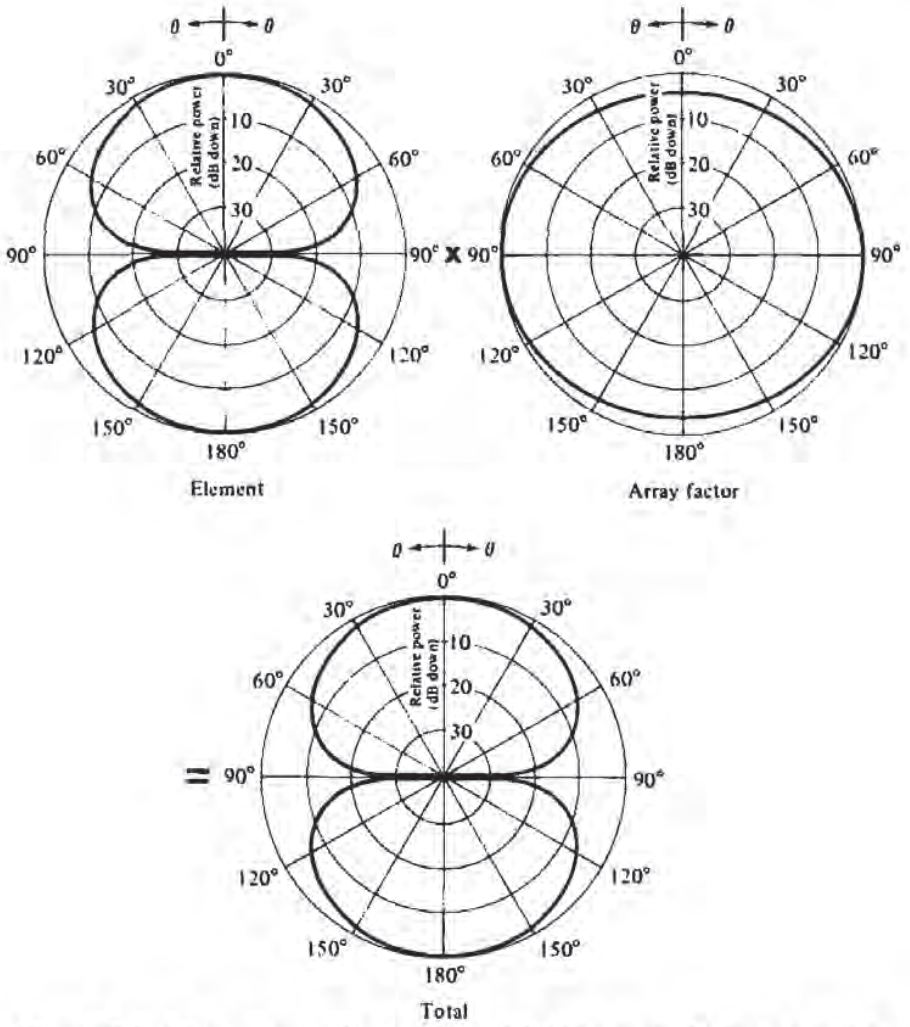


Figure 6.3 Element, array factor, and total field patterns of a two-element array of infinitesimal horizontal dipoles with identical phase excitation ($\beta = 0°$, $d = \lambda/4$).

Example 6.2

Consider an array of two identical infinitesimal dipoles oriented as shown in Figures 6.1(a) and (b). For a separation d and phase excitation difference β between the elements, find the angles of observation where the nulls of the array occur. The magnitude excitation of the elements is the same.

SOLUTION

The normalized total field of the array is given by (6-3) as

$$E_m = \cos\theta \cos\left[\tfrac{1}{2}(kd\cos\theta + \beta)\right]$$

INTEL-1045
U.S. Patent 7,151,430

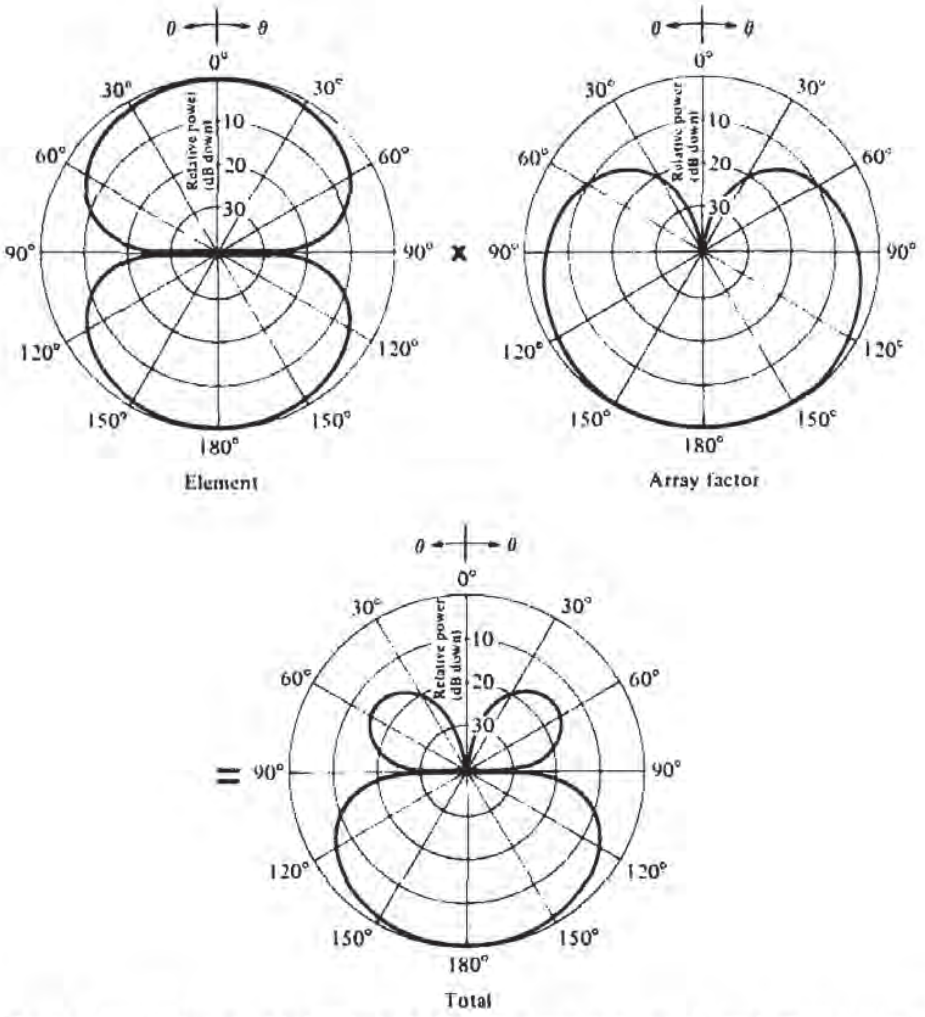


Figure 6.4 Pattern multiplication of element, array factor, and total array patterns of a two-element array of infinitesimal horizontal dipoles with (a) $\beta = +90°$, $d = \lambda/4$.

To find the nulls, the field is set equal to zero, or

$$E_{tn} = \cos\theta \cos[\tfrac{1}{2}(kd\cos\theta + \beta)]|_{\theta=\theta_n} = 0$$

Thus

$$\cos\theta_n = 0 \Rightarrow \theta_n = 90°$$

and

$$\cos\left[\frac{1}{2}(kd\cos\theta_n + \beta)\right] = 0 \Rightarrow \frac{1}{2}(kd\cos\theta_n + \beta) = \pm\left(\frac{2n+1}{2}\right)\pi$$

$$\Rightarrow \theta_n = \cos^{-1}\left(\frac{\lambda}{2\pi d}[-\beta \pm (2n+1)\pi]\right),$$

$$n = 0, 1, 2, \ldots$$

INTEL-1045
U.S. Patent 7,151,430

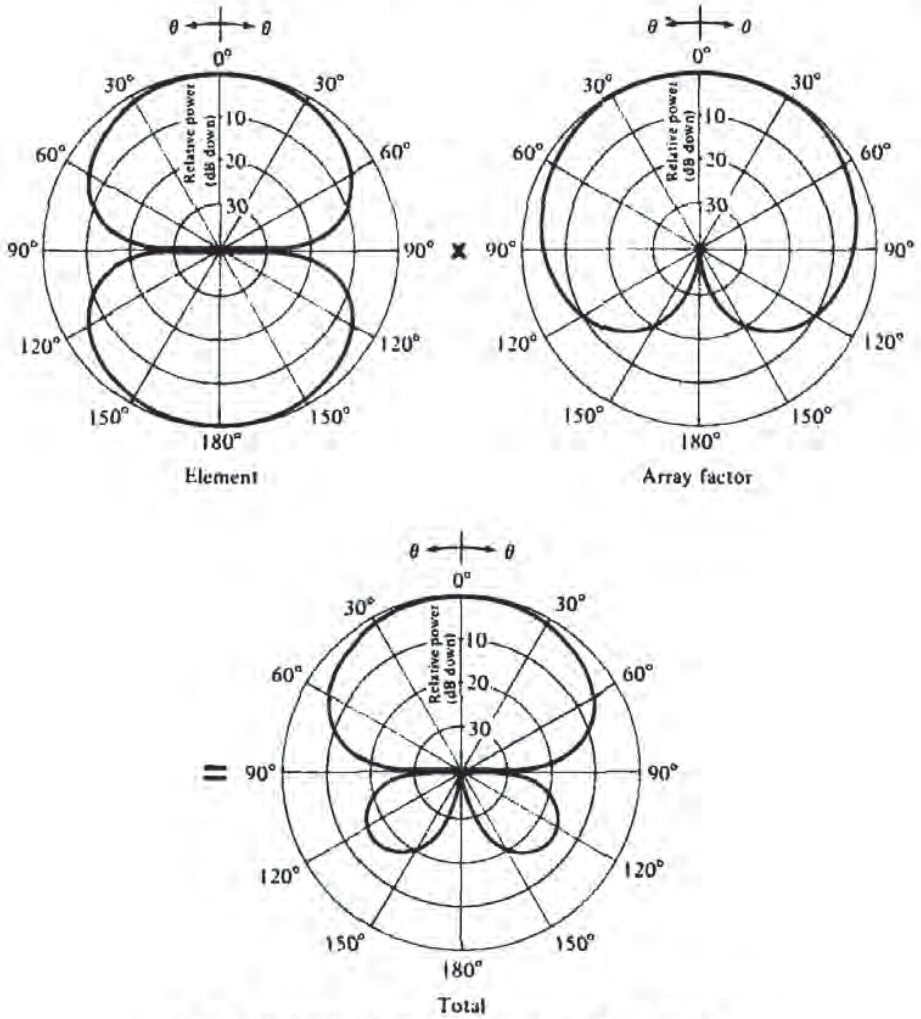


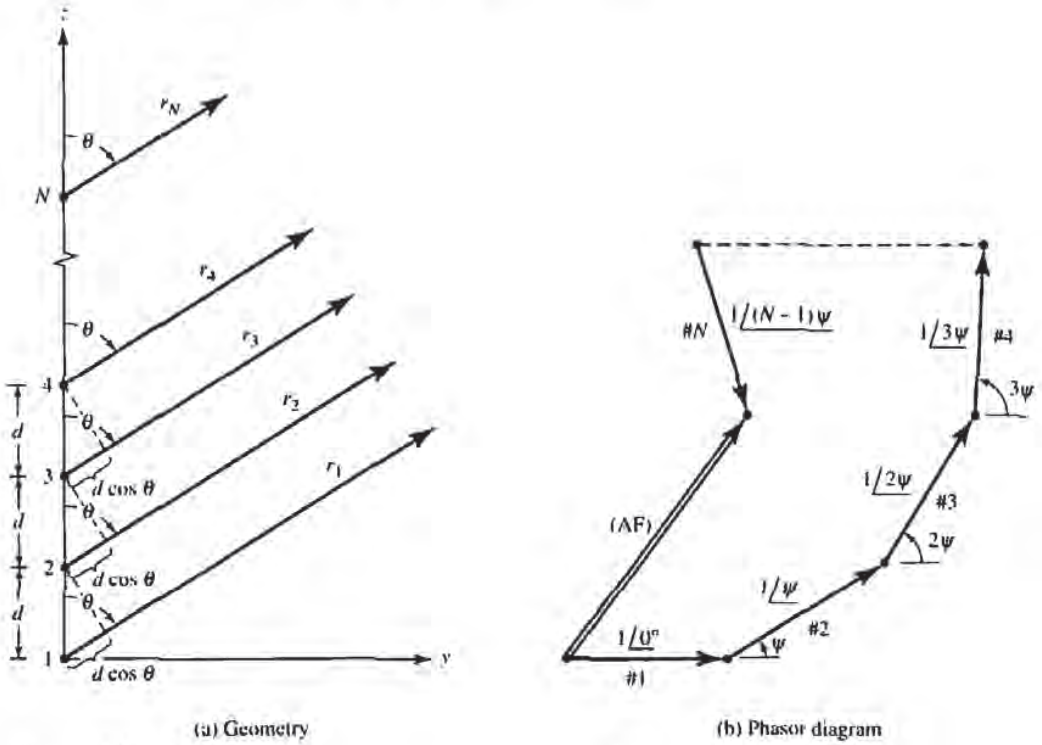
Figure 6.4 (b) Continued ($\beta = -90°$, $d = \lambda/4$).

The null at $\theta = 90°$ is attributed to the pattern of the individual elements of the array while the remaining ones are due to the formation of the array. For no phase difference between the elements ($\beta = 0$), the separation d must be equal or greater than half a wavelength ($d \geq \lambda/2$) in order for at least one null, due to the formation of the array, to occur.

6.3 *N*-ELEMENT LINEAR ARRAY: UNIFORM AMPLITUDE AND SPACING

Now that the arraying of elements has been introduced and it was illustrated by the two-element array, let us generalize the method to include N elements. Referring to the geometry of Figure 6.5(a), let us assume that all the elements have identical amplitudes but each succeeding element has a β progressive phase lead current excitation relative to the preceding one (β represents the phase by which the current

INTEL-1045
U.S. Patent 7,151,430



(a) Geometry (b) Phasor diagram

Figure 6.5 Far-field geometry and phasor diagram of N-element array of isotropic sources positioned along the z-axis.

in each element leads the current of the preceding element). *An array of identical elements all of identical magnitude and each with a progressive phase is referred to as a uniform array.* The array factor can be obtained by considering the elements to be point sources. If the actual elements are not isotropic sources, the total field can be formed by multiplying the array factor of the isotropic sources by the field of a single element. This is the pattern multiplication rule of (6-5), and it applies only for arrays of identical elements. The array factor is given by

$$\text{AF} = 1 + e^{+j(kd\cos\theta+\beta)} + e^{+j2(kd\cos\theta+\beta)} + \cdots + e^{j(N-1)(kd\cos\theta+\beta)}$$

$$\text{AF} = \sum_{n=1}^{N} e^{j(n-1)(kd\cos\theta+\beta)} \tag{6-6}$$

which can be written as

$$\boxed{\text{AF} = \sum_{n=1}^{N} e^{j(n-1)\psi}} \tag{6-7}$$

$$\boxed{\text{where} \quad \psi = kd\cos\theta + \beta} \tag{6-7a}$$

Since the total array factor for the uniform array is a summation of exponentials, it can be represented by the vector sum of N phasors each of unit amplitude and progressive phase ψ relative to the previous one. Graphically this is illustrated by the phasor diagram in Figure 6.5(b). It is apparent from the phasor diagram that the amplitude and phase of the AF can be controlled in uniform arrays by properly

INTEL-1045
U.S. Patent 7,151,430

selecting the relative phase ψ between the elements; in nonuniform arrays, the amplitude as well as the phase can be used to control the formation and distribution of the total array factor.

The array factor of (6-7) can also be expressed in an alternate, compact and closed form whose functions and their distributions are more recognizable. This is accomplished as follows.

Multiplying both sides of (6-7) by $e^{j\psi}$, it can be written as

$$(\text{AF})e^{j\psi} = e^{j\psi} + e^{j2\psi} + e^{j3\psi} + \cdots + e^{j(N-1)\psi} + e^{jN\psi} \tag{6-8}$$

Subtracting (6-7) from (6-8) reduces to

$$\text{AF}(e^{j\psi} - 1) = (-1 + e^{jN\psi}) \tag{6-9}$$

which can also be written as

$$\begin{aligned} \text{AF} = \left[\frac{e^{jN\psi} - 1}{e^{j\psi} - 1}\right] &= e^{j[(N-1)/2]\psi}\left[\frac{e^{j(N/2)\psi} - e^{-j(N/2)\psi}}{e^{j(1/2)\psi} - e^{-j(1/2)\psi}}\right] \\ &= e^{j[(N-1)/2]\psi}\left[\frac{\sin\left(\frac{N}{2}\psi\right)}{\sin\left(\frac{1}{2}\psi\right)}\right] \end{aligned} \tag{6-10}$$

If the reference point is the physical center of the array, the array factor of (6-10) reduces to

$$\text{AF} = \left[\frac{\sin\left(\frac{N}{2}\psi\right)}{\sin\left(\frac{1}{2}\psi\right)}\right] \tag{6-10a}$$

For small values of ψ, the above expression can be approximated by

$$\text{AF} \simeq \left[\frac{\sin\left(\frac{N}{2}\psi\right)}{\frac{\psi}{2}}\right] \tag{6-10b}$$

The maximum value of (6-10a) or (6-10b) is equal to N. To normalize the array factors so that the maximum value of each is equal to unity, (6-10a) and (6-10b) are written in normalized form as (see Appendix II)

$$\boxed{(\text{AF})_n = \frac{1}{N}\left[\frac{\sin\left(\frac{N}{2}\psi\right)}{\sin\left(\frac{1}{2}\psi\right)}\right]} \tag{6-10c}$$

INTEL-1045
U.S. Patent 7,151,430

and (see Appendix I)

$$\boxed{(AF)_n = \left[\frac{\sin\left(\frac{N}{2}\psi\right)}{\frac{N}{2}\psi}\right]} \tag{6-10d}$$

To find the nulls of the array, (6-10c) or (6-10d) are set equal to zero. That is,

$$\sin\left(\frac{N}{2}\psi\right) = 0 \Rightarrow \frac{N}{2}\psi\Big|_{\theta=\theta_n} = \pm n\pi \Rightarrow \theta_n = \cos^{-1}\left[\frac{\lambda}{2\pi d}\left(-\beta \pm \frac{2n}{N}\pi\right)\right] \tag{6-11}$$

$$n = 1, 2, 3, \ldots$$
$$n \neq N, 2N, 3N, \ldots \text{ with (6-10c)}$$

For $n = N, 2N, 3N, \ldots$, (6-10c) attains its maximum values because it reduces to a sin(0)/0 form. The values of n determine the order of the nulls (first, second, etc.). For a zero to exist, the argument of the arccosine cannot exceed unity. Thus the number of nulls that can exist will be a function of the element separation d and the phase excitation difference β.

The maximum values of (6-10c) occur when

$$\frac{\psi}{2} = \frac{1}{2}(kd\cos\theta + \beta)\Big|_{\theta=\theta_m} = \pm m\pi \Rightarrow \theta_m = \cos^{-1}\left[\frac{\lambda}{2\pi d}(-\beta \pm 2m\pi)\right]$$
$$m = 0, 1, 2, \ldots \tag{6-12}$$

The array factor of (6-10d) has only one maximum and occurs when $m = 0$ in (6-12). That is,

$$\theta_m = \cos^{-1}\left(\frac{\lambda\beta}{2\pi d}\right) \tag{6-13}$$

which is the observation angle that makes $\psi = 0$.

The 3-dB point for the array factor of (6-10d) occurs when (see Appendix I)

$$\frac{N}{2}\psi = \frac{N}{2}(kd\cos\theta + \beta)\Big|_{\theta=\theta_h} = \pm 1.391$$
$$\Rightarrow \theta_h = \cos^{-1}\left[\frac{\lambda}{2\pi d}\left(-\beta \pm \frac{2.782}{N}\right)\right] \tag{6-14}$$

which can also be written as

$$\theta_h = \frac{\pi}{2} - \sin^{-1}\left[\frac{\lambda}{2\pi d}\left(-\beta \pm \frac{2.782}{N}\right)\right] \tag{6-14a}$$

For large values of $d (d \gg \lambda)$, it reduces to

$$\theta_h \simeq \left[\frac{\pi}{2} - \frac{\lambda}{2\pi d}\left(-\beta \pm \frac{2.782}{N}\right)\right] \tag{6-14b}$$

INTEL-1045
U.S. Patent 7,151,430

The half-power beamwidth Θ_h can be found once the angles of the first maximum (θ_m) and the half-power point (θ_h) are found. For a symmetrical pattern

$$\Theta_h = 2|\theta_m - \theta_h| \tag{6-14c}$$

For the array factor of (6-10d), there are secondary maxima (maxima of minor lobes) which occur *approximately* when the numerator of (6-10d) attains its maximum value. That is,

$$\sin\left(\frac{N}{2}\psi\right) = \sin\left[\frac{N}{2}(kd\cos\theta + \beta)\right]\Big|_{\theta=\theta_s} \simeq \pm 1 \Rightarrow \frac{N}{2}(kd\cos\theta + \beta)\Big|_{\theta=\theta_s}$$
$$\simeq \pm\left(\frac{2s+1}{2}\right)\pi \Rightarrow \theta_s \simeq \cos^{-1}\left\{\frac{\lambda}{2\pi d}\left[-\beta \pm \left(\frac{2s+1}{N}\right)\pi\right]\right\}, \quad s = 1, 2, 3, \ldots \tag{6-15}$$

which can also be written as

$$\theta_s \simeq \frac{\pi}{2} - \sin^{-1}\left\{\frac{\lambda}{2\pi d}\left[-\beta \pm \left(\frac{2s+1}{N}\right)\pi\right]\right\}, \quad s = 1, 2, 3, \ldots \tag{6-15a}$$

For large values of $d (d \gg \lambda)$, it reduces to

$$\theta_s \simeq \frac{\pi}{2} - \frac{\lambda}{2\pi d}\left[-\beta \pm \left(\frac{2s+1}{N}\right)\pi\right], \quad s = 1, 2, 3, \ldots \tag{6-15b}$$

The maximum of the first minor lobe of (6-10c) occurs *appoximately* when (see Appendix I)

$$\frac{N}{2}\psi = \frac{N}{2}(kd\cos\theta + \beta)\Big|_{\theta=\theta_s} \simeq \pm\left(\frac{3\pi}{2}\right) \tag{6-16}$$

or when

$$\theta_s = \cos^{-1}\left\{\frac{\lambda}{2\pi d}\left[-\beta \pm \frac{3\pi}{N}\right]\right\} \tag{6-16a}$$

At that point, the magnitude of (6-10d) reduces to

$$(\mathrm{AF})_n = \left[\frac{\sin\left(\frac{N}{2}\psi\right)}{\frac{N}{2}\psi}\right]\Bigg|_{\substack{\theta=\theta_s \\ s=1}} = \frac{2}{3\pi} = 0.212 \tag{6-17}$$

which in dB is equal to

$$(\mathrm{AF})_n = 20\log_{10}\left(\frac{2}{3\pi}\right) = -13.46\ \mathrm{dB} \tag{6-17a}$$

Thus the maximum of the first minor lobe of the array factor of (6-10d) is 13.46 dB down from the maximum at the major lobe. More accurate expressions for the angle, beamwidth, and magnitude of first minor lobe of the array factor of (6-10d) can be obtained. These will be discussed in Chapter 12.

INTEL-1045
U.S. Patent 7,151,430

6.3.1 Broadside Array

In many applications it is desirable to have the maximum radiation of an array directed normal to the axis of the array (broadside; $\theta = 90°$ of Figure 6.5(a)). To optimize the design, the maxima of the single element and of the array factor should both be directed toward $\theta = 90°$. The requirements of the single elements can be accomplished by the judicious choice of the radiators, and those of the array factor by the proper separation and excitation of the individual radiators. In this section, the requirements that allow the array factor to "radiate" efficiently broadside will be developed.

Referring to (6-10c) or (6-10d), the maximum of the array factor occurs when

$$\psi = kd\cos\theta + \beta = 0 \tag{6-18}$$

Since it is desired to have the maximum directed toward $\theta = 90°$, then

$$\boxed{\psi = kd\cos\theta + \beta\big|_{\theta=90°} = \beta = 0} \tag{6-18a}$$

Thus to have the maximum of the array factor of a uniform linear array directed broadside to the axis of the array, it is necessary that all the elements have the same phase excitation (in addition to the same amplitude excitation). The separation between the elements can be of any value. To ensure that there are no principal maxima in other directions, which are referred to as *grating lobes*, the separation between the elements should not be equal to multiples of a wavelength ($d \neq n\lambda$, $n = 1, 2, 3\ldots$) when $\beta = 0$. If $d = n\lambda$, $n = 1, 2, 3, \ldots$ and $\beta = 0$, then

$$\psi = kd\cos\theta + \beta\Big|_{\substack{d = n\lambda \\ \beta = 0 \\ n = 1,2,3,\ldots}} = 2\pi n\cos\theta\Big|_{\theta=0°,180°} = \pm 2n\pi \tag{6-19}$$

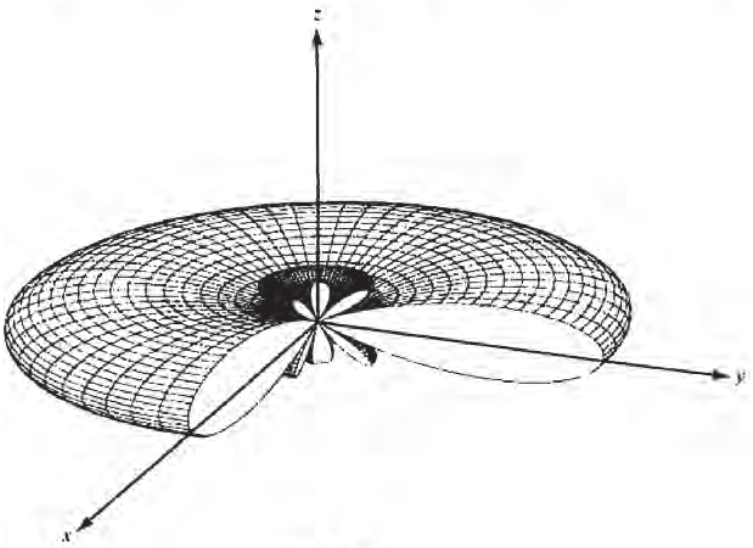
This value of ψ when substituted in (6-10c) makes the array factor attain its maximum value. Thus for a uniform array with $\beta = 0$ and $d = n\lambda$, in addition to having the maxima of the array factor directed broadside ($\theta = 90°$) to the axis of the array, there are additional maxima directed along the axis ($\theta = 0°$, $180°$) of the array (end-fire radiation).

One of the objectives in many designs is to avoid multiple maxima, in addition to the main maximum, which are referred to as *grating lobes*. Often it may be required to select the largest spacing between the elements but with no grating lobes. To avoid any grating lobe the largest spacing between the elements should be less than one wavelength ($d_{max} < \lambda$).

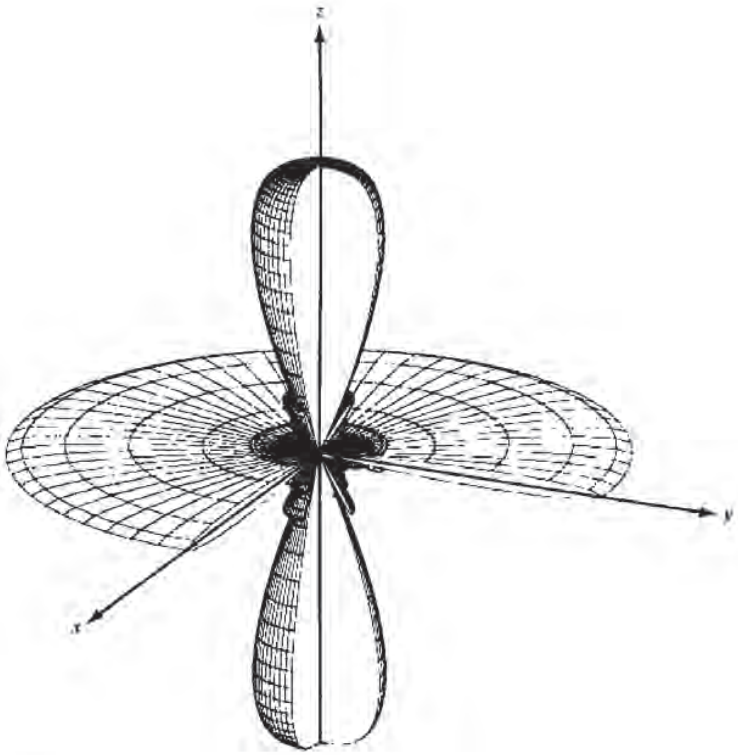
To illustrate the method, the three-dimensional array factor of a 10-element ($N = 10$) uniform array with $\beta = 0$ and $d = \lambda/4$ is shown plotted in Figure 6.6(a). A 90° angular sector has been removed for better view of the pattern distribution in the elevation plane. The only maximum occurs at broadside ($\theta = 90°$). To form a comparison, the three-dimensional pattern of the same array but with $d = \lambda$ is also plotted in Figure 6.6(b). For this pattern, in addition to the maximum at $\theta = 90°$, there are additional maxima directed toward $\theta = 0°$, 180°. The corresponding two-dimensional patterns of Figures 6.6(a,b) are shown in Figure 6.7.

If the spacing between the elements is chosen between $\lambda < d < 2\lambda$, then the maximum of Figure 6.6 toward $\theta = 0°$ shifts toward the angular region $0° < \theta <$

INTEL-1045
U.S. Patent 7,151,430



(a) Broadside



(b) Broadside/end-fire

Figure 6.6 Three-dimensional amplitude patterns for broadside, and broadside/end-fire arrays.

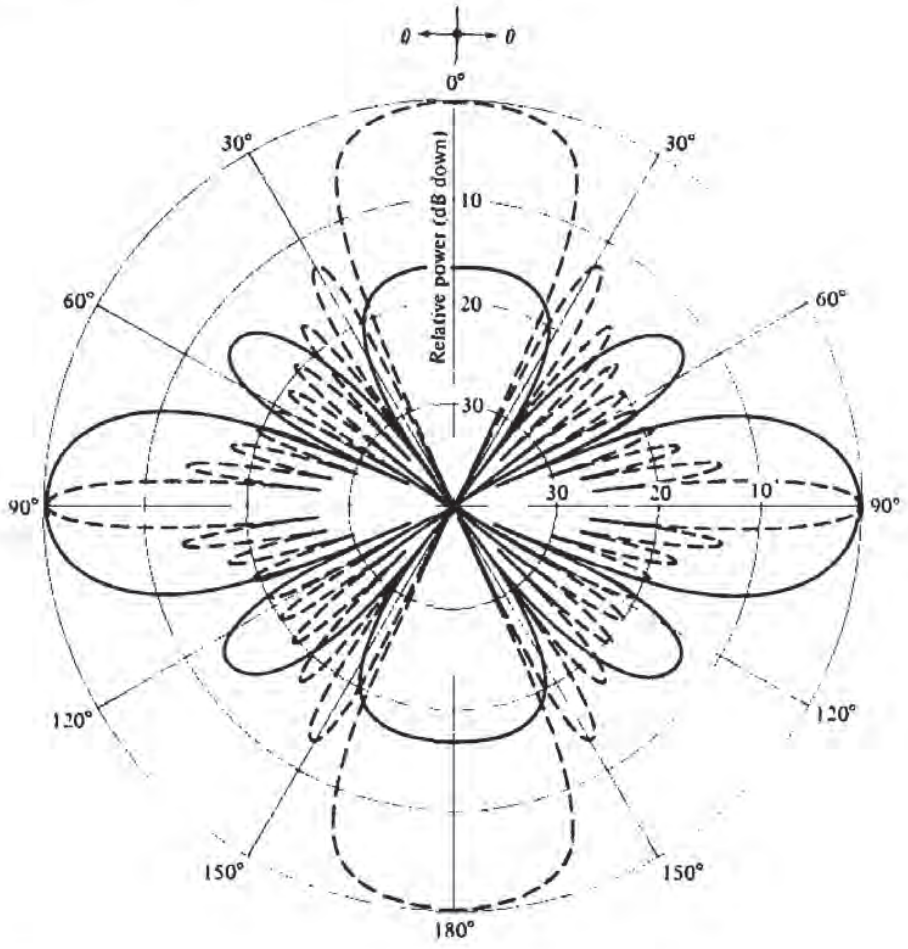


Figure 6.7 Array factor patterns of a 10-element uniform amplitude broadside array ($N = 10$, $\beta = 0$).

90° while the maximum toward $\theta = 180°$ shifts toward $90° < \theta < 180°$. When $d = 2\lambda$, there are maxima toward 0°, 60°, 90°, 120° and 180°.

In Tables 6.1 and 6.2 the expressions for the nulls, maxima, half-power points, minor lobe maxima, and beamwidths for broadside arrays have been listed. They are derived from the more general ones given by (6-10c)–(6-16a).

6.3.2 Ordinary End-Fire Array

Instead of having the maximum radiation broadside to the axis of the array, it may be desirable to direct it along the axis of the array (end-fire). As a matter of fact, it may be necessary that it radiates toward only one direction (either $\theta = 0°$ or 180° of Figure 6.5).

INTEL-1045
U.S. Patent 7,151,430

Table 6.1 NULLS, MAXIMA, HALF-POWER POINTS, AND MINOR LOBE MAXIMA FOR UNIFORM AMPLITUDE BROADSIDE ARRAYS

NULLS	$\theta_n = \cos^{-1}\left(\pm\frac{n}{N}\frac{\lambda}{d}\right)$ $n = 1, 2, 3, \ldots$ $n \neq N, 2N, 3N, \ldots$
MAXIMA	$\theta_m = \cos^{-1}\left(\pm\frac{m\lambda}{d}\right)$ $m = 0, 1, 2, \ldots$
HALF-POWER POINTS	$\theta_h = \cos^{-1}\left(\pm\frac{1.391\lambda}{\pi Nd}\right)$ $\pi d/\lambda \ll 1$
MINOR LOBE MAXIMA	$\theta_s = \cos^{-1}\left[\pm\frac{\lambda}{2d}\left(\frac{2s+1}{N}\right)\right]$ $s = 1, 2, 3, \ldots$ $\pi d/\lambda \ll 1$

To direct the maximum toward $\theta = 0°$,

$$\boxed{\psi = kd\cos\theta + \beta|_{\theta=0^\circ} = kd + \beta = 0 \Rightarrow \beta = -kd} \tag{6-20a}$$

If the maximum is desired toward $\theta = 180°$, then

$$\boxed{\psi = kd\cos\theta + \beta|_{\theta=180^\circ} = -kd + \beta = 0 \Rightarrow \beta = kd} \tag{6-20b}$$

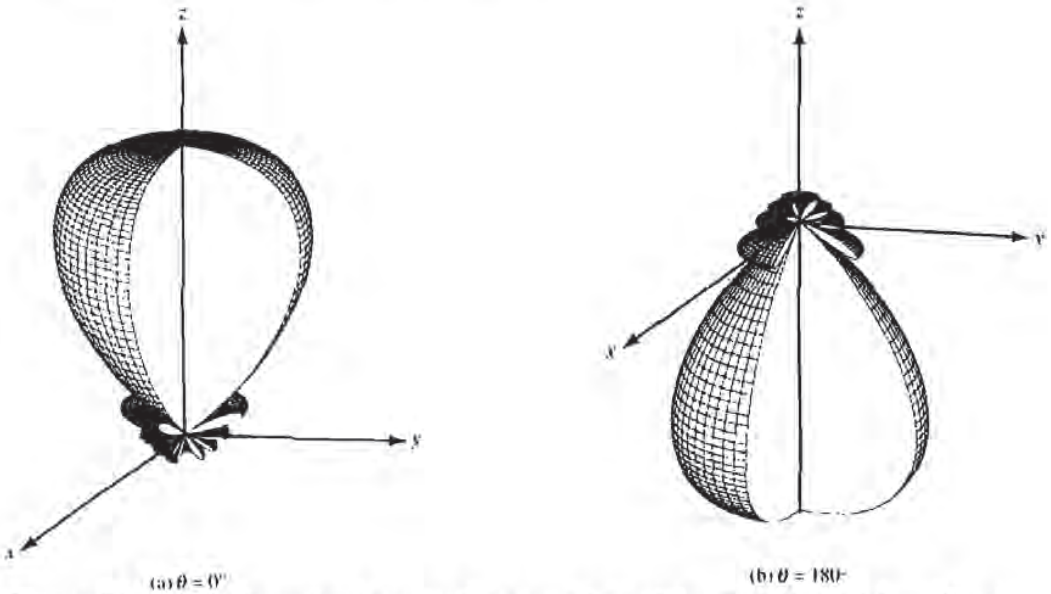
Thus end-fire radiation is accomplished when $\beta = -kd$ (for $\theta = 0°$) or $\beta = kd$ (for $\theta = 180°$).

If the element separation is $d = \lambda/2$, end-fire radiation exists in both directions ($\theta = 0°$ and $\theta = 180°$). If the element spacing is a multiple of a wavelength ($d = n\lambda$,

Table 6.2 BEAMWIDTHS FOR UNIFORM AMPLITUDE BROADSIDE ARRAYS

FIRST NULL BEAMWIDTH (FNBW)	$\Theta_n = 2\left[\frac{\pi}{2} - \cos^{-1}\left(\frac{\lambda}{Nd}\right)\right]$
HALF-POWER BEAMWIDTH (HPBW)	$\Theta_h = 2\left[\frac{\pi}{2} - \cos^{-1}\left(\frac{1.391\lambda}{\pi Nd}\right)\right]$ $\pi d/\lambda \ll 1$
FIRST SIDE LOBE BEAMWIDTH (FSLBW)	$\Theta_s = 2\left[\frac{\pi}{2} - \cos^{-1}\left(\frac{3\lambda}{2dN}\right)\right]$ $\pi d/\lambda \ll 1$

INTEL-1045
U.S. Patent 7,151,430



(a) $\theta = 0°$ (b) $\theta = 180°$

Figure 6.8 Three-dimensional amplitude patterns for end-fire arrays toward $\theta = 0°$ and 180°.

$n = 1, 2, 3, \ldots$), then in addition to having end-fire radiation in both directions, there also exist maxima in the broadside directions. Thus for $d = n\lambda$, $n = 1, 2, 3, \ldots$, there exist four maxima; two in the broadside directions and two along the axis of the array. To have only one end-fire maximum and to avoid any grating lobes, the maximum spacing between the elements should be less than $d_{max} < \lambda/2$.

The three-dimensional radiation patterns of a 10-element ($N = 10$) array with $d = \lambda/4$, $\beta = +kd$ are plotted in Figure 6.8. When $\beta = -kd$, the maximum is directed along $\theta = 0°$ and the three-dimensional pattern is shown in Figure 6.8(a). However, when $\beta = +kd$, the maximum is oriented toward $\theta = 180°$, and the three-dimensional pattern is shown in Figure 6.8(b). The two-dimensional patterns of Figures 6.8(a, b) are shown in Figure 6.9. To form a comparison, the array factor of the same array ($N = 10$) but with $d = \lambda$ and $\beta = -kd$ has been calculated. Its pattern is identical to that of a broadside array with $N = 10$, $d = \lambda$, and it is shown plotted in Figure 6.7. It is seen that there are four maxima; two broadside and two along the axis of the array.

The expressions for the nulls, maxima, half-power points, minor lobe maxima, and beamwidths, as applied to ordinary end-fire arrays, are listed in Tables 6.3 and 6.4.

6.3.3 Phased (Scanning) Array

In the previous two sections it was shown how to direct the major radiation from an array, by controlling the phase excitation between the elements, in directions normal (broadside) and along the axis (end-fire) of the array. It is then logical to assume that the maximum radiation can be oriented in any direction to form a scanning array. The procedure is similar to that of the previous two sections.

INTEL-1045
U.S. Patent 7,151,430

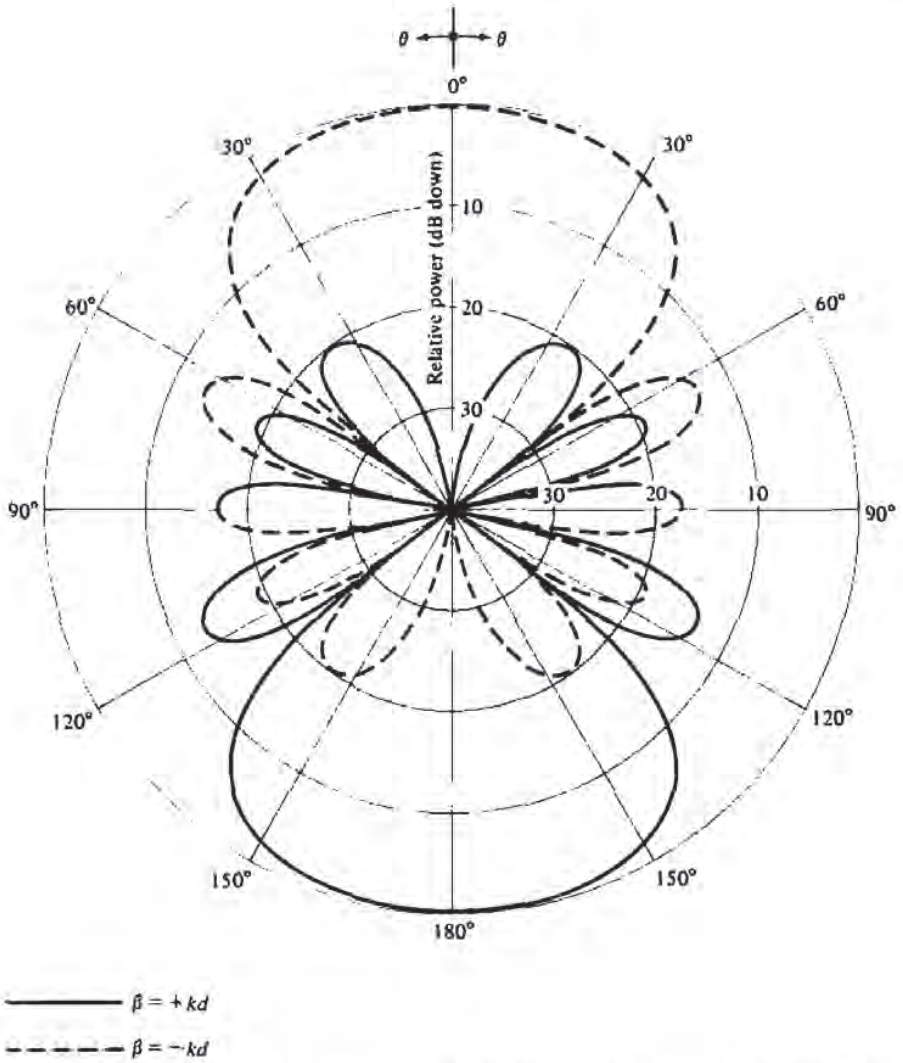


Figure 6.9 Array factor patterns of a 10-element uniform amplitude end-fire array ($N = 10$, $d = \lambda/4$).

Let us assume that the maximum radiation of the array is required to be oriented at an angle θ_0 ($0° \leq \theta_0 \leq 180°$). To accomplish this, the phase excitation β between the elements must be adjusted so that

$$\boxed{\psi = kd\cos\theta + \beta|_{\theta=\theta_0} = kd\cos\theta_0 + \beta = 0 \Rightarrow \beta = -kd\cos\theta_0} \quad (6\text{-}21)$$

Thus by controlling the progressive phase difference between the elements, the maximum radiation can be squinted in any desired direction to form a scanning array. This is the basic principle of electronic scanning phased array operation. Since in phased array technology the scanning must be continuous, the system should be capable of continuously varying the progressive phase between the elements. In practice, this is accomplished electronically by the use of ferrite or diode phase shifters. For ferrite phase shifters, the phase shift is controlled by the magnetic field

INTEL-1045
U.S. Patent 7,151,430

Table 6.3 NULLS, MAXIMA, HALF-POWER POINTS, AND MINOR LOBE MAXIMA FOR UNIFORM AMPLITUDE ORDINARY END-FIRE ARRAYS

NULLS	$\theta_n = \cos^{-1}\left(1 - \frac{n\lambda}{Nd}\right)$ $n = 1, 2, 3, \ldots$ $n \neq N, 2N, 3N, \ldots$
MAXIMA	$\theta_m = \cos^{-1}\left(1 - \frac{m\lambda}{d}\right)$ $m = 0, 1, 2, \ldots$
HALF-POWER POINTS	$\theta_h \simeq \cos^{-1}\left(1 - \frac{1.391\lambda}{\pi dN}\right)$ $\pi d/\lambda \ll 1$
MINOR LOBE MAXIMA	$\theta_s \simeq \cos^{-1}\left[1 - \frac{(2s+1)\lambda}{2Nd}\right]$ $s = 1, 2, 3, \ldots$ $\pi d/\lambda \ll 1$

within the ferrite, which in turn is controlled by the amount of current flowing through the wires wrapped around the phase shifter.

For diode phase shifter using balanced, hybrid-coupled varactors, the actual phase shift is controlled either by varying the analog bias dc voltage (typically 0–30 volts) or by a digital command through a digital-to-analog (D/A) converter [1].

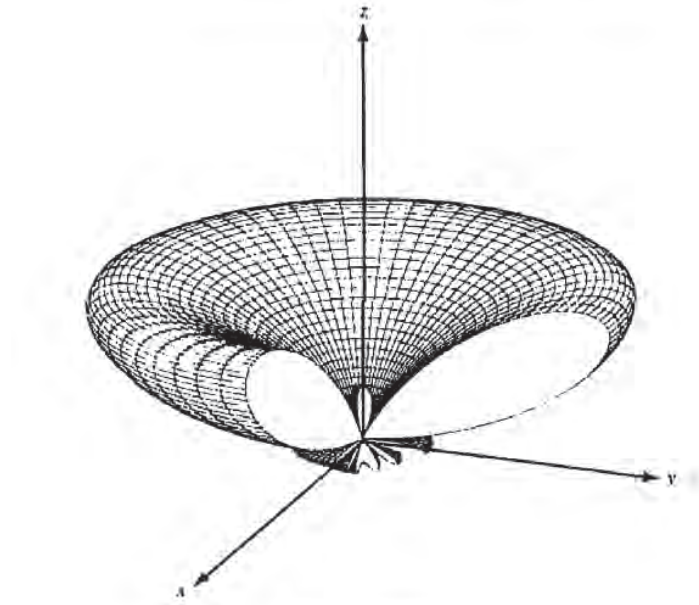
To demonstrate the principle of scanning, the three-dimensional radiation pattern of a 10-element array, with a separation of $\lambda/4$ between the elements and with the maximum squinted in the $\theta_0 = 60°$ direction, is plotted in Figure 6.10(a). The corresponding two-dimensional pattern is shown in Figure 6.10(b).

The half-power beamwidth of the scanning array is obtained using (6-14) with $\beta = -kd\cos\theta_0$. Using the minus sign in the argument of the inverse cosine function in (6-14) to represent one angle of the half-power beamwidth and the plus sign to

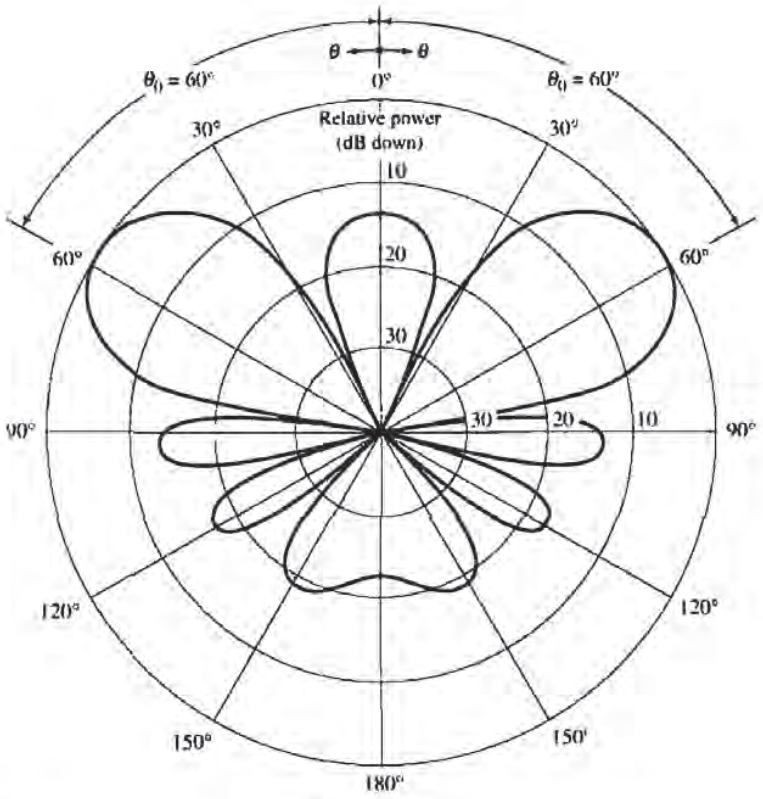
Table 6.4 BEAMWIDTHS FOR UNIFORM AMPLITUDE ORDINARY END-FIRE ARRAYS

FIRST NULL BEAMWIDTH (FNBW)	$\Theta_n = 2\cos^{-1}\left(1 - \frac{\lambda}{Nd}\right)$
HALF-POWER BEAMWIDTH (HPBW)	$\Theta_h \simeq 2\cos^{-1}\left(1 - \frac{1.391\lambda}{\pi dN}\right)$ $\pi d/\lambda \ll 1$
FIRST SIDE LOBE BEAMWIDTH (FSLBW)	$\Theta_s \simeq 2\cos^{-1}\left(1 - \frac{3\lambda}{2Nd}\right)$ $\pi d/\lambda \ll 1$

INTEL-1045
U.S. Patent 7,151,430



(a) Three-dimensional



(b) Two-dimensional

Figure 6.10 Three- and two-dimensional array factor patterns of a 10-element uniform amplitude scanning array ($N = 10$, $\beta = -kd\cos\theta_0$, $\theta_0 = 60°$, $d = \lambda/4$.)

INTEL-1045
U.S. Patent 7,151,430

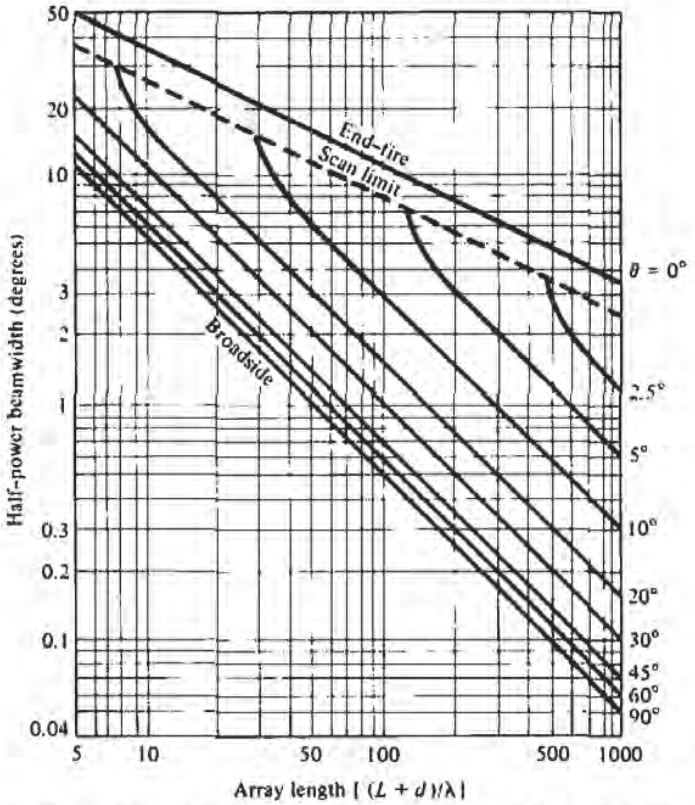


Figure 6.11 Half-power beamwidth for broadside, ordinary end-fire, and scanning uniform linear arrays. (SOURCE: R. S. Elliott, "Beamwidth and Directivity of Large Scanning Arrays," First of Two Parts, *The Microwave Journal*, December 1963)

represent the other angle, then the total beamwidth is the difference between these two angles and can be written as

$$\Theta_h = \cos^{-1}\left[\frac{\lambda}{2\pi d}\left(kd\cos\theta_0 - \frac{2.782}{N}\right)\right] - \cos^{-1}\left[\frac{\lambda}{2\pi d}\left(kd\cos\theta_0 + \frac{2.782}{N}\right)\right]$$
$$= \cos^{-1}\left(\cos\theta_0 - \frac{2.782}{Nkd}\right) - \cos^{-1}\left(\cos\theta_0 + \frac{2.782}{Nkd}\right) \tag{6-22}$$

Since $N = (L + d)/d$, (6-22) reduces to [2]

$$\boxed{\Theta_h = \cos^{-1}\left[\cos\theta_0 - 0.443\frac{\lambda}{(L+d)}\right] - \cos^{-1}\left[\cos\theta_0 + 0.443\frac{\lambda}{(L+d)}\right]} \tag{6-22a}$$

where L is the length of the array. Equation (6-22a) can also be used to compute the half-power beamwidth of a broadside array. However, it is not valid for an end-fire array. A plot of the half-power beamwidth (in degrees) as a function of the array

INTEL-1045
U.S. Patent 7,151,430

length is shown in Figure 6.11. These curves are valid for broadside, ordinary end-fire, and scanning uniform arrays (constant magnitude but with progressive phase shift). In a later section it will be shown that the curves of Figure 6.11 can be used, in conjunction with a beam broadening factor [2], to compute the directivity of nonuniform amplitude arrays.

6.3.4 Hansen-Woodyard End-Fire Array

The conditions for an ordinary end-fire array were discussed in Section 6.3.2. It was concluded that the maximum radiation can be directed along the axis of the uniform array by allowing the progressive phase shift β between elements to be equal to (6-20a) for $\theta = 0°$ and (6-20b) for $\theta = 180°$.

To enhance the directivity of an end-fire array without destroying any of the other characteristics, Hansen and Woodyard [3] in 1938 proposed that the required phase shift between *closely spaced elements of a very long array*† should be

$$\boxed{\beta = -\left(kd + \frac{2.92}{N}\right) \simeq -\left(kd + \frac{\pi}{N}\right) \Rightarrow \text{for maximum in } \theta = 0°} \quad (6\text{-}23a)$$

$$\boxed{\beta = +\left(kd + \frac{2.92}{N}\right) \simeq +\left(kd + \frac{\pi}{N}\right) \Rightarrow \text{for maximum in } \theta = 180°} \quad (6\text{-}23b)$$

These requirements are known today as the *Hansen-Woodyard conditions for end-fire radiation.* They lead to a *larger* directivity than the conditions given by (6-20a) and (6-20b). It should be pointed out, however, that *these conditions do not necessarily yield the maximum possible directivity.* In fact, the maximum may not even occur at $\theta = 0°$ or 180°, its value found using (6-10c) or (6-10d) may not be unity, and the side lobe level may not be -13.46 dB. Both of them, maxima and side lobe levels, depend on the number of array elements, as will be illustrated.

To realize the increase in directivity as a result of the Hansen-Woodyard conditions, it is necessary that, in addition to the conditions of (6-23a) and (6-23b), $|\psi|$ assumes values of

For maximum radiation along $\theta = 0°$

$$|\psi| = |kd\cos\theta + \beta|_{\theta=0°} = \frac{\pi}{N} \quad \text{and} \quad |\psi| = |kd\cos\theta + \beta|_{\theta=180°} \simeq \pi \quad (6\text{-}24a)$$

For maximum radiation along $\theta = 180°$

$$|\psi| = |kd\cos\theta + \beta|_{\theta=180°} = \frac{\pi}{N} \quad \text{and} \quad |\psi| = |kd\cos\theta + \beta|_{\theta=0°} \simeq \pi \quad (6\text{-}24b)$$

The condition of $|\psi| = \pi/N$ in (6-24a) or (6-24b) is realized by the use of (6-23a) or (6-23b), respectively. Care must be exercised in meeting the requirement of $|\psi| = \pi$

†In principle, the Hansen-Woodyard condition was derived for an infinitely long antenna with continuous distribution. It thus gives good results for very long, finite length discrete arrays with closely spaced elements.

INTEL-1045
U.S. Patent 7,151,430

for each array. For an array of N elements, the condition of $|\psi| = \pi$ is satisfied by using (6-23a) for $\theta = 0°$, (6-23b) for $\theta = 180°$, and choosing for each a spacing of

$$d = \left(\frac{N-1}{N}\right)\frac{\lambda}{4} \tag{6-25}$$

If the number of elements is large, (6-25) can be approximated by

$$d = \frac{\lambda}{4} \tag{6-25a}$$

Thus for a large uniform array, the Hansen-Woodyard condition can only yield an improved directivity provided the spacing between the elements is approximately $\lambda/4$.

To illustrate the principles, the patterns of a 10-element ($N = 10$) array with $d = \lambda/4$ ($\beta = -3\pi/5$) and $d = \lambda/2$ ($\beta = -11\pi/10$) have been plotted in Figure 6.12. In both cases the desired maximum radiation should be toward $\theta = 0°[\beta = -(kd + \pi/N)]$. It is apparent that the main lobe of the $d = \lambda/4$ pattern is much narrower when contrasted to its counterpart of Figure 6.9 using the ordinary end-fire conditions of (6-20a). In fact, the 3-dB beamwidth of the $d = \lambda/4$ pattern in Figure 6.12 is equal to 37° compared to 74° for that of Figure 6.9.

To make the comparisons more meaningful, the directivities for each of the patterns of Figures 6.9 and 6.12 have been calculated, using numerical integration, and it is found that they are equal to 11 and 19, respectively. Thus the Hansen-Woodyard conditions realize a 73% increase in directivity for this case.

As will be shown in Section 6.4 and listed in Table 6.7, the directivity of a Hansen-Woodyard end-fire array is always approximately 1.789 times (or 2.5 dB) greater than the directivity of an ordinary end-fire array. The increase in directivity of the pattern in Figure 6.12 for $d = \lambda/4$ over that of Figure 6.9 is at the expense of an increase of about 4 dB in side lobe level. Therefore in the design of an array, there is a trade-off between directivity (or half-power beamwidth) and side lobe level.

To show that (6-23a) and (6-23b) do *not* lead to improved directivities over those of (6-20a) and (6-20b) if (6-24a) and (6-24b) are not satisfied, the pattern for the same array ($N = 10$) but with $d = \lambda/2$ ($\beta = -11\pi/10$) that was plotted in Figure 6.12 will be discussed. Even though this pattern exhibits a very narrow lobe in the $\theta = 0°$ direction, its back lobes are larger than its main lobe. The $d = \lambda/2$ pattern fails to realize a larger directivity because the necessary $|\psi|_{\theta=180°} = \pi$ condition of (6-24a) is not satisfied. That is,

$$|\psi| = |(kd\cos\theta + \beta)|_{\substack{\theta=180° \\ \beta=-(kd+\pi/N)}} = |-(2kd + \pi/N)|_{\substack{d=\lambda/2 \\ N=10}} = 2.1\pi \tag{6-26}$$

which is not equal to π as required by (6-24a). Similar results occur for spacings other than those specified by (6-25) or (6-25a).

To better understand and appreciate the Hansen-Woodyard conditions, a succinct derivation of (6-23a) will be outlined. The procedure is identical to that reported by Hansen and Woodyard in their classic paper [3].

The array factor of an N-element array is given by (6-10c) as

$$(\mathrm{AF})_n = \frac{1}{N}\left\{\frac{\sin\left[\frac{N}{2}(kd\cos\theta + \beta)\right]}{\sin\left[\frac{1}{2}(kd\cos\theta + \beta)\right]}\right\} \tag{6-27}$$

INTEL-1045
U.S. Patent 7,151,430

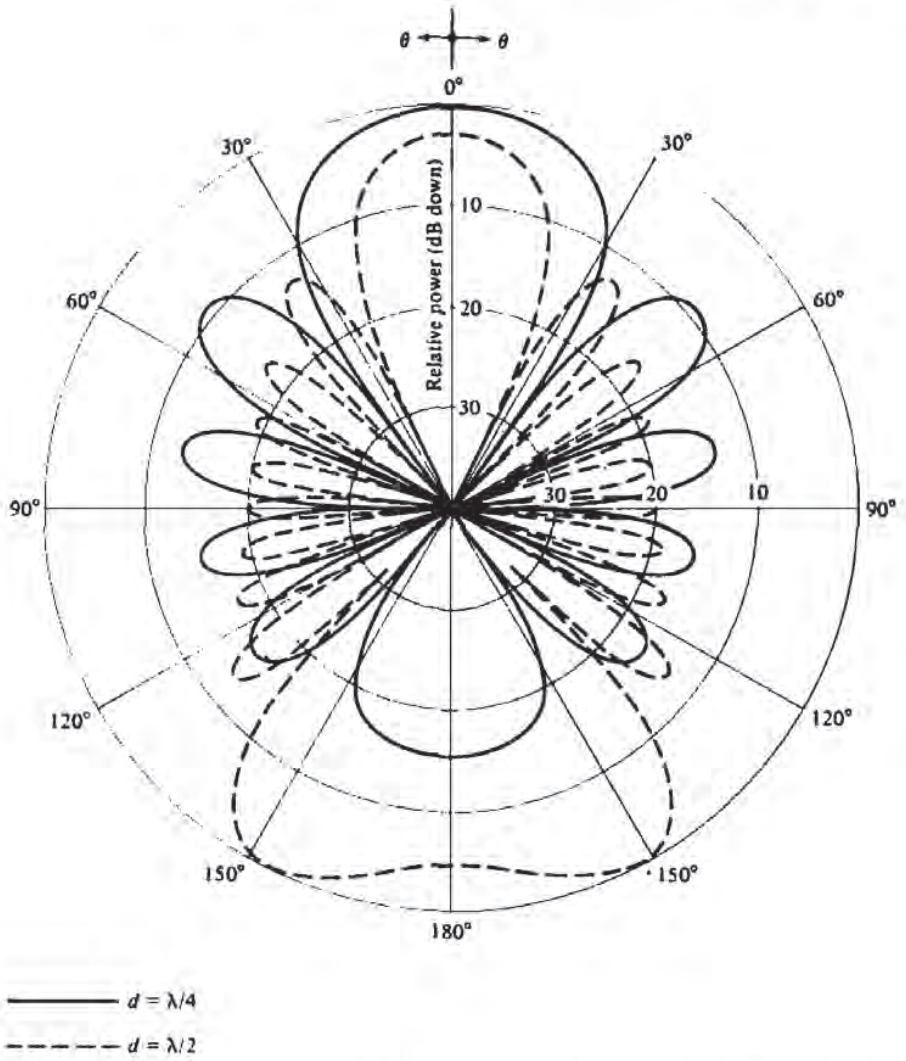


Figure 6.12 Array factor patterns of a 10-element uniform amplitude Hansen-Woodyard end-fire array [$N = 10$, $\beta = -(kd + \pi/N)$]

and approximated, for small values of ψ ($\psi = kd\cos\theta + \beta$), by (6-10d) or

$$(\mathrm{AF})_n \simeq \frac{\sin\left[\frac{N}{2}(kd\cos\theta + \beta)\right]}{\left[\frac{N}{2}(kd\cos\theta + \beta)\right]} \tag{6-27a}$$

If the progressive phase shift between the elements is equal to

$$\beta = -pd \tag{6-28}$$

where p is a constant, (6-27a) can be written as

$$(\mathrm{AF})_n = \left\{\frac{\sin[q(k\cos\theta - p)]}{q(k\cos\theta - p)}\right\} = \left[\frac{\sin(Z)}{Z}\right] \tag{6-29}$$

INTEL-1045
U.S. Patent 7,151,430

where

$$q = \frac{Nd}{2} \tag{6-29a}$$

$$Z = q(k\cos\theta - p) \tag{6-29b}$$

The radiation intensity can be written as

$$U(\theta) = |(\mathrm{AF})_n|^2 = \left[\frac{\sin(Z)}{Z}\right]^2 \tag{6-30}$$

whose value at $\theta = 0°$ is equal to

$$U(\theta)|_{\theta=0°} = \left\{\frac{\sin|q(k\cos\theta - p)|}{q(k\cos\theta - p)}\right\}^2\Bigg|_{\theta=0°} = \left\{\frac{\sin[q(k-p)]}{q(k-p)}\right\}^2 \tag{6-30a}$$

Dividing (6-30) by (6-30a), so that the value of the array factor is equal to unity at $\theta = 0°$, leads to

$$U(\theta)_n = \left\{\frac{q(k-p)}{\sin|q(k-p)|}\,\frac{\sin[q(k\cos\theta - p)|}{|q(k\cos\theta - p)|}\right\}^2 = \left[\frac{v}{\sin(v)}\,\frac{\sin(Z)}{Z}\right]^2 \tag{6-31}$$

where

$$v = q(k-p) \tag{6-31a}$$

$$Z = q(k\cos\theta - p) \tag{6-31b}$$

The directivity of the array factor can be evaluated using

$$D_0 = \frac{4\pi U_{\max}}{P_{\mathrm{rad}}} = \frac{U_{\max}}{U_0} \tag{6-32}$$

where U_0 is the average radiation intensity and it is given by

$$\begin{aligned} U_0 &= \frac{P_{\mathrm{rad}}}{4\pi} = \frac{1}{4\pi}\int_0^{2\pi}\int_0^{\pi} U(\theta)\sin\theta\,d\theta\,d\phi \\ &= \frac{1}{2}\left[\frac{v}{\sin(v)}\right]^2\int_0^{\pi}\left[\frac{\sin(Z)}{Z}\right]^2\sin\theta\,d\theta \end{aligned} \tag{6-33}$$

By using (6-31a) and (6-31b), (6-33) can be written as

$$U_0 = \frac{1}{2}\left[\frac{q(k-p)}{\sin[q(k-p)]}\right]^2\int_0^{\pi}\left[\frac{\sin[q(k\cos\theta - p)]}{q(k\cos\theta - p)}\right]^2\sin\theta\,d\theta \tag{6-33a}$$

To maximize the directivity, as given by (6-32), (6-33a) must be minimized. Performing the integration, (6-33a) reduces to

$$U_0 = \frac{1}{2kq}\left[\frac{v}{\sin(v)}\right]^2\left[\frac{\pi}{2} + \frac{[\cos(2v) - 1]}{2v} + S_i(2v)\right] = \frac{1}{2kq}g(v) \tag{6-34}$$

where

$$v = q(k-p) \tag{6-34a}$$

INTEL-1045
U.S. Patent 7,151,430

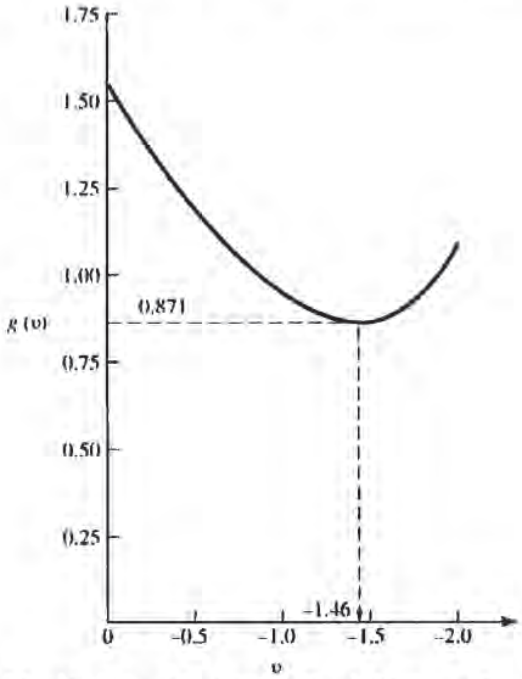


Figure 6.13 Variation of $g(v)$ (see Eq. 6-34c) as a function of v.

$$S_i(z) = \int_0^z \frac{\sin t}{t}\,dt \tag{6-34b}$$

$$g(v) = \left[\frac{v}{\sin(v)}\right]^2 \left[\frac{\pi}{2} + \frac{[\cos(2v) - 1]}{2v} + S_i(2v)\right] \tag{6-34c}$$

The function $g(v)$ is plotted in Figure 6.13 and its minimum value occurs when

$$v = q(k - p) = \frac{Nd}{2}(k - p) = -1.46 \tag{6-35}$$

Thus

$$\beta = -pd = -\left(kd + \frac{2.92}{N}\right) \tag{6-36}$$

which is the condition for end-fire radiation with improved directivity (Hansen-Woodyard condition) along $\theta = 0°$, as given by (6-23a). Similar procedures can be followed to establish (6-23b).

Ordinarily, (6-36) is approximated by

$$\beta = -\left(kd + \frac{2.92}{N}\right) \simeq -\left(kd + \frac{\pi}{N}\right) \tag{6-37}$$

with not too much relaxation in the condition since the curve of Figure 6.13 is very flat around the minimum point $v = -1.46$. Its value at $v = -1.57$ is almost the same as the minimum at $v = -1.46$.

The expressions for the nulls, maxima, half-power points, minor lobe maxima, and beamwidths are listed in Tables 6.5 and 6.6.

INTEL-1045
U.S. Patent 7,151,430

Table 6.5 NULLS, MAXIMA, HALF-POWER POINTS, AND MINOR LOBE MAXIMA FOR UNIFORM AMPLITUDE HANSEN-WOODYARD END-FIRE ARRAYS

NULLS	$\theta_n = \cos^{-1}\left[1 + (1 - 2n)\dfrac{\lambda}{2dN}\right]$ $n = 1, 2, 3, \ldots$ $n \neq N, 2N, 3N, \ldots$
MAXIMA	$\theta_m = \cos^{-1}\left\{1 + [1 - (2m + 1)]\dfrac{\lambda}{2Nd}\right\}$ $m = 1, 2, 3, \ldots$ $\pi d/\lambda \ll 1$
HALF-POWER POINTS	$\theta_h = \cos^{-1}\left(1 - 0.1398\dfrac{\lambda}{Nd}\right)$ $\pi d/\lambda \ll 1$ N large
MINOR LOBE MAXIMA	$\theta_s = \cos^{-1}\left(1 - \dfrac{s\lambda}{Nd}\right)$ $s = 1, 2, 3, \ldots$ $\pi d/\lambda \ll 1$

6.4 *N*-ELEMENT LINEAR ARRAY: DIRECTIVITY

The criteria that must be met to achieve broadside and end-fire radiation by a uniform linear array of N elements were discussed in the previous section. It would be instructive to investigate the directivity of each of the arrays, since it represents a figure-of-merit on the operation of the system.

6.4.1 Broadside Array

As a result of the criteria for broadside radiation given by (6-18a), the array factor for this form of the array reduces to

$$(\text{AF})_n = \frac{1}{N}\left[\frac{\sin\left(\frac{N}{2}kd\cos\theta\right)}{\sin\left(\frac{1}{2}kd\cos\theta\right)}\right] \tag{6-38}$$

which for a small spacing between the elements ($d \ll \lambda$) can be approximated by

$$(\text{AF})_n \simeq \left[\frac{\sin\left(\frac{N}{2}kd\cos\theta\right)}{\left(\frac{N}{2}kd\cos\theta\right)}\right] \tag{6-38a}$$

INTEL-1045
U.S. Patent 7,151,430

Table 6.6 BEAMWIDTHS FOR UNIFORM AMPLITUDE HANSEN-WOODYARD END-FIRE ARRAYS

FIRST NULL BEAMWIDTH (FNBW)	$\Theta_n = 2\cos^{-1}\left(1 - \frac{\lambda}{2dN}\right)$
HALF-POWER BEAMWIDTH (HPBW)	$\Theta_h = 2\cos^{-1}\left(1 - 0.1398\frac{\lambda}{Nd}\right)$ $\pi d/\lambda \ll 1$ N large
FIRST SIDE LOBE BEAMWIDTH (FSLBW)	$\Theta_s = 2\cos^{-1}\left(1 - \frac{\lambda}{Nd}\right)$ $\pi d/\lambda \ll 1$

The radiation intensity can be written as

$$U(\theta) = |(\mathrm{AF})_n|^2 = \left[\frac{\sin\left(\frac{N}{2}kd\cos\theta\right)}{\frac{N}{2}kd\cos\theta}\right]^2 = \left[\frac{\sin(Z)}{Z}\right]^2 \tag{6-39}$$

$$Z = \frac{N}{2}kd\cos\theta \tag{6-39a}$$

The directivity can be obtained using (6-32) where $U_{\max}$ of (6-39) is equal to unity ($U_{\max} = 1$) and it occurs at $\theta = 90°$. The average value U_0 of the intensity reduces to

$$U_0 = \frac{1}{4\pi}P_{\mathrm{rad}} = \frac{1}{2}\int_0^{\pi}\left[\frac{\sin(Z)}{Z}\right]^2 \sin\theta\, d\theta$$

$$= \frac{1}{2}\int_0^{\pi}\left[\frac{\sin\left(\frac{N}{2}kd\cos\theta\right)}{\frac{N}{2}kd\cos\theta}\right]^2 \sin\theta\, d\theta \tag{6-40}$$

By making a change of variable, that is,

$$Z = \frac{N}{2}kd\cos\theta \tag{6-40a}$$

$$dZ = -\frac{N}{2}kd\sin\theta\, d\theta \tag{6-40b}$$

(6-40) can be written as

$$U_0 = -\frac{1}{Nkd}\int_{+Nkd/2}^{-Nkd/2}\left[\frac{\sin Z}{Z}\right]^2 dZ = \frac{1}{Nkd}\int_{-Nkd/2}^{+Nkd/2}\left[\frac{\sin Z}{Z}\right]^2 dZ \tag{6-41}$$

INTEL-1045
U.S. Patent 7,151,430

For a large array ($Nkd/2 \rightarrow$ large), (6-41) can be approximated by extending the limits to infinity. That is,

$$U_0 = \frac{1}{Nkd}\int_{-Nkd/2}^{+Nkd/2}\left[\frac{\sin Z}{Z}\right]^2 dZ \simeq \frac{1}{Nkd}\int_{-\infty}^{+\infty}\left[\frac{\sin Z}{Z}\right]^2 dZ \tag{6-41a}$$

Since

$$\int_{-\infty}^{+\infty}\left[\frac{\sin (Z)}{Z}\right]^2 dZ = \pi \tag{6-41b}$$

(6-41a) reduces to

$$U_0 \simeq \frac{\pi}{Nkd} \tag{6-41c}$$

The directivity of (6-32) can now be written as

$$D_0 = \frac{U_{\max}}{U_0} = \frac{Nkd}{\pi} = 2N\left(\frac{d}{\lambda}\right) \tag{6-42}$$

Using

$$L = (N-1)d \tag{6-43}$$

where L is the overall length of the array. (6-42) can be expressed as

$$D_0 \simeq 2N\left(\frac{d}{\lambda}\right) \simeq 2\left(1 + \frac{L}{d}\right)\left(\frac{d}{\lambda}\right) \tag{6-44}$$

which for a large array ($L \gg d$) reduces to

$$D_0 \simeq 2N\left(\frac{d}{\lambda}\right) = 2\left(1 + \frac{L}{d}\right)\left(\frac{d}{\lambda}\right) \overset{L \gg d}{\simeq} 2\left(\frac{L}{\lambda}\right) \tag{6-44a}$$

Example 6.3

Given a linear, broadside, uniform array of 10 isotropic elements, ($N = 10$) with a separation of $\lambda/4$ ($d = \lambda/4$) between the elements, find the directivity of the array.

SOLUTION

Using (6-44a)

$$D_0 \simeq 2N\left(\frac{d}{\lambda}\right) = 5(\text{dimensionless}) = 10\log_{10}(5) = 6.99 \quad \text{dB}$$

INTEL-1045
U.S. Patent 7,151,430

6.4.2 Ordinary End-Fire Array

For an end-fire array, with the maximum radiation in the $\theta = 0°$ direction, the array factor is given by

$$(\text{AF})_n = \left[\frac{\sin\left[\frac{N}{2}kd(\cos\theta - 1)\right]}{N\sin\left[\frac{1}{2}kd(\cos\theta - 1)\right]}\right] \tag{6-45}$$

which, for a small spacing between the elements ($d \ll \lambda$), can be approximated by

$$(\text{AF})_n \simeq \left[\frac{\sin\left[\frac{N}{2}kd(\cos\theta - 1)\right]}{\left[\frac{N}{2}kd(\cos\theta - 1)\right]}\right] \tag{6-45a}$$

The corresponding radiation intensity can be written as

$$U(\theta) = |(\text{AF})_n|^2 = \left[\frac{\sin\left[\frac{N}{2}kd(\cos\theta - 1)\right]}{\frac{N}{2}kd(\cos\theta - 1)}\right]^2 = \left[\frac{\sin(Z)}{Z}\right]^2 \tag{6-46}$$

$$Z = \frac{N}{2}kd(\cos\theta - 1) \tag{6-46a}$$

whose maximum value is unity ($U_{\max} = 1$) and it occurs at $\theta = 0°$. The average value of the radiation intensity is given by

$$U_0 = \frac{1}{4\pi}\int_0^{2\pi}\int_0^{\pi}\left[\frac{\sin\left[\frac{N}{2}kd(\cos\theta - 1)\right]}{\frac{N}{2}kd(\cos\theta - 1)}\right]^2 \sin\theta\, d\theta\, d\phi$$

$$= \frac{1}{2}\int_0^{\pi}\left[\frac{\sin\left[\frac{N}{2}kd(\cos\theta - 1)\right]}{\frac{N}{2}kd(\cos\theta - 1)}\right]^2 \sin\theta\, d\theta \tag{6-47}$$

By letting

$$Z = \frac{N}{2}kd(\cos\theta - 1) \tag{6-47a}$$

$$dZ = -\frac{N}{2}kd\sin\theta\, d\theta \tag{6-47b}$$

INTEL-1045
U.S. Patent 7,151,430

(6-47) can be written as

$$U_0 = -\frac{1}{Nkd}\int_0^{Nkd}\left[\frac{\sin(Z)}{Z}\right]^2 dZ = \frac{1}{Nkd}\int_0^{Nkd}\left[\frac{\sin(Z)}{Z}\right]^2 dZ \qquad (6\text{-}48)$$

For a large array ($Nkd \rightarrow$ large), (6-48) can be approximated by extending the limits to infinity. That is,

$$U_0 = \frac{1}{Nkd}\int_0^{Nkd}\left[\frac{\sin(Z)}{Z}\right]^2 dZ \simeq \frac{1}{Nkd}\int_0^{\infty}\left[\frac{\sin(Z)}{Z}\right]^2 dZ \qquad (6\text{-}48a)$$

Using (6-41b) reduces (6-48a) to

$$U_0 \simeq \frac{\pi}{2Nkd} \qquad (6\text{-}48b)$$

and the directivity to

$$D_0 = \frac{U_{\max}}{U_0} \simeq \frac{2Nkd}{\pi} = 4N\left(\frac{d}{\lambda}\right) \qquad (6\text{-}49)$$

Another form of (6-49), using (6-43), is

$$D_0 \simeq 4N\left(\frac{d}{\lambda}\right) = 4\left(1 + \frac{L}{d}\right)\left(\frac{d}{\lambda}\right) \qquad (6\text{-}49a)$$

which for a large array ($L \gg d$) reduces to

$$D_0 \simeq 4N\left(\frac{d}{\lambda}\right) = 4\left(1 + \frac{L}{d}\right)\left(\frac{d}{\lambda}\right) \overset{L \gg d}{\simeq} 4\left(\frac{L}{\lambda}\right) \qquad (6\text{-}49b)$$

It should be noted that the directivity of the end-fire array, as given by (6-49)–(6-49b), is twice that for the broadside array as given by (6-42)–(6-44a).

Example 6.4

Given a linear, end-fire, uniform array of 10 elements ($N = 10$) with a separation of $\lambda/4$ ($d = \lambda/4$) between the elements, find the directivity of the array factor. This array is identical to the broadside array of Example 6.3.

SOLUTION

Using (6-49)

$$D_0 \simeq 4N\left(\frac{d}{\lambda}\right) = 10(\text{dimensionless}) = 10\log_{10}(10) = 10\ \text{dB}$$

This value for the directivity ($D_0 = 10$) is approximate, based on the validity of (6-48a). However, it compares very favorably with the value of $D_0 = 10.05$ obtained by numerically integrating (6-45) using the computer program at the end of Chapter 2.

INTEL-1045
U.S. Patent 7,151,430

6.4.3 Hansen-Woodyard End-Fire Array

For an end-fire array with improved directivity (Hansen-Woodyard conditions) and maximum radiation in the $\theta = 0°$ direction, the radiation intensity (for small spacing between the elements, $d \ll \lambda$) is given by (6-31)–(6-31b). The maximum radiation intensity is unity ($U_{max} = 1$), and the average radiation intensity is given by (6-34) where q and v are defined, respectively, by (6-29a) and (6-34a). Using (6-29a), (6-34a), (6-35), and (6-37), the radiation intensity of (6-34) reduces to

$$U_0 = \frac{1}{Nkd}\left(\frac{\pi}{2}\right)^2\left[\frac{\pi}{2} + \frac{2}{\pi} - 1.8515\right] = \frac{0.871}{Nkd} \tag{6-50}$$

which can also be written as

$$U_0 = \frac{0.871}{Nkd} = \frac{1.742}{2Nkd} = 0.554\left(\frac{\pi}{2Nkd}\right) \tag{6-50a}$$

The average value of the radiation intensity as given by (6-50a) is 0.554 times that for the ordinary end-fire array of (6-48b). Thus the directivity can be expressed, using (6-50a), as

$$D_0 = \frac{U_{max}}{U_0} = \frac{1}{0.554}\left[\frac{2Nkd}{\pi}\right] = 1.805\left[4N\left(\frac{d}{\lambda}\right)\right] \tag{6-51}$$

which is 1.805 times that of the ordinary end-fire array as given by (6-49). Using (6-43), (6-51) can also be written as

$$D_0 = 1.805\left[4N\left(\frac{d}{\lambda}\right)\right] = 1.805\left[4\left(1 + \frac{L}{d}\right)\frac{d}{\lambda}\right] \tag{6-51a}$$

which for a large array ($L \gg d$) reduces to

$$D_0 = 1.805\left[4N\left(\frac{d}{\lambda}\right)\right] = 1.805\left[4\left(1 + \frac{L}{d}\right)\left(\frac{d}{\lambda}\right)\right] \simeq 1.805\left[4\left(\frac{L}{\lambda}\right)\right] \tag{6-51b}$$

Example 6.5

Given a linear, end-fire (with improved directivity) Hansen-Woodyard, uniform array of 10 elements ($N = 10$) with a separation of $\lambda/4$ ($d = \lambda/4$) between the elements, find the directivity of the array factor. This array is identical to that of Examples 6.3 (broadside) and 6.4 (ordinary end-fire), and it is used for comparison.

SOLUTION

Using (6-51b)

$$D_0 = 1.805\left[4N\left(\frac{d}{\lambda}\right)\right] = 18.05(\text{dimensionless}) = 10\log_{10}(18.05) = 12.56\ \text{dB}$$

INTEL-1045
U.S. Patent 7,151,430

The value of this directivity ($D_0 = 18.05$) is 1.805 times greater than that of Example 6.4 (ordinary end-fire) and 3.578 times greater than that found in Example 6.3 (broadside).

Table 6.7 lists the directivities for broadside, ordinary end-fire, and Hansen-Woodyard arrays.

6.5 DESIGN PROCEDURE

In the design of any antenna system, the most important design parameters are usually the number of elements, spacing between the elements, excitation (amplitude and phase), half-power beamwidth, directivity, and side lobe level. In a design procedure some of these parameters are specified and the others are then determined.

The parameters that are specified and those that are determined vary among designs. For a uniform array, other than for the Hansen-Woodyard end-fire, the side lobe is always approximately -13.5 dB. For the Hansen-Woodyard end-fire array the side lobe level is somewhat compromised above the -13.5 dB in order to gain about 1.805 (or 2.56 dB) in directivity. The order in which the other parameters are specified and determined varies among designs. For each of the uniform linear arrays that have been discussed, equations and some graphs have been presented which can be used to determine the half-power beamwidth and directivity, once the number of elements and spacing (or the total length of the array) are specified. In fact, some of the equations have been boxed or listed in tables. This may be considered more of an analysis procedure. The other approach is to specify the half-power beamwidth or directivity and to determine most of the others. This can be viewed more as a design approach, and can be accomplished to a large extent with equations or graphs that have been presented. More exact values can be obtained, if necessary, using iterative methods.

Example 6.6

Design a uniform linear scanning array whose maximum of the array factor is 30° from the axis of the array ($\theta = 30°$). The desired half-power beamwidth is 2° while the spacing between the elements is $\lambda/4$. Determine the excitation of the elements (amplitude and phase), length of the array (in wavelengths), number of elements, and directivity (in dB).

SOLUTION

Since the desired design is a uniform linear scanning array, the amplitude excitation is uniform. However, the progressive phase between the elements is, using (6-21)

$$\beta = -kd\cos\theta_0 = -\frac{2\pi}{\lambda}\left(\frac{\lambda}{4}\right)\cos(30°) = -1.36 \text{ radians} = -77.94°$$

The length of the array is obtained using an iterative procedure of (6-22) or its graphical solution of Figure 6.11. Using the graph of Figure 6.11 for a scan angle of 30° and 2° half-power beamwidth, the approximate length plus one spacing ($L + d$)

INTEL-1045
U.S. Patent 7,151,430

Table 6.7 DIRECTIVITIES FOR BROADSIDE AND END-FIRE ARRAYS

Array	Directivity
BROADSIDE	$D_0 = 2N\left(\frac{d}{\lambda}\right) = 2\left(1 + \frac{L}{d}\right)\frac{d}{\lambda} \simeq 2\left(\frac{L}{\lambda}\right)$ $N\pi d/\lambda \to \infty, L \gg d$
END-FIRE (ORDINARY)	$D_0 = 4N\left(\frac{d}{\lambda}\right) = 4\left(1 + \frac{L}{d}\right)\frac{d}{\lambda} \simeq 4\left(\frac{L}{\lambda}\right)$ $2N\pi d/\lambda \to \infty, L \gg d$
END-FIRE (HANSEN-WOODYARD)	$D_0 = 1.805\left[4N\left(\frac{d}{\lambda}\right)\right] = 1.805\left[4\left(1 + \frac{L}{d}\right)\frac{d}{\lambda}\right] = 1.805\left[4\left(\frac{L}{\lambda}\right)\right]$ $2N\pi d/\lambda \to \infty, L \gg d$

of the array is 50λ. For the 50λ length plus one spacing dimension from Figure 6.11 and 30° scan angle, (6-22) leads to a half-power beamwidth of 2.03°, which is very close to the desired value of 2°. Therefore, the length of the array for a spacing of $\lambda/4$ is 49.75λ.

Since the length of the array is 49.75λ and the spacing between the elements is $\lambda/4$, the total number of elements is

$$N = \frac{L}{d} + 1 = \left(\frac{L + d}{d}\right) = \frac{50}{1/4} = 200$$

The directivity of the array is obtained using the radiation intensity and the computer program DIRECTIVITY at the end of Chapter 2, and it is equal to 100.72 or 20.03 dB.

6.6 N-ELEMENT LINEAR ARRAY: THREE-DIMENSIONAL CHARACTERISTICS

Up to now, the two-dimensional array factor of an N-element linear array has been investigated. Although in practice only two-dimensional patterns can be measured, a collection of them can be used to reconstruct the three-dimensional characteristics of an array. It would then be instructive to examine the three-dimensional patterns of an array of elements. Emphasis will be placed on the array factor.

6.6.1 N-Elements Along Z-Axis

A linear array of N isotropic elements are positioned along the z-axis and are separated by a distance d, as shown in Figure 6.5(a). The amplitude excitation of each element is a_n and there exists a progressive phase excitation β between the elements. For far-field observations, the array factor can be written according to (6-6) as

$$\text{AF} = \sum_{n=1}^{N} a_n e^{j(n-1)(kd\cos\gamma+\beta)} = \sum_{n=1}^{N} a_n e^{j(n-1)\psi} \tag{6-52}$$

$$\psi = kd\cos\gamma + \beta \tag{6-52a}$$

INTEL-1045
U.S. Patent 7,151,430

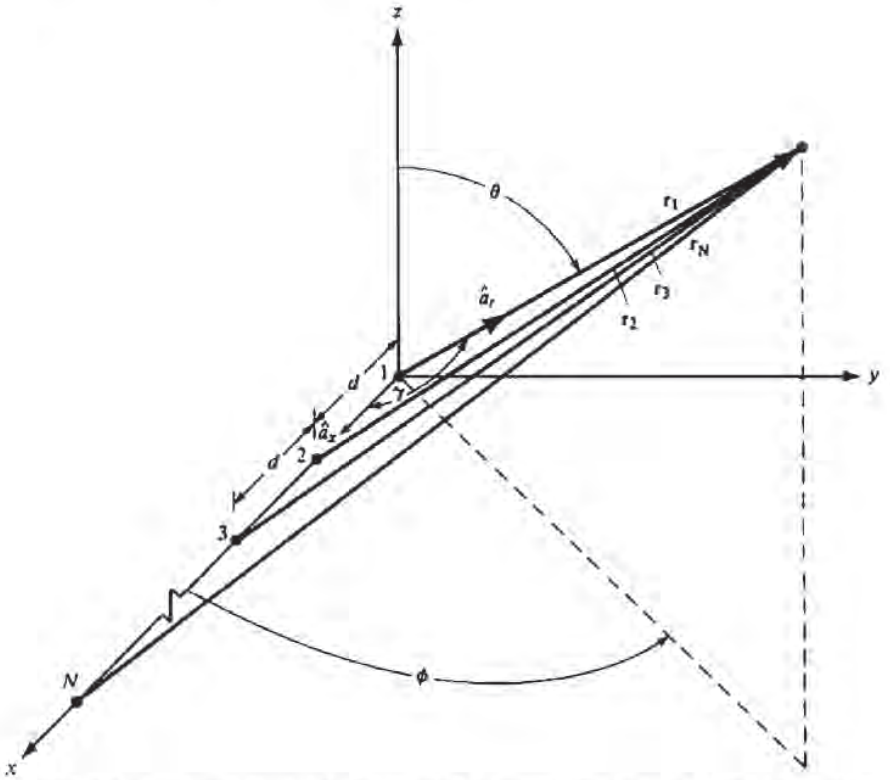


Figure 6.14 Linear array of N isotropic elements positioned along the x-axis.

where the a_n's are the amplitude excitation coefficients and γ is the angle between the axis of the array (z-axis) and the radial vector from the origin to the observation point.

In general, the angle γ can be obtained from the dot product of a unit vector along the axis of the array with a unit vector directed toward the observation point. For the geometry of Figure 6.5(a)

$$\cos\gamma = \hat{\mathbf{a}}_z \cdot \hat{\mathbf{a}}_r = \hat{\mathbf{a}}_z \cdot (\hat{\mathbf{a}}_x \sin\theta\cos\phi + \hat{\mathbf{a}}_y \sin\theta\sin\phi + \hat{\mathbf{a}}_z \cos\theta) = \cos\theta \Rightarrow \gamma = \theta \tag{6-53}$$

Thus (6-52) along with (6-53) is identical to (6-6), because the system of Figure 6.5(a) possesses a symmetry around the z-axis (no ϕ variations). This is not the case when the elements are placed along any of the other axes, as will be shown next.

6.6.2 *N*-Elements Along *X*- or *Y*-Axis

To demonstrate the facility that a "sound" coordinate system and geometry can provide in the solution of a problem, let us consider an array of N isotropic elements along the x-axis, as shown in Figure 6.14. The far-zone array factor for this array is identical in form to that of Figure 6.5(a) except for the phase factor ψ. For this geometry

$$\cos\gamma = \hat{\mathbf{a}}_x \cdot \hat{\mathbf{a}}_r = \hat{\mathbf{a}}_x \cdot (\hat{\mathbf{a}}_x \sin\theta\cos\phi + \hat{\mathbf{a}}_y \sin\theta\sin\phi + \hat{\mathbf{a}}_z \cos\theta) = \sin\theta\cos\phi \tag{6-54}$$

$$\cos\gamma = \sin\theta\cos\phi \Rightarrow \gamma = \cos^{-1}(\sin\theta\cos\phi) \tag{6-54a}$$

INTEL-1045
U.S. Patent 7,151,430

The array factor of this array is also given by (6-52) but with γ defined by (6-54a). For this system, the array factor is a function of both angles (θ and ϕ).

In a similar manner, the array factor for N isotropic elements placed along the y-axis is that of (6-52) but with γ defined by

$$\cos\gamma = \hat{\mathbf{a}}_y \cdot \hat{\mathbf{a}}_r = \sin\theta\sin\phi \Rightarrow \gamma = \cos^{-1}(\sin\theta\sin\phi) \tag{6-55}$$

Physically placing the elements along the z-, x-, or y-axis does not change the characteristics of the array. Numerically they yield identical patterns even though their mathematical forms are different.

Example 6.7

Two half-wavelength dipole ($l = \lambda/2$) are positioned along the x-axis and are separated by a distance d, as shown in Figure 6.15. The lengths of the dipoles are parallel to the z-axis. Find the total field of the array. Assume uniform amplitude excitation and a progressive phase difference of β.

SOLUTION

The field pattern of a single element placed at the origin is given by (4-84) as

$$E_\theta = j\eta\frac{I_0 e^{-jkr}}{2\pi r}\left[\frac{\cos\left(\frac{\pi}{2}\cos\theta\right)}{\sin\theta}\right]$$

Using (6-52), (6-54a), and (6-10c), the array factor can be written as

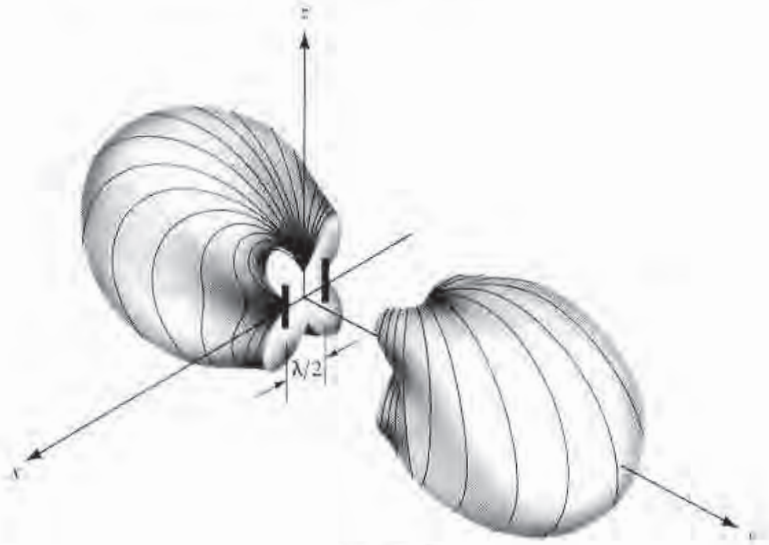
$$(\mathrm{AF})_n = \frac{\sin(kd\sin\theta\cos\phi + \beta)}{2\sin[\frac{1}{2}(kd\sin\theta\cos\phi + \beta)]}$$

The total field of the array is then given, using the pattern multiplication rule of (6-5), by

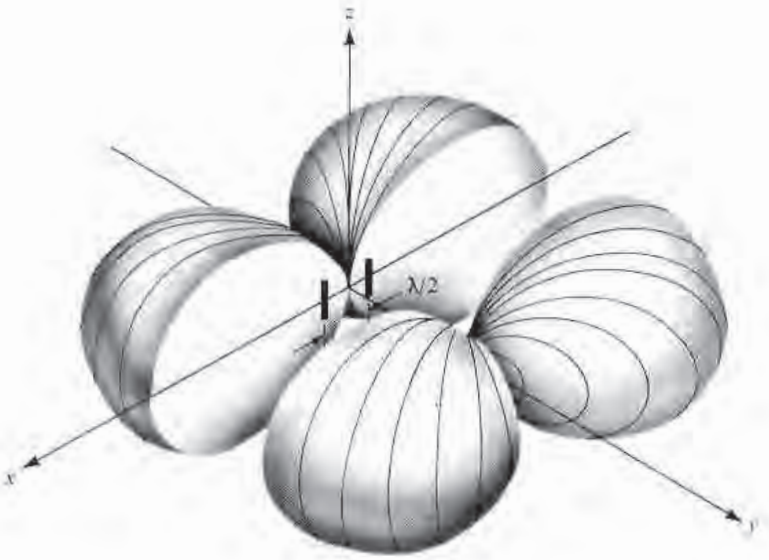
$$E_{\theta t} = E_\theta \cdot (\mathrm{AF})_n = j\eta\frac{I_0 e^{-jkr}}{2\pi r}\frac{\cos\left(\frac{\pi}{2}\cos\theta\right)}{\sin\theta}\left[\frac{\sin(kd\sin\theta\cos\phi + \beta)}{2\sin[\frac{1}{2}(kd\sin\theta\cos\phi + \beta)]}\right]$$

To illustrate the techniques, the three-dimensional patterns of the two-element array of Example 6.7 have been sketched in Figures 6.15(a) and (b). For both, the element separation is $\lambda/2$ ($d = \lambda/2$). For the pattern of Figure 6.15(a), the phase excitation between the elements is identical ($\beta = 0$). In addition to the nulls in the $\theta = 0°$ direction, provided by the individual elements of the array, there are additional nulls along the x-axis ($\theta = \pi/2$, $\phi = 0$ and $\phi = \pi$) provided by the formation of

INTEL-1045
U.S. Patent 7,151,430



(a) $\beta = 0°$



(b) $\beta = \pm 180°$

Figure 6.15 Three-dimensional patterns for two λ/2 dipoles spaced λ/2. (SOURCE: P. Lorrain and D. R. Corson, *Electromagnetic Fields and Waves*, 2nd ed., W. H. Freeman and Co., Copyright © 1970).

the array. The 180° phase difference required to form the nulls along the x-axis is a result of the separation of the elements [$kd = (2\pi/\lambda)(\lambda/2) = \pi$].

To form a comparison, the three-dimensional pattern of the same array but with a 180° phase excitation ($\beta = 180°$) between the elements is sketched in Figure 6.15(b). The overall pattern of this array is quite different from that shown in Figure 6.15(a). In addition to the nulls along the z-axis ($\theta = 0°$) provided by the individual elements, there are nulls along the y-axis formed by the 180° excitation phase difference.

INTEL-1045
U.S. Patent 7,151,430

6.7 RECTANGULAR-TO-POLAR GRAPHICAL SOLUTION

In antenna theory, many solutions are of the form

$$f(\zeta) = f(C \cos \gamma + \delta) \tag{6-56}$$

where C and δ are constants and γ is a variable. For example, the approximate array factor of an N-element, uniform amplitude linear array [Equation (6-10d)] is that of a $\sin(\zeta)/\zeta$ form with

$$\zeta = C \cos \gamma + \delta = \frac{N}{2}\psi = \frac{N}{2}(kd \cos \theta + \beta) \tag{6-57}$$

where

$$C = \frac{N}{2}kd \tag{6-57a}$$

$$\delta = \frac{N}{2}\beta \tag{6-57b}$$

Usually the $f(\zeta)$ function can be sketched as a function of ζ in rectilinear coordinates. Since ζ in (6-57) has no physical analog, in many instances it is desired that a graphical representation of $|f(\zeta)|$ be obtained as a function of the physically observable angle θ. This can be constructed graphically from the rectilinear graph, and it forms a polar plot.

The procedure that must be followed in the construction of the polar graph is as follows:

1. Plot, using rectilinear coordinates, the function $|f(\zeta)|$.
2. a. Draw a circle with radius C and with its center on the abscissa at $\zeta = \delta$.
   b. Draw vertical lines to the abscissa so that they will intersect the circle.
   c. From the center of the circle, draw radial lines through the points on the circle intersected by the vertical lines.
   d. Along the radial lines, mark off corresponding magnitudes from the linear plot.
   e. Connect all points to form a continuous graph.

To better illustrate the procedure, the polar graph of the function

$$f(\zeta) = \frac{\sin\left(\frac{N}{2}\psi\right)}{N \sin\left(\frac{\psi}{2}\right)}, \qquad \zeta = \frac{5\pi}{2}\cos\theta - \frac{5\pi}{4} \tag{6-58}$$

has been constructed in Figure 6.16. The function $f(\zeta)$ of (6-58) represents the array factor of a 10-element ($N = 10$) uniform linear array with a spacing of $\lambda/4$ ($d = \lambda/4$) and progressive phase shift of $-\pi/4$ ($\beta = -\pi/4$) between the elements. The constructed graph can be compared with its exact form shown in Figure 6.10.

From the construction of Figure 6.16, it is evident that the angle at which the maximum is directed is controlled by the radius of the circle C and the variable δ.

INTEL-1045
U.S. Patent 7,151,430

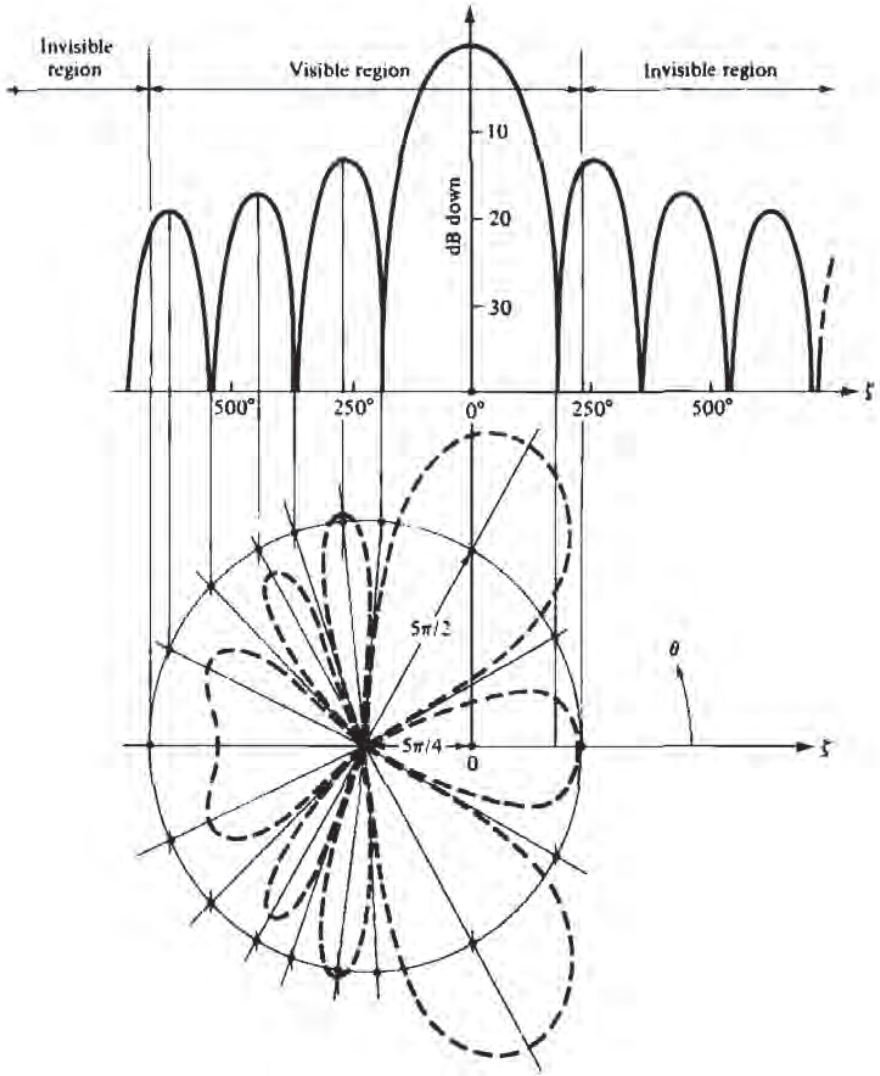


Figure 6.16 Rectangular-to-polar plot graphical solution.

For the array factor of Figure 6.16, the radius C is a function of the number of elements (N) and the spacing between the elements (d). In turn, δ is a function of the number of elements (N) and the progressive phase shift between the elements (β). Making $\delta = 0$ directs the maximum toward $\theta = 90°$ (broadside array). The part of the linear graph that is used to construct the polar plot is determined by the radius of the circle and the relative position of its center along the abscissa. The usable part of the linear graph is referred to as the *visible* region and the remaining part as the *invisible* region. Only the *visible* region of the linear graph is related to the physically observable angle θ (hence its name).

6.8 *N*-ELEMENT LINEAR ARRAY: UNIFORM SPACING, NONUNIFORM AMPLITUDE

The theory to analyze linear arrays with uniform spacing, uniform amplitude, and a progressive phase between the elements was introduced in the previous sections of

INTEL-1045
U.S. Patent 7,151,430

this chapter. A number of numerical and graphical solutions were used to illustrate some of the principles. In this section, broadside arrays with uniform spacing but nonuniform amplitude distribution will be considered. Most of the discussion will be directed toward binomial [4] and Dolph-Tschebyscheff [5] broadside arrays (also spelled Tchebyscheff or Chebyshev).

Of the three distributions (uniform, binomial, and Tschebyscheff), a uniform amplitude array yields the smallest half-power beamwidth. It is followed, in order, by the Dolph-Tschebyscheff and binomial arrays. In contrast, binomial arrays usually possess the smallest side lobes followed, in order, by the Dolph-Tschebyscheff and uniform arrays. As a matter of fact, binomial arrays with element spacing equal or less than $\lambda/2$ have no side lobes. It is apparent that the designer must compromise between side lobe level and beamwidth.

A criterion that can be used to judge the relative beamwidth and side lobe level of one design to another is the amplitude distribution (tapering) along the source. It has been shown analytically that for a given side lobe level the Dolph-Tschebyscheff array produces the smallest beamwidth between the first nulls. Conversely, for a given beamwidth between the first nulls, the Dolph-Tschebyscheff design leads to the smallest possible side lobe level.

Uniform arrays usually possess the largest directivity. However, superdirective (or super gain as most people call them) antennas possess directivities higher than those of a uniform array [6]. Although a certain amount of superdirectivity is practically possible, superdirective arrays require very large currents with opposite phases between adjacent elements. Thus the net total current and efficiency of each array are very small compared to the corresponding values of an individual element.

Before introducing design methods for specific nonuniform amplitude distributions, let us first derive the array factor.

6.8.1 Array Factor

An array of an even number of isotropic elements $2M$ (where M is an integer) is positioned symmetrically along the z-axis, as shown in Figure 6.17(a). The separation between the elements is d, and M elements are placed on each side of the origin. Assuming that the amplitude excitation is symmetrical about the origin, the array factor for a nonuniform amplitude broadside array can be written as

$$\begin{aligned}(\mathrm{AF})_{2M} = {} & a_1 e^{+j(1/2)kd\cos\theta} + a_2 e^{+j(3/2)kd\cos\theta} + \cdots \\ & + a_M e^{+j[(2M-1)/2]kd\cos\theta} \\ & + a_1 e^{-j(1/2)kd\cos\theta} + a_2 e^{-j(3/2)kd\cos\theta} + \cdots \\ & + a_M e^{-j[(2M-1)/2]kd\cos\theta}\end{aligned}$$

$$(\mathrm{AF})_{2M} = 2\sum_{n=1}^{M} a_n \cos\left[\frac{(2n-1)}{2} kd\cos\theta\right] \tag{6-59}$$

which in normalized form reduces to

$$(\mathrm{AF})_{2M} = \sum_{n=1}^{M} a_n \cos\left[\frac{(2n-1)}{2} kd\cos\theta\right] \tag{6-59a}$$

where a_n's are the excitation coefficients of the array elements.

If the total number of isotropic elements of the array is odd $2M + 1$ (where M is an integer), as shown in Figure 6.17(b), the array factor can be written as

INTEL-1045
U.S. Patent 7,151,430

$$(AF)_{2M+1} = 2a_1 + a_2 e^{+jkd\cos\theta} + a_3 e^{j2kd\cos\theta} + \ldots + a_{M+1} e^{jMkd\cos\theta} + a_2 e^{-jkd\cos\theta} + a_3 e^{-j2kd\cos\theta} + \ldots + a_{M+1} e^{-jMkd\cos\theta}$$

$$(AF)_{2M+1} = 2\sum_{n=1}^{M+1} a_n \cos[(n-1)\,kd\cos\theta] \tag{6-60}$$

which in normalized form reduces to

$$(AF)_{2M+1} = \sum_{n=1}^{M+1} a_n \cos[(n-1)\,kd\cos\theta] \tag{6-60a}$$

The amplitude excitation of the center element is $2a_1$.

Equations (6-59a) and (6-60a) can be written as

$$(AF)_{2M}\,(\text{even}) = \sum_{n=1}^{M} a_n \cos[(2n-1)u] \tag{6-61a}$$

$$(AF)_{2M+1}\,(\text{odd}) = \sum_{n=1}^{M+1} a_n \cos[2(n-1)u] \tag{6-61b}$$

where

$$u = \frac{\pi d}{\lambda}\cos\theta \tag{6-61c}$$

The next step will be to determine the values of the excitation coefficients (a_n's).

6.8.2 Binomial Array

The array factor for the binomial array is represented by (6-61a)–(6-61c) where the a_n's are the excitation coefficients which will now be derived.

A. Excitation Coefficients

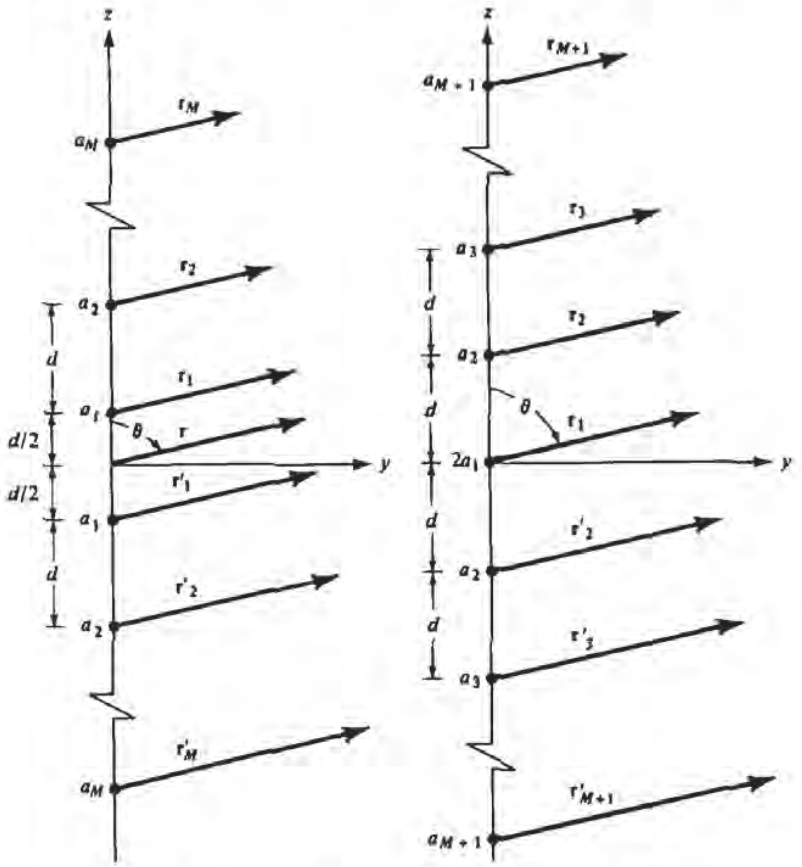
To determine the excitation coefficients of a binomial array, J. S. Stone [4] suggested that the function $(1+x)^{m-1}$ be written in a series, using the binomial expansion, as

$$(1+x)^{m-1} = 1 + (m-1)\,x + \frac{(m-1)(m-2)}{2!}x^2 + \frac{(m-1)(m-2)(m-3)}{3!}x^3 + \cdots \tag{6-62}$$

The positive coefficients of the series expansion for different values of m are

$$\begin{array}{lccccccccccc}
m=1 & & & & & & 1 & & & & & \\
m=2 & & & & & 1 & & 1 & & & & \\
m=3 & & & & 1 & & 2 & & 1 & & & \\
m=4 & & & 1 & & 3 & & 3 & & 1 & & \\
m=5 & & 1 & & 4 & & 6 & & 4 & & 1 & \\
m=6 & 1 & & 5 & & 10 & & 10 & & 5 & & 1 \\
m=7 & & 1 & & 6 & & 15 & & 20 & & 15 & \\
m=8 & & & 1 & & 7 & & 21 & & 35 & & \\
m=9 & & & & 1 & & 8 & & 28 & & 56 & \\
m=10 & & & & & 1 & & 9 & & 36 & & \\
\end{array} \tag{6-63}$$

INTEL-1045
U.S. Patent 7,151,430



(a) Even number of elements (b) Odd number of elements

Figure 6.17 Nonuniform amplitude arrays of even and odd number of elements.

The above represents Pascal's triangle. If the values of m are used to represent the number of elements of the array, then the coefficients of the expansion represent the relative amplitudes of the elements. Since the coefficients are determined from a binomial series expansion, the array is known as a *binomial array*.

Referring to (6-61a), (6-61b), and (6-63), the amplitude coefficients for the following arrays are:

1. Two elements ($2M = 2$)

$$a_1 = 1$$

2. Three elements ($2M + 1 = 3$)

$$2a_1 = 2 \Rightarrow a_1 = 1$$
$$a_2 = 1$$

3. Four elements ($2M = 4$)

$$a_1 = 3$$
$$a_2 = 1$$

INTEL-1045
U.S. Patent 7,151,430

4. Five elements ($2M + 1 = 5$)

$$2a_1 = 6 \hookrightarrow a_1 = 3$$
$$a_2 = 4$$
$$a_3 = 1$$

The coefficients for other arrays can be determined in a similar manner.

B. Design Procedure

One of the objectives of any method is its use in a design. For the binomial method, as for any other nonuniform array method, one of the requirements is the amplitude excitation coefficients for a given number of elements. This can be accomplished using either (6-62) or the Pascal triangle of (6-63) or extensions of it. Other figures of merit are the directivity, half-power beamwidth and side lobe level. It already has been stated that the binomial arrays do not exhibit any minor lobes provided the spacing between the elements is equal or less than one-half of a wavelength. Unfortunately, closed form expressions for the directivity and half-power beamwidth for binomial arrays of any spacing between the elements are not available. However, because the design using a $\lambda/2$ spacing leads to a pattern with no minor lobes, approximate closed form expressions for the half-power beamwidth and maximum directivity for the $d = \lambda/2$ spacing only have been derived [7] in terms of the numbers of elements or the length of the array, and they are given, respectively, by

$$\text{HPBW}\ (d = \lambda/2) \simeq \frac{1.06}{\sqrt{N-1}} = \frac{1.06}{\sqrt{2L/\lambda}} = \frac{0.75}{\sqrt{L/\lambda}} \tag{6-64}$$

$$D_0 = \frac{2}{\displaystyle\int_0^{\pi} \left[\cos\left(\frac{\pi}{2}\cos\theta\right)\right]^{2(N-1)} \sin\theta\, d\theta} \tag{6-65}$$

$$D_0 = \frac{(2N-2)(2N-4)\cdots 2}{(2N-3)(2N-5)\cdots 1} \tag{6-65a}$$

$$D_0 \simeq 1.77\sqrt{N} = 1.77\sqrt{1 + 2L/\lambda} \tag{6-65b}$$

These expressions can be used effectively to design binomial arrays with a desired half-power beamwidth or directivity. The value of the directivity as obtained using (6-65) to (6-65b) can be compared with the value using the array factor and the computer program DIRECTIVITY at the end of Chapter 2.

To illustrate the method, the patterns of a 10-element binomial array ($2M = 10$) with spacings between the elements of $\lambda/4$, $\lambda/2$, $3\lambda/4$, and λ, respectively, have been plotted in Figure 6.18. The patterns are plotted using (6-61a) and (6-61c) with the coefficients of $a_1 = 126$, $a_2 = 84$, $a_3 = 36$, $a_4 = 9$, and $a_5 = 1$. It is observed that there are no minor lobes for the arrays with spacings of $\lambda/4$ and $\lambda/2$ between the elements. While binomial arrays have very low level minor lobes, they exhibit larger beamwidths (compared to uniform and Dolph-Tschebyscheff designs). A major practical disadvantage of binomial arrays is the wide variations between the amplitudes of the different elements of an array, especially for an array with a large number of elements. This leads to very low efficiencies, and it makes the method not very desirable in practice. For example, the relative amplitude coefficient of the end elements of a 10-element array is 1 while that of the center element is 126. Practically, it would be difficult to obtain and maintain such large amplitude variations among

INTEL-1045
U.S. Patent 7,151,430

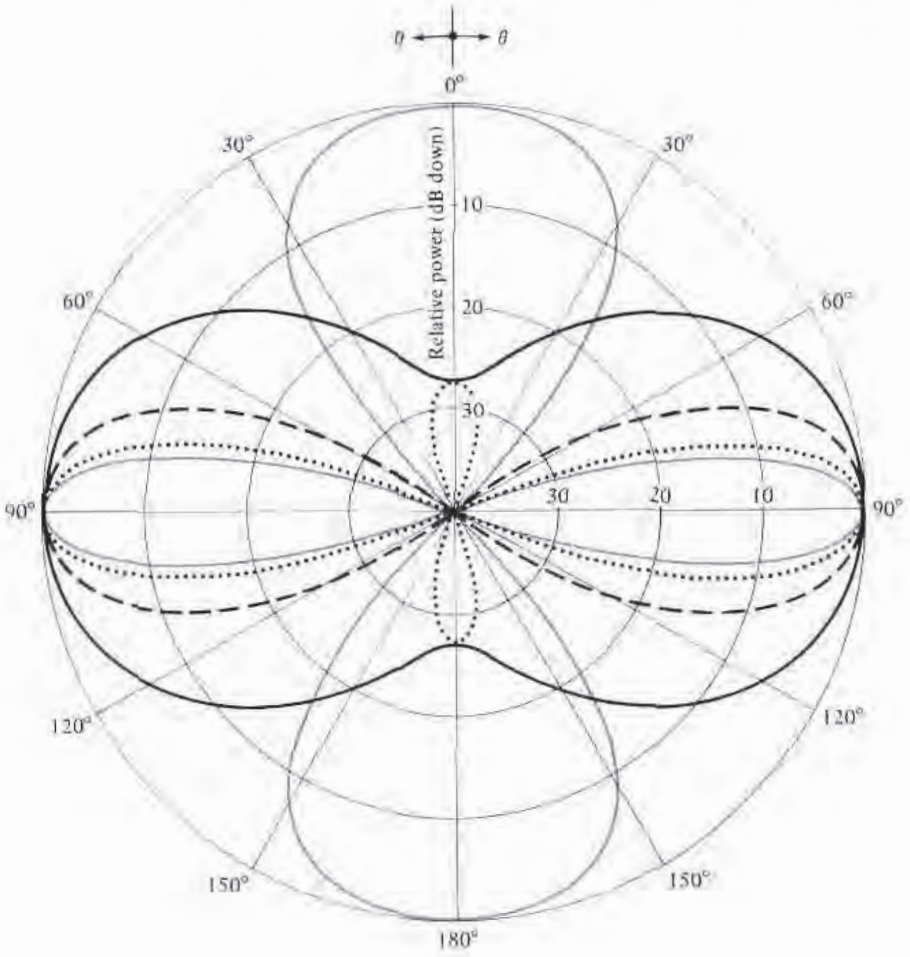


Figure 6.18 Array factor power patterns for a 10-element broadside binomial array with $N = 10$ and $d = \lambda/4, \lambda/2, 3\lambda/4$, and λ.

the elements. They would also lead to very inefficient antennas. Because the magnitude distribution is monotonically decreasing from the center toward the edges and the magnitude of the extreme elements is negligible compared to those toward the center, a very low side lobe level is expected.

Example 6.8

For a 10-element binomial array with a spacing of $\lambda/2$ between the elements, whose amplitude pattern is displayed in Figure 6.18, determine the half-power beamwidth (in degrees) and the maximum directivity (in dB). Compare the answers with other available data.

INTEL-1045
U.S. Patent 7,151,430

SOLUTION

Using (6-64), the half-power beamwidth is equal to

$$\text{HPBW} = \frac{1.06}{\sqrt{10-1}} = \frac{1.06}{3} = 0.353 \text{ radians} = 20.23^\circ$$

The value obtained using the array factor, whose pattern is shown in Figure 6.18, is 20.5° which compares well with approximate value.

Using (6-65a), the value of the directivity is equal for $N = 10$

$$D_0 = 5.392 = 7.32 \text{ dB}$$

while the value obtained using (6-65b) is

$$D_0 = 1.77\sqrt{10} = 5.597 = 7.48 \text{ dB}$$

The value obtained using the array factor and the computer program DIRECTIVITY is $D_0 = 5.392 = 7.32$ dB. These values compare favorably with each other.

6.8.3 Dolph-Tschebyscheff Array

Another array, with many practical applications, is the *Dolph-Tschebyscheff array*. The method was originally introduced by Dolph [5] and investigated afterward by others [8]–[11]. It is primarily a compromise between uniform and binomial arrays. Its excitation coefficients are related to Tschebyscheff polynomials. A Dolph-Tschebyscheff array with no side lobes (or side lobes of $-\infty$ dB) reduces to the binomial design. The excitation coefficients for this case, as obtained by both methods, would be identical.

A. Array Factor

Referring to (6-61a) and (6-61b), the array factor of an array of even or odd number of elements with symmetric amplitude excitation is nothing more than a summation of M or $M + 1$ cosine terms. The largest harmonic of the cosine terms is one less than the total number of elements of the array. Each cosine term, whose argument is an integer times a fundamental frequency, can be rewritten as a series of cosine functions with the fundamental frequency as the argument. That is,

$$\begin{aligned}
m &= 0 \quad \cos(mu) = 1 \\
m &= 1 \quad \cos(mu) = \cos u \\
m &= 2 \quad \cos(mu) = \cos(2u) = 2\cos^2 u - 1 \\
m &= 3 \quad \cos(mu) = \cos(3u) = 4\cos^3 u - 3\cos u \\
m &= 4 \quad \cos(mu) = \cos(4u) = 8\cos^4 u - 8\cos^2 u + 1 \\
m &= 5 \quad \cos(mu) = \cos(5u) = 16\cos^5 u - 20\cos^3 u + 5\cos u \\
m &= 6 \quad \cos(mu) = \cos(6u) = 32\cos^6 u - 48\cos^4 u + 18\cos^2 u - 1 \\
m &= 7 \quad \cos(mu) = \cos(7u) = 64\cos^7 u - 112\cos^5 u + 56\cos^3 u - 7\cos u \\
m &= 8 \quad \cos(mu) = \cos(8u) = 128\cos^8 u - 256\cos^6 u + 160\cos^4 u \\
&\qquad\qquad - 32\cos^2 u + 1 \\
m &= 9 \quad \cos(mu) = \cos(9u) = 256\cos^9 u - 576\cos^7 u + 432\cos^5 u \\
&\qquad\qquad - 120\cos^3 u + 9\cos u
\end{aligned} \tag{6-66}$$

INTEL-1045
U.S. Patent 7,151,430

The above are obtained by the use of Euler's formula

$$[e^{ju}]^m = (\cos u + j \sin u)^m = e^{jmu} = \cos(mu) + j \sin(mu) \tag{6-67}$$

and the trigonometric identity $\sin^2 u = 1 - \cos^2 u$.

If we let

$$z = \cos u \tag{6-68}$$

(6-66) can be written as

$$\begin{aligned}
m &= 0 \quad \cos(mu) = 1 = T_0(z) \\
m &= 1 \quad \cos(mu) = z = T_1(z) \\
m &= 2 \quad \cos(mu) = 2z^2 - 1 = T_2(z) \\
m &= 3 \quad \cos(mu) = 4z^3 - 3z = T_3(z) \\
m &= 4 \quad \cos(mu) = 8z^4 - 8z^2 + 1 = T_4(z) \\
m &= 5 \quad \cos(mu) = 16z^5 - 20z^3 + 5z = T_5(z) \\
m &= 6 \quad \cos(mu) = 32z^6 - 48z^4 + 18z^2 - 1 = T_6(z) \\
m &= 7 \quad \cos(mu) = 64z^7 - 112z^5 + 56z^3 - 7z = T_7(z) \\
m &= 8 \quad \cos(mu) = 128z^8 - 256z^6 + 160z^4 - 32z^2 + 1 = T_8(z) \\
m &= 9 \quad \cos(mu) = 256z^9 - 576z^7 + 432z^5 - 120z^3 + 9z = T_9(z)
\end{aligned} \tag{6-69}$$

and each is related to a Tschebyscheff (Chebyshev) polynomial $T_m(z)$. These relations between the cosine functions and the Tschebyscheff polynomials are valid only in the $-1 \le z \le +1$ range. Because $|\cos(mu)| \le 1$, each Tschebyscheff polynomial is $|T_m(z)| \le 1$ for $-1 \le z \le +1$. For $|z| > 1$, the Tschebyscheff polynomials are related to the hyperbolic cosine functions.

The recursion formula for Tschebyscheff polynomials is

$$\boxed{T_m(z) = 2zT_{m-1}(z) - T_{m-2}(z)} \tag{6-70}$$

It can be used to find one Tschebyscheff polynomial if the polynomials of the previous two orders are known. Each polynomial can also be computed using

$$\boxed{\begin{aligned}
T_m(z) &= \cos[m \cos^{-1}(z)] && -1 \le z \le +1 \qquad (6\text{-}71a) \\
T_m(z) &= \cosh[m \cosh^{-1}(z)]\dagger && z < -1, z > +1 \qquad (6\text{-}71b)
\end{aligned}}$$

In Figure 6.19 the first six Tschebyscheff polynomials have been plotted. The following properties of the polynomials are of interest:

1. All polynomials, of any order, pass through the point (1, 1).
2. Within the range $-1 \le z \le 1$, the polynomials have values within -1 to $+1$.
3. All roots occur within $-1 \le z \le 1$, and all maxima and minima have values of $+1$ and -1, respectively.

Since the array factor of an even or odd number of elements is a summation of cosine terms whose form is the same as the Tschebyscheff polynomials, the unknown coefficients of the array factor can be determined by equating the series representing

†$x = \cosh^{-1}(y) = \ln[y \pm (y^2 - 1)^{1/2}]$

INTEL-1045
U.S. Patent 7,151,430

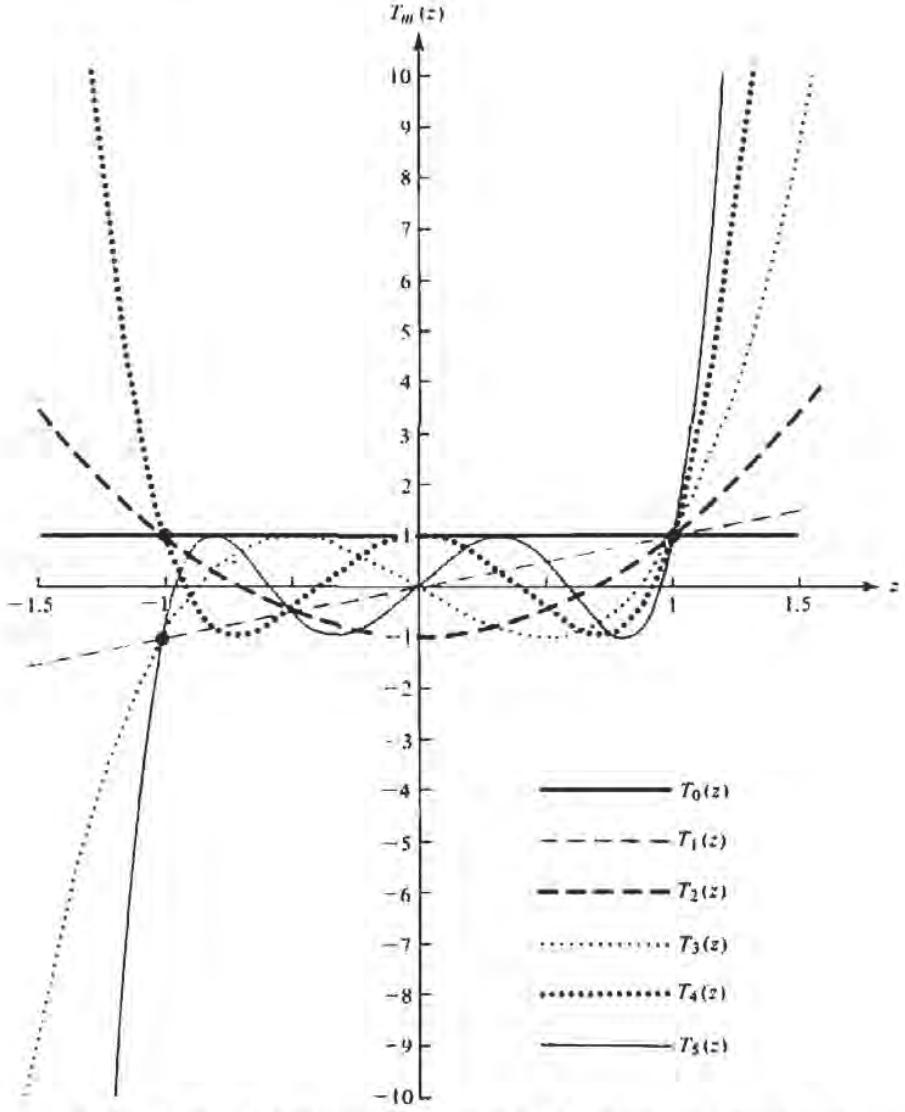


Figure 6.19 Tschebyscheff polynomials of orders zero through five.

the cosine terms of the array factor to the appropriate Tschebyscheff polynomial. *The order of the polynomial should be one less than the total number of elements of the array.*

The design procedure will be outlined first, and it will be illustrated with an example. In outlining the procedure, it will be assumed that the number of elements, spacing between the elements, and ratio of major-to-minor lobe intensity (R_0) are known. The requirements will be to determine the excitation coefficients and the array factor of a Dolph-Tschebyscheff array.

B. Array Design

Statement. Design a broadside Dolph-Tschebyscheff array of $2M$ or $2M + 1$ elements with spacing d between the elements. The side lobes are R_0 dB below the maximum of the major lobe. Find the excitation coefficients and form the array factor.

INTEL-1045
U.S. Patent 7,151,430

Procedure

a. Select the appropriate array factor as given by (6-61a) or (6-61b).

b. Expand the array factor. Replace each $\cos(mu)$ function ($m = 0, 1, 2, 3, \ldots$) by its appropriate series expansion found in (6-66).

c. Determine the point $z = z_0$ such that $T_m(z_0) = R_0$ (voltage ratio). *The order m of the Tschebyscheff polynomial is always one less than the total number of elements.* The design procedure requires that the Tschebyscheff polynomial in the $-1 \leq z \leq z_1$, where z_1 is the null nearest to $z = +1$, be used to represent the minor lobes of the array. The major lobe of the pattern is formed from the remaining part of the polynomial up to point z_0 ($z_1 < z \leq z_0$).

d. Substitute

$$\cos(u) = \frac{z}{z_0} \tag{6-72}$$

in the array factor of step 2. The $\cos(u)$ is replaced by z/z_0, *and not by* z, so that (6-72) would be valid for $|z| \leq |z_0|$. At $|z| = |z_0|$, (6-72) attains its maximum value of unity.

e. Equate the array factor from step 2, after substitution of (6-72), to a $T_m(z)$ from (6-69). The $T_m(z)$ chosen should be of order m where m is an integer equal to one less than the total number of elements of the designed array. This will allow the determination of the excitation coefficients a_n's.

f. Write the array factor of (6-61a) or (6-61b) using the coefficients found in step 5.

Example 6.9

Design a broadside Dolph-Tschebyscheff array of 10 elements with spacing d between the elements and with a major-to-minor lobe ratio of 26 dB. Find the excitation coefficients and form the array factor.

SOLUTION

1. The array factor is given by (6-61a) and (6-61c). That is,

$$(\mathrm{AF})_{2M} = \sum_{n=1}^{M=5} a_n \cos[(2n-1)u]$$

$$u = \frac{\pi d}{\lambda}\cos\theta$$

2. When expanded, the array factor can be written as

$$(\mathrm{AF})_{10} = a_1\cos(u) + a_2\cos(3u) + a_3\cos(5u) + a_4\cos(7u) + a_5\cos(9u)$$

Replace $\cos(u)$, $\cos(3u)$, $\cos(5u)$, $\cos(7u)$, and $\cos(9u)$ by their series expansions found in (6-66).

3. R_0 (dB) $= 26 = 20\log_{10}(R_0)$ or R_0 (voltage ratio) $= 20$. Determine z_0 by equating R_0 to $T_9(z_0)$. Thus

$$R_0 = 20 = T_9(z_0) = \cosh[9\cosh^{-1}(z_0)]$$

INTEL-1045
U.S. Patent 7,151,430

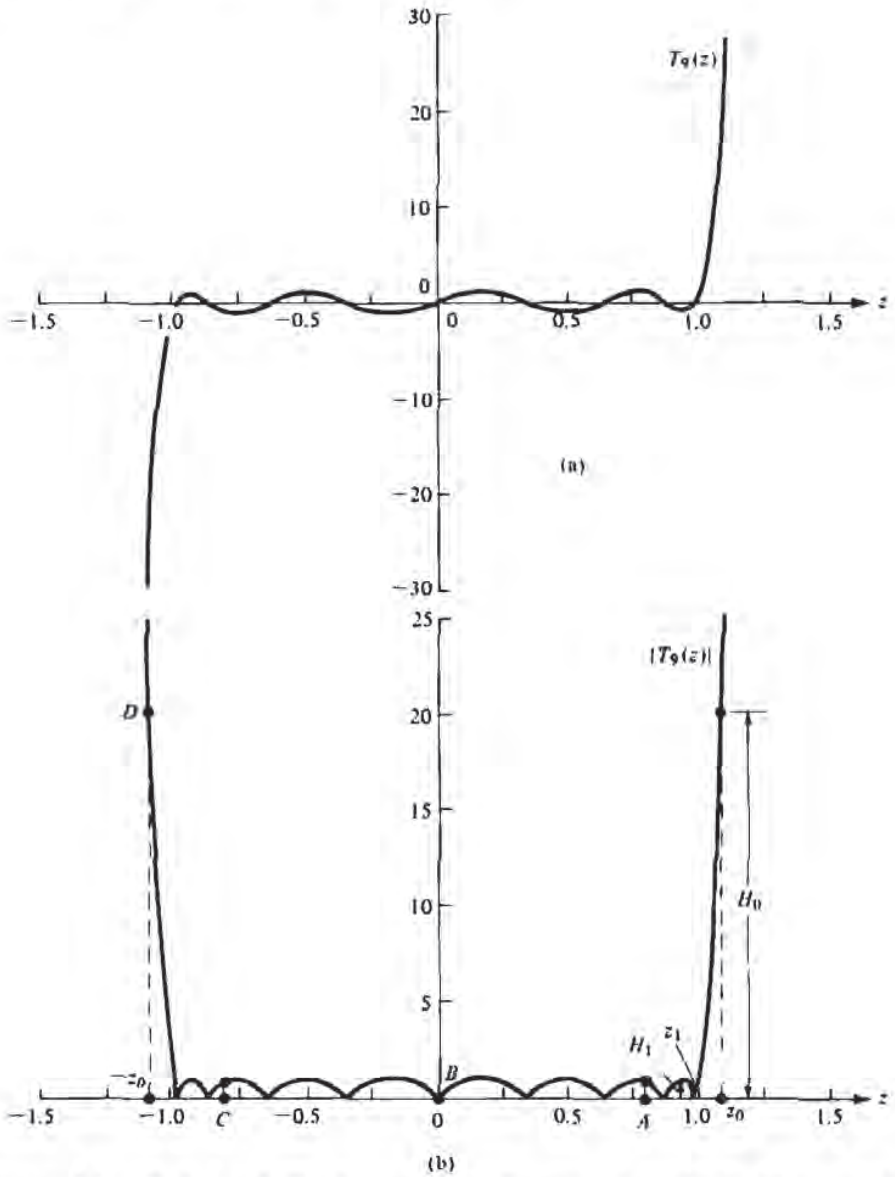


Figure 6.20 Tschebyscheff polynomial of order nine (a) amplitude (b) magnitude.

or

$$z_0 = \cosh[\tfrac{1}{9}\cosh^{-1}(20)] = 1.0851$$

Another equation which can, in general, be used to find z_0 and does not require hyperbolic functions is [8]

$$\boxed{z_0 = \frac{1}{2}\left[\left(R_0 + \sqrt{R_0^2 - 1}\right)^{1/P} + \left(R_0 - \sqrt{R_0^2 - 1}\right)^{1/P}\right]} \qquad (6\text{-}73)$$

where P is an integer equal to one less than the number of array elements (in this case $P = 9$). $R_0 = H_0/H_1$ and z_0 are identified in Figure 6.20.

INTEL-1045
U.S. Patent 7,151,430

4. Substitute

$$\cos(u) = \frac{z}{z_0} = \frac{z}{1.0851}$$

in the array factor found in step 2.

5. Equate the array factor of step 2, after the substitution from step 4, to $T_9(z)$. The polynomial $T_9(z)$ is shown plotted in Figure 6.20. Thus

$$\begin{aligned}(\mathrm{AF})_{10} = {} & z[(a_1 - 3a_2 + 5a_3 - 7a_4 + 9a_5)/z_0] \\ & + z^3[(4a_2 - 20a_3 + 56a_4 - 120a_5)/z_0^3] \\ & + z^5[(16a_3 - 112a_4 + 432a_5)/z_0^5] \\ & + z^7[(64a_4 - 576a_5)/z_0^7] \\ & + z^9[(256a_5)/z_0^9] \\ = {} & 9z - 120z^3 + 432z^5 - 576z^7 + 256z^9\end{aligned}$$

Matching similar terms allows the determination of the a_n's. That is,

$$\begin{aligned}256a_5/z_0^9 &= 256 && \Rightarrow a_5 = 2.0860 \\ (64a_4 - 576a_5)/z_0^7 &= -576 && \Rightarrow a_4 = 2.8308 \\ (16a_3 - 112a_4 + 432a_5)/z_0^5 &= 432 && \Rightarrow a_3 = 4.1184 \\ (4a_2 - 20a_3 + 56a_4 - 120a_5)/z_0^3 &= -120 && \Rightarrow a_2 = 5.2073 \\ (a_1 - 3a_2 + 5a_3 - 7a_4 + 9a_5)/z_0 &= 9 && \Rightarrow a_1 = 5.8377\end{aligned}$$

In normalized form, the a_n coefficients can be written as

$$\begin{array}{lll} a_5 = 1 & & a_5 = 0.357 \\ a_4 = 1.357 & & a_4 = 0.485 \\ a_3 = 1.974 & \text{or} & a_3 = 0.706 \\ a_2 = 2.496 & & a_2 = 0.890 \\ a_1 = 2.798 & & a_1 = 1 \end{array}$$

The first (left) set is normalized with respect to the amplitude of the elements at the edge while the other (right) is normalized with respect to the amplitude of the center element.

6. Using the first (left) set of normalized coefficients, the array factor can be written as

$$\begin{aligned}(\mathrm{AF})_{10} = {} & 2.798\cos(u) + 2.496\cos(3u) + 1.974\cos(5u) \\ & + 1.357\cos(7u) + \cos(9u)\end{aligned}$$

where $u = [(\pi d/\lambda)\cos\theta]$.

The array factor patterns of Example 6.9 for $d = \lambda/4$ and $\lambda/2$ are shown plotted in Figure 6.21. Since the spacing is less than $\lambda(d < \lambda)$, maxima exist only at broadside ($\theta = 90°$). However when the spacing is equal to $\lambda(d = \lambda)$, two more maxima appear (one toward $\theta = 0°$ and the other toward $\theta = 180°$). For $d = \lambda$ the array has four maxima, and it acts as an *end-fire* as well as a *broadside* array.

INTEL-1045
U.S. Patent 7,151,430

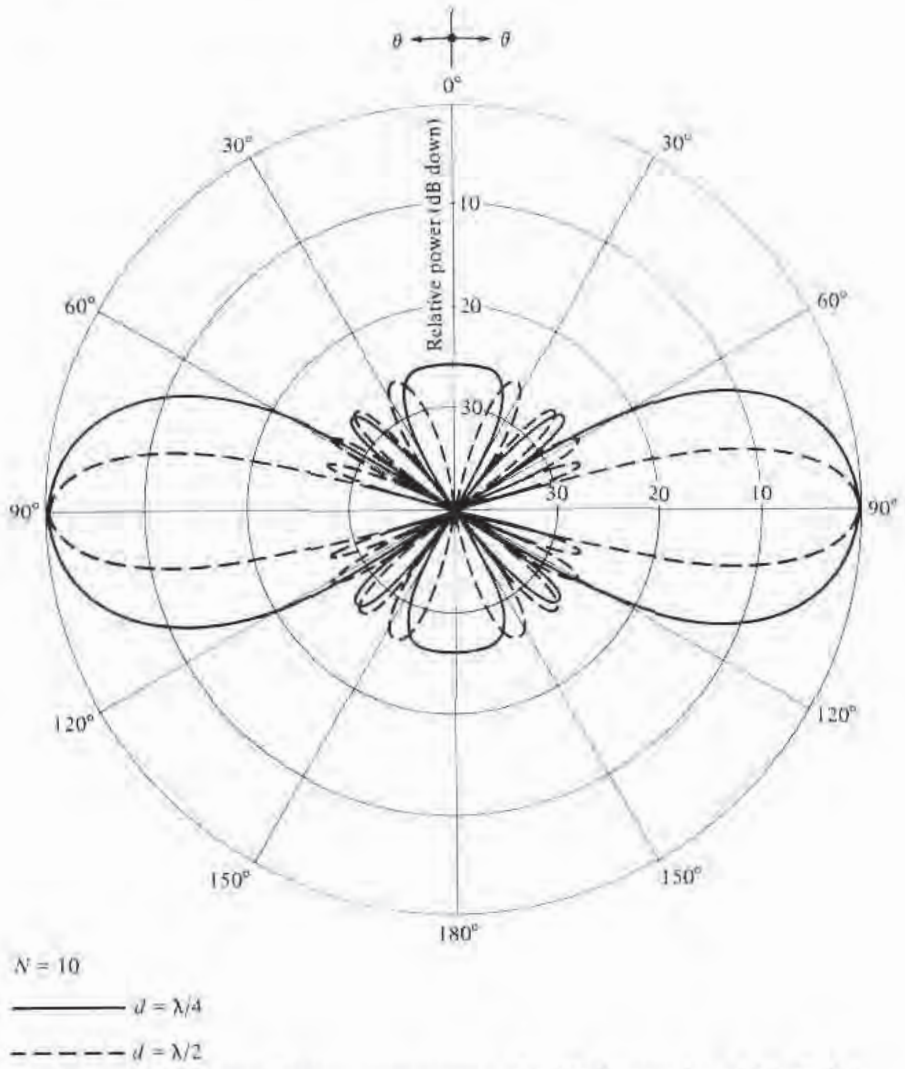


Figure 6.21 Array factor power pattern of a 10-element broadside Dolph-Tschebyscheff array.

To better illustrate how the pattern of a Dolph-Tschebyscheff array is formed from the Tschebyscheff polynomial, let us again consider the 10-element array whose corresponding Tschebyscheff polynomial is of order 9 and is shown plotted in Figure 6.20. The abscissa of Figure 6.20, in terms of the spacing between the elements (d) and the angle θ, is given by (6-72) or

$$z = z_0 \cos u = z_0 \cos\left(\frac{\pi d}{\lambda}\cos\theta\right) = 1.0851 \cos\left(\frac{\pi d}{\lambda}\cos\theta\right) \qquad (6\text{-}74)$$

For $d = \lambda/4$, $\lambda/2$, $3\lambda/4$, and λ the values of z for angles from $\theta = 0°$ to $90°$ to $180°$ are shown tabulated in Table 6.8. Referring to Table 6.8 and Figure 6.20, it is interesting to discuss the pattern formation for the different spacings.

1. $d = \lambda/4$, $N = 10$, $R_0 = 20$

At $\theta = 0°$ the value of z is equal to 0.7673 (point A). As θ attains larger values,

INTEL-1045
U.S. Patent 7,151,430

Table 6.8 VALUES OF THE ABSCISSA z AS A FUNCTION OF θ FOR A 10-ELEMENT DOLPH-TSCHEBYSCHEFF ARRAY WITH $R_0 = 20$

	$d = \lambda/4$	$d = \lambda/2$	$d = 3\lambda/4$	$d = \lambda$
θ	z (Eq. 6-74)	z (Eq. 6-74)	z (Eq. 6-74)	z (Eq. 6-74)
0°	0.7673	0.0	−0.7673	−1.0851
10°	0.7764	0.0259	−0.7394	−1.0839
20°	0.8028	0.1026	−0.6509	−1.0657
30°	0.8436	0.2267	−0.4912	−0.9904
40°	0.8945	0.3899	−0.2518	−0.8049
50°	0.9497	0.5774	0.0610	−0.4706
60°	1.0025	0.7673	0.4153	0.0
70°	1.0462	0.9323	0.7514	0.5167
80°	1.0750	1.0450	0.9956	0.9276
90°	1.0851	1.0851	1.0851	1.0851
100°	1.0750	1.0450	0.9956	0.9276
110°	1.0462	0.9323	0.7514	0.5167
120°	1.0025	0.7673	0.4153	0.0
130°	0.9497	0.5774	0.0610	−0.4706
140°	0.8945	0.3899	−0.2518	−0.8049
150°	0.8436	0.2267	−0.4912	−0.9904
160°	0.8028	0.1026	−0.6509	−1.0657
170°	0.7764	0.0259	−0.7394	−1.0839
180°	0.7673	0.0	−0.7673	−1.0851

z increases until it reaches its maximum value of 1.0851 for $\theta = 90°$. Beyond 90°, z begins to decrease and reaches its original value of 0.7673 for $\theta = 180°$. Thus for $d = \lambda/4$, only the Tschebyscheff polynomial between the values $0.7673 \le z \le 1.0851$ ($A \le z \le z_0$) is used to form the pattern of the array factor.

2. $d = \lambda/2$, $N = 10$, $R_0 = 20$

At $\theta = 0°$ the value of z is equal to 0 (point B). As θ becomes larger, z increases until it reaches its maximum value of 1.0851 for $\theta = 90°$. Beyond 90°, z decreases and comes back to the original point for $\theta = 180°$. For $d = \lambda/2$, a larger part of the Tschebyscheff polynomial is used ($0 \le z \le 1.0851$; $B \le z \le z_0$).

3. $d = 3\lambda/4$, $N = 10$, $R_0 = 20$

For this spacing, the value of z for $\theta = 0°$ is -0.7673 (point C), and it increases as θ becomes larger. It attains its maximum value of 1.0851 at $\theta = 90°$. Beyond 90°, it traces back to its original value ($-0.7673 \le z \le z_0$; $C \le z \le z_0$).

4. $d = \lambda$, $N = 10$, $R_0 = 20$

As the spacing increases, a larger portion of the Tschebyscheff polynomial is used to form the pattern of the array factor. When $d = \lambda$, the value of z for $\theta = 0°$ is equal to -1.0851 (point D) which in magnitude is equal to the maximum value of z. As θ attains values larger than 0°, z increases until it reaches its maximum value of 1.0851 for $\theta = 90°$. At that point the polynomial (and thus the array factor) again reaches its maximum value. Beyond $\theta = 90°$, z and in turn the polynomial and array factor retrace their values ($-1.0851 \le z \le +1.0851$; $D \le z \le z_0$). For $d = \lambda$ there

INTEL-1045
U.S. Patent 7,151,430